MICROBIAL DESULFURIZATION OF COALS BY ORGANISMS OF THE GENUS *PSEUDOMONAS*

CHARANJIT RAI AND JON P. REYNIERS

TEXAS A&I UNIVERSITY, KINGSVILLE, TEXAS 78363

INTRODUCTION

Organisms of the genus *Pseudomonas* are widely distributed in the environment and are found in high-sulfur content coals. These organisms are strictly aerobic chemolithotrophs which require minimal organics for growth.

Preliminary studies indicated that *P. aeruginosa* and *P. putida* may function in desulfurization of bituminous coals and lignite (1,2). However, *P. aeruginosa* was much less effective than *P. putida*. Incubation of these organisms at temperatures less than 37°C could favor growth of *P. putida* over *P. aeruginosa* since optimum growth of *P. putida* occurs at 26°C (3). Further, incubation of these organisms in the presence of semi-purified sources of inorganic sulfurs, such as pyrite (PYR), marcasite (MAR), and melanterite (MEL), or organic sulfur such as dibenzothiophene (DBT) could result in restricted growth of the organisms. Finally, differences in the enzymatic profile of the organisms could suggest possible mechanisms of sulfur processing.

The prupose of the present study was to characterize *P. aeruginosa* and *P. putida* in their ability to desulfurize coals and to evaluate their performance with specific natural sources of inorganic and organic sulfurs known to be constituents of coals. The results show that *P. aeruginosa* uniformly grows better that *P. putida* in the presence of the sulfur sources and coals and suggest that the mechanism of desulfurization is not similar to that of the genus *Thiobacillus*.

EXPERIMENTAL

Organisms

Pseudomonas aeruginosa (ATCC 27853) and *Pseudomonas putida* (ATCC 12633) were obtained in pure culture from the American Type Culture Collection, Rockville, MD.

Media

P. aeruginosa and *P. putida* were maintained at 5°C on minimal agar slants containing the following in g/l, final volume: solution A [potassium dihydrogen phosphate (3.0), disodium hydrogen phosphate (6.0), ammonium chloride (2.0), sodium chloride (5.0), agar (15.0) in 800 ml with deionized, distilled H_2O]; solution B [glucose (8.0), magnesium sulfate (0.1) in 200 ml with deionized, distilled H_2O]. Solutions A and B were autoclaved at 15 psi for 15 minutes and then aseptically combined after cooling. The final pH was 7.0. All reagents were obtained from MCB, except as noted. For experiments, HPLC-grade H_2O (Burdick & Jackson Laboratories, Inc.) was used, and agar was not incorporated. Where other materials were used as sulfur sources, magnesium sulfate was replaced by magnesium chloride. In shaker-flask experiments, the organisms were grown in a nutrient broth (DIFCO) containing beef extract (3.0 g/l) and peptone (5 g/l). Tryptic soy broth (DIFCO) served as a complete medium and contained the following in g/l: tryptone (17.0), soytone (3.0), dextrose (2.5), sodium chloride (5.0), dipotassium phosphate (2.5 g) in 1.0 l with deionized, distilled H_2O prior to autoclaving.

Coal and Sulfur Sources

Samples of Illinois #6 bituminous coal and lignite were obtained from Amax Coal Company. The coal samples were ground in a ball-mill and seived to 147-1651 μm particle size for shaker-flask experiments or to a fine powder for other experiments.

Samples of pyrite (FeS_2), marcasite (FeS_2), and melanterite ($FeSO_4 \cdot 7H_2O$) were obtained from the Department of Geology, Texas A&I University. These samples were ground to a fine powder equivalent in particle size to the coal samples. High-purity (>99.9%) pyrite was obtained from the Aesar Group, Seabrook, NH. The forgoing samples served as experimental sources of inorganic sulfur.

Dibenzothiophene (DBT)was obtained from Aldrich Chemical Company and served as a model organic sulfur source.

Organism and Enzyme Assays

Positive identifiaction and the purity of cultures of *P. aeruginosa* and *P. putida* was made prior to each experiment, using 20 standardized biochemical and carbon assimilation tests. Systematic and rapid semi-quantitative microanalysis of 19 enzymatic assays were obtained from DMS Laboratories, Inc., Farmington, NJ, and were performed according to standard protocols provided by the manufacturer.

Analytical Procedures

Illinois #6 coal and lignite samples were analyzed for total sulfur by the Eschka method and pyritic and sulfate sulfur content was determined by chemical procedures (D-2494-79) described by the American Society of Testing Materials (3,4).

Filtered coal samples were washed with dilute hydrochloric acid followed by distilled water to remove trace adsorbed sulfate and iron. The filtrate was analyzed for sulfate and total iron. The Eschka method was used to estimate total sulfur content in coals. Extraction of 1 g coal samples by dilute hydrochloric acid was followed by turbidimetric determination of sulfate (4). Extraction of weighed coal samples with 2N nitric acid was followed by titrimetric determination of iron (5) as a measure of pyritic sulfur content.

Microbial Methods

Shaker-flask experiments were conducted to determine the effectiveness of *P. aeruginosa* and *P. putida* in removal of pyritic sulfur from coals. Weighed samples of coal were placed into 250 ml Erlenmayer flasks and suspended in 75 ml nutrient broth. The flasks were charged with 5 ml of bacterial cells adjusted to 10^9 cells/ml. Incubation was allowed to proceed at 30°C for periods between 5-7 days in a shaker-bath. Following incubation, total and pyritic sulfur content of the coals were determined as previously described.

P. aeruginosa and *P. putida* were evaluated under various growth conditions for their response to the presence of saturating and dilute levels of pyrite, marcasite, melanterite, and dibenzothiophene. The organisms were also characterized with regard to their enzymatic patterns.

Preliminary growth experiments were performed in 13 x 100 mm screw-cap tubes containing 5.0 ml of complete medium and 0.1 g of pyrite, marcasite, or melanterite. The tubes containing the medium and sulfur sources were autoclaved (15 psi, 15 minutes), cooled, and inoculated with 0.1 ml of a suspension of an 18-hour mid-log phase culture of bacterial cells, adjusted to an optical density of 0.75 A_{540} (10^9 cells/ml) using a Baush and Lomb Spectronic 20 spectrophtometer. The tubes were incubated with occasional

shaking in water baths adjusted to temperatures between 20°C and 40°C. Growth of the organisms was monitored tuberidimetrically by following adsorbance at 540 nm. After 55 hours, the cells were removed by contrifugation (10,000 x g), and the pH of the medium was determined for each tube. In other experiments, growth of *P. aeruginosa* and *P. putida* was followed in tubes containing chemically-defined minimal medium and dilutions of the sulfur sources and coals. 0.1 g of pyrite, marcasite, melanterite, dibenzothiophene, bituminous coal, or lignite was added to 10 ml of HPLC-grade H_2O, autoclaved, and allowed to stand overnight. 0.5 ml of these suspensions was added to 4.0 ml of sterile solution A. The suspensions were clarified by centrifugation and the saturated supernate used to make 10-fold dilutions of the sulfur sources. 0.5 ml of these dilutions were added to 4.0 ml of sterile solution A. All tubes received 0.5 ml of solution B containing autoclaved glucose and magnesium chloride. Each tube received 0.1 ml of *P. aeruginosa* or *P. putida* grown to mid-log phase in 18 hours at 30°C in the chemically-defined minimal medium containing only magnesium sulfate as a sulfur source. Prior to inoculation, the organisms were washed with solution A without magnesium sulfate and the inoculous culture was adjusted to an optical density of 1.75 A_{540}. The tubes were incubated at 30°C and growth of the organism was followed spectrophotometrically for 45 hours. The cells were then removed by centrifugation and the pH of the medium in each tube was determined.

RESULTS AND DISCUSSION

1. Microbial Desulfurization of Coals by Organisms of the Genus *Pseudomonas*.

Preliminary investigations were conducted for pyrite desulfurization of Illinois #6 (Herrin Coal), Illinois #6 (Ziegler Coal) and Atascosa-McMullen lignite. The initial (As Received) pyritic sulfur content of Illinois #6 (Herrin Coal) was 4.9%; Illinois #6 (Ziegler Coal), 4.2%; and Atascosa-McMullen lignite, 1.9%. In the laboratory experiments *Pseudomonas aeruginosa* was found to be barely effective (about 28%), whereas *Pseudomonas putida* reduced the pyritic sulfur content of Illinois #6 (Herrin Coal) 147 µm particles and that of Atascosa-McMullen lignite 147 µm particles by approximately 75%. The desulfurization rate for the Herrin Coal was about 659 mg/liter x day, for the Ziegler Coal, 557 mg/liter x day and that for Atascosa-McMullen lignite about 288 mg/liter x day for the initial 6 day period. The data on the effect of particle size distribution on the rate of pyrite desulfurization is presented in Table 1 with organisms of Genus *Pseudomonas*.

2. Characterization of Organisms of Genus *Pseudomonas*.

P. aeruginosa is differentiated from *P. putida* in its production or use of nitrate, urease, geletin, n-acetylglucosamine, and adipate. All other biochemical and carbohydrate utilization tests were identical for both organisms.

Enzyme profiles were prepared on the organisms. No major differences were observed in the enzymatic profiles of the two organisms when grown in the absence of the sulfur or coal sources except those listed in Table 2. Incubation of the organisms in the presence of PYR, MAR, MEL or DBT as sulfur sources had no marked effect on any of the enzymes tested.

P. aeruginosa and *P. putida* were grown in complete medium in the presence of saturating levels of pyrite, marcasite, and melanterite at temperatures between 20 and 40°C. An objective of this experiment was to determine if these materials interfered with the growth of either organism and, if not, what temperatures would permit equivalent growth rates for both organisms.

The results of this experiment are summarized in Table 3.

TABLE 1

MICROBIAL DESULFURIZATION OF BITUMINOUS COALS
BY ORGANISMS OF GENUS *PSEUDOMONAS*

PSEUDOMONAS PUTIDA

COAL	PARTICLE SIZE	PYRITIC SULFUR, WT % BEFORE	PYRITIC SULFUR, WT % AFTER	DAYS	PYRITIC SULFUR REDUCTION, (%)	RATE, (MGS/LITER x DAY)
Illinois #6 Herrin Coal	+1397μm	4.10	1.25	5	69.15	586.75
Illinois #6 Herrin Coal	+1397μm	4.10	1.08	7	73.66	444.11
Illinois #6 Herrin Coal	- 147μm	5.13	1.47	5	71.34	753.52
Illinois #6 Herrin Coal	- 147μm	5.13	1.28	7	75.05	566.17
Illinois #6 Ziegler Coal	- 147μm	4.40	1.02	6	76.82	579.89
Illinois #6 Ziegler Coal	- 147μm	4.40	1.10	6	75.00	566.17
Lignite Atascosa-McMullen	- 147μm	2.22	0.54	6	75.67	288.23
Lignite Atascosa-McMullen	- 147μm	1.15	0.38	6	66.95	132.10
PSEUDOMONAS AERUGINOSA						
Illinois #6 Ziegler Coal	- 147μm	4.40	2.97	6	32.50	245.34
Illinois #6	- 147μm	4.40	3.25	6	26.14	197.30

These experiments were conducted at 70-85°F with continuous shaking.

TABLE 2. ENZYMATIC DIFFERENCES WITHOUT SULFUR AND COAL SOURCES.

ENZYME/SUBSTRATE	ACTIVITY[a] *P. aeruginosa*	*P. putida*
Lipase esterase/2-naphthyl-caprylate	30	5
Lipase/2-naphthyl-myristate	10	0
Acid phosphatase/2-naphthyl-phosphate	5	30
All enzymes/no substrate	0	0

[a] Nanomoles substrate hydrolyzed in 4 hours.

TABLE 3. INFLUENCE OF INORGANIC SULFUR SOURCES ON THE GROWTH OF *P. aeruginosa* and *P. putida*.

GROWTH TEMPERATURE, (°C)	GROWTH[1] *P. aeruginosa*	*P. putida*
20	R (PYR, MAR, MEL)	N
25	R (PYR, MAR, MEL)	R (PYR, MAR, MEL)
30	R (PYR, MAR, MEL)	R (PYR, MAR, MEL)
37	R (MAR, MEL)	R (PYR, MAR, MEL)
40	R (PYR, MEL)	N

[1] Relative to controls, without PYR, MAR or MEL as sulfur sources, growth of organisms is repressed (R) or not repressed (N) by saturating levels of the sulfur sources in complete mediums.

At 20°C, growth of *P. aeruginosa* was <0.4 A_{540}/45 hours and the presence of pyrite, marcasite, and melanterite further restricted growth ≦0.2 A_{540}/45 hours. At 25°C, the growth of *P. aeruginosa* improved. Maximum growth was reached with temperatures ≧30°C typically 1.5 A_{540}/45 hours. Stationary phase of growth was not reached until after 45 hours of incubation. The presence of the sulfur sources was generally restrictive at any incubation temperature. At or above 37°C, *P. aeruginosa* reached stationary phase between 15 and 20 hours of incubation.

P. putida grew slowly at 20°C, typically reaching ≦0.4 A_{540}/45 hours. Above 20°C, the presence of pyrite, marcasite, and melanterite was not restrictive to growth. *P. putida* grew better at 25°C with or without the sulfur sources. Maximum growth of *P. putida* was achieved ≧30C, typically being ≧1.4 A_{540}/45 hours. However, the growth of *P. putida* at temperatures ≧30°C in the presence of the sulfur sources was generally repressed, being typically ≦0.8 A_{540}/45 hours. Elevation of incubation temperature above 37°C resulted in low-level growth of *P. putida* (≦0.6A_{540}/45 hours) with or without the sulfur sources.

Following incubation of *P. aeruginosa* and *P. putida* with or without the sulfur sources, the pH of the medium was monitored. The results are shown in Table 4. Incubation of the organisms in the presence of the sulfur sources for 45 hours did not result in lowering of the pH of the medium relative to controls without the sulfur sources.

TABLE 4. EFFECT OF SULFUR SOURCES ON pH OF MEDIUM.

TREATMENT	pH OF MEDIUM[a] *P. aeruginosa*	*P. putida*
None	7.2 ± 0.1	7.3 ± 0.1
Pyrite	7.3 ± 0.1	7.0 ± 0.3
Marcasite	6.9 ± 0.4	7.3 ± 0.1
Melanterite	7.2 ± 0.1	7.1 ± 0.1

[a] Average of pH of all tubes (n = 20) of a given treatment for a given organism incubated between 20 and 40°C.

P. aeruginosa and *P. putida* were grown in a chemically-defined minimal medium containing various sulfur sources. The results are shown in Table 5. The presence of the sulfur sources or coals was, in general, repressive to the growth of both organisms and to *P. putida* more than *P. aeruginosa*. An attempt to limit availability of the sulfur sources by diluting from a point of solution saturation did not result in substantial effects to the growth of either organism. Growth of *P. putida* was better when the individual sulfur sources were provided rather than the coals. The pH of the medium after 55 hours of incubation remained near neutrality and was not significantly different from controls without the sulfur sources.

CONCLUSIONS

The results from the preliminary microbial desulfurization of Illinois #6 and Texas lignite by the organisms of the Genus *Pseudomonas* show that *P. putida* was much more effective than *P. aeruginosa*. The *P. putida* reduced the pyritic sulfur content of Illinois #6 as well as lignites by 69 to 76% in 5 to 7 days for coal particles from 147 μm to 1397 μm. Whereas *P. aeruginosa* was hardly effective (26 to 32.5%) in reducing the pyritic sulfur content of Illinois #6.

TABLE 5. GROWTH OF ORGANISMS IN CHEMICALLY-DEFINED MINIMAL MEDIUM.

TREATMENT[a]	ORGANISM[b]	AVERAGE GROWTH[c] SATURATED MEDIUM	AVERAGE GROWTH[c] DILUTED MEDIUM
PYR	P	0.40 ± 0.01	0.43 ± 0.01
	A	0.81 ± 0.01	0.58 ± 0.01
MAR	P	0.40 ± 0.02	0.48 ± 0.01
	A	0.68 ± 0.01	0.68 ± 0.02
MEL	P	0.50 ± 0.01	0.31 ± 0.02
	A	0.72 ± 0.02	0.60 ± 0.03
DBT	P	0.39 ± 0.01	0.53 ± 0.03
	A	0.59 ± 0.03	0.63 ± 0.02
BITU	P	0.34 ± 0.01	0.38 ± 0.01
	A	0.59 ± 0.02	0.64 ± 0.01
LIGN	P	0.39 ± 0.01	0.46 ± 0.03
	A	0.57 ± 0.01	0.64 ± 0.01

[a] Sulfur sources: pyrite (PYR), marcasite (MAR), melanterite (MEL), dibenzothiophene (DBT), bituminous coal (BITU), lignite (LIGN).

[b] Organisms: *P. aeruginosa* (A), *P. putida* (P).

[c] All A_{540} values averaged along growth curve for 55 hours at 30°C. These averages then averaged for saturated medium (n=4) contain particulate sulfur sources or dilutions (n=12) of the sulfur sources.

P. aeruginosa and *P. putida* were characterized by standard enzymatic and carbon assimilation tests to assure the purity of the microorganisms. Preliminary screening of other enzymatic activities indicated semiquantitative differences between the two microorganisms which could not explain the observed differences between their activities related to pyritic desulfurization of coals.

It was further observed that the equivalent growth for both *P. aeruginosa* and *P. putida* was obtained at 30°C, and this temperature was used in further studies. The presence of pyrite, marcasite, and melanterite, although not toxic to the organisms, was generally repressive to their growth with *P. putida* being qualitatively more labile than *P. aeruginosa*. Incubation of both *P. aeruginosa* and *P. putida* for long periods with or without the sulfur sources did not significantly alter the pH of the medium, suggesting that these organisms process sulfur by different mechanism than the organisms of the genus *Thiobacillus*.

ACKNOWLEDGEMENTS

This study was supported by research grants from the Texas Energy Corporation and Atlantic Richfield Foundation. The graduate students, T. J. Okeke, T. Balogun and S. Articharte conducted the experiments described in this paper. We thank them for their contributions.

REFERENCES

1. Rai, C. (1982), "Method for Removing Pyritic Sulfur from Coal by Using Aerobic Sulfur Reducing Microorganisms as Coal in Slurry Form is Transported Through a Pipeline," U. S. Patent filed in June 1982.
2. Rai, C. (1985), "Microbial Desulfurization of Coals and Texas Lignites, Presented at the AIChE Spring National Meeting, Houston, Texas (March 1985).
3. Buchanan, R. E. and N. E. Gibbons (1974). Bergey's Manual of Determinative Bacteriology," Eighth Edition, The Williams & Wilkins Company.
4. Karr, C. 1978. "Analytical Methods for Coal and Coal Products." Academic Press, N. Y., Vol. I, pp. 224, 280-321.
5. American Society of Testing Materials. Annual Book of ASTM Standards, Part 26, Methods D2492-79 and D3177-75, American Society of Testing Materials, (1979) Philadelphia, PA.

MICROBIAL DESULFURIZATION OF BITUMINOUS COALS

Charanjit Rai

Department of Chemical & Natural Gas Engineering
Texas A&I University
Kingsville, Texas 78363

INTRODUCTION

Our environment has constantly been polluted by the combustion of conventional fuels like petroleum, coal and natural gas. It is estimated that about 88 million tons of sulfur dioxide gas (SO_2) is discharged to the environment due to the combustion of fossil fuels. The Clean Air Act Amendment of 1977 set an emission limit of 1.2 lb SO_2 per million Btu of fuel combusted. Most bituminous coals contain 3 to 6 percent sulfur as inorganic or organic sulfur. The inorganic sulfur compounds are primarily metallic sulfides, pyrite or marcasite and sulfates formed by the air oxidation of metallic sulfides (1,2). The organic sulfur in coal is beleived to be in the form of monosulfide, disulfide or condensed thiophenes, benzothiophenes, dibenzothiophenes and thioxanthenes having varying reactivities. Physical and chemical processes have been developed for coal desulfurization, some of them operate at high temperatures and are energy intensive. Removal of organic sulfur by these processes is difficult. Microbial desulfurization offers an effective means of precombustion sulfur removal(3,4,5).

Colmer and Hinkle (6) identified *T. ferrooxidans* in acidic mine waters. Subsequent studies by Silverman *et al.* (7,8) confirmed that *T. ferrooxidans* could be utilized to oxidize FeS_2 in coal in 3 to 4 days and the rate of oxidative dissolution was a function of the particle size and rank of the coal. Dugan and Apel (4) showed that a mixed culture of *T. ferrooxidans* and *T. thiooxidans* was most effective at a pH of 2 to 2.5 when the nutrient was enriched with NH_4^+. They reported 97% removal of pyritic sulfur from a coal sample with 3.1 weight percent sulfur. Norris and Kelly (9) reported that another acidophillic bacteria, *Leptospirillum ferrooxidans* in mixed cultures with *T. thiooxidans* was effective for FeS_2 removal.

Hoffmann *et al.*(10) conducted a parametric study to determine the effect of bacterial strain, N/P molar ratio, the partial pressure of CO_2, the coal source and the total reactive surface area on the rate and extent of oxidative dissolution of iron pyrite at a fixed oxygen pressure. The bacterial desulfurization of high pyritic sulfur coal could be achieved in 8 to 12 days for pulp densities of $\leq$ 20%, and particle size $\leq$ 74 μm. The most effective strains of *T. ferrooxidans* were isolated from the natural systems and the most effective nutrient medium contained low phosphate levels, with an optimal N/P molar ratio of 90:1.

MECHANISM OF MICROBIAL DESULFURIZATION

The mechanism of microbial dissolution of pyritic sulfur in coal by acidophilic bacteria has been thoroughly investigated (10,11,12). The pyrite is readily oxidized by oxygen or the ferric ion resulting in the ferrous state as follows:

$$FeS_2 + 3.5\ O_2 + H_2O \rightarrow Fe^{++} + 2SO_4^{=} + 2H^+ \qquad 1)$$

$$FeS_2 + 2\ Fe^{+++} \rightarrow 3Fe^{++} + 2S \qquad 2)$$

Thiobacillus ferrooxidans derives energy by catalyzing the oxidation of the ferrous ions back to the ferric state (12):

$$Fe^{++} + 1/4\ O_2 + H^+ \rightarrow Fe^{+++} + 1/2\ H_2O \qquad 3)$$

Ferric sulfate, a reaction product, reacts with FeS_2 to form more ferrous sulfate which is again catalyzed by *T. ferrooxidans* to the ferric state.

$$FeS_2 + 14\ Fe^{+++} + 8H_2O \rightarrow 15\ Fe^{++} + 2\ SO_4^{=} + 16H^+ \qquad 4)$$

Elemental sulfur, likewise, is oxidized by *T. thioxidans* forming sulfuric acid.

$$2S + 2\ H_2O + 3O_2 \rightarrow 4H^+ + 2SO_4^{=} \qquad 5)$$

The oxidation reactions are dependent on the microbial reactions with the end result of accelerating the transformation of FeS_2 to ferrous sulfate and thus equation (1) precisely represents the overall reaction stoichiometry for kinetic purpose. Other reactions provide the possible mechanistic pathways for the microbial pyritic dissolution.

Most microbial desulfurization studies have been conducted in the laboratory shake-flask type experiments and the major drawback cited against such a process has been that the rates of pyritic sulfur removal were not high enough to reduce the reactor size to a reasonable capacity (2,5). In this study an attempt has been made to determine the effectiveness of *Thiobacillus ferrooxidans* under simulated pipeline conditions for pyritic sulfur removal. Since the microbial desulfurization process is conducted under acidic environment, an attempt has been made to determine the corrosion rates under dynamic conditions using Illinois #6 and Indiana #3 bituminous coals and to investigate the effectiveness of a commercial corrosion inhibitor for controlling the corrosivity.

EXPERIMENTAL

Coal Samples:

The samples of Illinois #6 and Indiana #3 were obtained from the Amax Coal Company's Delta and Midwest mines and Ziegler Coal Company's mine in the Randolph County of Illinois. The pyritic sulfur content data on the coal samples is shown in Table I. The samples were ground in a ball mill and then sieved to obtain the desired particle size distribution.

TABLE 1

Bituminous Coal Samples and Their Pyritic Sulfur Content

Coal Sample	FeS_2 (wt%)
1. Illinois #6, Delta Mine (CS-1280-004) Amax Coal Company	2.02

2.	Indiana #3, Ayrshire Mine (CS-1180-007) Amax Coal Company	2.60
3.	Illinois #6, Randolph County, Ziegler Coal Company	4.20
4.	Illinois #6 (C22024) Herrin Coal, Northern Illinois, Illinois State Geological Survey	4.90

The shake-flask and two-inch pipeline experiments were initially conducted with various particle sizes; such as: As Received, 417 to 1651 μm, 208 to 417 μm, 147 to 208 μm, and 43 to 147 μm. However, for detailed study a sample size, 74 to 147 μm, was selected.

Microbial Procedures:

A pure culture of *Thiobacillus ferrooxidans* obtained from the American Type Culture Collection (ATCC) was used in this study for the shake-flask experiments and the 2-inch slurry pipeline experiments. A mineral salts medium having the following composition was used in these experiments: $Fe(SO_4) \cdot 7\ H_2O$ 20 g/l; $(NH_4)_2\ SO_4$ 0.8 g/l; $KH_2\ PO_4$ 0.4 g/l; $Mg(SO_4) \cdot 7\ H_2O$ 0.16 g/l. The mineral salts were dissolved in distilled water and the pH was adjusted to 2.8 by addition of 1N H_2SO_4. The medium was autoclaved at 20 psia for one hour. The growth medium consisted of slurried coal samples consisting of Illinois #6 or Indiana #3 as desired.

Analytical Procedures:

The samples of bituminous coals were analyzed for pyritic sulfur, sulfate sulfur and total sulfur using conventional wet chemical procedures adapted from the American Society of Testing Materials (13,14). The Eschka method was used for the total sulfur, and D-2494-79 was used for sulfate and pyritic sulfur analysis.

The treated samples were filtered through a Whatman #2 filter paper to separate the coal particles from the liquid medium. The filtered sample was washed with 0.1 N HCl followed by distilled water to remove traces of absorbed sulfate and iron.

The total sulfur content of the coal samples was determined by the Eschka method. The sulfate sulfur content of the test samples was determined by extraction of a one gram sample with dilute hydrochloric acid followed by turbidimetric determination of sulfate (13). The pyritic sulfur content was determined by extraction of the weighed coal samples with 2N nitric acid followed by titrimetric or atomic absorption determination of iron in the extract (14).

Laboratory Corrosion Test:

The laboratory test procedure for the determination of corrosion rates of coal slurry used in this study was adapted from the method developed by Bomberger (15). The corrosion rates were determined by using ASTM Standard Corrosion Test,

also known as Total Immersion Method (16). The Bomberger technique consists of keeping coal slurry in suspension in a two-liter reaction vessel at a constant temperature. The corrosion rates are determined either by actual weight loss of steel coupons suspended in the reaction vessel or by the use of corrosometer probe over a 24 to 72 hour period. The weight loss of steel coupons is a measure of the corrosion rates expressed as Inch Per Year (IPY). In the case of corrosometer probe, it is initially calibrated by means of a weight loss measurement.

The ASTM Corrosion Test procedure by Total Immersion Method requires that all specimen in a test series should have the same dimensions when comparisons are to be made. In these experiments, carbon steel was used representing the pipeline material. The coupons were cleaned, polished and weighed. Coal-water slurry, 10 to 40 weight percent was used in the corrosion tests. Specimens were immersed in the reaction vessel maintained at a constant temperature of 86°F for 72 hours or the specified time. The coupons were removed, washed with deionized water, dried and weighed. The loss in weight of the specimen, before and after the test was attributed to corrosion. From the weight loss data, the corrosion rates were calculated as Inch Per Year (IPY) and also as gram per square centimeter per year. (g/cm^2. year).

RESULTS AND DISCUSSION

1. Shake-Flask Experiments with *Thiobacillus Ferrooxidans*.

A limited number of experiments were conducted using *Thiobacillus ferrooxidans* to determine the influence of process variables on the rate and extent of pyritic sulfur release from the coal samples in shake-flask experiments using a mechanical shaker. No attempt was made to optimize the mineral salts medium composition since the influence of NH_4^+, N/P molar ratio and the nitrogen requirements for the growth of *T. ferrooxidans* have been thoroughly investigated by other workers (4,7,8,10). A mineral salts medium with the composition described earlier in the Microbial Procedures section was used in all the experiments with *T. ferrooxidans*.

A number of samples of pulverized coals were used having the following particle sizes: As Received, 417 to 1651 μm, 147 to 208 μm, < 147 μm. Coal/water slurries (10 wt%) made from the sterilized coal samples in mineral salts medium were inoculated with a strain of *T. ferrooxidans* and were subjected to mechanical shaking from three to twelve days. At the end of the desired test period, 3, 6, 9 or 12 days, the coal samples were filtered, thoroughly washed with deionized water and analyzed for pyritic sulfur content. The data was plotted as mg/liter of pyritic sulfur realeased as a function of time as shown in Figure 1 for a coal sample of Illinois #6 from the Zeigler Coal mine. The data shows a maximum reduction in pyritic sulfur content was achieved with < 147 μm (-100 mesh) particle size, the average rate being 377.4 mg/liter x day during the nine day oxidation period versus 199.0 mg/liter x day for the 417 to 1651 μm (-10 to +35 mesh) particles. Indiana #3 coal from the Ayrshire mine exhibited similar trends, the average pyritic oxidation rate being 291.1 mg/liter x day for a 147 to 417 μm particles over an eight day period with *T. ferrooxidans*.

2. Two-Inch Slurry Pipeline Experiments:

(a) Slurry Pipeline System.

A two-inch PVC pipeline loop, 60 feet in length, was installed on a laboratory wall and a 2 horsepower positive displacement type Gould pump, Model 3196 was

incorporated in the flow system. The flow rate through the pipeline could be varied from a low of 2 ft/sec to 15 ft/sec. The system was designed to recirculate coal/water slurry through an open drum where air was bubbled in the line. A copper cooling coil was immersed below the slurry level in the drum for recirculating cold water through the medium in order to remove heat from the system. The flow rate in the pipeline was monitored by the use of a Polysonics flow meter, model UFM-P. The equipment was capable of continuous operation. The critical velocity for flow of slurries in the pipeline was calculated using a correlation developed by Oroskar and Turian (17). The critical velocity, defined as the minimum velocity needed to keep the coal particles susoended in the liquid medium, was calculated to be 5.5 ft/sec for a 50 wt% coal/water slurry for the two inch laboratory pipeline.

(b) Particle Size Distribution

A 6.6 wt% slurry consisting of Indiana #3 bituminous coal with 60.5% of 417 to 165 μm and 39.5% of 147 to 417 μm particles was recirculated through the pipeline loop for 6 hours at 5.6 to 5.8 ft/sec at 85-95°F using deionized water for preparation of the slurry. At the conclusion of the experiment, the coal particles were filtered, dried and sieved to determine the particle size distribution. The data for final size distribution of the slurried coal is shown in Table II.

TABLE II

Slurry Recirculation in Laboratory Pipeline

Indiana #3 (Ayrshire) (6.6% wt% slurry in deionized water)	417 to 1651 μm, 60.5%
	147 to 417 μm, 39.5%
Flow Rate:	5.6 to 5.8 ft/sec
Temperature:	85-95°F
Run, Hours:	6

Final Particle Size Distribution

Particle Size	Percent
+1651 μm	0.62
-1651 to +417 μm	4.69
-417 to +147 μm	40.45
-147 to +74 μm	39.40
-74 μm	14.79

(c) Microbial Desulfurization Experiments in the Two-Inch Pipeline.

Illinois #6 (Delta Mine) and Indiana #3 (Ayrshire Mine) bituminous coals were used in the slurry pipe desulfurization experiments using *T. ferrooxidans* for inoculating the coal/water slurry used in these experiments. A 10 wt% coal/water slurry was prepared using deionized water and the mineral salts medium described earlier, the coal particle size range was from 147 μm to 1981 μm. The slurry flow rate was kept at 6 to 6.2 ft/sec, and the temperature in the system was controlled by recirculating cold water through the copper cooling coils in the slurry drum. Duplicate samples of coal slurry were taken once a day for the determination of pyritic sulfur content in the slurry. The experiment was continued for seven days with recirculation of the slurry through the pipeline system for 8 hours/day. The experimental data with Illinois #6 (Delta) is shown in Table 3, and the rate of pyrite desulfurization is shown in Figure 2. The desulfurization rates in the slurry pipeline experiments and the

laboratory shake-flask experiments are in good agreement.

Another slurry pipeline desulfurization experiment was conducted using Indiana #3 (Ayrshire) coal in deionized water as a 25 wt% slurry. The other process variables were carefully controlled: flow rates 6-6.5 ft/sec, temperature, 70-90°F, and pH, 2.5-2.8. The experiment was continued for 14 days and the slurry samples for pyritic sulfur determination were taken daily. The desulfurization rates with Indiana #3 coal in the pipeline experiment are shown in Figure 4 and are in good agreement with the laboratory data and the results with Illinois #6 coal. As observed in the laboratory experiments, the rate of desulfurization of bituminous coals is directly proportional to the pyritic sulfur content and the particle size of the coal sample.

3. Corrosion Test Results:

The corrosion rates were determined using a 10 wt% to 40 wt% coal water slurry with 147 to 417 μm coal particles. The corrosion rates ranged from 1.223×10^{-3} IPY for Illinois #6 to 1.272×10^{-2} IPY for Indiana #3 coal slurry consisting of 40 weight percent each coal.

The addition of *T. ferrooxidans* in salt medium at the desired concentration to the coal/water slurry increased the corrosion rates for both the coals tested. The corrosion rates for 72-hour and 500-hour experiments in the presence of *T. ferrooxidans* in salt medium with 10 weight percent slurry of Illinois #6 ranged from 4.2×10^{-3} IPY to 1.41×10^{-2} IPY respectively. However, the introduction of upto 10 ppm of a commercial corrosion inhibitor, Calgon T G-10, inhibited the corrosion rates with Illinois #6 and Indiana #3 coals to very low levels approaching those obtained with the deionized water. Black Mesa pipeline has used this corrosion inhibitor on a regular basis with very satisfactory results.

CONCLUSIONS

About 80 to 85% pyritic sulfur removal has been achieved by microbial desulfurization of Illinois #6 and Indiana #3 coals using *Thiobacillus ferrooxidans* in laboratory shake-flask experiments and in a two-inch pipeline loop. The 10 to 25 wt% coal/water slurry was recirculated at 6-7 ft/sec for 5 to 12 days at 70-90°F. Results also show that the rates of bacterial desulfurization are higher in the pipeline loop under turbulent flow conditions for particle sizes, 43 to 200 μm as compared to the shake-flask experiments. It is visualized that the proposed coal slurry pipelines could be used as biological plug flow reactors under aerobic conditions. The laboratory corrosion studies show that use of a corrosion inhibitor will limit the pipeline corrosion rates to acceptable levels.

ACKNOWLEDGEMENTS

This study was supported by research grants from Texas Energy Corporation, Amax Foundation and Atlantic-Richfield Foundation. Their support is gratefully acknowledged. The graduate students Theresa Chang, Rasik Patel and Edward Eke conducted the experimental work described in this paper. Their contributions are much appreciated.

TABLE 3

SLURRY PIPELINE DESULFURIZATION
COAL/WATER SLURRY (10 WT%)
ILLINOIS #6 BITUMINOUS COAL (DELTA MINE)
(*Thiobacillus ferrooxidans*)

DAYS	PYRITIC SULFUR, WT%	PYRITIC SULFUR REDUCTION, %	RATE OF DESULFURIZATION MG/LITER X DAY
0	1.70	0.00	0.00
1	1.45	14.7	257.35
2	1.13	33.5	293.26
3	0.80	52.9	308.82
4	0.60	64.7	283.08
5	0.48	72.0	251.17
7	0.41	76.0	189.70

SLURRY FLOW RATE: 6 to 6.2 FT/SEC
SLURRY TEMPERATURE: 70-90°F
COAL PARTICLE SIZE: 147 μm to 1981 μm
pH OF SLURRY: 2.5 to 2.8

TABLE 4

SLURRY PIPELINE DESULFURIZATION
COAL/WATER SLURRY (25 WT%)
INDIANA #3 BITUMINOUS COAL (AYRSHIRE MINE)
(*Thiobacillus ferrooxidans*)

DAYS	PYRITIC SULFUR, WT%	PYRITIC SULFUR REDUCTION, %	RATE OF DESULFURIZATION MG/LITER X DAY
0	2.58	0	0.00
4	1.75	32	558.57
5	1.55	40	554.53
7	1.82	30	292.26
9	1.03	60	463.60
11	0.645	75	473.53
12	0.516	80	463.01
13	0.52	80	426.56

SLURRY FLOW RATE: 6 FT/SEC
SLURRY TEMPERATURE: 70-90°F
COAL PARTICLE SIZE: 147 μm to 1981 μm
pH OF SLURRY: 2.5 to 3.0

EFFECT OF PARTICLE SIZE ON PYRITIC DESULFURIZATION
(*Thiobacillus ferrooxidans*)

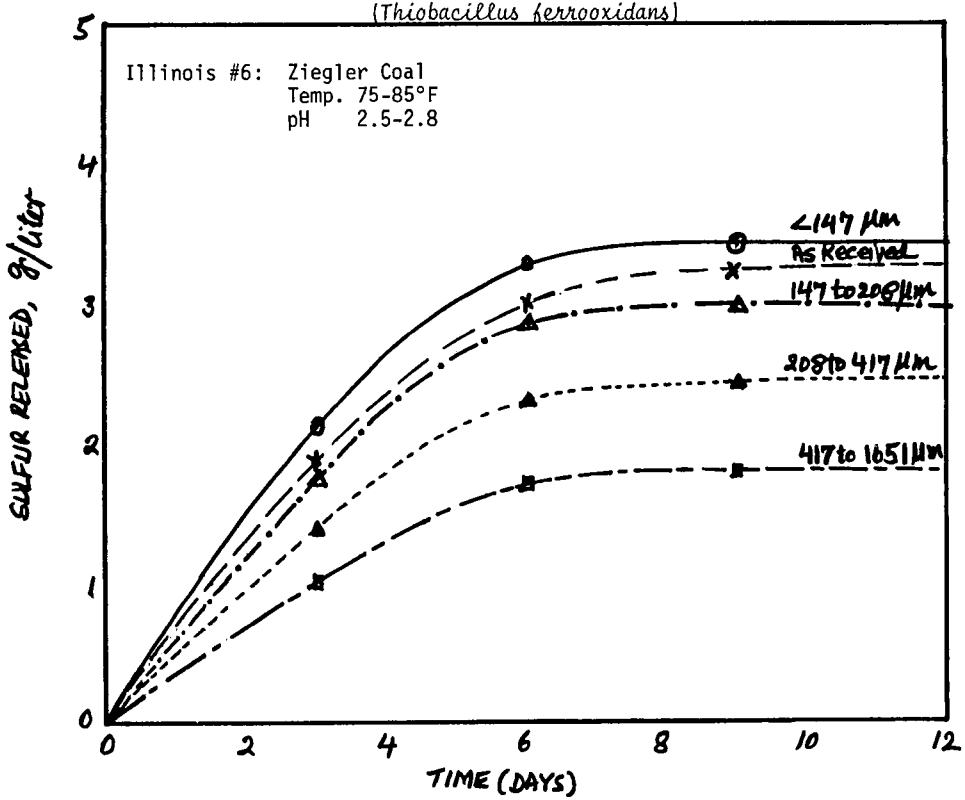

FIGURE 1.

SLURRY PIPELINE DESULFURIZATION

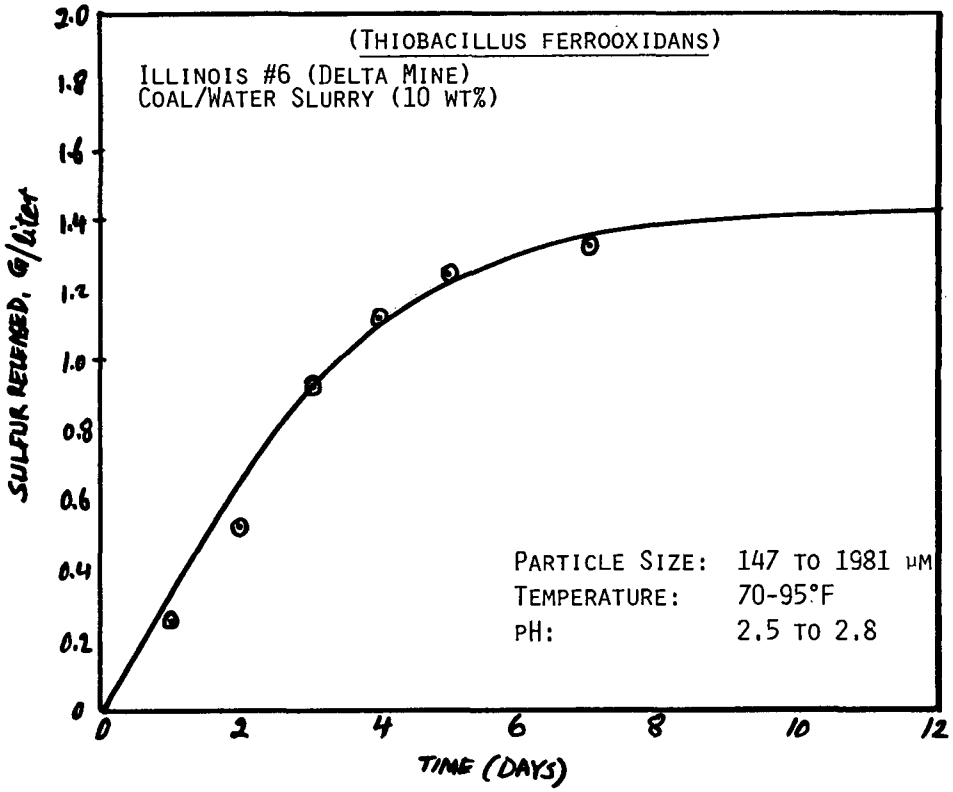

FIGURE 2

REFERENCES

1. Wheelock, T.D., Editor, 1977, "Coal Desulfurization Chemical and Physical Methods." ACS Symposium Series 64, Washington, D.C., p. IX-XI, 101-120.

2. Rofmann, H.K., Proc. Inst. Environ. Sci. 1979, pp. 266-270.

3. Robert C. Eliot, "Coal Desulfurization Prior to Combustion," Noyes Data Corporation, New Jersey, 1978, pp. V-VI, 33-42, 141-153.

4. Dugan, P.R. and W.A. Apel, 1978. "Micribial Desulfurization of Coal." In Metallurgical Application of Bacterial Leaching and Related Microbial Phenomenon." Editors, L.E. Murr, A.E. Torma and J.A. Brieley. Academic Press, N.Y. pp. 223-250.

5. Kargi, F. 1982, Microbial Coal Desulfurization, Microbial Enzyme Technol. 4(1): 13-20.

6. Colmer, A.R. and M.E. Hinkle, 1947. The Role of Microorganisms in Acid Mine Drainage, Science 106: 253-256.

7. Silverman, M.P. and D.G. Lundrgen, 1959. Studies on Chemosynthetic Iron Bacterium *Ferrobacillus ferrooxidans*. J. Bacteriol. 78: 326-331.

8. Silverman, M.P., M.H. Rogoff and I. Wender. 1963. Removal of Pyritic Sulfur from Coal by Bacterial Action. Fuel 42, 113-124.

9. Norris, P.R. and D.P. Kelly. 1978. Toxic Metals in Leaching Systems. p. 83-102. In L.E. Murr, A.E. Torma and J.A. Brierly (ed) Metallurgical Applications of Bacterial Leaching and Related Phenomena. Acadamic 85, Inc. New York.

10. Hoffmann, M.R., B.C. Faust, F.A. Panda, H.H. Koo and H.M. Tsuchiya. 1981. Kinetics of the Removal of Iron Pyrite from Coal by Microbial Catalysis. Applied & Environ. Microbiology. 42: 259-271.

11. Andrews, G.F. and J. Maczuga, 1984. Bacterial Removal of Pyrite From Coal, Fuel 63, 297-301.

12. Singer, P.C. and W. Stumm, 1970. Acidic Mine Drainage: The Rate Determining Step. Science 167: 1121-1123.

13. Karr, C. 1978. "Analytical Methods for Coal and Coal Products." Academic Press, N.Y., Vol. I, pp. 224, 280-321.

14. American Society of Testing Materials. Annual Book of ASTM Standards, Part 26, Methods D2492-79 and D3177-75, American Society of Testing Materials, (1979) Philadelphia, PA.

15. Bomberger, D.R., "Hexavalent Chromiom Reduces Corrosion in Coal-Water Slurry Pipeline." Materials Protection, Vol. 4, p. 43-49 (January 1965).

16. American Society of Testing Materials. Annual Book of ASTM Standards, Part 10, p. 913-943 (1979).

17. Oroskar, A.R. and R.M. Turian. 1980, "The Critical Velocity in Pipeline Flow of Slurries", AIChE J. 26, 550-558.

SEPARATION OF ULTRAFINE PYRITE FROM COAL BY SELECTIVE DISPERSION AND FLOCCULATION

Yosry A. Attia

The Ohio State University
Division of Mining Engineering
140 W. 19th Avenue
Columbus, Ohio 43210

- - -

ABSTRACT

A novel technique for separating ultrafine pyrite particles (minus 40 microns) from coal fines has been conceptually developed and tested. The technique involves the use of a selective polymeric dispersant for pyrite, while flocculating coal particles with a general polymeric flocculant. The suspended pyrite can be then removed from the flocculated coal fines which settle preferentially by gravity.

The key to this separation was the design and preparation of the selective dispersant for pyrite (PAAX). This was achieved by incorporating xanthate groups into the structure of a low molecular weight acrylic acid polymer (PAA). Testing this reagent on individual suspensions of coal and pyrite confirmed its selective dispersion action towards pyrite, while it had no dispersion action on coal suspension when using Purifloc-A22 flocculant. Preliminary tests on high sulfur coal from Kentucky No. 9 seam, also confirmed this selectivity. Further process development is needed however before this promising technique can be commercially feasible.

Introduction

Most of the Eastern U.S. coals, suffer from high sulfur content, which on burning emit sulfur dioxide in excess of EPA limit of 1.2 lb SO_2/million Btu. Specifically, there are three broad regions that suffer from severe sulfur problems. These are: Northern Appalachia (Pennsylvania, Ohio, West Virginia) with average sulfur content of about 3%; Midwest region (Indiana, Illinois, Kentucky) with average sulfur of 3.9%; and Central Midwest (Iowa, Missouri, Kansas, Oklahoma) with average sulfur of 5.25%.

The presence of sulfur in coal is generally attributed to two forms, organic sulfur and pyritic sulfur. The proportion of pyritic sulfur to organic sulfur varies significantly from one coal seam to another, but it appears that pyritic sulfur generally represents about 70 percent or more of the total sulfur (1). The pyrite is found in coal in a wide size distribution, with a significant proportion in the very fine size fraction (less than 25 microns). For example the mean particle size of pyrite in the Midwest region is about 37u (400 mesh) and for Central to Western Midwest region is about 107u (150 mesh), and in the Appalachian regions is about 68-100u. This can only mean that a significant amount of the pyrite is in the very fine to colloidal fractions. In fact, there are coal seams, such as Kentucky No. 9 where all the pyrite particles are often smaller than about ten microns (2).

It is believed therefore, that the separation-removal of pyrite from coal prior to its combustion would greatly reduce the sulfur dioxide emission and render many coal deposits within the EPA limits.

For separation of coal from relatively coarse shale and pyrite, gravity-based techniques have been effectively utilized. For sizes below 300 microns to about 100 microns, froth flotation has been used satisfactorily for separating coal from shales (3). Even separation of pyrite from coal has been achieved by flotation (4). However, most of these processes become less effective when the particle size of the coal suspension is significantly below 100 microns.

One of the promising new technologies for separation of very fine particles is selective flocculation. The selective flocculation process has been used effectively to separate very finely disseminated minerals from mixed ore suspension (5). The process is based on the preferential adsorption of an organic flocculant on the wanted minerals, thereby flocculating them, while leaving the remainder of the suspension particles dispersed. The dispersion of certain components in the suspension such as pyrite, can be enhanced by using more selective or powerful dispersants. Methods for achieving selective flocculation and dispersion have been recently described by Attia (6).

The objective of this research was to investigate the feasibility of separating coal fines from mixed suspensions with pyrite by selective flocculation. In this work, the separation of pyrite from coal was based on the distinct differences in their surface chemical properties. Pyrite being a sulfide mineral has an affinity for xanthate containing reagents, while coal does not have such an affinity towards xanthates. Therefore, if xanthate groups could be incorporated into the structure of long-chain polymers, selective polyxanthate flocculants or dispersants for pyrite might thus be achieved. The use of polyxanthates for selective flocculation of sulfide minerals, particularly for copper, was first reported by Attia and Kitchener (7). The separation of pyrite from coal using polyxanthate dispersants was demonstrated recently by Attia and Fuerstenau (8).

This article describes the progress made to achieve selective flocculation of coal from pyrite from a coal sample containing about 2.9% total sulfur.

Preparation and Testing of Polyxanthate Dispersants.

In a preceeding article (8) Attia and Fuerstaneu prepared polyxanthate dispersants by reacting low molecular weight polyacrylic acid solutions with sodium hydroxide and carbon disulfide. The presence of the xanthate groups (Dithio-carbonate) in the polymeric dispersant was ascertained from the UV - Spectra of the solution, where the absorption peak at 305 to 307 mμ was observed. This is very close to the UV-absorption peak of lower xanthate compounds of 303 mμ.

Selective flocculation of coal from pyrite was investigated using the newly developed polyxanthate dispersant in conjunction with a polystyrene sulfonate (purifloc A22) flocculant. The flocculation results on the individual mineral suspensions are shown in Figure 1 (A & B). These graphs show the effect of polyacrylic acid dispersant before (PAA) and after xanthation (PAAX) on the flocculation-dispersion behavior of individual suspensions of coal and pyrite with Purifloc-A22 flocculant.

From Figure 1(A), it appeared that PAA inhibited or restrained the flocculation action of Purifloc-A22 on both coal and pyrite suspensions at PAA concentrations of 100 mg/l and above. The dispersive action of PAA in this case was therefore unselective. However, the PAAX crude reaction product in Figure 1(B) only dispersed the pyrite suspension to the same level as PAA, while the coal suspension was totally flocculated even at high PAAX concentrations. The polyxanthate dispersant rather than improving the dispersion of pyrite, simply did not adsorb on the coal particles, thereby creating a selective dispersion action for the pyrite. These observations in Figure 1(B) were repeated and noted several times even with purified PAAX solutions. Selective dispersion of pyrite or selective flocculation of coal from pyrite using PAAX reagent appeared, therefore, possible.

Effect of Pyrite Particle Size on Dispersion: It was suspected that a lot of the non-dispersed pyrite particles, shown in Figure 1, was due to the settling of "coarse" particles between 10 and 37 microns. Pyrite has a specific gravity of about 5.4, while that of coal is around 1.6 to 1.8. Therefore, a pyrite suspensions of coal and pyrite of minus 37 microns size were also tested simultaneously. The results showed that the coal was almost totally flocculated as before, while the minus 10 micron pyrite suspension remained very stable, with only 10 - 20% weight of the particle, settled or flocculated. The minus 37 micron pyrite behaved in the same manner as in Figure 1. From these observations, it is believed that the se-

lective dispersion of pyrite will be more effective at the smaller particle sizes.

Selective Flocculation of High Sulfur Coal

Preliminary testing of the polyxanthate dispersant mentioned earlier, during the selective flocculation of high sulfur coal was conducted and described here. A sample of bituminous coal from Kentucky No. 9 seam was kindly supplied by the Occidental Research Corporation. The coal sample was wet ground in a steel ball mill and screened to obtain the minus 400 mesh (-37u) fraction for testing.

Single-step selective flocculation tests were conducted on dilute suspensions (about 3% wt) of the minus 37u coal particles, using 2 mg/l, F1029-D flocculant (a partially hydrophobic polymer prepared by Dai-Ichi Kogyo Sieyako, Japan), at pH 10. The test procedure was as follows: The coal suspension was dispersed at a moderate shear for 10 minutes, during which the required amounts of PAAX solution were added and the pH was adjusted to 10. The flocculant was then administered while the suspension was stirred at high shear for 10 seconds. The suspension was thereafter stirred at a low shear for one minute, followed by gentle rotation in an inclined cylinder for 5 minutes. At the end of this step the suspension was decanted off and the flocculated fraction was recovered. Both fractions were dried, weighed and analyzed for total sulfur. The results of this brief study is shown in Table 1 below.

Table 1: Material Balance for One-Step Selective Flocculation of High Sulfur Coal using PAAX Dispersant and F1029-D Flocculant.

Product	Weight %	Total Sulfur%	Total Sulfur Distribution %	Remarks
Dispersed	3.7	13.74	20.3	500 mg/l
Flocculated	96.3	2.08	79.7	PAAX
Feed	100.0	2.52	100.0	
Dispersed	2.7	9.96	9.7	300 mg/l
Flocculated	97.3	2.56	90.3	PAAX
Feed	100.0	2.76	100.0	

These results show that the sulfur content of the dispersed (reject) products was significantly higher than the feed or the flocculated fractions. This was specially evident at the higher PAAX dispersant concentration (500 mg/l) where the sulfur content in the dispersed fraction was 13.74% compared with 2.08% in the flocculated fraction. While these results present a definite evidence for the selectivity of flocculating coal and dispersing pyrite with the reagents mentioned above, the total sulfur removal was very low. The low sulfur removal could be due to the fact that pyrite is known to be very finely disseminated (~10 microns) in Kentucky No. 9 seams from which this sample was obtained. In the brief tests mentioned here no attention was paid to the liberation characteristics of pyrite from coal. It was hoped that grinding to minus 400 mesh (37 microns) would liberate a significant amount of pyrite. Another possible reason for the low sulfur removal was the presence of "coarse" pyrite or pyrite-containing coal particles which would settle at a similar rate as the pure coal flocs, thus, interferring in their separation. As mentioned earlier in this article, the process is expected to be more effective for the 10 microns size pyrite than for 37 microns size pyrite particles, if gravitational settling was used for separation of flocs from suspension. Other floc separation methods such as flotation might extend the effectiveness of this selective flocculation method to coarser sizes. Alternatively, the coarser pyrite particles (greater than 25 microns for example) could be separated by other technique prior to

applying selective flocculation.

Conclusions

From the foregoing discussion, it can be concluded that the addition of the polyxanthate dispersant (PAAX) during the selective flocculation of coal with F1029-D or Purifloc-A22, presents a promising approach for the removal of ultrafine pyrite particles from coal suspensions. This would specially be true however if future investigations could improve the overall pyrite removal, while still obtaining high coal (Btu) recovery. It is believed that by applying multi-stage selective flocculation (i.e., the flocs from the first separation step are re-dispersed and re-flocculated several times) more of the liberated pyrite particles would be removed.

Acknowledgment

The author would like to thank Mr. Steven Bright and Dr. S. Krishnan, both from Battelle-Columbus for their help in conducting the experiments on the high sulfur coal sample.

References

(1) "Analysis of Ohio Coal", Information circular No. 47, State of Ohio Department of Natural Sciences, Division of Geological Survey, 1978.

(2) Albaugh, E; Gulf Research and Development, Pittsburgh, Pennsylvania, Private communications with Y. Attia, 1982.

(3) Aplan, F.F.; "Fine Coal Preparation State of the Art - Problems and Predictions for the Future" in Beneficiation of Mineral Fines, Editors: P. Somasundaran and N. Arbiter, NSF workshop New York 1978.

(4) Miller, K.J.; "Flotation of Pyrite from Coal", U.S. Patent 3,807,557, April 30, 1974.

(5) Attia, Y.A.; "Selective Flocculation Technology, State of the Art Review", 111th AIME Annual Meeting, 1982, Dallas.

(6) Attia, Y.A.; "Fine Particle Separation by Selective Flocculation", Separation Science and Technology, 17 (3) (1982) 75-83.

(7) Attia, Y.A. and Kitchener, D.A.; "Development of Complexing Polymers for the Selective Flocculation of Copper Minerals", Eleventh Inter. Miner. Process. Cong., Cagliari, Italy (1975).

(8) Attia, Y.A. and Fuerstenau, D.W.; "Feasibility of Cleaning High Sulfur Coal Fines by Selective Flocculation", Fourteenth Inter. Miner. Process. Congr., Toronto, Canada (1982).

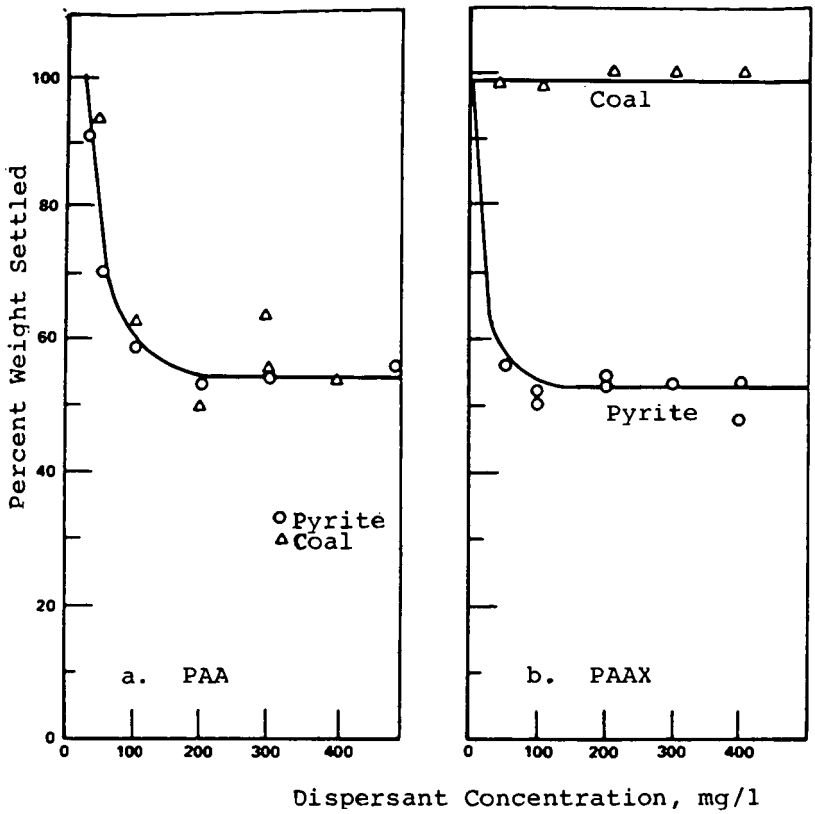

FIGURE 1. EFFECT OF PAA AND PAAX DISPERSANTS ON THE FLOCCULATION OF COAL AND PYRITE WITH PURIFLOC-A22 (4 mg/l) at pH10, AND 2% SOLIDS CONTENT IN SUSPENSIONS.

REMOVAL OF ORGANIC SULFUR FROM COAL BY SUPERCRITICAL EXTRACTION WITH ALCOHOLS

C. B. Muchmore, J. W. Chen, A. C. Kent, and K. E. Tempelmeyer

Department of Mechanical Engineering and Energy Processes
Southern Illinois University, Carbondale, Illinois 62901

INTRODUCTION

Growing concern over environmental effects of acid rain has resulted in increased interest in development of pre-combustion removal of sulfur from coal. Physical coal cleaning processes are effective for pyritic sulfur removal but do little to reduce the organic sulfur content of coal. This paper reports the selective removal of organic sulfur from coal, employing ethyl or methyl alcohols as the solvent/reactant. The process is based on the observation that, under supercritical conditions, organic sulfur is selectively removed from the coal matrix. The concentration of sulfur in the resulting solid product is thus reduced, while maintaining over 50% of the concentration of volatile matter compared to that of the parent coal. In addition to the desulfurized solid product, a high BTU gas is produced, and some conversion of coal to liquid products occurs.

LITERATURE REVIEW

Most work on supercritical extraction of coal reported in the literature has as a primary objective the maximum conversion of coal to liquid products. A 1975 article by Whitehead (6) [one of the first references to supercritical coal extraction presented in the literature] presented data on supercritical extraction of coal by coaltar or petroleum naphtha fractions. Tugrul and Olcay (5) reported in 1978 extraction yields and analytical results obtained by supercritical-gas extraction of 250 mesh lignite. They found extraction nearly complete after 30 minutes; extract yields of about 24% were reported. Gas chromatography/mass spectrometry analyses of several extract fractions indicated dozens of paraffins, alkylated hydrocarbons, phenolic and oxygenated compounds; however, no sulfur compounds were reported. A kinetic study of a high-volatile bituminous coal utilizing supercritical toluene was reported by Slomka and Rutkowski (4). A close fit of their experimental data on time dependence of extraction yield was found when a second order equation was used. The use of supercritical toluene extraction of coal in pilot plant studies supported by the British Coal Board was reported by Maddocks (2). The major objective of that study was also maximum conversion of coal to liquid products; reduction of sulfur in the unconverted solid was not reported.

Some work has been reported utilizing alcohols for supercritical extraction of coal. Makabe et al (3) reported extraction of coal with ethanol-sodium hydroxide with the objective of maximizing extraction yield; no sulfur data was reported. Methyl alcohol reaction with a low volatile Bituminous West Virginia coal at higher temperatures (460-600C) was reported by Garner et al (1). Promotion of coal gasification was the objective of that study; sulfur content of the resultant char was not reported.

In contrast to the previous reported work utilizing supercritical solvent extraction of coal, where major objectives have been the conversion of coal to liquid or gaseous products, the major objective of our research effort is to develop a desulfurization process that will result in a solid product suitable for combustion in existing coal fired utility boilers.

EXPERIMENTAL

Batch reactor studies

These experiments utilized a 300cc stirred autoclave reactor; a flow chart of the reactor is given in Figure 1. The coal, previously dried and ground to the desired particle size (generally -40 mesh), is charged to the reactor and alcohol is added. Heating the stirred mixture to above the critical temperature and pressure of the solvent (for ethyl alcohol 243C and 63 atm) results in a sequence of extraction and reaction processes that remove organic sulfur from the coal. After the desired reaction time (generally one hour) the fluid phase is vented from the reactor through a condenser system and liquid and gaseous products are collected. After cooling, the solid product is collected from the reactor.

For some experiments, treatment of the coal with KOH was utilized; two procedures were employed: a) charging the KOH to the reactor (5% of the weight of the coal charged) or b) soaking the coal for ten minutes in a 5% KOH/alcohol solution, followed by alcohol washes to remove essentially all of the potassium from the coal prior to supercritical reaction.

Semi-continuous reactor studies

The flow chart for the semi-continuous Berty gradientless reactor, equipped with a Magnedrive impeller and internal recirculation system, is given in Figure 2. The ground coal is held in a basket within the reactor, while solvent is pumped continuously through the system. After cooling following a run, the solid product is removed from the reactor basket for weighing and analysis. It is possible to maintain a constant pressure in this system, in contrast to the batch system where pressure increases during the course of a run, final pressure being determined by the temperature and charge size to the reactor.

RESULTS AND DISCUSSION

Batch reactor results

For one set of experiments, a comparison of ethyl and methyl alcohols as supercritical extractants was made over a temperature range of 275-450C, utilizing three different coals of varying ratio of organic to pyritic sulfur content. The coals were provided by the State of Illinois Geological Survey, and have been kept under a nitrogen atmosphere since the initial size reduction following mining of the coal. The organic sulfur/pyritic sulfur ratio varied from 0.72 to 2.82 for these coals. For all runs, the reaction time was 1 hr and a solvent/coal ratio of 1/1 was used. The results of these batch runs are summarized in Figure 3, where the sulfur reduction obtained (evaluated on a concentration basis, comparing the total sulfur in the product char to that of the original coal) is shown as a function of the organic sulfur/pyritic sulfur ratio of the original coal, with temperature as a parameter. Ethyl alcohol resulted in greater desulfurization (48%) than methyl alcohol at

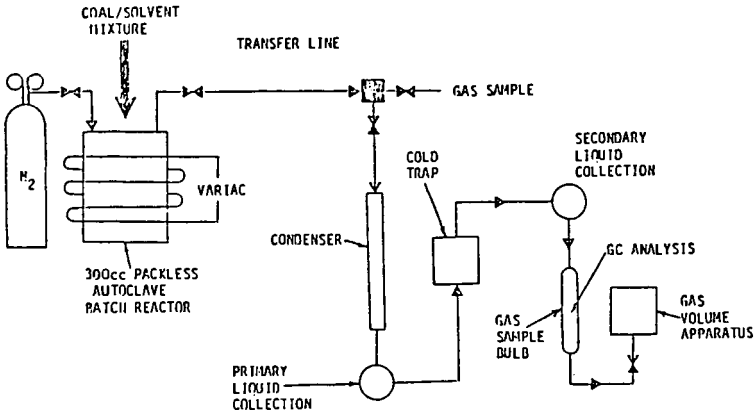

Figure 1. Flow diagram of batch reactor system.

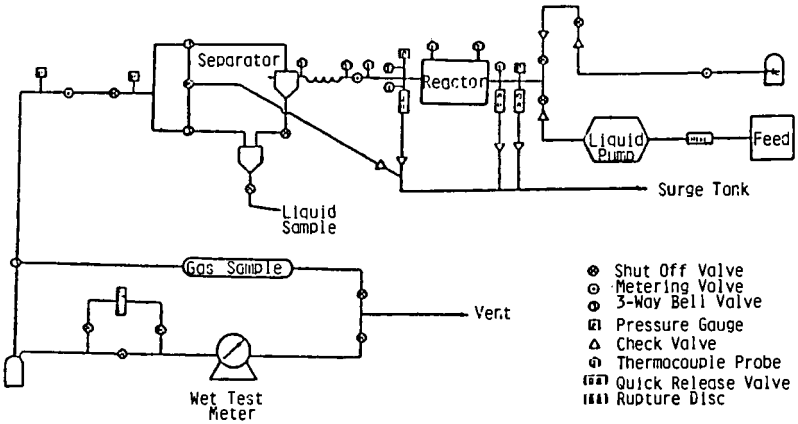

Figure 2. Flow diagram of semi-continuous reactor system.

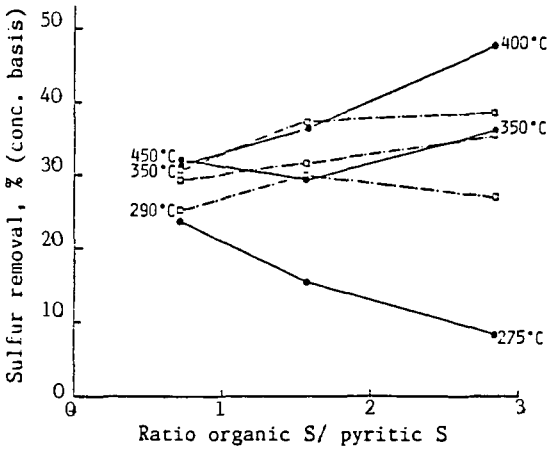

Figure 3. Comparison of ethyl and methyl alcohols as supercritical desulfurization fluids, for coals of varied organic sulfur/ pyritic sulfur ratio. (ethanol ——·——, methanol --·--)

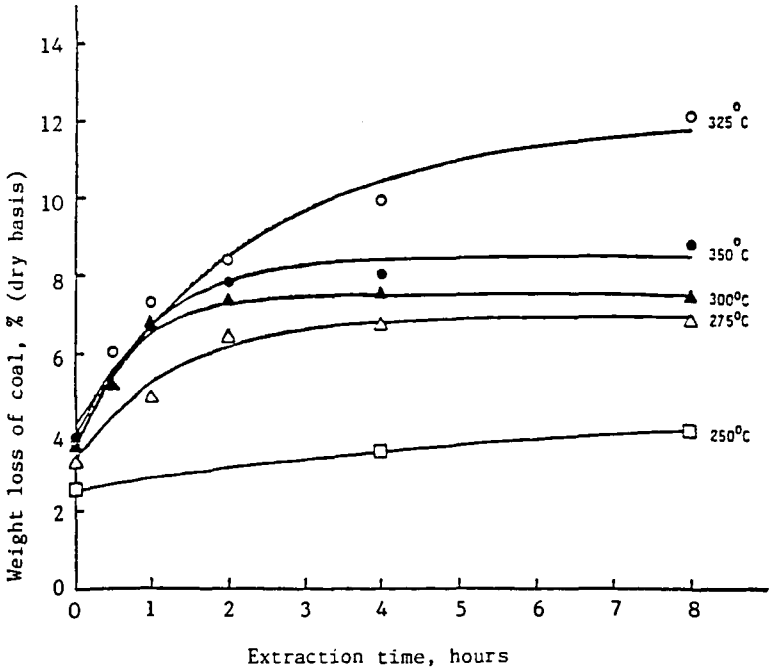

Figure 4. Weight loss of coal as a function of reaction time, semi-continuous reactor.

higher temperatures (400 C) with the higher organic sulfur content coal, and methyl alcohol gave comparable desulfurization to ethyl alcohol at the lower temperature investigated (300 C) with the lower organic sulfur content coal. The results confirm that organic sulfur is being removed by the supercritical extraction/reaction process.

Another series of four runs was performed to compare methyl and ethyl alcohols as supercritical fluid reactants, with and without KOH (5% of the coal charge). Previous studies had indicated enhanced desulfurization by pre-treatment of the coal with a potassium hydroxide-alcohol solution. Reaction time was 2 hours at a reaction temperature of 340C; maximum reaction pressures were 2500 to 4450psig. The high organic sulfur content coal (total sulfur content 4.23%, organic S/pyritic S ratio = 2.82) was used for these runs; results are summarized in Table 1.

Inspection of Table 1 indicates that addition of potassium hydroxide decreased solid product and liquid recoveries, and increased gas production; this was an anticipated result due to the reported influence of caustic on decomposition rates of alcohol at the reaction temperatures utilized. The greatest desulfurization (54.0% reduction in sulfur concentration) resulted in the methanol-KOH system. It is of interest to note that from 56 to 69% of the volatile matter is retained in the solid product compared to that of the original coal. Heating values of the solid products are one to seven per cent greater than the original coal, in spite of a slight increase in ash content. The higher ash resulting from the KOH treatment reflects the greater conversion of coal, as well as the KOH itself. Prior work with both the batch and semi-continuous systems established that comparable desulfurization is attained by both the KOH addition and pre-treatment soaking procedures.

Semi-continuous reactor results

A series of runs were performed using an Illinois No.6 coal having a total sulfur content of 3.0% and an organic S/pyritic S ratio of 2.43. Operating pressure was kept constant at 1750 psig, run temperatures covered the range of 250-350C, and extraction times at run temperature were up to eight hours. The observed weight loss of coal and sulfur removal as a function of extraction time are plotted in Figures 4 and 5, respectively. The conversions indicated at time zero on these plots represent extraction and/or reaction that occurs during the pre-heating time to reaction temperature.

An empirical first order kinetic model was used to fit the experimental data of the percent of coal extracted and the percent of sulfur removed, where concentrations remaining are based on the ultimate extractability at reaction conditions. An Arrhenius plot (Figure 6) reveals that the activation energy for coal extraction was about 30 K cal per mole and for desulfurization was about 17 K cal per mole, which compares favorably with the data in the literature. The selectivity of sulfur removal, as defined by the ratio of sulfur removal to coal extracted, was in the range of 2 to 4.

Gas and liquid product analyses

Analyses of the gas products resulting from the batch experiments reported in Table 1 are given in Table 2. The greater production of hydrogen resulting when KOH was used is evident for both the ethanol and methanol systems. As anticipated, no ethylene and much less ethane resulted from the methanol runs, compared to

TABLE 1

BATCH EXPERIMENTAL DATA

	Standard Coal C-22440	Ethanol, No KOH	Ethanol, 5% KOH	Methanol, No KOH	Methanol, 5% KOH
Maximum Reaction pressure (psig)		2500	3000	2650	4450
Char yield (% of coal charged)		83.0	81.9	89.5	86.8
Liquid yield (% of liquid charge)		83.5	74.8	90.3	59.8
Gas produced, l		10.0	13.0	6.2	26.8
% desulfurization (conc. basis)		36.3	37.6	30.5	54.0
Solid analyses (moisture free)					
% Volatile matter	41.6	23.8	23.2	28.8	25.0
% Ash	10.43	12.18	17.40	11.34	17.89
Btu/lb	12,375	13,263	12,990	12,826	12,501

Reaction Conditions: 60g coal, 60g ethanol, 2 hr. reaction at 340°C.

TABLE 2

GAS ANALYSIS (VOLUME %),
BATCH EXPERIMENTAL DATA

GAS PRODUCTS	ETHANOL		METHANOL	
	NO KOH	5% KOH	NO KOH	5% KOH
H_2	9	17	4	38
CH_4	35	23	68	31
C_2H_4	1	1	0	0
C_2H_6	30	27	7	3
CO_2	20	22	17	25
Other	5	10	4	3

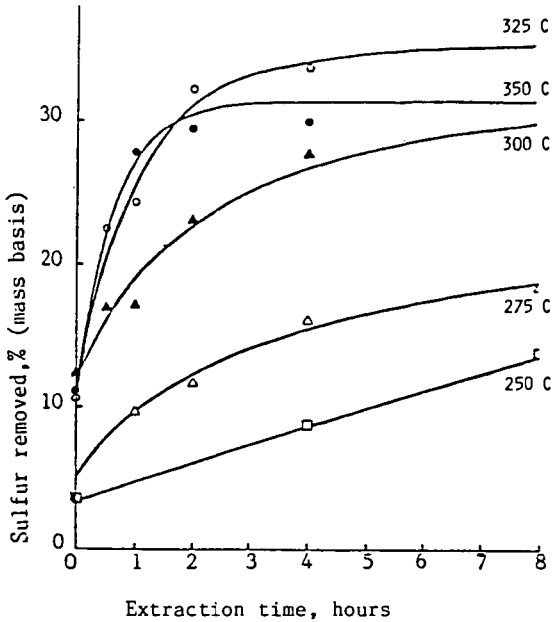

Figure 5. Sulfur removal (mass basis) as a function of reaction time.

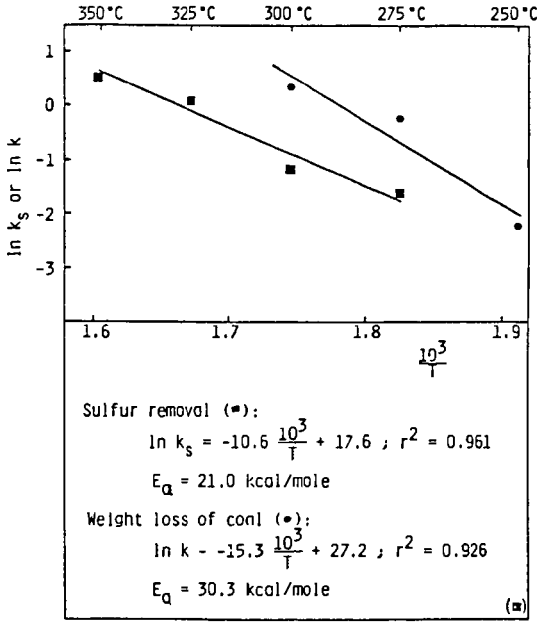

Figure 6. Arrhenius plot of weight loss of coal and sulfur removal data, semi-continuous reactor.

the ethanol runs; methane concentration was higher in the methanol runs.

Gas chromatograms of the liquid products resulting from two of the batch experiments reported in Table 1, where ethyl and methyl alcohols were used without KOH addition, are given in Figures 7 and 8, respectively. A capillary column was used for the analyses, and the sample was split to two different detectors after passing through the column, giving dual traces on each chromatogram. A flame photometric detector (FPD), specific for sulfur containing compounds, and a flame ionization detector (FID), sensitive to essentially all organic compounds, were used. Of the more than half dozen major sulfur containing compounds indicated in Figure 7, several have been identified; ethyl sulfide, ethyl disulfide, thioacetal, and thiophene were indicated by GC/MS analysis. The participation of the ethanol solvent (or a two carbon degradation product) in the desulfurization reactions is suggested by the structure of the sulfur containing products thus far identified. The gas chromatogram of the liquid product from the methanol run indicates only two major sulfur compounds, and lesser amounts of coal derived organic material, compared to the ethanol run.

CONCLUSIONS

It is apparent from the data thus far obtained that both ethyl and methyl alcohols are effective for desulfurization of high organic sulfur content coals when used as extractants/reactants under supercritical conditions. Since it is not known at this time if any significant amount of pyritic sulfur is being removed during the supercritical desulfurization reactions, this possibility must be recognized in any proposed model of the system. Figure 9 presents possible reaction pathways; the extent to which each may be contributing to the overall desulfurization observed under supercritical conditions has yet to be determined.

The potential for processing a typical high sulfur coal to produce a solid product with less than 1% total sulfur by a sequence of physical beneficiation for pyrite reduction, followed by supercritical extraction for removal of organic sulfur, is indicated by example in Figure 10. A 3% total sulfur coal, containing equal amounts of pyritic and organic sulfur, could be processed by existing technologies for removal of pyritic sulfur to give a total sulfur concentration of, say, 1.8%. An additional 50% reduction of the remaining total sulfur would then give a final total sulfur concentration of 0.9%. The initial attempt to attain this goal is also represented in Figure 10, where a coal processed by froth flotation was then subjected to supercritical extraction with the methanol-KOH system at 350C for one hour in the batch reactor. Although the final product total sulfur concentration of 1.37% fell short of the 1% goal, this initial result is encouraging in view of the fact that the froth flotation step has not yet been optimized for the coal used.

ACKNOWLEDGMENTS

This work was performed with grant support from the Illinois Coal Research Board and the U. S. Department of Energy.

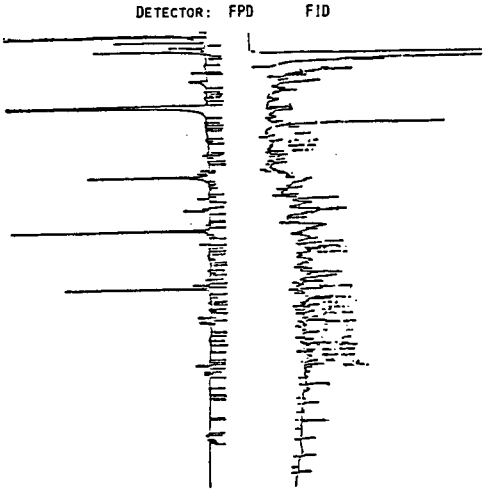

Figure 7. Gas chromatogram of liquid product from supercritical desulfurization of coal with ethanol at 350C. Flame photometric detector (FPD) response is on left; flame ionization detector (FID) response is on right.

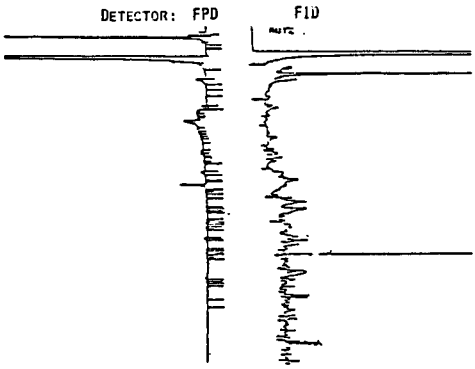

Figure 8. Gas chromatogram of liquid product from supercritical desulfurization of coal with methanol at 350C. Dual detectors as described above.

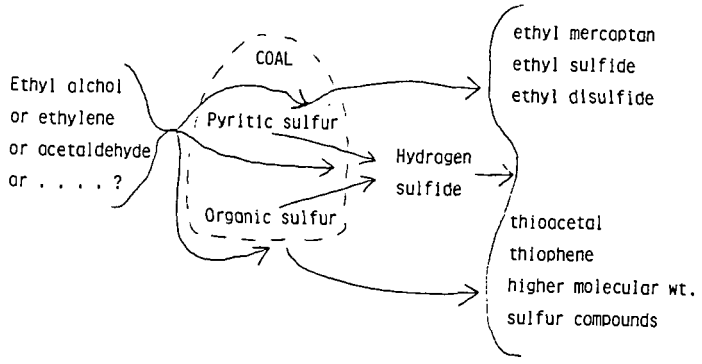

Figure 9. Possible reaction pathways for desulfurization of coal with ethyl alcohol under supercritical conditions.

SEQUENTIAL DESULFURIZATION
(EXAMPLE)
INITIAL EXPERIMENTAL DATA

	PYRITIC S	ORGANIC S	SULFATE S	TOTAL S
COAL · Run of Mine	1.5 %	1.5 %	—	3.0 %
	1.26 %	1.64 %	0.61 %	3.52 %
FROTH FLOTATION	0.3 %	1.5 %	—	1.8 %
	0.95 %	1.47 %	0.34 %	2.76 %
SUPERCRITICAL DESULFURIZATION	0.2 %	0.7 %	—	0.9 %
	0.05 %	0.98 %	0.34 %	1.37 %

Figure 10. Example of sequential processing of coal for removal of pyritic and organic sulfur.

REFERENCES

1. Garner, D.N., W.J. Huffman, and H.W. Parker, Coal Processing Using Methanol as a Reactant. Presented at 79th National Meeting, AIChE, 8th Petrochemical and Refining Exposition, Houston, TX (1975).

2. Maddocks, R.R., J. Gibson and D.F. Williams. Supercritical Extraction of Coal. Chem. Engr. Progress. (June 1979).

3. Makabe, M., Y. Hirano and K. Ouchi. Extraction Increase of Coals Treated with Alcohol-Sodium Hydroxide at Elevated Temperatures. Fuel, vol. 57 (May 1978).

4. Slomka, B. and A. Rutkowski. A Kinetic Study of the Supercritical Toluene Extraction of Coal at 9.8 MPa. Fuel Processing Technology, vol. 5 (1982).

5. Tugrul, T. and A. Olcay. Supercritical-Gas Extraction of Two Lignites. Fuel, vol. 57 (July 1978).

6. Whitehead, J.L. and D.F. Williams. Solvent Extraction of Coal by Supercritical Gases. Journal of the Institute of Fuel, (December 1975).

THE CHEMISTRY OF MOLTEN HYDROXIDE DESULFURIZATION USING MODEL SYSTEMS

Bruce R. Utz, Steven K. Soboczenski, and Sidney Friedman

U.S. Department of Energy
Pittsburgh Energy Technology Center
P.O. Box 10940
Pittsburgh, PA 15236

INTRODUCTION

The TRW "Gravimelt" Molten Hydroxide Desulfurization Process is being developed to remove sulfur from coal [1]. While the chemistry for removing inorganic sulfur is being examined actively [2], little research has been done on the removal of sulfur from organosulfur moieties in coal. The objective of this study is to determine how molten hydroxides remove organosulfur from coal. The two model compounds used initially to examine the chemistry of organosulfur removal are benzothiophene and dibenzothiophene. These model compounds were chosen because they simulate sulfur compounds in coal. Thermal decomposition reactions of intermediate products were also studied, and based on the results, a proposed pathway for desulfurization is suggested. The potential role of water in molten hydroxide desulfurization was determined by varying the amount of water present in the hydroxide mixture. Results demonstrate that water does not play an important role in the removal of sulfur from organosulfur moieties. Since both sodium hydroxide and potassium hydroxide have typically been used in the TRW Molten Hydroxide Desulfurization Process, the importance of each hydroxide was examined. It was found that the relative amount of each hydroxide may be critical in removing organosulfur and that potassium hydroxide is the important species. Continuing research will examine the importance of the cation in molten hydroxide reactions and the use of other molten salts for the removal of sulfur from organosulfur species.

EXPERIMENTAL

All molten hydroxide desulfurization reactions were performed using 1/2-inch Monel Swagelok unions as reactors. Similar 316-stainless-steel reactors developed cracks and leaks, resulting in loss of volatile components. In a typical reaction, 3.1 to 4.0 g of powdered sodium hydroxide and/or potassium hydroxide, 0.3 to 0.6 g organosulfur compound, and a 1/4-inch-diameter stainless-steel ball (to ensure adequate mixing) were added to the reactor under nitrogen. Product yields were slightly less without the stainless-steel ball. In some cases, the hydroxide mixture was added in two steps, to reduce the free volume of the reactor. Elimination of free volume ensured that the reactant would be in the condensed phase and in intimate contact with the molten hydroxide. This was accomplished by melting most of the powdered base in the reactor at 350°C, with subsequent addition of the organosulfur compound and 0.3 to 0.5 g of additional base. The end caps were then tightened to 35 ft lb.

The reactor was bolted to a bracket assembly and immersed in a Tescom SBL-2 fluidized sand bath that was preheated to reaction temperatures. Reaction temperatures ranged from 350°C to 400°C, and reaction times varied from 10 minutes to 3 hours. Vigorous mixing was accomplished by using a Burrell mechanical wrist-action shaker. The reactors were cooled rapidly by immersion in room-temperature water.

The reactors were opened, placed in 50 mL of CH_2Cl_2, and sonicated for 5 minutes. This allowed partial removal of neutral organics and, more important, minimal evaporative losses of volatile organics. The CH_2Cl_2 was decanted and 1 mL of a solution containing an internal standard was added (a solution containing an

internal standard was added to all CH_2Cl_2 extracts before GC analysis). The reactor was then sonicated with 50 mL of deionized water until all the base was dissolved (20-30 minutes). The basic solution was decanted and the reactor was washed with an additional 10 mL of water to ensure complete removal of its contents. The H_2O solutions were combined and extracted with two 25-mL portions of CH_2Cl_2 to remove any of the remaining neutral organics. Using litmus paper as the indicator, the water layer was neutralized with 4 to 6 mL of concentrated HCl. The neutralized solution contained acidic products that had previously remained in the aqueous phase as soluble salts. The neutralized water layer was then extracted with two 25-mL portions of CH_2Cl_2. Solutions containing internal standards were added to each portion to determine quantitatively the amounts of individual components and to determine material balances. Material balances of approximately 95% were achieved.

The three methylene chloride portions were analyzed using an HP 5740 gas chromatograph with a 50-meter SE-54 capillary column. In most cases, flame ionization was used to detect the individual components of the reaction. The CH_2Cl_2 was removed by rotoevaporation, and the products were further characterized by proton NMR; FTIR; and low-voltage, high-resolution MS. Some loss of the more volatile components was observed.

Thermal decomposition reactions were conducted using aromatic thiols and their respective salts. The aromatic thiol (0.2 g) and a stainless-steel ball(s) were added to the reactor, and the reactor was heated to 375°C for 30 minutes. Thermal decomposition of the salt of the aromatic thiol was examined by adding 0.2 g of the aromatic thiol, 3.5 g of powdered KOH and NaOH (60:40) and a stainless-steel ball to the reactor. Reaction conditions were the same as those for the aromatic thiol. Reaction products were dissolved in 50 mL of CH_2Cl_2 and quantified using capillary GC and an internal standard.

RESULTS AND DISCUSSION

Reaction of Benzothiophene

A weight ratio of 1:1 (KOH:NaOH) was chosen for the initial model-compound study, based on the ratio that the TRW process is using for bench-scale experiments with coal [1]. Preliminary experiments at 375°C and 30-minute reaction times indicated that benzothiophene, chosen as the initial model compound, had reacted partially with the molten hydroxide to form two principal products. Capillary GC, high resolution mass spectrometry, FTIR, and NMR identified the major product as o-thiocresol. The minor product was toluene.

Extending the reaction time to 3 hours gave a considerably different distribution of products. Not only had all the benzothiophene reacted, but the major product was toluene. These results indicate that the overall reaction of benzothiophene with molten hydroxide involves a ring opening and elimination of a carbon to form o-thiocresol, followed by a slower sulfur elimination to form toluene (Figure 1). These results are supported by the observations of Weissgerber and Seidler [3], who identified small amounts of o-thiocresol and formic acid when reacting benzothiophene with KOH at 300°-310°C. Apparently extended reaction times or higher temperatures are two means to remove sulfur from the sulfur species completely. The individual steps of the mechanisms are being examined.

Effect of KOH:NaOH Ratio

Because of some inconsistencies in product yield, a series of experiments was conducted using varying amounts of KOH and NaOH. Varying the relative amounts of KOH and NaOH clarified the problem and determined the importance of each hydroxide. Hydroxide mixtures having different ratios of KOH and NaOH were

prepared, and their activities were compared by determining the extent of benzothiophene conversion to the initial product, o-thiocresol, or the subsequent product, toluene. Weight percents of KOH:NaOH used for this study were the following: 0:100, 40:60, 45:55, 48:52, 50:50, 52:48, 55:45, 60:40, 75:25, 90:10, and 100:0. Figure 2 shows the results of these experiments. Note that at approximately a 45:55 ratio of KOH:NaOH, the conversion of benzothiophene to o-thiocresol increases dramatically. The lack of any significant reaction at lower percentages of KOH was unexpected. Increasing the weight percent of KOH in the hydroxide mixture resulted in an increase in the concentration of o-thiocresol and a corresponding increase in toluene formation, since the formation of toluene represented a decomposition of the intermediate product, o-thiocresol. Maximum yields of desulfurized product (toluene) were obtained by using pure KOH. Since conversions varied dramatically at approximately a 45:55 ratio, all subsequent experiments were done with a 60:40 ratio of KOH:NaOH.

From these results, it can be seen that the amount of KOH within the hydroxide mixture may be critical in removing organosulfur from coal. While the particular role of KOH has not been determined, evidence from the literature has shown that the size of the cation may be important in stabilizing intermediate carbanions. Wallace et al. [4] conducted a series of base-catalyzed, beta-elimination reactions with isopropyl sulfide and measured the amount of olefin production. The proposed mechanism involved an initial formation of a carbanion with subsequent elimination of the sulfur moiety (which can be considered a good leaving group) to form the olefin (Figure 3). It was shown that the rate of olefin production was dependent on the size of the metal cation (Li^+, Na^+, K^+, Rb^+, and Cs^+) of the base. The increase in olefin production with an increase in cation size was explained as a stabilization/solubilization effect, wherein the intermediate carbanion was more effectively stabilized by the larger cations, causing an increase in the rate of olefin production. Certain possible reaction pathways for the conversion of benzothiophene also require a carbanion intermediate. Increases in benzothiophene conversion with increasing amounts of K^+ support this type of intermediate.

Thiol Thermochemistry

The mechanism for the formation of o-thiocresol has not been clearly established, although evidence to support a pathway for the desulfurization of the aromatic thiol (o-thiocresol) has been obtained. Experiments using model compounds showed that the thermal decomposition of aromatic thiols is different from that of their respective salts (salt formation occurs in molten hydroxide). The thermal decomposition of thiols can be complicated because the incipient free-radicals tend to react with other thiol molecules and provide a variety of products. Reports in the literature demonstrate that certain aromatic thiols decompose thermally to form the corresponding sulfide [5]. Thermal decomposition reactions in our reactor (375°C for 30 minutes) using thiophenol or o-thiocresol produced diphenyl sulfide or 2,2'-dimethyldiphenyl sulfide respectively. Although the mechanism is not known, one can be suggested. The bond dissociation energy of the S-H bond for aromatics is approximately 75 kcal/mole, and at 375°C, the molecule most likely dissociates to Ar-S· and H· [6]. Attack of Ar-S· on the aromatic thiol with subsequent loss of the stable thiyl radical would produce a monosulfide and hydrogen sulfide (Figure 4).

The behavior of the aromatic thiol salt was studied by conducting thermal decomposition reactions in the molten hydroxide mixture (60%KOH:40%NaOH). It was assumed that hydroxide was present only to allow formation of the thiol salt. In molten hydroxide, the aromatic thiol loses a proton to form the conjugate base, which is not likely to lose an electron to form Ar-S· and a free solvated electron. The bond dissociation energy of the aromatic C-S bond is approximately 85 kcal/mole and represents a likely thermolysis pathway [6]. Thermal decomposition of the thiophenolate salt produced about 60%-70% insoluble material and

approximately 30% benzene. The formation of insoluble material may be a result of phenyl radical reactivity, leading to radical polymerization reactions. This hypothesis was tested by conducting the same reaction in the presence of formate ion. Formate ion is known to react with hydroxide and generate hydrogen, carbon monoxide, and carbonate salts [7]. In situ generation of H_2 might allow capping of intermediate free-radicals (phenyl radicals) and thus inhibit free-radical polymerization reactions. Thermal decomposition of the thiophenolate salt in the presence of formate yielded approximately 80% benzene, supporting the hypothesis that homolysis occurs at the C-S bond. Based on these results, it is suggested that the conjugate base of the intermediate product, o-thiocresol, undergoes thermal decomposition to toluene. The absence of polymer may be due to a low concentration of o-thiocresol at any given time.

Reaction of Dibenzothiophene

Dibenzothiophene was much less reactive than benzothiophene. Reactions at 375°C for 30 minutes in our laboratories demonstrated that dibenzothiophene was unreactive and quantitatively recovered. Maijgren and Hubner [8] observed, using dibenzothiophene as a model, that under similar reaction conditions (75%KOH and 25%NaOH, 370°C for 60 minutes), 81% of dibenzothiophene was recovered, but no reaction products were identified. Wallace et al. also found that dibenzothiophene was unreactive when heated at 200°C for 20 hours in a KOH - white oil mixture [9]. The severity of the reaction conditions in our laboratory was increased to 400°C for 3 hours. Under these conditions dibenzothiophene reacted quantitatively, producing approximately 50% CH_2Cl_2 insoluble material, 35% o-phenylphenol, and 10% biphenyl. These results indicate that dibenzothiophene will react with molten hydroxide and desulfurize if the reaction conditions are sufficiently severe.

Role of Moisture

Since A.C.S. reagent grade KOH has a moisture content of 13%-15%, it was thought reasonable to test whether water might be playing an important role in the desulfurization reaction using molten hydroxides. Reactions were conducted with a high-purity KOH that contained less than 1 wt.% of water, and the same results (complete conversion) were obtained. Also, an equivalent amount of water (13 wt.%) was added to experiments conducted in pure NaOH, and in each case, no conversion occurred. Based on these results, it appears that water has neither a deleterious nor an advantageous effect on the removal of sulfur from organosulfur compounds using molten hydroxides. These results also indicate that a considerable cost savings in the energy required for drying recycled caustic may be possible.

CONCLUSION

Experiments carried out in microautoclaves demonstrate that sulfur can be removed from organosulfur model compounds using molten hydroxides. Based on these results, it can be seen that the ratio of KOH and NaOH may be critical in removing sulfur from organosulfur moieties in coal and that the reaction temperatures and reaction times might determine which type of organosulfur species is being removed and to what extent. A large improvement in sulfur removal using the molten hydroxide desulfurization process might be possible by varying the amount of KOH and NaOH. While sulfur might be removed from benzothiophene moieties in coal at 375°C, it appears that more severe conditions are necessary to remove sulfur from dibenzothiophene moieties. Efficiency of organosulfur removal may be partially dependent on the type of organosulfur species in coal, and therefore continued efforts to characterize the types of organosulfur moieties in coal are necessary.

ACKNOWLEDGMENT

We gratefully acknowledge the technical assistance of Bonnie Brooks and Thomas Williams in obtaining technical data from the molten hydroxide experiments. We also acknowledge the Oak Ridge Associated Universities (ORAU) Postgraduate Research Associate Program, in which Steven K. Soboczenski participated.

REFERENCES

[1] "Gravimelt Process Development," Final Report, TRW Energy Development Group, Contract No. DOE/PC/42295-T7, June 1983.

[2] C.W. Fan, R. Markuszewski, and T.D. Wheelock, Am. Chem. Soc. Div. Fuel Chem. Preprints, 29(4), 319 (1984).

[3] R. Weissgerber and C. Seidler, Ber. Dtsch. Chem. Ges. B., 60, 2088 (1927).

[4] T.J. Wallace, J.F. Hofmann, and A. Schriesheim, J. Am. Chem. Soc., 85, 2739 (1963).

[5] E. Emmet Reid, "Organic Chemistry of Bivalent Sulfur," Vol. 6, pp. 27-29, Chemistry Publishing Company, Inc., N.Y. (1963).

[6] R. Shaw, in "The Chemistry of the Thiol Group," (S. Patai, ed.), Part 1, pp. 151-161, John Wiley and Sons, N.Y. (1974).

[7] M.C. Boswell and J.V. Dickson, J. Am. Chem. Soc., 40, 1779 (1918).

[8] Conf. on Coal Science, Pittsburgh, Pa., April 15-19, 1983, pp. 256-259.

[9] T.J. Wallace and B.N. Heimlich, Tetrahedron, 24, 1311 (1968).

DISCLAIMER

Reference in the report to any specific commercial product, process, or service is to facilitate understanding and does not necessarily imply its endorsement or favoring by the United States Department of Energy.

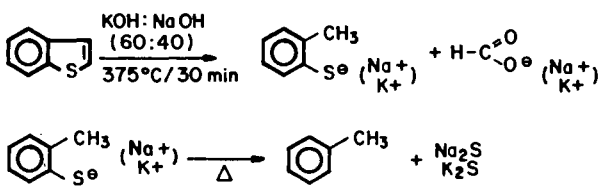

Figure I. Desulfurization of Benzothiophene in Molten Hydroxide

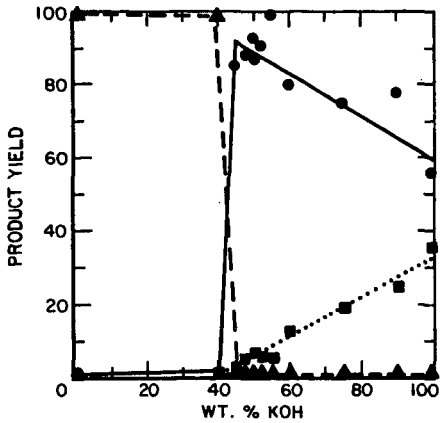

Figure 2. Reactions of Benzothiophene with Molten KOH/NaOH Mixtures at 375°C for 30 minutes.

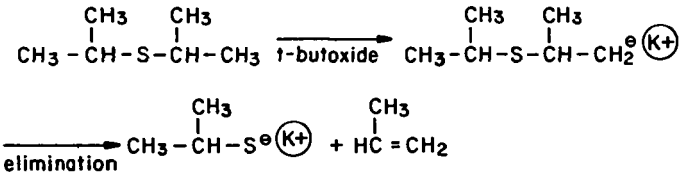

Figure 3. Base-Catalyzed Elimination of Sulfide [4]

Figure 4. Thermal Decomposition of Thiophenol

DESULFURIZATION AND DEMINERALIZATION OF COAL BY MOLTEN NaOH/KOH MIXTURES

R. Markuszewski, D. R. Mroch, G. A. Norton, and W. E. Straszheim

Ames Laboratory* - U.S. DOE, Fossil Energy Program
Iowa State University, Ames, IA 50011

INTRODUCTION

The use of molten caustic to remove pyrite and other mineral matter from coal was first reported by Masciantonio (1). He discovered that treating 1 part of coal with 4 parts of 1:1 NaOH/KOH mixture at 250°C or higher removed all of the pyrite within 5 minutes. At temperatures above 250°C, organic sulfur was also removed. In recent years, the technique was refined by TRW and became known as the Gravimelt Process (2-4). By using 10 parts of molten caustic to treat 1 part of coal at 370°C, followed by washing with dilute H_2SO_4, almost all of the pyritic sulfur and about 80% of the organic sulfur could be removed. In addition, the final ash contents were generally less than 1%. Further studies on the effects of retention time, temperature, coal-to-caustic and NaOH/KOH ratios, particle size, and rank of coal resulted in sulfur and ash reductions which met the New Source Performance Standards (5,6). The fundamental aspects of cleaning coal with molten caustic were also studied by Maijgren et al. (7, 8) who investigated the behavior of some organosulfur model compounds in addition to the effect of caustic composition, reaction time, temperature, and particle size.

The overall objectives of our own DOE-sponsored work at the Ames Laboratory are to propose, test, and develop methods for regenerating the spent caustic and other reagents used in the TRW Gravimelt Process in order to make this chemical cleaning method economical. As a preliminary step to our investigations, the thermodynamics, phase equilibria, and other properties of proposed reaction schemes were tested in order to develop flow diagrams incorporating the desulfurization and regeneration schemes (9). Furthermore, in order to ensure that our samples of cleaned coal and spent caustic are comparable to those produced by the Gravimelt Process, similar procedures were used in the cleaning steps. In the course of our work, the effect of various washing procedures as well as of particle size and recleaning was investigated. In addition, some fundamental chemistry and behavior of the mineral matter during cleaning were studied on our own samples and on samples provided by TRW.

EXPERIMENTAL

For our own work, channel samples of Pittsburgh No. 8 coal from the Grafton Mine, Churchville, WV, and Illinois No. 6 from the Captain Mine, Percy, IL, were used. Two separate batches, IL6 and IL6A, of the Illinois coal were used. The characteristics of the 2 bituminous coals are listed in Table 1.

The desulfurization experiments were run in a batch reactor designed and constructed at Ames Laboratory. The reaction crucible (8 in. x 3.5 in. o.d.) was constructed from Inconel tubing. A basket to hold the coal was fashioned from 20 mesh stainless steel screen. The chromel-alumel thermocouple was sheathed in stainless steel.

---

* Ames Laboratory is operated for the U. S. Department of Energy by Iowa State University under Contract No. W-7405-Eng-82.

Table 1. Analyses for Pittsburgh No. 8 (PT8) and Illinois No. 6 (IL6 and IL6A) Coal (on a dry basis, except for moisture)

	% H_2O	% Ash	% S	(Pyr.	Sulf.	Org.)	% V.M.	H.V., Btu/lb
PT8	2.18	7.02	3.12	(1.48	0.26	1.38)	39.27	13,482
IL6	8.25	13.26	4.10	(1.82	0.29	1.99)	36.55	11,833
IL6A	8.70	14.17	4.52	(2.21	0.23	2.08)	38.50	12,245

For the experiments, 50g of coal (usually 12 x 0 mesh) were placed in the basket and covered with 400g NaOH and 100g KOH. The basket, thermocouple, and stirring rod were placed in the crucible, and the crucible was lowered into the preheated furnace. The coal-caustic mixture was stirred and kept at 370°C for 1 hour while a continuous flow of nitrogen above the crucible provided an inert atmosphere. After the reaction, the basket containing the coal cake was removed from the reactor. The cake contained about 2 parts of caustic adhering to 1 part of coal by weight. The cake was first washed with 2L of water, followed by 1L of 10% H_2SO_4 or HCl, and then a final wash with 2 or 4L water.

The cleaned coal was dried at 110°C overnight and then sampled for analysis. Moisture, ash, and pyritic and sulfate S were determined by ASTM procedures (10). Total S was determined by high-temperature combustion using a Fisher Total Sulfur Analyzer. Organic sulfur was determined by difference.

For comparison, samples of another Pittsburgh No. 8 coal were obtained in March, 1983, from the TRW Gravimelt Benchscale Run #2 performed in California. The samples included raw coal, water-washed caustic-treated coal (intermediate product), and the final clean product (after additional acid and water wash) from the Gravimelt Process. In addition to the standard analyses described above, the samples were also analyzed directly for organic sulfur by a technique utilizing scanning electron microscopy (SEM) and energy-dispersive x-ray spectrometry as described by Straszheim et al. (11). Furthermore, they were characterized for various mineral phases and their distribution among different particle sizes by SEM and automated image analysis (SEM-AIA), a technique described previously by Straszheim and Markuszewski (12).

RESULTS AND DISCUSSION

Standard Conditions

The results for several cleaning experiments on the Pittsburgh No. 8 (PT8) and Illinois No. 6 (IL6 or IL6A) coals are presented in Table 2. For the Pittsburgh coal, under standard conditions (runs #3 and #16), 77-82% ash removal and 65-72% sulfur removal were achieved with recoveries around 85-90%. For the Illinois coal, (IL6 #6, IL6A #1, and IL6A #2), the ash and sulfur removal were better at 87-89% and 72-78%, respectively, while recoveries were lower at 75-79%.

Better Washings

When more water was used for the washing step (PT8 #10) and when the wash water

Table 2. Removal of Sulfur and Ash from Pittsburgh (PT8) and Illinois (IL6 or IL6A) Coals Under Standard[1] or Modified Conditions

Sample Run #	Conditions[1]	% H_2O	% Ash[2]	% Removal	% S[2]	% S Removed	% Rec.[3]
PT8	Untreated	2.18	7.02	----	3.12	----	----
PT8 #3		0.01	1.27	82.4	1.09	65.1	89.7
PT9 #9	Same as #3, but 10% HCl wash	0.16	2.27	67.6	0.91	70.8	87.9
PT8 #10	4L Wash	0.08	1.50	78.6	0.87	72.1	89.6
PT8 #12	4L Hot Wash	0.22	1.07	84.8	0.68	78.5	91.0
PT8 #16		0.18	1.61	77.0	0.89	71.5	84.6
PT8 #13	#10 recleaned	0.17	0.30	95.8	0.38	87.8	72.8 (overall) 81.1 (2nd step only
IL 6	Untreated	8.25	13.26	----	4.10	----	----
IL 6 #6	+60 mesh (80%)	0.33	1.79	86.5	1.16	71.7	74.5
IL6 #10	-60 mesh (85%)	0.48	0.56	95.8	0.57	86.1	64.7
IL6A	Untreated	8.70	14.17	----	4.52	----	----
IL6A #1		0.29	1.85	86.9	1.01	77.7	79.12
IL6A #2		0.25	1.53	89.2	1.12	75.2	79.12

[1] Standard conditions are: 10:1 caustic/coal ratio, 4:1 NaOH/KOH ratio, 370°C for 1 hour, 2L hot water (100°C) wash, 1L 10% H_2SO_4 wash (60°C), 4L hot H_2O wash (100°C). Only nonstandard conditions are listed.
[2] % Sulfur and % ash are reported on a dry basis.
[3] % Recovered = $\frac{\text{grams MAF coal out} \times 100}{\text{grams MAF coal in}}$

was heated to 100°C (PT8 #12), both ash and sulfur removals were improved for each step without appreciable decrease in recovery.

Different Acid

When 10% HCl was substituted for 10% H_2SO_4 (PT8 #9), the sulfur removal was improved, but the ash removal was worse than for run PT8 #3 in which 10% H_2SO_4 was used.

Recleaning

Best results were obtained when cleaned coal from run PT8 #10 was cleaned again under the same conditions. The final ash content of 0.30% and final sulfur content of 0.38% represent removals of 96 and 88%, respectively. The overall recovery, however, decreased to 73%. The lower recovery may be due partially to increased handling and the associated mechanical losses.

Finer Grind

The 12 x 0 mesh IL6 coal, sized as 80% plus 60 mesh, was used in run #6. When the sample was ground to 85% minus 70 mesh and used in run #10, the final ash content

of 0.56% and final sulfur content of 0.57% achieved represent significant improvements in removal, to 96% and 86%, respectively. The lower recovery of 65% can again be attributed in part to mechanical losses of the finer coal through the mesh of the basket.

Effect of Various Washings on Sulfur Forms

The decrease in the total sulfur content of cleaned PT8 coal was followed by observing the various sulfur forms after different washing procedures. Results of these analyses are presented in Table 3. Use of a 2L wash under standard conditions (run #3) showed an appreciable residue of sulfate in the cleaned coal, greater than the amount of sulfate present in the original, untreated coal. Such incorporation of sulfate after treatment with H_2SO_4 has been observed before in our laboratories (13). It may be due to the formation of organic sulfate esters or formation of inorganic sulfates or some other mechanism for adding sulfate. When more thorough washing was used in run #10, the sulfate content was decreased significantly. When 10% HCl was used for the acid wash in run #9, there was no chance of sulfate incorporation and thus the final sulfate content was almost zero.

Table 3. Effect of Washing Improvements on Sulfur Forms

Sample Run #	Conditions	% Pyritic Sulfur	Sulfatic Sulfur	Organic Sulfur	Total Sulfur
PT8	Untreated	1.48	0.26	1.38	3.12
PT8 #3	Standard 2L wash	0.02	0.47	0.60	1.09
PT8 #9	10% HCl wash	0.06	0.02	0.83	0.91
PT8 #10	4L wash	0.01	0.13	0.73	0.87

Effect of Molten Caustic on Particle Size

The Pittsburgh No. 8 coal used in run #3 was sized using sieves and a portable sieve shaker before and after the molten caustic treatment. The results of the sieve analyses are presented in Table 4. For the untreated coal, 20.1% of the particles were -60 mesh. After the treatment, 38.6% of the coal particles were -60 mesh, indicating severe comminution of the sample by action of the molten caustic. When the same cleaned and sieved sample was sieved again, the -60 mesh fraction increased to 44.4% indicating that the treated coal particles were friable and continued to break down further by even simple sieving. When the raw coal was sieved for a second time, results showed that the particle size distribution was unaffected. The degradation of coal matter by molten caustic can occur by pitting due to removal of mineral grains as well as by direct attack on the coal macerals. Observations of such attacks have been made by Oder et al. (14) on samples prepared by TRW. In addition, sudden release of moisture and volatile matter during contact with molten caustic can also contribute to the comminution process.

Effect of Gravimelt Process on Mineral Matter in Coal

The samples of Pittsburgh No. 8 coal obtained from TRW, representing raw coal, the intermediate product and the final cleaned coal, were analyzed by ASTM and other procedures. The results are presented in Table 5. In the final product, the total and organic sulfur were reduced by 70-80% from the levels observed in the raw coal, and the pyritic sulfur was reduced by about 99%, while levels of sulfate sulfur were

Table 4. Sieve Analysis for Pittsburgh No. 8 Coal Before and After Cleaning With Molten Caustic at Ames Laboratory

	RAW COAL		CLEAN COAL	
Mesh Size	PASS #1 Wt. %	PASS #2 Wt. %	PASS #1 Wt. %	PASS #2 Wt. %
>12	15.0	14.6	4.5	3.3
12-60	65.0	65.6	56.9	52.2
60-120	9.8	9.8	20.6	24.9
120-170	3.2	3.1	5.0	5.9
170-200	1.2	1.2	1.9	2.2
200-325	2.7	2.7	4.7	5.2
<325	3.2	3.0	6.4	6.2

Table 5. Analysis of Raw and Gravimelt Treated Pittsburgh No. 8 Coal. Values are in % unless otherwise noted and, except for moisture, are corrected to a dry basis).

	RAW			INTERMEDIATE PRODUCT			FINAL PRODUCT		
	TRW Data[a]	Ames Data	Org. S, by SEM[b]	TRW Data	Ames Data	Org. S, by SEM[b]	TRW Data	Ames Data	Org. S, by SEM[b]
Moisture	6.46	0.89	----	3.27	2.98	----	2.55	1.25	----
Ash	10.15	9.88	----	30.46	29.22	----	1.26	1.00	----
Total S	4.28	4.22	----	0.43	0.32	----	0.75	0.86	----
Pyritic S	2.20	1.78	----	----	0.02	----	----	0.01	----
Sulfate S	0.02	0.20	----	----	0.06	----	----	0.26	----
Organic S	2.06	2.24	1.99	----	0.24	0.08	----	0.59	0.41
Elemental S (ppm)	----	29	----	----	<1	----	----	4	----
Heat Value, BTU/lb	13,282	----	----	8,454	----	----	13,780	----	----
Mineral Matter[c]	12.50	12.00	----	----	33.03	----	----	1.13	----

[a] Analysis of head sample.
[b] Procedure in Reference 11.
[c] Mineral matter = (1.13 x ash) + (0.47 x pyritic S), as in Reference 12.

not significantly affected. The organic sulfur concentrations determined directly by the SEM technique were consistently lower than the indirect ASTM values. The deviation was most pronounced for the treated coals, which may indicate the formation of unusual minerals such as sulfides or jarosite during the Gravimelt process. Possibly, incomplete dissolution of pyrite in the ASTM method may also have inflated the ASTM organic sulfur values. These apparent discrepancies are being studied further. The magnitude of the reductions in levels of the various sulfur forms was generally better than the reductions for the Pittsburgh No. 8 coals observed at Ames Laboratory (see Tables 2 and 3).

In addition, the TRW samples were analyzed by the SEM-AIA technique described previously (12). The SEM-AIA data on the mineral phase identification and distribution between the size fractions are presented in Table 6 for all three samples of raw and treated coal. The SEM-AIA data show the nearly complete removal of many minerals and a reduction of more than 90% in the overall content of the coal as a result of the TRW Gravimelt Process. No major shifts in particle size distribution were observed, although the pyrite distribution shifted somewhat towards the coarse fraction after processing.

A significant change in mineralogy can be observed for the cleaned coals. The processed coals showed a much greater percentage of material classified as "miscellaneous" than did the raw coal, indicating formation of unusual minerals. For the washed, Gravimelt-treated coal, this miscellaneous portion contained significant amounts of Ca, K, and/or Na. SEM-EDX examination showed also a general enhancement of these cations in the coal rather than in a separate phase or in components enriched in these elements, indicating that they could be associated with the organic portion of coal (possibly with carboxylate or phenolate functions). Such enhancement of Ca ions in the organic portion of coal has been observed previously in coals after treatment by the Ames Oxydesulfurization Process (15) and in lower rank and severely weathered coals (16). In the final product from the Gravimelt treatment, the "miscellaneous" material contained appreciable amounts of Cr, Mn, and Ni or Fe (or both), suggesting contamination from nickel and stainless steel components. For many mineral categories, the relative weight percent decreased after the caustic treatment and then increased after the acid treatment. It appears that the caustic treatment altered much of the original mineral matter while forming unusual minerals. The iron-rich phase, for example, in the intermediate product could be $NaFeO_2$ which has been shown to be the principal product from the reaction of FeS_2 with fused NaOH (17). The subsequent acid treatment removed much of the unusual mineral matter in the "miscellaneous and unknown" category, thereby increasing the relative percentages in the other mineral categories.

CONCLUSIONS

Coal treated at Ames Laboratory with molten caustic by a procedure similar to that of the Gravimelt Process resulted generally in 80-90% reductions in ash and 70-80% reductions in total sulfur. The recoveries of coal on a moisture- and ash-free basis were 80-90%. The removal of sulfur and ash could be improved by better washing, finer grind, or additional cleaning. SEM-AIA data on samples treated by TRW showed the formation of unusual minerals in the treated samples, as well as enrichment of these minerals in certain elements. The decrease of 90% in the ash content could be explained by the removal of individual mineral phases in all particle sizes. Removal of organic sulfur was corroborated by a direct SEM-EDX technique.

ACKNOWLEDGEMENTS

This work was supported by the Assistant Secretary for Fossil Energy, Division of Coal Utilization, through the Pittsburgh Energy Technology Center, Coal Preparation Branch. The authors gratefully acknowledge Drs. R.A. Meyers and W.D. Hart at TRW Systems, for supplying samples of raw and chemically desulfurized coal on which our SEM-AIA analyses were performed.

Table 6. SEM-AIA Classification of Mineral Matter in Pittsburgh No. 8 Coal Samples Obtained from TRW. The mineral phases are described by chemistry and area-equivalent diameter (in μm), expressed as weight percent of the total coal.

Raw Coal

Mineral Phase	Particle size, μm < 6.3	6.3-20	20-63	63-200	Total
Pyrite	0.25	1.67	1.63	0.96	4.50
Kaolinite	0.15	0.75	0.62	0.50	2.02
Illite	0.29	0.92	0.71	0.51	2.43
Quartz	0.13	0.58	0.25	0.37	1.32
Iron-rich	0.01	0.04	0.22	0.71	0.98
Calcite	0.00	0.00	0.01	0.00	0.01
Silicates	0.08	0.13	0.03	0.14	0.39
Misc. & Unknown	0.10	0.21	0.02	0.00	0.34
Total	1.01	4.30	3.50	3.19	12.00

Water-Washed Gravimelt-Treated Coal (Intermediate Product)

Mineral Phase	Particle size, μm < 6.3	6.3-20	20-63	63-200	Total
Pyrite	0.13	0.18	0.08	0.00	0.40
Kaolinite	0.01	0.02	0.00	0.00	0.03
Illite	0.19	0.59	0.42	0.12	1.32
Quartz	0.01	0.07	0.00	0.00	0.08
Iron-rich	0.33	1.05	1.15	1.14	3.67
Calcite	0.05	0.07	0.00	0.00	0.11
Silicates	0.12	0.18	0.20	0.46	0.95
Misc. & Unknown	4.33	9.31	5.67	3.35	22.66
Total	5.17	11.46	7.53	5.07	29.22

Final Gravimelt Product

Mineral Phase	Particle size, μm < 6.3	6.3-20	20-63	63-200	Total
Pyrite	.006	.010	.074	.173	.262
Kaolinite	.019	.054	.025	.154	.252
Illite	.023	.030	.008	.000	.060
Quartz	.023	.037	.014	.017	.091
Iron-rich	.004	.004	.000	.000	.008
Calcite	.003	.005	.002	.000	.010
Silicates	.007	.007	.003	.000	.017
Misc. & Unknown	.093	.147	.060	.000	.300
Total	.176	.295	.185	.343	1.000

REFERENCES

1. P.X. Masciantonio, "The Effect of Molten Caustic on Pyritic Sulphur in Bituminous Coal," Fuel 44(4), 269-275 (1965).

2. R.A. Meyers and W.D. Hart, "Chemical Removal of Organic Sulfur from Coal," Symp. on Removal of Heteroatoms from Fuel, ACS Meeting, Houston, TX, March 23-28, 1980.

3. TRW, "Laboratory Study for Removal of Organic Sulfur from Coal," Final Report to U.S. DOE, DE-AC-80PC30141, July 1, 1981.

4. W.D. Hart, "Chemical Coal Cleaning," Proc. Resources from Coal, Coal Wastes, and Ash Workshop, Reston, VA, June 10-11, 1982, pp. 66-75.

5. TRW Energy Development Group, "Gravimelt Process Development, Final Report, DOE/PC/42295-T7 (DE84013743), Redondo Beach, CA, June 1983.

6. R.A. Meyers, "Gravimelt Process Applications and Economics," Proc. First Annual Pittsburgh Coal Conference, Pittsburgh PA, Sept. 17-21, 1984, pp. 381-384.

7. B. Maijgren, W. Hubner, K. Norrgard, and S.-B. Sundvall, "Determination of Organic Sulphur in Raw and Chemical Cleaning Coals by Scanning Electron Microscopy and Energy Dispersive X-ray Spectrometry," Fuel 62(9), 1076-1078 (1983).

8. B. Maijgren and W. Hubner, "Coal Cleaning by Molten Caustic," Proc. 1983 International Conference on Coal Science, Pittsburgh, PA, pp. 256-259.

9. R. Markuszewski and P. Chiotti, "Regeneration of Alkali in the Fused Salt Desulfurization System," Fossil Energy Annual Report (Oct. 1, 1981 - Sept. 30, 1982), IS-4816, Ames Laboratory, Iowa State University, Ames, IA, pp. 39-56.

10. Annual Book of ASTM Standards, Part 26, ASTM, Philadelphia, PA, 1982.

11. W.E. Straszheim, R.T. Greer, and R. Markuszewski, "Direct Determination of Organic Sulphur in Raw and Chemically Desulphurized Coals," Fuel 62(9), 1070-1075 (1983).

12. W.E. Straszheim and R. Markuszewski, "Automated Image Analysis of Mineral Matter in Raw and Supercleaned Coals," Am. Chem. Soc. Div. Fuel Chem. Preprints 29,(4), 310-318, (1984).

13. C.W. Fan, R. Markuszewski, and T.D. Wheelock, "Process for Producing Low-Ash, Low-Sulfur Coal," Am. Chem. Soc. Div. Fuel Chem. Preprints 29(1), 114-119 (1984).

14. R.R. Oder, B.N. Murthy, and E.L. McGinnis, "Chemical Coal Cleaning Assessments at Gulf," Separation Science and Technology 18 (12 & 13), 1371-1393 (1983).

15. R. Markuszewski, L.J. Miller, W.E. Straszheim, C.W. Fan, T.D. Wheelock, and R.T. Greer, "Evaluation of the Removal of Organic Sulfur from Coal," in New Approaches in Coal Chemistry, (ACS Symp. Series 169), B.D. Blaustein, B.C. Bockrath, and S. Friedman, eds., ACS, Washington, D.C., 1981, pp. 401-414.

16. F.E. Huggins and G.P. Huffman, "An EXAFS Investigation of Calcium in Coal," Proc. 1983 International Conference on Coal Science, Pittsburgh, PA, pp. 679-682.

17. P. Chiotti and R. Markuszewski, "Reaction of Pyrite with Fused Sodium Hydroxide," submitted to Ind. Eng. Chemistry, Process Design and Development, May 1984.

COAL DEMINERALIZATION WITH HOT ALKALINE SOLUTIONS

C.-Y. Chi, R. Markuszewski, and T. D. Wheelock

Chemical Engineering Department and Ames Laboratory[a]
Iowa State University, Ames, Iowa 50011

INTRODUCTION

A process for extracting most of the mineral matter from coal was demonstrated recently (1). It involves treating fine-size coal with a hot alkaline solution to dissolve quartz and to convert clay minerals and iron pyrite into acid-soluble compounds which are extracted with dilute acid in a second step. Although various alkalis and acids may be utilized, Na_2CO_3 and H_2SO_4 are advantageous because of low cost and ready availability. Preliminary work has shown that hot Na_2CO_3 solutions readily convert kaolinite into sodium hydroaluminosilicates which are acid-soluble (2). That work has also shown that hot sodium carbonate solutions will dissolve quartz and convert iron pyrite into hematite, but not as readily as sodium hydroxide solutions.

In this work, the characteristics of the two-step process were studied in greater detail using three different bituminous coals under a variety of conditions, with particular attention being given to the first step. The relative effectiveness of various alkalis was studied as well as the effects of alkali concentration, alkaline treatment time, and temperature. The alkali-treated coals were subsequently leached with hot HNO_3 to remove mineral matter. Nitric acid was employed because it dissolves iron pyrite and is used for that purpose in ASTM Method D2492 (3) for determining various forms of sulfur in coal. Since only organically bound sulfur should remain in coal which has been leached with HNO_3, it was possible to obtain an indication of how much organic sulfur was removed by the two-step treatment.

EXPERIMENTAL METHODS

Bituminous coals were obtained from several sources for this study (Table 1). Much of the work was done with high volatile C bituminous coal from the Lovilia No. 4 underground mine in Iowa. The other two coals were somewhat higher in rank. The different coals were ground to -200 mesh (U.S. Standard); a portion of each product was ball-milled further to approximately 90% -400 mesh. A sample of each prepared coal was leached with boiling dilute HNO_3 to remove inorganic sulfur so that the sulfur content of the residue would reflect the organic sulfur content of the raw coal. The leaching procedure was similar to that of ASTM Method D2492 (3) and was described in more detail elsewhere (4).

For the first step, 12 g. of ground coal and 120 ml. of alkaline solution were mixed and placed in a 300-ml. stainless steel autoclave equipped with a turbine agitator. The system was flushed with nitrogen and then heated to the desired temperature while the mixture was stirred continuously. After a period of treatment at constant temperature and pressure, the autoclave was cooled quickly, and the contents were filtered to recover the coal. The filter cake was washed with 400 ml. of distilled water, dried at 90°C for 4 hr., weighed, and analyzed for total sulfur and ash. A portion of the alkali-treated coal (usually 2.5-3.0 g) was leached for an additional 30 min. with boiling 2.1 $\underline{M}$ HNO_3 in a stirred, three-neck Pyrex flask fitted with a reflux condenser. In most cases, 250-300 ml. of acid was employed. After the acid treatment, the flask was cooled quickly to room temperature, and the

[a]Ames Laboratory is operated for the U.S. Department of Energy by Iowa State University under Contract No. W-7405-Eng-82.

contents were filtered. The filter cake was washed, dried, weighed, and analyzed as above. The ash content of the raw and treated coals was determined by ASTM Method D3174 (3), while the sulfur content was determined with a Fisher model 475 total sulfur analyzer.

REPORTING BASIS

The ash content of raw and treated coals is reported on a moisture-free basis and the sulfur content on both a moisture- and ash-free basis. The ash reduction achieved corresponds to the overall change in moisture-free ash content divided by the moisture-free ash content of the raw coal. The reduction in total sulfur content corresponds to the change in total sulfur content divided by the total sulfur content of the raw coal, all on a moisture- and ash-free basis. The apparent reduction in organic sulfur content corresponds to the difference between the sulfur content of the acid-leached raw coal and the final sulfur content of the acid-leached, alkali-treated coal divided by the sulfur content of the acid-leached raw coal, all on a moisture- and ash-free basis. Coal recovery corresponds to the mass ratio of coal recovered during the alkaline treatment step to coal charged, all on a moisture- and ash-free basis.

EXPERIMENTAL RESULTS

The results of leaching ground raw coals with HNO_3 alone are indicated in Table 1. The sulfur content of the acid-leached coal is indicative of the organically bound sulfur, while the ash content reflects the removal of iron pyrite and other minerals such as carbonates which are soluble in nitric acid. It can be seen that acid leaching alone reduced the sulfur content of Cherokee coal by 57%, Illinois No. 6 coal by 44-55%, and Lower Kittanning coal by 84-87%; also for these coals the ash conent was reduced by 63%, 44-56%, and 55-57%, respectively.

For the alkaline treatment experiments, a relatively long time was needed to heat the reactor and its contents to the required temperature. Typically, it took 20 min. to reach 150°C, 25 min. to reach 200°C, and 45 min. to reach 300°C. While the temperature was being raised, the alkaline attack on the coal and its mineral matter got underway. This attack can be seen from the changes which took place when ball-milled Cherokee coal was heated in 1.0 M Na_2CO_3 from room temperature to 300°C (Figure 1). Subsequent changes which occurred as the treatment was continued at 300°C are also reflected in Figure 1. The data in this diagram represent the results of nine different runs conducted for various time intervals. The results show that by the time the reaction mixture had reached 300°C the sulfur content of the coal had been reduced by 56% which was equivalent to removing all of the inorganic sulfur. As the treatment was continued at 300°C, the sulfur content of the coal was further reduced until a reduction of 69% was achieved. Further treatment was counterproductive as the sulfur content of the product actually increased slightly. Thus for maximizing sulfur removal, the optimum treatment time was 85 min. total or 40 min. beyond the initial heat up period. For the optimum treatment time, the total sulfur content of the alkali-treated coal was 27% below the apparent organic sulfur content of 1.13% indicated in Table 1 for the raw coal. Hence, it appeared that some of the organic sulfur had been removed.

The ash content of the alkali-treated coal was slightly higher than that of the raw coal which was probably due to the formation of sodium hydroaluminosilicates. Coal recovery on a moisture- and ash-free basis declined gradually as the treatment time was extended (Figure 1). Moreover, the rate of decline increased beyond a total treatment time of 70 min.

When the alkali-treated coal which had provided the data for Figure 1 was subsequently leached for 30 min. with boiling HNO_3, the overall results shown in Figure 2 were obtained for the two-step process. The time and temperature of the alkaline

treatment step are indicated. Since the HNO_3 leaching step by itself was capable of removing the inorganic sulfur and reducing the total sulfur content of the coal by 57%, treating the coal with alkali first had a relatively small effect on the total sulfur content of the coal after the combined treatment. For the optimum alkaline treatment time, the total sulfur content was reduced 77.5% by the combined treatment, as compared to 69% for the alkaline leaching step alone. On the other hand, the combined treatment seemed to account for a significant reduction in the apparent organic sulfur content. For an extended treatment time, the reduction in organic sulfur content exceeded 45% for the combined treatment which seemed significantly greater than the 27% reduction noted for the alkaline leaching step alone.

The alkaline treatment step had a pronounced effect on what happened to the ash content of Cherokee coal when it was subsequently leached with acid. As Figure 2 indicates, HNO_3 leaching of the raw coal reduced the ash content 63%. Pretreating the coal with alkali for short intervals at temperatures up to 200°C had little effect on the results of subsequent acid leaching. But pretreating the coal at 300°C for even a short time resulted in lowering the ash content 90% when the coal was leached with acid.

To determine the effect of the final temperature during the alkaline leaching of Cherokee coal, several runs were carried out in which different portions of the coal were treated with 1.0 M Na_2CO_3 for 1.0 hr. at various final temperatures. The alkali-treated coal was then leached with HNO_3. The results of the alkaline leaching step are indicated in Figure 3 and the overall results in Figure 4. As the treatment temperature was raised, the quantity of sulfur removed by the first step increased greatly while coal recovery declined. The decline in recovery was gradual up to 250°C and then more precipitous beyond. The overall reduction in total sulfur content for both steps increased slightly and the reduction in apparent organic sulfur content somewhat more as the temperature of the first step was raised. The overall reduction in ash content for both steps also rose but then reached a plateau at 250°C.

The effects of alkali type and concentration were studied by treating different portions of Cherokee coal with various alkaline solutions for 1 hr. at 300°C (Table 2) and then by leaching with HNO_3. The sulfur reduction achieved in the first step was nearly the same for a majority of the alkalis; however, it was slightly lower for coal treated with either $NaHCO_3$ or $KHCO_3$. Coal recovery in the first step was similar with most alkalis except that it was slightly higher for coal treated with Na_2HCO_3 and greatly lower for coal treated with NaOH. Because of the low recovery, the caustic-treated coal was not subjected to the second step. When the second step was applied to the other alkali-treated portions, the lowest sulfur and ash contents were obtained with coal treated with 1.0 M Na_2CO_3. Lower concentrations of Na_2CO_3 achieved similar overall reductions in sulfur and ash contents and provided a higher recovery.

Other coals were also subjected to the two-step treatment (see Table 3). The results obtained with ball-milled Illinois No. 6 coal were similar, in general, to those achieved with Cherokee coal. When the alkaline treatment step was applied to either coal, sulfur reduction increased and coal recovery declined as the temperature was raised. However, for any given temperature the recovery and sulfur content of the alkali-treated product were higher for Illinois coal than for Cherokee coal. The high sulfur content of the treated Illinois coal appeared to be largely due to the higher organic sulfur content of the raw coal, while the higher recovery of this material seemed to be related to a difference in coal rank. When the alkali-treated Illinois coal was treated with HNO_3, most of the ash-forming minerals were removed to give a low ash content. Also, the total sulfur content of the final product was lower than the apparent organic sulfur content of the raw coal, indicating removal of some organic sulfur. As for Cherokee coal, the results with Illinois coal were

not affected greatly by alkali concentration, but in both cases the final ash content achieved with the two-step process declined slightly as the alkali concentration increased. The results with Illinois coal were also not affected greatly by particle size. The first-step recovery was slightly lower and the ash-content of the final product was slightly higher for -200 mesh coal than for -400 mesh coal. The sulfur content of the final product was nearly the same in both cases.

Compared to the other coals, Lower Kittanning coal responded similarly in some ways to the two-step treatment but differently in other ways (Table 3). The differences seemed related to the high ash and sulfur contents of the coal and possibly to a difference in mineral species. Sulfur removal was affected by the alkaline treatment time and temperature much as for the other coals. However, because of the very high iron pyrite content, the alkaline leaching step never succeeded in reducing the total sulfur content to the level of the apparent organic sulfur content. On the other hand, after applying both steps, the final sulfur content was always below the apparent organic sulfur content of the raw coal again indicating organic sulfur removal. Sulfur removal in the first step was affected somewhat by alkali concentration and a 1.0 M concentration appeared optimum. Coal recovery was affected by changes in various parameters as for the other coals, but it was slightly higher for any given set of conditions in the case of Lower Kittanning coal. The greatest difference in results with this coal occurred with the removal of ash-forming minerals, because the alkaline treatment step appeared ineffective except under relatively mild conditions. The removal of ash-forming minerals by acid leaching was not improved by the first step in most cases. Only by carring out the first step at a relatively moderate temperature (i.e., 250°C) or with the smallest alkali concentration or for the shortest time did it appear to have a beneficial effect on the overall results. Consequently it seemed as though the Lower Kittanning coal was unique in containing some component which reacted with alkali under more rigorous conditions to form an acid insoluble material.

DISCUSSION AND CONCLUSIONS

A two-step process for extracting mineral matter and sulfur from coal was demonstrated with three different coals under a variety of treatment conditions. The first step involves treatment with a hot alkaline solution which extracts part of the sulfur and generally converts much of the mineral matter to an acid-soluble form. The second step involves leaching with an acid to extract the converted mineral matter. Although H_2SO_4 would likely be used in the second step of a commercial process, HNO_3 was chosen for the present study in order to shed some light on the disposition of organic sulfur.

A major concern of the present study was the effect of various parameters involved in the alkaline treatment step. Early in the investigation it was observed that Na_2CO_3, K_2CO_3, and NaOH were equally effective for removing sulfur in the first step while $NaHCO_3$ and $KHCO_3$ were less effective. On the other hand, coal recovery suffered greatly when NaOH was used. For the combined two-step treatment, the lowest sulfur and ash contents were achieved with Na_2CO_3. In view of this result and various economic advantages, Na_2CO_3 was selected for studying the effects of other parameters. The effects of alkali concentration appeared relatively minor in most instances. However, for Lower Kittanning coal an alkali concentration of 1.0 M appeared optimum for removing sulfur in the first step whereas a smaller concentration (0.2 M) resulted in a lower ash content overall for the two-step process.

Alkali-treatment time and temperature affected the results greatly. Sulfur removal increased and coal recovery decreased in the first step with rising temperature, and above 250°C coal recovery decreased disproportionately. Removal of mineral matter in the second step was affected by the temperature of the first step. With both the Iowa and Illinois coals, the overall reduction in ash content for both steps increased with temperature up to 300°C and then leveled off. But with Lower

Kittanning coal 250°C seemed to be the optimum temperature for reducing the ash content. Increasing the alkaline treatment time up to a point resulted in increasing sulfur removal in the first step, but beyond this point less sulfur was removed. Coal recovery declined as the alkaline treatment time was extended, and the rate of decline accelerated after prolonged treatment.

The apparent removal of organic sulfur by the two-step treatment observed with all three coals was of considerable interest. Since the total sulfur content of the treated coal was below that which could be achieved by leaching with HNO_3 alone, it appeared that the alkaline leaching step either removed a significant quantity of organic sulfur or converted some of the organic sulfur into a form which was extractable with HNO_3. In several instances the total sulfur content of Iowa or Illinois coal treated by the alkaline leaching step alone was below the apparent organic sulfur content of the raw coal indicating organic sulfur removal as well as inorganic sulfur removal, but usually the apparent reduction in organic sulfur content was slight and may not have been significant.

Lower Kittanning coal was unusual in that less rigorous alkaline treatment conditions were more effective than more rigorous conditions for converting the mineral matter into a form extractable with nitric acid. Additional work is needed to explain these unusual results.

ACKNOWLEDGEMENT

This work was supported by the Assistant Secretary for Fossil Energy, Division of Coal Utilization, through the Pittsburgh Energy Technology Center, Coal Preparation Branch.

LITERATURE CITED

1. Fan, C.-W., Markuszewski, R., and Wheelock, T. D., Process for producing low-ash, low-sulfur coal, Am. Chem. Soc. Div. of Fuel Chem. Preprints, 29(1):114-119 (1984).
2. Fan, C.-W., Markuszewski, R., and Wheelock, T. D., Behavior of mineral matter during alkaline leaching of coal, Am. Chem. Soc. Div. of Fuel Chem. Preprints, 29(4):319-325 (1984).
3. American Society for Testing and Materials, Annual Book of ASTM Standards, Part 26, Philadelphia, PA, 1975.
4. Markuszewski, R., Miller, L. J., Straszheim, W. E., Fan, C.-W., Wheelock, T. D., and Greer, R. T., Evaluation of the removal of organic sulfur from coal, in New Advances in Coal Chemistry (ACS Symp. Series 169), B. D. Blaustein, B. C. Bockrath, and S. Friedman, eds., Am. Chem. Soc., Washington, D.C., 1981, pp. 401-414.

Table 1. Bituminous coals used in leaching experiments

Coal Seam	Location	Size mesh	Ash, %	Tot. S %	HNO_3 leached	
					Ash, %	Tot. S %
Cherokee group	Monroe County, Iowa	-400	8.24	2.65	3.05	1.13
Illinois No. 6	Trivoli County, Illinois	-200	12.75	3.71	5.55	1.66
		-400	8.90	3.14	4.99	1.66
Lower Kittanning	Armstrong County, Pennsylvania	-200	18.07	10.44	7.94	1.88
		-400	18.44	10.24	8.29	1.69

Table 2. Results of treating Cherokee coal with different alkalis at 300°C for 1 hr. followed by leaching with HNO_3

Alkali	Alkaline treatment step				Product[a]		Overall reduction		
	Recov., %	Ash, %	Tot. S %	S redn., %	Ash, %	Tot. S, %	Ash, %	Tot. S, %	Org. S, %
0.2 M Na_2CO_3	85.8	10.04	0.94	64.5	1.21	0.62	85.3	76.6	45.1
0.6 M Na_2CO_3	85.4	10.32	0.84	68.3	0.95	0.62	88.5	76.6	45.1
1.0 M Na_2CO_3	78.7	11.90	0.92	65.3	0.88	0.62	89.3	76.6	45.1
1.0 M $NaHCO_3$	84.0	10.42	1.35	49.1	1.10	0.84	86.7	68.3	25.7
1.0 M K_2CO_3	79.4	11.84	1.02	61.5	1.63	0.83	80.2	68.7	26.5
1.0 M $KHCO_3$	75.4	13.13	1.27	52.1	2.15	0.80	73.9	69.8	29.2
2.8 M NaOH	35.6	13.42	1.02	61.5	--	--	--	--	--

[a]Ash and total sulfur contents of final acid-treated product.

Table 3. Results of applying different alkaline treatment conditions to coal followed by leaching with HNO_3.

Coal	Alkaline treatment step[a]							Acid trtd. prod.		Overall reduction		
	Na_2CO_3 M	Temp., °C	Time, min.	Recovery, %	Ash, %	Tot. S, %	S red., %	Ash, %	Tot. S, %	Ash, %	Tot. S, %	Org. S, %
Ill. No. 6	0.2	300	60	89.8	11.73	2.03	35.4	1.44	1.43	83.8	54.5	13.9
Ill. No. 6	0.6	300	60	89.5	11.66	1.68	46.5	1.04	1.43	88.3	54.5	13.9
Ill. No. 6	1.0	250	60	96.8	11.34	1.91	39.2	1.03	1.30	88.4	58.6	21.7
Ill. No. 6	1.0	300	60	86.8	12.09	1.78	43.3	0.77	1.44	91.3	54.1	13.3
Ill. No. 6	1.0	344	60	80.8	11.36	1.36	56.7	0.71	1.02	92.0	67.5	38.6
Ill. No. 6[b]	1.0	300	60	81.2	19.42	1.95	47.4	1.43	1.39	88.8	62.5	16.3
Low. Kit.	0.2	300	60	91.5	20.67	5.74	43.9	4.02	1.52	78.2	85.2	10.1
Low. Kit.	0.6	300	60	90.0	21.80	3.16	69.1	8.92	1.26	51.6	87.7	25.4
Low. Kit.	1.0	300	60	88.8	23.40	3.03	70.4	8.98	1.31	51.3	87.2	22.5
Low. Kit.	2.0	300	60	89.8	22.94	3.30	67.8	8.62	1.27	53.3	87.6	24.9
Low. Kit.	3.0	300	60	87.2	24.57	3.96	61.3	8.15	1.44	55.8	85.9	14.8
Low. Kit.	1.0	200	60	97.0	18.99	9.23	9.9	3.29	1.62	82.2	84.2	4.1
Low. Kit.	1.0	250	60	96.5	20.78	7.88	23.0	2.88	1.45	84.4	85.8	14.2
Low. Kit.	1.0	344	60	85.2	22.58	1.87	81.7	10.14	1.20	45.0	88.3	29.0
Low. Kit.	1.0	300	0	92.0	22.36	5.61	45.2	6.29	1.43	65.9	86.0	15.4
Low. Kit.	1.0	300	30	88.9	23.66	3.42	66.6	8.70	1.25	52.8	87.8	26.0
Low. Kit.	1.0	300	90	81.7	30.00	3.83	62.6	8.24	1.32	55.3	87.1	21.9
Low. Kit.[b]	1.0	300	60	87.8	23.85	4.21	59.7	7.96	1.36	56.8	87.0	27.7

[a]Net treatment time at constant temperature is indicated.

[b]-200 mesh.

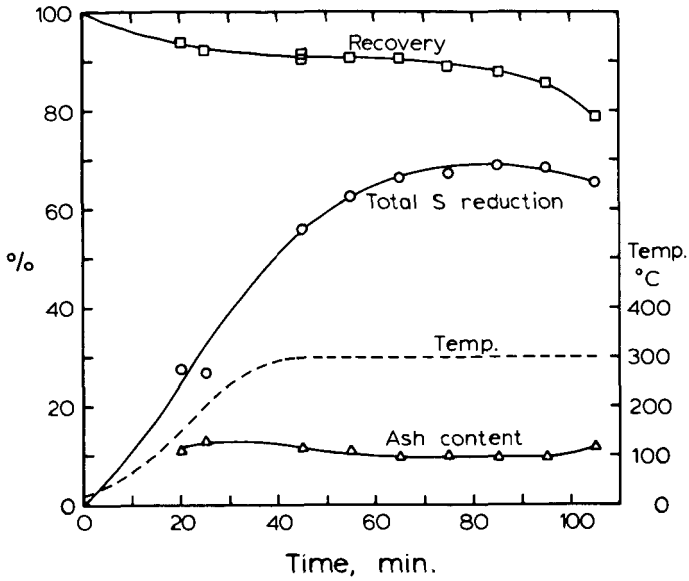

Figure 1. Results of treating -400 mesh Cherokee coal with 1 M Na_2CO_3.

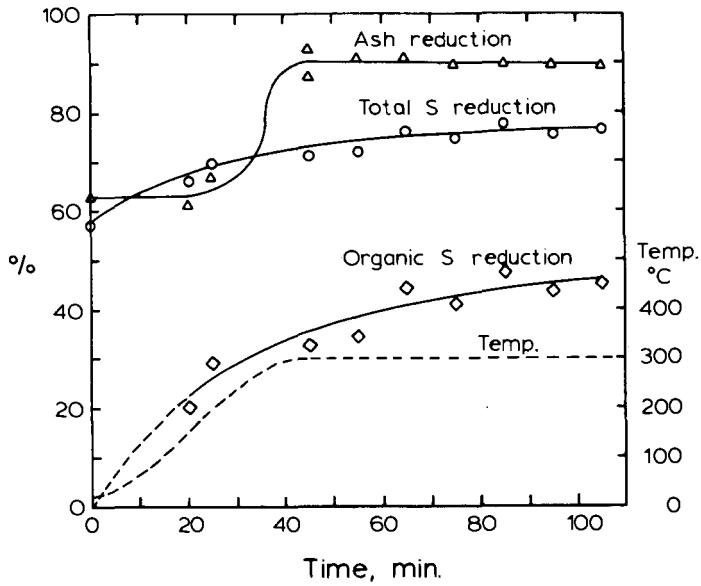

Figure 2. Overall results of applying the two-step process to Cherokee coal. Time and temperature are for the alkaline treatment step.

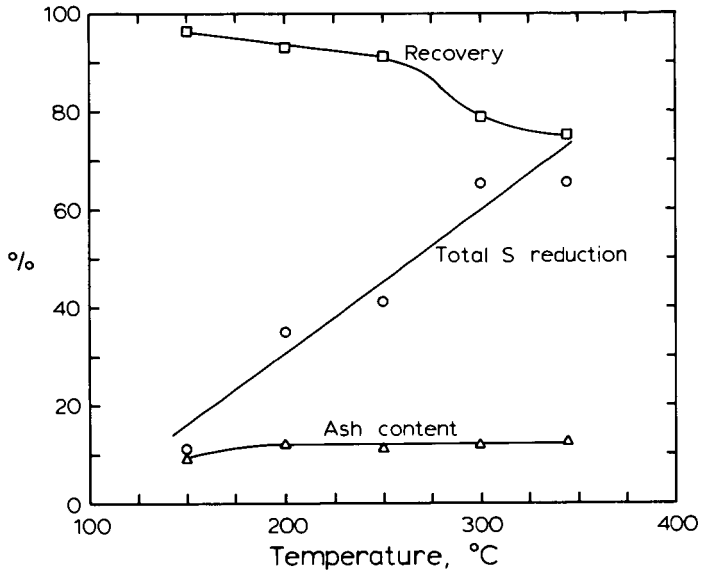

Figure 3. Results of treating -400 mesh Cherokee coal with 1 M Na_2CO_3 for 1 hr. at indicated temperature.

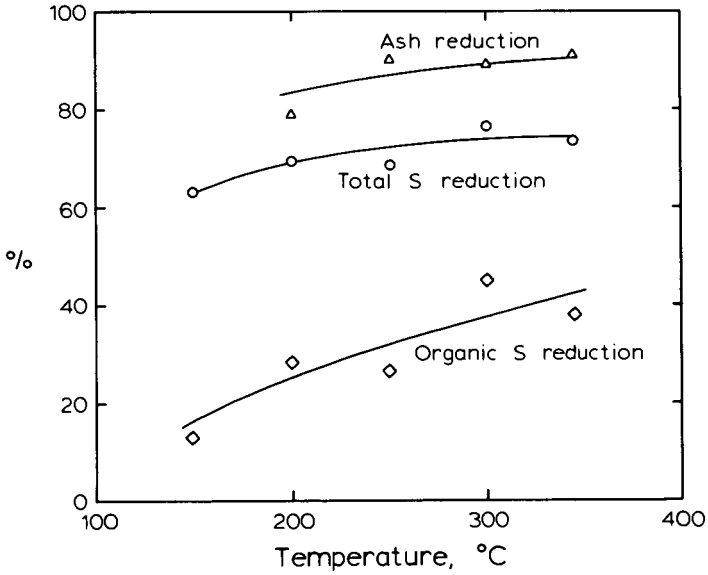

Figure 4. Overall results of applying the two-step process to Cherokee coal which was treated with Na_2CO_3 at the indicated temperature.

REMOVAL OF TRACE ELEMENTS DURING CHEMICAL CLEANING OF COAL

G. A. Norton, H. G. Araghi, and R. Markuszewski

Ames Laboratory*, Iowa State University, Ames, IA 50011

ABSTRACT

Different samples of Illinois No. 6 coal, which had been treated with aqueous Na_2CO_3 solutions at elevated temperatures and pressures and with molten NaOH/KOH mixtures at atmospheric pressure in order to remove sulfur and ash, were analyzed for trace elements before and after treatment. Although removal of sulfur and ash were the primary objectives of those treatments, the removal of trace elements by these chemical cleaning methods was investigated in this work. X-ray fluorescence, atomic absorption, and inductively coupled plasma-atomic emission spectroscopy were the instrumental methods used to determine levels of numerous trace elements in the raw and treated coals. In general, the aqueous Na_2CO_3 treatments reduced levels of Mn, Pb, and Zn by 75% or more, while levels of Cd and Ni were reduced by lesser amounts. In one run, significant reductions in the levels of Ba, Cr, Rb, Se, and Sr were also observed. The coals treated by the molten caustic showed substantial reductions in concentrations of As, Cd, Hg, Pb, Rb, Se, Sr, and Zn. However, levels of Cr and Ni were elevated in the treated coals, probably due to corrosion of the reactor components.

INTRODUCTION

Coal contains virtually every element, most of which are present in trace quantities of 100 ppm or less. Many of these trace elements are toxic to plant and animal life, even at low concentrations. Because power plants consume on the order of 600 million tons of coal annually for the production of electricity (1), coal combustion can mobilize thousands of tons of potentially hazardous trace elements into the environment each year. Because of the large quantities of coal combusted, even trace amounts of toxic elements can accumulate to hazardous levels. Also, potentially deleterious effects of particulate stack emissions from coal combustion may be enhanced since many trace elements are surface enriched (2) and concentrate preferentially in the smaller, more respirable particle sizes (3).

Aside from the detrimental environmental aspects of trace elements in coal, there are also adverse technological aspects of trace elements in coal, such as catalyst poisoning in catalytic hydrogenation and gasification reactions (4,5,6).

Physical methods can effectively remove some trace elements from coal, especially if deep cleaning methods are employed (7). However, such methods do not adequately remove finely disseminated minerals or organically bound elements, thereby necessitating chemical treatments for removing many of the deleterious elements in coal.

A literature survey was conducted to acquire information pertinent to the removal of trace elements from U.S. coals by chemical means. This survey included trace element associations with minerals and the affinities of trace elements for organic or inorganic components. Previous studies on chemical cleaning methods were also reviewed in order to ascertain any reductions in trace element contents. A thorough literature survey of all chemical cleaning methods revealed that caustic or alkaline treatments, especially when followed by an acid wash, are very effective in removing ash-forming minerals.

*Ames Laboratory is operated for the U.S. Department of Energy by Iowa State University under Contract No. W-7405-Eng-82.

In this study, the effectiveness of trace element removal by two chemical coal cleaning methods was examined. One method involved treatment with aqueous Na_2CO_3 solutions, and the other involved treatment with molten NaOH/KOH mixtures. In each case, acid washes were used as subsequent cleaning steps to decrease the ash content, followed by water washes in the final step.

BACKGROUND

Based on the reviewed literature, it is evident that modes of occurrence in U.S. coals vary considerably, although several generalizations can be made. Many elements of environmental concern, including As, Cd, Hg, Pb, and Zn, generally associate with the mineral portion of the coal and tend to associate with pyrite or accessory sulfide minerals. The element As has been found to occur in solid solution in pyrite (8), while Cd has been found in solid solution in sphalerite (9,10). The predominant mineral species containing a particular element can vary. In one example, Pb seems to be present mostly as PbSe in Appalachian Basin coals, but it tends to exist in the form of PbS in coals from other regions (8,11). Minerals in coal often occur, at least partially, as finely disseminated grains. Although most trace elements appear to be largely inorganically associated, several of them have a strong affinity for the organic portion of the coal and are believed to be present as metal chelates. Among the elements in the latter category are B, Be, and Ge. Many elements, such as Cr, Cu, Ni, and Se, appear to have a mixed or highly variable organic/inorganic affinity in some coals. Again, these are only generalizations, since organic/inorganic associations of trace elements can vary widely from coal to coal and can show both extremes in their affinities.

A literature review on trace element removal by chemical cleaning methods indicated that leaching coals with various acids to study trace element removal was common. In one study, various coals from eastern, central, and western coal regions were cleaned by a combination of physical and chemical means, and extraction efficiencies for numerous elements were ascertained by analyzing the raw and treated coals (12). Cleaning was performed by floating the coals at a specific gravity of 1.40, grinding the float fraction to -325 mesh, and then successively leaching with 10% HNO_3, 49% HF, and 25% HCl. Results of the analyses on the raw and cleaned coals showed that levels of Be were reduced by 90% or more, while levels of As, B, Cr, Cu, Mo, Ni, Se, and V were reduced by at least 70%. However, these are only average values, and standard deviations were sometimes larger than the averages. In that study, physical separation by flotation followed by acid leachings was found to be much more efficient at removing trace elements than flotation alone.

Results on trace element removal during desulfurization and demineralization by a chemical treatment are sparse. Only a few of the chemical cleaning processes studied in the past or currently being developed present trace element data in addition to the conventional sulfur, ash, and heating values.

One of these exceptions is the Jet Propulsion Laboratory Chlorinolysis Process, in which cleaning was generally accomplished by bubbling chlorine through a mixture containing 100 grams of finely ground coal, 200 grams of solvent (either methylchloroform, carbon tetrachloride, or tetrachloroethylene), and 20-70 grams of water (13). The chlorination step was conducted at 50-100°C at atmospheric pressure for 10-20 minutes. The coal was then hydrolyzed by washing with water for 60-120 minutes at 60-100°C and subsequently dechlorinated at 350-550°C in a steam atmosphere. For some coals treated under these conditions, levels of As, Be, Pb, and V were reduced by 50-90% (13,14).

In another one, the Battelle Hydrothermal Process (15,16), an aqueous slurry of finely ground coal, NaOH, and $Ca(OH)_2$ was heated for 10-30 minutes at 250-350°C at pressures of 600-2500 psig. Based on averages from several Ohio coals, this process reduced levels of As, B, Be, Pb, and V by 70-90% (16).

In yet another chemical cleaning process, the Meyers Process, crushed coal was leached with an acidic solution of ferric sulfate at 100-130°C for several hours (17). If the leaching time was long enough, almost all of the pyritic sulfur was extracted. At the same time the content of many trace elements, such as As, Cd, Cr, Mn, Ni, Pb, V, and Zn was significantly reduced (18). Still, the data discussed above represent only a small fraction of the chemical processes that have been studied.

EXPERIMENTAL

Because caustic or alkaline treatments are relatively effective at removing ash-forming minerals from coal, particularly when followed by an acid wash, the extraction efficiency of trace elements was assessed for several of these treatments in this study. Two samples of an Illinois No. 6 run-of-mine coal were obtained which had been treated for one hour with 1.0 M Na_2CO_3 at 250°C in an inert atmosphere (19). One of the samples was then washed with 2.0 M HCl to obtain the final product. The other sample was first pretreated with 0.2 M Na_2CO_3 at 150°C for one hour under 13.6 atm. oxygen, then treated as the above sample in an inert atmosphere, and subsequently washed with 1.8 M H_2SO_4. All the Na_2CO_3 treatments were performed under pressure in an autoclave.

Two additional samples were obtained from a different Illinois No. 6 coal used for molten caustic treatments at Ames Laboratory under conditions simulating the TRW Gravimelt Process. In that process, coal was treated with a molten 4:1 NaOH/KOH mixture for one hour at 370°C. After separating and washing the coal with water, the coal was treated with 10% H_2SO_4 and then with a final water wash. Two runs were made, one being made in the normal manner and the other with powdered reagent-grade iron included in the coal/caustic mixture. The iron was added in hopes that it would act as a sulfur scavenger and improve coal desulfurization.

In addition to these samples, several coal samples were provided by TRW Systems, Inc. (Redondo Beach, CA). The samples represented Illinois No. 6 and Pittsburgh No. 8 coals before and after treatment by the Gravimelt Process.

ANALYTICAL METHODOLOGY

All coals were analyzed at Ames Laboratory using energy-dispersive x-ray fluorescence (ED-XRF), inductively coupled plasma-atomic emission spectroscopy (ICP-AES), and atomic absorption spectrophotometry (AA).

For the determinations of Cd and Pb by AA, the coal samples were ashed at 500°C and the ashes were subsequently dissolved in accordance with procedures described in ASTM Method D-3683 (20). Basically, the ash was dissolved in a mixture of HNO_3, HCl, and HF in a tightly capped plastic bottle in a steam bath. Saturated H_3BO_3 solution was then added to the mixture to complex the excess fluoride and to improve flame properties during AA measurements. For the AA determinations of As, Sb, and Se, sample solutions were prepared by first treating the coal with hot HNO_3 and then with fuming H_2SO_4. For these dissolutions, an Erlenmeyer flask-reflux cap apparatus was used (21). Conventional flame AA was used for the Cd and Pb determinations, while hydride generation AA was used for the As, Sb, and Se. For the Hg determination, a portion of the coal was placed in a Parr bomb containing 10% HNO_3. After ignition, the contents of the bomb were washed into an Erlenmeyer flask, and $SnCl_2$ solution was added to the mixture to reduce the Hg for conventional cold vapor AA measurements. Corrections were made for reagent blanks in all analyses by AA.

For the coals analyzed by XRF, samples that were +60 mesh were first ground to -60 mesh with a boron carbide mortar and pestle. The samples were then prepared by mixing two grams of sample with 0.2 grams of Somar Mix, a granulated plastic binding

agent. If less than two grams of sample were available, the amount of binding agent was scaled down proportionally. The powder was then pressed into disks at a pressure of about 5000 psi. The XRF analyses were performed using a Mo-target x-ray tube.

Analyses by ICP were performed on the same dissolutions used for the AA analyses for Cd and Pb. The solutions were diluted as necessary and were then nebulized and introduced into the plasma. Line spectra were collected with a multi-channel analyzer and corrections were made for reagent blanks and background shifts. For all analyses, NBS Standard Reference Material 1632, a bituminous coal, was used for instrument calibration.

RESULTS AND DISCUSSION

Results of the analyses on coals before and after treatment with aqueous Na_2CO_3 solutions and molten NaOH/KOH mixtures at Ames Laboratory are shown in Table 1. Levels of Cd, Pb and Zn were relatively high in the raw Illinois No. 6 run-of-mine coal used for the Na_2CO_3 treatments. The elevated Cd levels correlate well with the high Zn levels, since Cd in coal is commonly associated with sphalerite (ZnS). The Pb was probably present largely as galena (PbS). For the alkali-treated coal washed subsequently with HCl, levels of Mn, Pb, Rb, Sr, and Zn were reduced by 75% or more, while levels of Ba, Cd, Cr, Ni, and Se, were reduced by 30-60%. The coal that had been pretreated showed reductions of 75% or more for Mn, Pb, and Zn, while Cd and Ni were reduced by 60% or more. It is interesting to note that every alkali and alkaline earth metal determined was enriched in the pretreated coal relative to the coal that was leached with no pretreatment. Some of these, such as Ba and Ca, were more concentrated in the pretreated coal than in the raw coal. The reason for the elevated levels of Ba, Cu, Se, and Sr in the pretreated coal is uncertain at this time.

Analysis of the XRF data on coals treated with molten caustic at Ames Laboratory (Table 1) showed that levels of Fe, which is predominantly associated with pyrite in coal, was reduced by about 90% for each of the two runs. Reductions in concentrations of other elements which form abundant minerals in coal, including Al, K, and Si, were also substantial. Because roughly 90% of the ash was removed, substantial concentration reductions in the major mineral-forming elements are expected. Of the trace elements, levels of Ba, Rb, Sr, and Zn were reduced by 70% or more and Se was reduced by 30% or more in the coal treated in the normal fashion (Run 1). In the coal from the test containing the iron additive (Run 2), levels of Rb, Sr, and Zn were also reduced by 70% or more. Pb levels remained essentially constant for each of the treated coals. The elevated Cr and Ni levels are believed to be corrosion byproducts from the reactor.

In the coal treated by molten caustic in Run 2, the Cr and Ni levels are significantly higher than in Run 1, suggesting a more severe attack in the second test. If the attack were more severe, then levels of Fe, Al, Si, and ash would be anticipated to be somewhat lower than in Run 1. As can be seen from these data, this is indeed the case. However, despite the apparently more severe attack in Run 2, overall trace element reductions did not seem to be significantly improved.

In the coals treated by the Gravimelt Process at TRW (Table 2), the ash content was decreased to 1% or less, and levels of As, Be, Cd, Hg, Pb, Se, Sr, and Zn were reduced by 75-95%. It is interesting to note that most of these elements are commonly associated with pyrite. Thus, substantial reductions in levels of these elements can be anticipated when most of the pyrite is removed (as indicated for both coal samples). In addition, the levels of Ba, Ge, Mn, and Rb were also reduced; however, the reduction levels are not as prominent nor as clear-cut.

Table 1. XRF Data on Coals Before and After Treatment.[a]

	Molten NaOH/KOH Treatment			Aqueous Na_2CO_3 Treatment		
	Raw Ill. No. 6	Run 1	Run 2[b]	Raw Ill. No. 6	Run 1	Run 2[c]
Ash (%)	14.17	1.24	1.02	13.24	2.61	2.97
Ag	<2	<20	<2	<20	<20	<20
Al (%)	1.9	0.72	0.29	2.0	0.70	0.79
As	3.4	1.0	3.8	<5	2.1	<1.0
Ba	49	<10	36	27	17	59
Br	1.7	<1.0	<1	2.7	6.3	5.7
Ca	5650	<284	<247	4560	264	7180
Cd	<2	<20	<2	49	<20	20
Cl (%)	<1100	<0.1	<0.5	<0.1	0.86	<0.1
Cr	27	58	144	26	18	98
Cu	12	<61	<113	38	53	2100
Fe (%)	1.19	0.189	0.142	1.50	0.87	0.12
Ga	2.9	5.4	1.4	<12	4.5	<4.5
Ge	<2	<1.0	<2	<17	5.1	5.3
K	1960	810	804	1775	65	1260
Mn	51	<18	22	62	14	9.5
Ni	20	241	344	24	14	<10
Pb	14	17	10	210	10	24
Rb	10	<1.0	<1	9.6	<1.0	7.5
S[d] (%)	4.52	0.96	0.84	3.71	2.40	1.84
Sb	<2	<20	<5	<20	<20	<20
Se	1.8	<1.0	<2	3.0	1.2	9.1
Si (%)	3.1	0.64	0.18	2.6	0.68	1.5
Sr	24	1.0	<2	11	<1.0	42
Ti	640	240	165	700	610	450
V	<150	<25	<19	<78	<61	<58
Zn	49	11	8.2	1100	36	<240

[a] Values are in ppm unless otherwise noted and are corrected to a dry basis.
[b] Powdered iron included in coal/caustic mixture.
[c] Pretreated with 0.2 M Na_2CO_3 and oxygen.
[d] Determined by a high-temperature combustion instrumental method.

Table 2. XRF, AA, and ICP Data on Raw and Chemically Cleaned Coals Received from TRW Systems, Inc.[a]

	Illinois No. 6		Pittsburgh No. 8		
	Raw	Cleaned	Raw	Cleaned	
Ash (%)	9.23	0.53	9.88	1.00	
Pyr. S (%)	1.04	0.02	1.78	0.01	
Hg	0.28	0.04	0.15	0.10	
Pb	5.8	1.4	5.6	1.4	A A
Cd	0.70	0.16	0.44	0.024	
As	0.33	0.14	3.9	0.18	D A T A
Sb	0.09	0.08	0.06	0.06	
Se	1.5	0.6	1.6	0.19	
Ag	<20	<20	<20	<20	
Al (%)	1.6	<0.7	1.2	<0.7	
As	<5	<10	<10	<5	
Ba	40	<40	~30	<40	
Ba*	<25	<0.4	13	<3.1	
Be*	0.77	<0.10	0.6	<0.06	
Br	9.9	16	7.9	3.4	
Ca (%)	0.16	0.015	0.18	0.027	
Ca*	978	63	545	72	
Cd	<20	<20	<20	<20	
Cl (%)	0.10	0.041	<0.02	0.053	
Cr	23	62	23	152	
Cr*	10	54	<6	110	
Cu	16	I(Ni)	20	I(Ni)	
Cu*	16	28	12	16	I C P
Fe (%)	0.968	0.078	1.54	0.107	
Fe* (%)	1.1	0.051	~1.3	0.033	a n d
Ga	<1	<1	~2.3	<1	
Ge	5.0	3.6	4.5	3.1	X R F
K	1500	360	1100	620	
Mn	49	9.9	51	21	D A T A
Mn*	42	1.7	23	4.4	
Ni	17	100	15	132	
Ni*	4.8	47	4.3	58	
Pb	<10	<10	<10	<10	
Rb	10	<5	7.4	<5	
S (%)	2.6	0.47	2.4	0.78	
Sb	<20	<20	<20	<20	
Se	<3	<3	<3	<3	
Si (%)	2.2	<0.2	2.0	0.23	
Sn	<20	<20	<20	<20	
Sr	17	<5	41	<5	
Ti	630	370	770	350	
Ti*	489	290	480	190	
V*	<2.5	<0.9	<14	1.5	
Zn	31	~3.9	23	~4	
Zn*	39	2.1	20	<0.6	

[a] Values are in ppm unless % is noted and are corrected to a dry basis. An "I" indicates an unsatisfactory determination due to an interference from another element (shown in parentheses).

* ICP data.

CONCLUSIONS AND RECOMMENDATIONS

The aqueous Na_2CO_3 and molten NaOH/KOH treatments, followed by acid washes, effectively remove many trace elements from the coals studied. However, due to corrosion of reactor components in the molten caustic system, levels of some elements, predominantly Ni and Cr, are substantially elevated in the treated coals. Similar tests should be conducted on a greater variety of coals in order to ascertain the general efficiency of trace element removal by these processes. In addition, reproducibility should be examined by making a number of runs using the same reaction conditions on different portions of the same raw coal.

ACKNOWLEDGEMENTS

This work was supported by the Assistant Secretary for Fossil Energy, Division of Coal Utilization, through the Pittsburgh Energy Technology Center, Coal Preparation Branch.

The authors gratefully acknowledge Dr. T.D. Wheelock and Dr. C-W. Fan at Iowa State University and Dr. Robert Meyers and Dr. Walter Hart at TRW Systems, Inc., for supplying samples of raw and chemically desulfurized coal on which our analyses were performed. Coals chemically cleaned at Ames Laboratory were provided by Mr. David Mroch.

LITERATURE CITED

1. R.D. Harvey, R.A. Cahill, C.-L. Chou, and J.D. Steele, "Mineral Matter and Trace Elements in the Herrin and Springfield Coals, Illinois Basin Coal Field," Illinois State Geological Survey, April, 1983.

2. R.W. Linton, A. Loh, and D.F.S. Natusch, "Surface Predominance of Trace Elements in Airborne Particles," Science 191, 852 (1976).

3. D.F.S. Natusch, J.R. Wallace, and C.A. Evans, Jr., "Toxic Trace Elements: Preferential Concentration in Respirable Particles," Science 183, 202 (1973).

4. M. Ihnatowicz and A. Worsztynowicz, "Poisoning and Regeneration of Catalysts for Hydrogenation of Coal Extracts," Proceedings: 1983 International Conference on Coal Science, pp. 790-793.

5. V. Valkovic, Trace Elements in Coal, Vol. 1, CRC Press Inc., Boca Ranton, Florida, 1983, p. 68.

6. R.R. Ruch, H.J. Gluskoter, and N.F. Shimp, "Occurrence and Distribution of Potentially Volatile Trace Elements in Coal," Illinois State Geological Survey, Environmental Geology Notes, Number 72, August 1974.

7. J.A. Cavallaro, A.W. Deurbrouck, G.A. Gibbon, E.A. Hattman, and H. Schultz, "A Washability and Analytical Evaluation of Potential Pollution from Trace Elements in Coal," in Analytical Methods for Coal and Coal Products, Vol. I, C. Karr, ed., Academic Press, New York, 1978, pp. 435-464.

8. R.B. Finkelman, "Modes of Occurrence of Trace Elements in Coal," Ph.D. Thesis, University of Maryland, Chemistry Dept., 1980.

9. D.J. Swaine, "Trace Elements in Coal," Trace Subst. Environ. Health 11, 107 (1977).

10. H.J. Gluskoter and P.C. Lindahl, "Cadmium: Mode of Occurrence in Illinois Coals," Science 181, 264 (1973).

11. C.B. Cecil, R.W. Stanton, S.D. Allshouse, and R.B. Finkelman, "Geological Controls On Mineral Matter in the Upper Freeport Coal Bed," Proceedings: Symposium on Coal Cleaning to Achieve Energy and Environmental Goals, (Sept. 1978, Hollywood, FL), EPA-600/7-79-098a, Vol. 1, 1979, pp. 110-125.

12. J.K. Kuhn, F.L. Fiene, R.A. Cahill, H.J. Gluskoter, and N.F. Shimp, "Abundance of Trace and Minor Elements in Organic and Mineral Fractions of Coal," Illinois State Geological Survey, Environmental Geology Notes #88, August 1980.

13. J.J. Kalvinskas and G.C. Hsu, "JPL Coal Desulfurization Process by Low Temperature Chlorinolysis," Proceedings: Symposium on Coal Cleaning to Achieve Energy and Environmental Goals, (Sept. 1978, Hollywood, FL), EPA-600/7-79-098b, Vol. 2, 1979, pp. 1096-1140.

14. G.C. Hsu, J.J. Kalvinskas, P.S. Ganguli, and G.R. Gavalas, "Coal Desulfurization by Low Temperature Chlorinolysis," in Coal Desulfurization: Chemical and Physical Methods, T.D. Wheelock, editor, ACS Symposium Series 64, 1977, pp. 206-217.

15. E.P. Stambaugh, H.N. Conkle, J.F. Miller, E.J. Mezey, and B.C. Kim, "Status of Hydrothermal Processing for Chemical Desulfurization of Coal," Proceedings: Symposium on Coal Cleaning to Achieve Energy and Environmental Goals (Sept. 1978, Hollywood, FL), EPA-600/7-79-098b, Vol. 2, 1979, pp. 991-1015.

16. E.P. Stambaugh, "Hydrothermal Coal Process," in Coal Desulfurization: Chemical and Physical Methods, T.D. Wheelock, editor, ACS Symposium Series 64, 1977, pp. 198-205.

17. R.A Meyers, Coal Desulfurization, Marcel Oekker,Inc. New York, 1977.

18. J.W. Hamersma, M.L. Kraft, and R.A. Meyers, "Applicability of the Meyers Process for Chemical Desulfurization of Coal," in Coal Desulfurization: Chemical and Physical Methods, T.D. Wheelock, editor, ACS Symposium Series 64, 1977, pp. 143-152.

19. C.-W. Fan, "Coal Desulfurization and Demineralization by Chemical/Physical Treatment," Ph.D. Dissertation, Iowa State University, Ames, Iowa 50011, 1984.

20. 1982 Annual Book of ASTM Standards, Part 26, American Society for Testing and Materials, Philadelphia, PA, 19103.

21. D.D. Slemer and H.G. Brinkley, "Erlenmeyer Flask-Reflux Cap for Acid Sample Decomposition," Anal. Chem. 53, 750 (1981).

MODELING FUTURE EMISSIONS OF ATMOSPHERIC POLLUTANTS

Kristin Graves
Edward H. Pechan

E.H. Pechan & Associates, Inc.
5537 Hempstead Way
Springfield, VA 22151

INTRODUCTION

In recent years, Federal, state, and local governments have shown increasing interest in studying air pollution, with particular emphasis on acid rain, visibility, and other pollution issues. To evaluate potential solutions to the problems at hand, considerable data and information must be gathered and examined: current levels and patterns of the dependent variables to be studied, potential future regulations and technologies, and expected levels of emissions and control costs based upon future regulations and technologies.

For air pollution, the five dependent variables of interest are typically emissions, atmospheric transport, deposition, effects or damage, and costs of control. Computer models have been developed that can predict the levels or patterns of these dependent variables for several years or decades into the future based on historical or current input data and information about other factors that may affect the level of the five variables of interest. These models vary in their purpose, their level of detail, their costs of development and use, and their capability to analyze the effect of alternative levels of various factors on the dependent variables. The usefulness of computer models, regardless of their composition, lies in their ability to examine the effects of alternative assumptions about independent variables on the dependent variables without requiring the model user to do all necessary recalculations by hand.

Several factors distinguish one model from another; such factors include the general structure of the model, the level of model detail (usually inversely related to the time frame over which the model makes its predictions), and the user-friendliness with which the model operates. In general, policy analysts use two structural types of models to make forecasts of future activity levels: econometric and engineering or process models. Econometric models use historic data and relationships to estimate future trends in variables of interest. Engineering or process models use the physical relationships of production processes (i.e., the relationship between inputs to a production process and its outputs) to predict levels of the dependent variables.

This paper selects one engineering/process model, the Environmental Trends Analysis Model II (ETAM II), and describes the methodology used to forecast emissions of a number of air pollutants from the electric utility sector. ETAM II uses exogenous activity level information (i.e., supplied from outside the model rather than produced within it), to which production relationships are applied as a means of generating estimates of pollutant emissions. ETAM was originally developed to provide environmental trend analyses in support of the U.S. Department of Energy's (DOE) 1983 National Energy Policy Plan (NEPP). Since then, it has been updated with modified algorithms and additional capabilities and new data have been added; the resultant model is known as ETAM II. ETAM II has been used for policy and sensitivity analysis in support of such programs as the Interagency Visiblility Task Force and the Interagency Prevention of Significant Deterioration Task Force.

ETAM II and the methodology it uses to forecast electric utility emissions of sulfur dioxide (SO_2) and nitrogen oxides (NO_x) are described in this paper. In addition, a brief comparison of the emission forecasting technique used

in ETAM II and those used in other models is given. Also included are sample results from ETAM II.

ETAM II METHODOLOGY

Introduction

ETAM II is a generalized forecasting system that can be used to project a variety of environmental indicators: 21 air pollutant species, 2 water pollutants, water withdrawal and consumption, 4 types of solid waste, and 5 measures of radiation. ETAM II is unique in that it both covers numerous residuals (i.e., emitted or discharged air, water, or solid waste pollutants) and all economic sectors discharging those residuals and is easy to use for policy analysis purposes. ETAM II is capable of measuring the indicators identified above from eight source sectors: electric utilities, industry, residential and commercial sources, transportation, agriculture, mining and minerals, synthetic fuels, and other sources. The "other" category includes sources such as forest fires and dust rising from gravel roads. Projections for the air, water, and solids pollution indicators can also be disaggregated by Federal region and energy use category (i.e., related or unrelated to energy production activities).

ETAM II is designed to be a scoping model, that is, a model that will provide quick results based on a number of different input assumptions. The model does not provide a great level of detail; for example, forecasts are made at the Federal region level of detail (the 50 states being aggregated into ten Federal regions) at 5-year intervals to the year 2030. Emission estimates are also available by end use sector and by industry type. Other models are available which, although providing more detail, such as electric utility plant or electric generating unit-specific emissions on a monthly or yearly basis, may not make forecasts so many years into the future or may be more difficult to run in terms of evaluating the effects of alternative input assumptions.

ETAM II also has been designed to allow users, even those with little or no computer experience, to make runs. For those interested users with a minimal amount of programming experience, the computer source code (i.e., the commands that constitute the model) can be altered to allow more complicated changes in input assumptions.

Data Sources and Methods

A number of external data bases and models have been incorporated into ETAM II, either in full or in part. These include the National Acid Precipitation Assessment Program (NAPAP) inventory of non-utility emissions (1), the electric utility Unit Inventory (2), the FORECAST electric utility emissions model (3, 4), data from the Residuals Accounting Model (5), DOE's NEPP (6), and DOE Secretary Hodel's testimony before the U.S. House of Representatives (7). In addition to the exogenous driving inputs listed above, ETAM II accepts a number of user-specified assumptions which affect its results. These are discussed in greater detail in the two volumes of ETAM II documentation (8, 9).

Utility Methodology

In general, ETAM II uses input data to estimate electricity generation in future years. Emission factors and the effects of alternative regulatory scenarios are then used to estimate the discharge of various environmental residuals. Alternative levels of economic or energy price growth affect emissions because economic factors and energy prices affect the demand and supply, and therefore the generation, of electricity.

The electric generating Unit Inventory (2) is a key component of the

projection process. It contains generating unit-specific data on unit type, size, age, capacity factor, emission rate, and fuel use. The model compiles these data by state and then derives certain summary statistics -- for example, the ratio of baseload to peaking capacity and the mix of fuels used in peaking generating units. The user of ETAM II, when running the utility component, provides input information on the forecast horizon, coal plant lifetimes, coal plant capacity factor, and environmental regulations (9).

ETAM II updates the 1980 generating Unit Inventory in 5-year increments. For each increment, SO_2 emissions from existing generating units are reduced to meet air regulations (i.e., State Implementation Plan targets). Generating units are retired according to announced retirement dates (10) occurring within each 5-year increment. If no retirement date has been announced, generating units are retired (after 1991) according to default retirement dates linked to plant lifetimes. Emission levels are further reduced to reflect these retirements.

Announced plans (10) to convert oil-fired capacity to coal are assumed to occur as scheduled. Additional conversions are assumed to occur in 19 states. Emission levels are increased to reflect these conversions.

If the user has so specified, ETAM II then adjusts the capacity factors of existing generating units. The capacity factors of oil and gas-fired generating units can be reduced to implicitly reflect their high fuel costs. The capacity factor of coal-fired generating units can either be increased to reflect utilities' success in efforts to reduce unusually high reserve margins or be decreased to reflect lowered availability as equipment ages. All generating units of a given fuel type are affected when an adjustment is made (i.e., the capacity factor of all existing coal-fired generating units, regardless of age or location, would be raised or lowered to the specified rate). Emission levels are adjusted accordingly.

National average growth rates for electricity demand, specified in the NEPP projections, are allocated to each state according to the ratios implied in 1980 North American Electric Reliability Council (NERC) forecasts. Within each state, demand is partitioned into baseload and peaking segments, using the state's 1980 ratio of baseload capacity to peaking capacity. This ratio is assumed to remain constant throughout the projection period. The fraction of total demand that can be accommodated by existing generating units is subtracted, and any remaining demand is assumed to be satisfied by new baseload or peaking generating units, depending on which segment is unable to meet demand.

New generating units are added according to the on-line dates specified in NERC's announced generating unit list and are assumed to operate at the default new unit capacity factors. The model will defer announced generating units in a particular state if they are not needed to meet the demand derived from NEPP. The new coal-fired generating units are assumed to comply with current revised New Source Performance Standards (NSPS) or Prevention of Significant Deterioration regulations, depending upon which are more stringent, or alternative regulations if specified in the input assumptions.

If a state's electricity demand is not met after all announced generating units have been put on-line, the model sites additional new generating units in the state to meet projected needs. The following assumptions are relevant to this decision:

- each state's 1980 ratio of baseload to peaking capacity remains constant;

- all additional baseload generating units built after the NERC announced generating unit list is satisfied but before the year

2000 are assumed to be coal-fired (except in California, where all new capacity is assumed to be from renewables);

- 80 percent of new baseload generating units built after the year 2000 are assumed to be coal-fired and 20 percent nuclear (except in California, where all new capacity is assumed to be from renewables);

- each state's 1980 mix of fuels used in peaking generating units remains constant; and

- new generating unit emission standards apply.

NEPP projections of utility sector fuel use are applied as "control totals" on ETAM II's initial calculations for each projection year. ETAM II determines each state's share of oil, coal, gas, nuclear, and alternative fuel use for 1980. ETAM II then uses these shares to proportionally disaggregate the NEPP national totals for each projection year to yield fuel-specific subtotals for each state. The NEPP subtotals available by fuel are then used to calibrate ETAM II's calculated subtotals by fuel and state. In effect, ETAM II makes marginal adjustments to the capacity factors of each generating unit (new and existing facilities) of a given fuel type in a particular state so that the model's fuel use totals equal the NEPP control totals. Emission levels are then adjusted in proportion to the fuel use adjustments.

The above methodology applies to forecasts made to the year 2010. For projections to 2030, each computational step is conducted in the same manner. Two differences should be noted: 1) the projection proceeds in 10-year increments so that each set of calculations combines the calculations for two increments in the 1980 to 2010 projection; and 2) the trends for the last 5-year increment (2005 to 2010) are extrapolated for the period 2010 to 2030. For example, capacity factors are assumed to remain at their 2000 level. ETAM II derives national-level electricity demand from NEPP and assumes state-level trends will continue linearly at the 2005 to 2010 rate. Note that for these longer-term projections, assumptions regarding plant lifetimes and emission standards become increasingly important.

ETAM II is unique because, due to its simplicity and structural design, it can be used to examine a number of alternative scenarios in a relatively short period of time. Scenarios examined can include the effects of different coal plant lifetimes, future environmental regulations, and energy and economic futures. By combining scenarios that result in high or low levels of residual discharge, ETAM II can provide its user with a range of emission levels, thus providing information about uncertainty in future residual discharge levels.

COMPARISON WITH OTHER MODELS

A number of other computer models are available for making predictions of pollutant emissions from electric utilities. These models include the Advanced Utility Simulation Model (AUSM), the National Coal Model (NCM), and the Optimization Model for Emission Generating Alternatives (OMEGA). Table 1 summarizes the relevant features of each of these models.

Advanced Utility Simulation Model

AUSM, sponsored by the U.S. Environmental Protection Agency in support of the National Acid Precipitation Assessment Program, is designed to project electricity demand, generation, and associated emissions. Considerable detail is included in the model in several areas, enabling in-depth analysis of the effects of various legislative scenarios. AUSM combines econometric modeling techniques

Table 1

Electric Utility Residual Discharge Models

Model	Program Type[a]	Regional Detail	Forecast Period	Residuals[d]	Developer[e]
AUSM	P, E	state	to 2009	TSP, SO_2, sulfate	EPA, URGE
ETAM II	P	10 Federal Regions	to 2030	TSP, SO_2, sulfate, NO_x, VOC, others	DOE, EHPA
NCM	P	state[b]	to 2010	TSP, SO_2, NO_x	DOE
OMEGA	P	state[c]	to 1995	SO_2	CMU

[a]P = process/engineering; E = econometric.

[b]NCM has 31 coal supply regions and 40 demand regions which approximate states in most cases.

[c]OMEGA uses 19 supply regions and 47 demand regions in a 31 state area.

[d]TSP = total suspended particulates; VOC = volatile organic compounds.

[e]EPA = U.S. Environmental Protection Agency; URGE = Universities Research Group on Energy (Public Policy Program, University of Illinois); CMU = Carnegie-Mellon University; EHPA = E.H. Pechan & Associates, Inc.

with process modeling techniques, resulting in a more complicated internal structure than that of ETAM II. AUSM's coal supply module contains distinct representations of coal costs and availability. The primary utility information data base used by AUSM has detail at the electric generating unit level. An annual recursiveness feature, which allows the projected price of electricity in one year to be reflected in the demand for electricity in the following year, is used in an econometric portion of the model to forecast electricity demand. A separate module within AUSM calculates control costs associated with any particular legislative alternative examined.

AUSM uses an extensive amount of input data. In addition to an inventory of generating units (the Unit Inventory) and an extensive file containing information on coal reserves and resources, a large quantity of input data must be specified by the user. Default values are available for these parameters, but a user needs to have some notion of appropriate values.

AUSM requires two user-specified scenario input files. One of these provides global parameters (e.g., inflation rate, flue gas desulfurization minimum size, etc.) and the other provides state-specific parameters (e.g., state emission limits, land use costs, etc.). In addition to these global and scenario parameters, each of the analysis modules within AUSM has a series of inputs which must be user-specified. The electricity demand module, for example, requires state-level forecasts of fuel prices, population, and economic activity indicators (i.e., personal income, earnings, and employment). The AUSM coal supply module requires the user to specify escalation rates for coal production costs at the mine-mouth and the costs of mining and cleaning coal (broken down by wages, capital costs, etc.). A separate module forecasts coal transportation costs, which can be up to 70 to 80 percent of the delivered price of coal.

Outputs from AUSM are more detailed than those from ETAM II and include state-level information on generation, peak load, prices, capacity additions, emissions and generation of residuals, coal use, and utility financial statements. Projections are made for 20 years into the future.

National Coal Model

NCM, sponsored by the U.S. Department of Energy for use in short and mid-term forecasting, is used to ascertain the impact of legislation on the coal and electric utility industries and to project coal production, consumption, and prices. The NCM is a process model that requires an extensive amount of data including information on utility operations costs, emission limits, capacity factors, coal demand and production, price and use of alternative fuels, and emission control costs. Outputs include coal production, transportation, blending, and consumption; generating capacity utilization; pollutant emissions; capital expenditures; and transmission of electricity. Each of these outputs is available by NCM region (approximately equal to state-level) and by Federal region to the year 2010. Proprietary variants of NCM are offered by some firms.

Optimization Model For Emission Generating Alternatives

OMEGA, a process model, was developed at Carnegie-Mellon University and examines emission control strategies of domestic coal-based electric utility plants. The current version examines only coal plants in a 31-state Eastern region. Due to its structure and computational algorithms, OMEGA is limited in the number of plant types, modes of transportation, coal types, and so forth that it can handle. The model is driven by an explicit listing of expected coal-fired startups from DOE's Generating Unit Reference File.

Required inputs to OMEGA are extensive and include coal-fired generation, use of coal by utilities, escalation rates for transportation costs, coal prices,

coal production, capacity factors, plant lifetime, discount rate, emission reduction target, and method of emission allocation among states. Model outputs include emissions and control costs at the state level to 1995.

SAMPLE RESULTS FROM ETAM II

To provide an illustration of the type of ouputs provided by these models, the results in Figure 1 are based on the examination of alternative coal plant lifetimes by ETAM II. Figure 1 shows a comparison of assumed 40 and 60 year utility plant lifetimes on emissions to 2030. As can be seen, these assumptions have no effect on emissions from non-utility sectors, but have a tremendous effect on both the pattern and the level of total emissions.

The significant impact of a plant lifetime assumption is due to the stringent controls placed on new plants through NSPS requirements; with earlier retirement of plants, the newer and more stringently-regulated plants come on-line much sooner. For SO_2 emissions, the assumption regarding coal plant lifetime affects the year in which industrial emissions become the primary contributor to total emissions. Under the 40-year lifetime assumption, utility SO_2 emissions fall below industrial emissions by 2010. If a 60-year lifetime is assumed, this switch will not occur until about 2030.

REFERENCES

1. Engineering-Science. "Development of the NAPAP Emission Inventory for the 1980 Base Year," prepared for the U.S. Environmental Protection Agency, 1984.

2. E.H. Pechan & Associates, Inc. "Electric Utility Unit Inventory: Database Technical Documentation," prepared for University of Illinois at Urbana-Champaign, Public Policy Program, May 1983.

3. E.H. Pechan & Associates, Inc. "FORECAST Model: Technical Documentation," June 1983.

4. E.H. Pechan & Associates, Inc. "FORECAST Model: User Documentation," July 1983.

5. The MITRE Corporation. "Scenario Reference Manual for the Residuals Accounting Model," MTR-81W180, September 1981.

6. U.S. Department of Energy, Office of Policy, Planning and Analysis, "Energy Projections to the Year 2010," DOE/PE-0029/2, October 1983.

7. Hodel, Donald Paul. U.S. Department of Energy, "Statement of Donald Paul Hodel, Secretary, U.S. Department of Energy, before the Subcommittee on Health and the Environment, Committee on Energy and Commerce, U.S. House of Representatives," March 29, 1984.

8. E.H. Pechan & Associates, Inc. "The Environmental Trends Analysis Model: Technical Documentation," March 1984.

9. E.H. Pechan & Associates, Inc. "The Environmental Trends Analysis Model: User Documentation," March 1984.

10. National Electric Reliability Council. "Electric Power Supply and Demand 1980-1989," July 1980.

Figure 1. Coal Plant Lifetime Scenario Results

(40 versus 60 year plant lifetimes)

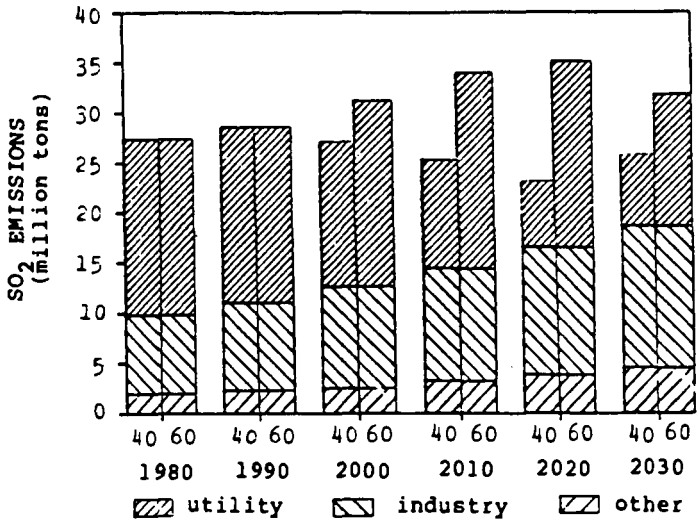

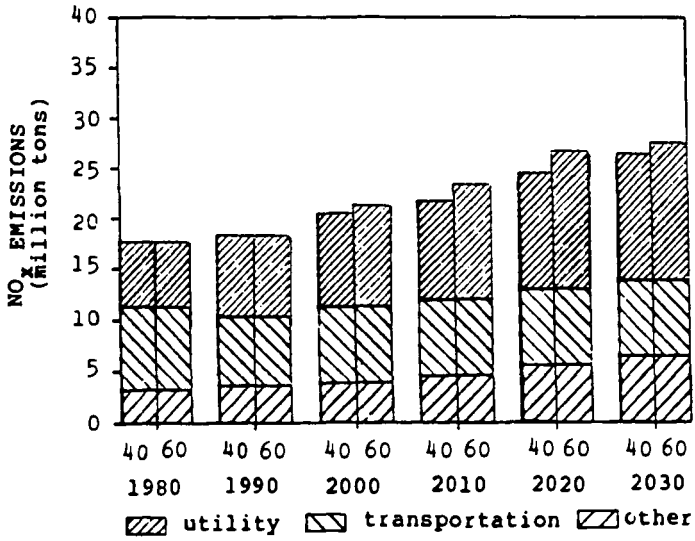

ISOTHERMAL FLAME STUDIES OF LIMESTONE PROPERTIES RELEVANT TO SO_2 REMOVAL FROM P.C. UTILITY BOILERS

J. A. Cole, J. C. Kramlich, W. R. Seeker

Energy and Environmental Research
18 Mason
Irvine, CA 92718

G. S. Samuelsen

Department of Mechanical Engineering
University of California
Irvine, CA 92717

Introduction

Dry-limestone injection provides an economically attractive means for SO_2 emissions control in pulverized-coal-fired (p.c.) utility boilers. The process is especially attractive as a retrofit for older boilers because of the potentially low capital costs relative to other SO_2 control technologies (1). In addition, the raw material is readily available and relatively inexpensive (2). Early demonstration tests, however, met with little success. For example, acceptable levels of SO_2 removal could not be achieved, even with a large stoichiometric excess of limestone (3).

In an attempt to enhance the capture of SO_2, research has been conducted under conditions representative of full-scale systems (4,5). Fundamental experimental and theoretical research has also been undertaken to examine the kinetics of calcination and sulfation (6-11).

The present effort was undertaken to investigate the conditions which will optimize SO_2 removal from flue gases by calcium-based dry sorbent injection. The conditions explored included time, temperature, and sorbent type and preparation. Sorbents were injected under experimental conditions which simulated, but did not duplicate, the environment of a p.c. utility boiler. The goal was to provide an environment representative of large-scale systems, but simultaneously well characterized, uniform and reproducible.

The approach to the present study was to utilize a laboratory-scale apparatus to study the sulfur capture reaction $CaO + SO_2 + 0.5\ O_2 \rightarrow CaSO_4$ under isothermal conditions in a flame-gas environment designed to simulate the radiant zone of a p.c. boiler. Powdered sorbents were injected and dispersed into a flow reactor doped with 3600 ppm SO_2 and down-fired by a flat-flame burner which provided residence times near 1.5 s for temperatures from 900-1200°C. SO_2 sorption was measured as a function of time, temperature, and sorbent characteristics.

Experimental

Reactor. The reactor is a dispersed-phase Isothermal Flow Reactor (ITR). The ITR provides a relatively long (up to 3.0 s) isothermal zone in which sorbent chemistry

can be studied as a function of time, temperature, and environment. This reactor is unique because it provides a large volume for dispersal of sorbents at reasonable feed rates. This is necessary to permit solids sampling for chemical analysis within practical time frames.

The ITR (Figure 1) is an electrically heated, gas-downfired drop-tube furnace. It has a heated length of 90 cm and accommodates a 10-cm diameter alumina reaction tube. Heating is provided by silicon carbide globars located in three independently regulated heating zones 22.5- 45- and 22.5-cm long. The ITR has a maximum wall temperature of 1500°C.

The ITR is downfired by a porous bronze plug water-cooled flat-flame burner. Limestone was injected into the ITR along the axis of the reactor through the burner. The limestones were injected from a 1.1-mm i.d. tube, which produced a turbulent jet, effectively dispersing the materials over a wide cross section of the reactor. Residence times and heating rates of the particle streams were calculated based on confined jet mixing theory (12) and convective and radiative heat transfer calculations. Heating rates were on the order of 10^4 K/s and total (end of reactor) residence times of 1.2 - 1.6 s were employed in the experiments described here. Solids sampling from the ITR was accomplished with an isokinetic water-cooled stainless steel probe. Sorbents were quenched rapidly and collected on a glass fiber filter located at the base of the probe. The probe is 1.2 m long and enables sample collection within 40 cm of the sorbent injection location.

Temperature profiles in the ITR are shown in Figure 2. Temperatures were measured using a 0.025-mm diameter butt-welded supported type S thermocouple. Radiation corrections to the thermocouple readings were applied only for non-isothermal reactor conditions, otherwise the corrections were smaller than +5°K. The profiles in Figure 2 are all for hydrogen-air flames. Methane was the fuel used for flame temperatures above 1350°C.

Sorbents. Limestone samples evaluated in this study are listed in Table 1. Each was characterized both before and after injection using several analytical techniques which are listed in Table 2. Most of the raw materials were analyzed for chemical composition, particle size distribution, and specific surface area. Samples collected from the reactors were analyzed for carbon (carbonate), hydrogen (hydroxide), total sulfur (sulfate) and total calcium. From these measurements the extent of calcination and calcium utilization (percent calcium as sulfate) were determined for most samples. In addition, the precalcined dolomite (D60) and precalcined Vicron 45-3 (V40) were characterized by specific surface area and pore size distribution before and after injection into the reactor.

Vicron 45-3 and D3002 served, respectively, as the baseline calcite and dolomite in this study. They both are comparable in mean size, specific surface area and both are high-purity minerals. It was from these limestones that the V40 and D60 precalcines were produced. Surface areas indicated for the precalcines are typical. However, the materials were produced in small batches and surface areas varied between batches. The type S material is a pressure-slaked dolomitic lime.

Table 1. PHYSICAL AND CHEMICAL PROPERTIES OF LIMESTONE SORBENTS

Material	Composition	Mean Size, m	Surface Area m^2/g	Chemical Analysis, wt% Ca	Mg
Vicron 45-3	$CaCO_3$	11	0.6	39.0	0.49
D3002 Dolomite	$CaCO_3 \cdot MgCO_3$	10	0.54	24.8	11.3
D60 Precalcine	$CaO \cdot MgO$	--	60.67	---	---
V40 Precalcine	CaO	--	41.45	---	---
Type S (Warner)	$Ca(OH)_2 \cdot Mg(OH)_2$	1.0	18.20	28.0	15.9

Table 2. ANALYTICAL PROCEDURES

PROCEDURES	DETERMINATION
Brunauer, Emmett, Teller N_2 absorption isotherm	Specific Surface Area
Pekin-Elmer 240B	Carbon, hydrogen det. extent of calcination, hydration
Leco SC32	Total Sulfur
ASTM D2795 Chelometric Tritration	Total Calcium
Sedigraph (X-ray sedimentation)	Particle size distribution, mean size
Mercury instrusion porisimetry	Pore size distribution, true porosity, porosity distribution

Results

Calcium utilization was measured as a function of residence time in the isothermal reactor (ITR) for the five sorbents at temperatures of 900, 1000, 1100 and 1200°C. In each case the initial SO_2 concentration in the burned gases was 3600 ppm and the sorbent feed rate was adjusted to ensure a calcium-to-sulfur ratio (Ca/S) less than 1.0 so that the measured calcium utilization would not be affected by SO_2 depletion in the reactor.

Sorbent Reactivity Ranking. At 900°C (Figure 3) the capture levels of the precalcines and type S are all greater than those of the raw sorbents, D3002 and Vicron 45-3. In part, this is due to the time required for the raw sorbents to calcine. At 1.6 s, the D3002 is still taking up SO_2 while the V40 capture profile has leveled off. The type S sorbent has a lower calcination temperature as well as a less endothermic calcination reaction than the raw sorbents. It may in fact calcine so quickly at 900°C that the calcination reaction presents no impediment to sulfation. Similarity in the reactivities of D60 and type S might be an indication of the surface area

attained by the type S material. The D60 and V40 are not expected to sinter (lose surface area) rapidly at this temperature.

At 1000°C (Figure 4) the relative order of reactivity has changed to Vicron 45-3 < V40 < D3002 < D60 < type S. This reflects a large increase in the relative reactivity of D3002. At 1.5 s, the calcium utilization of D3002 is approaching that of the D60 precalcine and from 0.75 s on the V40 remains just about 10 percent more reactive than Vicron 45-3. Both of the raw sorbents exhibit some delay in SO_2 uptake due to calcination, but it is not as severe as that experienced at 900°C. All five sorbents display a dramatic increase in reactivity between 900 and 1000°C.

At both 900 and 1000°C the data suggest that SO_2 capture occurs rapidly at first. The rate of sulfation then slows abruptly or, in some cases, approaches zero. Pore structure analyses of the D60 and V40 precalcines suggests an explanation for this behavior. The active surface area of the precalcines was found to occur in pores about 80 and 130 A° in diameter for the D60 and V40 precalcines, respectively. These pores represented porosities of 0.18 and 0.13 for the two sorbents. After low temperature sulfation (to avoid sintering) to about 25% utilization the porosities were reduced to 0.15 and 0.08 and the active pore diameter of the sulfated V40 was reduced to about 100 A°. Thus, pore plugging reduces the accessibility of the active sorbent surface to SO_2 thereby reducing the global sulfation reaction rate.

Temperature Effects. Figure 5 summarizes the ranking of reactivity of the five sorbents as a function of temperature. The data shown in Figure 5 were taken from smoothed-by-eye reactivity profiles at the residence time of 1.0 s. There is very little uncertainty associated with the ranking in Figure 5 because the slopes of calcium utilization profiles all were shallow at 1.0 s. What has not been taken into account is the delay of the onset of sulfation for Vicron 45-3 and D3002 due to slow calcination at 900 and 1000°C. Accounting for the delay would alter the shapes of the temperature/utilization profiles somewhat; however, it would not be reflective of the ultimate result of low-temperature injection into a p.c. utility boiler where calcination times may be a factor.

The most significant aspect of Figure 5 is the appearance of a maximum in the utilization achieved as a function of temperature. The location of the true maximum appears to be very near 1000°C but may be different for each sorbent. Although such a maximum might have been predicted as a result of the tradeoff between sintering and reaction kinetics, there was no suggestion that it would occur at the same temperature for five different sorbents.

Conclusions

For simultaneous calcination and sulfation under isothermal conditions, hydroxides and precalcines had the greatest initial reactivity. At longer times and higher temperatures, however, the advantages of precalcines diminished. In general, dolomitic materials were more reactive than calcitic stones. The advantage of the hydrated dolomitic lime may, in part, have been due to a small mean particle size. For all materials the optimal calcination and sulfation temperature was 1000°C, reflecting a balance of slow reaction kinetics at lower temperatures and sintering (surface area loss) at higher temperatures. Conversion profiles exhibited a knee, shifting from rapid to slow or zero rate of conversion, consistent with measured internal pore plugging due to sulfation.

Acknowledgments

This work was supported by the U.S. EPA under Contract 68-02-3633. D. B. Henschel was the EPA Project Officer. The efforts and contributions of EER Staff R. K. LaFond, T. C. Grogan and R. D. Blethen to this study are gratefully acknowledged.

References

1. M. E. Kelly and S. A. Shareef. Second Survey of Dry SO_2 Control Systems. Durham, NC: Radian Corporation, EPA-600/7-81-018 (NTIS PB81-157919), February 1981.

2. R. S. Boynton. Chemistry and Technology of Limestone. 2nd ed., New York: J. Wiley and Sons, 1980.

3. R. C. Attig and P. Sedor. Additive Injection for Sulfur Dioxide Control, A Pilot Plant Study: Babcock and Wilcox, APTD-1176 (NTIS PB226761), March 1970.

4. R. W. Coutant, et al. Investigation of the Reactivity of Limestone and Dolomite for Capturing SO_2 from Flue Gas, Columbus, OH: Battelle Columbus Laboratories, APTD-0802 (NTIS PB204385), October 1971.

5. Case, et al. Testing and Evaluation of Experimental Wall-Fired Furnaces to Determine Optimum Means to Reduce Emissions of Nitrogen and Sulfur Oxides, Irvine, CA: EER Corporation, Final Report, EPA Contract 68-02-3921, January 1984.

6. R. H. Borgwardt. AIChE Journal, In Press.

7. R. H. Borgwardt. "Kinetics of the Reaction of SO_2 with Calcined Limestone" Environmental Science and Technology Vol. 4, No. 1, January 1970, pp. 59-63.

8. R. H. Borgwardt and R. D. Harvey. "Properties of Carbonate Rocks Related to SO_2 Reactivity" Environmental Science and Technology, Vol. 6, No. 4, April 1972, pp. 350-60.

9. S. K. Bhatia and D. D. Perlmutter. "A Random Pore Model for Fluid-Solid Reactions: I. Isothermal, Kinetic Control," AIChE Journal, Vol. 26, No. 3., May 1980, pp. 379-86.

10. S. K. Bhatia and D. D. Perlmutter. "The Effect of Pore Structure on Fluid-Solid Reactions: Application to the SO_2-Lime Reaction," AIChE Journal, Vol. 27, No. 2, March 1981, pp. 226-34.

11. S. K. Bhatia and D. D. Perlmutter, "A Random Pore Model for Fluid-Solid Reactions: II. Diffusion and Transport Effects," AIChE Journal, Vol. 27, No. 2, March 1981, pp. 247-54.

12. M. A. Field, et al. Combustion of Pulverized Coal Leatherhead, England: British Coal Utilization Research Association, 1967.

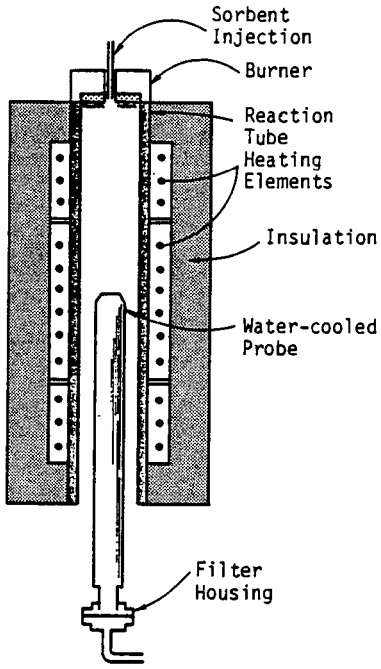

Figure 1. Schematic of the isothermal reactor with the burner and water-cooled probe installed.

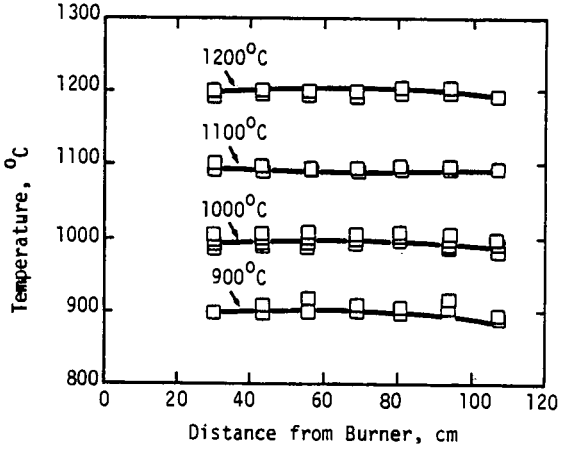

Figure 2. Temperature profiles in the isothermal reactor.

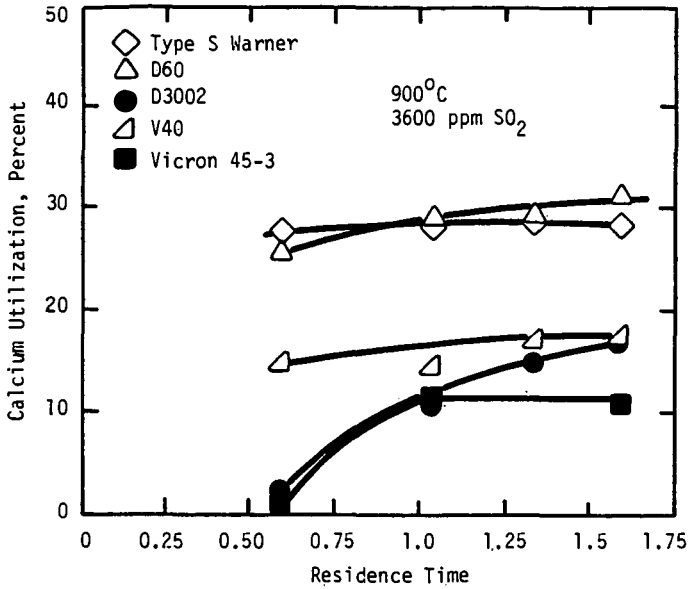

Figure 3. Calcium utilization profiles for five sorbents at 900°C, 3600 ppm SO_2.

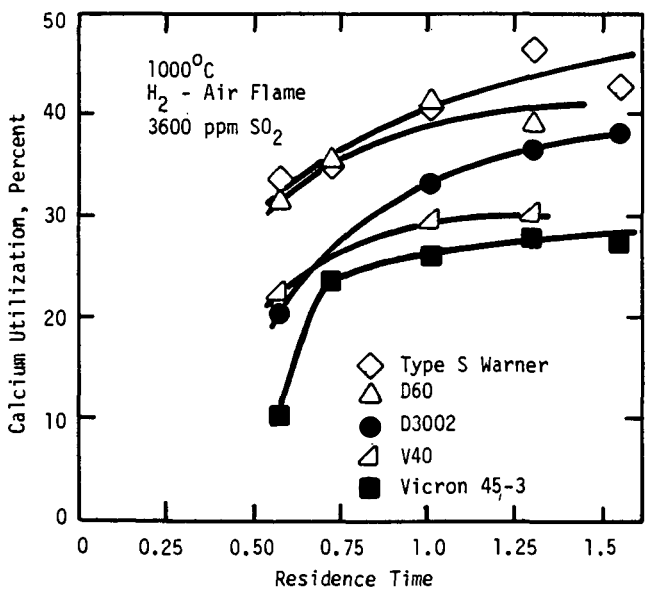

Figure 4. Calcium utilization profiles for five sorbents at 1000°C, 3600 ppm SO_2.

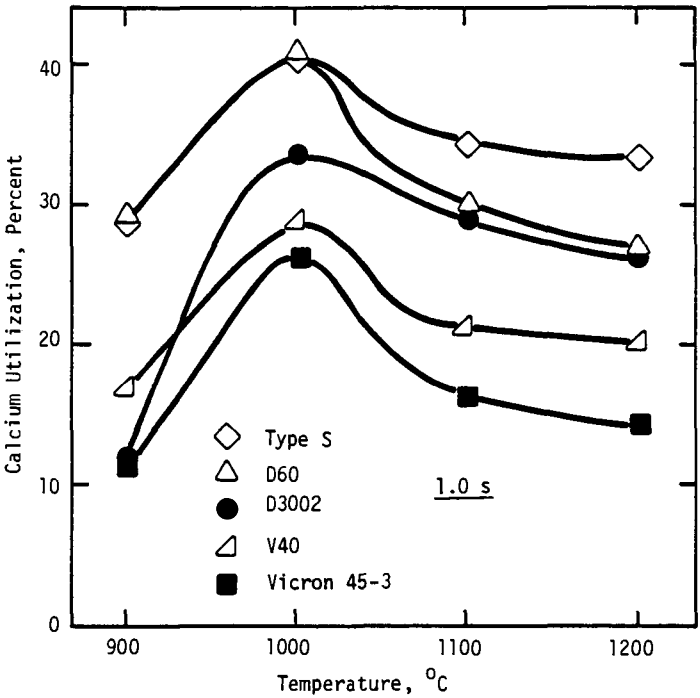

Figure 5. Relative levels of calcium utilization at 1.0 s by five sorbents as a function of isothermal reactor/calcination temperature.

SYMPOSIUM ON ENVIRONMENTAL SCIENCE OF FOSSIL FUELS
PRESENTED BEFORE THE DIVISION OF FUEL CHEMISTRY
AMERICAN CHEMICAL SOCIETY
189th National Meeting, April 28-May 3, 1985

SULFUR FIXATION OF COAL FINE AGGLOMERATES IN THE PRESENCE OF LIMESTONE AT OXIDIZING ATMOSPHERE

by

Felicia F. Peng and C. C. Young
Mineral Processing Engineering Department
West Virginia University
Morgantown, West Virginia 26506-6070

ABSTRACT

Utilization of coal fine agglomerates in the presence of limestone offers an advantage of in-situ sulfur fixation in the agglomerates during combustion and/or gasification to minimize the emission of SO_2 into the atmosphere. An experiment is carried out to study the kinetics of sulfur fixation in the coal fine-limestone agglomerates in air stream at temperature ranges of 500°- 900°C using a fixed bed reactor. Seventy percent of total sulfur reaction in the agglomerates can be achieved with Ca/S mole ratio of 3. The rate of sulfur fixation, in terms of total sulfur and sulfate sulfur retained, in the coal fine agglomerates can be represented by a coupled diffusion and zone reaction model. The activation energy of the overall sulfur fixation reaction is found to be 4 - 7 Kcal/mole.

INTRODUCTION

The most serious environmental problems in coal mining regions are the coal fine slurry impoundments. They not only present hazardous conditions to the local communities, but also restrict the use of land and water resources. Because of current concern over the impending energy shortages and environmental problems, the coal fine wastes must be recovered from tailing impoundments and waste streams of processing plants. This can be used to clean up the coal slurry impoundments and avoid need for impoundments to protect our environment. A potentially attractive method to recover and utilize these coal fines in producing clean energy with in-situ sulfur fixation has been developed. The proposed flow sheet is depicted in Fig. 1.(1) This process includes coal fine-limestone agglomeration and combustion steps.

A number of publications have disclosed the effectiveness of applying sulfur acceptor sorbents within sulfide ore pellets for in-situ sulfur fixation and used as a hydrogen sulfide scavenger. (2,3) The sulfur dioxide was formed and adsorbed by sorbent within the pellets as a hydrate ($CaSO_4$) during air roasting (~500°C). The hydrate was insoluable in acids and the sulfur was retained in the pellets during the subsequent acid leaching process. On the other hand, the hydrogen sulfide was generated and accepted by sorbent within the pellets in H_2 or steam atmosphere (600°- 800°C). The CaS in the pellets could be recovered as sulfur after the acid leaching process. Lime ($Ca(OH)_2$) was the only common sorbent that would adequately control SO_2 or H_2S evolution within the sulfide ore pellets during the roasting or reduction processes. Approximatley 90 percent of sulfur could be converted to CaS or $CaSO_4$ in the pellets in the presence of a stoichiometric amount of $Ca(OH)_2$.

The processes related to the in-situ sulfur fixation in the coal pellets in the presence of limestone were reported by LaRosa and Michaels (4), Buttermore (5), and Ban, et al. (6) Sixteen percent sulfur content of Illinois coal refuse was mixed with limestone and carbonized in the N_2 atmosphere. Sixty-two percent of sulfur converted to CaS and FeS within the pellets was reported by LaRosa, et al. Buttermore investigated the effect of various sorbents on the Ohio raw coal and West Virginia coal refuse for sulfur fixation in the pellets. The results showed

that a 100% sulfur retention efficiency in coal hydrated lime pellets and 93% in the coal-limestone pellets at the 180% stoichiometric CaO could be achieved. A clean pellet fuel process was developed by Ban, et al. Approximately 95% sulfur was retained during carbonization and about 75% of original sulfur was retained in the pellets in the presence of limestone with Ca/S mole ratio of 3 during combustion.

No kinetic data on the in-situ sulfur fixation reaction in the coal fine-limestone agglomerates has been reported. Therefore, it is the aim of this investigation to obtain rate data and to formulate the rate expressions for prediction and interpretation of the phenomena. The information is important in process design and operations. The mathematical model is also useful to apply in preparing the high sulfur coal to generate the clean energy and in predicting the sulfur fixation by calcium (as mineral matter in coal) in coal during the combustion and/or gasification.

EXPERIMENTAL

The coal fines were collected from a 9 year old coal slurry impoundment. The coal fine tailing contained 41.6% ash, 25.6% volatile matter, 1.62% total sulfur and 18,575 KJ/Kg (7,683 BTU/lb). The sulfur forms included 0.88% organic sulfur, 0.11 pyritic sulfur, and 0.63% sulfate sulfur. The low temperature ash analysis showed there was 2.96% CaO content in the coal ash. The Greer limestone was used as a SO_2 acceptor which contained 45.15% CaO. The coal fine tailing and limestone (Ca/S mole ratio 0 - 4) in the size range of 140M x 200M (106 - 75μm) were blended with 15% water by wt. and balled in a glass tubing by hand. All experiments were performed in a 26mm ID x 120mm L quartz tube which was used as a fixed bed reactor. The schematic diagram of the experimental apparatus is shown in Fig. 2. In a typical experimental run, the agglomerates (~1 g) were placed in a 60 mesh stainless steel sample holder and loaded in the cooling zone, while the reactor was continuously purging with air flow rate of 2 l/min, and maintained at a desired reaction temperature 500°, 700° or 900°C). To start the experiment, the coal sample was slid into the hot zone for combustion. The sample was slid back to the cooling zone at predesigned combustion time, while the air stream was switched to N_2 gas. The weight loss of the agglomerates were determined and sulfur forms of the agglomerates were analyzed by ASTM standard methods.

KINETIC MODELING

In the coal fine-limestone agglomerates, the solid reactants are visulized as being composed of a large number of spherical limestone particles and coal fine particles with the sulfur imbedded in the coal particles. In the overall agglomerate, the agglomerate is porous, the gaseous reactant, O_2, diffuses easily through the interstices between coal fine and limestone particles, and through the product layers surrounding the solid reactant grains in the particles. The chemical reaction then proceeds according to zone reaction model (7) in individual particles. The model is schematically shown in Fig. 3. The sulfur fixation reactions in the coal fine-limestone agglomerates involve the successive multiple solid-gas reactions. Three major chemical reactions, which contribute to the sulfur fixation in the agglomerates, can be represented by the following reactions:

$$S\ (\text{in coal}) + O_2 \rightarrow SO_2 \qquad 1)$$

$$CaCO_3 \rightarrow CaO + CO_2 \qquad 2)$$

$$SO_2 + CaO + \tfrac{1}{2}O_2 \rightarrow CaSO_4 \qquad 3)$$

If the order of reactions, with respect to the individual reactant, are first order, and the concentration of gaseous intermediate, SO_2, is much less than that of gaseous reactant O_2, the rate of mass transport of SO_2 within the solid product layers will become rate controlling. Therefore, application of a coupled diffusion and zone reaction models can be used in describing the mass transfers in the particles and agglomerates, and the successive multiple reactions for calcium sulfate formation. The rate expressions are:

$$\frac{dx_1}{dt} = \frac{A\,K_1\,x_{m1}(1-\frac{x_1}{x_{m1}})^{2/3}}{1+\frac{A\cdot K_1}{A\cdot D_1}(1-\frac{x_1}{x_{m1}})^{1/3}(1-(1-\frac{x_1}{x_{m1}})^{1/3})} = R_1 \qquad 4)$$

$$\frac{dx_2}{dt} = R_1 - R_2 \qquad 5)$$

$$\frac{dx_3}{dt} = \frac{B\,x_{m3}K_2\,(1-\frac{x_3}{x_{m3}})^{2/3}\,x_2\,x_4}{1+\frac{B\cdot K_2}{B\cdot D_2}(1-\frac{x_3}{x_{m3}})^{1/3}\,(1-(1-\frac{x_3}{x_{m3}})^{1/3})} = R_2$$

$$\frac{dx_4}{dt} = \frac{C\,D_3\,(1-x_4)^{1/3}}{1-(1-x_4)^{1/3}} \qquad 7)$$

With the conditions:

$x_1 = x_2 = x_3 = x_4 = 0$ at $t = 0$
$(1-x_1) + x_2 + x_3 = 1.0$ at $t > 0$

The rate expressions can be numerically analyzed by utilizing 4th order Runga-Kuta method.

where
x_1 = the fractional conversion of total sulfur
x_{1m} = the fractional conversion of total sulfur at steady state
x_2 = the fractional sulfur dioxide formed
x_3 = the fractional calcium sulfate formed
x_{3m} = the fractional calcium sulfate formed at steady state
x_4 = the fractional calcined limestone (CaO) formed

A,B,C = the parameters related to the physical properties of given particles and concentration of O_2
D_1 = a structural parameter includes the effective diffusivity of O_2 in ash product layer in coal fine particles
D_2 = a structural parameter includes the effective diffusivity of SO_2 in the product layer of limestone particles
K_1 = a kinetic parameter includes the rate constant of SO_2 formation
K_2 = a kinetic parameter includes the rate constant of calcium sulfate formation

RESULTS AND DISCUSSION

The effect of O_2 flowrate on the fulfur fixation rate was examined. The result showed that if the air flow rate was above 1.8 l/min, there was no effect on the rate of sulfur fixation. This indicates an negligible resistance to gas film diffusion above the flowrate of 1.8 l/min. The internal mass transfer in the agglomerate was also examined by varying the agglomerate sizes. The experimental results indicated that if the agglomerate size of less than 3/8-in. diameter were used, the SO_2- O_2- CaO reaction could be studied in the absence of pore diffusion resistance in the agglomerates. The reaction order for the SO_2 and limestone system was analyzed by varying the amount of limestone addition. Seventy percent of sulfur retention can be achieved at Ca/S mole ratio of 3 or higher. The correlation of initial rate and the concentration of limestone showed that the reaction was first order with respect to the concentration of limstone in the agglomerates. The calcination of limestone in the agglomerate was described by a diffusion model. Assumed that the calcination was controlled by the diffusion and the kinetic effect was negligible. Several coal fine agglomerates without limestone addition were also tested to determined the effect of CaO in the coal ash and the net effect of limestone addition on

the rate of sulfur fixation. The representative results of these studies are shown in Fig.4. The kinetic and structural parameters in the rate expressions were obtained for the given experimental conditions, and determined by trial and error as the one that best fit the experimental data. The comperision of predicted and observed values are depicted in Fig.5. Good agreement between predicted and obseved experimental data was obtained. A slower initial rate of sulfur fixation was noted, which could attribute to the time required for calcination of limestone and evolution of SO_2 from the surface of the agglomerates. An enhancement of the combustion rate in the presence of limestone was also detected. Drastic changes in the structure of the agglomerates can be predicted as temperature increase through the structure parameters in the kinetic models. The rate constant for the overall sulfur fixation obtained from experimental data can be expressed as follows.

$$k_i = 21.0667\ \mathrm{Exp}(-7{,}300/RT) \qquad \text{for } 500^\circ\text{-}700^\circ\ C \qquad 8)$$

$$K_i = 3.5057\ \mathrm{Exp}(-3{,}860/R) \qquad \text{for } 700^\circ\text{-}900^\circ\ C \qquad 9)$$

CONCLUSION

Kinetic studies are reported here on the in-situ sulfur fixation in the coal fine-limestone agglomerates during combustion. The sulfur is first oxidized to form SO_2 while limestone is calcined to form CaO, and the intermediate gaseous product, SO_2, subsequently reacts with calcined limestone and oxygen to form calcium sulfate. Diffusion is found to play an important role in sulfur fixation rate. The unusually low activation energy found for the sulfur fixation reaction is thought to be due to the time requirement for limestone calcination and emission of SO_2 from the surface of the agglomerates at initial stage. The sulfur fixation rate data have been interprepted based on a coupled diffusion and zone-reaction model, and the kinetic and structural parameters obtained for the temperature ranges of 500°- 900°C.

REFERENCES

1. Peng,F.F., Young,C.C., and Cai,Z., "Combustion Characteristics of Coal Fine Refuse-Linestone agglomerates for Sulfur Fixation," 1984 AIME-SME Annual meeting, Los Angeles, CA, 1984.
2. Haung,H.H., and Bartlett,R.N., "Oxidation Kinetics of Lime-Copper Concentrate Pellets," Metallurgical Trans., B, vol.7B, 1976, pp. 369-374
3. Rajamani,K., and Sohn,H.Y., "Kinetics and Sulfur Fixation in the Reduction or oxidation of Metal Sulfides Mixed with Lime," Metallurgical Trans., B, vol.14B,1983, pp. 175-180
4. LaRose,P.J., and Michaels,J.J., "Study of Sulfur Recovery from Coal Refuse," Final Report for the Environmental Protection Agency, Contract #14-12-929, 1971, Black, Sivallas and Bryson, Inc., Pittsburgh, PA.
5. Buttermore,W.H., "The Sulfur Process: A Technique to Minimize Sulfur Emissions," Coal Research Bureau Technical Report No.168, 1979, West Virginia University
6. Ban,T.E., Johnson,E., and Marlowe,W.H., "Development of the Clean Pellet Fuel Process - A Progress Report," Mining Engineering, Jan., 1981, pp. 71-80
7. Wen,C.Y., "Noncatalytic Heterogeneous Solid Fluid Reaction Models," I & C.E., 1968, pp. 34-54

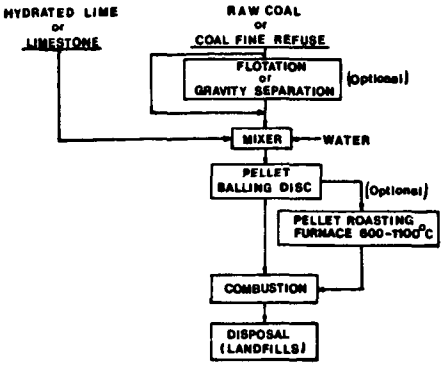

FIG.1 FLOWSHEET FOR COAL FINE REFUSE-LIMESTONE COMBUSTION PROCESS

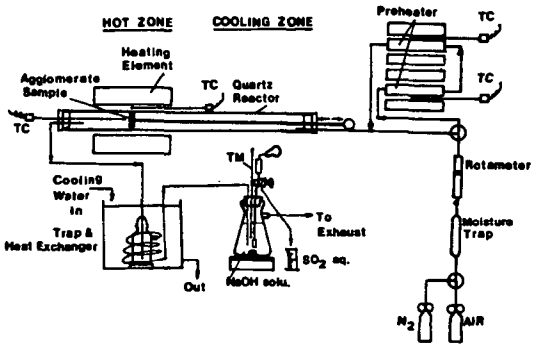

FIG.2 SCHEMATIC DIAGRAM OF COMBUSTION SYSTEM FOR COAL FINE REFUSE-LIMESTONE AGGLOMERATE

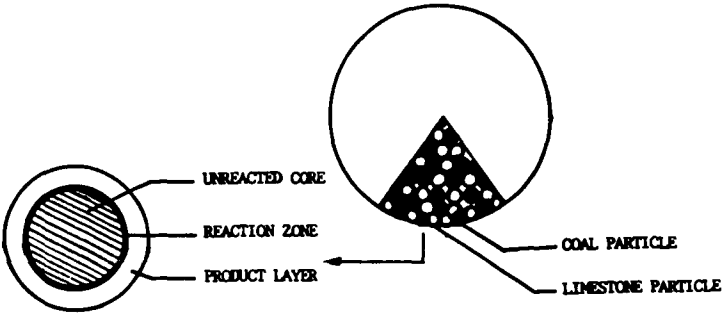

zone Reaction Model

FIG.3 A COUPLED DIFFUSION-ZONE REACTION MODEL

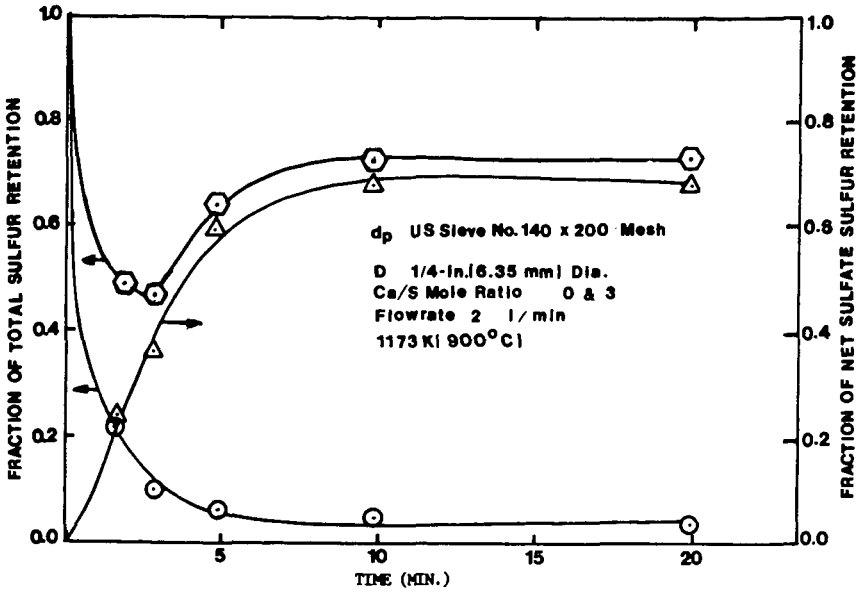

FIG.4 THE RATES OF SUCCESSIVE SULFUR FIXATION REACTIONS - FRACTIONAL TOTAL SULFUR RETAINED AND FRACTIONAL SULFATE SULFUR RETAINED IN THE 1/4-in. (6.35mm) COAL FINE AGGLOMERATE IN THE PRESENCE/ABSENCE OF LIMESTONE AT 1173K (900 DEG. C) AND 1 ATMOSPHERE

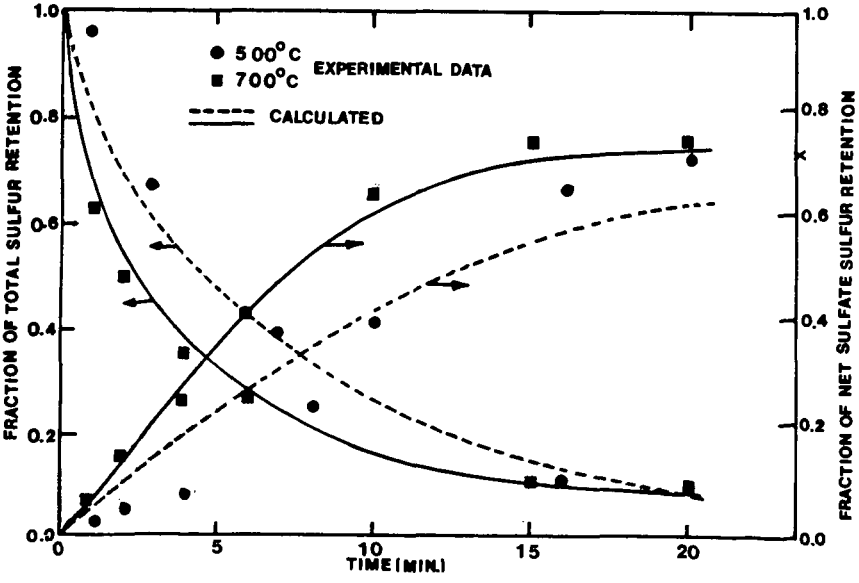

FIG.5 Comparison of the Calculated Curves with Experimental Data for the Sulfur Fixation in the Coal Fine-Limestone Agglomerates

EFFECT OF DELIQUESCENT SALT ADDITIVES ON THE REACTION OF SULFUR DIOXIDE WITH DRY $Ca(OH)_2$

Rosa N. Ruiz-Alsop and Gary T. Rochelle

Dept. of Chemical Engineering, University of Texas at Austin, Austin, TX 78712

ABSTRACT

The effect of deliquescent salt additives in the reaction of SO_2 with dry $Ca(OH)_2$ solids dispersed in a sand reactor was studied. Small amounts of the deliquescent salts (1 to 10 mole %) were added to the $Ca(OH)_2$ by a slurrying, drying process. The reaction rate was studied at relative humidities of 54 and 74 % and other conditions similar to those encountered in bag filters during flue gas desulfurization by spray drying. The reaction solids were characterized by Scanning Electron Microscopy, powder X-ray diffraction, coulter counter size distribution, BET (N_2) surface area, energy dispersive spectrometry, and differential scanning calorimetry. Most of the deliquescent salts tested increased the reactivity of the lime. The most effective additives were: LiCl, KCl, NaCl, NaBr and $NaNO_3$.

INTRODUCTION

Spray drying has become increasingly important in recent years as an alternative to wet scrubbing for sulfur dioxide control. In the spray dryer the sulfur containing flue gas is contacted with a fine mist of an aqueous solution or a slurry of an alkali (typically lime or soda ash). The sulfur dioxide is then absorbed in the water droplets and neutralized by the alkali. Simultaneously, the thermal energy of the gas evaporates the water in the droplets to produce a dry powdered product. After leaving the spray dryer the dry products including the fly ash are removed with collection equipment such as fabric filters or electrostatic precipitators.

Fabric filters are the preferred collection equipment as additional sulfur dioxide removal takes place in the bag house [6, 7]. Typically, under conditions such that 80 % of SO_2 is removed, about 60 to 70 % of the removal takes place in the spray dryer and 10 to 20 % removal takes place in the bag filters [14, 9, 2]. Parametric studies in spray dryer pilot plants have demonstrated that the main variable affecting the SO_2 removal in the bag filters beside the stoichiometric ratio of lime to SO_2 is the approach to the adiabatic saturation temperature of the gases [14, 2, 15, 12, 1]. The approach to the adiabatic saturation temperature in turn is correlated with the moisture content of the solids. Additives that will modify the moisture content of the lime solids in equilibrium with a gas phase of a given relative humidity would then be expected to change the reactivity of the lime towards SO_2.

A few additives have been tested in spray drying systems. $CaCl_2$ has proven effective in increasing the reactivity of limestone and lime towards SO_2 [5]. Adipic acid was also tested [10] with mixed results. Sodium sulfite, Fe^{++} compounds, Ethylenediaminetetra-acetic acid and disodium salt (EDTA) had been used as additives during simultaneous SO_2 and NO_x removal (Niro Process) [4]. The emphasis in the Niro process was to improve the removal of NO_x.

The present work was undertaken to investigate in a systematic manner the kind of additives that could be used to improve lime reactivity towards SO_2. A small fixed bed reactor was used to simulate the conditions encountered in the bag filters during spray drying flue gas desulfurization. Three different kind of additives were tried: buffer acids, organic deliquescents and inorganic deliquescents. The inorganic salts were selected according to their deliquescent properties, or the lowering of the vapor pressure of water over their saturated solutions. Of these three types of additives the deliquescent salts were the only ones that increased

the lime reactivity.

EXPERIMENTAL

Apparatus

The general scheme of the experimental apparatus is given in Figure 3. Simulated flue gas was synthesized by combining nitrogen and sulfur dioxide from gas cylinders. The gas flow rates were measured using rotameters. Water was added by means of a syringe pump and evaporated at 120 °C before mixing with the gas stream. The glass reactor (4 cm diameter, 12 cm height) was packed with a mixture of silica sand and powdered reagent $Ca(OH)_2$ in a weight ratio of 40:1. The addition of sand is necessary to avoid channeling caused by lime agglomeration [5]. The silica sand, obtained from Martin Marietta Aggregates, was 100 mesh. The reactor was immersed in a water bath that maintained the temperature within 0.1 °C. Tubing upstream from the reactor was heated to prevent the condensation of moisture in the walls. Before going to analysis the gas was cooled and the water then condensed by cooling water and an ice bath . The gas was analyzed for SO_2 in a pulsed fluorescent SO_2 analyzer (Thermoelectron Corporation model 40) and the concentration continuously recorded. The reactor was equipped with a bypass, to allow the bed to be preconditioned and then after, to allow the gas flow to be stabilized at the desired SO_2 concentration before beginning the experiment. Prior to each experimental run the bed was humidified by flushing with pure nitrogen at a relative humidity of about 98 % for 10 minutes then later with pure nitrogen at the relative humidity at which the experiment was to be performed for 8 minutes. This was done to better simulate the conditions encountered in the bag filters where the solids are originally slurry droplets.

Preparation of the Samples

An aqueous solution containing the desired additive was prepared. Five ml of this solution were then added to 1 g of lime and slurried. The sample was then placed in a oven to dry at 75 °C for about 14 hours then later sieved to separate the individual lime particles prior to mixing with the silica sand and being placed in the reactor.

Analysis

The fraction of $Ca(OH)_2$ reacted at any given time can be calculated by integrating the SO_2 versus time curve obtained by the recorder on the SO_2 analyzer and doing a mass balance in the reactor. As a backup, the reacted solids are analyzed for sulfite and hydroxide using acid/base and iodine titrations.

Characterization of the reactant

The lime used in these experiments was calcium hydroxide powder reagent. The particle size distribution of the lime was determined by means of a Coulter Counter model T_{AII} using as electrolyte a solution of 4 wt % $CaCl_2$, saturated with $Ca(OH)_2$. The surface area was determined using Brunauer Emmett and Teller (BET) nitrogen absorption isotherms. Table 1 shows the particle size distribution and surface area of the lime used. The surface area was also measured for the lime after being slurried (5 ml water/g lime) and dried overnight at 75 °C. There was a small decrease in the surface area due to this slurrying process. Figures 1 and 2 show Scanning Electron Micrographs of the lime that was used as the reactant. From these pictures it can be seen that the lime particles are in the micron range size, are highly nonspherical and have considerable surface roughness.

The samples of lime with additives that were prepared in the way discussed above were characterized using x-ray powder diffraction, scanning electron microscopy (SEM), energy dispersive spectroscopy (EDS), and BET surface area. According to x-ray diffraction analysis most of the additives precipitate as a separate phase after slurrying with the lime then drying. The exception is $CaCl_2$, where the $Ca(OH)_2.CaCl_2.H_2O$ phase is formed. This finding agrees with the result reported in the literature for the equilibrium of the $Ca(OH)_2$-$CaCl_2$-H_2O system [13]. In the case of $Ca(NO_3)_2$, the formation of the solid phase $Ca_2N_2O_7.2H_2O$ has been reported [13]. This could not be confirmed using x-ray analysis as the diffraction pattern of the $Ca_2N_2O_7.2H_2O$ was not available.

EDS was used to analyze individual particles and it was found that the additives precipitate together with the lime and are, more or less, uniformly distributed through the lime particles. SEM micrographs of the particles of lime with additives showed no significant difference in size or shape from the pure lime particles. The BET surface areas of the lime with different salt additives were also measured. The surface areas ranged from 7.0 to 9.6 m^2/g depending on the additive used. No correlation was found between lime reactivity and surface area.

RESULTS

Effects of Additive Type

The additives tried can be classified as three types: buffers, organic deliquescents and inorganic deliquescents. Column 1 of Table 3 shows the experimental results for these three types of additives, expressed as percentage of lime reacted after 60 minutes of reaction. The experiments shown in column 1 were all run at a relative humidity of 74 % and other conditions as indicated in the table. The buffers added were adipic and glycolic acid in concentrations of 1 and 5 wt % respectively. The addition of buffers proves to be detrimental to the reaction of SO_2 and lime, a conversion lower than the pure lime case was observed. The organic deliquescents tried were monoethanolamine, ethylene glycol, and triethylene glycol all at concentrations of 5 wt %. A small decrease in lime reactivity was found in these cases as can be seen from Table 3. At a 74 % relative humidity all the deliquescent salts tried were successful in increasing the reactivity of the lime, but some salts were more effective than others.

Influence of the relative humidity on effectiveness of additives

Column 2 of Table 3 shows the effect of selected deliquescent salts on the lime reactivity at a relative humidity of 54 %. As can be seen by comparing columns 1 and 2 of Table 3 the effectiveness of some salts change with relative humidity, for example $Ca(NO_3)_2$ was very effective at 74 % relative humidity but behaved poorly at a lower relative humidity. At a lower relative humidity the salts that behave the best were K, Li and Na Chlorides, NaBr, and $NaNO_3$.

Influence of Salt Concentration

A series of experiments were performed to determine the influence of the salt concentration on the SO_2 reaction rate. The salts used were NaCl and $NaNO_3$ in concentrations ranging from 1 to 15 mole %. The experiments were carried out at 54 % relative humidity, and a reactor temperature of 66 °C. As can be seen from Figure 4, the conversion increases with increasing concentration of additive until about 10 mole %. After this the curve levels off. The optimum concentration of additive is then about 10 mole % for 1:1 salts like NaCl and $NaNO_3$.

Effect of Prehumidification at 98 % Relative Humidity

To investigate the effect of prehumidifying the bed on the reactivity of the lime with additives towards SO_2 some experimental runs were made omitting this step. Table 2 shows the results obtained at 54 and 17.4 % relative humidity with and without prehumidification of the bed at 98 % relative humidity. The additives used were NaCl, $NaNO_3$ and KCl. At 54 % relative humidity even when some decrease of the lime conversion was found without the prehumidification, the results are still far superior to the pure lime case. At 17.4 % relative humidity all the beneficial effect in the case of the NaCl appears to be due to the prehumidification of the bed i. e. due to an hysteresis phenomena.

DISCUSSION

Columns 3 and 4 of Table 3 show the deliquescent properties of the salts, expressed as water activity in saturated solutions of the salt at 25 and 100 °C and 1 atm. The water activity is approximately equal to the relative humidity of the gas phase in equilibrium with the saturated solution. When examining the deliquescent properties of the salts it is apparent that if the improvement of reactivity was due solely to deliquescence, $NaNO_3$ and all the chlorides tried, with the exception of the LiCl, should not work at a relative humidity of 54 %. Furthermore, the most deliquescent of all the additives tried, NaOH does not perform as well as some of other less deliquescent salts. We can see that some salts are effective at a lower relative humidity than would be predicted by the vapor pressure of water over saturated solutions of these salts. A possible explanation would be a hysteresis phenomena affecting the amount of absorbed water in the solid phase. Strong hysteresis effects have been reported in NaCl aerosols [17]. From the experimental results presented in Table 2, it can be concluded that even when the hysteresis effects can explain the improvement in reactivity at a very low relative humidity (17.4 %) it can not explain all the improvement observed at 54 % relative humidity. An alternate explanation proposed is that the chlorides and $NaNO_3$ modify the properties of the product $CaSO_3.1/2H_2O$ layer that is formed as the reaction takes place thereby facilitating the access of the SO_2 to the unreacted lime which remains in the center of the particle. NaCl and $CaCl_2$ have been reported to enhance the sulfur dioxide reactivity of limestones in fluidized bed combustion by affecting the the pore structure of the lime during calcination, which then increases the extent of sulfation of the limestone [3].

For an additive to be effective it is necessary that the hydroxide of the cation be very soluble, otherwise the cation will precipitate as the hydroxide and the anion as the Ca salt. For example $Co(NO_3)_2$ is very deliquescent but $Co(OH)_2$ is insoluble so Co precipitates as $Co(OH)_2$ and adding cobalt nitrate becomes equivalent to adding calcium nitrate, which is not very effective.

Table 1

PROPERTIES OF THE $Ca(OH)_2$ USED AS A REACTANT

Particle size (μm)	50 % below 5.6 90 % between 1.5 - 15
BET Surface Area (m^2/g)	9.4 (non slurried lime) 8.8 (slurried lime)

Table 2

EFFECT OF PREHUMIDIFICATION OF THE BED ON LIME REACTIVITY
Inlet SO_2 concentration = 500 ppm
Nitrogen Flow Rate = 4.6 l/min (0°C, 1 atm)
Amount of Lime = 1.0 g

	Lime Conversion after 60 Minutes			
	54 % Relative Humidity 66 °C		17.4 % Relative Humidity 95 °C	
Additive	Prehumidified	Nonprehumidified	Prehumidified	Nonprehumidified
None	11.2	-	4.0	-
10 mole % NaCl	27.0	23.2	9.7	4.0
10 mole % $NaNO_3$	27.2	23.7	11.9	-
10 mole % KCl	37.3	19.3	3.4	-

Table 3

EFFECT OF ADDITIVES ON LIME REACTIVITY AND DELIQUESCENT PROPERTIES OF SALTS
Inlet SO_2 Concentration = 500 ppm
Nitrogen Flow Rate = 4.6 l/min [0 °C, 1 atm]
Amount of Lime = 1.0 g

Additive	Lime Conversion at 60 min. 74 % R.H. 64.4 °C	54 % R.H. 66 °C	a_w at 25 °C	a_w at 100 °C
None	22.4	11.8	-	-
BUFFERS				
5 wt % Glycolic Acid	11.3	-	-	-
1 wt % Adipic Acid	20.3	-	-	-
ORGANIC DELIQUESCENTS				
5 wt % Monoethanolamine	19.6	-	-	-
5 wt % Ethylene Glycol	20.3	-	-	-
5 wt % TEG	20.5	-	-	-
INORGANIC DELIQUESCENTS				
5 mole % Na_2SO_4	28.3	-	-	.902 [8]
5 mole % Na_2SO_3	29.8	16.1	-	-
5 mole % $CaCl_2$(***)	34.6	16.4	.850 [8]	.686(*) [8]
10 mole % NaCl	38.5	27.0	.753 [16]	.735 [8]
10 mole % NaOH	38.8	17.3	.0703 [16]	.004 [11]
5 mole % $Ca(NO_3)_2$(***)	39.4	12.3	-	.553 [8]
10 mole % $NaNO_2$	40.0	-	-	.496(**)
10 mole % $NaNO_3$	41.5	27.2	.738 [16]	.549 [8]
$BaCl_2.2H_2O$	-	19.4	.902 [16]	.71(**)
$Na_2S_2O_3$	-	21.6	-	.52(**)
KCl	-	37.3	.842 [16]	.745 [8]
$NaBr.2H_2O$	-	42.0	.577 [16]	.502 [8]
LiCl	-	43.9	.112 [16]	.085 [8]
100 % SO_2 Removal	48.2	48.2		

(*) Data at 75 °C.
(**) Extrapolated from data reference [8]
(***) Solid phases are $CaCl_2.Ca(OH)_2.H_2O$ and $Ca_2N_2O_7.2H_2O$ respectively.

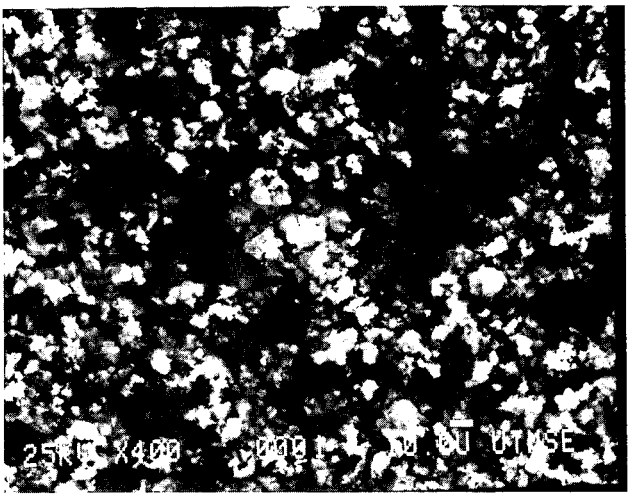

FIGURE 1. $Ca(OH)_2$ SEM MICROGRAPH, 400 MAGNIFICATIONS.

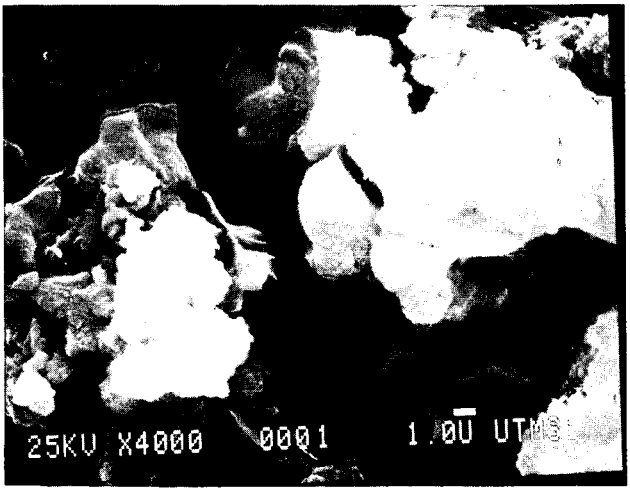

FIGURE 2. $Ca(OH)_2$ SEM MICROGRAPH, 4000 MAGNIFICATIONS

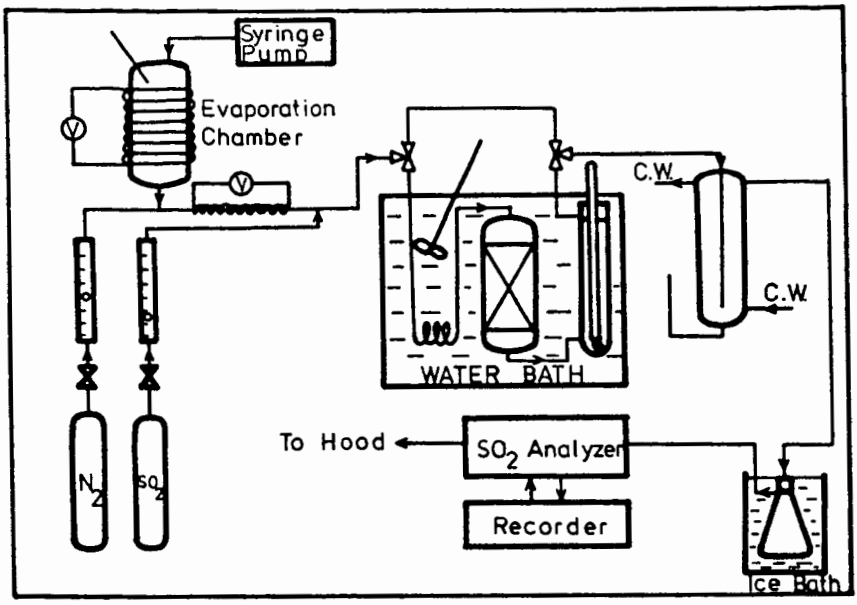

Figure 3. Experimental Apparatus

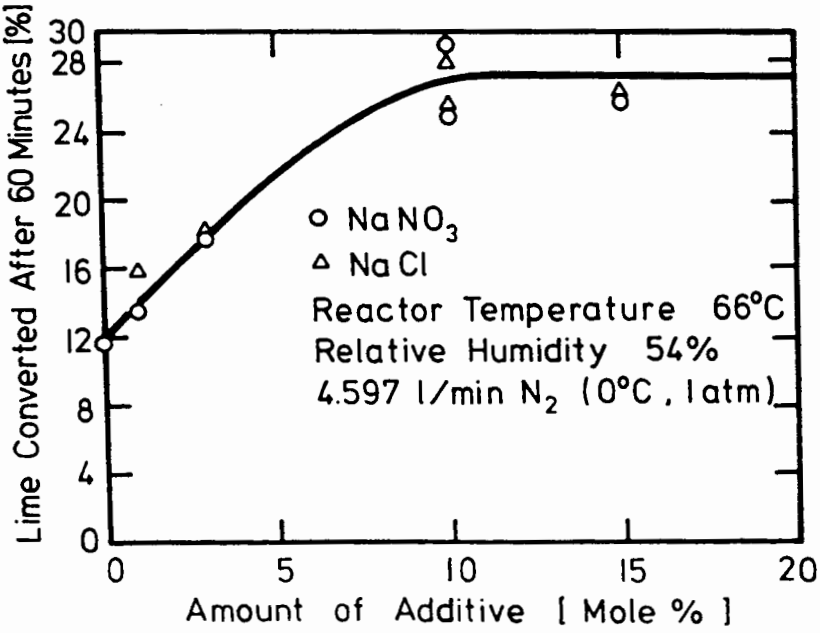

Figure 4. Effect of Amount of Additive on Lime Reactivity.

REFERENCES

[1] Blythe, G. M. and Rhudy, R. G., EPRI Spray Dryer/Baghouse Pilot Status and Results, Presented at the EPA/EPRI Symposium on FGD, (New Orleans, November 1983).

[2] Bresowar, G. E.; Borsare, D. C. and Walki, K. W., Dry Scrubber Design and Application. The C-E Approach, Presented at the Joint Power Generation Conference, (St. Louis, Missouri, October 1981).

[3] Chopra, O. K.; Smith, G. W.; Lenc, J. F.; Shearer, K. M.; Myles, K. M. and Johnson, I., Effect of Salt Treatment of Limestone on Sulfation and on the Corrosion behavior of Materials in AFBC Systems, The Proceedings of the Sixth International Conference on Fluidized bed Combustion, (Atlanta, Georgia, April 1980).

[4] Felsvang, K.; Morsing, P. and Veltman, P., Acid Rain Prevention Thru New SO_x/NO_x Dry Scrubbing Process, Presented at the EPA/EPRI Symposium on FGD, (New Orleans, November 1983).

[5] Karlsson, H. T.; Klingspor, J.; Linne, M. and Bjerle, I., Activated Wet-Dry Scrubbing of SO_2, APCAJournal 33, 1 (1983), 23.

[6] Kelly, M. E. and Dickerman J. C., Current Status of Dry Flue Gas Desulfurization Systems, pp. 761, Proceedings: Symposium on FGD, (Washington, D. C., 1981).

[7] Kelly, M. E.; Kilgroe, J. D.and Brna, T. G., Current Status of Dry SO_2 Control Systems, pp. 550, Proceedings: Symposium on FGD, (March 1983).

[8] National Research Council, International Critical Tables, (Mc Graw Hill, New York, 1930).

[9] Parsons, E. L.; Hemenway, LL. F.;Krag, O. T.; Brna, T. G. and Ostop, R. L., SO_2 Removal by Dry FGD, pp. 801, Proceedings: Symposium on FGD, (Washington, D. C., 1981).

[10] Parsons, E. L.; Boscak, V.; Brna, T. G. and Ostop, R. L., SO_2 Removal by Dry Injection and Spray Absorption Techniques, Presented at the U. S. Third Symposium on the Transfer and Utilization of Particulate Control Technology, (Orlando, Florida, March 1981).

[11] Perry, R. H. and Chilton, C. H., Chemical Engineer's Handbook, (Mc Graw Hill, N. Y., 1973).

[12] Samuel, E. A.; Lugar, T. W.; Lapp, D. E.; Fortune, O. F.; Brna, T. G. and Ostop, R. L., Dry FGD Pilot Plant Results: Lime Spray Absorption for High Sulfur Coal and Dry Injection of Sodium Compounds for low Sulfur Coals, pp. 574, Proceedings: Symposium on FGD, (March 1983).

[13] Seidell, A. and Linke, W. F., Solubilities of Inorganic and Metal Organic Compounds, (Van Nostrand Co. Inc., Washington, D. C., 1958).

[14] Stevens, N. J., Dry Scrubbing Pilot Plant Results, pp. 777, Proceedings:Symposium on FGD, (Washington, D. C., 1981).

[15] Stevens, N. J.; Manavizadeh, G. B.; Taylor, G. W. and Widico, M. J., Dry Scrubbing SO_2 and Particulate Control, Presented at the U. S. Third Symposium on the Transfer and Utilization of Particulate Control Technology, (Orlando,

Florida, March 1981).

[16] Stokes, R. H. and Robinson, R. A., Standard Solutions for Humidity Control at 25 °C., Ind.Eng.Chem. 41 (1949), 2013.

[17] Tang, I. N.; Munkelwitz, H. R. and Davis, J. G., Aerosol Growth Studies. II Preparation and Growth Measurements of Monodisperse Salts Aerosols, J.AerosolSci. 8 (1977), 149-159.

ACTIVITY COEFFICIENTS PREDICTED BY THE LOCAL COMPOSITION MODEL FOR AQUEOUS SOLUTIONS USED IN FLUE GAS DESULFURIZATION

Charles E. Taylor and Gary T. Rochelle

The University of Texas at Austin
Department of Chemical Engineering
Austin, Texas 78712

SCOPE

The major objective of this work is to extend the predictability of solution equilibra models for flue gas desulfurization processes by employing an activity coefficient technique which is accurate over a wide concentation range. Current FGD equilibrium models use a Davies technique for activity coefficient prediction. The Davies technique is useful only up to ionic strengths of 1 molal, thus, limiting the application of FGD equilibrium models to low ionic strength. In this work a data base and methods have been developed to use the local composition model (LCM, 1,2) for the prediction of activity coefficients in aqueous FGD solutions. The LCM was used to predict the solubilities in various multicomponent systems for gypsum, calcium sulfite, magnesium sulfite, calcium carbonate, and magnesium carbonate; SO_2 vapor pressure over sulfite/bisulfite solutions; and, CO_2 vapor pressure over carbonate/bicarbonate solutions.

CONCLUSIONS AND SIGNIFICANCE

Accurate prediction of activity coefficients over a 0-6 molal ionic strength range will allow for improvement of available FGD equilibrium models. This will provide accurate equilibrium calculations for low ionic strength lime/limestone processes and higher ionic strength processes as dual alkali or regenerative sodium scrubbing. Additionally, improved accuracy will be available for more complex FGD simulations which use equilibrium models as a means of establishing the inlet scrubber solution composition and to calculate driving forces for rate processes (3).

A data base of necessary binary parameters and equilibrium constants for activity coefficient prediction by the LCM is presented. The LCM has proven to be accurate from 0-6 molal ionic strength for typical FGD aqueous solutions. In general, the LCM is slightly less accurate than the Davies technique from 0-1 molal ionic strength. The advantages of the LCM over the current Davies technique are clearly seen when predicting over the entire concentration range.

C. E. Taylor is presently with
General Electric Environmental Services, Inc., Lebanon, PA 17042

INTRODUCTION

It is often desirable to perform equilibrium calculations in the design or operation of a FGD facility. By using the fundamental principles of conservation of mass and charge, and chemical equilibrium expressions, the concentration of individual species in solution (sometimes called the "species distribution") can be calculated. The available equilibrium models for lime or limestone based FGD are the Bechtel-modified Radian equilibrium program (BMREP, 4) and the species distribution model (SDM, 5). The SDM is the most current equilibrium model and has been improved considerably over earier models to make it more general in nature. Some simple uses of equilibrium models inclnde predicting the saturation or solubility of gypsum to indicate scaling potential, predicting SO2 vapor pressure to trouble-shoot problems with SO2 removal, and predicting dissolved alkalinity or capacity of a solution. However, the BMREP and SDM have limitations which restrict their use to low ionic strength processes.

The practical limit for using the BMREP, SDM, or any equilibrium model for electrolytic solutions normally stems from the lack of correlations for electrolyte thermodynamics (e.g. activity coefficient techniques). The BMREP and SDM currently use the Davies technique for activity coefficient prediction. The Davies technique is a combination of the extended Debye-Huckel equation (6) and the Davies equation (7). The Davies technique (and hence both equilibrium models) is accurate to ionic strengths of 0.2 molal, and may be used for practical calculations up to ionic strengths of 1 molal (8). Ion-pair equilibria are incorporated for species that associate (e.g. 1-2 and 2-2 electrolytes). The activity coefficients (γ_i) are calculated as a simple function of ionic strength (I), and are represented as:

$$\log\gamma_i = AZ_i^2\left[\frac{-I^{1/2}}{1+Ba_iI^{1/2}} + b_iI\right] \qquad 1)$$

where A and B are constants at a given temperature. Depending on the input values of a_i and b_i, Equation 1 can represent either the extended Debye-Huckel or Davies equations, or an extension of the two.

Both the BMREP and SDM approximate activity coefficients of uncharged species (e.g. ion-pairs, molecular species) by the following expression:

$$\log\gamma_i = U_iI \qquad 2)$$

where U_i is an empirical constant.

To improve the BMREP and SDM in eqnilibrium calculations requires an activity coefficient technique which is accnrate over a wide concentration range. Rosenblatt (9,10) identified the inherent limitations of the BMREP and SDM, and investigated the use of the modified Pitzer equation as an activity coefficient technique for FGD solutions. The modified Pitzer equation (11-13) was noted as the most elaborate and successful activity coefficient technique in use (14). Rosenblatt concluded that Pitzer's equations offered a promising approach for thermodynamic modeling of FGD chemistry. Currently, Radian is incorporating the Bromley method (15) as a new activity coefficient technique in the SDM (16). Recently, Chen and co-workers (17-19) developed the local composition model (LCM) for activity coefficient prediction. The LCM is a semi-theoretical model with a minimum number of adjustable parameters, and is based on the Non-Random Two Liquid (NRTL) model for nonelectrolytes (20). The LCM does not have the inherent drawbacks of virial-expansion type equations as the modified Pitzer, and proved to be more accurate than the Bromley method. Some advantages of the LCM are that the binary parameters are well defined, have weak temperature dependence, and can be regressed from various thermodynamic data sources. Additionally, the LCM does not require ion-pair equilibria to correct for activity coefficient prediction at higher ionic strengths. Thus, the LCM avoids

defining, and ultimately solving, ion-pair activity coefficients and equilibrium expressions necessary in the Davies technique. Overall, the LCM appears to be the most suitable activity coefficient technique for aqueous solutions used in FGD, hence, a data base and methods to use the LCM were developed.

THE LOCAL COMPOSITION MODEL

The local composition model (LCM) is an excess Gibbs energy model for electrolyte systems from which activity coefficients can be derived. Chen and co-workers (17-19) presented the original LCM activity coefficient equations for binary and multicomponent systems. The LCM equations were subsequently modified and used in the ASPEN process simulator (Aspen Technology, Cambridge, MA) as a means of handling chemical processes with electrolytes. The LCM activity coefficient equations are explicit functions, and require computational methods. Due to length and complexity, only the salient features of the LCM equations will be reviewed in this paper. The "Aspen Plus Electrolyte Manual" (1), and Taylor (21) present the final form of the LCM binary and multicomponent equations.

The approach taken by Chen and co-workers in developing the LCM was to account for the excess Gibbs energy of electrolyte systems as the sum of long-range (ion-ion) interactions, and short-range (ion-ion, ion-molecule, and molecule-molecule) interactions. The extended Debye-Huckel equation proposed by Pitzer (22) was used to account for the long-range interactions, and the local composition concept was used to account for the short-range interactions of all kinds. The excess Gibbs energy expression is therefore the sum of the unsymmetric Pitzer-Debye-Huckel expression and the unsymmetrical local composition expression. The equation has the general form:

$$\frac{g^{ex^*}}{RT} = \frac{g^{ex^*,pdh}}{RT} + \frac{g^{ex^*,lc}}{RT} \qquad 3)$$

Similarly, the activity coefficient equations (which can be derived from the excess Gibbs energy expression) have the general form:

$$\ln\gamma_i^* = \ln\gamma_i^{pdh^*} + \ln\gamma_i^{lc^*} \qquad 4)$$

The long-range Pitzer-Debye-Huckel equation calculates activity coefficients as a function of ionic strength, and no adjustable parameters are necessary. The short-range local composition equation calculates activity coefficients by accounting for all short-range interactions, and requires a minimum of adjustable parameters. For binary systems, two adjustable binary parameters are necessary: salt-molecule and molecule-salt. For multicomponent systems three types of adjustable parameters are necessary: salt-molecule, molecule-salt, and salt-salt. Therefore, the regressed parameters of the LCM data base are specifically for the short-range contribution to the activity coefficient equation.

The approach to using the LCM for FGD applications involves some assumptions and simplifications. Since the concentrations of all molecular species in solution are negligible with respect to water, only salt-water and water-salt binary parameters are necessary. All salt-molecule and molecule-salt binary parameters for molecular species other than water are set equal to salt-water and water-salt binary parameters. All molecule-molecule interactions are assumed equivalent to water-water interactions, and are set equal to zero. Additionally, all salt-salt parameters are set to zero. Lastly, the temperature dependence of all binary parameters is neglected.

RESULTS AND DISCUSSIONS

The results of applying the LCM to typical FGD solutions are summarized in tables 1 and 2. Table 1 preaents the final regressed LCM binary parameters for typical FGD solutions. The implied formation reactions, and temperature dependent parameters for the equilibrium constants are shown in table 2.

Regression of the necessary LCM binary parameters required various thermodynamic data. The Powell method (23), an unoonstrained nonlinear code, was used to minimize a nonlinear function $f(x)=f(x,...,x_n)$ of n variables. The function f(x) normally represented the standard deviation of the thermodynamic property (e.g. activity coefficients, osmotic coefficients, solubility products, or vapor pressure) being regressed using the LCM for activity coefficient prediction. The n variables represent the final regressed binary parameters. Default values were used for binary parameters representing interactions of species present in low concentration, or when no thermodynamic data were available. Default values were determined by averaging binary parameters regressed by Chen and co-workers (18) for each type of electrolyte (e.g. 1-1, 1-2, 2-1, and 2-2). This approach should yield a minimum error, since the binary parameters are well defined for each type of electrolyte.

The LCM has proven to be useful in predicting data of molal ionic activity coefficients, and vapor pressure depression of various single electrolyte, single solvent systems. The standard deviation of the natural logarithm of the mean activity coefficient was 0.01 for uni-univalent aqueous single electrolytes (17). Similar results were found for uni-bivalent and bi-bivalent electrolyte activity coefficient prediction. Figure 1 compares the LCM with the Davies technique for a sodium sulfate-water system (24). The LCM is accurate over the entire concentration range of 0-6 molal. Two curves are shown for the Davies technique. The upper curve assumes the salt to be totally dissociated, and activity coefficients are calculated directly from Equation 1. The lower curve assumes the ion-pair NaSO4- is present, and activity coefficients are calculated from the SDM, which incorporates the additional ion-pair equilibium. Figure 1 demonstrates the necessity of ion-pair equilibria to insure an accurate activity coefficient prediction in the low concentration range (0-0.2 molal) for salts that associate.

The LCM also predicted activity coefficients of bi-univalent electrolytes (e.g. MgCl2 and CaCl2), which exhibit the experimentally observed reversal of slope and dramatic increase in the activity coefficient at higher ionic strengths. For bi-univalent electrolytes, regressing binary parameters over a 0-6 molal range causes some inaccuracy in the low concentration region. However, regressing the LCM binary parameters over a smaller concentration range (0-2.5 molal) improves the LCM accuracy.

The solubility of gypsum in various salt solutions, ranging in ionic strength from 0-6 molal, was predicted accurately by the LCM. Figure 2 compares the LCM and SDM in predicting gypsum solubility with the addition of sodium sulfate at 25, 50, and 75°C (25). A relative saturation of unity would indicate accurate prediction of the experimental data, since the solutions are known to be saturated to gypsum. The LCM predicted the solubility of gypsum in sodium sulfate solutions within 10 percent error in relative saturation at 50 and 70°C, and within 20-30 percent error in relative saturation at 25°C. In magnesium sulfate solutions at 25°C (26), the LCM predicts gyspum relative saturation from 0-6 molal within 30 percent error. The solubility of gypsum in calium chloride (27) and sodium chloride at 25°C (28) was predicted within 10 percent error in relative saturation from 0-6 molal. In general, the Davies technique, and hence the SDM, gives accurate prediction of gypsum relative saturation only in the low concentration range (0-1 molal). Increasing the ionic strength causes the SDM to yield high relative saturation (as seen in figure 2).

The solubility of magnesium sulfite hexahydrate in water with the addition of magnesium sulfate was accurately predicted by the LCM from 0-6 molal (29). The relative saturation of the magnesium sulfite hexhydrate was predicted within 10 percent error at 40 and 50°C, and within 20 percent error at 60°C.

The LCM accurately predicted the vapor pressure of SO2 and CO2 over sulfite/bisulfite and carbonate/bicarbonate solutions, respectively, for salts of sodium, calcium, and magnesium. Figure 3 plots the LCM predictions of SO2 vapor pressure as a function of the total SO2 to sodium ratio for a sodium sulfite/bisulfite system at 50°C (30). The LCM was accurate within 20 percent error in SO2 vapor pressure for the 50°C data, as well as data at 35, 70, and 90°C. The solid line shows the general trend of the LCM predictions. Figure 4 plots the apparent equilibrium constant as a function of ionic strength for a calcium sulfite/bisulfite system at 25, 50, and 60°C (31). The LCM predicts the SO2 vapor pressure within 6 percent error for this system at all temperatures. Similar results were obtained for a system of magnesium sulfite/bisulfite with the addition of magnesium sulfate at 48.3 and 70.6°C (32). The SO2 vapor pressure was predicted within 17 percent error for this system. Data for CO2 vapor pressure analogous to the SO2 systems discussed are available to a lesser extent. CO2 vapor pressure over sodium carbonate/bicarbonate solutions (33) from 35-65°C at constant ionic strength (1 molal) were predicted within 10 percent error. CO2 vapor pressure over calcium (34) and magnesium (35) carbonate/bicarbonate solutions varying in temperature from 25-70°C, and at low ionic strength (< 1.5 molal), were predicted within 5 percent error.

NOTATION

A	Debye-Huckel constant for osmotic coefficient
B	Temperature dependent parameter
I	Ionic strength
R	Gas constant
T	Temperature (°K)
Z	Absolute value of ionic charge
a	Mean distance of closest approach
b	Empirical constant (normally 0.3)
g^{ex}	Molar excess Gibbs free energy
m	Molality

Greek Letters

γ	Activity coefficient
τ	LCM binary interaction parameter

Subscripts

ca	Salt "ca" of cation c and anion a
m	Molecular species

Superscripts

*	Unsymmetric convention
lc	Short-range local composition contribution
pdh	Long-range Pitzer-Debye-Huckel contribution

LITERATURE CITED

[1] Aspen Technology, "Aspen Plus Electrolytes Manual," June 1983 (draft).

[2] Chen, C-C, et al., "A Local Composition Model for the Excess Gibbs Energy of Multicomponent Aqueous Systems," AIChE Annual Meeting, San Francisco, November 1984.

[3] Chan, P.K., and G.T. Rochelle, "Modeling of SO2 Removal by Limestone Slurry Scrubbing: Effects of Chlorides," EPA/EPRI Symposium on Flue Gas Desulfurization, New Orleans, November 1983.

[4] Epstein, H., U.S. EPA, Environmental Protection Technology Series, EPA-650/2-75/047,PB-244901, June 1975.

[5] Faist, M.B., et al., Radian Corporation, DOE Contract No. DE-AC21-80mc14549 (1981).

[6] Harned, H.S., and B.B. Owens, The Physical Chemistry of Electrolyte Solutions, 3rd ed., Reinhold Publishing Corp. (1958).

[7] Davies, C.W., Ion Association, Butterworths, Washington, D.C. (1962).

[8] Lowell, P.S., et al., Radian Corporation, Final Report For Contract PHS CPA-22-69-138 To National Air Pollution Administration (HEW), PB 193-029 (1970).

[9] Rosenblatt, G.M., AIChE J., 27, 619 (1981).

[10] Rosenblatt, G.M., ACS Symp. Ser., 188, 57 (1980).

[11] Pitzer, K.S., J. Phys. Chem., 77, 268 (1973).

[12] Pitzer, K.S., and G. Mayorga, J. Phy. Chem., 77, 2300 (1973).

[13] Pitzer, K.S., and J.J. Kim, J. Am. Chem. Soc., 96, 5701 (1974).

[14] Maurer, G., Fluid Phase Equilibria, 13, 269 (1983).

[15] Bromley, L.A., AIChE J., 19, 313 (1973).

[16] Radian Corporation, Communication with M.B. Faist (1984).

[17] Chen, C-C, Sc.D. Thesis, Dept. of Chem. Eng., Mass. Inst. of Tech.(1980).

[18] Chen, C-C, et al., AIChE J., 25, 820 (1979).

[19] Chen, C-C, et al., AIChE J., 28, 588 (1982).

[20] Renon, H., and J.M. Prausnitz, AIChE J., 14, 135 (1968).

[21] Taylor, C.E., M.S. Thesis, Dept. of Chem. Eng., Univ. of Texas at Austin (1984).

[22] Pitzer, K.S., ACS Symp. Ser., 133, 451 (1980).

[23] Himmelblau, D.M., Applied Nonlinear Programming, McGraw-Hill, New York (1972).

[24] Robinson, R.A., and R.H. Stokes, Electrolyte Solutions, 2nd ed., Butterworths (1959).

[25] Hill, A.E., and J.H. Wills, J. Amer. Chem. Soc., 24, 674 (1902).

[26] Cameron, F.K., and J.M. Bell, J. Phys. Chem., 10, 210 (1906).

[27] Cameron, F.K., and A. Seidell, J. Phys. Chem., 5, 643 (1901).

[28] Marshall, W.L., and R. Slusher, J. Phys Chem., 70, 12 (1966).

[29] Pinaev, V.A., J. Appl. Chem. USSR, 37, 1953 (1964).

[30] Johnstone, H.F., et al., Ind. Eng. Chem., 30, 101 (1938).

[31] Kuzminykh, I.N., and M.D. Babushkina, J. Appl. Chem. USSR, 29,1601 (1956).

[32] Kuzminykh, I.N., and M.D. Babushkina, J. Appl. Chem. USSR, 30, 495 (1957).

[33] Mai, K.L., and A.L. Babb, Ind. Eng. Chem., 47, 1749 (1955).

[34] Miller, J.P., Am. J. Sci., 250, 161 (1952).

[35] Kline, W.D., J. Am. Chem. Soc., 51, 2093 (1929).

[36] CRC, Handbook of Chemistry and Physics, 59th ed., The Chemical Rubber Co., Cleveland, Ohio (1978-79).

[37] ICT, International Critical Tables of Numerical Data, Physics, Chemistry and Technology, Vols. I-VII, McGraw-Hill Book Company, Inc., New York and London (1933).

[38] Haehnel, O., J. Prakt. Chem. [2], 107, 165 (1924).

Cation	Anion	$\tau_{ca,m}$	$\tau_{m,ca}$	Data Type	Ref.
H+	SO3-2	-4.667	8.452	D	19
H+	SO4-2	-4.667	8.452	D	19
H+	HSO3-	-4.279	8.489	D	19
H+	CL-	-5.212	10.090	A	24
H+	HCO3-	-4.279	8.489	D	19
H+	CO3-2	-4.667	8.452	D	19
H+	OH-	-4.279	8.489	D	19
H+	HSO4-	-5.448	11.045	V	36
H+	AD-2	-4.667	8.452	D	19
H+	HAD-	-4.279	8.489	D	19
H+	S2O3-2	-4.667	8.452	D	19
H+	S3O6-2	-4.667	8.452	D	19
CA+2	SO3-2	-6.861	11.398	D	19
CA+2	SO4-2	-3.795	7.343	S	25
CA+2	HSO3-	-5.685	11.748	V	31
CA+2	CL-	-4.125	8.319	S	27
CA+2	HCO3-	-6.958	9.467	V	34
CA+2	CO3-2	-6.861	11.398	D	19
CA+2	OH-	-5.799	10.441	D	19
CA+2	HSO4-	-5.799	10.441	D	19
CA+2	AD-2	-6.861	11.398	D	19
CA+2	HAD-	-5.799	10.441	D	19
CA+2	S2O3-2	-4.795	9.542	V	37
CA+2	S3O6-2	-6.861	11.398	D	19

Cation	Anion	$\tau_{ca,m}$	$\tau_{m,ca}$	Data Type	Ref.
MG+2	SO3-2	-3.857	7.814	S	29
MG+2	SO4-2	-4.205	8.492	S	26
MG+2	HSO3-	-4.137	8.292	V	32
MG+2	CL-	-5.400	11.217	V	37
MG+2	HCO3-	-5.437	10.691	V	38
MG+2	CO3-2	-6.861	11.398	D	19
MG+2	OH-	-5.799	10.441	D	19
MG+2	HSO4-	-5.174	10.044	V	37
MG+2	AD-2	-6.861	11.398	D	19
MG+2	HAD-	-5.799	10.441	D	19
MG+2	S2O3-2	-6.861	11.398	D	19
MG+2	S3O6-2	-6.861	11.398	D	19
NA+	SO3-2	-2.745	5.703	V	30
NA+	SO4-2	-3.830	7.824	A,O,V	36,37,24
NA+	HSO3-	-2.735	7.779	V	30
NA+	CL-	-4.125	6.988	S	28
NA+	HCO3-	-7.196	13.109	V	33
NA+	CO3-2	-4.041	8.077	V	37
NA+	OH-	-4.816	9.644	A,O,V	36,37,24
NA+	HSO4-	-3.987	7.622	V	36,37
NA+	AD-2	-4.667	8.452	D	19
NA+	HAD-	-3.108	5.631	A,O	24
NA+	S2O3-2	-4.218	8.643	A,O,V	36,37,24
NA+	S3O6-2	-4.144	8.214	V	37

Table 1 LCM Data Base: Final Regressed Binary Parameters. (A-activity coefficient data, D-default parameters, O-osmotic coefficient data, V-vapor pressure data)

Equilibrium Constant	Implied Formation Reaction	Temperature Dependent Parameters A	B	C	D
Ksp1	CaSO4*2H2O = Ca+2 + SO4-2 + 2H2O	4096.0521	31.3476	0.0	-86.9037
Ksp2	CaSO3* ½H2O = Ca+2 + SO3-2 + ½H2O	-4646.4154	31.8594	0.0	100.2073
Ksp3	MgSO3*6H2O = Mg+2 + SO3-2 + 6H2O	8121.4199	54.1774	0.0	-157.5713
Ksp4	MgSO3*3H2O = Mg+2 + SO3-2 + 3H2O	-3181.3288	-16.6579	0.0	55.3001
Ksp5	CaCO3 (calcite) = Ca+2 + CO3-2	13797.9724	108.4748	0.0	-306.2902
Ksp6	MgCO3*3H2O = Mg+2 + CO3-2 +3H2O	-21134.1076	-143.5699	0.0	431.1240
K1	SO3-2 + SO2(aq) + H2O = 2HSO3-	2280.8662	19.6510	0.0	-60.6891
K2	SO2(aq) + H2O = H+ + HSO3-	276.8176	0.0000	0.006572	0.8521
K3	HSO3- = H+ + SO3-2	-2004.0486	-19.6510	0.006572	61.5412
HSO2	SO2(aq) = SO2(gas)	2422.8421	8.7615	0.0	-29.7136
K4	CO3-2 + CO2(aq) + H2O = 2HCO3-	-147.4864	1.2997	0.0	-6.6947
K5	CO2(aq) + H2O = H+ + HCO3-	5251.5323	36.7816	0.0	-102.2685
K6	HCO3- = H+ + CO3-2	5399.0187	35.4819	0.0	-95.5739
HCO2	CO2(aq) = CO2(gas)	2948.4426	11.4519	0.004540	-41.0371

Table 2 LCM Data Base: Implied Formation Reactions And Temperature Dependent Parameters For Equilibrium Constants. Equation form:

$$-\log K = A/T + B \log T + CT + D$$

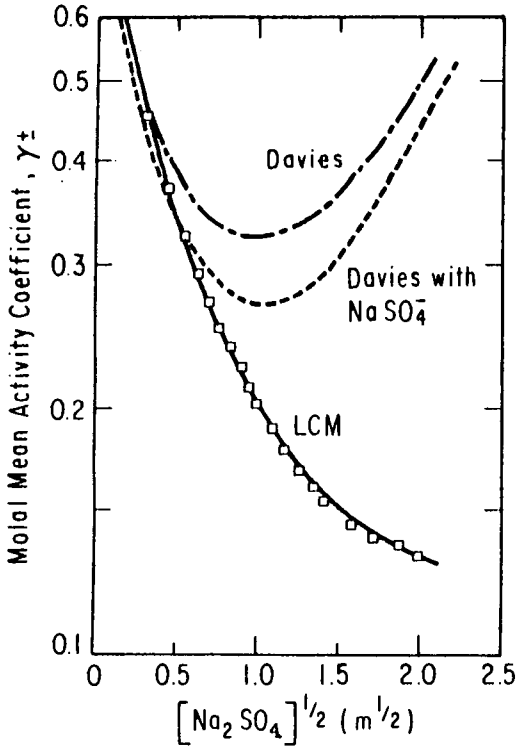

Figure 1 Comparison of SDM Davies Technique and LCM in Predicting Molal Mean Activity Coefficient (1-2 electrolyte) at 25°C. Data from Robinson and Stokes (24).

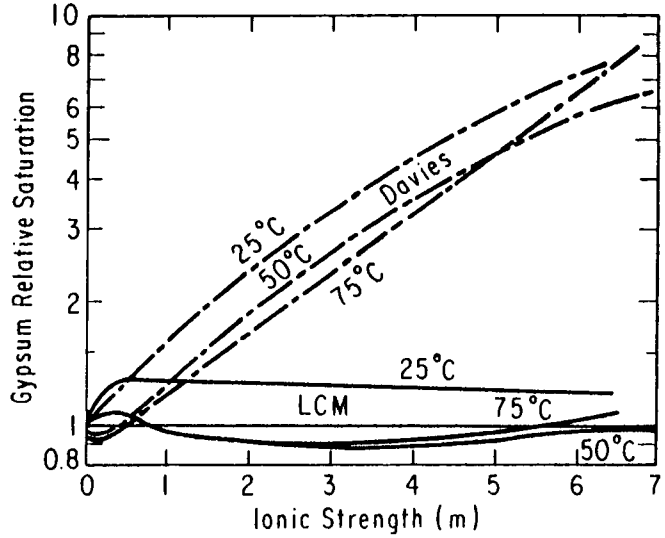

Figure 2 Comparison of SDM Davies Technique and LCM in Predicting Gypsum Relative Saturation with the Addition of Sodium Sulfate. Data from Hill and Wills (25).

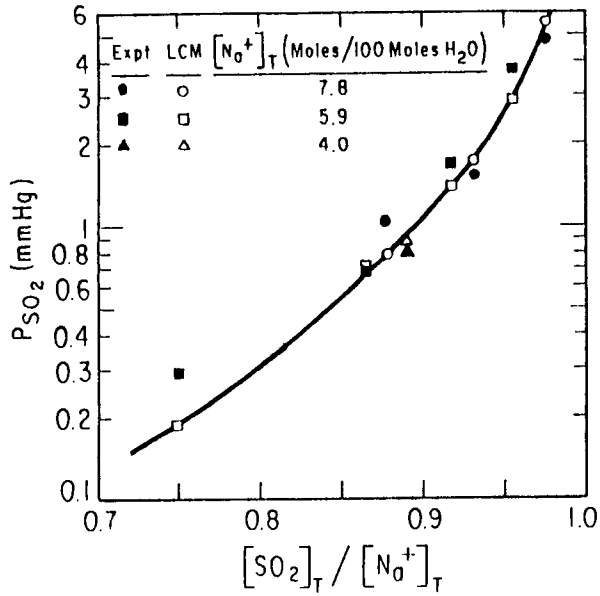

Figure 3 LCM Prediction of SO2 Vapor Pressure Over Sodium Sulfite/Bisulfite Solutions at 50°C. Data from Johnstone, et al. (30).

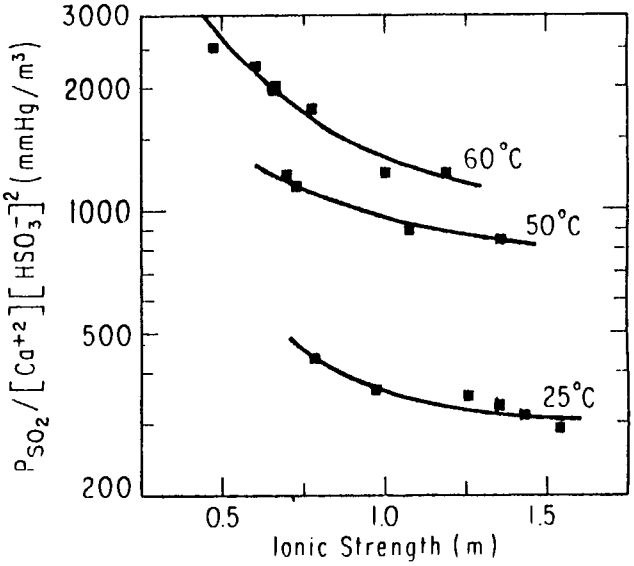

Figure 4 LCM Prediction of Apparent Equilibrium Constant in Calcium Sulfite/Bisulfite Solutions. Data from Kuzminykh and Babushkina (31).

OXIDATIVE DEGRADATION OF ORGANIC ACIDS IN FGD PROCESS

Joseph Y. Lee and Gary T. Rochelle

Dept. of Chemical Engineering, University of Texas at Austin, Austin, Texas 78712

ABSTRACT

Organic acid degradation coupled with sulfite oxidation has been studied under flue gas desulfurization (FGD) conditions. The ratio of the reaction rate constants (degradation to oxidation) was used to characterize the degradation behavior of organic acids. The ratio was shown to be independent of pH, dissolved oxygen, and dissolved sulfite/bisulfite. However, this ratio was increased by certain transition metal ions such as Co, Ni, and Fe, and was decreased by Mn and halides. Hydroxyl and sulfonated carboxylic acids degraded approximately three times slower than saturated dicarboxylic acids, while unsaturated dicarboxylic acids degraded an order of magnitude faster. A wide spectrum of dicarboxylic acid degradation products were found, including carbon dioxide, hydrocarbons, lower molecular weight mono- and dicarboxylic acids, and other carbonyl compounds.

INTRODUCTION

Currently, limestone scrubbing is the dominant commercial technology for flue gas desulfurization (FGD) (1). The performance of limestone scrubbing is chemically limited by two pH extremes: (a) low pH near the gas/liquid interface which decreases the SO_2 solubility and absorption rate; and (b) high pH near the liquid/solid interface which decreases the limestone solubility and dissolution rate (2, 3). Organic acids that buffer between pH 3.0 and pH 5.5 enhanced SO_2 removal efficiency and limestone utilization at concentrations of 5 to 10 mM (2-10).

Adipic acid was the first buffer successfully and generally applied to the FGD process (3, 9, 11, 12). It has been replaced commercially by dibasic waste acid (DBA), a waste from adipic acid and cyclohexanone production, containing primarily adipic, glutaric, and succinic acids. The effectiveness of DBA is equivalent to adipic acid (3, 9). Other potential alternatives include hydroxycarboxylic acids and sulfonated carboxylic acids (10, 13, 14). They are of interest because of reduced volatility and potentially lower degradation rates.

In addition to the expected loss of organic acid additive by entrainment of solution in waste solids, chemical degradation (15) and coprecipitation (16) losses are also observed. Chemical degradation, which is conjugated with sulfite oxidation (15), is the most important mechanism of buffer loss under forced oxidation conditions (3, 9)

A rate expression for adipic acid degradation under scrubber conditions was derived by Rochelle (15). Assuming that both sulfite oxidation (17) and organic acid degradation (18) are free radical reactions proceeding by a common radical, R• :

$$d[A]/dt = k_1 [A] [R\bullet] \qquad 1)$$

$$d[S(IV)]_t/dt = k_2 [S(IV)]_d [R\bullet] \qquad 2)$$

where, A and S(IV) stand for organic acid, sulfite/bisulfite and the subscripts d and t denote 'dissolved' and 'total' respectively, then the rate of degradation is give by

$$d[A]/dt = k_{12}([A]/[S(IV)]_d)(d[S(IV)]_t/dt) \qquad 3)$$

where $k_{12} \equiv k_1/k_2$. Previous works have correlated rates by the degradation rate constant k_d, defined as $k_{12}/[S(IV)]_d$. The most probable free radical here is $SO_4^{\bullet-}$, because of its reactivity toward alcohols which are inhibitors of sulfite oxidation (19) and because it has been cited as the active specied in the decarboxylation/oxidation of organic acids by persulfate (S_2O_8) (20, 21).

Valeric acid, glutaric acid, and hydrocarbons from ethane to butane were identified as degradation products of adipic acid (15, 16). Low pH, especially in the presence of manganese reduced the degradation of adipic acid (22). It was also found that high dissolved S(IV) reduced the degradation (23).

It is desirable to understand the degradation kinetics, the mechanism, and the additional environmental impact caused by degradation. This paper covers the degradation kinetics and products. Since decarboxylation is the major degradation pathway, and it is decarboxylation that significantly affects the buffering capacity, CO_2 evolution rate instead of the actual degradation rate is of greater interest. Furthermore, k_{12}, the ratio of k_1 to k_2 instead of k_d, will be used for most kinetic studies, since this ratio excludes the effect of $[S(IV)]_d$.

EXPERIMENTAL

The reactor used for this study was a closed system, semibatch reactor (continous to gas but batch to solution or slurry). Figure 1 gives the block diagram of the experimental apparatus.

In a typical experiment, 1.0 M synthesized $CaSO_3$ solids were slurried and oxidized in a solution containing 10 mM organic acid and 0.1 M $CaSO_4.2H_2O$ seed crystals. All experiments were performed at a constant temperature of 55°C. pH was maintained constant throughout a given experiment.

Total S(IV) was analyzed by iodometric titration of the slurry sample. Filtered samples were reheated to 55°C, the experimental temperature, and the pH was adjusted back to the original pH (4.5 - 5.5±0.01) with sodium sulfite or air oxidation. Then iodometric titration was applied to measure the dissolved S(IV). CO_2 was monitored continuously by an infrared CO_2 detector. Hydrocarbons, organic acids and liquid degradation products were analyzed by ion chromatograph exclusion (ICE, Dionex 14), gas chromatography (GC, Varian 3700), and/or gas chromatograph - mass spectrometer (GC/MS, Finnigan 4023). More detailed procedures and conditions are available elsewhere (10).

For better control of dissolved S(IV), some experiments were run with sodium sulfite solution in the presence of 10 mM organic acid and 0.3 M sodium sulfate to prevent any dramatic change in ionic strength. Only the CO_2 evolution rate was measured. The oxidation rate was fixed by the sodium sulfite titration rate. k_d and k_{12} were then calculated according to Equation 3.

RESULTS AND DISCUSSIONS

Most of the experiments were performed with adipic acid or glutaric acid. It was found that these acids degraded at practically identical rates and that the molar rate of CO_2 evolution was equal to the molar rate of degradation at the initial stage.

Sulfite Oxidation Rate - The effect of the sulfite oxidation rate on adipic acid degradation was studied in sodium sulfite solution system at pH 5.0, without addition of metal ions. When the oxidation rate, controlled by the sodium sulfite feedrate, increased from 0.0082 to 0.024 M/hr, $[S(IV)]_d$ changed from 0.74 to 1.2 mM, and the carbon dioxide evolution rate changed from 0.13 to 0.20 mM/hr. Accordingly, k_d changed from 1.58 to 0.82 M^{-1}, while k_{12} only changed from 1.17×10^{-3} to 0.99×10^{-3}. Therefore, the organic acid degradation rate is directly proportional to the sulfite oxidation rate.

pH and Dissolved S(IV) - It was generally observed that little organic acid degradation occurred in the calcium sulfite slurry system at low pH (22). However, dissolved S(IV) is significantly affected by pH in this system (Table 1). Therefore, sodium sulfite solution at pH 5.0 was used for better control of dissolved S(IV). The dissolved S(IV) variation caused by oxidation was reflected by pH change :

$$HSO_3^- + 1/2\ O_2 = H^+ + SO_4^= \qquad 4)$$

Therefore, the addition of sodium sulfite to maintain constant pH would keep dissolved S(IV) constant. The same approach has been used for the studies of limestone dissolution (24), sulfite oxidation (17, 25), and calcium sulfite dissolution /crystallization (26). The experimental data followed the rate expression nicely, and k_d was found to be inversely proportional to $[S(IV)]_d$ without addition of metal ions (Figure 2). In other words, as predicted, k_{12} was independent of $[S(IV)]_d$ which itself was a strong function of pH in calcium sulfite slurry. Further studies confirmed the null effect of pH on k_{12} (Figure 3). Therefore, it was very clear that in calcium sulfite slurry, it was $[S(IV)]_d$, not pH, that significantly controlled organic acid degradation rate. Figure 3 also indicates that k_{12} declines, in the presence of 0.1 mM Fe, as the pH increases over 5.0. Also different values of k_{12} are obtained for different catalyst conditions. These catalyst effects will be discussed later in the section on transition metals.

Oxygen - The sulfite oxidation rate can be expressed in terms of the oxygen absorption rate as :

$$R = k'(P^*_{O2} - P_{O2}) \qquad 5)$$

where P^*_{O2} and P_{O2} are vapor pressures corresponding to the saturation and bulk concentration, respectively. Experimentally, P^*_{O2} was controlled by mixing oxygen and nitrogen. The experiments shown in Figure 4 were performed with very low oxidation rate. Therefore, the solution was practically saturated to O_2 at the partial pressure in the feed gas. Figure 4 shows that k_{12} is independent of P_{O2}. Again, k_{12} values were different for different catalyst conditions.

Transition Metals - It was shown above that k_{12} is a strong function of catalyst environment. Among the transition metals, Mn and Fe are of greater interest because of their presence in the scrubbing system. Both Mn and Fe are effective catalysts for sulfite oxidation (17), and are predicted theoretically to catalyze oxidation with 0.5 power (19, 27, 28). It was observed that organic acid degradation was increased by Fe but decreased by Mn. Probably the degradation rate varied with Fe and Mn to the first and zero order, respectively. If this hypothesis is correct, k_{12} should vary with Fe to the 0.5 power and with Mn to the -0.5 power. The solubility of ferrous sulfate was limited by pH (Table 1). This limitation justifies the declining k_{12} in Figure 3. Slurry experiments using iron-free synthesized calcium sulfite solids with known amounts of added ferrous sulfate within its solubility showed that the adipic acid degradation rate constant, k_d, varied with dissolved iron to the power of 0.6 (Figure 5). However, slurry experiments with varying Mn were less quantitative but demonstrated reduced k_{12} at higher Mn (Figure 6).

The first series of transition metals except Sc and Zn were studied in sodium sulfite clear solution system. All of these transition metals except Ti and Cr, caused an increment of k_{12} (Table 2). Titanium dioxide might have a solubility problem, and chromium sulfate might interfere dissolved S(IV) measurement.

Mn is capable of two-electron transfer. Thallium (Tl), another transition metal able to transfer two electrons, was studied in calcium sulfite slurry because of the interference with dissolved S(IV) measurement. With the addition of 1 mM Tl, k_d decreased from 1.5 and 2.5 to 0.6 and 0.7 M^{-1} for pH 5.0 and pH 5.5, respectively. The mechanism is still unclear. But there is a trend that transition metals transfering one electron increase degradation while transition metals transfering two electrons decrease degradation.

Halides - It has been reported that decomposition of carboxylate salts during sulfite oxidation is suppressed by the presence of 2 to 10% by weight of chloride ion in the aqueous absorbent (29). Table 3 lists the resulting k_{12} values of adipic acid with different concentration of chloride, bromide, and iodide. Manganese effects are included for the convenience of comparison. In clear sodium sulfite solution system, chloride reduces k_{12} significantly only when its concentration is as high as 100 mM. On the other hand, the iodide effect is so strong that even in the presence of 0.1 mM Fe, 0.1 mM iodide reduces k_{12} to 0.1×10^{-3}. The corresponding value for Mn in the

absence of Fe is approximately 0.7×10^{-3}. Bromide behaves moderately. Its effect is between chloride and iodide.

Alternatives - The potential buffer additives covered here can be grouped into dicarboxylic (adipic, glutaric), hydroxycarboxylic (4-hydroxycarboxylic), sulfonated carboxylic (sulfosuccinic), and unsaturated carboxylic (maleic) acids. Sulfosuccinic acid is not commercially available, but can be easily synthesized by reaction of maleic acid with sodium sulfite (10, 30)

k_{12} is found to be a strong function of functional group (Table 4). Unsaturated maleic acid degrades about seven times faster than dicarboxylic acids, probably due to the presence of conjugated double bonds. In reducing the degradation of maleic acid, Mn is not as effective as in the case of dicarboxylic acids. Fe is inert to maleic acid degradation. On the other hand, 4-hydroxybutyric acid degrades about three times slower than dicarboxylic acids probably due to the formation of an intramolecular hydrogen bond. Sulfosuccinic acid behaves more or less in the same way as 4-hydroxybutyric acid except that Fe has no significant effect on the degradation of sulfosuccinic acid.

Degradation Products - The degradation products of adipic acid are widely distributed. They can be classified as dicarboxylic acids, monocarboxylic acids, hydroxy-carboxylic acids, keto-acids, furans, hydrocarbons, and carbon dioxide (Table 5). The degradation product distribution is also a strong function of catalyst environment. In the presence of 1 mM Mn, glutaric and valeric acids are the major products except for carbon dioxide which is the primary degradation product for all cases. In the absence of Mn, 4-formylbutyric acid is the major liquid phase product. Although oxygen would be required to generate a smaller dicarboxylic acid, the dissolved oxygen in the presence of 1 mM Mn should be practically zero because of the mass transfer-controlled sulfite oxidation. Probably, Mn is an effective carrier of oxygen to the degradation product(s).

DISCUSSIONS

The proposed rate expression for organic acid degradation is very useful for comparing the degradation behavior of different organic acids. The degradation of organic acid is directly proportional to its concentration, to the sulfite oxidation rate and inversely to the concentration of dissolved sulfite/bisulfite. However, the rate expression needs modification under different catalyst environment. In general, sulfonated organic acids and hydroxycarboxylic acids degrade much slower than adipic or glutaric acids, while unsaturated carboxylic acids, especially with conjugated doubled bonds degrade much faser.

In summary, the degradation rate constant ratio, k_{12}, is independent of dissolved sulfite/bisulfite, dissolved oxygen or pH. However, it is reduced by transition metals with two-electron transfered capability, such as Mn and Tl. It is also inhibited by halides. Mn is very effective in reducing k_{12}. Iodide is even more efficient in inhibiting degradation. On the other hand, k_{12} is enhanced by one electron-transfered transition metals, especially by Fe. It should be emphasized that pH affects the solubility of iron and calcium sulfite, which both affect the degradation. However, the effects of iron solubility and dissolved S(IV) are opposite on organic acid degradation. Therefore, low pH will not necessarily reduce organic acid degradation, even in the calcium sulfite slurry system.

The degradation product pattern of adipic acid is a strong function of catalyst environment. Manganese gives glutaric and valeric acids as the major liquid phase products, while 4-formylbutyric acid is the major corresponding product in the absence of manganese. Carbon dioxide is the major degradation product in all cases. In addition, other mono- and dicarboxylic acids, hydrocarbons, hydroxycaroxylic acids and other carbonyl compounds such as 4-oxopentanoic acid are observed as degradation products of adipic acid.

Table 1 The Effects of pH and Sulfite Oxidation Rate on the Solubility of $MnSO_4$, $FeSO_4$, and $CaSO_4 \cdot 1/2H_2O$

pH	Fe^a(mM)		Mn^b(mM)		$[S(IV)]_d$(mM)	
	Rox^c=0	Rox=0.5	Rox=0	Rox=0.5	Rox=0	Rox=0.5
4.0	0.15	0.13	0.43	0.43	34.2	27.0
4.5	0.12	0.12	0.45	0.46	24.8	14.5
5.0	0.02	0.02	0.46	0.46	9.3	5.9
5.5	≤0.01	≤0.01	0.47	0.46	3.9	1.3

a 0.1 mM was added
b 0.5 mM was added
c Rox = sulfite oxidation rate (M/hr)

Table 2 Effects of Transition Metals on k_{12} in Sodium Sulfite Solution by CO_2 Evolution from 10 mM Adipic Acid at pH 5.0, 55°C

Conc (mM)	Degradation to Oxidation Constant Ratio, $k_{12} \times 10^3$					
	Co	Ni	Cu	Ti	V	Cr
0	0.81	0.89	0.87	0.86	1.10	0.99
0.03	0.84	-	0.89	-	-	-
0.1	0.76	1.18	0.93	-	1.23	1.03
0.3	0.82	-	1.00	0.90	1.43	1.02
1.0	0.99	2.48	1.31	0.86	1.46	1.02
3.0	1.60	-	1.33	0.84	1.54	-
10.0	3.30	-	-	-	-	-
oxidation state	2,3	2,3	1,2	3,4	2,3,4,5	2,3,6

Table 3 Effects of Halide on k_{12} in Sodium Sulfite Solution by CO_2 Evolution from 10 mM Adipic Acid at pH 5.0, 55°C

Conc.(mM)	Degradation to Oxidation Constant Ratio, $k_{12} \times 10^3$			
	KCl	KBr*	KI*	$MnSO_4$
0	1.0	2.7	3.1	1.0
0.1	-	2.3	0.1	0.7
0.3	-	2.0		0.3
1	-	1.5		0.3
10	-	0.2		
30	0.8			
100	0.6			
300	0.3			

* with 1.0 mM Fe

Table 4 Comparison of Organic Acids as Buffer Additives in Terms of k_{12} at pH 5.0, 55°C, in Sodium Sulfite Solution by CO_2 Evolution

Organic Acid	Degradation to Oxidation Rate Constant Ratio, $k_{12} \times 10^3$		
	with 1 mM Mn	No Catalyst	with 0.1 mM Fe
Adipic	0.3	1.0	3.0
Glutaric	0.3	1.0	3.0
4-Hydroxybutyric	0.1	---	1.4
Sulfosuccinic	0.1	0.3	0.3
Maleic	3.6	6.7	7.0

Table 5 Degradation Products from 80% Degradation of 10 mM Adipic Acid in Calcium Sulfite Slurry with 0.1 mM Mn at pH 5.0, 55°C in Terms of the Percentage of the Initial Concentration (mM C)

	Dicarboxylic	Monocarboxylic	Hydroxycarboxylic	Hydrocarbons	Others
C6	Adipic (20)				Tetrahydro2,5furan Dicarboxylic(*)
C5	Glutaric (1.5)	Valeric (0.7)	5-Hydroxyvaleric (2.5)		4-Formylbutyric (6.7) 4-Dxopentanoic (0.3)
C4	Succinic (0.1)	Butyric (0.4)	4-Hydroxybutyric (2.5)	Butane (1.0)	3-Formylpropionic (*) Furane (0.6)
C3	Malonic (2.3)	--		Propane (*)	
C2		--		Ethane (*)	
C1		Formic (2.0)		Methane (*)	Formaldehyde (*) CO_2(49)

* less than 0.1%

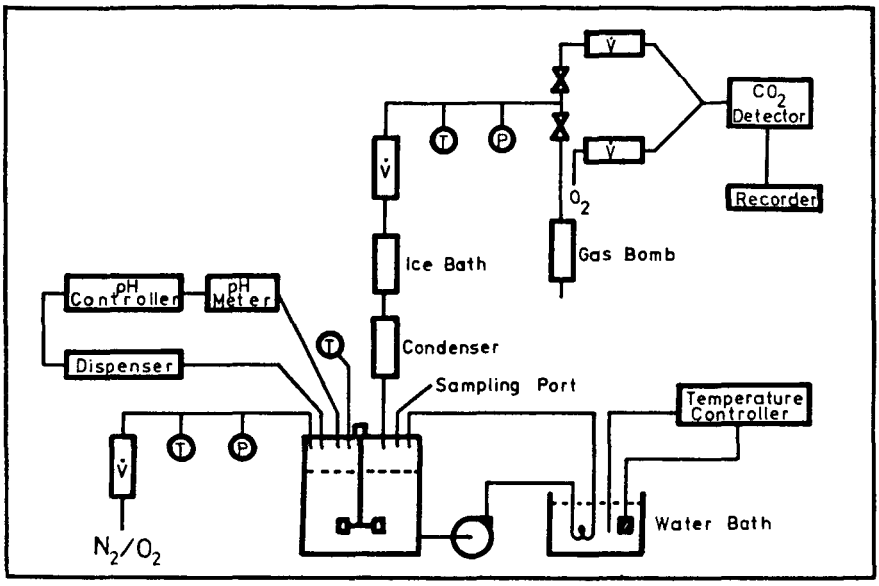

Figure 1 The Apparatus for Oxidative Degradation of Organic Acids

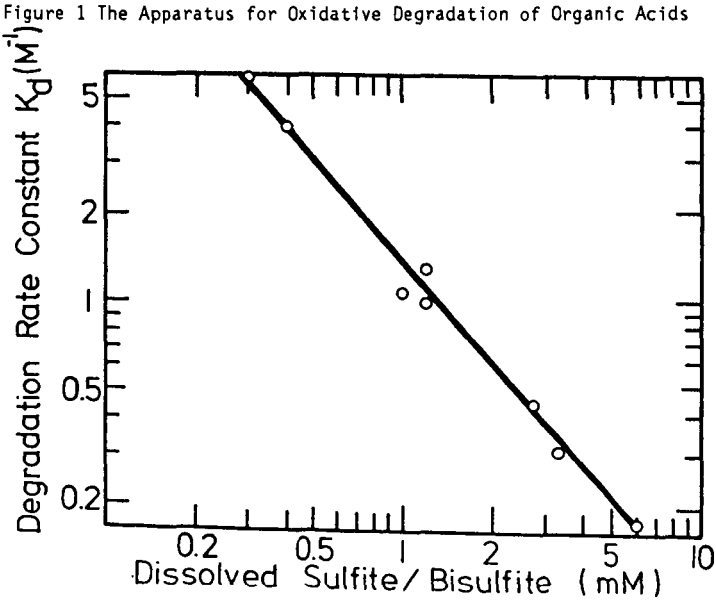

Figure 2 The Effects of Dissolved Sulfite/Bisulfite on k_d in Sodium Sulfite Solution at pH 5.0, 55°C, by CO_2 Evolution

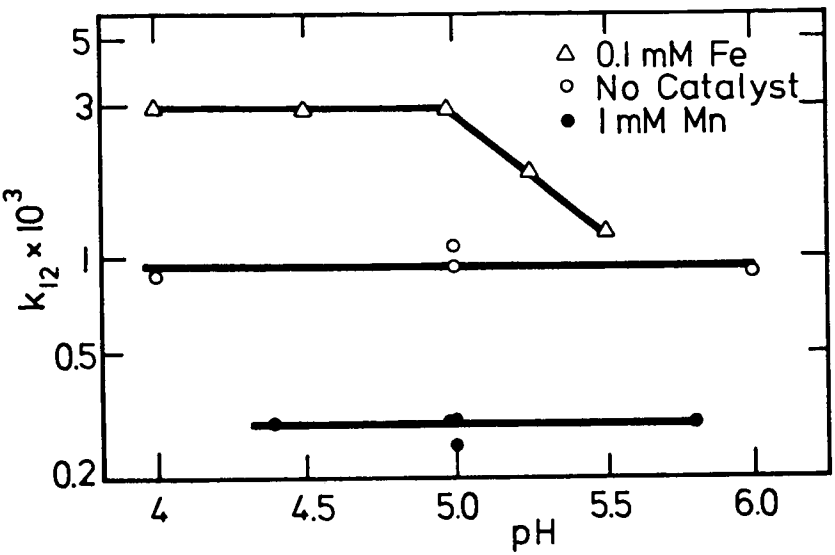

Figure 3 The Effect of pH on k_{12} in Sodium Sulfite Solution at pH 5.0, 55°C by CO_2 Evolution

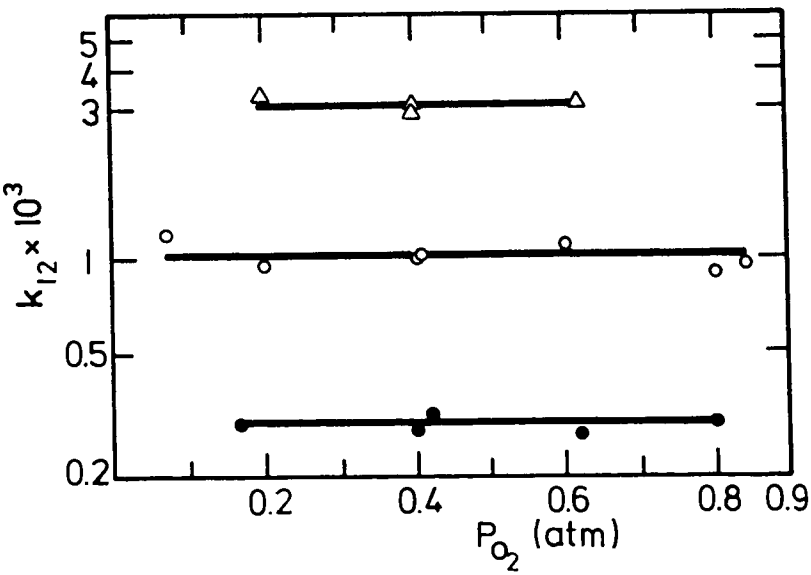

Figure 4 The Effect of Oxygen Vapor Pressor on k_{12} in Sodium Sulfite Solution at pH 5.0, 55°C by CO_2 Evolution

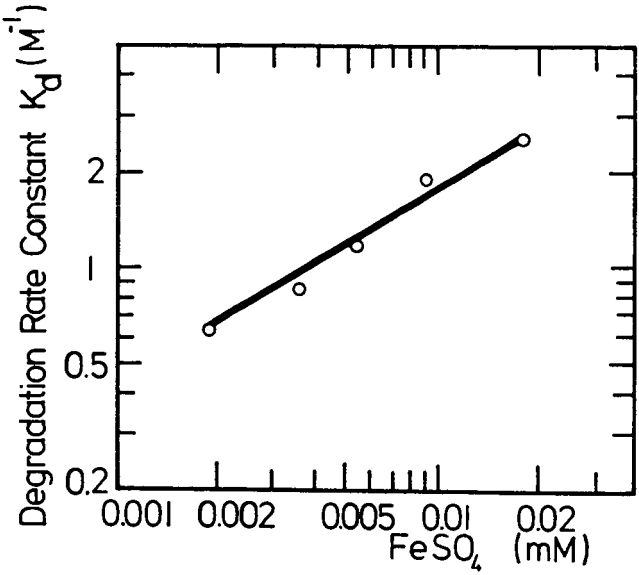

Figure 5 The Effect of Iron on k_d in Calcium Sulfite Slurry at pH 5.0, 55°C by CO_2 Evolution

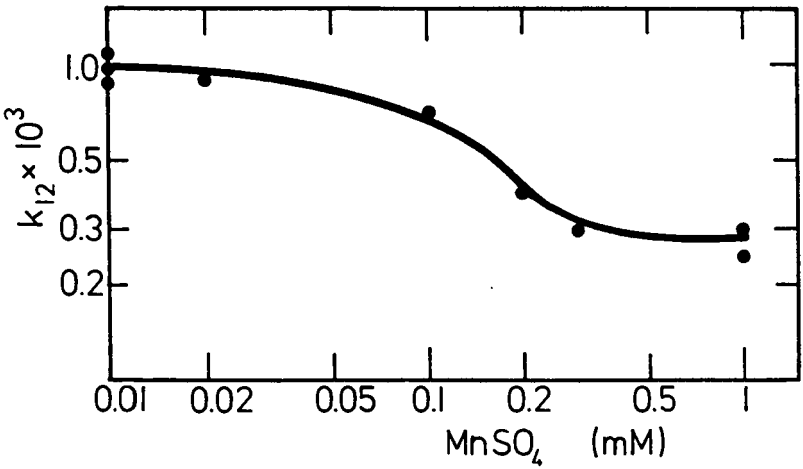

Figure 6 The Effect of Manganese on k_{12} in Calcium Sulfite Slurry at pH 5.0, 55°C by CO_2 Evolution

REFERENCES

1. Laseke, B.A., M.T. Melia, and N. Kaplan, "Trends in Commercial Applications of FGD," presented at the EPA/EPRI Symposium on Flue Gas Desulfurization, New Orleans, November (1983)

2. Rochelle, G.T. and C.J. King, "The Effect of Additives on Mass Transfer in $CaCO_3$ or CaO Slurry Scrubbing of SO_2 from Waste Gases," Ind. Eng. Chem. Fundam, 16, 67 (1977)

3. Chang, C.S. and J.D. Mobley, "Overview of EPA's Testing of the Adipic Acid Enhanced Limestone FGD Process," presented at EPA's Industry Briefing on the Adipic Acid Enhanced Limestone FGD Process, Springfield, Missouri, July (1981)

4. Burbank, D.A., S.C. Wang, R.R. McKinsey, and J.E. Williams, "Test Results on Adipic Acid Enhanced Limestone Scrubbing at the EPA Shawnee Test Facility - Third Report," Proceedings : Symposium on Flue Gas Desulfurization, Houston, EPA-600/9-81-019a, October (1980)

5. Hargrove, O.W., J.D. Colley, and J.D. Mobley, "Adipic Acid-Enhanced Limestone Flue Gas Desulfurization System commercial Demonstration," presented at Coal Technology '81, Houston, TX, November (1981)

6. Glover, R.L., G.E. Brown, N.D. Hicks, D.M. Fraley, and J.D. Moley, "Results of the First Two Years of Commercial Operation of an Organic Acid Enhanced FGD System," presented at EPA's Industry Briefing on Organic Acid Enhanced Limestone FGD Process, San Antonio, July (1984)

7. Burke, J.M. and J.D. Mobley, "Technical and Economic Evaluation of Organic Acid Addition to the San Miguel FGD System," presented at EPA's Industry Briefing on the Organic Acid Enhanced Limestone FGD Process, San Antonio, July (1984)

8. Rochelle, G.T., et al., "Buffer Additives for Lime/Limestone Slurry Scrubbing," ACS Symposium Ser. 188, 243-66 (1982)

9. Rochelle, G.T., "Buffer Additives for Limestone Scrubbing : A Review of R&D Results," presented at the EPA/EPRI Symposium on Flue Gas Desulfurization, Hollywood, FL, May (1982)

10. Rochelle, G.T., et al., "Buffer Additives for Lime/Limestone Scrubbing : Synthesis, Mass Transfer, and Degradation," EPA-60017-84-052, April (1984)

11. Borgwardt, R.H., "Significant EPA/IERL-RTP Pilot Plant Results," Proceedings : Industry Briefing on EPA's Lime/Limestone Wet Scrubbing Test Programs, EPA-600/7-79-092, March (1979)

12. Head, H.N., S.C. Wang, D.T. Rabb, R.H. Borgwardt, J.E. Williams, and M.A. Maxwell, "Recent Results from EPA's Lime/Limestone Scrubbing Program - Adipic Acid as a Scrubber Additive," Proceedings : Symposium on Flue Gas Desulfurization, Las Vegas, Nevada, EPA-600/7-70-167a, 343, July (1979)

13. Chang, C.S., "Mass Transfer with Equilibrium Chemical Reaction : Sulfur Dioxide Absorption in Aqueous Solutions", Ph.D. Dissertation, University of Texas at Austin (1979)

14. Weems, W.T., "Enhanced Absorption of Sulfur Dioxide by Sulfite and Other Buffers," M.S. Thesis, The University of Texas at Austin (1981)

15. Meserole, F.B., D.L. Lewis, A.W. Nichols, and G.T. Rochelle, "Adipic Acid Degradation Mechanism in Aqueous FGD Systems," EPA-600/7-79-224, September, (1979)

16. Jarvis, J.B., J.C. Terry, S.A. Schubert, D.L. Utley, "Effect of Trace Metals and Sulfite Oxidation on Adipic acid Degradation in FGD System," EPA-60017-82-067 (NTIS PB83-148379), Radian Corporation, Austin, Texas, December (1982)

17. Ulrich, R.K., "Sulfite Oxidation Under Flue Gas Desulfurization Conditions : Enhanced Oxygen Absorption Catalyzed by Transition Metals", Ph.D. Dissertation, The University of Texas at Austin (1983)

18. Denisov, E.T., N.I. Mitskevich, and V.E. Agabekov, "Liquid-Phase Oxidation of Oxygen Containing Compounds," Consultants Bureau, New York, (1977)

19. Hayon, E., A. Treinin, and J. Wilf, "Electronic Spectra, Photochemistry, and Autoxidation Mechanism of the Sulfite-Bisulfite-Pyrosulfite Systems : The SO_2 , SO_3 , SO_4 , and SO_5 Radicals," J. Ame. Chem. Soc. 94, 47 (1972)

20. Vasudeva, W.C., and S. Wasif, "A Kinetic Study of the Oxidation of Malonic Acid by Peroxydisulfate," J. Inorg. Nucl. Chem. 34, 3153 (1972)

21. Vasudeva, W.C., "An Electron Spin Resonance Study of Reactions of Carboxylic Acid with the Sulphate Radical-anion," J. Chem. Soc. Perkin II, 697 (1975)

22. Hsiang, M.W., "Degradation of Adipic Acid Conjugation with Sulfite Oxidation," M.S. Thesis, University of Texas at Austin (1981)

23. Chang, C.S., "Effect of Scrubbing Operating Conditions on Adipic Acid Degradation," EPA-600/7-78-017, (1981)

24. Chan, P.K., "$CaCO_3$ Dissolution in SO_2 Scrubbing Solution, Mass Transfer Enhanced by Chemical Reactions," M.S. Thesis, The University of Texas at Austin (1981)

25. Owens, D.R., "Sulfite Oxidation Inhibited by Thiosulfate," M.S. Thesis, The University of Texas at Austin (1984)

26. Tseng, C.P., "Calcium Sulfite Hemihydrate Dissolution and Crystallization," Ph.D. Dissertation, The University of Texas at Austin (1984)

27. Backstrom, H., "Der Kettenmechanisms bei der Autoxydation von Natriumsulfitlosungen," Z. Physik Chem. 25B: 122 (1934)

28. Chen, T.I., and C.H. Barron, "Some Aspects of the Homogeneous Kinetics of Sulfite Oxidation," Ind. Eng. Chem. Fundam. 11: 466 (1972)

29. Kureha Chemical Industry Co., Ltd. UK Patent Application GB 2 082 159 A

30. Smith, R.J., "Synthesis of Organic Acids for Stack Gas Desulfurization by Aqueous Scrubbing," M.S. Thesis, The University of Texas at Austin (1981)

The Potential of a Wet Process for Simultaneous Control of SO_2 and NO_x in Flue Gas†

S. G. Chang* and D. Littlejohn

Lawrence Berkeley Laboratory
University of California
Berkeley, CA 94720

Power plants release oxides of sulfur and nitrogen into the air as a result of the burning of fossil fuels. At high concentration these gases directly affect human health, and when further oxidized and hydrolyzed, they are converted into sulfuric and nitric acids and fall to earth as acid rain to corrode metals and etch buildings and monuments made of calcareous rock. Acid rain will also acidify surface and ground water to a point where toxic trace metals reach concentrations that make the water unfit for human consumption or unsuitable for aquatic animals, and inhibit crop and forest productivity. Therefore, oxides of sulfur and nitrogen in power plant flue gas should be removed before they are released to the atmosphere.

While the development of flue gas clean-up processes has been progressing for many years, a satisfactory process is not yet available. Lime/limestone wet flue gas desulfurization scrubber is the most widely used process in the utility industry at present. The wide use of this type of process is due primarily to the fact that these processes are the most technically advanced and generally the most economically attractive. In spite of this, it is expensive and accounts for about 25-35% of the capital and operating costs of a power plant. Techniques for the control of nitrogen oxides emissions in the post combustion have not been developed as extensively as those for control of sulfur dioxide emissions. Several approaches have been proposed. Among these, ammonia-based selective catalytic reduction (SCR) has received the most attention. But, SCR may not be suitable for U.S. coal-fired power plants because of reliability concerns and other unresolved technical issues. These include uncertain catalyst life, water disposal requirements, and the effects of ammonia by-products on plant components downstream from the reactor. The sensitivity of SCR processes to the cost of NH_3 is also the subject of some concern.

The development of a process that is simple and can allow an efficient removal of both SO_2 and NO_x simultaneously in one system could provide economical advantage. In the 70's, Japanese pursued this approach and developed several types of wet flue gas simultaneous desulfurization and denitrification processes which were demonstrated to be highly efficient in SO_2 and NO_x removal (about 90% for NO_x and 99% for SO_2). However, these wet processes have not reached the commercial stage yet because they are uncompetitive economically, according to cost evaluation. These cost evaluations, however, were made based on design and knowledge available at that time. Critiques have indicated that these wet processes are in their early stages of development and with their maturation, they could become competitive in cost.

The most promising type of wet process developed so far, such as Asahi process, is based on the addition of ferrous chelates in scrubbing liquor to enhance the absorption of NO by forming ferrous nitrosyl chelates in aqueous solutions. Ferrous nitrosyl chelate can then react with dissolved SO_2 to produce N_2, N_2O

† This work was supported by the Assistant Secretary for Fossil Energy, Office of Coal Research, U.S. Department of Energy under Contract Number DE-AC03-76SF00098 through the Pittsburgh Energy Technology Center, Pittsburgh, Pennsylvania.

dithionate, sulfate and various N-S compounds, while some ferrous chelate is oxidized to ferric chelates, which are inactive. Therefore, this type of process requires regeneration of scrubbing liquors by removing dithionate, sulfate, and N-S compounds from the solutions and reduction of ferric chelate back to ferrous chelates. The chemistry of this type of process is complicated and has not been well investigated. Therefore, an optimum design of a system of this type can not be achieved. This paper discusses some important factors that should be considered in identifying an optimum metal chelate catalyst and in developing an efficient scrubber for the simultaneous desulfurization and denitrification of a power plant stack gas. The kinetics and products of the reaction of ferrous nitrosyl chelates with aqueous SO_2 have been investigated. The effect of this reaction on scrubber operation is also discussed.

Thermodynamic Equilibrium and Kinetics of NO and SO_2 Absorption

The solubility of NO in aqueous solutions is very small. The solubility coefficients is 1.93 x 10^{-3} mol/L-atm at 25° C and zero ionic strength (μ). The solubility decreases with increasing temperature; the enthalpy of solution is ΔH = -2.94 Kcal/mol. The solubility of NO decreases with increasing ionic strength; this decrease amounts to approximately 8% for μ = 0.1 mol/L. The solubility of NO in aqueous solution was found to be independent of pH over the range 2-13. For 1000 ppm of NO in equilibrium with aqueous scrubbing solution at 50° C and μ = 0.1 mol/L, the concentration of NO in the aqueous phase is only 1.2 x 10^{-6} mol/L. The absorption of NO is enhanced by some water-soluble metal chelate compounds which forms complexes with NO. We have determined the equilibrium constants, enthalpy, and entropy for the coordination of NO to several ferrous chelates using a laboratory scale gas absorption apparatus and a temperature-jump apparatus. For an aqueous scrubbing solution initially containing 0.1 mol/L $Fe^{2+}(NTA)$ at 50° C, μ = 0.1 mol/L, the fraction of the iron chelate that is converted to $Fe^{2+}(NTA)NO$ is about 36% when the solution is in equilibrium with a gas containing 1000 ppm of NO at 1 atm. Thus, the presence of the $Fe^{2+}(NTA)$ increases the capacity of the scrubbing solutions of NO by a factor of 30,000 or more.

With the temperature-jump technique, we have directly measured the formation and dissociation rate constants of several ferrous nitrosyl chelates. For both $Fe^{2+}(EDTA)NO$ and $Fe^{2+}(NTA)NO$, the relaxation times due to the temperature jump were too fast to be measured. However, an upper limit of 10 μs was established for the relaxation times for both complexes.

Sulfur dioxide is moderately soluble in water. The solubility coefficient of SO_2 is 1.24 mol/L-atm at 25° C. Hydrated SO_2 can ionize to form bisulfite and sulfite ions. The equilibrium constants of these ionizations are known. The equilibrium concentrations of total aqueous S(IV) species increases with increasing solutions pH at a given partial pressure of SO_2. The rate constants of ionization of hydrated SO_2 has been measured to be very fast (3.4 x 10^6 sec^{-1} at 20° C) by Eigen et al. by using a relaxation technique.

Reaction of $Fe^{2+}(L)NO + SO_3^{=}/HSO_3^{-}$

A number of studies have been made of the reaction of ferrous nitrosyl chelates with sulfite and bisulfite ion in recent years. Reports of the reaction have indicated that is is complicated, and have not provided a complete understanding of the reaction mechanisms. There are contradictions in the literature as to what the reaction products are, as well as the kinetic behavior. We have recently studied the reaction using several different analytical techniques. The observed reaction products are Fe(III), SO_4^{2-}, $S_2O_6^{2-}$, N_2, N_2O, and N-S compounds.

Gaseous products were analyzed by an Aerograph A700 gas chromatograph with a Porapak Q column. SF_6 was used over most solutions and as a carrier gas to allow determination of N_2 generated by the reaction mixtures. Occasionally, gas samples were withdrawn and run on an A.E.I. MS12 mass spectrometer to check the results obtained by gas chromatography.

Ferrous ion concentrations were determined by the 1,10 phenanthroline method. Test solutions were acidified to pH ~ 2.5 to avoid interference from the ligands used in the reaction mixtures.

We have developed a laser Raman spectroscopic and ion chromatographic techniques that can be successfully used in the determinations of N-S compounds in reaction mixtures. Both techniques require only a small amount of the sample and allow simple, rapid and simultaneous determination of these compounds. Figure 1 shows Raman spectra of the N-S compounds along with the sulfate ion reference peak at 980 cm^{-1}. The spectra can be quantified by adding a known amount of a reference compound, such as ClO_4^-, to the sample and comparing peak heights. The peak heights must be corrected for the relative scattering efficiencies of the compounds (Table 1). Using a Dionex 2010i Ion Chromatograph with a conductivity detector, we can make determinations of N-S compounds. Figure 2 shows composite ion chromatogram of the N-S compounds.

The kinetics of the disappearance of the ferrous nitrosyl complex was monitored by observing one of the visible absorption bands of the complex with a Cary 219 spectrophotometer interfaced to an Apple II+ computer. The rate expression we obtained is:

$$\frac{d[Fe(II)(L)NO]}{dt} = k_1[HSO_3^-] + k_2[SO_3^{2-}][Fe(II)(L)NO] \qquad 1)$$

For L = EDTA at 55° C and pH 4 to 8, $k_1 = 9.0 \times 10^{-5}\ sec^{-1}$ and $k_2 = 0.60\ M^{-1}\ sec^{-1}$. These values are valid for $10^{-4}\ M < [Fe(II)(EDTA)NO] < 10^{-3}\ M$ and $10^{-3}\ M < [S(IV)] < 10^{-1}\ M$.

From the reaction products observed and their behavior, we have developed the following reaction mechanism:

$$Fe(II)(L)NO = Fe(II)(L) + NO \qquad a$$

$$NO + SO_3^{2-} \rightarrow (NO)SO_3^{2-} \qquad b$$

$$NO + NOSO_3^{2-} \rightarrow (NO)_2SO_3^{2-} \qquad c$$

$$(NO)_2SO_3^{2-} \rightarrow N_2O + SO_4^{2-} \qquad d$$

$$Fe(II)(L)NO + SO_3^{2-} = Fe(II)(L)NOSO_3^{2-} \qquad e$$

$$Fe(II)(L)NOSO_3^{2-} \rightarrow Fe(II)(L)(NO)_2SO_3^{2-} \qquad f$$

$$Fe(II)(L)(NO)_2SO_3^{2-} = Fe(II)(L) + (NO)_2SO_3^{-2} \qquad g$$

$$Fe(II)(L) + Fe(II)(L)(NO)_2SO_3^{2-} \rightarrow 2\,Fe(III)(L) + N_2O_2^{2=} + SO_3^{2-} \qquad h$$

$$Fe(II)(L)NO + HSO_3^- = Fe(II)(L)NOHSO_3^- \qquad i$$

$$2Fe(II)(L)NOHSO_3^- \rightarrow 2\,Fe(II)(L) + HON(SO_3^-)_2 + HNO \qquad j$$

$$Fe(II)(L)NOHSO_3^- + Fe(II)(L)NO \rightarrow 2Fe(II)(L) + NOSO_3^- + HNO \qquad k$$

$$HSO_3^- + NOSO_3^- \rightarrow HON(SO_3^-)_2 \qquad l$$

$$NO^- + H_2O \;=\; HNO + OH^- \qquad m$$

$$2\,HNO \;\rightarrow\; H_2N_2O_2 \qquad n$$

$$2NO^- \;\rightarrow\; N_2O_2^{2-} \qquad o$$

$$H_2N_2O_2 \;\rightarrow\; N_2O + H_2O \qquad p$$

$$N_2O_2^{2-} + H^+ \;\rightarrow\; N_2O + OH^- \qquad q$$

$$\mathrm{Fe(III)(L)} + HSO_3^- \;\rightarrow\; \mathrm{Fe(II)(L)} + SO_3^- + H^+ \qquad r$$

$$2SO_3^- \;\rightarrow\; S_2O_6^{2-} \qquad s$$

$$\mathrm{Fe(III)(L)} + SO_3^- + OH^- \;\rightarrow\; \mathrm{Fe(II)(L)} + SO_4^{2-} + H^+ \qquad t$$

This mechanism provides an explanation of the complexity of this reaction system and helps explain the results obtained by others.

Regeneration of Scrubbing Liquors

The scrubbing liquors leaving an absorber must be regenerated before being recycled back to the absorber. Ferric chelates, produced as a result of the oxidation of ferrous chelate catalysts by residual oxygen in flue gas and $^-ONNOSO_3^-$ in the system, are inactive and must be reduced back to ferrous chelates. It is known that ferric ion can react with bisulfite ion to form ferrous ion and dithionate (r and s). This reduction method has been employed in the Asahi process. Also the sulfate, dithionate, and N-S compounds produced from the reaction of ferrous nitrososulfonates and ferrous nitrosyl chelates (j, k and l) in the scrubbing liquors must be removed to prevent its buildup in the scrubbing solutions.

In the Asahi process, the flue gas enters a packed-bed absorber where it flows countercurrent to a 6.3 pH sodium-salt scrubbing solution containing $Fe^{2+}(EDTA)$. The liquid effluent from the absorber is then pumped to a reducing tank. Most of the scrubbing liquors leaving the reducing tank is recycled to the absorber. Only about 10-20% of liquors is pumped to an evaporator system in the regeneration section. The concentrated solution from the evaporators is then pumped to a cooling crystallizer where hydrated sodium dithionate and sulfate crystals are produced under vacuum. These crystals are separated from the mother liquor in a screw decanter and sent to a dryer operating at 250° F-300° F in which the hydrated crystals are converted to anhydrous sodium salts. Most of the mother liquor from the decanter is recycled to the reducing tank and a smaller stream is passed through a N-S compounds treatment section. The N-S compounds are converted to relatively insoluble potassium salts by reaction with potassium sulfate. The potassium salts of N-S compounds are separated in a screw decanter and sent to a thermal cracker for the decomposition at about 930° F.

The high capital investment cost of the Asahi process is due to the necessity for large absorbers, evaporators, crystallizers, dryers, rotary kiln crackers and screw decanter separators. The major operating and maintenance costs are electricity, fuel oil, steam and chemicals such as soda ash, EDTA and limestone. The requirement for consumption of large amount of utilities is associated with the operation principle and design of the Asahi process.

Further research areas where improvement of this type of process such as the Asahi process might be made to provide economic advantage will be discussed.

Table 1

Species	Raman Shift (cm^{-1})	Relative Molar Intensity[a]
NO	1877	-
N_2O	1285	~0.18
NO_2^-	818	0.053
	1240	~0.025
	1331	0.125
NO_3^-	1050	0.95
$N_2O_2^{2-}$	892[b]	weak[b]
	1115[b]	weak[b]
	1383[b]	strong[b]
SO_3^{2-}	967	0.12
HSO_3^-	1023	~0.10
	1055	~0.13
$SO_2 H_2O$	1152	-
$S_2O_5^{2-}$	710	0.47
	1092	1.48
SO_4^{2-}	455	~0.07
	981	1.00
HSO_4^-	1050	0.05
$(NO)_2SO_3^{2-}$	932	0.19
	1051	0.31
	1130	0.51
HADS	700	0.13
	1084	1.43
HAMS	760	0.075
	1058	0.48
ATS	1097	1.80
ADS	1084	1.02
HA (pH 7)	1004	0.21
HA (pH 9)	918	0.09
SA (pH 3)	1049	0.41
H_3BO_3	876	0.22

a. SO_4^{2-} 981 cm^{-1} = 1.000

b. J. E. Rauch and J. C. Decius, Spectochim. Acta 22, 1963 (1966)

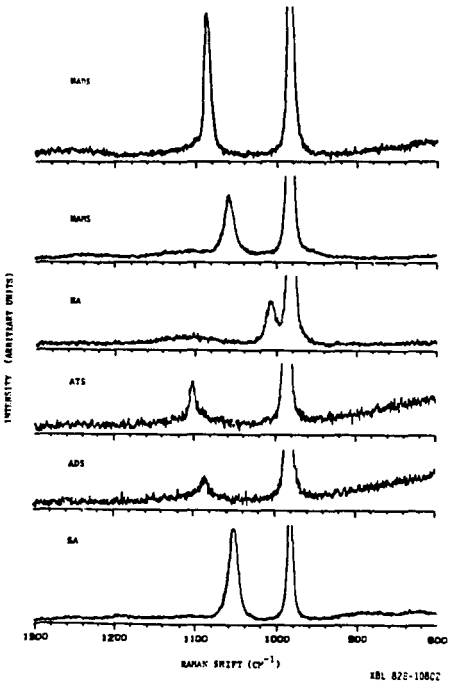

Figure 1 Raman spectra of (from top to bottom) HADS, HAMS, HA, ATS, ADS, and SA, along with $SO_4^=$ reference peak at 980 cm^{-1}.

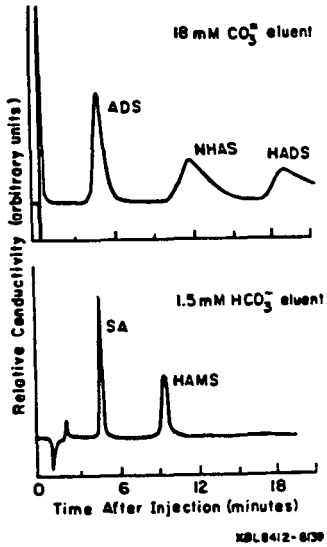

Figure 2 Ion chromatograms of ADS and HADS with 18 mM $CO_3^=$ eluent (upper trace) and SA and HAMS with 1.5mM HCO_3^- eluent (lower trace).

Chemical Kinetics of Intermediates in the Autoxidation of SO_2

Robert E. Huie

National Bureau of Standards
Gaithersburg, MD 20899

The autoxidation of aqueous solutions of sulfur dioxide (sulfite, bisulfite) is a classic problem in chemistry. Basic features of this reaction have been known since early in this century, when it was established that the reaction is trace metal ion catalyzed (1) and most likely involved free radicals (2). Certain chemical effects associated with sulfite autoxidation were noted also. Before the turn of the century, it was reported that sulfite would induce the oxidation of transition metal ions (3) and it was reported later that the oxidation of organic compounds was brought about during sulfite autoxidation (4). Conversly, it was reported also that organic compounds could serve as inhibitors of sulfite autoxidation (5).

Over the past century there have been a great many studies on sulfite autoxidation (6), including studies on the rate of the reaction in the presence of catalysts and inhibitors, measurements of the amounts of sulfite and dithionate found under various conditions, the determination of the products arising from the addition of organic (including biochemical) compounds, and studies on the effects of mixed catalysts. Yet, a quantitative understanding of the reaction has been elusive (7,8). This is due largely to a lack of quantitative data on the elementary steps in the overall reaction, including data on the rates of the free radical reactions likely to be important.

Recently, we have carried out studies on the free radical chemistry of sulfite. These studies have included kinetic measurements on the reactions of organic and inorganic free radicals with sulfite and bisulfite, and on the reactions of the sulfite derived radicals SO_3^- and SO_5^- with organic and inorganic substrates. In this paper, I will review some of our results and results from other laboratories on the radical chemistry of sulfite and discuss these results in relation to the problem of SO_2 autoxidation.

Rate constants for the radical reactions were carried out using pulse radiolysis. Briefly, a N_2O saturated solution is pulse irradiated, with high energy electrons, producing OH radicals.

$$H_2O \qquad OH,\ H,\ e^-_{aq}$$

$$e^-_{aq} + N_2O + H_2O \rightarrow N_2 + OH + OH^-$$

(The small amount of H atoms produced usually does not interfere.) The OH reacts with sulfite or bisulfite to produce the $\dot{S}O_3^-$ radical

$$OH + HSO_3^- \rightarrow H_2O + \dot{S}O_3^-$$

$$OH + SO_3^{2-} \rightarrow OH^- + \dot{S}O_3^-$$

or with some other organic or inorganic substrate to produce another desired radical

$$OH + S \rightarrow OH^- + \dot{S}^+$$

The optical absorption of $\dot{S}O_3^-$ exhibits λ_{max} = 225 nm with ϵ_{max} = $1000M^{-1}cm^{-1}$ (9). This absorption is not convenient for following the reactions of $\dot{S}O_3^-$ with other substrates since the uv absorption of most other substrates or their radicals mask this relatively weak absorption. Therefore, the optical absorption of the other radical product (or reactant) was monitored. For example, in the reaction of $\dot{S}O_3^-$ with ascorbate, the ascorbate radical absorption at 360 nm was monitored; the reaction of the radical I_2^- with HSO_3^-/SO_3^{2-} was monitored at 380 nm, the absorption maxima for I_2^-.

Oxidation of sulfite and bisulfite by free radicals

We have found that sulfite and bisulfite undergo one-electron oxidation by many free radicals to produce $\dot{S}O_3^-$. Rate constants determined for selected radicals are given in Table 1. Measurement of the rate constant over a wide range of pH has, in some cases, allowed the separate determination of rate constants for the oxidation of sulfite and bisulfite. The very strong oxidants OH and SO_4^- react very rapidly and oxidize bisulfite faster than sulfite. For radicals are weaker oxidants, the reaction with sulfite is the faster. For example, with Br_2^- the ratio of rate constants for sulfite to bisulfite is about 4; for the even weaker oxidant I_2^- the ratio is about 200. For the dimethylaniline radical cation, the reaction with sulfite is very fast ($k \sim 10^9 M^{-1}s^{-1}$) while the reaction with bisulfite is too slow to measure ($k<8x10^5 M^{-1}s^{-1}$).

These observations on both the relative and absolute rates of reaction of radicals with sulfite and bisulfite can be compared with observations made on the reactions of transition metal ions with SO_2 solutions. Typically, a strong, positive pH dependence is measured for these reactions. This usually is interpreted as suggesting that sulfite, not bisulfite, is the important reactant. Since these metal ions are relatively weak oxidants (E < 1V), this conclusion would appear to be justified. For Mn(III), which is a strong oxidant ($E_o \sim 1.4V$), reaction with bisulfite appeared to be important (10).

Reactions of sulfite radicals

Rate constants for the reactions of $\dot{S}O_3^-$ with a wide variety of organic compounds have been measured; some of these results are summarized in Table 2. The sulfite radical was found to oxidize ascorbate, trolox (a water soluble tocopherol derivative), methoxyphenol, hydroquinone and other phenolic compounds, sulfonated hydroquinones, phenylenediamines, and phenothiazines with rate constants ranging to $10^9 M^{-1}s^{-1}$.

Rate constants for one-electron redox reactions depend upon the relative reduction potentials of the reactants. We have been able to derive the one-electron reduction potential of $\dot{S}O_3^-$ by measuring the equilibrium constant for its reaction with chlorpromazine

$$SO_3^- + ClPz \rightleftarrows SO_3^{2-} + ClPz^+$$

This led to a reduction potential of 0.84V v. NHE at pH 3.6 for the couple SO_3^-/HSO_3^-. The reduction potential of the SO_3^-/SO_3^{2-} couple in basic solution is calculated (from the pKa of $HSO_3^- \rightleftarrows H^+ + SO_3^{2-}$) to be 0.63V. This change in potential helps explain why SO_3^{2-} is oxidized by the same oxidant more readily than HSO_3^-.

Using the reduction potential for SO_3^- we can calculate the one-electron reduction potential for SO_4^{2-}. In basic solution, this can be done by subtracting $E(SO_3^-)$=0.63V from twice the two-electron reduction potential for sulfite

$$SO_4^{2-} + H_2O + 2e^- \rightarrow SO_3^{2-} + 2OH^-, \; E = -0.92V.$$

This leads to

$$SO_4^{2-} + H_2O + e^- \rightarrow SO_3^- + 2OH^-, \; E= -2.47V.$$

Although this suggests that $\dot{S}O_3^-$ can act as a strong reductant, this calculation possibly seriously overstates its actual reducing power. This is because the initial product of the electron transfer would be SO_3, not SO_4^{2-} which results from subsequent hydrolysis. The enthalpy difference between $SO_3{\cdot}_{aq}$ and SO_4^{2-} is not known, but probably is greater than that between $SO_2{\cdot}_{aq}$ and SO_3^{2-} (3.24V) (11). If this is correct, the one electron potential for the SO_3/SO_3^- couple would be greater than 0.77 V and $\dot{S}O_3^-$ would therefore be a very poor reductant.

Possibly the most important reaction of the sulfite radical in autoxidation systems is with molecular oxygen. The reaction has been suggested to lead either to O_2^- or to the peroxy radical $S\dot{O}_5^-$

$$\dot{S}O_3^- + O_2 \rightarrow SO_3 + O_2^-$$

$$\dot{S}O_3^- + O_2 \rightarrow S\dot{O}_5^- \quad .$$

By determining the reactivity of the product radical with ascorbate, we were able to demonstrate that the former reaction is very unlikely and concluded that the product is the peroxy radical, $S\dot{O}_5^-$.

Reactions of the peroxysulfate radical

In Table 3 are listed some rate constants for reactions of $S\dot{O}_5^-$, along with some values for $\dot{S}O_3^-$ and $S\dot{O}_4^-$ for comparison. The results show that $S\dot{O}_5^-$ is a stronger oxidant than $\dot{S}O_3^-$ (but weaker than $S\dot{O}_4^-$) and we have estimated its one-electron reduction potential to be about 1.1V at pH

7. Of particular interest is the ability of $S\dot{O}_5^-$ to oxidize certain substances (aniline and dimethylaniline, for example) which form radicals which are capable of oxidizing sulfite. This can lead to the enhancement of the autoxidation of sulfite through the chain

$$SO_3^- + O_2 \rightarrow SO_5^-$$

$$SO_5^- + X \rightarrow SO_5^{2-} + X^+$$

$$X^+ + SO_3^{2-} \rightarrow X + SO_3^- \ .$$

In sulfite autoxidation, an exceedingly important reaction is that of SO_5^- with SO_3^{2-}/HSO_3^-. We have been able to derive a rate constant for this reaction, but have not been able to establish its mechanism.

Three paths are possible for this reaction

$$SO_5^- + SO_3^{2-} + H^+ \rightarrow HSO_5^- + SO_3^-$$

$$\rightarrow SO_4^- + SO_4^{2-} + H^+$$

$$\xrightarrow{H_2O} 2SO_4^- + OH + 2H^+$$

Since both OH and SO_4^- very rapidly oxidize SO_3^{2-} to SO_3^-, these paths are indistinguishable in our experiments. The identity of the correct path is quite important since the production of HSO_5^- can lead to possible chain branching steps. We do know that SO_5^- undergoes this one-electron reduction by a host of organic compounds. Further, the rate constants for these reactions are consistant with that derived for the reaction of $S\dot{O}_5^-$ with SO_3^{2-}. I therefore conclude that the mechanism producing HSO_5^- is the most likely.

This product of the one-electron reduction of $S\dot{O}_5^-$ (HSO_5^-, peroxymonosulfate, Caro's acid), is a strong oxidant with a standard two-electron reduction potential of 1.82V (12). A product with the properties of peroxymonosulfate has been observed with a yield up to 30% upon bubbling oxygen through a solution of sodium sulfite (13). This compound can undergo many possible subsequent reactions. From the present point of view, the most important would be the further production of free radicals, most likely upon reaction with transition metal ions, for example

$$Fe^{2+} + HSO_5^- \rightarrow Fe^{3+} + OH + SO_4^{2-}$$

$$\rightarrow Fe^{3+} + OH^- + SO_4^-$$

In a mechanism for the iron catalyzed autoxidation of sulfite, this would be a chain branching step. We have some evidence that the reaction of Fe^{2+} with HSO_5^-, in acid, does lead to free radicals, but is somewhat more complex than written above (14).

Conclusions

It has been apparent for some time that the inhibition of sulfite autoxidation by organic compounds is due to reaction of free radical intermediate with these compounds. Further, it seems likely that the chemical effects associated with SO_2 autoxidation are due to these or other reactive intermediates. Now that the reactivities of many of these intermediates are known, the mechanism of these effects can be begun to be understood. For many organic compounds, like hydroquinone and other phenolic species, reaction with SO_3^- and SO_5^- is possible. Indeed, they prove to be the most efficient inhibitors of SO_2 autoxidation. For other organic compounds like mannitol or fumarate, only reactions with SO_4^- or OH are likely. In some cases, inhibition by direct reaction with HSO_5^- might be possible.

The results we have obtained on the one-electron oxidation of sulftie and bisulfite by free radicals also are important in understanding possible chain initiation and chain carrying steps in SO_2 autoxidation. This is particularly true in systems which do not consist simply of SO_2 and a catalyst. For example, the production and subsequent reaction of halide free radicals could be important in any system containing halogen ions. The observation that many organic free radicals can react with sulfite also could be important in understanding these complex systems. Some organic free radicals can be formed easily by reaction of the parent with O_2. If these radicals react with sulfite but are otherwise stable, they could provide new, efficient, catalysts for SO_2 autoxidation.

Although the study of SO_2 autoxidation is over 100 years old, the direct study of the reactive intermediates is just beginning. In real-world systems, ranging from atmospheric droplets to flue-gas scrubbers, these reactions will take place under a wide range of pH, temperature, and ionic strength. As these reactions become better understood, they can be used to model these sytems and, ultimately to control them.

References

(1) Titoff, A.; Z. Phys. Chem. (Liepzig) 1903, 45, 641.
(2) Mathews, J. H.; Weeks, M. E., J. Am. Chem. Soc. 1917, 39, 635.
(3) For a discussion of some of this early work, see, Jorissen, W. P., "Induced Oxidation", Elsevier, Amsterdam, 1959.
(4) Kharasch, M. S.; May, E. M.; Mayo, F. R., J. Org. Chem. 1938, 3, 175.
(5) Bigelow, S. L., Z. Phys. Chem. 1898, 28, 493.
(6) Westley, F., NBS Special Pub. 630, 1982.
(7) Huie, R. E.; Peterson, N. C., in "Trace Atmospheric Constituents", S. E. Schwartz, ed.; Wiley, New York, 1983; Chapter 2.
(8) Hoffmann, M. R.; Boyce, S. D., in "Trace Atmospheric Constituents", S. E. Schwartz, ed.; Wiley, New York, 1983; Chapter 3.
(9) Hayon, E.; Treinin, A.; Wilf, J., J. Am. Chem. Soc. 1972, 94, 47.
(10) Siskos, P. A.; Peterson, N. C.; Huie, R. E., Inorg. Chem. 1984, 23, 1134.
(11) Wagman, D. D.; Evans, W. H.; Parker, V. B.; Halow, I.; Bailey, S. M.; Schumm, R. H., NBS Tech. Note 270-3, 1968.
(12) Steele, W. V., Appelman, E. H., J. Chem. Thermodynamics 1982, 14, 337.
(13) Deuvyst, E. A.; Ettel, V. A.; Mosolu, M. A., CHEMTECH, 1979, 426.
(14) Peterson, N. L; Ouellette, P. A; Huie, R. A., unpublished work.

Table 1 . Rate Constants for Reactions of Sulfite with Radicals

Reaction	pH	$k(M^{-1}s^{-1})$	reference
$OH + HSO_3^-$	-	9.5×10^9	a
$OH + SO_3^{2-}$	-	5.5×10^9	a
$SO_4^- + HSO_3^-$	-	$\geq1\times10^9$	b
$SO_4^- + SO_3^{2-}$	-	$\geq5\times10^8$	b
$Cl_2^- + SO_3^{2-}/HSO_3^-$	7	3.3×10^7	c
$Br_2^- + HSO_3^-$	4.2	6.9×10^7	d
$Br_2^- + SO_3^{2-}$	10	2.6×10^8	d
$I_2^- + HSO_3^-$	3	1.1×10^6	d
$I_2^- + HSO_3^-/SO_3^{2-}$	6.7	1×10^7	d
$I_2^- + SO_3^{2-}$	11	1.9×10^8	d
$NH_2 + SO_3^{2-}$	11	NR	d
$C_6H_5O + SO_3^{2}$	11	1×10^7	d
$C_6H_5NH_2^+ + HSO_3^-$	2.5	4.8×10^6	d
$C_6H_5NH_2^+ + SO_3^{2-}$	*	4×10^9	d
$C_6H_5NH + SO_3^{2-}$	13	$<3\times10^4$	d
$C_6H_5N(CH_3)_2^+ + HSO_3^-$	3.6	$<8\times10^5$	d
$C_6H_5N(CH_3)_2^+ + SO_3^{2-}$	10.9	9.9×10^8	d
$(chlorpromazine)^{\bullet+} + HSO_3^-$	3.6	$\sim5\times10^5$	e

NR No reaction detected ($k<10^5M^{-1}s^{-1}$). The redox potentials for NH_2 and SO_3^- radicals appear to be very similar, judging from rate constants for their reactions with several reactants.

* Calculated from the pH dependence of the rate constant.

(a) Adams, G. E.; Boag, J. W., Proc. Chem. Soc. 1964, 112.
(b) Hayon, E.; Treinin, A.; Wilf, J., J. Am. Chem. Soc. 1972, 94, 47.
(c) Hasegawa, K.; Neta, P., J. Phys. Chem. 1978, 82, 854.
(d) Neta, P.; Huie, R. E., J. Phys. Chem., submitted.
(e) Huie, R. E.; Neta, P., J. Phys. Chem., 1984, 88, 5665.

Table 2. Rate constants for Reactions of SO_3^- Radicals with Various Reactants

Reactant	pH	$k(M^{-1}s^{-1})$	reference
ascorbic acid	<3	$<10^6$	a
ascorbate ion	5-10	$9x10^6$	a
ascorbate dianion	>12	$3x10^8$	a
trolox	9	$\sim10^6$	a
phenol	11.1	$6x10^5$	b
p-methoxyphenol	9.2	$4x10^7$	b
p-methoxyphenol	12.4	$1.2x10^8$	b
hydroquinone	8.9	$4.5x10^6$	c
hydroquinone	10.5	$5.4x10^7$	c
hydroquinone	12.9	$3.2x10^8$	c
p-phenylenediamine	3.4	$<5x10^5$	d
p-phenylenediamine	5.3	$4.2x10^6$	d
p-phenylenediamine	9.3	$5.0x10^7$	d
N,N,N',N'-tetramethyl-p-phenylenediamine	4.5	$8.2x10^6$	d
N,N,N',N'-tetramethyl-p-phenylenediamine	9.5	$5.2x10^8$	d
chlorpromazine	3.6	$\sim5x10^6$	b
O_2	6.8	$1.5x10^9$	b

(a) Huie, R. E.; Neta, P., Chem. Biol. Interact., 1985, in press.
(b) Huie, R. E.; Neta, P., J. Phys. Chem., 1984, 88, 5665.
(c) Huie, R. E.; Neta, P., manuscript in preparation.
(d) Neta, P.; Huie, R. E., J. Phys. Chem., submitted

Table 3. Comparison of Some Rate Constants for Reactions of SO_3^-, SO_5^-, and SO_4^- with Organic Compounds (in $M^{-1}s^{-1}$)

Reactant	SO_3^-	SO_5^-	SO_4^-
ascorbic	$<10^6$	$2x10^6$ [a]	*
ascorbate	$9x10^6$	$1.4x10^8$ [a]	*
trolox	$\sim10^6$	$1.2x10^7$ [a]	*
aniline	(reverse)	$3x10^6$ [b]	*
N,N-dimethylaniline	(reverse)	$1x10^7$ [b]	*
tyrosine	$<10^6$		$\sim3x10^9$ [c]
tryptophan	$8x10^4$		$\sim2x10^9$ [c]
histidine	NR		$\sim2.5x10^9$ [c]
i-ProH	$<10^3$		$\sim8x10^7$ [c]
ethanol		$<10^3$ [d]	$\sim3x10^7$ [c]
fumarate	$<10^5$		$\sim2x10^7$ [c]
succinate	-	-	$7.1x10^6$ [c]
allyl alcohol	NR		$1.5x10^9$ [c]
glycine	$<10^3$		$\sim9x10^6$ [c]
HSO_3^-	-	$3x10^6$ [e]	$\sim10^9$ [c]

(a) Huie, R. E.; Neta, P., Chem. Biol. Interactions, 1985, in press.
(b) Neta, P.; Huie, R. E., J. Phys. Chem., submitted.
(c) Ross, A. B.; Neta, P., NSRDS-NBS-65, 1979
(d) Hayon, E.; Treinin, A.; Wilf, J., J. Am. Chem. Soc. 1972, 94, 47.

Acoustic Agglomeration of Power Plant Fly Ash for Environmental and Hot Gas Clean-Up

Gerhard Reethof

The Pennsylvania State University, University Park, PA 16802

INTRODUCTION AND STATEMENT OF PROBLEM

Current techniques to remove particulates in coal fired power plant flues are based on electrostatic precipitators, bag houses and wet scrubbers. Typical collection efficiencies of such devices and the far less efficient cyclones are shown in Figure 1. Of interest is the fact that below 1 μm the efficiencies drop off rather precipitously. Work presented by Davies [1], Figure 2, has shown that the human lower pulmonary system is unfortunately most efficient in absorbing and retaining particles in the 1 μm range. These particles are the primary cause of such respiratory ailments as bronchitis, emphysema and lung cancer.

Observations indicate that currently, approximately 50% of the particles suspended in an urban atmosphere are smaller than 1 μm [2]. This fact appears to be in part the result of the low efficiency of particle collection devices for the removal of these small particles. Therefore, legislation has been under consideration at the Federal level which will include recognition of particle size rather than just mass removal which is the sole criterion in current Federal legislation. California and Maryland have already legislation in effect which, as a result of a "no visible emission" statement, provides some control of submicron particulates.

The agglomeration or growth of the submicron and low micron sized particles into 5 to 20 micron sized agglomerates using high intensity acoustic fields for subsequent efficient removal by conventional particle removal devices, such as those mentioned earlier, is one of the most attractive alternatives and the subject of this paper. Acoustic agglomerators would, therefore, be aerosol conditioning devices in clean-up trains consisting for example, of a first stage of cyclones to remove the largest particles followed by an acoustic agglomeration device with the resulting enlarged particles being removed by any one of the conventional cleaning devices.

Accelerated agglomeration of particles in sound fields is not a new idea. William Ostwald first suggested the use of acoustic agglomeration to collect liquid particles as early as 1866. Notable among the early studies is the work of Smoluchowski [3], in Germany in 1915; Andrade [4]; Brandt, Freund and Hiedeman in Germany [5,6] in 1936; St. Clair [7] in the United States between 1938 and 1950; Stokes [8] in the United States in 1950. Of much interest is the work of Neumann, Danser and Soderberg and Fowle (9-14], at Ultrasonic Corporation in Cambridge, Massachusetts during the early 1950's, who developed commercially available acoustic coagulators for such diverse applications as cement plants, open hearth gas dust removal, calcinated soda removal, molybdenum disulfate, ammonium chloride, carbon black and other dust as well as liquid aerosol agglomeration. The most thorough and often quoted work was done by Mednikov [15], and other in Russia in the 1960's. More recent work by Volk [16,17] in the United States at Penn State University has shown significant agglomeration of carbon black, white lead, kaolin clay and fly ash dusts at rather modest acoustic levels, between 100 and 120 dB with frequencies in the 1000 to 6000 Hz range, representative dust loadings between 0.5 to 2 gm/m^3, and exposure times varying from 10 to 40 seconds. Scott [18], in Canada performed very interesting and important studies on the effect of nonlinear acoustic effects on agglomeration. Shaw [19 - 20], and his associates at the State University of New York at Buffalo have performed research of both a theoretical and experimental nature on acoustic agglomeration with special emphasis on the phenomena of

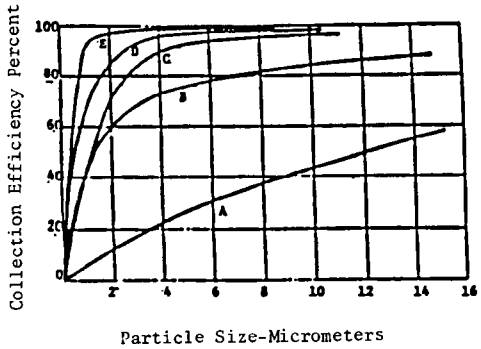

Figure 1. Collection efficiencies of seceral particle removal devices

A. High Throughout Cyclone
B. High Efficiency Cyclone
C. Dry Electrostatic Precipitator
D. Spray Tower
E. Scrubber

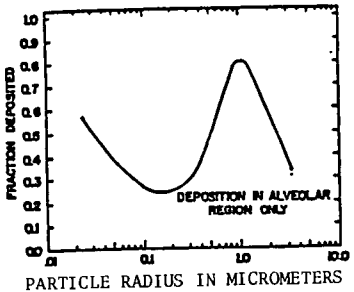

Figure 2. Absorption of particles in the human pulmonary system

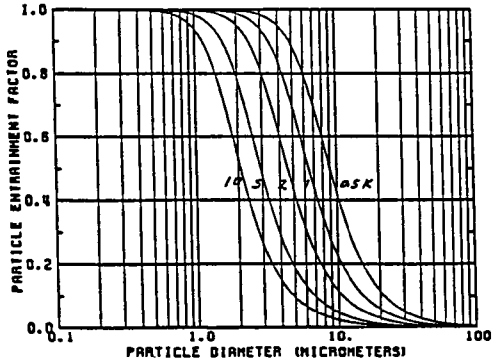

Figure 3

acoustically induced turbulence at very high levels of acoustic intensities and also the effects of acoustically induced shock waves. Research at Penn State over the last two years under the authors direction, has not been able to identify such high acoustically generated turbulence levels under similar conditions. This important subject will be discussed in the paper. On the other hand, very effective agglomeration of submicron sized particles of fly ash at flue temperatures was obtained by us with similar acoustic levels of 155-165 dB but at frequencies in the 2500 Hz range and exposure times of about 4 seconds. The details of these experiments and the theoretical foundation will also be discussed in this paper.

Recent very successful demonstrations of the high efficiencies that can be achieved with combined cycle gas turbine-steam turbine power plants using pressurized, fluidized bed coal combustion heat sources have shown that gas turbine life is severely limited because even the most efficient available hot clean-up devices cannot remove the small erosive particles from the 6 to 10 atmosphere, 1600°F gas streams. Acoustic agglomeration in conjunction with high efficiency cyclone trains appears to be the only viable means of making this promising new power plant concept feasible. We must also mention the acoustic agglomeration experiments conducted by the Braxton Corporation [22] in 1974 which did not give good results. In fact, essentially no agglomeration was experienced in this rather large scale facility. These tests which were supported by EPA, were performed at a frequency of 366 Hz and intensities of 165 dB. Redispersed cupola dust of about 4 μm mean size and fly ash of about 6 μm mean size were used as dusts. The results of our research and Dr. Shaw's work clearly show that for the type and size of dust used, frequencies on the order of 2500 Hz and 3000 Hz provide optimum agglomeration. It is, therefore, not surprising that very poor results were obtained by the Braxton experiments.

From these introductory remarks it is apparent that much work has been done on both the theoretical and the practical aspects of acoustic agglomeration.

The research results to date at Penn State University show conclusively that acoustic agglomeration of fly ash can be accomplished yet further research is required on several important acoustic and coagulation phenomena before large scale demonstration of the technical and economic viability of the process can be accomplished. Th eowrk reported has been supported by the Pittsburgh and Morgantown Energy Technology centers of the U.S. Department of Energy.

THE FUNDAMENTALS OF ACOUSTIC AGGLOMERATION OF SMALL PARTICULATES

Let us consider a polydisperse aerosol consisting of submicron and micron sized particles. The mean separation distance between particles would typically be about 100 microns. Brownian movement of the particles is caused by the collision of the thermally agitated air molecules with the particles. Also any convection currents or turbulence in the carrier gas will of course cause the particles to be partially entrained and moved in the air. If we next impose an acoustic field of acoustic pressure p, the acoustic velocity u will be given by

$$u = \frac{p}{\rho_o c} \qquad 1)$$

where ρ_o is the air density and c is the speed of sound in the air. For a typical acoustic sound pressure level of 160 dB the acoustic velocity will be about 5 m/sec (for 150 dB the acoustic velocity will drop to 0.5 m/sec, on tenth this value). For a typical acoustic frequency of 2000 Hz a fully entrained particle might flit back and forth 2000 times a second over a distance of about 600 μm. Let us next apply Newton's second law to a spherical particle equating the particle mass times its acceleration to the Stokesian or viscous drag forces

$$\frac{d}{dt}(u_p) = (u_g - u_p)\frac{18\,\mu}{\rho_p d_p^{\,2}} = (u_g - u_p)\frac{1}{\tau} \qquad 2)$$

where u_p is the particle velocity, ρ_p the particle density, d_p the particle diameter u_g the gas velocity, μ the gas dynamic viscosity and τ the particle relaxation time. The particle Reynolds number for these conditions is rather low in the range 2-10. Solution of equation (2) with $u_g = U_g \sin(\omega t-\phi)$ where ω is the acoustic frequency and t is time is of the form

$$u_p = \mu_p\, u_g \sin(\omega t-\phi) \qquad 3)$$

where η_p is the entrainment factor of the particle and ϕ is the phase angle between particle and gas motion. The factor η_p is then given by

$$\eta_p = 1/(1+\omega^2\tau^2)^{1/2} \qquad 4)$$

Thus for $\eta_p = 1$ full entrainment occurs and for $\eta_p = 0$ no entrainment occurs meaning the particle stands still. For a particle density of 2300 kg/m^3 corresponding to fly ash dust and frequencies of 500, 1000 2000, 5000, 10,000 Hz, the entrainment factor η_p is plotted for various particle diameters in Figure 3. For each of the frequencies there is a cut particle size below which particles are almost fully entrained. For example, for the 2000 Hz case the cut particle size is about 4.5 µm. The large particles compared to the cut size are essentially still, the small particles are moving through large displacementscolliding with the large particles, adhering the these particles because of the large Van der Waal forces. In a slowly convecting field we can, therefore, think of the large particles as cleaning out the small particles thereby generating empty spaces. One of the long standing unanswered questions in this field has been how the refill of these swept out volumes occurs? Every investigator in this country and abroad has assumed either explicitly or tacitly that the swept out volume would be refilled in just one cycle without giving a justification. Penn State's most recent agglomeration analytical model also is based on this premise and, as will be shown later, gives good agreement between our measurements and prediction.

We recently completed an analytical investigation of the flow field near slowly drifting spheres at Reynolds numbers from 0-10. The interaction of flow fields between two moving spherical particles of unequal size required the solution of the uncoupled Navier Stokes Equations using 5th and 6th order Runge-Kutta-Verner method and applying experimentally obtained expressions for the drag coefficient as a function of Reynolds number. Typical results are shown in Figure 6 for a 10 micron and a 1 micron particle exposed to an acoustic field of 150 dB at 2500 Hz for several acoustic cycles. The 120 micron particle remains essentially stationary and is shown at the origin of the plot. The trajectory of the central position of 9 different (one at the time) particles entering from the right side are shown with each little circle depicting the particle after each acoustic cycle. The larger the spacing between little circles along a trajectory the larger the velocity. The important conclusion to be drawn is that the flow field around the large particle causes the small particles which are vertically higher than 10 microns to assume a significant orthogonal velocity to the acoustic velocity thereby being able to refill the swept-clear volumes. Actually the particles sweep through about 250 microns during each cycle as shown in Figure 5. Our calculations show that this phenomenon explains about 85% of the refill, the rest resulting from gravitational and turbulent diffusion processes.

In a separate investigation we have determined that the agglomerates up to modest sizes are sufficiently robust to withstand the rigors of the flow through cyclones and electrostatic precipitators. The research is based on experimental

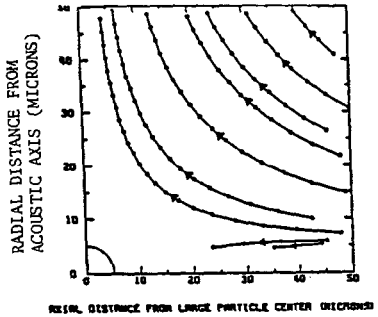

Figure 4. Hydrodynamic interaction of particles shown for several cycles

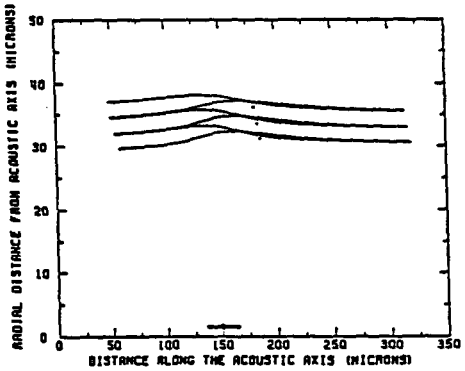

Figure 5. Hydrodynamic interaction of particles for 3 acoustic cycles. Acoustic waves of 2500 Hz frequency and 150 dB sound pressure level, particles of 1 and 10 micrometer diameter. The circles show mean positions during the acoustic cycles.

ACOUSTIC AGGLOMERATOR MODELING

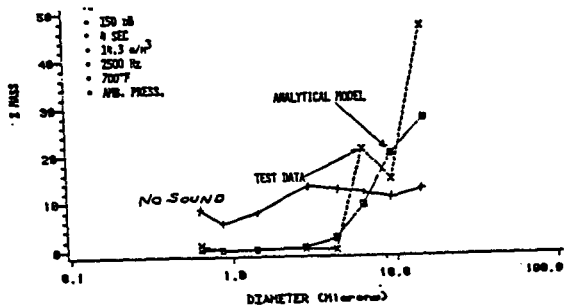

Figure 6. Results of Acoustic Agglomeration Model and Comparison with Test Data

results with inertial separation devices (impactors) and comparing the experienced shear stresses in impactors as determined from theory, with the shear stresses expected in cyclones.

A further experimental investigation has established that acoustically generated turbulence at these high acoustic intensities is not the dominant mechanism of agglomeration and that the acoustic velocities as explained earlier are the primary kinetic sources.

We have recently developed a computer code for the simulation of the agglomeration processes using these just mentioned advances in our knowledge. The principal mechanism is the orthokinetic process including also Brownian movement and several other factors. The code is in effect a simulation of the agglomeration process. The initially log normally distributed particle size distribution is divided into a number (75) of particle size ranges. As particles within ranges and particles from one range collide with particles from another range, the code moves the agglomerated particles into the range containing particles of the particular agglomerate size. The code assumes that all collisions result in agglomerations and that no break-up of agglomerates occur. Furthermore, the results of several other earlier investigations performed by us are included in the model. For example; the results of our fragility study permit us to exclude fractional agglomerate break-ups; the acoustically generated turbulence studies permit us to consider only acoustic velocity caused aerodynamic flow field; our recent results with the fluid mechanics of the flow near spheres at low Reynold's numbers permit us to assume that refill of swept out volumes occurs within just a very few oscillatory periods. A typical result is given in Figure 6 comparing experimental results from impactor measurements with our prediction. The agreement is indeed most encouraging. What is also evident from this one example is that indeed we do obtain very significant agglomeration; in fact the particles smaller than 6 microns are essentially eliminated. More on the matter later. We must point out, however, that the agreement between our idealized model and experiment is not as good for higher acoustic intensities and longer time exposures. We are continuing our research toward improving the model.

DESCRIPTION OF THE 700°F ACOUSTIC AGGLOMERATOR

We have developed and used several acoustic agglomerators over the past 11 years that we have been working in this field. We are describing here the currently operating atmospheric pressure agglomerator which permits temperatures up to 700°F, sound pressure levels from 130-165 dB, sound frequencies from 1000-4000 Hz, dust loadings from 2 gr/m^3 to 30 gr/m^3, flow rates from 0.4 to 4 ft/sec in the 8 foot long agglomeration section. Noise exposure times therefore range from 2 seconds to 20 seconds.

The agglomerator is shown in the partial sectional view in Figure 7 and the system is shown in Figure 8. Starting from the left we have the 600 acoustic watt siren designed and built at Penn State. Compressed air is provided by a Roots-type blower. Pressure to the siren is controlled by means of a bypass valve. We note that the siren is acoustically coupled to the 8-inch internal diameter agglomerator chamber by an exponential type acoustic coupler. The 9.25 inch long tubular section has 16 - 0.5 inch diameter exhaust holes for the siren air. The acoustically transparent barrier prevents the cold siren air from flowing into the heater section. The sheet of felted, woven and sintered stainless steel has a flow resistance of 110 MKS rayls giving an acoustic transmission loss of only 4 dB. By automatically controlling the pressure drop across the barrier to about 1 inch of water, we are able to minimize cold siren air flow into the agglomeration chamber. Control is obtained by an automatically controlled damper valve in the final exhaust section of the system. We sense the pressure drop by means of a Valedyne differential pressuresensor which in turn, through appropriate electronics, controls the stepping motor activated damper valve. A sluice type gate valve is installed as noted to

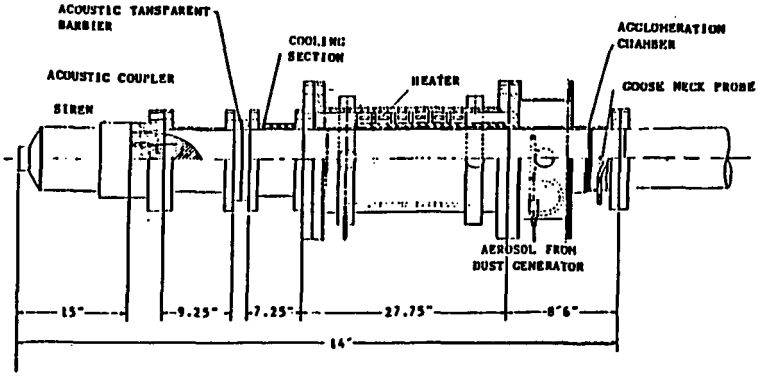

Figure 7. Moderate Temperature Acoustic Agglomerator

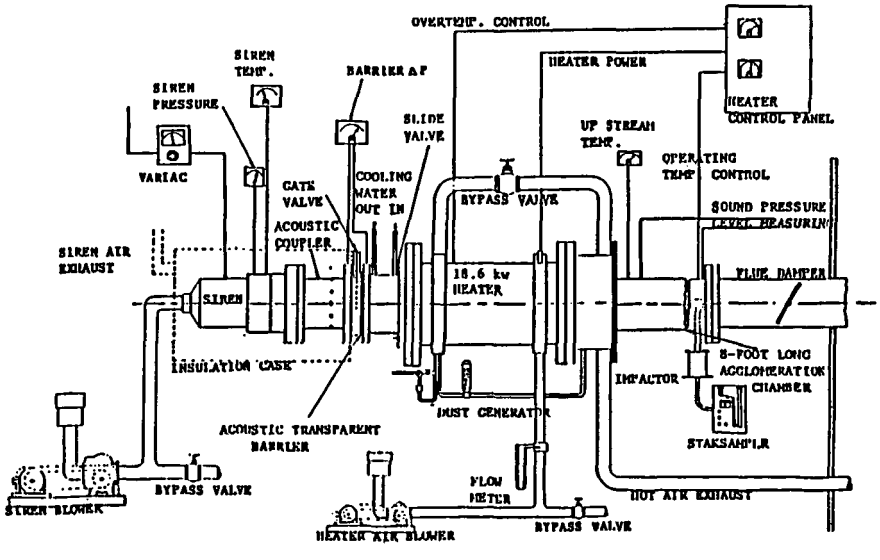

Figure 8 . Final Setup of Moderate Temperature Acoustic Agglomerator Facility

prevent hot air backflow during the many hours of heater-only time to reach the desired system temperature.

The 7.25 jacketed, water cooled section prevents heat conduction to the siren system thus protecting the wooden horn and siren from over-temperature. The heater section consists of a 14 inch schedule 40 pipe with 150 lb. flanges welded to each end. Six Chromolox Model KSEF-Koilfin electric heating elements generate 18.6 KW of heating power which is transferred to the airflow by convection. The system can be cycled at 3 Hz holding the temperature within just a few degrees. Air velocity over the heaters is 10 ft/sec. to maintain proper heating element temperatures. System schematic diagram Figure 10 shown the Roots-type blower with bypass flow control and orifice meter flow sensor providing the heating air to the system. Only about 10% to 20% of the heated air actually enters the agglomerator through 24-1/8 inch diameter angled holes. An adjustable sleeve valve controls the exposure of these holes. The excess hot air is then passed through the bypass control valve into the aerosol distribution section to heat the aerosol to the gas temperature. Finally the hot air is exhausted to the out-of-doors. The aerosol concentrate distribution system is attached to the heater flange as shown in Figure 7. Four equal length copper tubes from the aerosol manifold are connected to the four 90° spaced holes on the 8 inch diameter tube.

The aerosol generator is a simple plated standard aspirator of the type used in laboratories to obtain a vacuum source from a water supply. It is modified by removing the original vacuum line attachment and is connected to a cylindrical glass tube as the reservoir for the dust. A pulse of air traveling through the aspirator creates a short time duration low pressure which causes a controlled amount of dust from the reservoir to be sucked down the pipe line and into the agglomeration chamber. The pulsed air is produced by passing the compressed air through a solenoid valve. The time that the air is permitted to flow through the aspirator (pulse time) and the pulse frequency are controlled by a Pulse/Lapse Timer connected to the solenoid valve.

Agglomeration takes place in the 8 foot long, 8 inch schedule 40 pipe. A 1/2 inch gooseneck sampling probe is located in the end of the section. Isokinetic samples were drawn by the RAC Staksampler into an Anderson Mark III particle-sizing stack impactor which is designed for use up to 1500°F. The impactor consists of a series of plates with a number of holes arranged as shown in Figure 9 . The holes are displaced on successive plates so that a gas stream, after going through the holes in a plate, impacts a surface and must make a sharp turn to enter the holes in the next plate. The impactor operates on the theory that at each stage smaller particles flow with the air stream during the sharp turn; larger particles, due to their greater inertia, will go straight the deposit on to the plate. As shown in Figure 9 each plate has holes smaller than those in the previous plate and, therefore, the velocity increases at each stage, depositing particles of given size ranges at each level. A final filter collects any particles which remain after the last plate. A glass fiber substrate with properly located cutouts is placed on each stage as the collection medium. Each substrate is weighed before and after exposure to determine the mass of particles of each size collected; and it is dehydrated before weighing to eliminate the factor of the weight of moisture. The range of particle diameters that will collect on a plate at each stage is determined by the aerosol flow rate through the impactor.

The impactors are preheated in a small furnace to the temperature of the aerosol being tested.

The piping from the upstream heater flange to the end of the 8 foot agglomeration tube is covered completely with 2 inch thick thermal insulation (calcium silicate or Epytherm) and aluminum sheeting to reduce heat loss, increase acoustic transmission loss and reduce temperature gradients in the test section.

The acoustic pressure sensors were attached to small water jacketed coolers which were screwed into the hot agglomeration chamber pipe wall to provide protection from the high temperatures.

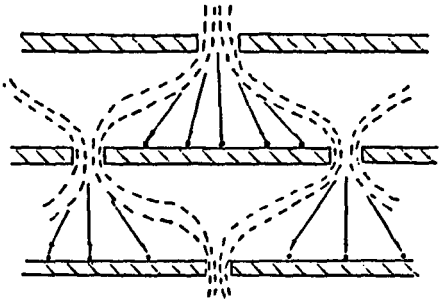

Figure 9 Schematic of Impactor Stage

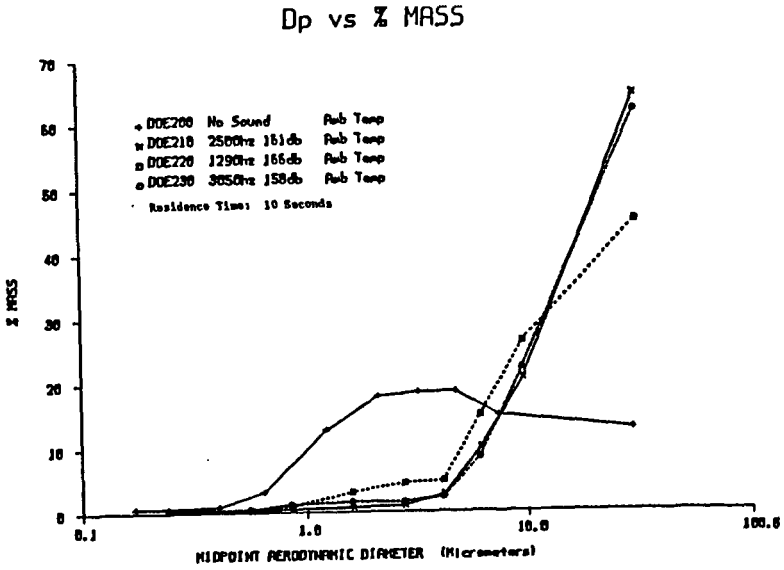

Figure 10

Because of the importance of the sound source in terms of its overall efficiency, reliability and cost, we shall describe the siren design in somewhat greater detail. Before deciding on the siren as a very promising sound source, we investigated several other potential high acoustic sound pressure sources. Hartmann Whistles (generators) provide efficiencies of about 5%. Air powered, electrically driven oscillating sleeve valve type drivers are on the market with acoustic outputs in the 2 KW to 40 KW range. Their efficiencies are in the 8% to 10% range. These latter sound sources can provide the broad band sound required in the acoustic fatigue test installations for which they were designed. Generally, they are not designed for long life applications. These sources work at considerably lower frequencies than needed for acoustic agglomeration. Another well-known high power source is the St. Clair generator which is basically a resonant cylinder vibrating in an axial mode. Kilowatt range powers in the 1 to 15 KHz range have been produced with overall efficiencies in the vicinity of 6%. Sirens have been shown to be the only sound source which promises to provide the high overall efficiencies of from 50 to 60% required for economically viable acoustic agglomerators in power plant applications. Also, properly designed sirens offer the promise of the required long life, high reliability, low operating costs and relatively low initial cost compared to other systems.

Almost all commerical sirens are used for fire and air raid warning systems. They have frequencies in the 250-500 Hz range and produce acoustic power in the 100-1000 watt range and are not very efficiency sound producers. We have, therefore, developed the technology to design high efficiency reliable sirens. Our work is built on a foundation of research at Penn State in the 1950's, some recent excellent work in Poland, Russia and in Japan. The siren used in this research develops about 600 acoustic watts in the desired frequency range giving us sound pressure levels in the 8 inch duct up to 165 dB. Almost all the energy is contained in the fundamental frequency.

Recent Experimental Results

The agglomerator has performed reliably and the results were quite repeatable. We have used a processed fly ash dust consisting primarily of Silica, Alumina and Iron Oxide particles. A typical set of results in shown in Figure 10 for a dust loading of about 2 gr/m^3 and an exposure time of 10 seconds. The results show that the maximum agglomeration for this density of dust and this particular size distribution does occur near the predicted value of 2500 Hz with clearly less agglomeration at 1290 Hz. Earlier experiments with heavier white lead dust followed prediction and gave an optimum frequency of about 1500 Hz.

Space limitations do not permit to show the full range of parametric effects.

CONCLUSIONS

Our theoretical and experimental work has shown conclusively that acoustic agglomeration does result in shifting the particle size distribution from submicron sizes into the 10 micron and above size range. In order to achieve the desired 150 to 160 dB specific acoustic powers of from 0.1 to 1 watt/cm^2 are required for plane wave propagation and less than that for standing wave chambers.

We have reached an understanding of the fundamental processes and an ability to model the process permitting us to perform approximate trade-off studies for various clean-up train strategies involving various types of clean-up devices at different locations in the system. For example, a hot gas clean-up system consisting of a pressurized, fluidized bed coal burner producing 10 atmospheres, 1650°F gas with a loading of 10,000 parts per million by weight with a particular size distribution followed by a Stairmand cyclone, an acoustic agglomerator which is followed by a high efficiency Van Tongeren cyclone. To meet the required 25 ppmw dust loading requirement we predict exposure times of 9 seconds at 155 dB, 5 seconds at 160 dB

and 3 seconds at 165 dB. Since long exposure times mean large agglomeration chambers and high acoustic intensities require more power from the power plant cost trade off optimization studies can be performed. As a general statement, we can say that the power required to operate the acoustic agglomeration system is about 0.02 to 0.5% of the power plant output. For a 250 megawatt power plant we would need anywhere from 50 KW to 1250 KW for the acoustic agglomeration system. At 50% overall efficiency the acoustic power would range from 25 KW to 625 KW. These are very large acoustic powers when compared to the acoustic power output of a 4 engine commercial jet aircraft of about 36 KW on take-off.

We are continuing our research with U.S. Department of Energy support to further improve our understanding of several important aspects of acoustic agglomeration such as acoustic energy absorption by hot gases and large particle concentrations, nonlinear acoustic phenomena, output and efficiency, the effect of acoustic agglomeration chamber geometry on the acoustic field. We are also involved in several other applications of acoustic agglomeration for dust control.

REFERENCES

1. Davies, R.N., "Dust is Dangerous", Faker & Faker Limited, London, 1953.

2. National Air Pollution Control Administration, "Air Quality Criteria for Particulate Matter", AP-69, 1969.

3. Smoluchowski, M.V., "Versuch Einer Mathematischen Theorie der Koagulationskinetik Kolloider Losungen", Z. Physik Chem., Vol. 195, 129-168, (1918).

4. Andrade, E.N. dac, "The Coagulation of Smoke by Supersonic Vibrations", Pro. Royal Society, Vol. 134, 1111-1115, (1936).

5. Brandt, O., Freund, H. and Heidemann, E., "Schwebstoffeim Schallfeld", Z. Phys., Vol. 104, No. (7-8), 511-533, (1937).

6. Brandt, O., Freund, H. and Hiedemann, E., "Zur Theorie der akustischen Koagulation", Kolloid Z, Vol. 77, No. 1, 103-115, (1936).

7. St. Clair, H.W., "Agglomeration of Smoke, Fog or Dust Particles by Sonic Waves", Industrial Engineering Chem., 2434-2438, (1949).

8. Stokes, C.A., "Sonic Agglomeration of Carbon Black Aerosols", Chemical Engineering Process, Vol. 46, No. 8, 423-432, (1950).

9. Neumann, E.P., Soderberg, C.R. and Fowle, A.R., "Design Application, Performance and Limitations of Sonic Type Flocculators and Collectors", International Committee on Air Pollution, Washington, D,C,M Air Pollution Proc. - U.S. Technical Conference, 388-393, (1950).

10. Newmann, E.P. and Norton, R.L., "Application of Sonic Energy to Commercial Aerosol Collection Problems", Chem. Eng. Progr. Symp. Sec. 1, Vol. 47, No. 1, 4-10, (1951).

11. Danser, H.W., "Eliminate Stack Dusts and Mists", Chemical Engineering, 158-160, (1950).

12. Danser, H.W. and Newmann, E.P., "Industrial Sonic Agglomeration and Collection Systems", Industrial Engineering Chem., Vol. 41, No. 11, 2439-2442, (1949).

13. Soderberg, C,R., Jr., "Industrial Application of Sonic Energy", Iron Steel Engr., Vol. 29, No. 2, 87-94, (1952).

14. Neumann, E.P. and Norton, J.L., "Application of Sonic Energy to Commercial Aerosol Collection Problems", Chemical Engineering Symposium Series No. 1, Vol. 47, 4-10 (1951).

15. Mednikov, E.P., "Acoustic Coagulation and Precipitation of Aerosols", Translated from Russian, Consultants Bureau, (1965).

16. Volk, Jr., M and Moroz, W.J., "Aerosol Coagulation in an Acoustic Field", CAES Technical Report Number 354-74, The Pennsylvania State University, University Park, Pennsylvania, 80 pages, (1974).

17. Volk, Jr., M. and R. Hogg, "Sonic Agglomeration of Aerosol Particles", CAES Report 465-77, The Pennsylvania State University, March 1977.

18. Davidson, G.A. and Scott, D.S., "Finite-Amplitude Acoustics of Aerosols", J Acoustic Soc. AM. 53 (6), pp. 1717-1729, (1973).

19. Shaw, D.T., "Recent Developments in Aerosol Science", Wiley Inter-Science, pp. 279-319, (1978).

20. Shaw D. T., and Tu, K.W., "Acoustic Particle Agglomeration Due to Hydrodynamic Interaction Between Monodisperse Aerosols", SUNY at Buffalo, NY (1979).

21. Lee, P.S., Cheng, M.T. and Shaw, D.T., "The Acoustic and Hydrodynamic Turbulence-Turbulence Interaction and Its Influence on Acoustic Particle Agglomeration", Report DOE/MC/11842-T9, 1982.

22. Braxton Corporation, "Sonic Agglomeration", Report to Environmental Protection Agency, Report No. PB234146, 1974.

EFFECTS OF MAGNESIUM AND CHLORIDE IONS ON LIMESTONE DUAL ALKALI SYSTEM PERFORMANCE

BY
John C. S. Chang
Acurex Corporation
P. O. Box 13109
Research Triangle Park, NC 27709

Norman Kaplan and Theodore G. Brna
U. S. Environmental Protection Agency
Industrial Environmental Research Laboratory
Research Triangle Park, NC 27711

ABSTRACT

Pilot plant tests have been conducted to evaluate the effects of magnesium and chloride ions on system performance of limestone-regenerated dual alkali processes under closed-loop operating conditions. It was found that limestone reactivity and solids dewatering properties are very sensitive to magnesium ion concentrations. The total magnesium ion concentration should be maintained below 1000 ppm for satisfactory performance under normal operation. A model which assumes competitive surface adsorption of calcium and magnesium ions was used to interpret the data. Limestone reactivity and solids dewatering properties decreased with the increase of chloride ion concentration. However, the effect of chloride ion accumulation was not significant until the concentration reached 80,000 ppm.

INTRODUCTION

Sodium-based dual alkali (DA) flue gas desulfurization (FGD) processes have the features of clear solution scrubbing, high SO_2 removal efficiency, low liquid-to-gas (L/G) ratio and high reliability[1]. Recent testing has demonstrated the feasibility of using limestone instead of lime for scrubbing liquor regeneration which makes DA processes more competitive with slurry scrubbing processes[2].

Since the limestone DA process uses concentrated sodium sulfite solution as the absorbent for SO_2 removal, closed water loops are desired to minimize the sodium makeup requirements. However, the closed-loop operation (i.e., the only water leaving the FGD system is through evaporation and filter cake moisture) also promotes the buildup of soluble salts in the recirculating scrubbing liquor. The primary sources of soluble salts include makeup water, reagents, and flue gas. Previous findings indicate that the accumulation of soluble salts, especially chloride ions, can have significant effects on system chemistry and scrubber performance of lime/limestone slurry FGD processes[3,4]. The most significant effects observed include decreases of equilibrium pH, SO_2 removal efficiency, and solids settling rate, and increase in gypsum scaling potential.

In order to broaden the data base of the limestone DA process and to evaluate the impacts of closed-loop operation, a series of pilot plant tests was conducted under the sponsorship of U.S. Environmental Protection Agency's (EPA) Industrial Environmental Research Laboratory in Research Triangle Park, NC (IERL-RTP). The testing concentrated on evaluating the effects of magnesium and chloride ions since appreciable accumulations of soluble salts containing these two species are expected in a limestone DA system under closed-loop operating conditions.

The current trend in power plant design is to use plant waste water (e.g., cooling tower blowdown) for FGD system makeup. Magnesium and chloride are the primary ingredients of soluble salts which enter the FGD system with plant waste water. Additional chloride ions may enter the scrubbing liquor through the absorption of HCl produced during the coal combustion process. In addition to makeup water, limestone is also an important source of magnesium ions. If closed-loop operation is used, the dissolved salts from either of the above sources can be concentrated to levels which are considerably higher than those presently observed in most systems. This paper summarizes selected results from the pilot plant study of the limestone DA process with total magnesium ion concentration up to 2000 ppm and chloride ion concentration to 150,000 ppm.

TEST FACILITIES

The IERL-RTP pilot facilities include a three-stage tray tower with 7.5 m^3/min (approximately 0.1 MW) flue gas capacity (Figure 1). The flue gas is drawn from a gas-fired boiler (no flyash is present). Pure SO_2 is injected to achieve the desired concentration in the flue gas. Regeneration of spent scrubbing liquor is performed in the four-tank-in-series reactor train with a total residence time of 80 minutes. Limestone is fed to the first reactor as 45% slurry. The feed rate is manually set as required for either pH or reactant stoichiometry control. Soda ash is added to the fourth reactor as sodium makeup. Reactor effluent slurry flows by gravity to the thickener centerwell. Clarified liquor overflows from thickener to the forward feed hold tank from which it is pumped to the tray tower. A horizontal belt filter is used for further dewatering of the thickener underflow solids.

Ultraviolet spectrophotometry (DuPont 400 SO_2 analyzer) was used to monitor the gas phase SO_2 concentrations and SO_2 removal efficiencies. The pH of scrubbing liquor in each reactor was measured hourly during pilot testing. Solid dewatering properties were characterized by hold tank slurry settling rate and filter cake insoluble solids concentration. Detailed descriptions of the test facilities and analytical procedures were reported earlier[5].

EFFECTS OF MAGNESIUM IONS

For the study of magnesium ion (Mg^{2+}) effects on the system performance of limestone dual alkali process, epsom salt ($MgSO_4 \cdot 5H_2O$) was added to adjust the Mg^{2+} concentration in the scrubbing liquor. The base case system performance was established without the addition of epsom salt; the steady-state concentration of Mg^{2+} was 355 ppm. In subsequent tests, all operating conditions -- except for Mg^{2+} concentration --were maintained constant; the concentration of Mg^{2+} was gradually increased by epsom salt addition to the first reactor. The maximum total Mg^{2+} concentration reached during this test series was 2000 ppm. The principal results of these tests are listed in Table 1. Summaries of liquor and solid analyses are listed in Tables 2 and 3.

Effects of 1000 ppm Mg^{2+}

A comparison of results obtained from run MG-1 with those from MG-2 indicated that the most significant change observed with the increase of total Mg^{2+} concentration up to 1000 ppm is the deterioration of solids dewatering properties as reflected by the decrease of insoluble solids in the filter cake. The base case (run MG-1) filter cake contained 52% solids; however, only 45% solids was obtained in the filter cake generated at 1000 ppm total Mg^{2+} concentration.

No magnesium sulfate was added to the system for run MG-3. The objective of this run was to evaluate the system performance with decreasing Mg^{2+} concentration. The mass balance indicated that the total Mg^{2+} concentration should drift down to

below 500 ppm. During the run, the total Mg^{2+} concentration decreased from 1000 ppm to about 625 ppm toward its end. A leak was discovered at the scrubber bleed/quench recirculation pump inlet which introduced air into the process stream and therefore caused high oxidation. The high oxidation, as confirmed by solids analysis results in Table 3, was reflected by increases of the sulfate-to-sulfite ratio to above 2.5. After the air leak problem was corrected, the sulfate-to-sulfite ratio decreased, but the test average was 2.4.

Very stable operation was maintained for run MG-4 without magnesium sulfate addition with the total Mg^{2+} concentration stabilizing at about 350 ppm. The sulfate-to-sulfite ratio decreased to 2.0, the filter cake insoluble solids reached 53%, and the slurry settling rate was 2.0 cm/min. The results confirmed the base case solids quality and scrubber performance obtained from run MG-1.

Effects of 2000 ppm Mg^{2+}

Epsom salt was then added to the first reactor to raise the Mg^{2+} concentration for run MG-5. No significant changes of system performance were observed except the deterioration of filter cake quality when the total Mg^{2+} concentration reached 1000 ppm. The filter cake insoluble solids dropped from 53% to 47% at 1000 ppm total Mg^{2+} concentration and confirmed the results observed during runs MG-1 and MG-2. However, a further increase of the Mg^{2+} concentration caused significant changes in system performance. When the total Mg^{2+} concentration exceeded 1500 ppm, pH decreases were observed throughout the system. The SO_2 removal efficiency also decreased. Filter cake quality deteriorated further to below 40% insoluble solids. The solids settling rate also began to drop. At 2000 ppm total Mg^{2+} concentration, a system upset with non-settling solids occurred. The solids settling rate dropped to below 0.1 cm/min, while only 28% insoluble solids were obtained from the filter cake. The pH of the regenerated liquor was 6.2 (base case pH was 6.6) and SO_2 removal efficiency was 85% (base case removal efficiency was 92%). The solids content of slurries in the reactors reached 4.7% (base case solids content was 2.1%) due to the solids carryover in the thickener overflow.

Results of Chemical Analysis

Several sets of samples were taken from each reactor and hold tank for liquid and solids analyses to characterize the system chemistry at various Mg^{2+} concentrations. Results of the chemical analyses are shown in Figures 2 to 8. Figure 2 shows the profile of total Mg^{2+} concentration across the pilot plant system. A slight drop of Mg^{2+} concentration was observed from the scrubber bleed hold tank (V-102) to the first reactor (V-105), especially for the high Mg^{2+} concentration runs. The concentration drop was not very significant since the changes were within ± 5% (the range of experimental error). However, a magnesium loss across the reactors is implied. Magnesium lost in this manner is probably coprecipitated with calcium sulfite/sulfate.

The pH profile is shown in Figure 3. A significant drop in the system pH was obtained when the total Mg^{2+} concentration was increased from 1000 to 2000 ppm. The scrubber bleed hold tank pH decreased from 6.3 to 5.6 and the forward feed hold tank pH also decreased from 6.7 to 6.2. However, the increase of pH across the reactors was observed even at 2000 ppm total Mg^{2+} concentration, indicating that the limestone dissolution was not completely stopped by increasing the Mg^{2+} concentration.

The total oxidizable sulfur (TOS) and sulfate ion concentrations are shown in Figures 4 and 5, respectively. Similar concentration levels and concentration trends were observed for both species at the three Mg^{2+} concentrations tested. Figures 4 and 5 confirm that the concentrations of important species, such as TOS and sulfate ion, were not altered by increasing the Mg^{2+} concentration by epsom salt addition.

Figure 6 shows the total alkalinity concentrations across the system. Since the TOS concentrations were maintained at about the same levels for all runs (Figure 4), the decrease of total alkalinity when total Mg^{2+} concentration was increased from 1000 to 2000 ppm reflects the pH drop caused by the increase of magnesium ion concentrations.

The calcium ion (Ca^{2+}) and total carbonate concentrations are shown in Figures 7 and 8, respectively. The concentration levels and the trends of Ca^{2+} and total carbonate profiles obtained at the three Mg^{2+} concentrations are very similar.

Solids Analysis

The product solids obtained at various magnesium ion concentrations were examined under a scanning electron microscope (SEM) to observe the detailed morphology of the individual solid particles. As can be seen in the SEM photomicrographs reproduced in Figures 9 through 12, the product solids were physically different. Figure 9 shows the solids taken at the base case conditions where the particles gave a 50 to 55% solids filter cake with agglomerates of well-defined platelets. The thickness of each platelet can be seen clearly in Figure 9b which was taken at a magnification of 5000x.

Photomicrographs of solids produced at the 1000 ppm total Mg^{2+} concentration are shown in Figure 10. Compared with the base case solids (Figure 9), the solid particles in Figure 10 were composed of thinner, smaller platelets. This was reflected in poorer filter cake qualities (45 to 50% insoluble solids).

Photomicrographs of solids produced at 2000 ppm total Mg^{2+} concentration are shown in Figure 11 which indicates the solid particles are composed of ill-defined, needle-like platelets. Furthermore, Figure 11b reveals serious crystal defects. The poor crystal properties were evidenced by an extremely low settling rate (less than 0.1 cm/min) and very few filter cake insoluble solids (less than 30%).

In summary, two significant effects of Mg^{2+} concentration on DA system performance were observed. First, the pilot plant data indicated that the solid product dewatering properties are very sensitive to Mg^{2+} concentration. Photomicrographs show that the deterioration of solids dewatering properties is caused by crystal morphology changes comprising crystal size decreases and crystal defects. Second, the limestone dissolution rate decreased as reflected by the system pH drop. This effect is not very significant until the total Mg^{2+} concentration reaches about 1000 ppm.

Surface Adsorption Model

The effect of Mg^{2+} on the dissolution rate of $CaCO_3$ has been investigated with a pH-stat laboratory experiment[6]. The results indicated that the presence of Mg^{2+} in the solution reduces the $CaCO_3$ dissolution rate. To interpret the data, it was assumed that Mg^{2+} can be adsorbed on the surface of $CaCO_3$ particles to form a surface Ca-Mg-carbonate. The adsorption reduces the dissolution rate since the surface is partially blinded by adsorbed Mg^{2+}. It was also assumed that the reduction of the dissolution rate is proportional to the fraction of the surface (θ) occupied by the adsorbed Mg^{2+}, which can be expressed by the Langmiur adsorption isotherm:

$$\theta = ac/(1 + bc) \qquad (1)$$

where a and b are constants and c is the concentration of adsorbed species.

The dissolution rate (R) can be determined from:

$$R = kA\,(1 - r^{1/2})^n \qquad (2)$$

where k is the apparent rate constant, A is the active surface area, r is the degree of $CaCO_3$ saturation, and n is a constant. In the presence of Mg^{2+}, the active surface area A is related to Θ by:

$$A = (1 - \Theta) \qquad (3)$$

The inhibition effect of Mg^{2+} on $CaCO_3$ dissolution rate can be described by the following correlation derived from Equations 1, 2 and 3.

$$(1 - R/R_0) = 1.38 \times 10^5\,[Mg^{2+}]/(1 + 1.68 \times 10^5\,[Mg^{2+}]) \qquad (4)$$

where R_0 is the dissolution rate in the absence of Mg^{2+} and $[Mg^{2+}]$ is the concentration of total magnesium in moles cm^{-3}.

In wet flue gas desulfurization processes, either dual alkali or limestone slurry, the combined effects of calcium and magnesium actually determine the limestone dissolution rate. Sjoberg's results[6] indicated that Ca^{2+} can inhibit $CaCO_3$ dissolution rate much more effectively than Mg^{2+} by the same surface adsorption phenomenon. The combined effects of Ca^{2+} and Mg^{2+} can be described as competitive adsorption, and the limestone surface will act as an ion-exchanger. The fraction of surface occupied by adsorbed Ca^{2+} and Mg^{2+} can be expressed as:

$$\Theta = \Theta_{Ca} + \Theta_{Mg} = \sum_{i=1}^{n} a_i c_i \,/\, (1 + \sum_{i=1}^{n} b_i c_i) \qquad (5)$$

where a_i and b_i are constants and c_i is the concentration of the adsorbed species i. The reduction of dissolution rate is proportional to Θ, or:

$$(1 - R/Ro) \;\alpha\; \Theta \qquad (6)$$

In the ideal case, a_i and b_i are constants independent of c_i. Therefore,

$$\frac{\Theta_{Mg}}{\Theta_{Ca}} = K' \frac{[Mg^{2+}]}{[Ca^{2+}]} \qquad (7)$$

where K' is a constant with a value of 0.033 as obtained by Sjoberg[6].

Equation (7) indicates that the relative effectiveness of Mg^{2+} and Ca^{2+} in inhibiting the limestone dissolution rate depends on the ratio of Mg^{2+} concentration to Ca^{2+} concentration. On the other hand, the sensitivity of limestone dissolution rate to the Mg^{2+} concentration is determined by the Ca^{2+} concentration. As indicated by Equation (7), when the minimum ratio (Θ_{Mg}/Θ_{Ca}) of 0.5 is required for Mg^{2+} to effectively inhibit limestone dissolution rate, dual alkali processes need only 908 ppm Mg^{2+} since the normal Ca^{2+} concentration in the first reactor is about 100 ppm. Furthermore, if competitive adsorption of Mg^{2+} and Ca^{2+} also occurred on the $CaSO_3$ surface, the adsorbed Mg^{2+} can act as an impurity which causes crystal defects and inhibits crystal growth. As a result, the properties of the solid product deteriorate with the increase of Mg^{2+} concentration as reflected by the decrease of slurry settling rate and filter cake insoluble solids obtained from pilot plant testing.

EFFECTS OF CHLORIDE IONS

Chloride ions (Cl^-) accumulating in the scrubbing liquor will be balanced by cations such as sodium (Na^+) and Mg^{2+}. Since previous data indicated that high magnesium ion concentrations are not desirable, it is expected that Na^+ will be the cation associated with the Cl^- in limestone dual alkali scrubbing solutions.

The pilot evaluation test was started on the base case (no chloride addition) conditions with 183 ppm Cl^- concentration. Industrial grade sodium chloride was then added to the third reactor to raise the Cl^- concentration to 20,000, 50,000, and 80,000 ppm, respectively. The principal results of these tests are listed in Table 4. Summaries of liquor and solids analyses are listed in Tables 5 and 6. The most significant change observed with the increase of Cl^- concentration was the decrease of system pH. While all the other variables (limestone feed rate, SO_2 feed rate, active sodium concentration, sulfate-to-sulfite ratio, etc.) were maintained at approximately constant levels, the pH of regenerated liquor decreased from 6.6 to 6.5, 6.3, and 6.2 as the Cl^- concentration increased from the base case to 20,000, 50,000, and 80,000 ppm, respectively. Correspondingly, the SO_2 removal efficiency also dropped slightly from 93 to 92, 91, and 90%, respectively. In order to maintain constant total alkalinity concentrations, the soda ash make-up rate was increased by more than 50%. No significant changes in solids quality were observed with the increase of Cl^- concentration when the Cl^- concentration was below 80,000 ppm. The filter cake insoluble solids content fluctuated between 50 and 55% and the sulfate-to-sulfite ratio dropped slightly from 1.9 to 1.8. Filter cake analyses indicated that the overall oxidation decreased from 6.9% to 4.0% as the Cl^- concentration increased from the base case level to 80,000 ppm.

Chloride ion concentrations of 100,000 ppm and 150,000 ppm were also tested. Corresponding to these Cl^- concentrations, the Na^+ concentrations reached 116,900 ppm and 140,500 ppm, respectively. As observed in previous runs, the system pH dropped with the increase of Cl^- concentration. The base case (no chloride addition) regenerated liquor pH was 6.7. At 100,000 ppm Cl^- concentration, the regenerated liquor pH fell to 6.1. The regenerated liquor pH further decreased to 5.9 when the Cl^- concentration was increased to 150,000 ppm.

The most significant operating problem encountered during runs with 100,000 and 150,000 ppm Cl^- was scaling in the absorber. The quench nozzle scaled and plugged, and a very high pressure drop (over 10 in. H_2O) across the absorber was obtained. Layers of hard scale composed of $CaSO_3/SO_4$ were found on the absorber walls. A large quantity of water soluble sodium scale was deposited beneath the middle and the bottom trays. Neither scale contained significant amounts of chloride.

In addition to scaling, system performance also deteriorated. Only 86% SO_2 removal efficiency was obtained at 150,000 ppm chloride, significantly lower than the 93% at base case conditions. Filter cake insoluble solids also decreased to 39% compared with 50 to 55% for the base case. Decreases of TOS and total alkalinity concentrations were observed and reflected the increased liquor loss and sodium consumption.

SUMMARY

In summary, the pilot plant data indicate that:

- The solid product dewatering properties are very sensitive to Mg^{2+} concentration. Significant drops (5% or more) of filter cake insoluble solid concentrations were obtained with the increase of total Mg^{2+} concentration from 500 ppm to 1000 ppm. Solids quality deteriorated rapidly after the

total magnesium ion concentration exceeded 1000 ppm. At a total Mg^{2+} concentration of 2000 ppm, a system upset with non-settling solids occurred. The solids settling rate dropped below 0.1 cm/min, and only 28% insoluble solids were obtained from the filter cake. Scanning electron micrographs showed that the deterioration of solids dewatering properties was caused by crystal morphology changes reflecting crystal size decreases and crystal defects.

- The limestone dissolution rate decreased as shown by decreasing system pH with increasing Mg^{2+} concentration. This effect is relatively small until the total magnesium ion concentrations reach about 1000 ppm.

- The effect of Mg^{2+} concentration on limestone dissolution rate can be explained by a surface adsorption model. The adsorption of Mg^{2+} reduces the limestone dissolution rate because the surface is partially blinded by the adsorbed magnesium ions. The competitive adsorption of calcium and magnesium ions was described by a mathematical model based on the Langmuir adsorption isotherm. The model was used to explain the sensitivity of limestone dissolution rate to magnesium ion concentration under limestone dual alkali operating conditions.

- When the chloride ion concentration is below 80,000 ppm, the most significant change observed with the increase of Cl^- concentration was the decrease of system pH. Correspondingly, slight drops of SO_2 removal efficiency were also obtained.

- When the chloride ion concentration is above 100,000 ppm, system performance deteriorated with the increase of chloride ion concentration. In addition to the decreasing scrubbing solution pH and SO_2 removal efficiency, the filter cake insoluble solids also decreased and resulted in increased liquor losses and sodium consumptions.

REFERENCES

1. Kaplan, N., "Summary of Utility Dual Alkali Systems," Proceedings: EPA Flue Gas Desulfurization Symposium (Las Vegas, March 1979), Volume 2, EPA-600/7-79-1676, July, 1979.

2. Chang, J. C. and N. Kaplan, "Pilot Evaluation of Limestone Regenerated Dual Alkali Process," presented at the 8th EPA/EPRI Flue Gas Desulfurization Symposium, New Orleans, LA, November, 1983.

3. Chang, J. C., "Pilot Plant Tests of Chloride Ion Effects on Wet FGD System Performance," EPA-600/15-7-84-039, May 1984.

4. Laslo, D., J. C. Chang, and J. D. Mobley, "Pilot Plant Tests on the Effects of Dissolved Salts on Lime/Limestone FGD Chemistry," Presented at the 8th EPA/EPRI Flue Gas Desulfurization Symposium, New Orleans, LA, November, 1983.

5. Chang, J. C., J. H. Dempsey, and N. Kaplan, "Pilot Testing of Limestone Regeneration in Dual Alkali Processes," Proceedings: Symposium on Flue Gas Desulfurization," EPRI CS-2897, March, 1983.

6. Sjoberg, E. L., "Kinetics and Mechanism of Calcite Dissolution in Aqueous Solutions at Low Temperatures," Stockholm Contributions in Geology, 32(1), 1981.

TABLE 1. MAGNESIUM-ION-EFFECT TEST CONDITIONS

Run	MG-1	MG-2	MG-3	MG-4	MG-5
Mg^{2+} concentration, ppm	355	1060	625	356	2000
Tower pressure drop, in. H_2O	8.1	8.4	7.9	7.8	8.2
Liquor forward feed, gpm	1.4	1.4	1.4	1.4	1.4
Scrubber feed pH	6.6	6.6	6.6	6.6	6.2
Scrubber effluent pH	6.2	6.2	6.2	6.2	5.6
Inlet SO_2 concentration, ppm	3010	2990	2990	3050	3020
SO_2 feed rate, lb/hr	6.7	6.7	6.6	6.7	6.6
SO_2 absorption, wt. %	92.7	91.8	91.0	92	85
SO_2 make-per-pass, mmol/l	139	137	132	138	125
Limestone slurry feed rate, lb/hr	23	23	22	22	22
Limestone slurry solids, wt. %	45	45	45	45	45
Flue gas O_2, vol. %	6.4	7.0	6.1	6.9	7.2
Thickener solids, wt. %	19	18	16	20.1	7.8
Filter cake solids, wt. % (insoluble)	52	45	48	53	28
Filter wash rate (nominal), gph	3	3	3	3	3
Na concentration, g/l	57	55.6	57.4	54.0	49.7
TOS, gmol/l	0.72	0.67	0.70	0.74	0.67
Ca concentration, ppm	88	52	74	62	58
Total alkalinity, gmol/l (V-113)	0.42	0.41	0.38	0.42	0.28
Na in filter cake, mg/g[a]	15.5	18.6	16.9	12.6	(d)
Run time, hours	81	78	85	92	67
Limestone stoichiometry[b]	1.07	1.08	1.06	1.03	1.13
Settling rate (reactor), cm/min	2.0	1.9	2.2	2.2	<0.1
Settling test % solids	2.1	2.1	2.6	2.1	4.7
Active Na, gmol/l[c]	1.14	1.08	1.08	1.16	0.95
SO_4/sulfite	2.05	2.15	2.4	2.0	3.2

[a] Washed in the belt filter
[b] Mass balance
[c] Active Na = TOS + Total Alkalinity, gmol/l
[d] Data not available

TABLE 2. SUMMARY OF THICKENER LIQUOR ANALYSIS FROM MAGNESIUM-ION-EFFECT TESTS

Run No.	MG-1	MG-2	MG-3	MG-4	MG-5
Component, g/l					
Ca	0.088	0.052	0.074	0.062	0.058
Mg	0.355	1.06	0.625	0.356	2.02
Na	57.0	55.6	57.4	54.0	49.7
TOS as SO_3	57.6	53.6	55.6	59.3	53.6
SO_4	82.6	84.5	86.4	80.6	86.4
CO_3	2.73	2.54	2.35	2.1	2.03
Cl^-	0.165	0.174	0.192	0.182	0.175
pH	6.7	6.7	6.6	6.7	6.2

TABLE 3. SUMMARY OF FILTER CAKE ANALYSIS FROM MAGNESIUM-ION-EFFECT TESTS

Run No.	MG-1	MG-2	MG-3	MG-4	MG-5
Component, mg/g					
Total S as SO_3	529	522	525	509	511
TOS as SO_2	379	378	363	382	376
Carbonate as CO_2	42	47	43	42	56
Ca	294	297	298	296	298
Mg	2.6	3.4	2.8	2.5	3.6
Na	5.7	5.8	5.8	4.4	5.3
Oxidation, %	10.4	9.5	13.6	6.2	8.0
L/S Utilization, %[a]	89.9	87.8	88.1	86.0	85.7

[a] SO_3/Ca
[b] data not available

TABLE 4. CHLORIDE-ION-EFFECT TEST CONDITIONS

Run No.	CL-1	CL-2	CL-3	CL-4	CL-5	CL-6
Cl^- concentration, ppm	Base Case	20000	50000	80000	100000	150000
Tower pressure drop, in. H_2O	8.0	8.1	8.1	8.2	8.9	10.2
Liquor forward feed, gpm	1.4	1.4	-(d)	1.4	1.4	1.4
Scrubber feed pH	6.6	6.5	6.3	6.2	6.1	5.9
Scrubber effluent pH	6.2	6.1	5.9	5.8	5.7	5.5
Inlet SO_2 concentration, ppm	3040	3010	3060	3010	3030	3010
SO_2 feed rate, lb/hr	6.6	6.7	6.7	6.6	6.6	6.7
SO_2 absorption, %	93	92	91	90	89	86
SO_2 make-per-pass, mmol/l	137.1	137.7	-	122.7	131	129
Limestone slurry feed rate, lb/hr	22	22	22	22	22	22
Limestone slurry solids, wt. %	45	45	45	45	45	45
Flue gas O_2, vol. %	5.6	5.1	5.3	4.7	5.2	5.1
Thickener solids, wt. %	22.8	19.8	23.4	22.1	18.1	20.2
Filter cake solids, wt. % (insoluble)	53	52	51	52	48	39
Filter wash rate (nominal), gph	3	3	3	3	3	3
Na concentration, g/l	47.8	59.6	78.8	96.9	116.9	140.5
TOS, gmol/l	0.70	0.65	0.66	0.64	0.61	0.47
Ca concentration, ppm	61	57	58	49	51	36
Total alkalinity, gmol/l (V-113)	0.44	0.41	0.40	0.39	0.34	0.29
Na in filter cake, mg/g[a]	8.2	9.4	13.3	14.6	17.7	24.5
Run time, hours	85	62	68	58	84	72
Limestone stoichiometry[b]	1.03	1.03	1.04	1.07	1.08	1.10
Settling rate (reactor), cm/min	2.3	2.1	1.8	1.9	1.8	1.7
Settling test % solids	2.0	1.9	2.7	1.8	2.1	2.4
Active Na, gmol/l[c]	1.14	1.06	1.06	1.03	0.95	0.76
SO_4/Sulfite	1.9	1.9	1.8	1.8	1.84	1.72

[a] Washed in the belt filter
[b] Mass balance
[c] Active Na = TOS + Total Alkalinity, gmol/l
[d] Flowmeter not operational

TABLE 5. SUMMARY OF THICKENER LIQUOR ANALYSIS FROM CHLORIDE-ION-EFFECT TESTS

Run No.	CL-1	CL-2	CL-3	CL-4	CL-5	CL-6
Component, g/l						
Ca	0.061	0.057	0.058	0.049	0.051	0.036
Mg	0.344	0.298	0.333	0.247	0.176	0.072
Na	47.8	59.6	78.8	96.9	116.9	140.5
TOS as SO_3	56.0	52.0	52.8	51.2	48.6	37.6
SO_4	80.3	76.2	69.1	67.3	60.2	48.0
CO_3	2.68	2.25	2.12	1.95	1.25	0.96
Cl	0.183	20.1	50.3	80.2	100.0	150.0
pH	6.6	6.5	6.3	6.2	6.1	5.9

TABLE 6. SUMMARY OF FILTER CAKE ANALYSIS FROM CHLORIDE-ION-EFFECT TESTS

Run No.	CL-1	CL-2	CL-3	CL-4	CL-5	CL-6
Component, mg/g						
Total S as SO_3	513	498	503	505	501	491
TOS as SO_2	382	372	381	388	383	372
Carbonate as CO_2	40	42	43	46	56	61
Ca	295	286	292	298	308	307
Mg	2.4	2.3	2.4	3.2	3.0	2.6
Na	5.9	(b)	6.2	5.8	6.5	5.9
Oxidation, %	6.9	6.6	5.3	4.0	4.4	5.3
L/S Utilization, %(a)	86.9	87.1	86.1	84.7	81.3	80.0

(a)SO_3/Ca
(b)data not available

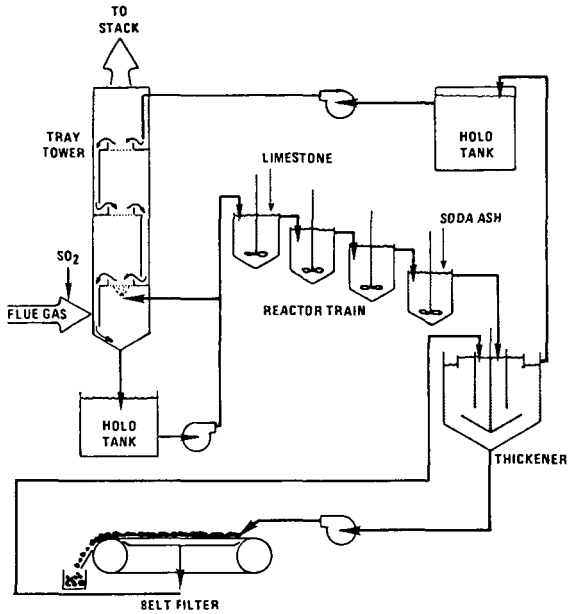

Figure 1. Flow diagram of IERL-RTP dual alkali pilot plant.

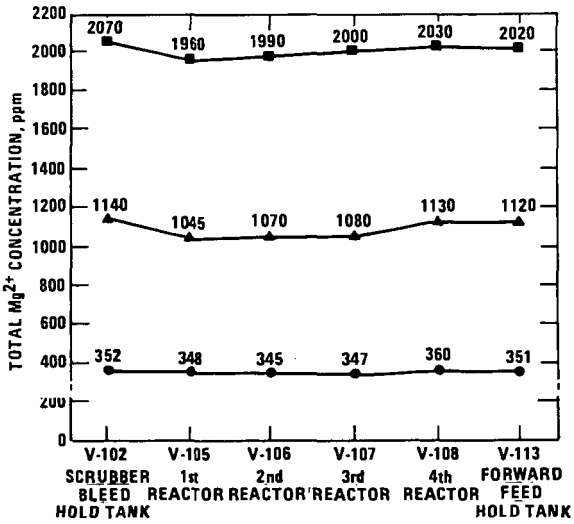

Figure 2. Distribution of magnesium ion concentration in limestone DA pilot plant.

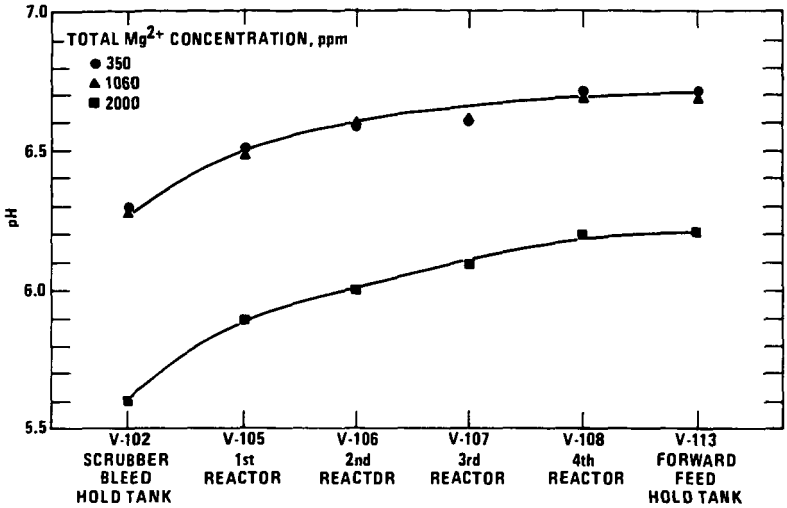

Figure 3. Profiles of pH values in limestone DA pilot plant.

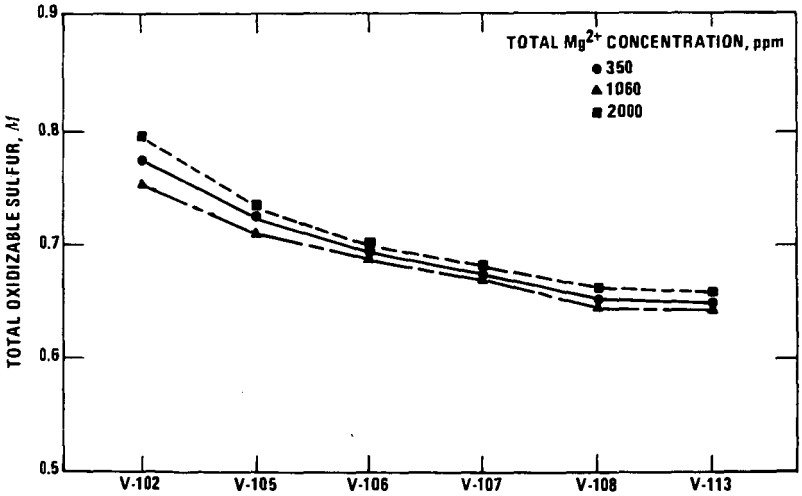

Figure 4. Total oxidizable sulfur concentrations in limestone DA pilot plant.

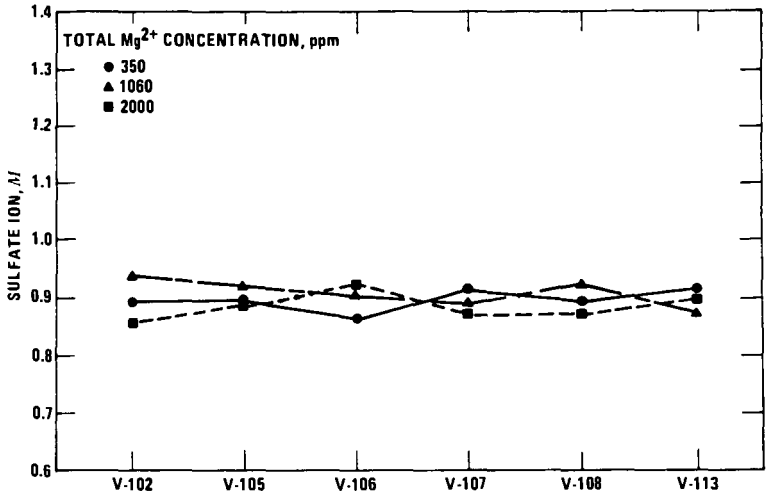

Figure 5. Distribution of sulfate ion concentration in limestone DA pilot plant.

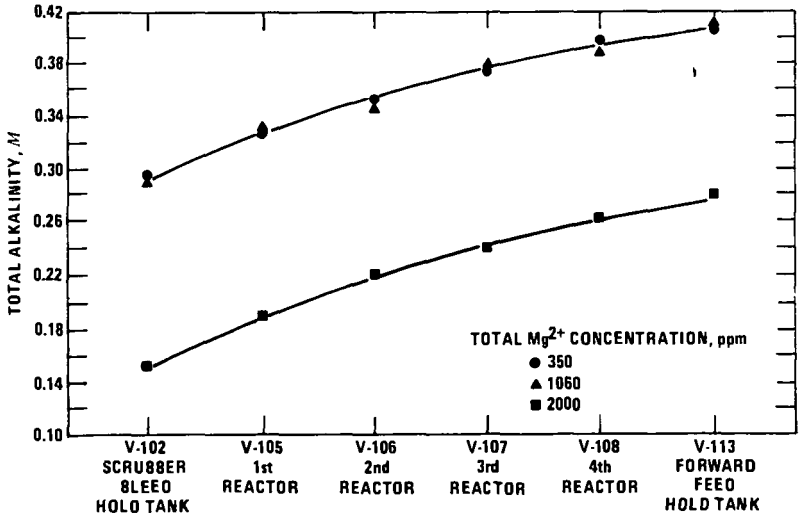

Figure 6. Total alkalinity concentrations in limestone DA pilot plant.

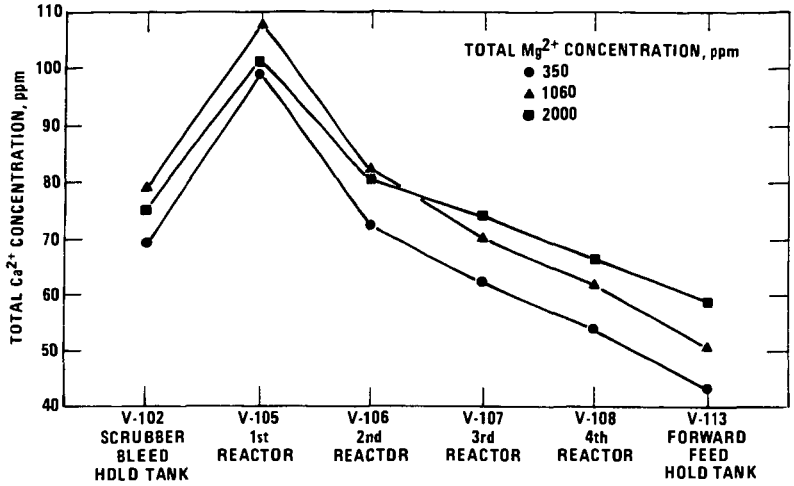

Figure 7. Distribution of total calcium ion concentration in limestone DA pilot plant.

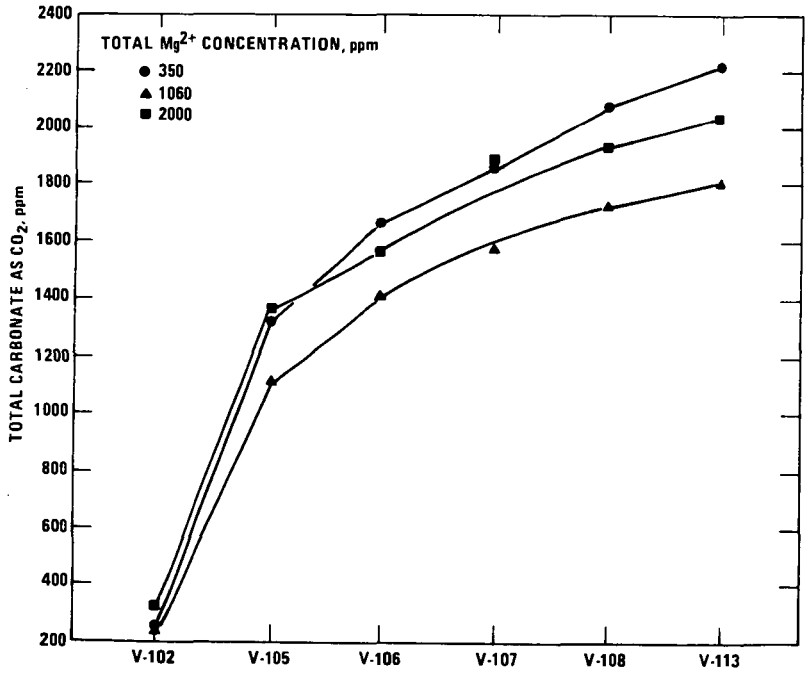

Figure 8. Distribution of carbonate ion concentration in limestone DA pilot plant.

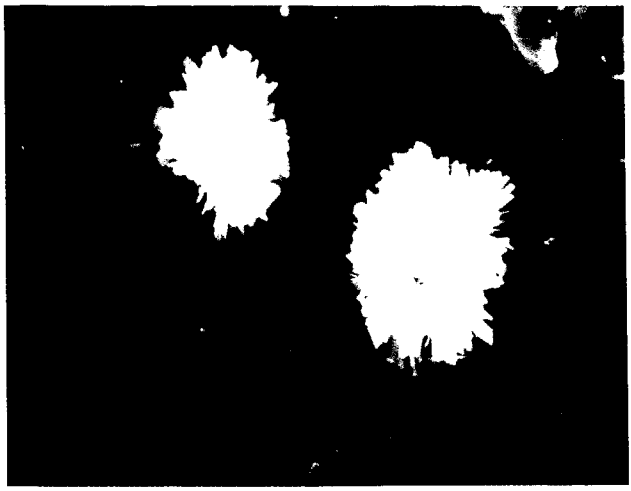

(a) 1000X

(b) 5000X

Figure 9. Scanning electron micrograph of base case solid products.

(a) 1000 X

(b) 5000 X

Figure 10. Scanning electron micrograph of solid products at 1000 ppm Mg^{2+} concentration.

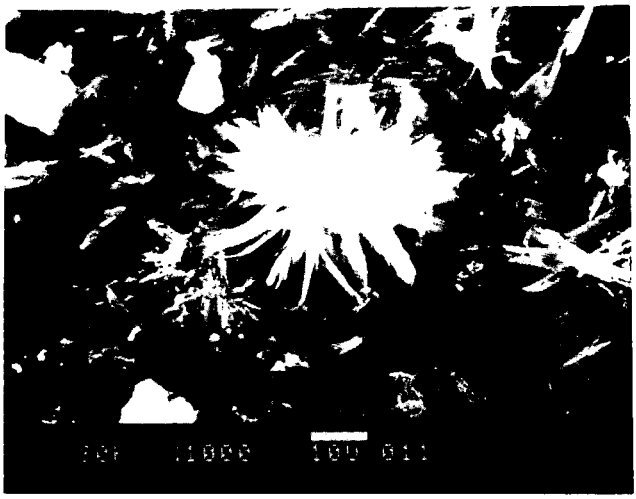

(a) 1000X

(b) 5000X

Figure 11. Scanning electron micrograph of solid products at 2000 ppm Mg^{2+} concentration.

APPLICATION OF THE SODIUM DUAL ALKALI SCRUBBING PROCESS TO HIGH CHLORIDE GAS STREAMS

William H. Mink

Battelle's Columbus Laboratories
505 King Avenue
Columbus, Ohio 43201

INTRODUCTION

The methods used for disposing of military chemical agents, such as VX, GB, and H, have been changed from land and sea burial to chemical neutralization and incineration due to environmental constraints and legislative restrictions.

As an approach to munitions disposal, the Army has developed a Chemical Agent Munitions Disposal System (CAMDS) facility at the Tooele Army Depot, Tooele, Utah. This is a prototype for other lethal chemical demilitarization plants expected to be built in the future.

The CAMDS facility was especially designed for the safe handling, disassembly, destruction, and decontamination of chemical agents VX, GB, and H, and munitions containing these chemical agents. These disposal operations must include adequate emission control technology. The emissions of concern include not only the agents themselves, but also certain species produced in the disposal process, such as sulfur oxides (SO_2 and SO_3), phosphorus oxides (e.g., P_2O_5), hydrogen chloride (HCl), and particulate matter.

Although the present method of gas treatment is believed to have excellent reliability, it is costly to operate because of its raw material requirements and its material handling procedures. A particularly expensive step in the overall gas treatment procedure is the required evaporative drying of salts which results from the use of the CAMDS single alkali scrubbing system. Alternatives to the evaporative drying of the salts have been investigated in order to reduce the energy consumption of the facility.

After demilitarization of a munition at the CAMDS facility, the metal parts are conveyed into the metal parts furnace (MPF), a roller hearth furnace, where residual agent on metal parts is thermally destroyed. Bulk mustard is also destroyed in the MPF. Exhaust from this furnace is treated in an extensive control system comprising (a) an oxidizing section for thermally decomposing any residual agents at 1600 F, (b) a quench venturi, and (c) a packed column where the exhaust gases are contacted with NaOH or Na_2CO_3 solution. Exhaust from the packed tower exits through a stack to the atmosphere.

To avoid buildup of phosphates, sulfates, and chlorides in the scrubber solution, a portion of the scrubber stream is removed from the system and evaporated to dryness. The resultant dry salts are then placed in drums for storage. The evaporation step requires large amounts of energy. The use of dual alkali scrubbing technology could avoid the need to evaporate large amounts of water to produce a solid waste.

In the sodium-based dual alkali process, the acid gases are absorbed by a solution of sodium salts at a pH range of 5-8. The solution is regenerated outside the scrubber with lime or limestone to produce a solid waste containing calcium sulfate and calcium sulfite. Some sodium salts are lost with the waste and must be made up by the addition of NaOH or Na_2CO_3. The principal chemical reactions are as follows:

Scrubber:

$$2NaOH + SO_2 \longrightarrow Na_2SO_3 + H_2O \qquad 1)$$

$$Na_2SO_3 + 1/2\ O_2 \longrightarrow Na_2SO_4 \qquad 2)$$

Regenerator: $Ca(OH)_2 + Na_2SO_3 \longrightarrow CaSO_3 + 2NaOH$ 3)

$Ca(OH)_2 + Na_2SO_4 \longrightarrow CaSO_4 + 2NaOH.$ 4)

One consideration in specifying a dual alkali system for the MPF is the relatively high concentration of HCl in the flue gas during mustard operations. The NaCl resulting from the reaction of NaOH and HCl cannot be regenerated with $Ca(OH)_2$ and must be purged from the system. In order to avoid a liquid purge stream which would have to be dried, the process in Figure 1 was designed to remove the NaCl with the liquid in the filter cake.

Dual alkali systems have been extensively applied to scrubbing SO_2 from boiler flue gas. In most of these applications, the objective in using a dual alkali system as compared to a single alkali system, is to minimize the use of the more expensive sodium as compared to the calcium in lime. However, the most cost-effective operation for the system on the MPF is one that will eliminate the expensive drying process. The design shown in Figure 1 may actually require considerably more alkali than the minimum required in order to increase the solids content in the waste filter cake and thereby allow the NaCl to be purged with the liquid attached to the filter cake. In order to minimize this quantity of liquid, the chloride content is allowed to build up to very high levels.

The principal advantage of a dual alkali process applied to the MPF is the substitution of a relatively inexpensive filtering step for the expensive drying step in the single alkali system.

RESULTS AND DISCUSSION

After assembling the sodium dual alkali pilot plant shown in Figure 1, it was operated at several different conditions to explore the scrubbing efficiency, the effect of chloride buildup in the scrubbing liquor, and to obtain a material balance. Tables 1A and 1B summarize the data obtained in the 13 runs made in the pilot plant.

Scrubbing Efficiency

The effect of the stoichiometric ratio of total alkali [$Ca(OH)_2$ plus NaOH] to total acid gas (SO_2 plus HCl) is shown in Figure 2. The theroretical limit for reaction of the alkali with the acid gases is indicated in the figure. (Actually, some removal of HCl can be expected with no alkali present.) Sulfur dioxide removal efficiencies were found to exceed 99 percent when alkali/acid stoichiometric ratios were greater than about 1.9. HCl removal efficiencies generally exceed SO_2 removal at any given alkali/acid stoichiometric ratio.

Effect of Chloride Buildup

Removal Efficiency. The outlet stream from the regeneration tanks was filtered to remove the solids. A typical filtrate composition at the higher chloride concentration range is presented in Table 2. The filtrate was recycled to the system, mixed with additional sodium hydroxide, and pumped back into the column as scrubbing liquor. Chloride built up as the scrubbing reaction occurred.

Figure 3 shows percent SO_2 remaining in the scrubbed gas as a function of alkali/acid gas stoichiometric ratio. The numbers beside each point are chloride concentration in the scrubber liquor. From an examination of this figure, it does not appear that chloride concentration has any significant effect on SO_2 removal in the range studied.

Solids Precipitation. Although chloride concentration in the scrubber liquor has little effect on removal efficiency, it has a significant effect on the operation of the column. Chloride concentrations greater than about 6.6 percent (see Table 3), lead to some deposit of salts in the scrubber column. Nevertheless, it appears that if chloride level is maintained below about 8-1/2 to 9 percent, column operation

would not be impaired. Figure 4 shows chloride concentration of the last nine runs together with an indication of the degree of column plugging.

Precipitation occurs when solubility limits of the components in solution are exceeded. This is the case when Cl^- concentration in the scrubbing liquor reaches values above 6.6 percent. These salts redissolve in the liquor, indicating that they are most likely sodium salts.

Chloride is removed with the moisture in the cake, thus maintaining a steady-state concentration. Essentially no chloride is removed as a solid as shown in a typical dry cake analysis (Table 4).

The other type of salt precipitating in the column is calcium-based. Elimination or reduction of calcium ions in the liquor is critical if the temperature in the system drops. A larger amount of precipitate was observed in the pilot plant when overnight temperature dropped to about 60 F. Most of these salts returned to solution after the system was reheated to operating temperatures. This relationship between the temperature and precipitation must be taken into consideration in the design and operation of a full-scale plant. As indicated by the analysis and postulated composition shown in Table 5, these salts are believed to be primarily calcium sulfite and sulfate.

Operation of a dual alkali plant would be significantly impaired if precipitation is allowed in the system. For example, as observed during pilot plant operation, precipitation present at the nozzle and in the column sometimes limited the amount of liquor input to the column.

Tower and packing designs also affect the accumulation of insoluble matter in the column. A spray tower design would considerably reduce the plugging potential, but at the expense of scrubbing efficiency. The packing size, shape, and height are also critical to the plugging problem. Large size, open shape, and low packing height would all minimize plugging. However, the large size has a reduced surface area per unit volume which may cause a reduction in scrubbing efficiency. The low packing height would also reduce the scrubbing efficiency. During the pilot plant operation, no attempt was made to optimize the packing material.

The area of scrubber plugging has been the subject of intense study by investigators of conventional limestone and dual alkali scrubbing systems.

Material Balance

In Pilot Plant Run No. 10, all the materials in and out of the system were accounted for in order to calculate a material balance. The balance is shown in Table 6. Note that most of the values closed within 10 percent with the exception of calcium. The discrepancy in calcium may have resulted from accumulation in the scrubber column or other parts of the system and losses in the filter washwater.

Solids Removal

Some problems were found during the pilot plant operation which were directly related to the filtration step. The first problem was the filter cloth size. The initial filter cloth installed plugged with the solids causing equipment malfunction. This problem was overcome by using a coarser weave filter cloth.

A second problem encountered with the filtration step was the additional water introduced in the system most likely as a result of the continuous washing of the filter cloth. This problem would probably be minimized with larger-scale equipment.

An alternative to the horizontal belt filter for solids separation is the use of a centrifuge or centrifugal filter. A continuous decanter centrifuge may be acceptable for the operation. The separation of solids is controlled by the centrifugal force, the bowl radius, and the effective length. The specification depends on the desired product: maximum clarification, classification, or solids dryness.

The degree of dryness in this system is determined by the amount of water necessary in the cake to carry out sufficient Cl^- for an 8-1/2 to 9 percent chloride concentration in the filtrate.

A centrifugal filter was used in the pilot plant to remove excess liquor from the cake collected in the material balance run (Run 10) prior to analysis and disposal. The filter operated well, reducing the wet cake to about 30 percent moisture.

pH Control and Monitoring

The pH of the scrubbing solution was monitored during the pilot plant operation. An unsuccessful attempt was made to control pH by use of pH controllers. The pH varied greatly with small additions of NaOH until it reached a value of about 12. At this level, the system appeared to be buffered. Higher pH levels were not reached during operation. Because of the difficulty in controlling the pH, the effect of pH on scrubbing was not determined and the method of NaOH addition changed to pump feeding at a selected rate.

Continuous monitoring of the pH in the regeneration tank was also accompanied with difficulties. Apparently, the higher concentration of solids and extremely high pH's in localized areas (from the lime feed) adversely affected the electrodes and the meter. However, spot monitoring was accomplished with a portable unit.

The scrubber discharge pH (see Table 3) varied from less than 1 to over 4. This wide range probably results from the absence of a strong buffering effect at the column discharge. The discharge pH does not appear to correlate with either column plugging or removal efficiency.

Corrosion

Soon after the pilot plant started operation, the column solution turned purple, dark green, and black. The colors were a result of the corrosion occurring in the gas feed lines. It was originally believed that the dry acid gases could be retained in the stainless steel lines at least during the course of the study. However, moisture from the compressed air, uniting with the acid gases, caused corrosion at the point where the gases and air mixed. To alleviate this problem, the junction of the gas line and the air line was moved to just ahead of the column inlet. This is an indication of the need for corrosion-resistant pipes for a larger plant.

The column should also be made of corrosion-resistant material to avoid corrosion problems. The pH in the tower is expected to change from very basic at the top (pH 12) to acidic (down to about pH 1) before the liquor reaches the bottom of the scrubber.

CONCLUSIONS

Laboratory and pilot plant studies on the sodium dual alkali scrubbing process indicate that it is a feasible method of scrubbing the products of combustion of mustard agent. High removal efficiencies (over 99 percent) of both HCl and SO_2 may be obtained at stoichiometric ratios of alkali-to-acid gas of about 1.9 or higher. Removal efficiencies appear not to be affected by chloride in the scrubber liquor with loadings as high as 8.6 percent Cl^- (14.3 percent NaCl). Plugging of the scrubber occurs at chloride loadings of over about 9 percent Cl^- (15 percent NaCl); however, the solids redissolve as the chloride content falls. Cake moisture content at this chloride level was about 35 percent.

ACKNOWLEDGEMENT

The author wishes to acknowledge the assistance of Mr. E. A. Coale of the Army Toxic and Hazardous Materials Agency and their support of this work.

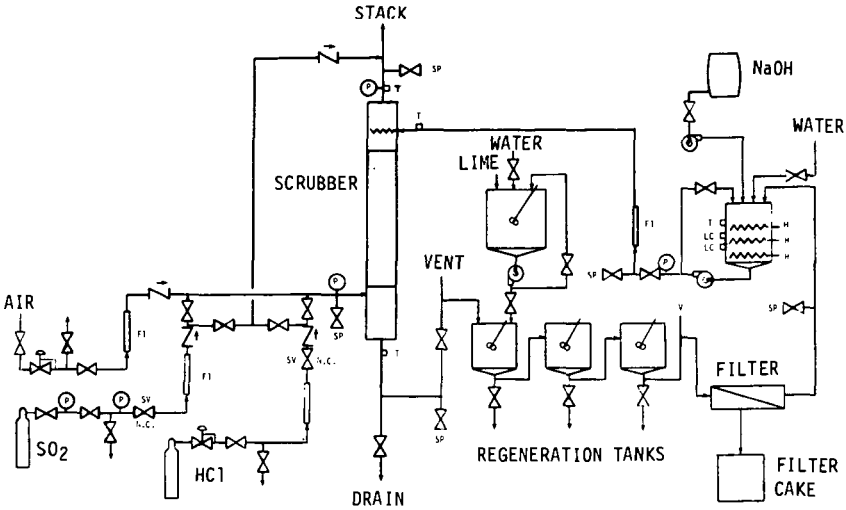

FIGURE 1. PILOT PLANT PROCESS FLOW DIAGRAM

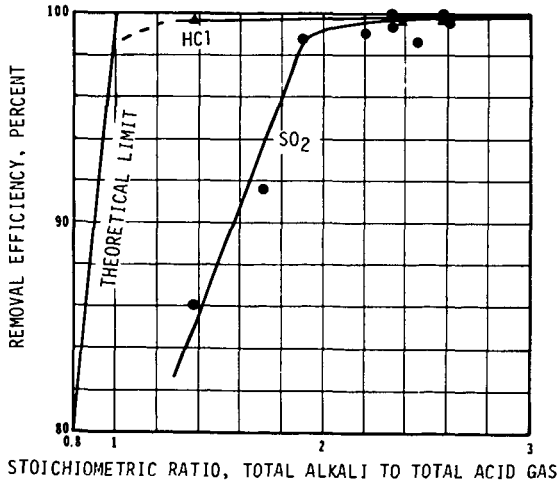

FIGURE 2. SO_2 AND HCl REMOVAL EFFICIENCY

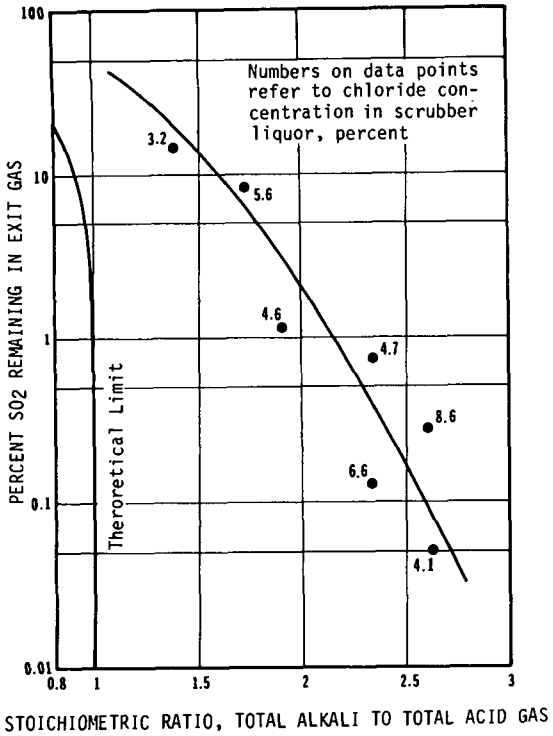

FIGURE 3. SO_2 REMOVAL

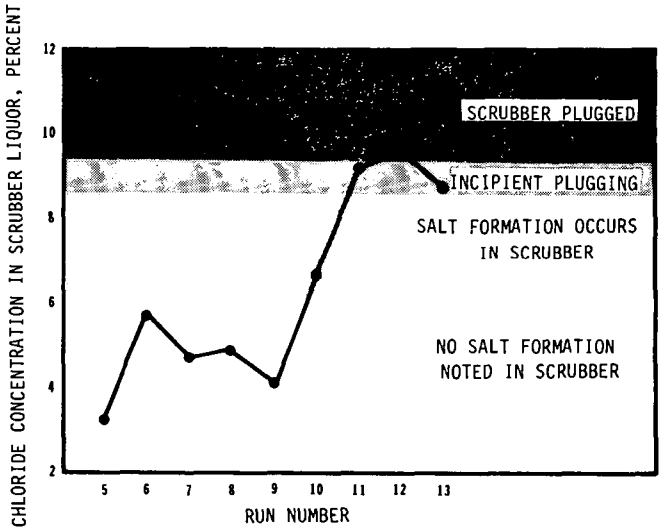

FIGURE 4. EFFECT OF CHLORIDE CONCENTRATION ON SCRUBBER OPERATION

TABLE 1A. RUN CONDITIONS

Run No.	Liquor Recirculation rate GPM	Gas Rate CFM	Column Temperature Inlet	Column Temperature Outlet	Column pH Inlet	Column pH Outlet	$Ca(OH)_2$ feed #/hr	NaOH feed #/hr	Purpose of Run
1	1.0	31.4	158 F	108 F	10.4	-	5.46	*	To build concentration of liquor
2	1.7	31.0	158	108	9.5	-	10.98	*	To build concentration of liquor
3	1.4	30.6	160	99	12.0	10.4	6.18	3.9	To build concentration of liquor
4	0.9	30.6	160	96	10.9	5.2	9.44	4.2	To build concentration of liquor
5	1.3	30.6	158	106	10.9	2.3	6.18	0	Build concentration and removal efficiency data
6	0.9	31.1	163	94	11.0	1.3	6.18	4.25	Obtain removal efficiency data
7	1.2	31.1	162	95	10.4	1.2	7.72	3.65	Obtain removal efficiency data
8	0.9	31.1	159	95	12.0	4.2	9.44	4.65	Obtain removal efficiency data
9	0.6	31.1	161	96	12.1	4.1	10.98	4.75	Obtain removal efficiency data
10	0.4	31.1	159	96	12.1	1.9	9.44	4.65	Material Balance Run - removal efficiency data
11	1.1	32.4	161	-	12.1	0.2	9.44	11.5	Determine effect of high concentration of salts in liquor
12	0.6	32.4	163	-	12.2	0.6	9.44	11.5	Determine effect of high concentration of salts in liquor
13	0.7	32.4	160	-	12.1	3.5	9.44	5.4	Determine effect of high concentration of salts in liquor Obtain removal efficiency data

* NaOH added to maintain pH

TABLE 1B. RUN GAS CONCENTRATIONS AND RESULTS

Run No.	SO_2 Concentration PPM In	SO_2 Concentration PPM Out	HCl Concentration PPM In	HCl Concentration PPM Out	Stoichiometric Ratio total alkali/total acid gas	Removal Efficiency, % SO_2	Removal Efficiency, % HCl
1	5,290	-	25,700	-	-	-	-
2	4,450	-	15,600	-	-	-	-
3	4,500	50	15,800	-	2.20	98.89	-
4	4,500	68	15,800	-	2.46	98.49	-
5	4,500	632	15,800	24	1.38	85.96	99.85
6	8,290	700	15,600	-	1.72	91.56	-
7	8,290	95	15,600	-	1.89	98.95	-
8	8,290	60	15,600	-	2.34	99.28	-
9	8,290	4	15,600	26	2.61	99.95	99.83
10	8,290	10	15,600	138	2.34	99.88	99.12
11	8,290	-	54,300	-	1.03	-	-
12	8,290	-	54,300	-	1.03	-	-
13	12,560	34	37,800	-	2.61	99.73	-

TABLE 2. FILTRATE COMPOSITION
(Run 11)

SPECIES	PPM
Ca^{++}	1,490
Na^{+}	41,200
Cl^{-}	83,200
$SO_3^{=}$	100
$SO_4^{=}$	1,300

TABLE 3. CHLORIDE CONCENTRATION OF SCRUBBER LIQUOR IN VARIOUS RUNS

Run Number	Cake Moisture Percent	Average Chloride Concentration in Scrubber Liquor, %	Scrubber Liquor pH: Scrubber Feed	Scrubber Liquor pH: Scrubber Discharge	Comments
5	50.7	3.2	10.5	2.0	No salt formation noted in scrubber.
6	55.7	5.6	11.0	1.4	No salt formation noted in scrubber.
7	47.9	4.6	10.4	1.2	No salt formation noted in scrubber.
8	50.9	4.7	12.0	4.2	No salt formation noted in scrubber.
9	48.3	4.1	12.1	1.6	No salt formation noted in scrubber.
10	43.0	6.6	12.1	2.0	Some salt formation noted.
11	35.3	9.2	12.2	0.2	Intermittent plugging in column.
12	-	9.5	12.2	0.4	Scrubber full of salts.
13	-	8.6	12.2	1.3	Salt formation reduction noted.

TABLE 4. TYPICAL DRY CAKE SOLIDS COMPOSITIONS (RUN 11)

A. Analysis

Species	PPM
Ca^{++}	338,000
Na^{+}	32,100
Cl^{-}	512
$SO_3^{=}$	336,000
$SO_4^{=}$	390,000

B. Postulated Dry Cake Composition

Species	%
NaCl	1.6
Na_2SO_4	7.9
Na_2SO_3	14.8
$CaSO_3$	42.3
$Ca(OH)_2$	20.9
Unaccounted for	12.5
	100.0

TABLE 5. SCRUBBER DEPOSIT

Analysis

Species	Percent
Ca	24.3
Na	3.17
Cl	0.52
SO_3	23.4
SO_4	16.1
Total S	21.1

TABLE 6. MATERIAL BALANCE (lb/hr)

Run 10

	S	Cl	Ca	Na
IN				
Gas	1.32	2.68	0	0
Alkali	0	0	5.10	2.67
TOTAL	1.32	2.68	5.10	2.67
OUT				
Gas	0	0.02	0	0
Cake Solids	0.96	0	2.67	1.38
Cake Liquor	0.04	2.92	0.01	1.37
Wash Solids	0.39	0	1.08	0.05
TOTAL	1.39	2.94	3.76	2.80
OVER (UNDER) lb/hr	0.07	0.26	(1.34)	0.13
OVER (UNDER) percent of material in	5.3	9.7	(26.3)	4.9

ORGANIC COMPOUNDS IN EFFLUENTS RELATED TO COAL COMBUSTION

G. A. Junk, J. J. Richard and M. J. Avery

Ames Laboratory, US DOE, Iowa State University, Ames, IA 50011

ABSTRACT

Organic compounds in the various effluents from the efficient combustion of coal at power plants do not appear to be an environmental problem. This conclusion is based on interpretation of results obtained during a five-year study of samples of stack gas, sluice water, and fly, stack and grate ash from the combustion of coal alone and mixtures of coal and refuse derived fuel (RDF). Dioxins and furans were not present in these samples at the detection limit of 10 ppT. Alkanes, chlorinated benzenes, polychlorinated biphenyls (PCBs), polycyclic aromatic hydrocarbons (PAHs), aliphatic acids and other miscellaneous compounds were found but the amounts were below those found in ambient urban air. These low levels of organic compounds are obtained only under steady state conditions of high combustion temperature, excess oxygen, small fuel particles and sufficient residence time. An added benefit of coal combustion was the removal, presumably by adsorption, of aromatic contaminants from the water used to sluice the fly and grate ash.

INTRODUCTION

The release of organic pollutants into the environmental from the burning of coal has been of periodic concern ever since the industrial revolution in England. This concern has resurfaced recently due to the shift to coal as the major fuel for generating electricity in the U.S.A.

Because of this environmental concern, an extended study of the Ames power plant for generating electricity was begun in 1977. This study included all types of pollutants such as NO_x, SO_x, total suspended particles, fly ash, grate ash, and trace elements as well as the organic compounds from the combustion of coal alone and mixtures of coal and refuse derived fuel (RDF). The results in this report are confined to the organic compounds found in all of the solid, liquid and gaseous effluents related to the combustion processes.

At the start of this study in 1977, the analytical methodology was inadequate for the characterization of organic compounds in the various effluents. Thus, priority was given to: 1) identifying the analytical difficulties; 2) devising methods to resolve the most critical problems; and 3) using evolving methodologies to determine those components judged to pose a threat to the environment.

As an aid in establishing the analytical problems, published data were compiled and reviewed for coal combustion and waste incineration (1). Important conclusions drawn from this review were: 1) only a limited number of organic components had been identified in the effluents; 2) the identified components reflected analytical capabilities and interests rather than a true distribution; 3) reliable quantitative data were not available; and 4) the data base was insufficient for predicting the probable environmental effects associated with the combustion of coal.

A critical examination of the analytical procedures used prior to 1977 showed these to be inadequate for the determination of organic compounds in combustion effluents; of special concern were the short-comings in sample collection methods. These short-comings are delineated in a review published recently (2). Because of these sampling uncertainties, the continuous development and validation of new procedures and sampling systems was an essential element of this study.

Coincident with the development of sampling procedures were the constant iterative improvements in extraction, separation, identification and quantitation of organic compounds. Special emphasis was placed on selected compound classes such as the polycyclic aromatic hydrocarbons (PAHs), polychlorinated biphenyls (PCBs),

chlorinated benzenes, and chlorinated dibenzo-p-dioxins (dioxins). The best available procedures were used to determine these components because they have known acute or chronic effects and previous studies suggested that they might be present in effluents from the combustion of coal alone and combination coal/RDF.

EXPERIMENTAL SECTION

SAMPLING PROCEDURES

Stack Vapor.-Vapor phase organic components present in the stack effluent were sampled by three different procedures. An EPA Method 5 train was equipped with an organic module and used during the early stages. This sampler allowed the stack gas to pass over the accumulated particles during the entire sampling period and thus gave rise to the possibilities of adsorption, sublimation and chemical transformations of organic components. When the equipment became available, the Method 5 train was supplanted by a Source Assessment Sampling System (SASS). This system allowed larger volumes of gas to be sampled and reduced the contact between accumulated particles and the stack gas. The complexity of the SASS made this system undesirable for use when the only goal was to obtain a sample of vapor phase components. A third sampling system was the Ames Vapor Sampling System (AVSS) described by Junk and Richard (3). This sampling system largely eliminated contact between vapor phase components and particles. The AVSS provided a simple and effective accumulation of organic components from very mild atmospheres such as ambient air and very severe atmospheres such as stack gas.

Stack Ash.-Samples of stack ash were obtained using the EPA Method 5 and the SASS. On occasion, large amounts of stack ash were collected conveniently by placing a custom-designed tray into the stack for 24 hours. This tray collected the particles that settled from the disturbed gas stream.

Fly Ash.-Fly ash samples were collected directly from the hoppers of the cyclone and electrostatic precipitator used for particle control.

Grate Ash.-Grate ash samples from stoker-fired units were collected from hoppers located below the grates. Grate ash from the tangentially-fired units was removed from the boilers by sluicing so samples were obtained by filtering the sluice water collected at the outlet of the pipe used to transport the sluiced ash to a settling pond. Additional ash samples were collected from the settling pond as sediment samples.

EXTRACTION PROCEDURES

Adsorbents.-A macroreticular resin, XAD-2, was used as the adsorbent in the AVSS, the SASS and the EPA Method 5 sampling train. Organic compounds accumulated on the resin were recovered by elution with methylene chloride. Diethyl ether was used as an eluent, instead of methylene chloride, when subsequent determinations were performed by gas chromatography with electron capture detection. Other eluents and desorption techniques were tested and found to offer no significant advantages (3).

Water Condensates.-When stack gas was cooled during sampling, water vapor condensed. The organic components in these condensates were extracted with methylene chloride. Diethylether, pentane and isooctane were used as alternative extraction solvents when subsequent gas chromatographic determinations required the use of electron capture detectors.

Ashes (Particles).-Because there were no standard and accepted procedures among the many described in the literature for the extraction of organic components from particles, several techniques were critically evaluated. Soxhlet extraction with benzene,

benzene-methanol, benzene saturated with hydrogen chloride, toluene, toluene-methanol, and methylene chloride were evaluated. Sonic extractions using a probe or a bath with a variety of solvents and pretreatment procedures using aqueous acids and water were also tested. No technique resulted in significant improvement in the extraction of the cross-section of different organic components associated with the various particle effluents. Consequently, the traditional soxhlet extraction using benzene-methanol was used most frequently.

CLASS SEPARATIONS

Chromatographic and solvent partitioning procedures were used to separate organic components recovered from particles into chemical classes to facilitate their ultimate determinations in less complex mixtures. The procedure included the separation of PAHs on Sephadex (4) and the separation of components on the basis of polarity using alumina (5), silica gel (6), Florisil (7), the polystyrene-divinylbenzene resin XAD-4 (8), and the traditional solvent partitioning into acid, base and neutral fractions. Preparatory scale, normal-phase, high-performance liquid chromatography with amine and cyano columns was used to separate mixtures on the basis of polarity and to partially separate PAHs (9).

The Soxhlet extraction of particles with benzene-methanol yielded PAHs plus many non-polar and polar organic compounds which interfered with the gas chromatographic separations. The interfering compounds were removed using standard solvent partitioning with DMSO (10), DMF (11), or nitromethane (12).

COMPOUND SEPARATIONS

Gas chromatography was used for the separation of individual organic components. Columns packed with Dexsil 300 (Supelco Inc., Bellefonte, PA) provided the separation of the high boiling point PAHs during the early stages of this study. Later, as the column technology advanced rapidly, capillary columns coated with SE-52 and SE-54 (J&W Scientific, Rio Rancho, CA) were used almost exclusively. These columns were found to be applicable to the efficient separation of a diverse assortment of organic components in complex mixtures.

IDENTIFICATION AND QUANTITATION

Combination gas chromatography/mass spectrometry (GC/MS) was used for the identification of the organic components extracted from the various combustion effluents. Quantitation of organic components was normally obtained using external standards and gas chromatography. The quantitation by gas chromatography was periodically checked on randomly chosen samples using appropriate techniques of combination GC/MS.

CONFIRMATIONS AND VALIDATIONS

For positive identifications by GC/MS, the full mass spectrum of a tentatively identified component was compared to the mass spectrum of an authentic sample. If the spectra were identical, within experimental error, and if the gas chromatographic retention times of standard and unknown components on a 30-meter SE-54 fused silica capillary column agreed within two seconds, the identification was considered positive. When the amount of material present was insufficient for detection using full scan GC/MS techniques, the more sensitive single and multiple ion monitoring techniques were employed. Confirmation in these cases consisted of coincidences of retention times of mass chromatograms of the unknown and of the authentic sample. For chlorinated materials, the molecular ions contained additional information about the chlorine isotope distribution. Confirmation in those cases included the correct isotope ratios for the number of chlorines in the molecule.

Validation of the methodology used for components that could not be detected in extracts of particle samples was obtained by extraction of surrogate samples. The

surrogate sample for PAHs was soot generated from an air-starved methane flame. The positive results obtained from this soot sample have been reported elsewhere (13). The surrogate sample for dioxins was an incinerator ash obtained from Dow Chemical Company. Results obtained from analysis of extracts of this ash sample were ±50% of the published values for the tetra-, hexa-, hepta- and octachloro- isomers (14). This agreement substantiated the validity of the analytical protocol used to screen the effluent samples for dioxin compounds.

RESULTS AND DISCUSSIONS

IDENTIFIED COMPONENTS

A combined listing of all the compounds identified in extracts of the vapor and particles in the stack, fly and grate ash effluents from the combustion of coal at the Ames power plant are listed in Table I. Similar compounds have been observed for extracts from a second coal-fired power plant located at Iowa State University. Therefore, this list may be partially representative of coal combustion in semi-modern boilers. Certainly, many more organic compounds than the listed 78 are present in these effluents but so far these have not been positively identified. Indeed, a 1980 review of organic compounds from coal combustion (1) taken from all the literature reports had only 106 compounds identified.

Table I. List of Organic Compounds Present in Effluents From Coal Combustion

ALKANES - Methane, Decane, Undecane, Hexadecane, Heptadecane, Octadecane, Nonadecane, Eicosane, Heneicosane, Docosane, Tricosane, Pentacosane, Hexacosane, Octacosane, Triacontane, Dotriacontane, Trimethylcyclohexane, Dimethylcyclohexane

AROMATICS - Toluene, Xylene, Propylbenzene, Butylbenzene, Biphenyl, Terphenyl, Naphthalene, 1-Methylnaphthalene, 2-Methylnaphthalene, Methylindene, Acenaphthene

PAHs - Benz(a)pyrene, Anthracene, Fluoranthene, Fluorene, Pyrene

ACIDS - 2-Ethylbutanoic, Nonanoic, Decanoic, Dodecanoic, Tridecanoic, Tetradecanoic, Pentadecanoic, 9-Hexadecenoic, Hexadecanoic, Heptadecanoic, Octadecanoic, Benzoic

PHENOLS - Phenol, o-Cresol, Ethylphenol, Butylphenol, 2,4-Dichlorophenol, 2,4,6-Trichlorophenol

CL COMPOUNDS - Tetrachloroethylene, Tetrachloroethane, 1,2-Dichlorobenzene, 1,3-Dichlorobenzene, 1,4-Dichlorobenzene, 1,2,4-Trichlorobenzene, 1,2,3-Trichlorobenzene, 1,2,3,4-Tetrachlorobenzene, 1,2,3,5-Tetrachlorobenzene, Pentachlorobenzene, Hexachlorobenzene, 2,3,2',5'-Tetrachlorobiphenyl[a], 2,5,3',4'-Tetrachlorobiphenyl, 2,4,5,2',5'-Pentachlorobiphenyl, 2,4,5,2',4',5'-Hexachlorobiphenyl

O, N, P, S COMPOUNDS - Acetophenone, Methylacetophenone, Phthalic Anhydride, Methylbenzoate, Indanone, Dibenzofuran, Diethylphthalate, Dibutylphthalate, Diisobutylphthalate, Di(2-ethylhexyl)phthalate, Diphenylamine

[a] The characteristic Arochlor 1254 profile was observed but only four isomers were positively confirmed.

QUANTITATION

It was not possible to obtain exact quantitative values for all the identified components associated with each of the effluents from coal combustion. The amounts varied because of the analytical problems mentioned in the experimental section and different firing conditions. However, semi-quantitative values have been obtained for many of the components and these values are proposed to be reasonable estimates of the amounts of organic compounds expected from the efficient combustion of coal in a modern power plant. A discussion of some important compound classes and the amounts in the various effluents is given below. In general, the amounts are much lower than would be predicted from a review of the limited quantitative data available in the literature.

Polycyclic Aromatic Hydrocarbons (PAHs).-The most highly studied class of compounds in combustion effluents is the PAHs. However, very little information about the amounts present in the vapor phase and on particles in the effluents from the efficient combustion of coal is available. The data in Table II partially fills this informational gap. The amounts in the vapor phase varied according to the firing conditions and the stack temperature that was ~ 240°C. Even if all these PAHs were to condense on the particles, the amounts are well below the multiple μg/g quantities present on ambient air particles.

Table II. Summary of PAHs in Effluents From Coal-Fired Power Plants

Compound	Concentration Range (ng/g)		Conc. Range Vapor Phase (ng/M^3)[b]
	Respirable Particles	Non-Respirable Particles	
Naphthalene	ND[a]-18	0.5-23	10-1800
Phenanthrene			26-640
Anthracene			0.4-100
Fluoranthene	0.2-0.3	0.05-1.5	0.5-240
Pyrene	0.2-7	0.08-1.1	0.2-2850
Chrysene	ND	ND-4	0.1-28
Benz(a)pyrene	ND	ND	0.1-120
Benz(a)anthracene	ND	ND-0.3	NM[c]
Benz(ghi)perylene	NM	NM	3-22

[a] ND = Not detected at the limit of 0.05 ng/g.
[b] Includes values reported by Midwest Research Institute (15, 16).
[c] NM = Not measured.

Alkanes and Aromatics.-The distinction between aromatic and polycyclic was arbitrarily set at three conjugated six-member rings in Table I. With this definition the alkane and aromatic hydrocarbons with 30 entries dominate the list of identified components. These compounds are also present in the highest concentration in the different effluents. Ordinarily their concentrations were not measured because of a low interest in these kinds of compounds but in those instances where measurements were made, the amounts ranged from 10-1500 ng/M^3 in the vapor phase and from 10-90 ng/g on the suspended particles in the stack effluents. These hydrocarbons were not quantitated for any of the fly and grate ash samples.

Aliphatic Acids and Phenols.-Eleven aliphatic acids and six phenols were determined as constituents of the vapor phase and associated with particle effluents. These acidic compounds and the amounts are listed in Table III. A range of values from 20 different sampling runs is shown for the C9, C12, C14, C16 and C18 acids and phenol to illustrate the fluctuations that can occur in the amounts of organic acids in the effluents. The extent of the variation attributed to changes in firing conditions and analytical difficulties in the determinations is unknown and needs further study.

Polychlorinated Biphenyls (PCBs).-The PCBs were observed in the stack effluents during the combustion of coal but these compounds were not produced in the combustion process by a de novo synthesis or from precursor compounds. The source of the PCBs was the air used to support the combustion. This indoor air contained 0.13 $\mu g/M^3$ of PCBs; the concentration of PCBs in the stack gas was only 0.02 $\mu g/M^3$ when coal containing no detectable level of PCBs was burned. For perspective, this emission level should be compared to the average ambient air level of about 0.006 $\mu g/M^3$.

When the coal fuel was supplemented with RDF containing 8500 μg of PCBs/Kg of RDF, the amount of PCBs in the stack remained at the low level of 0.02 $\mu g/M^3$.

Table III. Summary of Acidic Compounds in Effluents From Coal-Fired Power Plants

Acid	Concentration Range[a]	
	Vapor	Particles
2-Ethylbutanoic	200	NM[b]
Nonanoic	20-250	NM
Decanoic	10	20
Dodecanoic	80-800	90
Tridecanoic	NM	10
Tetradecanoic	100-300	8-600
Pentadecanoic	90	50
9-Hexadecenoic	50	NM
Hexadecanoic	40-300	40-270
Heptadecanoic	NM	20
Octadecanoic	80	40-150
Phenol	20-200	25-1000
o-Cresol	NM	NM
Butylphenol	NM	NM
2,4-Dichlorophenol	NM	0.1
2,4,6-Trichlorophenol	NM	0.05
Pentachlorophenol	NM	0.2

[a] ng/M^3 for vapors and ng/g for particles. Where a range is listed, these selected components were measured in 26 extracts.
[b] NM = Not measured.

Calculations based on fuel inputs, stack gas flow, support gas input and PCBs in all the inputs and effluents showed that 99+% of the PCBs in the input RDF were destroyed in the combustion process. The details of this investigation of the co-combustion of coal and RDF containing PCBs have been published elsewhere (17).

The explanation of the high destruction efficiency for the PCBs in the RDF is efficient combustion based on a combination of high temperature (~ 2000°F), excess oxygen at 22%, and adequate residence time and sufficient turbulence for the small coal and RDF particles in the combustion zone. This same combination of combustion conditions is the probable explanation for the undetectable levels of TCDD discussed below.

2,3,7,8-Tetrachlorodibenzo-p-dioxin (TCDD).-At the detection limit of ten parts per trillion, no TCDD was found in the effluents from the combustion of coal in three different boilers at the Ames power plant (see summary table in reference 16 for description of boilers). This observation was confirmed at a second smaller coal-fired power plant located at Iowa State University. Even when the coal fuel was supplemented with RDF, which should contain the precursor compounds, no dioxins were observed in the vapor and particle samples taken from the effluents. Thus no de novo synthesis occurred during the combustion of coal alone and if dioxins were formed from precursor compounds in the co-combustion of coal and RDF, they were destroyed in the efficient combustion as explained above for the thermal destruction of the PCBs present in the RDF. The PCBs are destroyed at 1200°F (18) and a similar temperature is expected for the dioxins. This is well below the 2000°F operation of the boilers used for this study (19).

Chlorinated Benzenes.-Ten chlorinated benzenes were targeted for analysis in the stack effluents. The analytical results when coal alone was combusted are shown in Table IV. When the coal fuel was supplemented with RDF up to 20%, no consistent increase in the amounts of the chlorinated benzenes occurred although barely

detectable amounts of the tetra-, penta- and hexa- isomers were observed during some of eleven different combustions of coal with 20% RDF. Based on these results it appears as if the dichlorobenzenes, reported to be present in the RDF at the 8000 μg/Kg level (15, 16), were thermally destroyed with high efficiency in much the same manner as that documented above for the PCBs present in the RDF.

Table IV. Chlorinated Benzenes in Stack Effluent From Coal-Fired Power Plants

Chlorobenzene Isomer	Concentrations ng/M^3
1,2-Dichloro-	0.5
1,3-Dichloro-	ND[a]
1,4-Dichloro-	80
1,2,3-Trichloro-	3.9
1,2,4-Trichloro-	1.2
1,2,3,4-Tetrachloro-	ND
1,2,3,5-Tetrachloro-	ND
1,2,4,5-Tetrachloro-	ND
Pentachloro-	ND
Hexachloro-	ND

[a] ND = Not detected at limit of 0.03 ng/M^3; average of three runs.

The environmental effects from the emission of these chlorinated benzenes are estimated to be insigificant because of the low levels and the further dilution by factors of 10^3 to 10^5 in the atmosphere before any human or plant exposure.

Sluice Water.-There is a legimate concern over the release of pollutants into the water environment following the utilization or disposal of the huge amounts of fly and grate ash produced during the combustion of coal. Our studies were restricted to the investigation of the possible release of organic pollutants only when fly and grate ash are sluiced to settling ponds and retained there as a disposal site. The water in the settling pond was checked periodically for organic compounds known to be present at low concentrations on the ash.

None of these known components were detected in the water at the conservative limit of one ppB. Indeed, this pond water did not contain any gas chromatographable organic compounds at the detection limit of 0.1 ppB even though the well water used for sluicing contained multiple ppB levels of aromatic compounds indicative of the coal tar that had contaminated the aquifer (19). Thus, the ash effluents from coal combustion appear to adsorb rather than release organic compounds into the water.

This adsorption feature was examined in an experiment where water containing 20 to 50 ppB of five aromatic hydrocarbons was mixed with fly ash for ten minutes at a water to ash weight ratio of 10 to 1. In this short contact time, the fly ash completely removed the organic components; this is vividly illustrated by the two gas chromatograms shown in Figure 1. The effective adsorption is probably due to the active forms of carbon, aluminum and silicon expected to be present in fly ash. For organic compounds then, fly ash provided desirable clean-up rather than undesirable contamination of water.

ACKNOWLEDGEMENTS

The technical assistance of Ray Vick, Al Joensen, Jerry Hall, Brian Jerome and Jennings Capellen is gratefully acknowledged. The administrative assistance of H. J. Svec, V. A. Fassel, R. W. Fisher and H. R. Shanks is also appreciated. In addition, the thoughtful assistance and cooperation of Mr. Donald Riggs, Mr. Gary Titus, Mr. Arnold Chantland, and other personnel from the City of Ames made this study possible. This work was supported financially by the U. S. Department of Energy under Contract

No. W-7405-Eng-82 through the Office of Health and Environmental Research, Office of Energy Research, and the Assistant Secretary for Fossil Energy, Division of Coal Utilization, through the Morgantown Energy Technology Center.

REFERENCES

1. G. A. Junk and C. S. Ford, Chemosphere, 9(11), 187 (1980).
2. G. A. Junk and B. A. Jerome, Amer. Lab, 15(12), 16 (1983).
3. G. A. Junk and J. J. Richard, "Vapor Phase Sampling of Organic Compounds," Chapter 5 in Identification and Analysis of Organic Pollutants in Air, L. H. Keith, ed., Butterworth Publishers, Boston, MA, 1984.
4. H. J. Klimisch, Z. Anal. Chem., 264, 275 (1973).
5. L. H. Klemm, D. Reed, L. A. Miller, and B. T. Ho., J. Org. Chem., 24, 1468 (1959).
6. H. J. Cahnmann, Anal. Chem., 29, 1307 (1957).
7. G. U. Dinneen, J. R. Smith, R. A. VanMeter, C. S. Albright, and W. R. Anthony, Anal. Chem., 27, 185 (1955).
8. T. J. Spitzer, J. Chromatogr., 150, 381 (1978).
9. S. A. Wise, W. J. Bonnet, and W. E. May, "Polynuclear Aromatic Hydrocarbons: Chemistry and Biological Effects," Bjorseth and Dennis, eds., Battelle Press, Columbus, OH, 781, (1980).
10. A. Bjorseth, Anal. Chim. Acta., 94, 21 (1977).
11. B. A. Tomkins, H. Kuboxa, W. H. Griest, J. E. Caton, B. Clark, and M. R. Guerin, Anal. Chem., 52, 1331 (1980).
12. D. Hoffman, and E. L. Wynder, Anal. Chem, 32, 295 (1960).
13. R. D. Vick and M. J. Avery, "Extraction and Identification of Organic Materials Present in Soot from a Natural Gas Flame," ISU Journal, IS-4329, 1978.
14. L. L. Lamparski, and T. J. Nestrick, Anal. Chem., 52, 2045 (1980).
15. C. Haile, Midwest Research Institute, Personal Communication (1983).
16. D. Redford, US EPA, Personal Communication (1982, 1983).
17. J. J. Richard, and G. A. Junk, Environ. Sci. Technol., 15, 1095 (1981).
18. F. P. Sebastian, G. F. Kronenberger, L. A. Lombana, and J. M. Napoleon, Proc. Am. Ind. Chem. Eng. Workshop, 5, 67 (1974).
19. A. L. Joensen, Iowa State University, Personal Communication (1981).
20. A. K. Burnham, G. V. Calder, J. S. Fritz, G. A. Junk, H. J. Svec, and R. Willis, Anal. Chem., 44, 139 (1972).

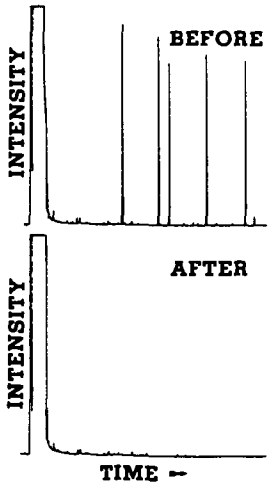

Figure 1.
Clean-up of water by coal combustion fly ash. BEFORE - capillary column GC chromatogram with left to right major peaks being indan, 3-methylindene, naphthalene, 1-methylnaphthalene and acenaphthylene at 50 to 80 ppB in water before contact with fly ash.
AFTER - same chromatogram after water contacted with fly ash for ten minutes.

EXHAUST GAS SAMPLING AND ANALYSIS IN SMALL-SCALE SYNFUEL COMBUSTION.

G.A. Gibbon, C.M. White, and L.J. Douglas

U.S. Department of Energy
Pittsburgh Energy Technology Center
P.O. Box 10940
Pittsburgh, PA 15236

The Coal Science Division of the Pittsburgh Energy Technology Center has undertaken the development of a method for determining the trace level organics present in the hot exhaust gases from the combustion of liquid synfuels. This method development is part of a larger task to assess the possible environmental impact of substituting such synfuels for petroleum fuels in utility and industrial boilers. The studies were conducted in a fully instrumented 20-hp firetube boiler capable of burning any liquid fuel with handling and combustion properties ranging from those for No. 2 fuel oil to those for No. 6 fuel oil [1]. In addition, the boiler could be operated over a wide range of combustion conditions while varying such parameters as air/fuel ratio, fuel consumption rate, and steam generation rate. To achieve a consistent data base, all results of the combustion runs for all the fuels studied were compared to the base-line case of No. 2 fuel oil.

The sampling of the hot exhaust gases for trace level organics was accomplished by drawing a stream of the gases from the exhaust duct at a point about 10 feet above the firebox [1]. The duct surface temperature at the sampling point ranged from 210°C to 250°C depending on the combustor operating conditions. The gas sample stream was passed through a particulate knock-out that was maintained at 140°C to remove large particles, and then through a glass spiral and an adsorbent resin bed maintained at 70°C [2,3].

Before use, the adsorbent resin was rigorously cleaned by exhaustive Soxhlet extraction with water, methanol, diethyl ether, pentane, and methylene chloride. The organic solvents were either spectroscopic or liquid chromatographic grade.

During a typical sampling run, 150-180 ft^3 of the exhaust gases were drawn through the sampler during 5-6 hours of combustor operation. The sampling was considered successful only if there were no upsets in combustion operating during the run and if there was no visible deposit of particulates on the resin bed.

Upon completion of a sampling run, the resin was removed from the sampler and Soxhlet-extracted with methylene chloride. The extraction solvent was then removed by evaporation, and the concentrate was analyzed by Gas Chromatography/Mass Spectrometry (GC/MS). An SE-50 capillary column (0.30 mm x 19 m, 0.25-μm film) was used with helium as a carrier gas. Split-mode injection was used with the splitter operating at 275°C. All the alkanes and polycyclic aromatic hydrocarbons (PAH) reported here were

identified by their mass spectral patterns and by cochromatography with authentic samples.

The table summarizes the qualitative results for the reference No. 2 fuel oil and for 5 additional fuels, including No. 6 fuel oil, several coal-derived liquids, and a biomass-derived liquid. Estimated relative amounts for the compounds are denoted in the table as follows: L = low, M = medium, H = high, VL = very low, and ND = not detected. The chromatograms represent the total sample eluting from the column, with a minimum detectable amount of about 1 ng (VL) and a full scale response (H) of approximately 100 ng. While quantitation of the amounts of the compounds is not possible because the samples were not taken isokinetically, an indication of the total hydrocarbons present in the exhaust gases, approximately 1 ppm, was obtained by a flame ionization detector mounted adjacent to the sample port used for this study.

The No. 2 fuel oil used was a purely aliphatic material, and the PAH observed in the exhaust gases are thought to be formed during the combustion process. The presence of the alkanes suggests that small amounts of the fuel are unaffected by their passage through the combustion firebox. The same observations hold for the No. 6 fuel oil, suggesting that the molecular weight of the fuel is not an important variable when both fuels are burned under comparable conditions.

All three coal-derived fuels (SRC, EDS, and H-Coal) give similar results, showing PAH present in the original fuels as well as those formed during the combustion of the fuel oils. The biomass-derived fuel shows less PAH than either the fuel oils or the coal-derived oils. This is presumably the result of the high oxygen level of the fuel. This hypothesis is supported by the fact that no PAH are observed when methanol is burned.

The combustion of methanol in the boiler was originally done to confirm the hypothesis that high oxygen levels in the fuel resulted in a low PAH level in the exhaust gases, and to verify the sampling and analytical procedures [4]. The first methanol combustion test results showed the presence of saturated and aromatic hydrocarbons as well as detectable amounts of organic sulfur compounds, e.g., dibenzothiophene. To account for these observations, an extensive set of combustion experiments, using No. 2 fuel oil and No. 2 fuel oil spiked with diisopropylnaphthalene, was conducted. The exhaust duct was rigorously cleaned between runs. These experiments showed that the unexpected results could be attributed to a "memory effect" in the exhaust duct and/or the soot deposits on the interior surfaces of the duct [4].

The results for the EDS and H-Coal fuels given in the table were obtained after the methanol and spiked-fuel experiments. The exhaust duct was cleaned between each set of runs for each fuel to avoid the "memory effect" described above.

All the extracts were retrospectively examined for the presence of nitro-polycyclic aromatic hydrocarbons (nitro-PAH) using electron impact GC/MS. No nitro-PAH were found in any of the extracts. The limit of detection for the analysis was about 3 ng. It is possible that any nitro-PAH present were lost on the surface of the sample container during storage; however, this is

deemed unlikely as no nitro-PAH have been found in extracts analyzed immediately after preparation.

While the absence of quantitation makes rigorous comparison of the fuels impossible, it is valid to suggest that PAH are present in the exhaust gases when any of the fuels listed in the table are burned. The levels of the PAH emissions from the exhaust duct to the atmosphere were not measured in this study; however, they should not exceed the levels in the duct itself. In addition, the small experimental combustor had no exhaust gas cleanup equipment such as might be used on a large commercial apparatus. Thus the change from petroleum-derived liquid fuels to coal-derived liquids should not significantly increase the emission of PAH to the environment.

REFERENCES

1. Gibbon, G.A., Ekmann, J.M., White, C.M., Navadauskas, R.J., Joubert, J.I., and Retcofsky, H.L. Small-Scale Combustion Testing of Synthetic Fuels, DOE/PETC/TR-82/1, available at the Technical Information Center, P.O. Box 62, Oak Ridge, TN 37830.

2. Jones, P.W., Giammar, R.D., Strup, P.E., and Stanford, T.B. Efficient Collection of Polycyclic Aromatic Hydrocarbons from Combustion Effluents. Environmental Sci. Technol., 10, 806 (1976).

3. Strup, P.E., Wilkenson, J.E., and Jones, P.W., "Trace Analysis of Polycyclic Aromatic Hydrocarbons in Aqueous Systems Using XAD-2 Resin and Capillary Column Gas Chromatography-Mass Spectrometry Analysis," in Carcinogenesis. Vol. III, edited by P.W. Jones and R.I. Freudenthal, Raven Press, New York, 1978.

4. Douglas, L.J., Gibbon, G.A., and White, C.M., "Stack Contamination Effects During Small-Scale Combustion Testing of Synthetic Fuels," DOE/PETC/TR-84/4, available at the Technical Information Center, P.O. Box 62, Oak Ridge, TN 37830.

DISCLAIMER

Reference in this report to any specific commercial product, process, or service is to facilitate understanding and does not necessarily imply its endorsement or favoring by the United States Department of Energy.

Summary of GC/MS Data Obtained
from Combustion Emissions Collected on XAD-2

Compound	Detected in Combustion Emissions of					
	No. 2 Fuel Oil	No. 6 Fuel Oil	SRC-II	Biomass	EDS	H-Coal
Naphthalene	H	H	M	M	H	H
2-Methylnaphthalene	L	L	H	L	H	L
1-Methylnaphthalene	L	L	L	L	H	L
Biphenyl	M	L	M	L	M	L
2-Ethylnaphthalene	L	L	H	ND	L	L
2,6- & 2,7-Dimethylnaphthalene	M	L	H	ND	M	L
1,3- & 1,7-Dimethylnaphthalene	L	L	M	ND	M	L
1,6-Dimethylnaphthalene	L	L	L	ND	L	L
1,5-Dimethylnaphthalene	L	L	L	ND	VL	L
Acenaphthene	L	L	L	H	M	L
1,2-Dimethylnaphthalene	L	L	L	ND	L	VL
Acenaphthylene	ND	ND	M	ND	L	VL
Dibenzofuran	L	L	M	L	M	L
Fluorene	M	M	H	H	M	L
9-Methylfluorene	ND	ND	M	ND	ND	ND
2-Methylfluorene	ND	ND	M	ND	L	VL
1-Methylfluorene	ND	ND	ND	ND	VL	VL
Dibenzothiophene	M	L	M	M	VL	VL
Phenanthrene	H	VH	H	H	M	M
Anthracene	L	L	L	L	L	VL
Carbazole	ND	VL	M	ND	ND	ND
1-Phenylnaphthalene	L	L	L	L	L	L
3-Methylphenanthrene	M	M	M	L	VL	VL
2-Methylphenanthrene	H	M	H	L	L	L
4-H-Cyclopento[def]phenanthrene	L	M	L	H	L	L
9- & 4-Methylphenanthrene	L	M	L	L	VL	L
1-Methylphenanthrene	M	M	L	VL	VL	L
2-Phenylnaphthalene	L	L	L	M	L	L
Fluoranthene	H	H	L	H	L	L
Benz[e]acenaphthalene	ND	VL	VL	M	L	ND
Benzo[def]dibenzothiophene	H	M	L	L	L	ND
Pyrene	H	H	H	H	L	L
Retene	ND	ND	VL	ND	ND	ND
Benzo[b]fluorene	L	L	M	VL	ND	VL
4-Methylpyrene	VL	L	L	ND	VL	VL
2-Methylpyrene	VL	L	L	ND	VL	VL
Benzo[ghi]fluoranthene	M	VL	ND	L	VL	VL
Benzo[a]anthracene	L	VL	ND	ND	VL	VL
Chrysene/Triphenylene	L	VL	ND	ND	VL	VL
Alkanes	H	H	L	VL	L	L

EVALUATION OF COAL DERIVED LIQUIDS AS UTILITY BOILER FUELS EASTERN TEST

David P. Burford

Research and Development Department
Southern Company Services, Inc.
P.O. Box 2625
Birmingham, Alabama 35202

INTRODUCTION

The synthetic fuels evaluation at Mississippi Power Company's Plant Sweatt is just one of a number of tests, sponsored by the Electric Power Research Institute (EPRI) under project RP 2112, to assess the potential of coal derived, liquid synthetic fuels as an alternative or substitute for liquid petroleum fuels. Specifically, the work done at Plant Sweatt examined the applicability of six liquid synthetic fuels to a full scale, wall fired utility boiler. EPRI sponsored testing with synthetic fuels at other sites included small scale combustors, a Combustion Engineering wall-fired utility boiler, a Combustion Engineering tangentially-fired utility boiler, a combustion turbine and diesel piston engines with generally favorable results.

The testing at Plant Sweatt was sponsored by EPRI, Mississippi Power Company (MPC) and Southern Company Services, Inc.(SCS). EPRI also contributed the 27,700 barrels of synthetic fuel to the test effort.

OBJECTIVES

The objectives of the test were to:

- Demonstrate the use of coal derived liquids as potential substitutes for petroleum fuel oil in a full scale, wall fired utility boiler.
- Assess the potential for minimizing nitrogen oxide (NO_x) emissions from the six, high fuel-bound nitrogen liquids.
- Obtain data on the quantity and composition of other emissions from the combustion of the synthetic fuels such as particulate loading, particulate morphology, hydrocarbons, chlorides and flue gas acid dew point temperature.
- Assess the future utilization of coal derived liquids as a possible replacement fuel for other existing boilers or as a design basis for new boilers.
- Compare and contrast the combustion characteristics of the two baseline fuels and the six synthetic fuels in terms of combustion efficiency, regulated emissions and fuel handling.

At the original writing of this paper, a large portion of the data require additional reduction and analysis. Therefore, the results and conclusions that follow have not yet been subject to the thorough investigation that remains to be done as part of the EPRI contract.

FACILITIES

Mississippi Power Company's Plant Sweatt is located on Valley Road,

approximately five miles south of Meridian, Mississippi, in Lauderdale County. This station has two identical steam units labeled 1 and 2 which were placed in service in 1951 and 1953, respectively. Although rated at 40 MW, each unit is capable of generating 49 MW and with the onsite 39.4 MW combustion turbine, represent 4.5% of Mississippi Power's generating capacity. The boilers are Babcock & Wilcox (B&W), balanced draft, front wall fired (2 vertical x 3 horizontal burner matrix) units with welded cases. Each is designed to produce 425,000 pounds of steam per hour at 850 psig and 900°F. Both are currently fired on either natural gas or No. 6 oil and have no environmental controls of any type. While this plant is normally restricted to providing peaking capability during the summer, arrangements were made to isolate Unit 1, the test unit, from economic dispatch and to set load based on testing requirements from September 1983 through December 1983 to accommodate the project schedule.

PROJECT ORGANIZATION

The project at Plant Sweatt was organized with Southern Company Services as EPRI's prime contractor responsible for project management, project direction and subcontractor performance. Subcontracted to Southern Company Services were Babcock & Wilcox(B&W) and KVB. B&W provided technical consultation and boiler performance evaluations, KVB provided combustion gas emission characterizations and supplementary technical consultation. Although not directly subcontracted to SCS, Radian, Inc. provided fuel logistics support and Control Data Health Care Services assisted with the industrial hygiene program as part of the multi-site EPRI work with synthetic fuels, RP 2112.

PLANT MODIFICATIONS

Before testing could begin in September of 1983, minor modifications to Plant Sweatt were required to accommodate the objectives of the work. Five areas were addressed:

(1) Fuel forwarding system
(2) Rail transloading site
(3) Burner air registers
(4) Exterior ductwork
(5) Industrial hygiene program

The well documented aggressiveness of the synthetic fuels toward rubber-based gasketing material dictated the design of a redundant fuel forwarding system of predominantly welded joints. The few joints that were gasketed were done so with Flexitalic gaskets(asbestos/metal) which are resistant to deterioration from synthetic fuels. This redundant fuel system allowed Unit 1 to operate concurrently on natural gas and a liquid fuel in any configuration. It also provided the flexibility to transition online from liquid synthetic fuel to either baseline fuel at the burner front should Plant Sweatt have been needed for a production type emergency. This redundant fuel system was designed to provide the same liquid pressures and flow rates to the existing Racer burner components at the boiler front as in normal No. 6 fuel oil operation.

The onsite surge capacity for storing synthetic fuels was accomplished through the use of four, 7800 gallon commercial fuel hauling trailers which were manifolded into the synthetic fuel forwarding system. When emptied, each trailer was pulled out for refilling at the rail transloading site.

The six synthetic fuels were delivered to Plant Sweatt in 23,500 gallon

"jumbo" railcars from their various origins. These cars were temporarily sited on Illinois Central & Gulf Railways Okatibbee siding approximately 1/4 mile from the plant. This railsiding was the location for the second set of modifications. An area approximately 200'x20' was graded and paved to support the transloading operation from railcar to mobile trailer. Curbing and a drainage sump were included to prevent any ground water contamination. The transloading was done with the fuel transporter's tractor power-take-off pump, gravity fed from the railcar's bottom discharge. Fuel transloading was a continuous process during any testing over 25 MW due to synthetic fuel consumption rates.

The third area of modification was in the boiler windbox. Although B&W had reworked the burners on Unit 1 in 1974, moderate to severe warpage and misalignment were noted during the B&W Field Service Engineer's inspection in November of 1982. Consequently, the air register vanes in all six burners were replaced and individually aligned for reliable air flow control. Partial shrouds were also added around each burner to augment the control of combustion airflow.

Corrosion penetrations in the flue gas ductwork downstream of the air preheater caused the replacement of some ductwork to be the fourth modification. Although air inleakage on the suction side of the ID fan was not operationally troublesome, any dilution of the flue gas upstream of the proposed emission extraction grid would discredit the analytical procedures for measuring combustion emissions. When this ductwork was replaced, an access platform for the sampling crews was added around the flue gas extraction ports.

The last area of modification actually took place in several locations around the plant to support the industrial hygiene program. First, the plant employee locker room area was subdivided into a clean side/dirty side concept similar to that found at nuclear installations. All equipment or personnel involved in synthetic fuel handling were segregated on the dirty side. In order to pass to the clean side where street clothing was stored, personnel were required to take a shower at the end of their shift. A daily change of coveralls and laundry service were also mandatory for synthetic fuel handlers. Personnel not involved in handling the synthetic fuels were denied access to those areas where spills and contamination were most probable; the redundant fuel system/trailer pad, the boiler front, the rail transloading area and the dirty side locker room. Barricade tape and signs were appropriately placed as a reminder. In order to contain any large spillage, the stationary trailer pad and the rail transloading area were paved and curbed. Fuel handling personnel were equipped with hard hats, eye protection, face masks with organic vapor filters, coveralls, a bib rainsuit, and elbow-length gloves. They were reimbursed for their work boots if contaminated at the project end. Personnel involved in the testing were given baseline medical examinations and classes on personal hygiene as a part of the industrial hygiene philosophy of "no contact" with the synthetic fuels. Fortunately, no spills or gross contamination occurred during the four months of testing.

TEST PLAN

Six synthetic fuels from three major research firms were provided by EPRI for testing at Plant Sweatt:

Gulf Research/Tacoma, Washington
- Solvent Refined Coal-II (Full Range Mixture)
- Solvent Refined Coal-II (Middle Distillate Fraction)

Ashland Oil/Catlettsburg, Kentucky

H-Coal (Light Fraction)
H-Coal (Heavy Fraction)
H-Coal (Blended Mixture)

Exxon Research/Baytown, Texas
Exxon Donor Solvent

Mississippi Power Company provided the baseline fuels:
Natural Gas
No. 6 Fuel Oil

In satisfying the test objectives, it was necessary to "test" the single gaseous fuel and seven liquid fuels on as common a basis as possible for a meaningful comparison. Generally, the areas of investigation were:

(1) Limits of operability,
(2) operability at repeatable conditions, and
(3) adaptability for combustion optimization.

The test points contemplated were based on each fuel's "smoke point" as the boundary between complete and incomplete combustion. Smoke point was operationally defined as the flue gas excess oxygen level measurement at which drastic upswings in carbon monoxide and opacity occurred on B&W and KVBs instantaneous monitors. This level is a function of each fuel's molecular composition and is somewhat dependent on a boiler's particular combustion dynamics. This level may be influenced by burner type, tip placement, combustion air distribution, fuel atomization and other physical factors. By operating just above the smoke point, the combustion loss due to excess air is minimized, which results in higher boiler efficiencies. Three test points for each liquid fuel were originally established based on a fuel's smoke point:

(1) Low Excess Air - "LEA"
Smoke point plus 0.5% excess oxygen in the flue gas

(2) Normal Excess Air - "NEA"
Smoke point plus 1.0% excess oxygen in the flue gas

(3) High Excess Air - "HEA"
Smoke point plus 2.0% excess oxygen in the flue gas

A fifth test point was also established later to give the test results commonality at one excess oxygen level. This test point was to be at a comparable excess oxygen level found for the baseline liquid fuel (No. 6 fuel oil) known as the Oil Comparable (OC) test point. These five points were established with normal burners in service at three loads; 40 megawatts, 25 megawatts and 15 megawatts and again with burners out of service. This satisfied the three areas of investigation outlined earlier. In some cases, however, testing was limited by unstable combustion or combustion air availability (fan limited). This caused the early termination of some tests.

Coal liquefaction processes are designed to chemically clean coal by removing ash, sulfur and to a lesser extent, nitrogen from the feed coal. The principal differences between the fuels tested at Plant Sweatt and their petroleum counterparts are that synthetic fuels have a higher carbon/hydrogen ratio and higher fuel-bound nitrogen content. A high C/H ratio is sometimes an indication of increased soot formation. This, however, was not found in the Plant Sweatt

testing. Increased fuel-bound nitrogen in coal derived fuels can serve as the precursor for another currently regulated emission, nitrogen oxides (NO_x). One of the objectives of the Plant Sweatt testing was to measure and reduce NO_x emissions through combustion modifications. These modifications were limited to changes in the combustion process within the boiler. No equipment such as selective catalytic reduction devices was added. This was done to demonstrate the feasibility of "no cost" options for NO_x reduction in existing liquid fueled boilers.

The conversion of nitrogen to NO_x is predominantly a conversion of fuel nitrogen as opposed to the conversion of combustion air nitrogen. This conversion (combustion) is stoichiometrically limited by the presence of available oxygen. The work at Plant Sweatt relied mainly on "burners out of service" (BOOS) as the combustion modification to reduce NO_x emissions. This was done, of course, in combination with operation at minimum excess oxygen levels. The BOOS configuration that gave the least NO_x emission on each fuel and each load was subjected to the full testing matrix of excess oxygen levels.

BOOS owes its success to the resulting segregation of the boiler into two zones: oxygen rich and oxygen lean. The BOOS concept objective is to force the combustion reaction to occur in the oxygen lean zone. By optimizing each burner flame with air register adjustments and then simply closing the fuel valve on selected burners, the BOOS technique is accomplished. Burners without fuel (the BOOS) are producing fuel lean/oxygen rich zones by still contributing combustion air. The burners remaining in service become fuel rich/oxygen lean in two ways:

(1) The aggregate fuel flow to maintain load remains constant but increases proportionately to those burners remaining in service with no increase in available combustion air. This causes the burners remaining in service to be less stoichiometrically excessive in oxygen.

(2) It is also theorized that air flow increases slightly in the BOOS as there is no flame back pressure at these burners. This makes the burners still in service even less stoichiometrically excessive in oxygen.

Of course, it is still necessary to maintain an excess oxygen level sufficient to complete combustion by maintaining air vane settings in the BOOS. It is also desirable that particulate emissions (measured as opacity) and carbon monoxide levels be held within acceptable limits rather than optimizing the NO_x reduction at the expense of other considerations.

DATA ACQUISITION

The data acquisition role at Plant Sweatt was performed by Babcock & Wilcox and KVB. B&W used their Computerized Boiler Diagnostic System (CBDS) programmed into a Hewlett-Packard portable computer in gathering and calculating boiler operating data. This automated system was complemented by the traditional checklist approach for non-automated control room information. The CBDS recorded approximately 200 data points every sixty seconds for refinement into ten minute averages for each test. Data measurement devices included extensive thermocouple grids, differential pressure transmitters and extractive flue gas analysis both before and after the air preheater. Instantaneous scan values could be read on a CRT screen while data values and averages were stored on a non-volatile, magnetic disk. These averages were combined later to provide a single, boiler efficiency value for each test. B&W also calibrated the plant's combustion air flow orifice

readings with their Velocity/Pressure Averaging System (VPAS) prior to testing.

KVB acquired real time data on several emissions and gathered many samples for later analysis. Included in their matrix were the continuous monitoring of carbon monoxide, carbon dioxide, excess oxygen, nitrogen oxides and sulfur dioxide. Gas sampling for sulfur trioxides and chlorides was done intermittently as was measurement of acid dew point, particulate loading, particulate morphology and particulate size distributions.

At the original writing of this paper, a large portion of both B&W and KVBs data require additional reduction and analysis. Therefore, the results and conclusions that follow have not yet been subject to the thorough investigation that remains to be done as part of the EPRI contract.

RESULTS AND CONCLUSIONS

The testing of the six synthetic fuels at Plant Sweatt was very successful. Results on the first three synthetic fuels(SRC-II(Full range mixture), H-Coal(Heavy fraction) and H-Coal(Blended mixture)) indicate that all three have higher boiler efficiencies and produced fewer emissions than the baseline No. 6 fuel oil. Results of testing on the last three synthetic fuels(SRC-II(Middle distillate fraction), H-Coal(Light fraction) and Exxon Donor Solvent) indicate comparable findings but lack the depth of data taken on the first three fuels. The burners out of service technique in combination with reduced excess combustion oxygen was also very successful, providing as much as a 50% reduction in NO_x levels. These coal derived liquid fuels appear to be quite adequate for petroleum liquid replacement in existing units and should certainly be considered in the design basis for liquid fuel boilers of the future. The only drawbacks to the use of these fuels are in their material aggressiveness toward standard gasketing materials and their implied human toxicity. Both problems should be surmountable through simple design accommodations.

Combustion efficiency for the fuels ranged from a low of 83.6% for natural gas at 15 MW to a high of 91.2% for SRC-II at 25 MW (Figures 2 and 3). The efficiencies calculated for SRC-II, H-Coal(Heavy) and H-Coal(Blend) are on the order of one to two percentage points higher than No. 6 fuel oil and five to seven percentage points higher than natural gas. This is strongly associated with the higher amount of excess combustion oxygen required for natural gas and No. 6 fuel oil to operate above their smoke points. Table I illustrates this point.

Table I
Ranking Of Low Excess Air (LEA) Levels (40 MW, 6 burners)

(1) 2.7% H-Coal(Heavy)	(5) 3.0% H-Coal(Blend)
(2) 2.7% H-Coal(Light)	(6) 3.5% SRC-II(Middle Distillate)
(3) 2.7% EDS	(7) 4.0% Natural Gas
(4) 2.9% SRC-II(Full Range)	(8) 5.8% No. 6 Fuel Oil

As anticipated, the nitrogen oxide emissions from the coal derived liquids were higher than that of No. 6 fuel oil or natural gas (Figure 1). However, the combination of BOOS and LEA reduced NO_x emissions as much as 50% in some cases (Figures 4 and 5). Table II lists some typical results.

TABLE II
Selected NO_x Reduction Results

Fuel	Load	Burners	Excess O_2 Level	NO_x	% Reduction
SRC-II(Full Range)	25MW	no BOOS	HEA	403ppm	
					25%
		no BOOS	LEA	301ppm	53%
					37%
		2 BOOS	LEA	191ppm	
H-Coal(Blend)	40MW	no BOOS	HEA	398ppm	
					21%
		no BOOS	LEA	316ppm	51%
					30%
		1 BOOS	LEA	195ppm	
No. 6 Fuel Oil	40MW	no BOOS	HEA	275ppm	
					21%
		no BOOS	LEA	217ppm	33%
					15%
		1 BOOS	LEA	185ppm	

It is interesting to note that NO_x emissions from the synthetic fuels could be lowered to a level approximating the NO_x emission from optimized No. 6 fuel oil combustion. From another perspective, optimized synthetic fuel combustion resulted in considerably less NO_x than unoptimized No. 6 fuel oil operation (HEA, no BOOS).

Particulate emissions from the synthetic fuels were very low, on the order of 0.01 lb per million Btu. This is approximately one order of magnitude less than particulate emissions from No. 6 fuel oil. Also, LEA and BOOS operation did not significantly contribute added particulate emissions. Data on particulate morphology and submicron particle size distributions are still undergoing analysis.

The difficulty in fuel handling was somewhat self-imposed by the project philosophy of, "no human contact" with the synthetic fuels. The personal hygiene requirements (clothing changes, mandatory raingear/facemask/gloves, and restricted areas) were more burdensome than problematic. At a plant designed specifically to use synthetic fuels, the potential for contact with the fuel could be minimized through bulk liquid storage, welded pipe joints, dry disconnect couplings and backflushing filters. This would limit potential spillage (and human contact) to infrequent fuel transfer operations and emergencies.

Overall, the consensus of the participants is that any of the six coal derived liquids could be used as a replacement for liquid petroleum fuel in this utility boiler with no equipment modifications, equipment additions or environmental variances. The relatively small modifications required at Plant Sweatt indicate that few design criteria would be affected if these synthetic fuels were to be included in the fuel specifications of future design criteria.

When all the data have been reduced and analyzed, a final EPRI report on the work at Plant Sweatt(RP 2112-02) will be published. Further specific inquiries will be welcomed pending the distribution of this final report.

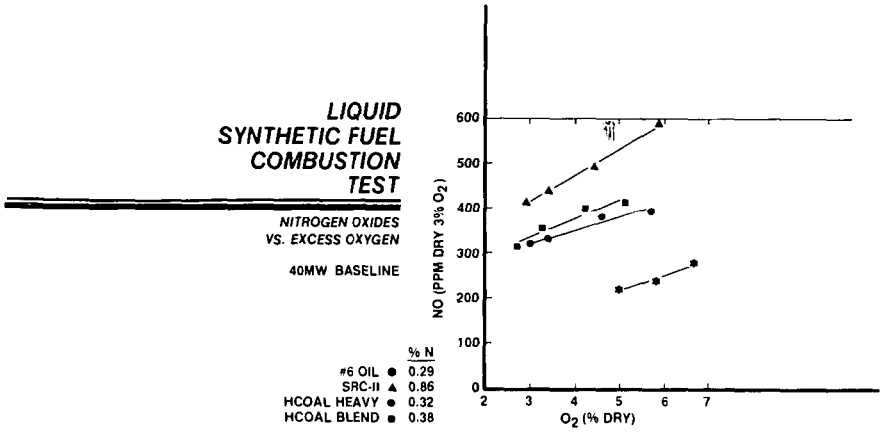
LIQUID
SYNTHETIC FUEL
COMBUSTION
TEST
NITROGEN OXIDES
VS. EXCESS OXYGEN
40MW BASELINE
% N
#6 OIL ● 0.29
SRC-II ▲ 0.86
HCOAL HEAVY ● 0.32
HCOAL BLEND ■ 0.38
NO (PPM DRY 3% O2)
600
500
400
300
200
100
0
2
3
4
5
6
7
O2 (% DRY)

FIGURE 1

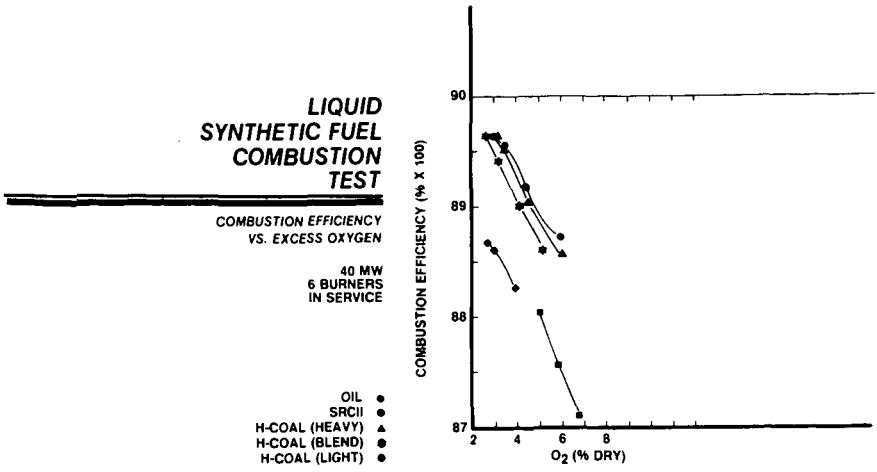

FIGURE 2

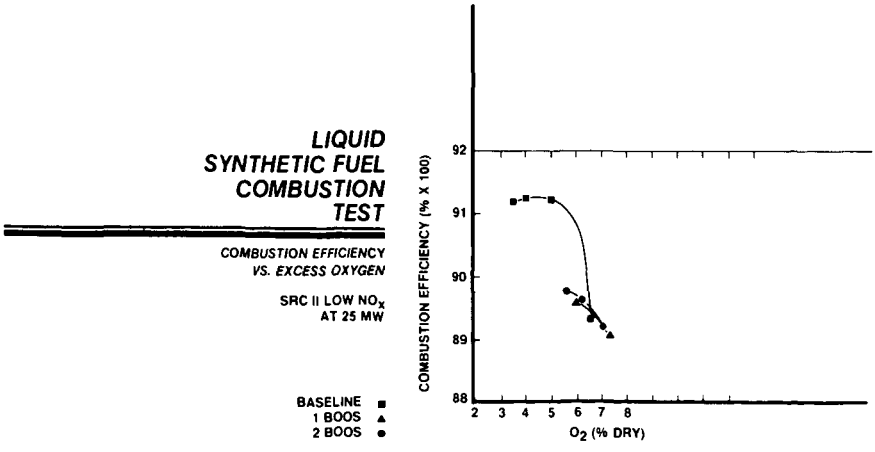

FIGURE 3

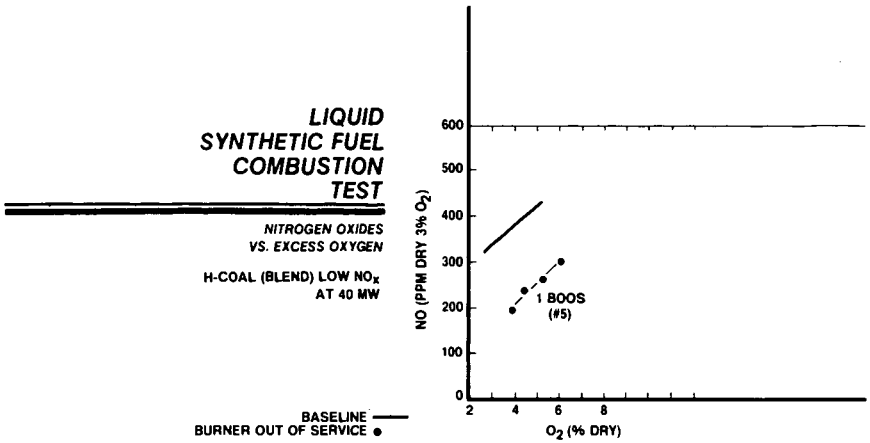

FIGURE 4

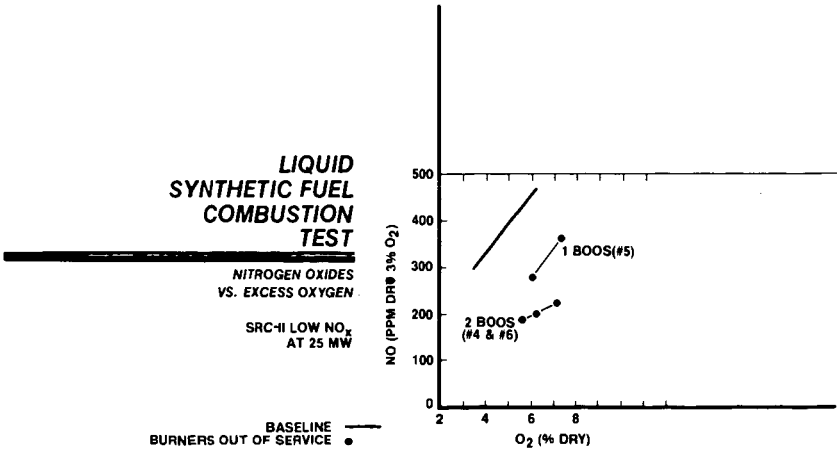

FIGURE 5

EMISSIONS SAMPLING OF COMBUSTION EFFLUENTS FROM A STATIONARY DIESEL BURNING A COAL DERIVED LIQUID FUEL

W. Piispanen, P. Webb, D. Trayser

Battelle Columbus Laboratories
505 King Avenue
Columbus, Ohio 43201

Introduction

The purpose of this study was to evaluate the performance of a utility diesel generator when burning a middle distillate Exxon Donor Solvent (EDS) coal derived liquid fuel. While coal derived liquid fuels have been successfully fired in external combustion sources (1,2), their use in internal combustion sources is limited by 1) low octane number, 2) high distillation range 3) high nitrogen and sulfur content and 4) high aromatic content. These factors may influence both the engine performance and the emissions of particulates and gaseous products of combustion.

Technical Approach

For this program a Cooper LSV-16-GDT 16-cylinder, 4-stroke, turbocharged engine was used to evaluate various blends of EDS and a standard DF-2 fuel. The engine was owned and operated by a public utility company. Cooper Energy Services designed a test matrix for the evaluation of fuel blends at different engine operating conditions and supervised the actual engine test operations. Basically three operating parameters were varied: the fuel blend ratio as EDS/DF-2, the air manifold temperature (AMT) and the engine/speed load conditions as kilowatts (KW) of electrical power at rated speed. In addition a specially designed sampling system was used to evaluate extreme blend ratios and test engine modifications applied to only one of the 16 cylinders. Baseline tests on the DF-2 fuel were made at the various test conditions for comparative purposes.

Sampling for gaseous emissions was conducted at two locations of the engine exhaust. In one location a rake type probe with a heated sampling line was used to continuously withdraw samples of the exhaust gas before it entered the silencer. A special check-valve sampling probe was installed for the single cylinder exhaust gas monitoring. Provision for SO_2/SO_3 sampling was included in both sample lines. A schematic of this system is shown in Figure 1.

The sampling for SO_2/SO_3 was by a controlled condensation system based on an original design by Goksoyr and Ross in 1962, followed by a hydrogen peroxide impinger train. This system is now referred to as the Goksoyr-Ross train and methods for operation are documented by both the U.S. EPA and the APHA.

Sampling for particulates was by a standard EPA Method 5 probe and impinger train. The method was modified by adding NaOH to the second impinger to allow determination of chloride emissions. The Method 5 sampling was conducted at the outlet of the silencer using two perpendicular sampling ports and multiple point traverses.

For the program, replicate tests were conducted when feasible. Duplicate measurements were made of SO_2 (EPA Method 6 and on NDIR instrument) and of NO_x (EPA method 7 and chemiluminescence instrument). Analyses of particulate, SO_3/SO_2 and Cl were made onsite. All gas monitoring instruments were zeroed and spanned daily using certified span gases.

Test Results

Fuel Analyses. Prior to actual sampling the fuel blends were analyzed by Southwest Research Institute (SWRI) and reported in their report to EPRI on this project (3). The octane number of the fuel blends ranged from 49.6 for 100% DF-2 to 21.0 for 100% EDS. The higher heating values (HHV) ranged from 19,500 Btu/lb to 18,569 Btu/lb (for 100% EDS). The nitrogen and sulfur content were variable but reported by SWRI as 0.09 percent sulfur and 0.12 percent nitrogen. This sulfur content is lower and the nitrogen is higher than most conventional diesel fuels. The DF-2 sulfur content was also low at 0.15 percent. The H/C ratio of the EDS was somewhat lower than the DF-2 (approximately 0.11 compared to 0.16) indicating a higher degree of aromatic constituents.

Baseline Tests. Baseline diesel tests were conducted at constant rated speed (360 rpm) and four generating loads, No Load, 1800 KW, 2600 KW, and 3600 KW. All tests were conducted at 110 F AMT except for the 3600 KW condition which also included 150 F AMT and 95 F AMT tests.

The gaseous emissions were comparable to those reported in other tests of diesel generators burning No. 2 diesel fuel.[4] The O_2 ranged from 10.8 percent at 3600 KW to 18.2 percent at FSNL. As expected, the CO_2 increased with increasing load. The CO was slightly higher than expected, up to 195 ppm at 3600 KW, indicating less than optimum performance. The SO_2 concentrations were low, reflecting the low sulfur content of the fuel.

Gaseous Emissions from Blend Tests. Tests were conducted for the various blend ratios and load conditions. The results from the stack emissions measurements for the full engine tests are summarized in Table 1. This table provides averages for each engine load condition as measured at the baseline fuel condition and for the three blend ratios. As was observed in the baseline tests, the CO_2 increased with engine load while O_2 decreased. There was no observed effect of blend ratio on SO_2 emissions, although SO_2 did increase slightly with increasing load as would be expected. The NO_x, when corrected to 15 percent O_2 (dry), showed a significant increase as load was increased to 1800 KW and then a more gradual increase up to the maximum load of 3600 KW.

The results of gaseous monitoring for the blend tests at AMT of 95 F and 150 F were compared to the 110 AMT tests. The 3600 KW baseline emission tests for 95 F and 150 F AMT were comparable to the 110 F AMT tests. The gaseous emissions showed no significant changes between operating temperatures except that the corrected NO_x appeared to increase slightly at 110 F AMT compared to 95 F AMT but to decrease when the AMT was raised to 150 F.

Particulate Emissions from Blend Tests. The stack particulate emissions for the baseline and three blend ratios were measured. The effect of blend ratios

on the particulate emission rate is shown graphically in Figure 2. In this representation the percent increase of the particulate emission rate over the baseline value for the various blend ratios is plotted for the two higher engine loads at 110 F AMT.

The effect of blend ratio on the particulate emissions is significant. The increase in the rate over baseline is approximately the same for the two conditions load at 110 F AMT. The increase over baseline is greater at 150 F AMT and less at 95 F AMT. In terms of actual emissions rate based on mass of particulate per heat input, the 50 percent blend at 2600 KW and 110 F AMT was lowest while the 66.7 percent at 3600 KW and 110 F AMT was the highest. A test of 75 percent blend at 3600 KW and 150 F AMT was observed to have a lower particulate emission rate than the reported highest value and similarly a baseline test of 3600 KW and 150 F AMT showed a 42 percent lower particulate emission rate than either the 95 F AMT or the 110 AMT baselines. This suggests that increasing the AMT may reduce the particulate emission rate.

Other Gaseous Emissions. Emissions samples for SO_3 and chlorides measurements were also included in this program. In total, 12 samples for SO_2/SO_3 measurement were obtained; 6 were in the stack location and 6 were in the single cylinder configuration. No SO_3 was detected in any of the samples by the standard titration with 0.02 N NaOH. In each of the tests for particulate emissions conducted in this program, an impinger sample was collected for Cl determination by AgCl gravimetric method. In all cases there was no precipitate formation indicating chlorides were less than the detectable limit.

Conclusions

The use of EDS/DF-2 fuel blends in utility diesels provides an acceptable alternative to conventional petroleum based fuel operation. A blend ratio of approximately 66.7 percent EDS and 33.3 percent DF-2 can be used without engine knocking at an AMT of 110°F. At an AMT of 150 °F this ratio can be extended to 75 percent EDS. The major impact of the use of EDS blends appears to be an increase in the particulate emissions rate. The effect of EDS/DF-2 blends on particulate emissions was significantly influenced by both blend ratio and engine load. Increasing one or ther other or both resulted in an increase in the particulate emissions, though an increase in AMT may reduce the particulate emissions rates. No information on particle size or morphology was obtained in this program.

The results of the exhaust stack measurements of gaseous emissions indicate that the use of EDS/DF-2 fuel blends under engine load conditions resulted in a moderate increase in CO emissions (25%) and a moderate decrease in THC emissions (26-31%) when compared to baseline (0%) tests. The EDS/DF-2 fuel blends all showed substantial increases in both CO and THC emissions at the no-load condition.

The emissions of NO_x from EDS blends are less than or equal to the baseline over all engine loads except for the maximum EDS/DF-2 blend where NO_x levels were slightly higher at lower loads. A 150 F AMT slightly increased the NO_x for baseline and the 66.7 percent blend at 3600 KW but lowered the 2600 KW concentration. The overall average percentage of NO_2 in the NO_x at baseline conditions was approximately 9 percent. Due to problems with the NO analyzer the effect of AMT and blend ratio on NO_2 could not be determined.

There was little correlation between blend ratios and SO_2 emissions, all of which were relatively low. Measurements of SO_3 and Cl were below the expected lower limits and thus the potential for corrosion should be minimal in the use of EDS/DF-2 blends.

Acknowledgements

This work was supported by EPRI through the Advanced Power Systems Division. Mr. Henry Schreiber was the Project Manager. Field Sampling was conducted by Battelle Columbus personnel Paul Webb, Harry Leonard and William Baytos. Cooper Energy Services and Easton Utilities provided technical assistance and operated the fuel handling and engine systems during the tests.

References

1. Piper, B. F., Hersch, S., and Nazimowitz, W., "Combustion Demonstration of SRC II Fuel Oil in a Tangentially Fired Boiler", KVB, Inc., Final Report No. EPRI FP-1029, Projects 1235-5 and 1412-2. Prepared for Electric Power Research Institute, May 1979.

2. Downs, W. and Kubasco, A. J., "Characterization and Combustion of SRC II Fuel Oil", The Babcock and Wilcox Company, Final Report No. EPRI FP-1028, Projects 1235-3, -4, and 1412-1. Prepared for Electric Power Research Institute, June, 1979.

3. Ariga, S. and Baker, Q. A. "Evaluation of Exxon Donor Solvent (EDS) Coal Liquid as a Utility Diesel Fuel". Appendix C, EPRI Report AP-3224, October, 1983.

4. Shih, C. C., Hammersma, J. W., Ackerman, D. G., Beimer, R. G., Kraft, M. L., and Yamada, M. M., "Emission Assessment of Conventional Stationary Combustion Systems: Volume II, Internal Combustion Sources", U.S. EPA Report No. EPA-600/7-79-029C, February, 1979.

5. Piispanen, W., Webb, P. and Trayser, D. "Emissions Sampling for Utility Diesel Synfuel Tests" Appendix B in EPRI Report AP-3224, October, 1983.

TABLE 1

AVERAGE STACK GASEOUS EMISSIONS DATA SUMMARY FOR FULL ENGINE TESTS
(From Reference 5)

Load (KW)	CO_2 (percent)	CO (ppm)	O_2 (percent)	SO_2 (ppm)	NO (ppm)	NO_x (ppm)	THC (ppm)
			0 Percent Blend, AMT = 110 F				
FSNL	1.8	178	18.2	67	--*	388	206
1800	5.6	87	13.2	73	803	835	142
2600	6.2	93	12.0	72	833	915	153
3600	7.2	161	10.8	80		986	166
			25 Percent Blend, AMT = 110 F				
FSNL	1.8	345	18.5	54		516	273
1800	7.8	105	13.3	60	776	835	155
2600	6.6	105	12.0	58	--	895	160
3600	7.2	175	11.1	55	--	962	205
			50 Percent Blend, AMT = 110 F				
FSNL	1.9	725	18.3	56		601	390
1800	6.0	110	13.0	56	--	850	117
2600	6.7	124	12.0	64	--	878	120
3600	7.4	162	11.0	62	--	991	128
			66.7 Percent Blend, AMT = 110 F				
FSNL	1.8	1200	18.5	50		540	750
1800	6.1	110	12.9	59	974	1007	108
2600	6.9	116	11.8	61	--	1004	105
3600	7.3	170	11.2	62	--	917	122

*Indicates data deleted due to malfunction of instrument.

Note: NO and NO_x data are corrected to 15 percent O_2.

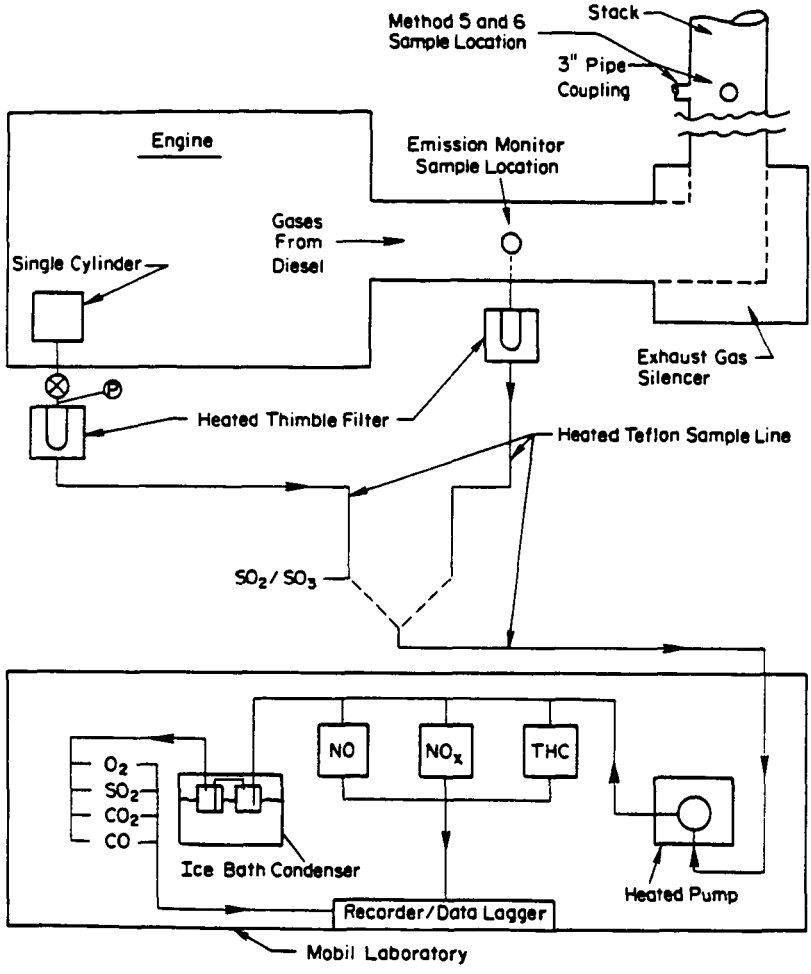

FIGURE 1. SCHEMATIC OF BATTELLE MONITORING AND SAMPLING EQUIPMENT

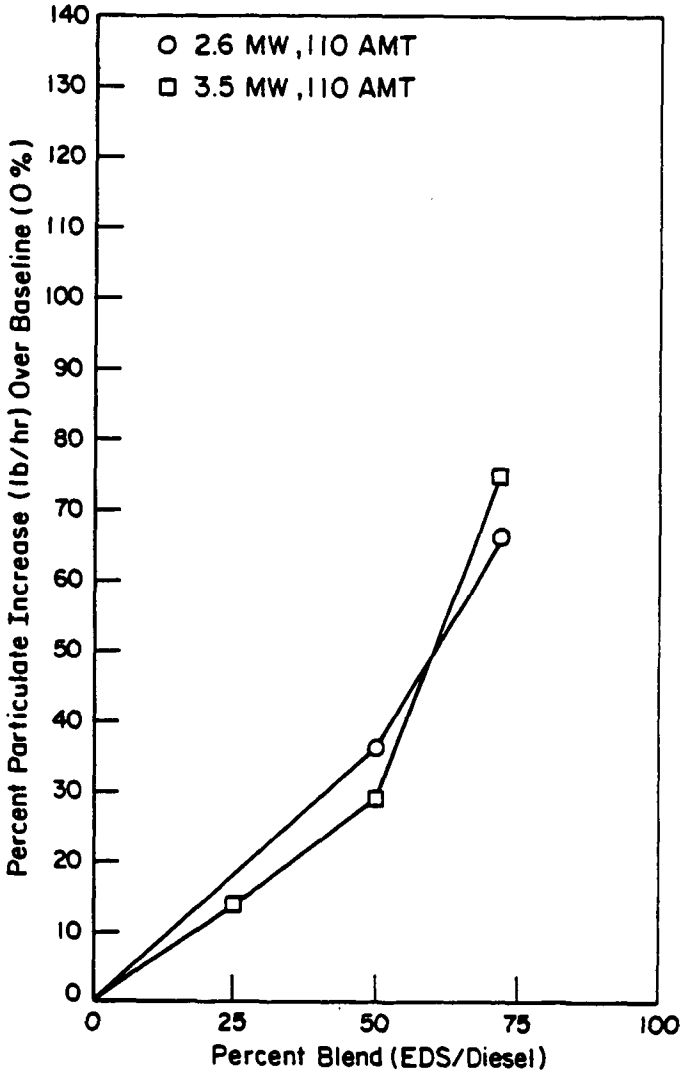

FIGURE 2. PARTICULATE MASS RATE INCREASE AS AFFECTED BY BLEND RATIO, ENGINE LOAD, AND AMT

SORBATE AND LEACHATE CHARACTERISTICS OF FLY ASH

John W. Liskowitz, James M. Grow, Mung S. Sheih, Richard B. Trattner

Industry/University Cooperative Center for
Research in Hazardous and Toxic Substances
New Jersey Institute of Technology, Newark, New Jersey 07102

James A. King

Lincoln University, Lincoln, Pennsylvania 19352

John Kohut and Melvin Zwillenberg

Public Service Electric & Gas, 80 Park Plaza, Newark, New Jersey 07101

Increased reliance on coal combustion can give rise to significant fly ash storage or disposal problems. Most fly ash is presently used as a low cost material for construction purposes and also as cover material for landfills. Other, more economically advantageous uses for this inexpensive material would be desirable. One such use for fly ash could be to treat ash pond effluent for reuse by power plants as cooling tower makeup water. Another application could be as sorbents of the heavy metals, toxic anions and organic substances commonly found in leachates emanating from landfills. Over the past several years, our laboratory has developed, under EPA Grants R803-717-91 and R803-717-02 a method for the treatment utilizing fly ash alone or in combination with other inexpensive sorbents for the removal of heavy metals, toxic anions and organics from industrial sludge leachates and industrial waste stream effluents. During the course of these investigations, two types of fly ash were repeatedly collected at different times from the some electrostatic precipitator at a coal burning boiler of a large east coast electric utility. These fly ashes exhibited different leaching and sorbent characteristics; i.e. one type produced an acidic leachate while the other leached basic. Although both fly ashes initially leached both cations and anions, the leaching eventually ceased and removal of these species occured. For example, the fly ash whose effluent was initially acidic leached copper (0.69 micrograms/gram of fly ash) and zinc (0.32 micrograms/grams of fly ash) when this material was placed in a lysimeter and eluted with industrial sludge leachate. After a period of time the leaching ceased and both copper and zinc in the treated effluent were reduced from about 2.5 mg/l and 0.4 mg/l, respectively, to 0.01 mg/l.[1] Since each fly ash type exhibited different sorbent characteristics, a mixture of both types was found to be more effective in the treatment of industrial sludge leachates. Up to this point, the availability of the different types of fly ash from the power plant could not be predicted. One simply had to collect what was available and determine its characteristics by testing. This lack of an adequate supply of fly ashes with the desired sorbent characteristics inhibited the further development of this low cost technology for the treatment of industrial waste effluent and leachate from industrial landfills. Therefore, an investigation was carried out in order to correlate the sorbent and leaching characteristics of fly ash produced with the composition of the coal and the combustion conditions that existed during the production of these fly ashes.

Three different types of coal fired boilers were utilized in this study. One type (A), a dry bottom boiler, was operated with flame temperatures below the ash fusion temperature of the coal ash. The second type (B), a wet bottom boiler, was operated at flame temperatures which exceeded the ash fusion tem-

perature of the coal ash. The third boiler types (C&D), dry bottom tangentially fired boilers, were operated with flame temperatures that were comparable to the ash fusion temperatures of the coal.

Six high fusion coals and five low fusion coals were burned in these three different boiler types under closely monitored conditions. Table 1 gives a listing of these coals by mine name and location.

TABLE 1

COAL BURNED UNDER TEST CONDITIONS

Mine		Location
	High Fusion Coal	
Militant		Pennsylvania
Deep Hollow		West Virginia
Upshur		West Virginia
Badger		West Virginia
Mine Mouth C		Pennsylvania
Mine Mouth D		Pennsylvania
	Low Fusion Coal	
Wellmore Cactus		Virginia
Wellmore Ackiss		Virginia
Ellsworth		Pennsylvania
Nora		Pennsylvania
Blend		Not known

Table 2 gives the temperature profile observed in the boilers along with the coal, natural gas and oil feed rates when co-fired or relative power outputs when the coal feed rate was unavailable, boiler additive feed rates, percent excess air, ambient air temperature, barometric pressure and power generation level.

During the combustion of the test coal, coal samples were collected at the entrance to each pulverizer just prior to being burned. The collection of fly ash was timed to correspond to the coal being burned. Different size distributions of the fly ash were obtained by the collection of samples from both the front and back row of electrostatic precipitators. The coals and their ashes were analyzed for %C, %S, %SiO_2, %Al_2O_3, %Fe_2O_3, %CaO, %K_2O, %Na_2O, %M_gO, ppm of Ti, Cd, Cu, Cr, Pb, Zn, Sn, Ni, Mn, ash content and ash fusion temperatures according to ASTM procedures.

The difference in leaching of Cadmium, Boron, Tin, Molybdenum, Nickel, Lead, Copper, Chromium, Zinc, Manganese and Iron from both the high fusion and low fusion fly ashes in general were found to be dependent upon the differences in trace amounts of these elements present in the fly ash, the differences in the size of the fly ash particles and the differences in boiler temperatures encountered by the fly ashes during their generation.

The differences in the amount an element is leached from the fly ashes was found to be related directly to the concentration in the fly ash for a majority of the elements examined. The differences in the amount of an element present in the high fusion fly ashes in turn is determined by its concentration in the coal and the size of the fly ash particles. The smaller fly ash particles were found to contain greater amounts of specific element than the larger particles. In comparison, the differences in the amount of a specific element found in the low ash fusion was observed to be dependent on its concentration

in the coal, its particle size as well as boiler temperatures. The smaller low fusion fly ash particles and lower boiler temperatures, when compared to the larger particles and higher boiler temperatures, contained the greater amounts of the majority of the above elements.

TABLE 2

Upper Reading Conditions of Coal Fired Boilers

Boiler A Generation Station

Coal	Coal (TPH)	Oil %	Gas (MCF)	Pressure (MM/S)	Excess O_2 %	Additive Feed Rate LPH-40 Gal/hr	Additive Feed Rate CTRL M Lbs/hr	Power	Boiler Temperature (F) Flame	Above Basket	Super Heater
Militant	110	0	2900	30.8	5.4	18	25	full	-	-	-
Militant	108	0	400	30.5	8.0	18	25	min.	-	-	-
Militant	102	0	1125	30.5	6.6	18	25	int.	-	-	-
Militant	110	0	3145	30.5	3.9	17.5	25	full	-	-	-
Deep Hollow	140	32	0	29.65	5.4	14	25	full	-	-	-
Deep Hollow	114	0	0	29.65	8.0	14	25	low	-	1450	-
Deep Hollow	142	0	0	29.65	6.8	16	20	int.	-	1550	-
Upshur	198	0	0	29.8	4.7	18	0	full	2470	1590	1565
Badger	188	0	0	29.3	3.1	18	25	full	2550	1750	1440

Boiler B Generation Station

Coal	Relative Power output %	Pressure (mmHg)	% Excess O_2	Additives Feed Rates LPA-40 gal/hr	Control M lbs/hr	#11 Boiler Temp. Above Flame	Basket	Arch	#12 Reheater Temp. Above Flame	Basket	Arch
Wellmore Cactus #1	89	-	3.8	32	0	3150	1620	2080	3150	1530	1480
Wellmore Cactus #2	100	27.8	3.3	28	0	3125	1400	1680	2970	1400	1320
Blend	95	27.8	3.4	28	0	3100	1815	2250	3100	1737	1835
Ellsworth	98	27.7	3.5	0	0	3100	1815	2240	3100	1740	1820
Wellmore	94	27.8		16	0	3050	1900	2180	2950	1725	1500
Ackiss	50	27.8	5.0	16	0	2870	1590	1780	2950	1620	1500
Nora	97	-	3.5	20	0	3100	1850	2175	3250	1700	1700

Boiler C and Boiler D Generation Station

Coal	Coal (TPH)	Pressure (mmHg)	% Excess O_2	Additive Feed Rate LPA-40 gal/hr	Control M lbs/hr	Power	Boiler Temperature Flame	Above Basket	Arch
Boiler C	313	-	4.2	0	0	full	-	2600	-
Boiler D	303	-	4.7	0	0	full	2650	2700	2700

There appears to be some correlation between the differences in trace element leaching observed for the fly ashes and the concentration of these elements at the surface of the fly ash particles provided that greater than 50% of the element is concentrated at the surface. Hansen and Fischer [2] have shown that the major portion of the Cd, Cu, Zn, Cr, Pb, and Mo present in the fly ash particles are concentrated at the surface of the fly ash particles. Our results reveal that the difference in leaching of the Cd, Cu, Zn, Cr, Pb and Mo by a majority of the fly ashes can be correlated with the differences in the amounts of those elements present in the fly ashes. However, when the trace elements are not concentrated at the surface, as was reported by Hansen and Fischer to be the case for Ni and Fe[2], our results indicate no correlation between the difference in leaching by the fusion fly ashes and the differences in the amounts of these elements present in these fly ashes.

The exceptions to the above correlations is Mn. Although, the concentration of Mn at the surface of the fly ash particles was reported by Hansen and Fischer to be less than 50%, our results show that most of the differences in leaching exhibited by the Blend, Wellmore Cactus #1, Militant, Deep Hollow and Wellmore Ackiss fly ashes can be correlated with the differences in the amount of manganese present in these fly ashes.

Differences in the leaching of the above elements as they relate to particle size and boiler temperatures is explained as follows. A comparison of the elements leached from small fly ash particles and large fly ash produced from the same coal under the same boiler conditions show the smaller particles in general leach greater quantities of the above elements than the larger particles. If the distribution of leachate elements within the different phases present in the fly ash are the same, the smaller particles would expose a greater leachable surface area.

Boiler temperatures probably influence the leaching characters of the fly ashes by fixation of the leachable elements. The different leaching results obtained with the low fusion fly ashes produced from the same coal at the same time indicated that operation of the boiler at temperatures above the ash fusion temperatures, along with the ash remaining in the fused state for longer lengths of time can reduce the leaching exhibited by the fly ashes. Apparently, these temperatures, lead to some fixation of these elements into the non-soluble portion of the fly ash. The leaching results suggest that the leachable elements are contained to some extent within a water soluble component located at the surface of the ash which is eventually removed when the fly ash is brought in contact with the aqueous ash pond effluent. The leachable amounts of each element can be in general related to 1) the amount of this element present in the fly ash (provided that a major portion to the element is located at the surface), 2) the surface area of the fly ash particles and 3) the boiler temperature encountered by the fly ashes during their formation.

Three separate ash pond samples were used to evaluate the effectiveness of the fly ash in treating fly ash pond effluent. Analysis of these ash pond samples are presented in Table 3.

The results show that fly ash can be used for treatment of Cd, B, Sn, Mo, Ni, Pb, C, Cu, Zn, Mn, Fe, As and organics in these ash pond effluents. Removals of greater than 75 percent were achieved for all of the above elements with the exception of Boron and Molybdenum where removals of only 21% and 43%, respectively were obtained. For example, Figure 1 shows that the concentration of lead remaining in the treated ash pond sample remained below detectable levels with no indication of breakthrough even after passing 36 liters of ash pond sample through the fly ash generated from the Nora coals. These removals

were achieved even though the concentration of lead in the ash pond sample was increased to 3.0 mg/1 (see dotted line in Fig.1). The maximum allowable primary drinking standard for lead is 0.05 mg/1. The exceptional removal of lead does not appear to be due to precipitation since the concentration of lead in the ash pond sample was kept below the maximum solubility of the lead as measured as a function of pH (See Fig. 2). Also, the pH measured in the treated ash pond effluent ranged from an alkaline value of 10 down to an acidic value of 6 during the removal of lead from 36 liters of ash pond sample. (See Fig. 3).

TABLE 3

Elemental Concentration of Actual Ash Pond Effluent Used In Fly Ash Sorbate Characterization

Element	Sample A mg/1	Sample B mg/1	Sample C mg/1
Cadmium	N.D.*	N.D.*	0.02
Boron	3.30	3.30	2.80
Tin	0.90	2.07	1.01
Molybdenum	3.0	2.70	0.41
Nickel	0.26	0.11	0.09
Lead	1.80	0.35	0.62
Copper	.01	0.01	0.09
Chromium	.48	0.18	0.09
Zinc	.16	0.06	1.48
Manganese	.24	0.24	0.40
Iron	0.22	0.05	0.10
Arsenic	0.16	0.15	0.13

*N.D. - below measurable limits

The general sorbate characteristics of the fly ashes are favored by low ash fusion temperatures, combustion temperatures that favor the fusion of the fly ash during formation and the time that the fly ashes remain in the fused state. No correlation could be established between the sorbate characteristic of the fly ashes and their bulk major, minor and trace elemental compositions nor with their major and minor elemental surface compositions. Also, no correlation could be established between the treatment achieved with the fly ashes and particle size of the fly ash particles. Only the carbon content of the fly ash could be related to its organic removal properties.

The sorbate capacities of the fly ashes, identified in this investigation to provide the best treatment, average about 80 ug/gm for the Cadmium, Copper and Zinc, 3.4 ug/gm for Arsenic and 700 ug/gm for the organics. However, the sorbate capacity for Arsenic may be increased with further washing of the fly ashes.

These capacities were found to be independent of pH in the range from about 6 to 10. Also, the removals of Cadmium, Copper, Lead and Zinc were observed to be independent of their inlet concentrations in the ranges from 0.52 mg/1 to 2.0 mg/1, 0.52 mg/1 to 3.5 mg/1, 0.30 mg/1 to 3.0 mg/1 and 0.56 mg/1 to 4.0 mg/1, respectively.

Greater than 75 percent removals of the Cadmium, Copper and Zinc present in the ash pond samples were achieved within a 15 minute contact time between the fly ash and the sample. The results indicate that removal of the above elements in ash pond effluent can be achieved with the same fly ash that origi-

nally leached these elements. The washed fly ash was observed to have a significant excess of sorbative capacity beyond that required to treat the elements originally leached from the fly ash.

Financial support for this work was provided by the U.S. Department of Energy, University Coal Research Programs PETC, Pittsburgh, Pennsylvania under Grant No. DE-FG22-80PC30231.

REFERENCES

1. Chan, P., Dresnack, R., Liskowitz, J.W., Perna, A. and Trattner, R. "Sorbents for Fluoride Metal Finishing and Petroleum Sludge Leachate Contaminant Control," EPA 600/2-78-824. March (1978).

2. Hansen, R.D., and Fischer, G.L. "Elemental Distribution in Coal Fly Ashes," Env. Sci. & Tech., 14, pp. 1111-1117 (1980).

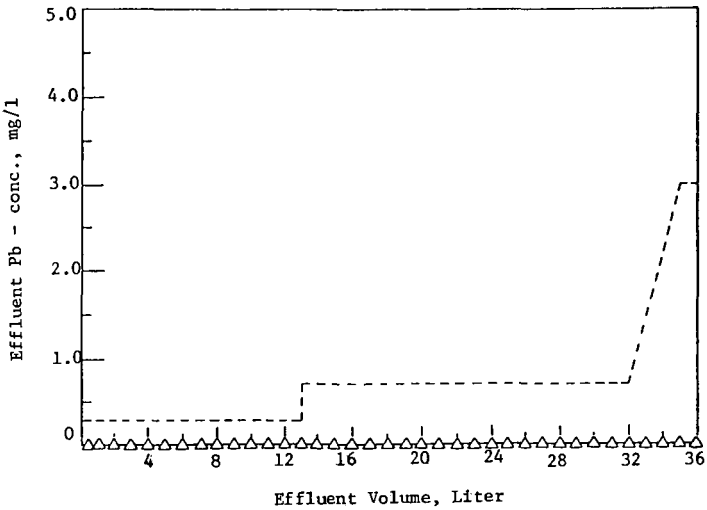

Fig. 1 Concentration of Lead Remaining After Treatment with Nora Fly Ash, 500 grams

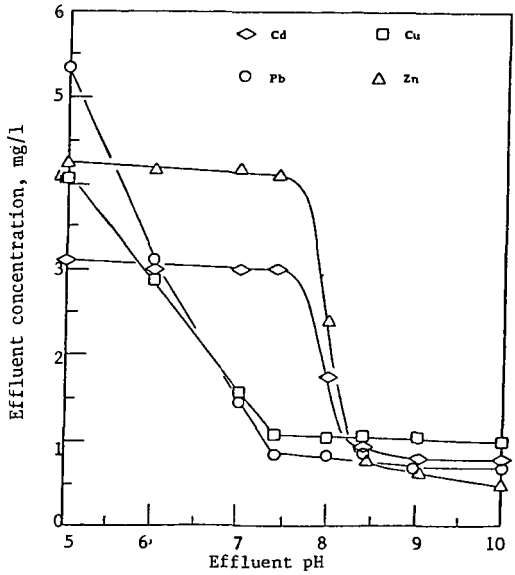

Fig. 2. pH Effect on Cadmium, Copper, Lead and Zinc Solubility in Ash Pond Sample D.

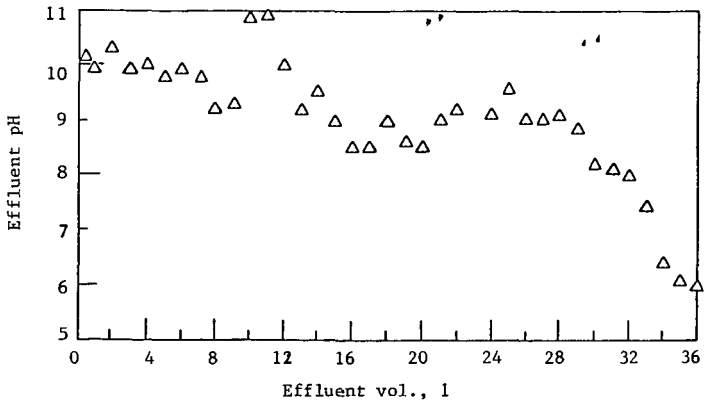

Figure 3. pH of Treated Ash Pond Sample Using Nora Fly Ash

OXYGEN ISOTOPIC STUDY OF THE OXIDATION OF SO_2 BY H_2O_2 IN THE ATMOSPHERE

B. D. Holt and R. Kumar

Argonne National Laboratory, Argonne, Illinois 60439

INTRODUCTION

Considerable interest has been shown in the possibility of using oxygen isotopy to elucidate the role of H_2O_2 in the oxidation of SO_2 to sulfates in the atmosphere (1). The potential importance of H_2O_2 lies in the view that aqueous-phase oxidation of SO_2 to H_2SO_4 probably accounts for a major fraction of the observed SO_4^{2-} in the precipitation occurring in the northeastern United States. The key reactants responsible for the this oxidation are not well known, although a large number of possible catalysts and oxidants exist in the atmosphere, including carbon, transition metal ions, hydroxyl and organic free radicals, hydrogen peroxide and ozone. Of these, the last two are the only ones believed to be present in sufficient quantity to produce the observed amounts of SO_4^{2-} in wet deposition. It is quite possible that the atmospheric oxidation of SO_2 is limited by the availability of one or both of these oxidants, rather than by the availability of SO_2 itself. It is therefore important to determine if indeed H_2O_2 has a pivotal role in acid formation and deposition from the atmosphere.

Oxygen isotopic studies are useful in distinguishing between the different oxidation mechanisms effective in the atmosphere. Laboratory simulation of several different atmospheric reaction sequences has shown that the oxygen isotope ratio in the product SO_4^{2-} is uniquely related to the reaction pathway followed in its formation (2). It may therefore be possible to determine if the atmospheric hydrogen peroxide is responsible for significant oxidation of SO_2 to sulfate, and if it is this oxidant that limits the aqueous-phase formation of sulfuric acid. The results of these studies could have significant implications for energy technology, particularly if they indicate that it may be more important to reduce the ambient concentrations of H_2O_2 than of SO_2.

In the 1981 JASON committee report to the U. S. Department of Energy (1), some recommendations for further research were based, at least in part, on our earlier work on SO_2 oxidation by H_2O_2 (3). In those studies the $\delta^{18}O$ [deviation in parts per thousand (‰) of the $^{18}O/^{16}O$ ratio of the sample from that of the standard reference material, Standard Mean Ocean Water (SMOW)] of sulfates produced by H_2O_2 oxidation were significantly lower than the $\delta^{18}O$ of sulfates found in rainwater. However, the $\delta^{18}O$ of the reagent-grade H_2O_2 used in those experiments was not known. The results suggested the need for isotopic analysis of H_2O_2 in dilute solutions, and for a methodology whereby the $\delta^{18}O$ values of H_2O_2, H_2O, and SO_4^{2-} in rainwater could be compared in order to assess the importance of H_2O_2 in the formation of sulfate-constituted acid rain.

EXPERIMENTAL

The plan of this investigation was to develop a method for the determination of the $\delta^{18}O$ of H_2O_2 in dilute aqueous solutions (simulating rainwater); to prepare solutions of H_2O_2 of various ^{18}O enrichments; to use the freshly prepared solutions of H_2O_2 to oxidize SO_2 to SO_4^{2-} for evaluation of the relationship between $\delta^{18}O_{SO_4^{2-}}$ and $\delta^{18}O_{H_2O_2}$; and to apply this relationship to the measured $\delta^{18}O_{H_2O_2}$, $\delta^{18}O_{SO_4^{2-}}$, and $\delta^{18}O_{H_2O}$ in precipitation water, for assessment of the importance of H_2O_2 in the atmospheric transformation of SO_2 to sulfate.

Development of Analytical Method

No suitable analytical method was available for the quantitative extraction of the oxygen in H_2O_2, (dissolved in water in the ppb range), for isotopic analysis. A 4-step method was developed (4). It consisted

of the removal of dissolved O_2 from 20-liter samples of water by a combination of evacuation, ultrasonic agitation, and sparging with helium; oxidation of the dissolved H_2O_2 to O_2 in the water with $KMnO_4$; removal of the newly formed O_2 from the water in a carrier-gas stream; and conversion of the O_2 to CO_2 by reaction with platinum-catalyzed carbon at 600°C. The CO_2 was then mass spectrometrically analyzed for its $\delta^{18}O$ (identical to that of the oxygen in the original H_2O_2).

To confirm the absence of appreciable isotopic interference by oxygen exchange between the H_2O and either the H_2O_2 or the O_2, before, during, or after the oxidation reactions, the reaction was carried out in the presence of three different water supplies of various $\delta^{18}O$. The results in Fig. 1 show that the $\delta^{18}O$ of the CO_2 product was unaffected by the $\delta^{18}O$ of the water solvent.

Synthesis of $\delta^{18}O$-enriched H_2O_2

Hydrogen peroxides of various $\delta^{18}O$ were not commercially available. A suitable method of synthesis was identified and successfully applied to the laboratory preparations of four stock solutions of H_2O_2 of different $\delta^{18}O$. By this method(5), H_2O_2 is formed by exposure of different supplies of water vapor (each differing in $\delta^{18}O$) to a high-voltage ($\sim$1.4 kV) discharge in $\sim$100 cm of 10-mm o.d. glass tubing between two water-cooled aluminum electrodes. Some of the HO radicals formed by the dissociative reaction

$$2H_2O \rightleftarrows 2HO + 2H \qquad 1)$$

are condensed in a liquid-nitrogen cold trap where they combine to form H_2O_2, leaving the H radicals to combine in formation of H_2 and be pumped away through the vacuum line.

Other techniques which we experimentally found to give inadequate yields of H_2O_2 were conduction of an electric arc across a stream of aerosolized water droplets (6), excitation of water vapor by a radio-frequency silent discharge in a glass chamber (7.5 cm dia $\times$ 20 cm long) in a commercially available plasma cleaner unit, and excitation by a glow-discharge unit (4.8 cm dia $\times$ 70 cm long) that had uncooled aluminum disk electrodes (7).

Oxidation of SO_2 to SO_4^{2-} by H_2O_2

Using the four stock solutions of hydrogen peroxide, each of different $\delta^{18}O$, sulfate solutions of correspondingly different $\delta^{18}O$ were prepared by oxidation of SO_2 (of constant $\delta^{18}O$) in water ($\delta^{18}O$= $-7.9‰$). In Fig. 2 the $\delta^{18}O$ of each resulting sulfate is plotted versus the $\delta^{18}O$ of the H_2O_2 and the equation of the best-fit regression curve is

$$\delta^{18}O_{SO_4^{2-}} = 0.43\,\delta^{18}O_{H_2O_2} + 3.5‰ \qquad 2)$$

The regression curve of the previously determined (3) relationship between $\delta^{18}O_{SO_4^{2-}}$ and $\delta^{18}O_{H_2O}$ in aqueous-phase oxidation of SO_2 by H_2O_2 was

$$\delta^{18}O_{SO_4^{2-}} = 0.57\delta^{18}O_{H_2O} - 2.4‰ \qquad 3)$$

Assuming that all significant effects of the $\delta^{18}O$ of the SO_2 on the $\delta^{18}O$ of the SO_4^{2-} are lost by rapid isotopic exchange between the SO_2 and the large excess of water, prior to appreciable oxidation (3), $\delta^{18}O_{H_2O}$ and $\delta^{18}O_{H_2O_2}$ remain as the only two complementary variables in the equation for $\delta^{18}O_{SO_4^{2-}}$; therefore, the comprehensive regression curve for $\delta^{18}O_{SO_4^{2-}}$ is

$$\delta^{18}O_{SO_4^{2-}} = 0.57\,\delta^{18}O_{H_2O} + 0.43\,\delta^{18}O_{H_2O_2} + C \qquad 4)$$

$$= \sim\frac{3}{5}\,\delta^{18}O_{H_2O} + \sim\frac{2}{5}\,\delta^{18}O_{H_2O_2} + C \qquad 5)$$

The constant, C, was evaluated at 8.4‰ from the data given in Fig. 2 by substituting the corresponding measured values for $\delta^{18}O_{SO_4^{2-}}$ and $\delta^{18}O_{H_2O_2}$, and −7.9‰ for $\delta^{18}O_{H_2O}$.

The comprehensive equation then became

$$\delta^{18}O_{SO_4^{2-}} = 0.57\ \delta^{18}O_{H_2O} + 0.43\ \delta^{18}O_{H_2O_2} + 8.4‰ \qquad 6)$$

and can now be used to calculate $\delta^{18}O_{SO_4^{2-}}$ from $\delta^{18}O_{H_2O_2}$ and $\delta^{18}O_{H_2O}$ of rainwater for comparison with corresponding measured values of $\delta^{18}O_{SO_4^{2-}}$. This comparison may prove to be uniquely useful in the assessment of the importance of H_2O_2 in the oxidation of SO_2 to SO_4^{2-} in the atmosphere.

The slope of 0.43 (approximately 2/5) in Equation 2 of the regression curve through the data of Fig. 2 confirms the evidence of the intermediate species, $H_2O_2 \cdot SO_3^{2-}$, which was previously proposed (3). Apparently, the $\delta^{18}O$ of the sulfate product is 2/5-controlled by the two oxygens in the H_2O_2 of the adduct, and 3/5-controlled by the SO_3^{2-}, which, in turn, is isotopically controlled by rapid oxygen exchange with the large excess of water with which it is associated.

PRELIMINARY RESULTS

The thrust of this paper is to report the readiness of a new isotopic method for studying the oxidation of SO_2 by H_2O_2 in the atmosphere. So far, the analytical procedure has been applied to samples of rainwater from only two rain events at Argonne, IL. We recognize the uncertainty of the significance of results from so few samples; however, we present them as suggestive of what may follow in more comprehensive sampling programs.

The rainwater was collected by four 1-m^2 dish-shaped plastic funnels. The funnels were inverted skylights, fitted with drainage connections. Enough water was collected to provide duplicate 20-liter samples from each of the two rains. The first duplicate of each rain was analyzed as soon as operationally practical after collection; the second, a few days later, after storage in the polyethylene bottles in a "cool," unrefrigerated location. The analytical procedure was also applied to a dilute solution of H_2O_2 from a reagent-bottle supply of 30% H_2O_2 (Fisher Scientific Company, H-325 Lot 720017), added to 20 liters of distilled water.

The results of these analyses are given in Table I. The concentrations of H_2O_2 in rainwater (derived from measurement of the CO_2 formed from the O_2 of H_2O_2 origin) ranged from 55 ppb and 35 ppb in the first duplicates of each sample, to 16 ppb and 5 ppb in tbe second duplicates. The decrease in concentration during storage for each sample was apparently caused by autodecomposition of the H_2O_2. The $\delta^{18}O$ of the H_2O_2 (~31‰ for each sample) was relatively high in comparison to that of air oxygen (23.5‰) and very high in comparison to the reagent-bottle H_2O_2 (~−6‰).

The measured values of $\delta^{18}O$ for sulfate in the first duplicate sample of each rain appeared to be significantly less (2–3‰) than the values calculated from the $\delta^{18}O$'s of H_2O and H_2O_2, using Equation 6. This suggests that the SO_4^{2-} in a fresh sample of rain may be a mixture of SO_4^{2-} formed by H_2O_2 oxidation of SO_2 and SO_4^{2-} formed by other mechanisms known to yield lower $\delta^{18}O$ values (3). The apparent decrease in $\delta^{18}O_{H_2O_2}$ (and correspondingly the calculated $\delta^{18}O_{SO_4^{2-}}$) with autodecomposition of the H_2O_2 during storage is surprising and not yet fully understood. Whether the $\delta^{18}O$ of the residual H_2O_2 increases or decreases during autodecomposition may depend on the catalyst(s) involved in the reaction (8-10).

TABLE I

SUMMARY OF RESULTS, H_2O_2 IN 20-L SAMPLES: REAGENT, RAIN

Sample	Duplicate	Storage Time (days)	H_2O_2 Concentration (ppb)	H_2O_2 Recovery (%)	$\delta^{18}O_{H_2O}$ (measd) (‰)	$\delta^{18}O_{H_2O_2}$ (measd) (‰)	$\delta^{18}O_{SO_4^{2-}}$ (calcd)* (‰)	$\delta^{18}O_{SO_4^{2-}}$ (measd) (‰)
Reagent	1	0	425	95		−5.4		
FSC	2	0	425	96		−6.5		
Rain	1	3	55	–	−4.1	31.1	19.5	16.2
9-25/84	2	8	16	–		22.4	15.7	
Rain	1	1	35	–	−3.3	30.8	19.7	17.6
10-18-84	2	5	5	–		22.4	16.1	

* $\delta^{18}O_{SO_4^{2-}\,(calcd)} = 0.57\ \delta^{18}O_{H_2O\,(measd)} + 0.43\ \delta^{18}O_{H_2O_2\,(measd)} + 8.4$.

LITERATURE CITED

(1) Chamberlain, J. C., Foley, H., Hammer, D., MacDonald, G., Rothaus, O., and Ruderman, M., Technical Report JSR-81-25, prepared for the Office of Energy Research, U. S. Department of Energy (1981).

(2) Holt, B. D., Kumar, R., and Cunningham, P. T., *Science*, **217**, 51 (1981).

(3) Holt, B. D., Kumar, R., and Cunningham, P. T., *Atmos. Environ*, **15**, 557 (1981).

(4) To be published elsewhere.

(5) Vol'now, I. I., Tsentsiper, A. B., Chamova, V. N., Latysheva, E. I., and Kuznetsova, Z. I., *Russian J. Phys. Chem.* **38**, 645–648 (1964).

(6) Kok, G. L., "The Production of Hydrogen Peroxide by Lightning," presented at the 1982 American Geophysical Union Meeting, San Francisco.

(7) Jarnagan, R. C. and Wang, J. H., *J. Amer. Chem. Soc.* **80**, 786–787 (1958).

(8) Taylor, H. S. and Gould, A. J., *J. Amer. Chem. Soc.* **56**, 1823 (1934).

(9) Malcolm, D., Rudd, D. P., Muchow, G. R. and Comte, C., *J. Chem. Phys.*, **20**, 961 (1952).

(10) Cahill, A. E. and Taube, H., *J. Amer. Chem. Soc.* **74**, 2312 (1952).

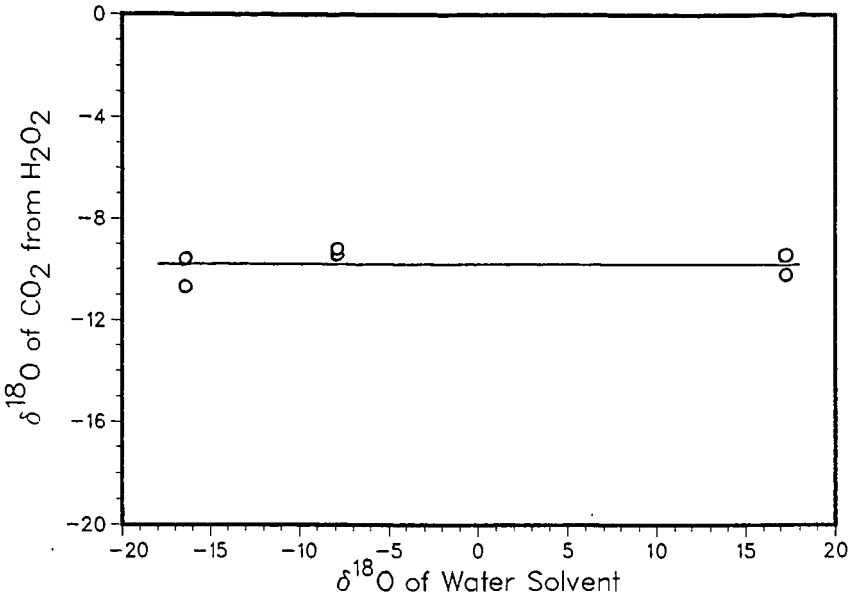

Figure 1. Isotopic influence of water solvent on CO_2 of H_2O_2 origin.

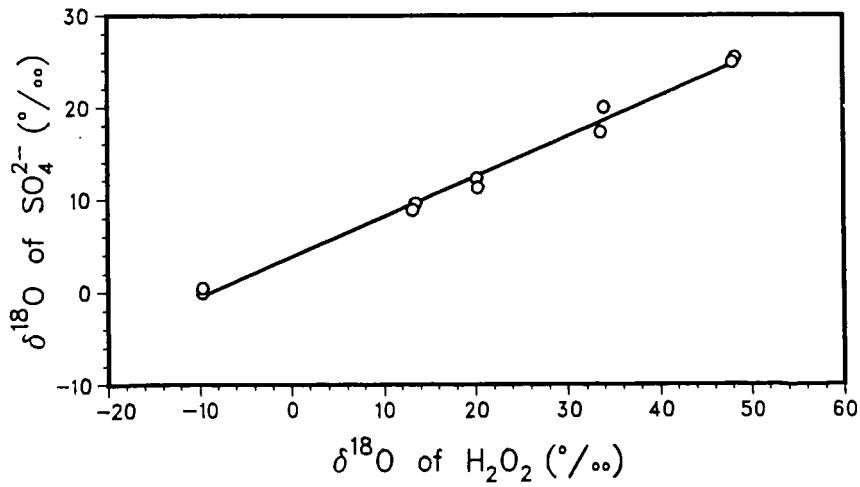

Figure 2. Isotopic influence of the H_2O_2 oxidant on the SO_4^{2-} product.

COAL COMBUSTION AND FOREST ECOSYSTEM HEALTH

William H. Smith

School of Forestry and Environmental Studies
Yale University
370 Prospect Street
New Haven, CT, 06511

Abstract

Historically, the combustion of fossil fuels has directly or indirectly been the source of air contaminants at three levels; local, regional, and global. Pollutants of importance at the local level have included sulfur dioxide and trace metals. Local forest damage is confined to a zone of a few km immediately surrounding a facility and for a distance of several to tens of km downwind. Regional air pollutants may be deposited over expansive forest areas because they are transported tens or hundreds of km from point of release due to small size or snythesis in the atmosphere from precursors introduced into the troposphere. Regional air pollutants of potential influence for forests include; oxidants, trace metals, and acid deposition. Global pollutants influence the entire atmosphere of the earth, e.g. halocarbons and carbon dioxide. The latter is important because of the potential it has to influence global climate. Risks associated with regional and global air pollution and forest health are high. The evidence available to describe the total boundaries of the problem for all pollutants is incomplete.

Introduction

A challenge of developed nations throughout the temperate zone is air quality policies that protect natural resources as well as human health. Throughout Europe and North America, the decade of the Eighties will be recorded as a period of profound decisions regarding atmospheric contamination and natural resource quality. The central issues for those interested in forest health are as follows. Is air pollution influencing the growth of forests or individual species, changing the species composition of forest communities or destroying certain tree species, associated plants or animals over significant forest areas? In an effort to answer this question, I shall discuss the spatial scales of air pollution stress and what we know about the response of trees to pollutants at these scales.

Local, regional and global-scale air pollutants

Local-

During the first two thirds of the twentieth century, research and regulatory efforts were focused on local air pollutants and acute vegetative effects. Pollutants of primary concern were sulfur dioxide, particulate and gaseous fluoride compounds and numerous heavy metals such as lead, copper, and zinc. Occasional interest was expressed in other inorganic gases including ammonia, hydrogen sulfide and chloride, and chlorine. The sources of these pollutants were and are typically discrete and stationary facilities for: energy production, for example, fossil-fuel electric generating plants, gas purification plants; metal related industries, for example, copper, nickel, lead, zinc or iron smelters, aluminum production plants; and diverse other industries, for example, cement plants, chemical and fertilizer plants and pulp mills.

It is appropriate for us to consider the above pollutants local-scale because forest areas directly affected by these facilities are typically confined to a zone of a few km immediately surrounding the plant and for a distance of several to tens of km downwind. The dimensions of the surrounding and downwind zones of influence are variable and primarily controlled by source strength of the effluent, local meteorology, regional topography and susceptibility of vegetation. In any case, the forest influence is confined to a region generally less than a thousand hectares.

Regional-

During the past three decades we have become increasingly aware of regional-scale air pollutants. The regional designation is applied because these contaminants may affect forests tens, hundreds, or even thousands of kilometers from their site of origin. The regional air pollutants of greatest documented or potential influence for forests include: oxidants, most importantly ozone; trace metals, most importantly heavy metals - e.g. cadmium, cobalt, copper, lead, mercury, molybdenum, nickel, vanadium, zinc; and acid deposition, most importantly sulfuric and nitric acids. Ozone, sulfuric and nitric acids are termed secondary air pollutants because they are synthesized in the atmosphere rather than released directly into the atmosphere. The precursor chemicals, released directly into the atmosphere and causing secondary pollutant formation, include hydrocarbons and nitrogen oxides in the case of ozone, and sulfur dioxide and nitrogen oxides in the case of sulfuric and nitric acid. The combustion of the fossil fuels coal, oil, gas release some hydrocarbons and sulfur dioxide. The heat of combustion causes nitrogen and oxygen to react and form nitrogen oxides. Many activities generate small particles (approximately 0.1 - 5 μm diameter). Those activities associated with combustion (particularly coal burning) can preferentially contaminate these small particles with trace metals. Because the formation of secondary air pollutants may occur over tens or hundreds of km from the site of precursor release, and because small particles may remain airborne for days or weeks, these pollutants may be transported 100 to more than 1000 km from their origin. Eventual wet and dry deposition of the pollutants onto lakes, fields, or forests may occur over large rather than small areas.

The U.S. Environmental Protection Agency and the U.S. Department of Agriculture, Forest Service established a network of air monitoring stations to measure ozone concentrations in remote areas of National Forests. Analysis of selected high ozone events during 1979 suggested that long-range transport of air masses contaminated by urban centers contributed to peak concentrations at remote sites (3). In a study of rural ozone episodes in the upper-midwest, Pratt et al. (18) presented evidence that ozone and precursors were transported 275 km from Minneapolis-St. Paul. Studies of trace metal concentrations, in the atmosphere in remote northern and southern hemispheric sites revealed that the natural sources include the oceans and the weathering of the earth's crust, while the major anthropogenic source is particle air pollution (23). Murozumi et al. (13) showed that long range transport of lead particles from automobiles significantly polluted polar glaciers. We estimated the annual lead deposition on a remote northern hardwood forest in New Hampshire to be 266 g per hectare. This caused lead contamination of the forest floor 5-10 times greater than the estimated pre-industrial concentration (20).

Evidence is available, satellites, surface deposition of aerosol sulfate and reduced visibility (2, 22, 28), for long-range transport of acidifying pollutants from numerous sources. During the winter, approximately 20 percent of the emissions from tall power plant stacks in northeastern United States may

remain elevated and relatively coherent for more than a day and 500 km (24).

The long distance transport of regional pollutants means they may have interstate, international and even intercontinental significance. It means further that the forests subject to their deposition exceed tens of thousands of km^2.

Global-

In the past 25 years, we have become concerned with a third scale of air pollution--global. Global pollutants affect the entire atmosphere of the earth. Two global air pollutants of special note include carbon dioxide and halocarbons.

Careful monitoring of carbon dioxide during the past two decades in Hawaii, Alaska, New York, Sweden, Austria and the South Pole has firmly established that carbon dioxide is steadily increasing in the global atmosphere. This increase is due to anthropogenic activities including fossil fuel combustion. It may also be caused by altered land use management, such as, forest destruction in the tropics. The atmospheric carbon dioxide concentration has been estimated to have been approximately 290 ppm (5.2×10^4 $\mu g\ m^{-3}$) in the middle of the nineteenth century. Today, the carbon dioxide concentration approximates 340 ppm (6.1×10^5 $\mu g\ m^{-3}$) and is increasing about one ppm (1.8×10^3 $\mu g\ m^3$) per year. In 1977-78 it increased 1.5 ppm (2.7×10^3 $\mu g\ m^{-3}$). In the year 2020, if the increasing rate continues, the carbon dioxide amount in the global atmosphere may be nearly two times the present value (5).

Naturally occurring stratospheric ozone is important because it screens the earth from biologically damaging ultraviolet radiation -- light with wavelengths between 290 and 320 nanometers — released by the sun. Halocarbons released by humans can deplete the natural ozone layer surrounding the earth. In summary, halocarbon molecules, especially chlorofluoromethanes, released by various human activities, are transported through the troposphere. They pass through the tropopause and lower stratosphere and are decomposed in the mid- to upper-atmosphere. Free chlorine, resulting from decomposition, causes a rapid, catalytic destruction of ozone. In 1979, the National Academy of Sciences estimated that release of halocarbons to the atmosphere, at rates inferred for 1977, would eventually deplete stratospheric ozone 5 to 28 percent, most probably 17 percent (14). In 1982, the National Academy revised its previous estimate and suggested a depletion from 5 to 9 percent (17).

Affect of local-scale, regional-scale and global-scale air pollution on forest ecosystems

Local-

High deposition of local air pollutants has caused documented forest destruction. High sulfur dioxide or fluoride doses, severely injure or kill forest trees. The ecosystems, of which the trees are a part, are simplified, lose nutrients, sustain soil erosion, have microclimates and hydrologic patterns altered and ultimately they are destroyed or converted to more resistant seral stages. Miller and McBride (12) reviewed the forests destroyed by local air pollution. Early in this century, it was clearly documented in numerous locations throughout North America that sulfur dioxide and trace metal pollution destroyed forests surrounding metal smelting facilities. Smelting centered in Ducktown, Tennessee devastated the southern hardwood forest over 27 km^2 (10.5

mi^2) surrounding the plant, coverted an additional 68 km^2 (17,000A) to grassland and created a 120 km^2 (30,000A) transition zone with altered species composition. Smelters in the Sudbury, Ontario, Canada area have caused simplification of the surrounding mixed boreal forest and have caused eastern white pine mortality in a 1865 km^2 (720 mi^2) zone to the northeast.

Aluminum reduction plants have also caused local forest destruction. In Montana, fluoride pollution killed or severely injured ponderosa pine and lodgepole pine on 8 km^2 (2000A) surrounding a plant. In Washington, ponderosa pine mortality and morbidity resulted over a 130 km^2 (50 mi^2) area in the vicinity of an aluminum plant.

Local pollution has caused extensive forest destruction throughout Europe. Examples are in Austria, Germany, Hungary, Norway, Poland and Sweden. Industrial operations along the northern border of Czechoslovakia have caused extensive forest destruction.

Regional-

Deposition of regional pollutants subject forests to different perturbations then local- pollutants because the doses are less. Rather than severe tree morbidity or mortality with dramatic symptoms, regional pollutants subtly change tree metabolism and ecosystem processes. Smith (19) provided a comprehensive review of subtle air pollution forest stress.

Regional air contaminants may influence reproductive processes, nutrient uptake or retention, metabolic rates (especially photosynthesis), and insect pest and pathogen interactions of individual trees. At the ecosystem level, regional air pollutants may influence nutrient cycling, population dynamics of arthropod or microbial species, succession, and biomass production. In the instance of high-dose local-scale pollution, the symptoms are typically acute, dramatic and obvious (severe disease, mortality, forest simplification). In the case of lower-dose regional-scale pollution, the symptoms are typically not visible (at least initially), undramatic and not easily measured. The integration of regional pollutant stresses is slower growth, altered competitive abilities and changed susceptibility to pests. Ecosystem symptoms may include altered rates of succession, changed species composition and biomass production. Symptom development is, of course, much slower at the regional scale. Evidence of the relative importance of regional pollutants is variable, caused in part by the length of time that has been devoted to the study of individual pollutants and in part by the subtleness and complexity of the pollutant interactions. The toxicity of trace metals has been studied for approximately 60 years, of ozone approximately 25 years and of acid deposition approximately 10 years.

Table 1 suggests the relative strength of evidence for forest responses to regional pollutants. A review of the column totals suggests we know most about the regional effects of oxidants, less about regional effects of trace metals and least about regional effects of acid deposition. A review of the row totals suggests tree and ecosystem processes especially vulnerable to air pollution stress. The processes with a total of five or more include; litter decomposition, seedling survival, photosynthesis, foliar necrosis, tree growth, microbial pathogen activity, and ecosystem succession plus species composition. These are the tree and ecosystem processes at particular risk from regional air pollution. Fig. 1 provides an overview of regional air pollution influence on forest trees and ecosystems.

Global-

Increasing carbon dioxide concentration and decreasing stratospheric ozone concentration of the atmosphere may alter global radiation fluxes. Presumably a primary result of more carbon dioxide in the air will be warming. While incoming solar radiation is not absorbed by carbon dioxide, portions of infrared radiation from earth to space are. Over time, the earth would become warmer. While the forces controlling global temperature are varied and complex, the increase of 0.5°C since the mid-1800s is generally agreed to be at least partially caused by increased carbon dioxide. By 2000 it may increase an additional 0.5°C. Numerous models advanced to estimate the average global warming per doubling of carbon dioxide project 0.7 to 9.6°C. Natural impacts on climate, such as solar variability, remain important and of unclear relationship to anthropogenic causes. A mean global average surface warming, however, of 3 ± 1.5°C appears reasonable (National Academy of Sciences 1982 a, b).

The consequences of a warmer global climate, with even a very modest temperature increase, on the development of forest ecosystems, could be profound. Warming, with increased carbon dioxide in the atmosphere, might enhance forest growth. Manabe and Stouffer (8) have estimated that a doubling of atmospheric carbon dioxide would cauae a 3°C warming at the U.S.-Canadian border, while Kellogg (6) has suggested that a rise of 1°C in mean summer temperature extends the growing season by approximately 10 daya. Other changes associated with global warming, however, may restrict foreat growth. Physiological processes of plants, especially photosynthesis, transpiration, respiration and reproduction are sensitive to temperature. With warming, respiration and decompositon may increase faster than photosynthesis. Transpiration and evaporation increases may enhance stress on drier sites. Reproduction may be altered by changes in dynamics of pollinating insects, changes in flower, fruit or seed set, or changes in seedling production and survival. The geographic or host ranges of exotic microbial pathogens or insect pests may expand. Previously innocuous endemic microbes or insects may be elevated to important pest status following climatic warming. Precipitation changes are associated with global warming, and certain areas will receive more and others less. Those areas receiving less precipitation will also experience increased evaporation and transpiration. Waggoner (26) has estimated that the projected change in weather by the year 2000 caused by increased atmospheric carbon dioxide, will cause moderate decreases of 2-12 percent in yield of wheat, corn and soybeans in the American grain belt due to increased dryness. While agriculturists may be able to adopt new crop varieties to a drier climate, forests cannot be similarly manipulated. Increased drought stress over widespread forest areas would be expected to initiate new rounds of progressive tree deterioration termed dieback/decline disease. Drought is the most common and important initiator of forest tree decline. Forest stresses caused by other air pollutants and other agents must be evaluated against this background of forest change caused by climatic warming.

A serious consequence of anthropogenic release of halocarbons to the atmosphere is the depletion of naturally occurring stratospheric ozone. Some reduction in halocarbon release has been achieved in the United States and a few other countries. Immediate termination of all release worldwide, however, would still leave the world with important stratospheric ozone reductions during the next decade. Reduced upper-air ozone would increase ultraviolet radiation reaching the surface of the earth. Current understanding does not allow an inventory of the impacts of increased ultraviolet radiation on forests. Studies of more than 100 agricultural species showed that increased ultraviolet exposure reduces plant dry weight and changes the proportion of root, shoot and leaf

tissue. Studies of more than 60 aquatic organisms showed that many were quite sensitive to current levels of ultraviolet radiation at the water surface (9). Chlorofluorocarbons can also contribute to global warming in a manner similar to carbon dioxide.

Regional air pollutants are the most important concern of forest managers.

The effects of local air contaminants on forests have stabilized in the vicinity of existing point-sources of air pollutants. In numerous cases improvements have been achieved. In the case of sulfur dioxide, increasing stack heights and use of scrubbers have reduced ground level concentrations of sulfur dioxide. New industries and electrical plants in the U.S. can employ the best available air quality technology.

On the global-scale, the destruction of ozone by halocarbons was addressed in the U.S. by banning chlorofluorocarbons in aerosol products. The release of carbon dioxide to the atmosphere from fossil fuel combustion will continue well into or through the twenty-first century. Energy requirements of nations of the temperate zone will require combustion of gas, oil and coal and the atmospheric burden of carbon dioxide will continue to increase with uncertain consequences.

Regional-scale air pollutants, on the other hand, exhibit both increasing trends and known and probable effects on forest ecosystems over large portions of the temperate region. The integration of stresses imposed by regional pollutants has the potential to cause growth reductions in some forest species and, ultimately, dieback/decline symptoms in susceptible tree species at ambient levels. At the ecosystem level this has or will cause changes in species composition and increases or decreases in biomass production depending on the specific ecosystem (Fig. 1). Documentations of decreased tree growth and increased decline symptoms due to air quality in the field are very limited because the changes are subtle, not continuous but patchwork in character, and extremely difficult to separate from other factors that control tree growth (eg. age, competition, moisture, temperature, nutrients, insects, pathogens) and that induce dieback/decline symptoms (eg. drought, other climatic stresses, insects, pathogens). In addition, species composition and patterns of forest succession are regulated by numerous determinants (eg. vegetative site alterations, plant species interactions, insect/pathogen activities, windstorms, fires and human cultural activities) and forest ecosystem production is influenced by several variables (system age, competition, species composition, moisture, temperature, nutrients, insects, pathogens). A review of the current evidence available to support the importance of air pollution induced forest change has been provided by Smith (19). The comprehensive study of oxidant pollution in portions of the San Bernardino National Forest, California demonstrated air pollution effects on forest growth and succession (11). Additional evidence of reduced forest growth imposed by oxidant pollution in the west, mid-west and east has been provided (23). For various forest ecosytems we are at, or near, the threshold of trace metal impact on nutrient cycling processes. Lead will continue to accumulate in forest floors as long as it is released into the atmosphere (U.S.E.P.A. 1983). Although adverse effects on forest ecosystems from acid deposition have not been conclusively proven by existing evidence, we cannot conclude that adverse effects are not occurring. Presently, tree mortality and tree morbidity and growth rate reductions in European and North American regions do occur where regional air pollution, including acid deposition, is generally high. Temporal and spatial correlations between wet acidic deposition and forest tree growth rates has been provided. Numerous hypotheses for adverse forest effects from acid deposition, worthy of testing, have been proposed (7, 21). Under natural conditions, forest ecosystems are exposed to multiple air pollutants

simultaneously or sequentially and interactive and accumulative influences are important. It is inappropriate to consider the effects of any regional pollutant on forests in isolation. The growth reductions and decline symptoms of the forests of the Federal Republic of Germany are dramatic and should warn all nations that the resiliency of forest ecosystems has limitations. Until the cause of this decline is more clearly understood, prudent natural resource science should not reject nor indict any single stress.

Conclusion

A sensitive and convenient forest parameter must be found to monitor the extent and intensity of stress on expansive forest systems. Waring (27) suggested that monitoring canopy leaf area and its duration of display is a very appropriate general index of forest ecosystem stress. Canopy quantity and quality is an indicator of productivity. Inventory techniques from the air (multispectral scanning, microwave transmission, radar, laser) and ground (correlations with stem diameter, sapwood cross-sectional area) for canopy leaf area are available. At a given site, detection of an increase in leaf area would suggest an improving environment, a decrease in leaf area would infer the system is under stress. Baes and McLaughlin (1) have proposed that trace metal analyses of tree rings can provide information on temporal changes in air pollutant deposition and tree health.

Implimentation of wide-area forest monitoring of any nature involves two challenges. First, detection of stress does not suggest cause. We are keenly aware that tree and forest health are controlled by many factors in addition to air quality—age, competition, environment (moisture, temperature, nutrition), insect and pathogen activity. We desperately need procedures to partition the relative importance of influencing variables for a given site. Fortunately we are making research progress toward this resolution (4, 10, 27). The second challenge is to convince foresters that the time and cost of systematic forest health monitoring is justified. I feel it is not only justified, but essential for intelligent decisions regarding regulation of regional air pollutants.

Air pollution has been killing trees locally for centuries. We have been keenly aware of this in the United States for over 100 years. We now realize that in addition to mortality, regional air pollutants may be capable of causing alterations in species composition and growth-rate reductions in certain forest ecosystems over large areas and across national boundaries.

Forests are variable in species, topography, elevation, soils and management. Air pollution deposition and influences are also variable and poorly documented in the field. Monitoring of species dynamics and productivity, necessary to detect effects of regional air pollutants, or any other environmental stress, are presently rarely available. Dendrochronological or other tree-ring analytical techniques are subject to enormous difficulty when they attempt to partition the relative importance of forces that may influence tree growth. Growth is regulated by precipitation, temperature, length of growing season, frost, drought, by developmental processes such as succession and competition, and to stochastic events such as insect outbreaks, disease epidemics, fire, windstorms and anthropogenic activities such as thinning, fertilization, harvesting <u>and</u> finally air quality.

For a long time, dieback and decline of specific forest species, somewhere in the temperate zone, has been common. Age, climate, or biotic stress factors have frequently been judged to be the principal causes for declines. Again, however, it is difficult to assign responsibility for specific cause and effect.

Trees are large and long-lived and their health integrates all the stresses to which they are exposed over time.

The risks associated with regional and global air pollution stress and forest ecosystem health are high. The evidence available to describe the total boundaries of the problem for all pollutants is incomplete. There is enormous uncertainty about specific effects on forests of regional and global air pollutants. We do know, however, that coal combustion will provide more than 50 percent of America's electricity by 1990. We further know that without management or control, coal combustion is a source of numerous regional and global pollutants identified as important, or potentially important, to the health of forest ecosystems. Natural ecosystem health, along with human health, must be recognized in assessments, economic and otherwise, of pollution abatement strategies.

References

1. Baes and McLaughlin. 1984. Trace elements in tree rings: Evidence of recent and historical air pollution. Science 224: 494-497.

2. Chung, Y.S. 1978. The distribution of atmospheric sulfates in Canada and its relationship to long-range transport of pollutants. Atmos. Environ. 12:1471-1480.

3. Evans, G., P. Finkelstein, B. Martin, N. Possiel and M. Graves. 1983. Ozone measurements from a network of remote sites. Jour. Air Pollu. Cont. Assoc. 33:291-296.

4. Fritts, H.C. and M.A. Stokes. 1975. A technique for examining non-climatic variation in widths of annual tree rings with special reference to air pollution. Tree-Ring Bull. 35:15-24.

5. Holdgate, M.W., M. Kassas and G.F. White. 1982. World environmental trends between 1972 and 1982. Environ. Conserva. 9:11-29.

6. Kellogg, W.W. 1977. Effects of human activities on global climate. Technical Note No. 156. WHO-No. 486. World Meteorol. Org., Geneva.

7. Linthurst, R.A. (ed.) 1984. Direct and Indirect Effects of Acidic Deposition on Vegetation. Vol. 5. Acid Precipitation Series. J.I. Teasley, ed. Butterworth Publishers, Boston, 117 pp.

8. Manabe, S. and R.J. Stouffer. 1980. Sensitivity of a global climate model to an increase of CO_2 concentration in the atmosphere. Jour. Geophys. Res. 85:5529-5554.

9. Maugh, T.H. 1980. Ozone depletion would have dire effects. Science 207:394-395.

10. McLaughlin, S.B., T.J. Blasing, L.K. Mann and D.N. Duvick. 1983. Effects of acid rain and gaseous pollutants on forest productivity: A regional scale approach. Jour. Air Pollu. Cont. Assoc. 33:1042-1049.

11. Miller, P.R., O.C. Taylor and R.G. Wilhour. 1982. Oxidant Air Pollution Effects on a Western Coniferous Forest Ecosystem. U.S. Environmental Protection Agency, Publica. No. EPA-600/D-82-276. Corvallis, OR, 10 pp.

12. Miller, P.R. and J.R. McBride. 1975. Effects of air pollutants on forests. In, J.B. Mudd and T.T. Kozlowski, eds., Responses of Plants to Air Pollution. Academic Press, N.Y., pp. 195-235.

13. Murozumi, M. T. Chow and C. Patterson. 1969. Chemical concentrations of pollutant lead aerosols, terrestrial dusts and sea salts in Greenland and Antarctic snow strata. Geochim. Cosmochim. Acta 33:1247-1294.

14. National Academy of Sciences. 1979. Stratospheric Ozone Depletion by Halocarbons. National Academy of Science, Washington, D.C., 249 pp.

15. National Academy of Sciences. 1982a. Solar Variability, Weather, and Climate (Studies in Geophysics). ISBN No. 0-309-03284-9. National Academy Press, Washington, D.C., 120 pp.

16. National Academy of Sciences. 1982b. Carbon Dioxide and Climate: A Second Assessment. ISBN No. 0-309-03285-7. National Academy Press, Washington, D.C., 92 pp.

17. National Academy of Sciences. 1982c. Stratospheric Ozone Depletion by Halocarbons. National Acsdemy of Science, Washington, D.C., pp.

18. Pratt, G.C., R.C. Hendrickson, B.I. Chevone, D.A. Christopherson, M.V. O'Brien, and S.V. Krupa. 1983. Ozone and oxides of nitrogen in the rural upper-midwestern U.S.A. Atmos. Environ. 17:2013-2023.

19. Smith, W.H. 1981. Air Pollution and Forests. Springer-Verlag, N.Y., 379 pp.

20. Smith, W.H. and T.G. Siccama. 1981. The Hubbard Brook Ecosystem Study: Biogeochemistry of lead in the northern hardwood forest. Jour. Environ. Qual. 10:323-333.

21. Society of American Foresters. 1984. Acid Deposition and Forest Ecosystems. Task Force on the Effects of Acid Deposition on Forest Ecosystems. Report prepared for the Society of American Foresters, Bethesda, MD, 51 pp.

22. Tong, E.Y., G.M. Hidy, T.F. Lavery and F. Berlandi. 1976. Regional and local aspects of atmospheric sulfates in the northeastern quadrant of the U.S. Proceedings, Third Symposium on Turbulence, Diffusion and Air Quality. Amer. Meteor. Soc., Boston, MA.

23. U.S. Environmental Protection Agency. 1983a. Air Quality Criteria for Lead. Vol. I. Publica. No. 600/8-83-028A. U.S.E.P.A., Research Triangle Park, N.C. 169 pp.

24. U.S. Environmental Protection Agency. 1983b. The Acidic Deposition Phenomenon and Its Effects. Vol. I. Atmospheric Sciences. Publica. No. 600/8083-016A. U.S.E.P.A., Washington, D.C. p. 3-92.

25. U.S. Environmental Protection Agency. 1984. Air Quality Criteria for Ozone and Other Photochemical Oxidants. U.S.E.P.A., Research Triangle Park, N.C. (in press).

26. Waggoner, P.E. 1984. Agriculture and carbon dioxide. Amer. Scient. 72:179-184.

27. Waring, R.H. 1983. Imbalanced ecosystems - Assessments and consequences. In: Dynamics of Forest Ecosystems. Proc. Workshop held in Uppsala, Sweden, March, 1983 (in press).

28. Wolff, G.T., N.A. Kelly, M.A. Furman. 1981. On the sources of summertime haze in the eastern United States. Science 211:703-705.

Table 1. Relative strength of evidence (quantity/quality)* available to support forest ecosystem interaction with regional+ air pollutants.

ecosystem process/component perturbation	air contaminants: oxidants	trace metals	acid deposition	TOTAL
I. nutrient cycling				
1. increase nutrient availability				
a. increase input (fertilization)	0	1	2	3
b. increase soil weathering	0	0	1	1
2. decrease nutrient availability				
a. reduce litter decomposition	0	4	1	5
b. increase soil acidification	0	0	2	2
c. increase soil (cation) leaching	0	0	2	2
d. decrease microbial symbioses	0	3	1	4
II. primary producers (trees)				
1. reproductive physiology				
a. reduce flowering	1	1	0	2
b. reduce pollen production/metabolism	2	1	1	4
c. reduce cone/seed set	2	0	0	2
d. reduce seedling survival	3	3	1	7
2. foliar physiology				
a. reduce photosynthesis	4	1	0	5
b. increase (cation) leaching	0	0	2	2
c. increase necrosis	4	2	0	6
3. root physiology				
a. decrease water/nutrient uptake	0	1	1	2
b. increase necrosis	0	1	2	3
4. reduce tree growth	4	1	1	5

III. consumers				
1. arthropod pest activity				
a. increase	4	0	0	4
b. decrease	0	0	0	0
2. microbial pathogen activity				
a. increase	4	1	1	6
b. decrease	1	2	0	3
3. other pest activity (viruses, bacteria, nematodes, mistletoes, weeds)				
a. increase	0	0	0	0
b. decrease	0	0	0	0
4. wildlife (bird/mammal) activity				
a. reduce food	2	0	0	2
b. reduce habitat	2	0	0	2
c. increase morbidity/mortality	0	2	0	2
IV. ecosystem succession/species composition (cause alteration)	4	1	0	5
V. ecosystem productivity (increase/decrease biomass accumulation)	4	0	0	4
TOTAL	41	25	18	

*evidence scale

0 - extremely limited evidence or hypotheses only
1 - slight evidence
2 - more evidence
3 - greater evidence
4 - considerable evidence including field evidence

+exclusive of local air pollution effects within several km of point sources

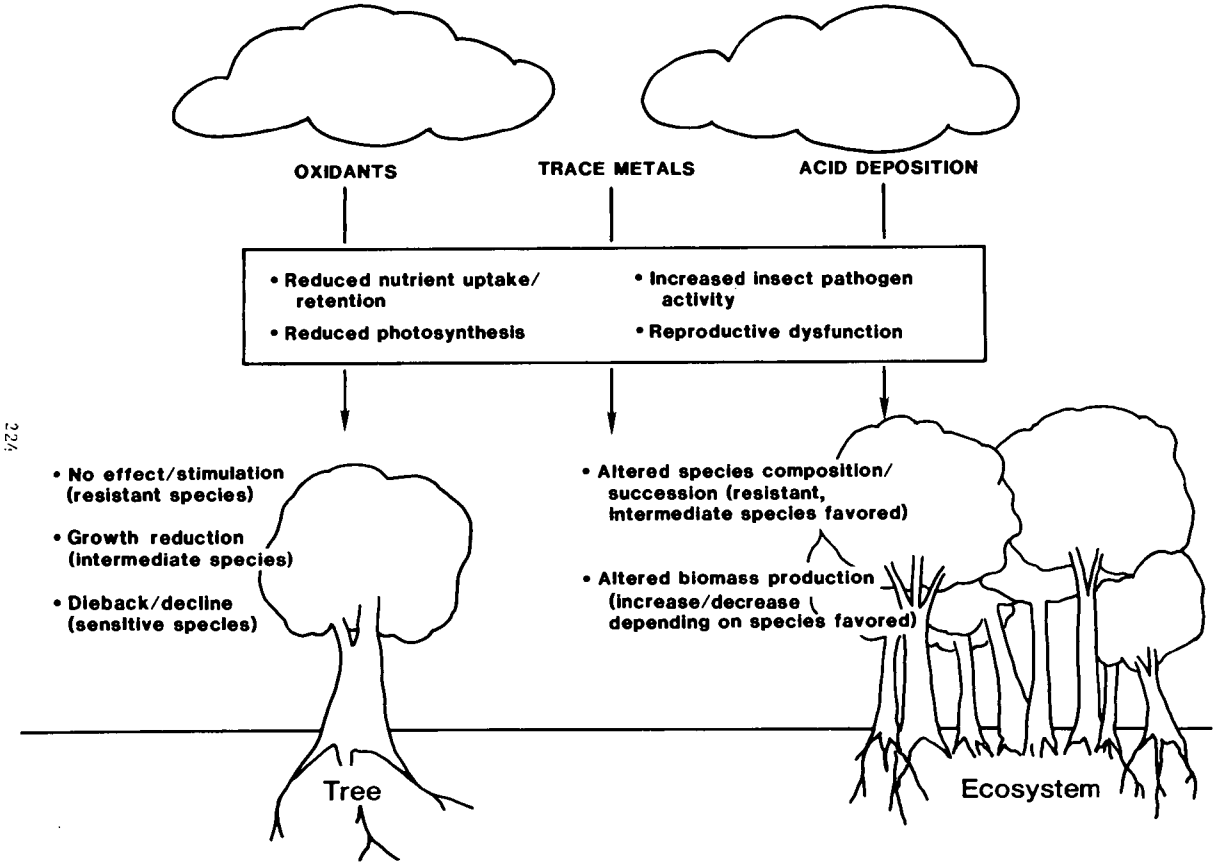
OXIDANTS
TRACE METALS
ACID DEPOSITION
• Reduced nutrient uptake/ retention
• Reduced photosynthesis
• Increased insect pathogen activity
• Reproductive dysfunction
• No effect/stimulation (resistant species)
• Growth reduction (intermediate species)
• Dieback/decline (sensitive species)
• Altered species composition/ succession (resistant, intermediate species favored)
• Altered biomass production (increase/decrease depending on species favored)
Tree
Ecosystem

ELECTRON-MICROSCOPICAL IDENTIFICATION OF COAL FLY ASH AT A REMOTE SITE IN THE NORTHEASTERN UNITED STATES

Liaquat Husain, James S. Webber, Vincent A. Dutkiewicz, and Edmondo Canelli

Wadsworth Center for Laboratories and Research, New York State Department of Health, Albany, New York 12201

ABSTRACT

Individual microparticles collected before, dnring and after an episode of high sulfate concentration at Whiteface Mountain, NY (26-30 July 1983) were characterized by scanning, transmission and high-voltage electron microscopy. Consistent with findings from an earlier episode, submicrometer spheres common in coal fly ash were abnndant during the high-sulfate period but were absent before or after the episode. Minerals identified in iron-rich spheres by electron diffraction were magnetite, maghemite, and hematite. Equally abundant at the same time were silicon spheres which were probably glass since they yielded no diffraction patterns. Also common in high-sulfate samples were submicrometer spheres composed of varying proportions of iron, silicon, aluminum, potassium, calcium and titanium. No evidence of particles from oil combustion was observed. Additional support for coal combustion as the sonrce of the high-sulfate concentration was given by Mn/V ratios which were consistent with air from the coal-burning Midwest rather than the oil-burning East Coast. Prevailing meteorologic conditions also indicated air flow from the Midwest. Preliminary evaluation of a new chemical signature, V/Ni ratio, is also presented. Although observed ratios were also consistent with coal rather than oil combustion, additional evaluation of this tracer is needed.

INTRODUCTION

It is widely assumed that the industrial Midwest, because it has the highest SO_2 emissions, is largely responsible for the widespread acid-stressed conditions in the Northeast. Indeed, studies that related daily sulfate concentration ($[SO_4^{2-}]$) with backward air trajectories at Whiteface Mountain, NY, have invariably found that the highest $[SO_4^{2-}]$ were associated with air masses passing through the Midwest (1,2,3). While trajectory-based studies themselves do not unequivocally prove this assumption, more recent investigations have shown with increasing clarity that coal-burning in the industrial Midwest is indeed the major sonrce of SO_4^{2-} aerosols reaching the acid-stressed Adirondack region. Husain et al. (4) used samples collected at 6-hour intervals from a network of sites to trace high-SO_4^{2-} air masses from the Midwest across New York State. These air masses retained Mn/V ratios characteristic of the Midwest (>> 1) even after traveling more than 500 km. Conversely, when trajectories passed through coastal regions, Mn/V ratios were distinctly lower (< 0.5), consistent with the region's dependence on oil. Although the Mn/V ratio technique has some limitations (5), it can be a very useful indicator of air mass history, particularly when used in conjunction with other tracers. Most recently, electron microscopy (EM) was used to identify coal fly ash in a high-SO_4^{2-} air mass at Whiteface Mountain (6). Both the meteorology and the Mn/V ratios indicated a midwestern origin for this air mass. The combination of microparticle identification, meteorology and chemical tracers has provided the clearest fingerprint to date of the sources of SO_4^{2-} in northern New York.

During the summer sampling campaign in 1983 a second high-SO_4^{2-} episode was observed at Whiteface Mountain. EM analysis of samples collected during this episode are presented and discussed along with the measurement of selected trace metals in simultaneous high-volume samples.

EXPERIMENTAL

Dnring summer 1983 airborne particulate samples were collected with high-volume pumps on Whatman 41 filters at the summit of Whiteface Mountain (WFM), at Mayville (MAY) in the southwestern corner of New York, at Alexandria Bay (AXB) on

the northeastern shore of Lake Ontario, and at West Haverstraw (WHV) in the lower Hudson River Valley (Figure 1). While the first three sites are rural, WHV is a suburban site located near the metropolitan New York City area. This site was selected primarily to characterize East Coast aerosols because of its proximity to two oil-burning power plants. Samples were collected for 6-hour intervals at WFM and MAY and for 12-hour intervals at WHV and AXB. These were analyzed for SO_4^{2-} by ion chromatography and for Al, Mn, V, and Ni by atomic absorption spectrophotometry as detailed elsewhere (4). Microparticles were collected simultaneously with the high-volume samples at WFM on carbon-coated Nuclepore filters in an automatic dichotomous sampler (6). These filters with collected particles were transported in airtight containers to the lab where a thin carbon film was vacuum evaporated over the collection surface to immobilize the particles and to reduce excess charge produced by the electron beam. In addition to the EM analyses performed on the earlier samples (6), sections of filter were shadowed with Au-Pd at an angle of ~30 degrees to allow 3-dimensional interpretation of particle morphology by transmission EM (7).

During the period of interest (26-30 July 1983), air flow across New York State was dominated by a slow-moving high-pressure system from the Great Lakes. Although air trajectories are not available at this time, this pattern in the past has produced air flow from the Midwest across the state and is generally associated with high-SO_4^{2-} periods in upstate New York (8). This high centered over southern Pennsylvania early on 27 July may produce air flow from the Midwest at MAY while AXB and WFM should be under the influence of Canadian air. By the next day, the high had moved off the coast of Virginia, where it remained stationary for two days (Figure 1). A cold front with a large mass of leading showers was trailing the high. (The leading edge of the showers can be seen in the upper left hand corner of Figure 1.) During 28 July, precipitation began in the western part of the state and by the next day, was widespread throughout the upstate area.

RESULTS

Chemistry

On 27 July [SO_4^{2-}] began to increase throughout the state, first at MAY and 12 hours later at AXB and WFM (Figure 2). This is consistent with the beginning of midwestern air flow on the backside (western edge) of the high pressure system. At AXB and WFM, maximum concentrations, 46 and 49 μg/m³ respectively, were observed in the afternoon of 28 July but decreased dramatically on 29 July when precipitation was widespread throughout the state. The onset of precititation is also indicated by the trace metal data. Al concentrations at WFM, for example, were ~340 ng/m³ during the peak [SO_4^{2-}] period but decreased abruptly to 90 ng/m³ for the first sample on 29 July. Such an abrupt decrease is consistent with the washout of aerosols. At MAY [SO_4^{2-}] leveled off at ~25 μg/m³ for 30 hours beginning with the first sample on 28 July. However, the leading edge of showers shown in Figure 1, which began affecting the western part of the state on the 28th, may have significantly affected the [SO_4^{2-}]. The variations in trace metal concentrations are consistent with this assumption. [SO_4^{2-}] at WHV also peaked in the last sample on 28 July, but the concentration was much lower, 15 μg/m³. Because this site was much closer to the center of the high, it may very well have been influenced by air from a different area than the upstate sites. This has been the case in episodes previously studied (4).

The ranges of Mn/V ratios (crustal corrected as described earlier (4)) are shown in Figure 2. Throughout the episode, Mn/V ratios at the three upstate sites were consistently >2. While [SO_4^{2-}] was > 20 μg/m³ at MAY, Mn/V ratios ranged from 3.3 to 21 and averaged 11. At WFM during the peak [SO_4^{2-}] period, Mn/V ratios averaged 6 which is within the range of values observed at MAY although only about half the mean. Larger ratios at MAY compared to WFM are, however, consistent with previous data (4,6). At both sites the Mn/V ratios are clearly within the range for midwestern air and much too high to suggest any significant influence from heavy oil-burning areas. At AXB, Mn/V ratios were only slightly >2, much lower than at WFM. While [SO_4^{2-}] were comparable at the two sites, AXB

had much higher V concentrations. Although the Mn/V ratios at AXB were within the range of coal-burning regions, the fact that the ratios were much lower than at WFM suggests a larger influence from oil-combustion at AXB. However, since the highest V concentration was only 6.7 ng/m³ and Mn/V ratios do remain >2, the high-[SO_4^{2-}] period still seemed to be dominated by coal-combustion aerosols.

While Mn/V ratios at WHV have been included for completeness, its proximity to oil-burning power plants precludes the usefulness of Mn/V ratios as tracers at this site (5). As in previous studies (4,6), Mn/V ratios at WHV were almost invariably <0.5 as expected. On 28 July the Mn/V ratio increased to 0.53. Since it is generally around 0.2, this indicates that a component from some coal-combustion source may be present.

To reinforce the Mn/V ratio data we also considered V/Ni ratios in these samples. V/Ni ratios are different in coal and oil fly ash. [V] is markedly enriched in oil fly ash while [Ni] is also enriched, not to the extent of V (9). In contrast, [Ni] is increasingly enriched with decreasing particle size in coal fly ash whereas [V] is not (10,11). Henry and Knapp (12) analyzed 6 oil fly ash samples and 6 coal fly ash samples and found average V/Ni ratios to be 5.2 and 1.2 respectively. Analysis of the data of Davison et al. (11) reveals that V/Ni is very low (<0.5) in coal fly ash which is less than 2 μm. This is the particle size range expected to be transported long distances.

V/Ni ratios are shown in Figure 2. At WHV on 26-27 July, the V/Ni ratio averaged 3.0. This site is strongly influenced by oil emissions ([V] averaged 30 ng/m³) and the V/Ni ratio is approaching that measured in oil fly ash. During the [SO_4^{2-}] episode, however, the ratio averaged 1.6 and returned to near 3 on the 30th. The decreased V/Ni ratios are consistent with increased influence from coal-burning regions during the high-SO_4^{2-} period. At WFM, episodic ratios averaged 1.2 and nonepisodic ratios averaged 1.3, near that for coal, again indicating that oil-combustion aerosols were not dominant at these times. V/Ni ratios at MAY and AXB were similar to WHV with nonepisodic ratios averaging 2.1 and and 2.4 respectively and episodic ratios averaging 1.4 and 2.0. At none of the sites was the episodic V/Ni ratio large enough to be associated with purely oil-fired combustion products and, except at WFM where the ratio was already near that of coal, the V/Ni ratio decreased during the high-SO_4^{2-} episode, as expected for increased contributions from coal-burning areas. Consistent with Mn/V ratios, V/Ni ratios were higher at AXB than WFM during the episode supporting the earlier conclusion that AXB has an oil-derived aerosol component. AXB is on the St. Lawrence Seaway, approximately 100 km NE of a large oil-burning power plant on the southeast shore of Lake Ontario. While further study is needed, this data suggests that V/Ni ratios may provide another useful indicator of coal and oil combustion emissions.

Microparticles

More than 200 particles collected at WFM in the fine fraction (<2.5 μm) on 27 July I and IV, 28 July II,III and IV and 29 July I (where I=0000-0600 h, II=0600-1200 h, III=1200-1800 h, IV=1800-2400 h) were characterized by electron diffraction (ED), energy-dispersive x-ray spectroscopy (EDXRS) and morpholgy with transmission and high-voltage EM.

The most abundant particles were S-rich particles, usually much smaller than 0.8 μm. These particles were electron transluscent and occasionally the S x-ray peaks were accompanied by much smaller K, Ca or Fe x-ray peaks. Interesting morphological features were highlighted by Au-Pd shadowing (Figure 3). S particles collected on 27 July IV ([SO_4^{2-}]=6μg/m³)and 29 July I ([SO_4^{2-}]=29 μg/m³) were dome shaped and generally larger than in other periods. Those collected on 28 July II and III ([SO_4^{2-}]=14 and 41 μg/m³ respectively) were not flattened, but rather had cluster morphologies similar to N in Figure 3b. Ferek et al. (7) revealed that $(NH_4)_2SO_4$ collected on SiO films with an impactor had cap-like morphologies. Particles were collected in the present study at a face velocity orders of magnitude lower than that encountered with an impactor. Hence, the S-rich clusters seen by us were probably $(NH_4)_2SO_4$

clusters which had retained their solid morphology rather than being flattened by high-velocity impaction. Ferek et al. also found that H_2SO_4 impacted on SiO films formed a large central drop with multiple satellite droplets. This phenomenon had been reported earlier by Frank and Lodge (13), who concluded that this was caused by dehydration of the H_2SO_4 on the hydrophobic SiO rather than by impaction forces. One reason that cap-like spheres with satellites were not seen by us might be that the carbon film used for collection was less hydrophobic than SiO and thus satellite formation was not favored during dessication. Furthermore, our samples were given a second carbon coat soon after collection and this probably slowed dessication and certainly prevented changes in morphology during any subsequent dessication/oxidation. Hence the domelike spheres were probably H_2SO_4. This hypothesis is reinforced by the bubbling seen within these domes during electron-beam heating. This bubbling was not evident in the clusters thought to be $(NH_4)_2SO_4$. The S particles collected during the peak $[SO_4^{2-}]$ ranged from clusters to domes, with small domes often concentrated around the 0.4 μm pores (Figure 3b). This collection pattern is not unusual for smaller particles which have insufficient inertia to be impacted uniformly on the filter face but have too much inertia to pass over the lip of the pore (14). These small domes are morphologically similar to the H_2SO_4 and their contents did bubble in the electron beam. The collection of the smaller H_2SO_4 near the pores during peak $[SO_4^{2-}]$ as compared to the collection of the larger H_2SO_4 between the pores in the earlier and later samples may indicate a less aged SO_4^{2-} component in the aerosol during the peak period (15).

Spheres similar to those seen in the episode one month earlier and identified as coal fly ash (6) were less numerous than the SO_4^{2-} particles. The total number of spheres is larger than shown in Figure 4 because spheres in clusters were often too small or too agglomerated to allow individual enumeration. The abundance of these spheres varied dramatically, ranging over more than two orders of magnitude. Spheres were almost absent before the episode but were abundant during the high-SO_4^{2-} period. A strictly quantitative relationship between $[SO_4^{2-}]$ and fly-ash particles was not expected because of opposing forces during transport: fly ash spheres could only decrease during transport because of sedimentation whereas $[SO_4^{2-}]$ could increase because of SO_2 oxidation.

All spheres and sphere clusters were <1 μm. This would suggest a distant source in that supramicrometer spheres would have settled out during extended transport. Their spherical morphology points to combustion evolution, e.g., cooled silicate and metal droplets.

The abundance of spheres composed primarily of Fe (and called ferrospheres after Lauf (16)) generally followed $[SO_4^{2-}]$ but peaked 12 hours earlier. Whereas magnetite (Fe_3O_4) was the most common ferrosphere mineral in the episode studied earlier, maghemite (γ-Fe_2O_3) was the most abundant mineral in ferrospheres in this episode (Figure 5a,b). Magnetite (or Fe-rich spinels) and hematite (α-Fe_2O_3) were also present. These minerals have been commonly reported in coal fly ash studies (17,18,19). The x-ray spectra of these spheres occasionally revealed traces of Mn, Zn, Si, K, Ca, Cr or Se. The first-row transition metals are possibly isomorphic substitutions in the spinel structure (19) whereas Se may be a surface-enriched volatile as reported by others (11).

Spheres composed primarily of Si were as abundant as the ferrospheres and their numbers correlated with $[SO_4^{2-}]$. In addition to the Si x-rays, these spheres often yielded smaller x ray peaks of Fe, K, Ti, Al, Mn, Zn, Cd or Se. Like the Si spheres collected one month earlier, these did not yield diffraction patterns, again making them likely candidates for the glass spheres found in coal fly ash (16,19).

Spheres which did not fit neatly into the Fe or Si group usually were composed of a mixture of Al, Si, Fe and/or Ti. One sphere (Figure 5c) was identified by its EDXRS and ED as mullite ($3(Al_2O_3).2SiO_2$), a high-temperature mineral found in coal fly ash (16,17,19). Fe has been previously identified in mullite coal

fly ash (19). The mixed-element sphere in Figure 5d is the largest sphere collected and identified at WFM.

The above spheres are typical of coal fly ash but have not been characterized in oil fly ash. Oil fly ash is generally platy or honeycombed carbon which is enriched in V and Ni (9,12,20). A few particles collected before, during and after the episode yielded very small V x-ray peaks but these peaks were not associated with a specific particle type or elemental combination. Hence microparticle analysis provides no evidence of an increase of oil fly ash during the elevated [SO_4^{2-}] period.

Common, though never abundant, were Si-rich fragments which were identified as quartz, K feldspars and plagioclase (Figure 4). These ranged in size from slightly less than 1 μm to 3 μm. Abundance varied only a little more than an order of magnitude. These were most likely local crustal fragments since the three identified mineral groups are the most common minerals in the Adirondack region (21).

Pb-rich particles ranging from 0.1 to 1.0 μm were detected in the episodic samples. These Pb x-ray peaks were always associated with larger S peaks and $PbSO_4$ was the most commonly identified mineral. Br x rays were not seen with any of these Pb particles but the more volatile Br may have been lost by aging or by the heat of the electron beam. These particles were seen only when [Pb] exceeded 30 ng/m³ and the concentration of Pb particles correlated closely with [Pb].

CONCLUSION

The variety of evidence outlined above demonstrated that SO_2 emissions from the industrial Midwest rather than emissions in the Northeast were the major source of a high-SO_4^{2-} episode in the acid-sensitive regions of New York State. The movement of the high-pressure system during this episode was identical to previous meteorological conditions when trajectory analyses revealed flow of air masses from the Midwest across the state. Mn/V ratios were distinctly midwestern during this episode. V/Ni ratios reinforced the interpretation of Mn/V ratios and hold promise as another regional signature. The mineralogy, morphology and elemental composition of spheres collected during the episode were typical of coal fly ash but not of oil fly ash. The submicrometer size range of these spheres pointed to a distant source. While this coal fly ash was virtually absent before the episode, it became abundant when [SO_4^{2-}] increased.

ACKNOWLEDGEMENTS

The authors are grateful to Adil Khan, Edward LeGere, Jill Spierre, David Teiger and Joan Fleser of this center for their assistance in collecting, preparing or analyzing the samples. Analysis was assisted by PHS grant number RR01219 supporting the New York State High-Voltage Electron Microscope as a National Biotechnology Resource, awarded by the Division of Research Resources, DHHS. The authors are grateful to Professor Volker Mohnen for the use of the Atmospheric Sciences Research Center, State University of New York at Albany facilities atop Whiteface Mountain and to Dan Sullivan for sample collection. The authors are also grateful to Chautauqua County for the use of their facilities at Mayville and to Steve Johnson and Bob Lincoln for their assistance in sample collection. The cooperation of Dr. Fuhs and the staff of the NYS Health Department field laboratories for sample collection at West Haverstraw and Alexandria Bay is also gratefully acknowledged.

REFERENCES

(1) Galvin, P.J., Samson, P.J., Coffey, P.E. Environ. Sci. Technol. 1978, 12, 580.
(2) Samson, P.J. Atmos. Environ. 1978, 12, 1889.
(3) Parekh, P.P., Husain, L. Geophys. Res. Lett. 1982, 9, 79.
(4) Husain, L., Webber, J.S., Canelli, E., Dutkiewicz, V.A., Halstead, J.A. Atmos. Environ. 1984, 18, 1059.
(5) Husain, L., Webber, J.S., Canelli, E. J. Air Poll. Control Assoc. 1983, 33, 1185.
(6) Webber, J.S., Dutkiewicz, V.A., Husain, L. Atmos. Environ. 1985, (in press).
(7) Ferek, R.J., Lazrus, A.L., Winchester, J.W. Atmos. Environ. 1983, 17, 1545.
(8) Dutkiewicz, V.A., Halstead, J.A., Parekh, P.P., Khan, A., Husain, L. Atmos.e Environ. 1983, 17, 1475.
(9) Cheng, R.J., Mohnen, V.A., Shen, T.T., Current, M., Hudson, J.B. J. Air Poll. Control Assoc. 1976, 26, 787.
(10) Weissman, S.H., Carpenter, R.L., Newton, G.J. Environ. Sci. Technol. 1983, 17, 65.
(11) Davison, R.L., Natusch, D.F.S., Wallace, J.R., Evans, C.A. Jr. Environ. Sci. Technol. 1974, 8, 1107.
(12) Henry, W.M., Knapp, K.T. Environ. Sci. Technol. 1980, 14, 450.
(13) Frank, E.R., Lodge, J.P. Jr. J. Microscopie 1967, 6, 449.
(14) Hinds, W.C., ''Aerosol Technology'', John Wiley and Sons, New York, NY, 1982.
(15) Whitby, K.B. Atmos. Environ. 1978, 12, 135.
(16) Lauf, R.J. Application of Materials Characterization Techniques to Coal and Coal Wastes, ORNL/TM-7663, Oak Ridge National Laboratory, TN, 1981.
(17) Hansen, L.D., Silberman, C., Fisher, G.L. Environ.Sci.Technol. 1981, 5, 1057.
(18) Cabaniss, G.E., Linton, R.W. Environ. Sci. Technol. 1984, 18, 271.
(19) Hulett, L.D. Jr., Weinburger, A.J., Northcutt, K.J., Ferguson, M. Science 1980, 210, 1356.
(20) McCrone, W.C., Delly, J.G. ''The Electron Microscopy Atlas'',In The Particle Atlas, Ed. Two, V. III, Ann Arbor Science, Ann Arbor, MI., 1973, 773-789.
(21) Whitney, P., N.Y. State Geol. Survey, personal communication.

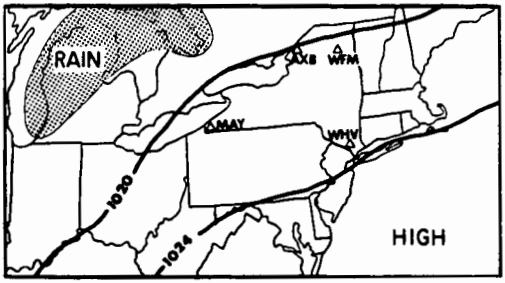

Figure 1. Simplified surface meteorlogic conditions in the northeastern United States at 0730 EST on 28 July 1983. Sampling sites are Mayville (MAY), Alexandria Bay (AXB), Whiteface Mountain (WFM) and West Haverstraw (WHV).

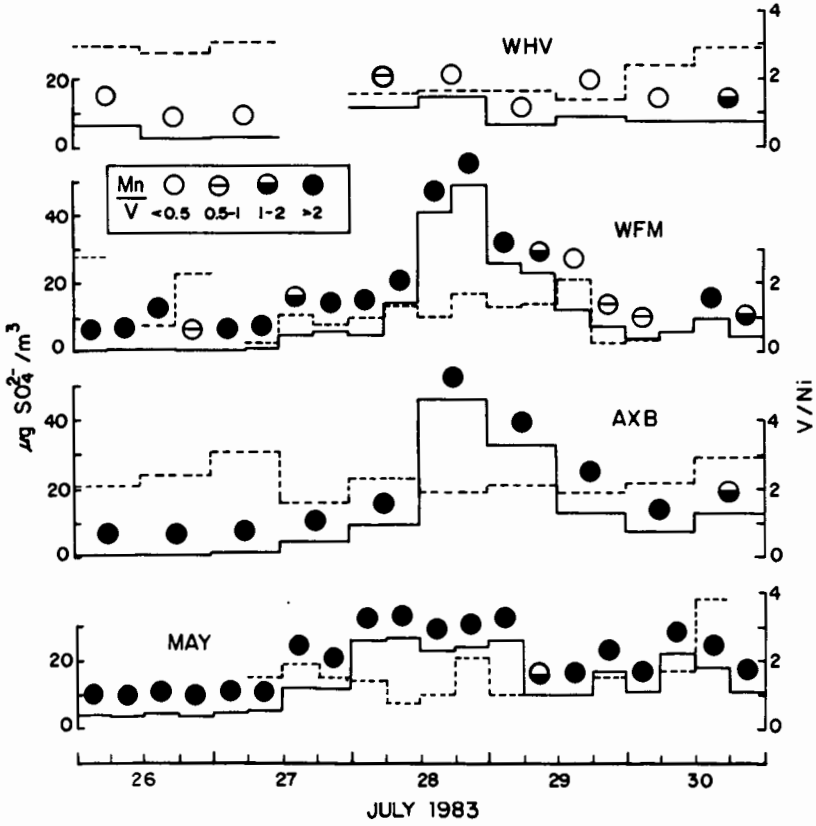

Figure 2. Sulfate concentrations (solid bars), V/Ni ratios (dashed bars) and Mn/V ratios at four sites in New York State. Metal ratios omitted for samples with one or both metals below detection limit or with excessive crustal correction.

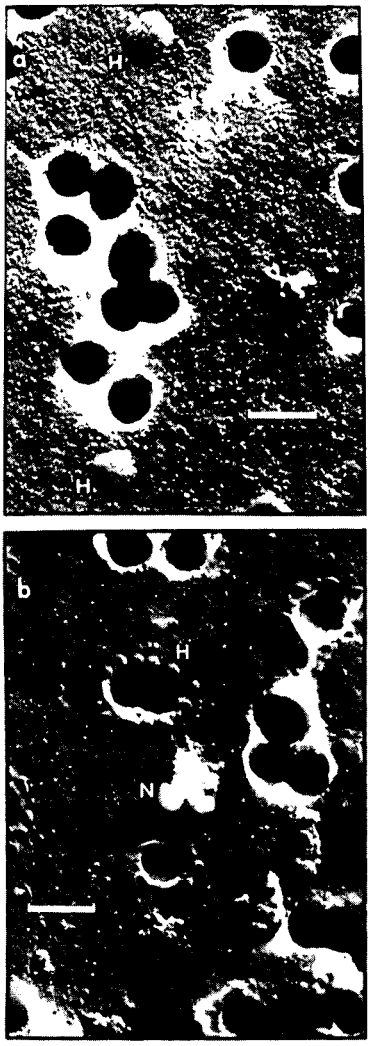

Figure 3. Transmission electron micrographs of sulfate particles collected on Nuclepore filters at WFM and shadowed with Au/Pd. (a) 27 July IV 1983. H denotes cap-like particles which are probably H_2SO_4.
(b) 28 July IV 1983. N denotes cluster which is probably $(NH_4)_2SO_4$.

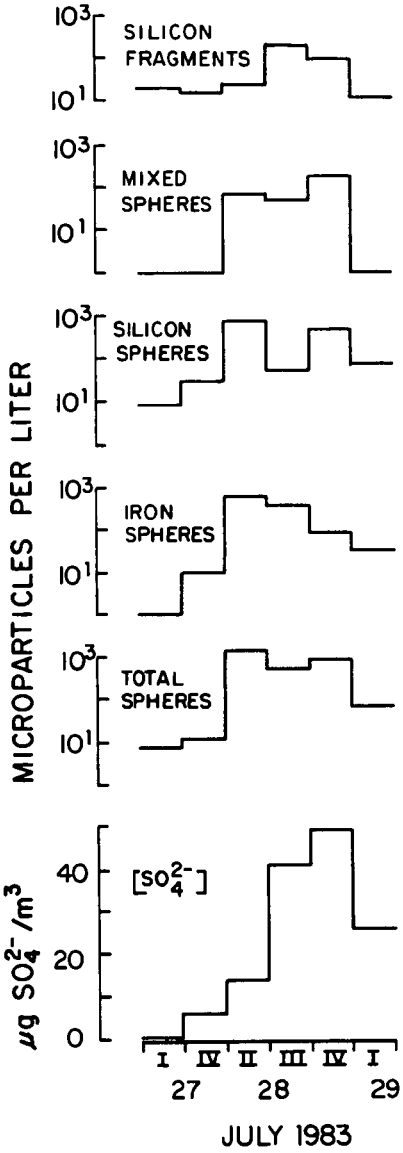

Figure 4. Sulfate and microparticle concentrations at WFM during selected periods from 27-29 July 1983.

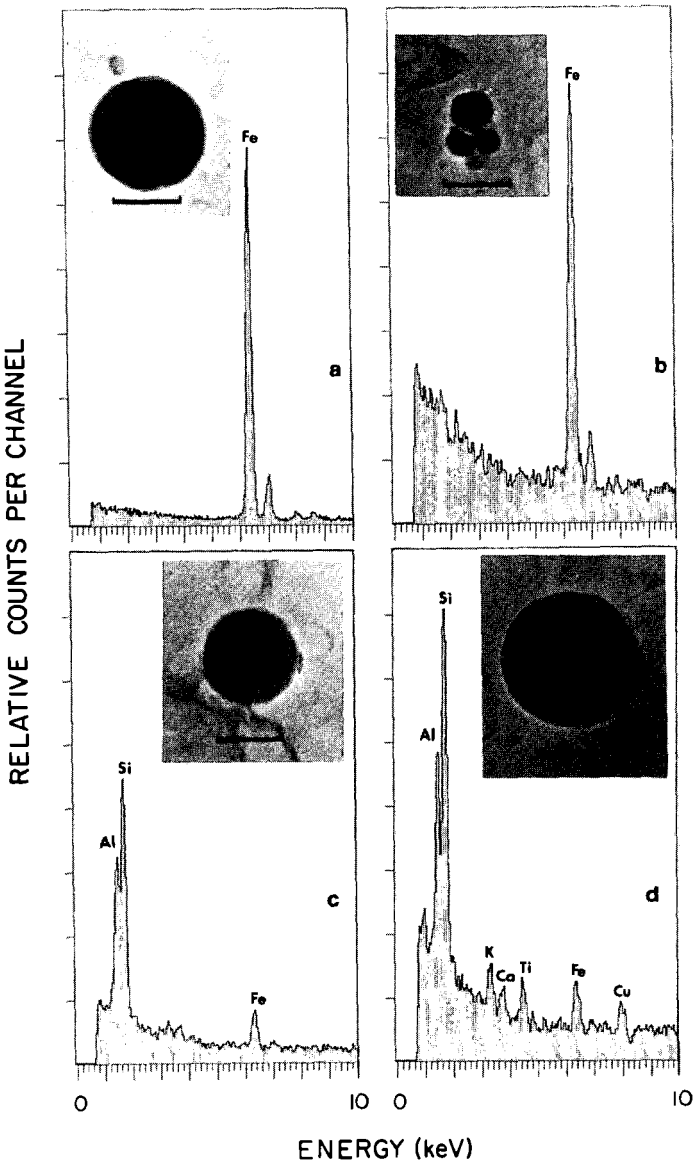

Figure 5. High-voltage electron micrographs and x-ray spectra of microparticles collected at WFM in 1983. Scale bar equals 0.5 μm. (a) γ-Fe_2O_3 sphere collected 28 July II. (b) γ-Fe_2O_3 sphere cluster collected 28 July IV. (c) Mullite sphere collected 28 July IV. (d). Mixed-element sphere collected 28 July III.

USE OF CASCADE IMPACTORS IN THE CHEMICAL AND PHYSICAL CHARACTERIZATION OF COAL-COMBUSTION AEROSOL PARTICLES

John M. Ondov

Martin Marietta Environmental Systems
9200 Rumsey Road
Columbia, Maryland 21045

ABSTRACT

Aerosol particles from combustion of pulverized coal are typically distributed bimodally with respect to size, and contain particles ranging from about 0.01 μm to over 100 μm in diameter. Development of control technology, emissions testing, and prediction of health and environmental effects often require characterization of the size distributions of aerosol particulate mass or the various chemical components. Cascade impaction provides a relatively simple and fundamental measurement of the mass-vs-size distribution and can yield size-segregated material in quantities adequate for determining the distributions of chemical, physical, or biologically active constituents. This paper briefly reviews impactor theory, considers the merits and shortcomings of four cascade impactors, and reviews the principal problems involved in using cascade impactors to measure properties of coal combustion aerosols. These problems include errors in measuring narrow distributions, effects of particle bounce and reentrainment, diffusive deposition of fine particles, and deposition of condensible/adsorbable gases. Ambiguities in data reduction will also be discussed.

INTRODUCTION

Cascade impactors have been used extensively to provide size-segregated particulate samples for characterizing the distributions of mass and chemical constituents in both ambient and source aerosols. In principal, conventional inertial impactors can provide accurate data on particle distributions in the range of 0.2 to 50 μm (1,2). The lower size limit has been reduced to 0.05 μm with low-pressure impactors (3,4,5) and, more recently, to 0.026 μm with a microorifice impactor (6,7,8). Large errors in estimates of the distribution parameters can result, however, in cases where the size distribution is narrow (such as that for aerosols modified by highly efficient particulate-control devices), from the effects of particle bounce and reentrainment, and from the deposition of particles and gases from boundary streams onto impaction substrates. These problems are especially important in sampling the bimodal aerosols produced in the combustion of pulverized coal, which contain condensible gases, enormous concentrations of submicrometer particles, and predominantly dry, glassy aluminosilicate spheres that tend to stick poorly to impaction substrates. Because of particle bounce, contamination of submicrometer-particle fractions with larger particles is an especially important problem in sampling both source and ambient aerosols. These problems are reviewed below.

The Principle of Inertial Impaction

The underlying principle of inertial impaction is embodied in the concepts of relaxation time and stopping distance. When the velocity of a particle-containing gas is changed, for example, by accelerating the gas through a nozzle or by changing the direction of its flow, the suspended particle, with its greater inertia, lags behind the gas. The time required for equilibrium to become reestablished is known as the relaxation time, and the distance the particle travels while equilibrating is known as the stopping distance. In an impactor, placement of an obstruction (impaction plate) normal to the direction of flow forces the gas to change direction. A particle is deposited (i.e., collected) on the impaction plate if the size of the plate is large with respect to the stopping distance of the particle.

The stopping distance (S) of an aerosol particle is a function of the diameter (D_p), velocity (V_p), and density (ρ_p) of the particle, and the viscosity of the gas (μ), as shown in Equation 1 (9):

$$S = \frac{\rho_p V_p C D_p}{18\mu} \qquad (1)$$

where C is the Cunningham slip correction factor, which accounts for discontinuity in the transfer of momentum to the particle (as a result of collisions with gas molecules at the particle surface) that occurs for particles of size near that of the mean free path of the gas molecules (9).

Typical cascade impactors consist of a series of nozzle plates, each followed by an impaction plate; each set of nozzle plate plus impaction plate is termed a stage. The sizing characteristics of an inertial impactor stage are determined by the efficiency with which the stage collects particles of various sizes. Collection efficiency is a function of three dimensionless parameters: the inertial parameter (Stokes number), the ratio of the jet-to-plate spacing to the jet width, and the jet Reynolds number. The most important of these is the inertial parameter, which is defined by Equation 2) as the ratio of the stopping distance to some characteristic dimension of the impaction stage (10), typically the radius of the nozzle or jet (D_j).

$$\text{Stokes} = \frac{\rho_p V_p C D_p / 18\mu}{D_j/2} \qquad (2)$$

Particle collection efficiency is a monotonically increasing function of the inertial parameter and has been determined experimentally (1,11,12). Customarily, this function is represented by a single value, that is, the value of the Stokes number that corresponds to a collection efficiency of 50%. Thus by rearranging Equation 2), the diameter of the particle collected with 50% efficiency (D_{50}) is expressed in terms of the Stokes number for 50% collection (Stk_{50}) as follows:

$$D_{50} = \sqrt{Stk_{50}} \times \sqrt{\frac{D_j 9\mu}{\rho_p V_p C_p}} \qquad (3)$$

Particles with large enough stopping distances will be deposited on the first impaction plate; those with somewhat smaller stopping dis-

tances will be carried to the next stage; and so on. By increasing the velocity of the aerosol in sucessive stages, the stopping distance of the particle is likewise increased, and progressively smaller particles are collected. The jet velocity can be increased either by reducing the number or size of the jets or by increasing the overall flow rate of the aerosol.

Data Reduction

In typical aerosols, particle size is distributed lognormally. The distribution parameters (median and the geometric standard deviation) may be estimated graphically from cumulative plots of mass vs particle size, or mathematically, by fitting the data to a lognormal distribution function.

Gravimetric or chemical analysis of the individual impaction plates is used to determine the aerosol mass or the amount of some chemical constituent associated with the range of particle sizes collected on the plate. The size distribution of the measured variable can then be deduced by plotting the data against the appropriate impactor stage parameter, usually the D_{50} as determined by Equation 3). The D_{50}, however, is a measure of the diameter of a particle collected with 50% efficiency, and not the size of the particle collected on the impactor stage. The true distribution of particles actually collected on the stage is a function of the distribution of the aerosol sampled and the efficiency-vs-size curves for the individual stages; only by chance would the D_{50} be equal to the median diameter of particles on the stage. The use of D_{50}s in determining actual distributions therefore contains an intrinsic error. If efficiency curves are available, this intrinsic error can be reduced by using data-inversion techniques (13,14). These techniques determine the distribution that, after multiplication by the appropriate sets of calibration curves, best reproduces the amounts of particulate mass collected on each impactor stage.

In general, if the aerosol distribution is wide enough and the mass median diameter (MMD) is within the range of the device, D_{50}s can provide reasonably accurate estimates of the aerosol-distribution parameters. Efficiency curves for impactors are sigmoidal, however, and collection efficiency for particles of all sizes is non-zero. Thus, when the size distribution is narrow, as in aerosols modified by particulate-control devices, the amount of mass attributed to the larger particles may be incorrect. As a rule, the size of the largest particle collected on the first stage of the impactor should be determined by microscopy or by inference from other measurements. Additional sizing errors, resulting from nonideal behavior, are discussed below.

Nonideal Behavior

The principal problems in determining size distribution parameters with cascade impactors are wall losses, inefficient collection due to particle bounce, deposition of gas-phase species on impaction substrates, and deposition of fine particles from boundary layers. As discussed above, an intrinsic error can result from using D_{50}s to infer size distributions from the impactor data. Depending on the sampling conditions and on the chemical and physical properties of the aerosol sampled, each of the other errors can also be significant, and generally must be considered in sampling coal combustion aerosols.

Wall losses. Ideally, all of the aerosol sampled in an impactor should be deposited on the collection plates or be captured by the afterfilter. In practice, some of the particles collect on other interior surfaces and are typically excluded from the analysis. Wall losses result from diffusion of particles in turbulent eddies, from sedimentation of large particles (especially in large-particle stages with large internal volume and corresponding low gas velocities), from electrostatic effects, and from particle bounce. Wall losses appear to depend on size and hence on stage. Therefore, if they are significant, both the total mass concentration of the aerosol and its inferred size distribution will contain an error. Experience has shown that wall losses are greater for large, hard, dry particles, typically composed of aluminosilicate materials, than for small (submicrometer) carbonaceous or sulfate particles.

Particle bounce. When particles bounce off the collection surface, they may be carried to subsequent stages, where they may stick or again bounce off. The result is that subsequent stages collect more mass than is appropriate, and the inferred particle-size distribution is biased towards the smaller particles. Apparently, because of increasing velocity, particles that bounce off an earlier stage of the impactor quite often continue to bounce off the subsequent stages and are finally collected on the afterfilter. As discussed below, such collection can severely limit the utility of afterfilter data. Typically, sticky substances are applied to impaction surfaces to reduce particle bounce. Compounds that can be "wicked" by the collected particles tend to be the most effective.

The significance of these and other real-world difficulties are discussed below for sampling coal combustion aerosols.

Problems in Measuring Coal Combustion Aerosols

In an earlier study (15) we addressed some of the problems in obtaining accurate concentration-vs-particle-size distributions for elements in stack aerosols collected downstream of an electrostatic precipitator and a Venturi wet scrubber at a coal-fired power plant. The problems investigated were error associated with the use of the D_{50}s, wall losses, and contamination of afterfilters by particle bounce. In a later study, we observed the artifactual deposition of gas-phase components during sampling (16). In both studies we used the University of Washington Mark III and Mark V Source Test Cascade Impactors (17). Our specific objectives were to verify the sizes of particles collected on impaction stages and afterfilters and to estimate impactor efficiency relative to collection on filters. The ultimate goal was to determine elemental emission rates as a function of particle size.

The Mark III and Mark V impactors used in these studies are, respectively, 7- and 11-stage multicircular jet units with integral backup filters. These were operated isokinetically, in-stack, with Nuclepore™ polycarbonate impaction substrates coated with vacuum grease. Elemental constituents of the particles collected were determined by neutron activation analysis, and number-size distributions (for each stage) were determined by counting particles in discrete size ranges after sonic dispersion in hexane. Particle sizes were determined from scanning electron microscope (SEM) photographs or by use of a Quantimet image analyzer with an interface to the SEM.

In Figure 1 are plotted both the cumulative mass distributions of Al in fly-ash particles as determined from stage D_{50}s and the distribution parameters for each stage as determined from SEM analyses. The SEM number-distribution (nmd) parameters for each stage were transformed to the corresponding volume parameters and adjusted for the measured particle density (2.44 g/cm^3) and slip correction factor to obtain estimates of the mass median aerodynamic diameters (mmad) for the stage. Neither the nmds nor the mmads determined from the microscopy analysis are directly comparable to the D_{50} stage parameters. Values corresponding to the D_{50}s can, however, be interpolated from the cumulative curves (Fig. 1) and are listed in Table 1. Comparison of these data shows that use of the D_{50}s supplied with the impactor (these are calculated values, and generally agree well with calibrations) results in serious overestimation of the amount of mass associated with large particles. As indicated in Fig. 1, aerosol MMAD was overestimated by a factor of two when the D_{50}s were used, and the estimated geometric standard deviation was 40% too large. In this case, the aerosol contained relatively few particles with diameters comparable to the D_{50}s of the first impactor stages. The presence of particles with diameters much smaller than the D_{50}s is attributed to their low, but significant, collection efficiency.

Wall losses were estimated by comparing the mass concentrations of various elemental constituents of aerosols collected with a series of alternately collected filter and impactor samplers. For samples collected downstream of an electrostatic precipitator (ESP), where the aerosol MMAD was 11.5 µm, the average amount of mass collected in the impactors was about 60% of that collected by the filters (Table 2). When fine (MMAD <2 µm), wet particles were collected downstream of a Venturi wet scrubber, the impactor and filter data typically agreed to within 20%, which was well within the uncertainty of the comparison. We concluded, therefore, that wall losses were lower for small, wet particles than for larger, dry fly-ash particles.

Afterfilter data. As indicated in Table 1, the minimum D_{50} in this study was about 0.5 µm, and particles smaller than this were collected on an afterfilter. Aerosols from combustion of pulverized coal typically are distributed bimodally, with a fine-particle mode at about 0.1 µm and a large-particle mode at supermicrometer sizes; the modal diameter of the latter depends strongly on the efficiency characteristics of the control device. The elemental concentrations in the fine-particle mode are of interest in health-impact and source-apportionment studies because of the typically high enrichment of the concentrations of many potentially toxic elements and useful tracer elements in particles in this size range. Large-particle contamination of the afterfilter due to particle bounce can, however, limit the value of these data.

To investigate the importance of afterfilter contamination by particle bounce, particle-size distributions were determined by SEM techniques for afterfilters from three impactors (15). With a final-stage D_{50} of 0.5 µm, we would expect to see particles as large as about 0.94 µm on the afterfilters; however, the afterfilters actually contained particles as large as 4 µm. Cumulative mass distributions for the observed particles are plotted in Fig. 2. Curves a and b represent data for samples collected downstream of an ESP. Impactor stages were coated with vacuum grease (curve a) or not coated (curve b). Curve c represents afterfilter data for a coated impactor run downstream of a Venturi wet scrubber. As indicated in Fig. 2, large particles accounted

for about 96% of the particulate mass on the afterfilter from the coated ESP impactor and 98% of that from the uncoated ESP impactor. A somewhat lower value (87%) for large-particle mass on the third afterfilter indicates that particle bounce and reentrainment were only slightly reduced for the small (<2 μm), wet particles collected downstream of the Venturi scrubber.

The mmads for the distribution of particles on these afterfilters, which ranged from about 1.4 to 3 μm, were far larger than the D_{50} for the final impactor stage and could not have been inferred without SEM measurement. Since neither the correct mass nor the correct particle size can be determined without SEM measurements, afterfilter data should usually be excluded from the analysis when SEM analyses are not made. However, there are some exceptions. For example, the concentrations of certain trace elements are typically much higher in submicrometer particles than in supermicrometer particles. In this study, the concentrations of Mo, Sb, As, and Se in the large particles were so low that a high degree of large-particle contamination could be tolerated. As shown in Table 3, we used the microscopy data and chemical analyses to estimate the true concentrations of elements in the fine-particle component of one of the afterfilters. Except for Mo, Sb, As, Se, and Ba, the elemental concentrations determined in particles on the afterfilter (which would normally be assigned a size less than the final-stage D_{50}) ranged from 40% to over 200% higher than our estimates of their bounce-off-corrected concentrations.

Although we have not formally investigated the deposition of condensible gases, the overall concentrations of Br and Se in impactor samples collected downstream of a hot-side ESP at a large western coal-fired power plant far exceeded their concentrations as determined by filter sampling (16). In addition, the concentrations of Br and Se were nearly uniform on all stages of an impactor (16). Both of these elements tend to be distributed inversely with respect to particle size, and concentrations typically differ by a factor of 10 between particles of 0.1 μm and 1 μm diameter. The surface area available for vapor adsorption is dominated by the substrate rather than by the particles collected on the substrates. Therefore we concluded that the flat concentration-vs-size distributions for Br and Se resulted from the adsorption of vapor-phase components of these elements.

Another phenomenon that we have observed in sampling coal-combustion aerosols is the collection of numerous fine particles on large-particle impaction stages. Figure 3 is an SEM photograph of the third stage of an impactor located downstream of an ESP at a large western coal-utility boiler. Although the D_{50} was 6 μm, hundreds of tenth-micrometer particles are visible. In treated off-gas streams from combustion of pulverized coal, concentrations of submicrometer particle are typically about $10^7/cm^3$, while supermicrometer particle concentrations typically are three or four orders of magnitude lower. We attribute the collection of these fine particles to diffusive deposition from flow streams passing near the collection surface. Since these fine particles typically contain much higher concentrations of many trace elements, their collection may significantly bias the reported size distributions of these elements towards large particles.

Submicrometer Aerosol Measurements

Impactors that size-segregate particles via a series of stages operating at sucessively higher nozzle velocities have been designed by

numerous investigators (11,17,18,19). There is a practical upper limit to jet velocity (3,000-4,000 cm/s), above which particles tend to rebound from the collection plate and no longer stick to it (3). Further, given conventional drilling techniques, it is difficult to make jets with diameters less than about 0.025 cm. As a result, the lower limit of sizing by these impactors is about 0.4 μm (3). Particles below this size are typically collected on a backup filter, but are not size-segregated. Fresh aerosols from high-temperature combustion sources typically contain accumulation modes with modal diameters of about 0.1 μm. Thus the distribution characteristics of these aerosols cannot be determined with conventional cascade impactors operated at near-atmospheric pressure.

From Equation 3), it is clear that the size of particles collected on an impaction stage can also be reduced by increasing the value of the slip correction factor (C) or by reducing the diameter of the jets. The value of C is increased by reducing the gas pressure, and such an increase is the basis for low-pressure and high pressure-drop impactors such as those designed by McFarland et al. (3), Hering et al. (4), and Pilat et al. (5). The McFarland and Hering impactors use commercially available preimpactors for supermicrometer sizing and have three and four additional stages, respectively, for sizing submicrometer particles. The submicrometer sizing stages operate at a final stage pressure of 24.3 mm Hg (McFarland impactor) or 8 mm Hg (Hering impactor). The lower limit diameter for both impactors is 0.05 μm. The McFarland impactor samples at a rate of 28 ℓpm and, by using multiple jets (600 or 1,762), achieves jet velocities within the range required for acceptable particle bounce. Unfortunately, however, the unit requires a vacuum pump weighing between 400 and 500 lb to support the 28-ℓpm sampling rate at the low final-stage pressure. Because of its large size and power requirements, the unit has not been adopted for routine field use and has never been fully evaluated.

The Hering impactor is more portable and has been used to study the distribution of submicrometer sulfate aerosols (20). In this impactor a critical orifice separates the atmospheric and low-pressure stages and determines the 1-ℓpm sampling rate. The low-pressure stages each use a single jet, which even at the relatively low sampling rate produces jet velocities ranging from 9,300 to 30,000 cm/s. These jet velocities are so high that particle bounce is severe for the submicrometer particles (21). The single-jet design is not conducive to analysis by x-ray fluorescence, and the low flow-rate hampers the collection of sufficient material for analyses of trace constituents in ambient air.

In another study (22), we used a University of Washington Mark V impactor to determine the distributions of trace elements in submicrometer combustion aerosols from a 430-MW(e) coal-fired power plant. The Mark V is similar in design to the Mark III, but it has 11 impactor stages and may be operated as a high pressure-drop impactor. The orifice plates of the last four stages of the Mark V are quite similar to those of the University of Washington Mark IV, which was designed specifically for low-pressure operation. The unit can provide up to six submicrometer particle-size fractions. The Mark V was operated at flow rates of about 7 ℓpm at final-stage pressures no lower than 345 mm Hg.

Theoretical values of stage cutoff diameters can be calculated for the impactor if the gas pressures can be accurately estimated or measured. Pilat et al. (23) have extensively measured the pressures on each stage of the Mark IV and have prepared theoretical curves giving stage cutoff diameters as a function of gas temperature and sampling rate for a speci-

fic final-stage pressure. Because of the constraints of isokinetic sampling and the somewhat high pressure-drop filter required for our chemical analyses, and possibly because the amount of gas leakage around the jet stages in our study may have differed from that in the study of Pilat et al. (23), we were unable to obtain the final-stage pressures and sample flow rates called for by the theoretical curves. Because the degree of leakage between stages was unknown, and because the effects of particle bounce are not accounted for by theory, we relied on SEM techniques to determine the size distributions of particles collected on individual stages. The mmds for individual stages that collected submicrometer particles ranged from 0.77 to 0.11 μm. In this study we used Teflon®-fiber afterfilters to achieve the desired flow rate, but these could not be analyzed by SEM. The size distributions observed for the last four stages (Fig. 4) were generally "well behaved"--i.e., they fit well the lognormal distribution function, and tended to be free of the large particles that should have been collected on previous stages. We believe that the use of coated substrates and the numerous impactor stages helped to minimize the effects of particle bounce.

More recently, Kuhlmey et al. (6) developed a uniform-deposit microorifice impactor in which nozzles with diameters of 100 μm were made in 50-μm-thick plates by a photochemical etching process. The original impactor used 200 jets per stage and could collect 0.1-μm particles at a flow rate of 10 ℓpm with an overall pressure drop of only a few inches of Hg. Because of the large number of nozzles, the relatively high flow rate is achieved at quite low jet velocities. The nozzles were placed in a spiral pattern and the collection plate was rotated to achieve uniform deposition. The advantages of uniform deposition are that particles do not pile up under the nozzles and alter the jet-to-plate spacing, thus changing the cutoff diameter; and that x-ray fluorescence can be used for analysis. A later, horizontally configured five-stage design with up to 2,000 jets per stage permitted sampling at 30 ℓpm with a minimum cutoff size of 0.06 μm. Marple (8) has recently built two vertically configured microorifice impactors having a final cutoff size of 0.026 μm. These vertically configured units use four-stage conventional atmospheric-pressure preimpactors to remove supermicrometer particles, and they also operate at 30 ℓpm. All of these microorifice impactors can be used with standard low-volume rotary carbon-vane vacuum pumps.

We have used both the horizontally and vertically configured impactors to sample coal-combustion aerosols in elevated plumes and in plumes at ground level near Deep Creek Lake in western Maryland. Aside from the usual difficulty with the effects of particle bounce, few problems were encountered. Particle bounce could not be evaluated for ambient samples because the individual submicrometer particles could not be discerned. Marple and Rubow (8) have performed extensive calibrations with monodisperse aerosols; these show that impaction plates covered with aluminum foil have slightly larger D_{50}s than plates covered with Teflon-fiber filters.

References

1. Ranz, W. E., and Wong, J. B., Impaction of Dust and Smoke Particles on Surface and Body Collectors. Indust. Eng. Chem. 44, 1371-1381 (1952).

2. Mercer, T. T., The Interpretation of Cascade Impactor Data. Amer. Indust. Hyg. Assoc. J. 26, 236-241 (1965).

3. McFarland, A. R., Nye, H. S., Erikson, C. H., Development of a Low Pressure Impactor. U.S. Environmental Protection Agency, Report no. EPA-650/2-74-014 (1973).

4. Hering, S. V., Flagan, R. C., Friedlander, S. K., Design and Evaluation of New Low-Pressure Impactor. I. Environ. Sci. Technol. 12 667-673 (1978).

5. Pilat, M. J., Powell, E. B., Carr, R. C., Submicron Particle Sizing with UW Mark 4 Cascade Impactor. Proc. 70th Annual Meeting, Air Pollut. Control Assoc. 4, 35.2 (1977).

6. Kuhlmey, G. A., Liu, B. Y. H., Marple, V. A., A Micro-Orifice Impactor for Sub-Micron Aerosol Size Classification. Amer. Indust. Hyg. Assoc. J. 42, 790-795 (1981).

7. Marple, V. A., Liu, B. Y. H., Kuhlmey, G. A., A Uniform Deposit Impactor. J. Aerosol Sci. 12, 333-337 (1981).

8. Marple, V. A., Rubow, K. L., Development of a Microorifice Uniform Deposit Cascade Impactor. Univ. of Minnesota, Particle Technology Laboratory Publ. No. 532 (1984).

9. Fuchs, N. A., The Mechanics of Aerosols. Macmillan Co., New York, (1964). p. 71.

10. Hidy, G. M., Brock, J. R., The Dynamics of Aerocolloidal Systems. Pergamon Press, Oxford (1970). Vol. 1, p. 72.

11. May, K. J., The Cascade Impactor: An Instrument for Sampling Coarse Aerosols. J. Sci. Instrument. 22, 187-195 (1945).

12. McFarland, A. R., Zeller, H. W., Study of a Large Volume Impactor for High Altitude Aerosol Collection. Report of the Division of Technical Information Extension of the U.S. Atomic Energy Commission, TID-18624 (1963).

13. Cooper, D. W., Spielman, L. A., Data Inversion Using Nonlinear Programing with Physical Constraints: Aerosol Size Distribution Measurement by Impactors. Atmos. Environ. 10, 723-729 (1976).

14. Dzubay, T. G., Hasan, H., Size Distributions of Species in Fine Particles in Denver Using a Micro-Orifice Impactor. In preparation.

15. Ondov, J. M., Ragaini, R. C., Biermann, A.H. Elemental Particle-Size Emissions from Coal-Fired Power Plants: Use of an Inertial Cascade Impactor. Atmos. Environ. 12, 1175-1185 (1978).

16. Ondov, J. M., Biermann, A. H., Ralston, H. R., Composition and Distribution Characteristics of Aerosols Emitted from a Coal-Utility Boiler Equipped with a Hot-Side Electrostatic Precipitator. Presented at the Annual ACS Meeting, Miami Beach, FL, Sept. 10-15 (1979).

17. Pilat, M. J., Ensor, D. S., Bosch, J. C., Source Test Cascade Impactor. Atmos. Environ. 4, 671-679 (1970).

18. Andersen, A. A., A Sampler for Respiratory Health Hazard Assessment. Amer. Indust. Hyg. Assoc. J. 27, 160-165 (1966).

19. Marple, V. A., Impactors with Respirable Cut-Off Characteristics. Amer. Ind. Hyg. Conf. Abs. N.P. p. 24 (1977).

20. Hering, S. V., Friedlander, S. K., Origins of Aerosol Sulfur Size Distributions in the Los Angeles Basin. Atmos. Environ. 16, 2647-2656 (1982).

21. Hering, S. V., Personal communication (1981).

22. Ondov, J. M., Biermann, A. H., Heft, R. E., Koszykowski, R. F., Elemental Composition of Atmospheric Fine Particles Emitted from Coal Burned in a Modern Electric Power Plant Equipped with a Flue-Gas Desulfurization System. American Chemical Society Symposium Series no. 167, 173-186 (1981).

23. Pilat, M. J., University of Washington, Personal communication (1979).

Table 1. Comparisons of D_{50} values for a University of Washington Mark III in-stack impactor and observed particle sizes in a sample collected downstream from the electrostatic precipitator of a 750-MW coal-fired electrical power unit (15)

Stage	mg Al	nmd[a]	σ_g	mmad	Interpolated[b] D_{50}	D_{50}
1	2.01	8.14	1.88	34.4	18.5	38.3
2	1.75	2.91	2.10	11.7	8.06	16.7
3	0.985	2.21	1.71	6.72	4.70	6.40
4	0.586	1.39	1.65	4.24	3.01	3.17
5	0.428	1.00	1.35	2.24	1.70	1.77
6	0.179	0.64	1.38	1.37	0.99	0.94
7	0.0837	0.34	1.35	0.73	d	0.50

[a]Number median diameters (nmd) determined from SEM observation. [b]Diameter taken from mmad curve (Fig. 1) corresponding to cumulative mass points of impactor D_{50} values. [c]50% cutoff diameters taken from calibration curves provided with the impactor and adjuster to reflect a particle density of 2.44 $g \cdot cm^{-3}$. [d]Value not determined.

Table 2. Comparisons of selected elemental concentrations in samples collected on filters and on impactors located downstream from the electrostatic precipitator of a 750-MW coal-fired electrical power unit

	Average impactor ($\mu g/m^3$)	Average filter ($\mu g/m^3$)	Collection efficiency (impactor/filter)
Al	230,000 ± 21,000	402,000 ± 46,000	0.57 ± 0.08
As	72.3 ± 4.9	118 ± 8	0.61 ± 0.06
Ba	3,640 ± 490	5,990 ± 420	0.62 ± 0.09
Br	10.2 ± 0.7	81 ± 34	0.13 ± 0.05
Ce	210 ∓ 29	381 ± 28	0.55 ± 0.09
Co	25.4 ∓ 3.9	43.1 ± 3.5	0.59 ± 0.10
Sb	12.4 ± 0.7	19.5 ± 1.2	0.63 ± 0.05
Sc	24.7 ± 2.7	45.9 ± 3.2	0.54 ± 0.07
Se	55 ± 18	44 ± 22	1.27 ± 0.75
Sr	738 ± 28	1,320 ± 20	0.56 ± 0.02
Ta	3.74 ± 0.14	7.73 ± 0.57	0.48 ± 0.04
Th	45.9 ± 5.7	86.5 ± 8.5	0.53 ± 0.08
Ti	10,500 ± 900	17,500 ± 2,300	0.60 ± 0.09
U	25.5 ± 2.4	42.0 ± 3.5	0.61 ± 0.08
V	268 ± 18	498 ± 28	0.54 ± 0.05
		Average collection efficiency[a] (±σ)(excluding Br and Se)	0.60 ± 0.05
		Range	0.47 - 0.71

[a] Includes additional data reported in reference 15

Table 3. Ratios of observed elemental masses on a typical afterfilter to those adjusted for particle bounce

Element	Ratios
Mo, Sb, As, Ba	1.0±0.3; 1.18±0.08; 1.19±0.08; 1.3±0.1
Se, W, V, In	1.3±0.1; 1.4±0.2; 1.5±0.2; 1.9±0.3
Zn, Fe, U, Sr	2.1±1.1; 2.9±1.0; 2.5±1.2; 2.9±1.4
Mn	3.8±2.6
Ca, Ce, Co, Cr Hf, K, Lu, Sc Sm, Ta, Yb	>1.0
Ga, Ti, Eu, Al Dy, Th, La, Na	>1.4, >1.7, >2.0, >2.1 >2.2, >2.6, >2.7, >3.3

Adapted from reference 15

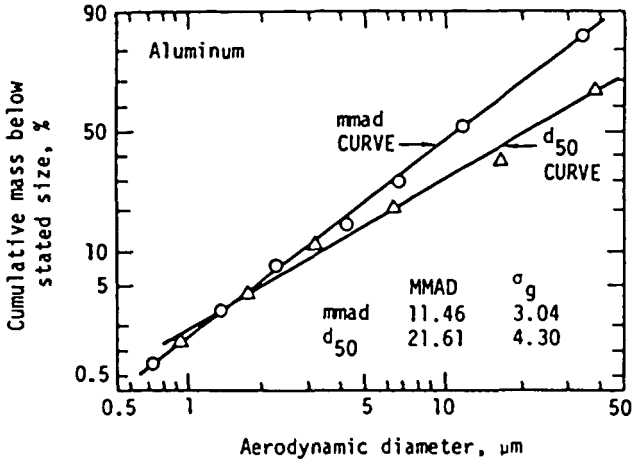

Figure 1. Cumulative mass distributions of the element Al plotted using using impactor D_{50} values and mmads derived from SEM analyses. The impactor was run downstream from an ESP with uncoated impaction stages.

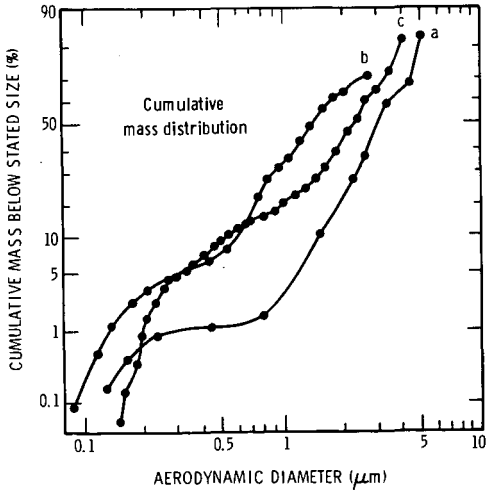

Figure 2. Curve a - cumulative mass distribution for coal combustion particles collected on an afterfilter of a coated impactor. Curve b - cumulative mass distribution for particles collected on an afterfilter of an uncoated impactor. Curve c - cumulative mass distribution for particles collected on an afterfilter at the outlet of a wet scrubber.

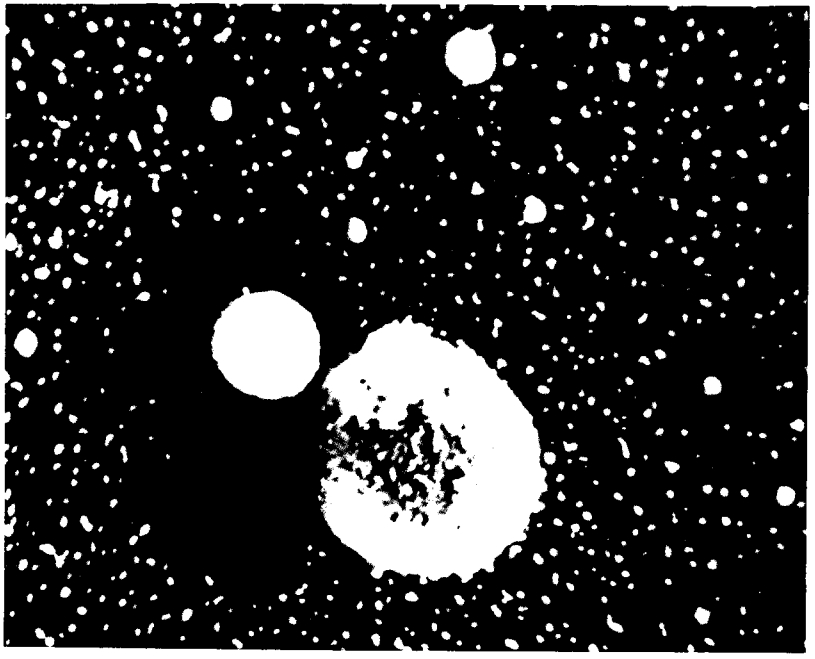

Figure 3. Particles collected on an impactor stage with a D_{50} of 6.4 μm; 4000X magnification.

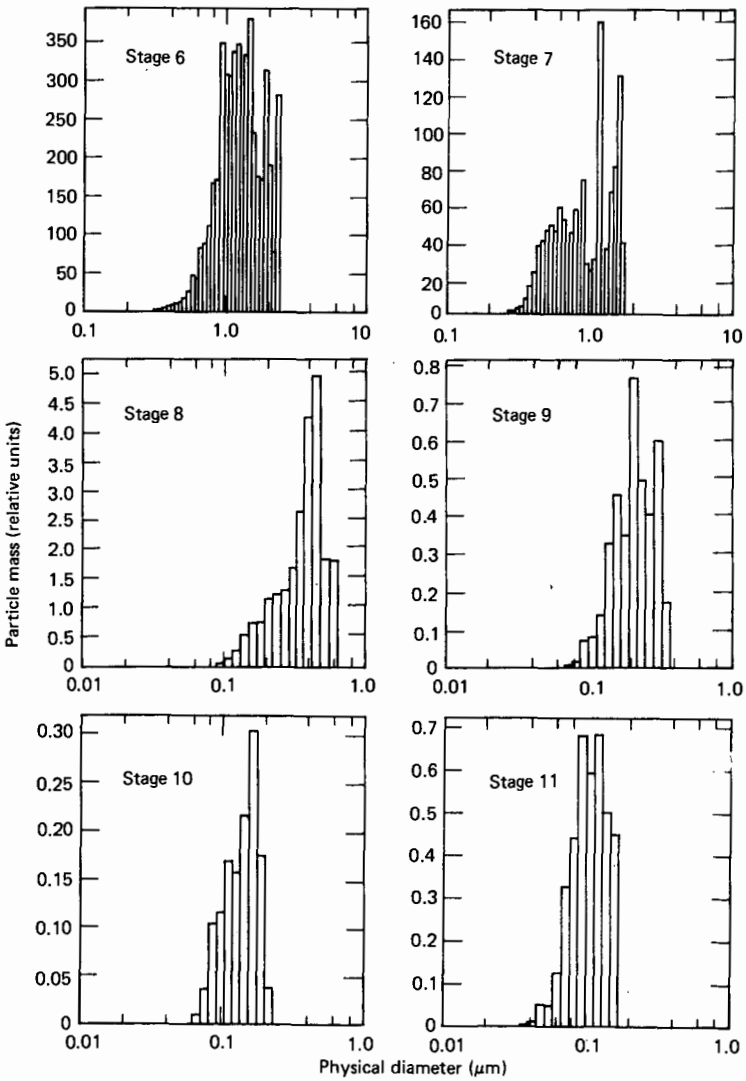

Figure 4. Distribution of particles on stages of a high pressure-drop impactor with submicrometer cut off diameters.

VARIABILITY OF COMPOSITIONS OF PARTICLES RELEASED BY COAL-FIRED POWER PLANTS

Glen E. Gordon and Ann E. Sheffield

Department of Chemistry, University of Maryland, College Park, MD 20742

Introduction

Methods are needed for determining contributions of emissions from coal-fired power plants to atmospheric pollution problems ranging from total suspended particulate matter (TSP) on a local scale (10s of km) to sulfates and acid precipitation on a regional scale (100s of km). One of the best approaches is receptor modeling (1), in which unique chemical and other characteristics of emissions are used to identify contributions from various sources. According to the most widely used receptor model, "chemical mass balances" (CMBs), the composition of airborne particles is expressed as a linear combination of the composition patterns for all important sources:

$$C_i = \sum_j m_j x_{ij}, \qquad 1)$$

where C_i is the concentration of element (or species) i in an ambient particulate sample, m_j is the mass concentration contributed by source j, and x_{ij} is the concentration of element i in particulate matter from source j. Concentrations of many species, C_i, in the atmosphere and compositions of particles from many sources, the x_{ij}s, are measured and a least-squares fit to the C_i values is performed to obtain the source-strength terms, the m_js. The CMBs are most successful if the measured elements include some, often called "marker elements", that are contributed mainly by certain sources, e.g., Pb and Br from motor vehicles, V and Ni from oil combustion, As and Se from coal-fired plants (2).

Progress in this field, especially on an urban scale, has been good (3), but to make receptor modeling more precise and to extend it to a regional scale, we need greatly to improve our knowledge of source-composition terms, the x_{ij}s, for use in CMB calculations. For this reason, we have assembled a source-composition library, which includes data from the literature and our group's research on compositions of particles from important types of air-pollution sources. Here we report on 21 studies of compositions of particles released by coal-fired power plants.

Source-Composition Library

We have tried to make the source-composition library as useful as possible for interpretation of existing large data sets. Therefore, whenever size data were available, we entered the compositions of "fine", "coarse", and "total" particles. We define fine particles as those of diam <2.5 μm and coarse particles as those with diameters from 2.5 μm up to the maximum collected in a given experiment, usually 15 to 20 μm. Most data were taken with different size cuts, so it was necessary to group data in different ways and

interpolate around the 2.5-μm region. The "total" category (a properly weighted combina tion of fine and coarse particles) was included for CMB treatments of many otherwise excellent ambient particle data sets containing no size information. The "total" component also contains data from source studies in which no size information was obtained. Some source categories would contain few entries if restricted only to size-segregated data.

Most recent data sets are accompanied by estimates of errors of the measurements or observed sample-to-sample fluctuations, which we have entered into the library, as it is important to weight various data sets by some inverse function of the uncertainty (traditionally $1/\sigma^2$, which we have used) to compute overall averages and their uncertainties. The latter are important, as modern CMB programs use uncertainties of source compositions in weighted least-squares fitting procedures. We excluded fluctuations arising from variations of mass loading of the stacks or errors in the air volume sampled. For receptor modeling, the appropriate errors for weighting are those of the concentrations of the species in the particulate mass (or relative to that of some normalizing element, if mass was not measured). For each source type, we normalized concentrations of all elements to that of a prominent element, e.g., Al for emissions from coal-fired plants. However, when a data set contains reliable information on mass, we enter a value for mass relative to the normalizing element to retain that information. Data for 21 studies of coal-fired plants (including more than one study of some plants) are included in the library.

Compositions of Particles from Coal-Fired Plants

When coal burns, elements present in the carbonaceous phase tend to be liberated to the gas phase, whether or not they are volatile. Aluminosilicate fragments, the "ash" of coal, melt and outgas volatile species, but are only slightly vaporized (4). When the exhaust stream leaves the combustion zone and cools, major portions of the moderately volatile elements condense on pre-existing particle surfaces and, as finer particles present more surface area, these elements become preferentially associated with fine particles (5). Fine particles also tend to be transmitted through pollution-control devices more readily than large particles. Thus, moderately volatile elements tend to be enriched relative to lithophiles such as Al and Si with respect to the input coal.

Instead of considering raw compositions of particles from coal combustion, we use enrichment factors, EF, which are easier to interpret:

$$EF_{crust} = (C_X/C_{Al})_{partic}/(C_X/C_{Al})_{crust}, \qquad 2)$$

where Cs are concentrations of element X and Al, respectively, in the particles and average crustal material of the earth (6). (Note that Al is not a unique choice of normalizing element; others such as Si or Fe can and have been used.)

The EF_{crust} values are plotted in Fig. 1 for the "total" category for all elements for which there are significant data. We assume that distributions are log-normal and have plotted logs of the (unweighted) geometric means plus

and minus the log of the geometric standard deviations to show the variability of compositions.

In Fig. 1, many elements (mostly lithophile) are only slightly, if at all, enriched with respect to the crust: the alkaline earths, the higher alkali metals, the rare earths, Sc, Ti, Fe, Zr, Hf and Th. That is, these elements occur in the same relative concentrations in coal emissions as in soil or rocks, so they are of little value in distinguishing between coal emissions and airborne soil in CMB calculations. Some elements are depleted relative to the crust because they were washed out of the forming coal in the ground: Na, K and Mn. (Tantalum is probably not depleted; rather, the crustal abundance is incorrectly large.) Many elements are enriched up to ten-fold, especially transition elements V, Cr, Co, Ni, Cu and Zn. The highest EFs, up to 10,000, are for elements that are volatile or have volatile compounds: B, P, S, Cl, As, Se, Br, Mo, Ag, Cd, In, Sb, I, Hg and Pb. In general, the elements of this group will be the most useful for tracing emissions from coal-fired plants unless greater amounts are released by other sources: Pb, Br and Cl from combustion of leaded gasoline; Mo from oil in eastern U.S. cities; Ag, Cd, In and Sb from incinerators, if they are in use; halogens from sea salt in marine areas.

A major problem with these highly volatile elements is that appreciable fractions remain in the gas phase beyond the pollution-control devices, but portions of the vapor may condense when the stack gases are cooled and diluted by ambient air. Thus, concentrations of many of these elements on particles may be greater at the ambient sampling site than in the hot stack. Major portions of S, Cl, Se, Br and Hg are known to be in the gas phase in stacks (7); Se (8) and, of course, S are known to become more strongly associated with particles in ambient air. New sampling methods are needed to obtain particles more similar to those that exist after some time spent in ambient air. Dilution source sampling, in which stack gases are mixed with filtered ambient air before sampling (9), is a step in the right direction, but studies far downwind in plumes are more satisfactory, e.g., the collection of particles from the Four Corners plant on a mesa 8 km from the stack by Wangen (10). Although the gas-phase problem is a nuisance for determining appropriate particle compositions, vapor-phase species could serve as useful tracers if more work were done on them.

Concentrations of some of the most highly enriched elements in Fig. 1 also have some of the highest variabilities, the EF values often covering more than an order of magnitude. In part, the variability may result from fluctuations in the amount of vapor-phase species collected by the particles before they are sampled. However, much of the variation arises because the library contains data for a wide range of plants, some burning eastern (mostly bituminous) coal, some burning western (subbituminous and lignite) coal, some equipped with electrostatic precipitators (ESPs), others with scrubbers. We can attempt to eliminate variations caused by fluctuations of composition of the input coal by considering enrichment factors with respect to input coal, EF_{coal}, the same as Eq. 2, except with $(C_X/C_{Al})_{coal}$ in the denominator. (Note that the population of plants drops to about half, as coal was not analyzed in the others.) We have listed EF data for several of the enriched elements in Table 1. The key measure of variability, independent of the magnitude of the mean value, is σ_g. Much as in our earlier investigation with

fewer data (11), we see that the use of EF_{coal} instead of EF_{crust} reduces fluctuations for some elements (V, I, W, U and, especially, Se and Mo), but increases them for the others, so this technique is not a complete solution to the problem of variability.

Another approach involves the realization that, for receptor modeling in a given region, the component should not include data from all plants investigated, but from those most representative of the types of plants present in the region. For example, for study of eastern U.S. cities or the acid rain problem in the northeast U.S., the component should be made up mainly from data for eastern plants equipped with ESPs. Note in Table 1 that, except for Br, Mo and Pb, there are reductions in σ_g, some quite significant, when we consider only this group of plants. The removal of plants with scrubbers helps especially in the case of Se, as scrubbers greatly increase the EF of Se (and S) on released particles.

Another possible source of fluctuation is the efficiency of the ESP as a function of particle size. Some of this variability should be removed if we consider only fine particles. Data in Table 2 show that there are further reductions of σ_g in most cases that can be tested (along with expected increases in mean EF) when we consider only fine particles. In the final columns, we show the arithmetic average and standard deviation for the fine particles, in this case, properly weighted by $1/\sigma^2$ of the individual measurements. By thus restricting the data, we have obtained rather small variations; however, very few data sets are included in this group, so more studies are needed to establish reliable composition patterns. Some of the remaining fluctuation, e.g., for Se, surely results from variation in the amount of vapor-phase species that condensed before particles were collected.

Recommendations

More data on compositions of particles and vapors from coal-fired plants are needed for receptor-modeling calculations. Special efforts shoud be made to analyze for the highly enriched elements, which provide the best tracers of emissions from coal-fired plants. Particles should be collected in at least two size fractions and samples of the input coal should be analyzed. More effort is needed to collect particles representative of those collected at receptor sites, e.g., by dilution source sampling or, preferably, sampling as far as possible downwind in plumes.

References

1. Glen E. Gordon, Environ. Sci. Technol. 14, 792 (1980).

2. G. S. Kowalczyk, G. E. Gordon and S. W. Rheingrover, Environ. Sci. Technol. 16. 79 (1982).

3. R. K. Stevens and T. G. Pace, Atmos. Environ. 18, 1499 (1984) and following five papers of that issue report on the Quail Roost II Workshop on Mathematical and Empirical Receptor Models.

4. B. S. Haynes, M. Neville, R. J. Quann and A. F. Sarofim, J. Colloid Interface Sci. 87, 266 (1982).

5. R. D. Smith, Prog. Energy Combust. Sci. 6, 53 (1980).

6. K. H. Wedepohl, in Origin and Distribution of the Elements, L. H. Ahrens, ed. (Pergamon Press. London, 1968) pp. 999-1016.

7. M. S. Germani, Ph.D. Thesis, Dept. of Chemistry, Univ. of Maryland, College Park, MD, 1980.

8. K. K. S. Pillay and C. C. Thomas, J. Radioanal. Chem. 7, 107 (1971).

9. R. J. Heinsohn, J. W. Davis and K. T. Knapp, Environ. Sci. Technol. 14, 1205 (1980).

10. L. E. Wangen, Environ. Sci. Technol. 15, 1080 (1981).

11. G. E. Gordon, W. H. Zoller, G. S. Kowalczyk and S. W. Rheingrover, in Atmospheric Aerosol: Source/Air Quality Relationships, E. S. Macias and P. K. Hopke, eds., Amer. Chem. Soc. Symp. Series No. 167 (ACS, Washington, D. C., 1981).

Table 1. Enrichment Factors for Selected Elements Borne by Total Particles from Coal-Fired Power Plants.

Element	All Plants						Eastern Plants with ESPs		
	EF_{crust}			EF_{coal}			EF_{crust}		
	x_g	σ_g	n	x_g	σ_g	n	x_g	σ_g	n
V	3.6	2.8	15	2.5	2.0	8	2.8	1.8	8
Ni	3.5	2.8	16	2.8	3.6	9	2.45	1.6	7
Zn	8.3	3.1	20	7.0	2.5	12	7.0	3.4	8
As	90	4.4	18	2.8	5.6	8	135	2.1	8
Se	1400	6.3	18	8.4	3.1	9	950	3.4	8
Br	27	6.7	6	1.4	8.3	2	13	7.2	3
Mo	76	4.5	9	4.6	4.6	10	34	-	1
Cd	64	3.5	7	7.4	3.8	4	520	-	1
I	190	6.8	3	4.0	2.2	2	570	1.4	2
W	4.0	1.2	4	2.7	1.02	2	4.1	1.0	2
Pb	9.7	3.2	18	4.0	4.0	9	5.7	4.0	7
U	2.6	2.7	5	1.7	2.2	4	-	-	-

Table 2. Enrichment Factors for Selected Elements Borne by Fine Particles from Eastern Coal-Fired Power Plants with Electrostatic Precipitators.

Element	EF_{crust}			
	Geometric			Weighted Arithmetic
	x_g	σ_g	n	$x \pm \sigma$
V	3.1	1.6	6	1.7±0.9
Ni	4.2	1.2	5	4.0±1.0
Zn	5.5	1.7	6	4.1±1.1
As	280	2.0	6	205±80
Se	1440	2.5	6	990±690
Br	41	10	3	6.8±2.9
Mo	97	-	1	97±35
Cd	-	-	0	-
I	1180	1.0	2	1180±45
W	9.1	1.1	2	9.2±0.6
Pb	9.9	1.9	4	14±5

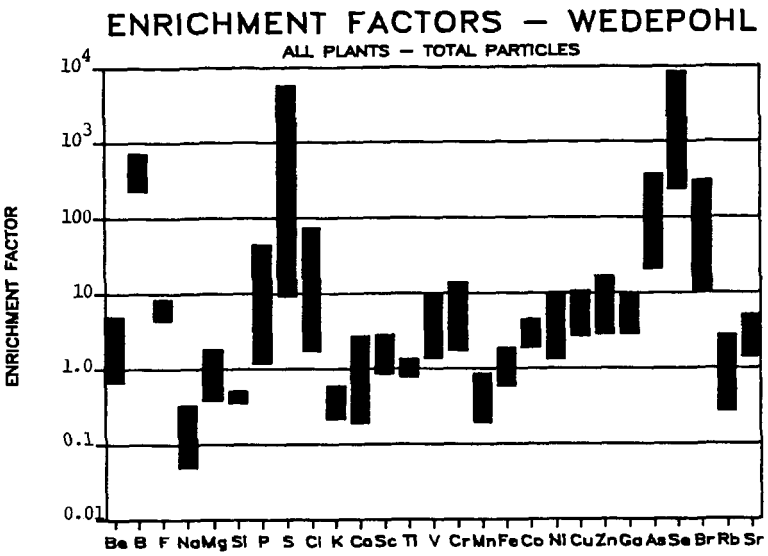

Fig. 1.(a) Enrichment factors for total suspended particles from coal-fired power plants of all types with respect to Wedepohl's crustal abundances (6): Be-Sr.

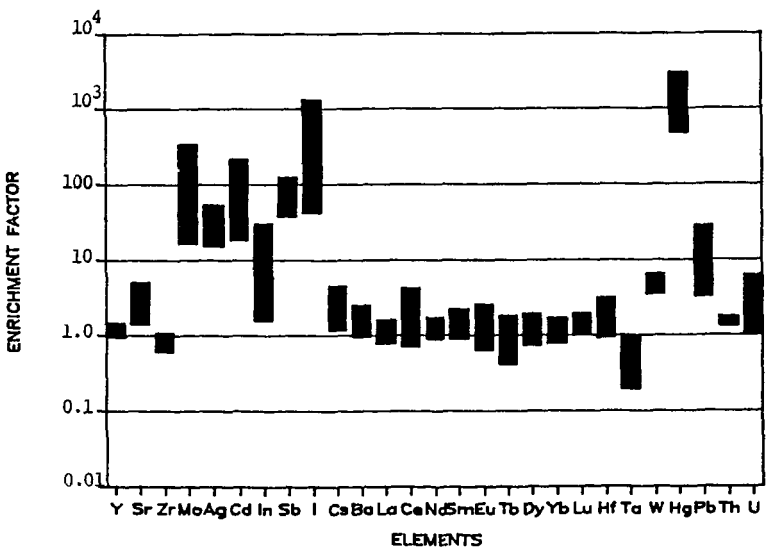

Fig. 1. (b) Same for Y-U.

CHEMICAL REACTIVITY OF POLYCYCLIC AROMATIC COMPOUNDS VAPOR-ADSORBED ON COAL STACK ASH

A. A. Garrison, R. A. Yokley, R. J. Engelbach, E. L. Wehry, and G. Mamantov

Department of Chemistry, University of Tennessee,
Knoxville, Tennessee 37996-1600

INTRODUCTION

Chemical reactions of polycyclic aromatic hydrocarbons (PAHs) under environmental conditions recently have received considerable attention (1-5), but much remains to be learned about the fate of PAHs in the atmosphere. Coal ash is a complex inhomogeneous mixture of many particle sizes, shapes and colors (6,7). It contains virtually every chemical element. The dominant elements are Si, Al, O, Fe, and C, along with significant concentrations of Ca, K, Mg, and Ti. The manner in which coal ash surfaces influence the chemistry of adsorbed PAHs undoubtedly represents a complex interplay of chemical and physical parameters. Their study is complicated by the heterogeneous, complex composition of coal ash and the extreme difficulty of detecting adsorbed organic compounds by optical or particle spectroscopic methods.

The chemical reactivities of five polycyclic aromatic hydrocarbons, as adsorbates on coal stack ash surfaces, have been examined. Each of the indicated compounds is deposited (from the vapor phase) on seven well-characterized coal stack ashes of diverse origins, physical properties, and chemical composition. A significant aspect of the research is the use of vapor-deposition techniques. PAHs were deposited from the vapor phase in a nitrogen atmosphere using diffusion cell and expanded adsorbent bed procedures decribed in detail elsewhere (8,9). This method was selected, as the photochemical behavior of PAHs adsorbed on coal fly ash may be significantly different from that of PAHs in liquid form, in the form of pure solids, or as adsorbates on alumina or silica (10-12).

The reactivity of adsorbed PAHs exposed to gaseous co-pollutants also is not well understood. For example, there appears to be a possibility that some nonphotochemical nitration reactions reported for adsorbed PAHs in the presence of NO_2 actually result from reactions with HNO_3 present as a contaminant in commercial NO_2 (13). The manner in which the reactivity of adsorbed PAHs with NO_2 is influenced by the nature of the adsorbate surface or the presence of light has not been established.

We have generally observed that coal stack ash surfaces stabilize polycyclic aromatic hydrocarbons with respect to both photochemical and nonphotochemical oxidative transformation processes. However, there are significant variations in the abilities of different ashes to exhibit such stabilizing effects. The chemical and physical characteristics of the various stack ashes which may play important roles in altering the chemical behavior of organic compounds adsorbed from the vapor phase are discussed below.

MATERIALS AND METHODS

Aromatic Hydrocarbons

Anthracene (hereafter abbreviated A), phenanthrene (Ph), pyrene (Py), benzo[a]-pyrene (BaP), and benzo[a]anthracene (BaA) were obtained from commercial sources and, when necessary, purified by vacuum sublimation.

Adsorbents

Six ashes (from combustion of Eastern Appalachian (EA), East Tennessee (ET), Western Kentucky (WK), and Illinois (IL) bituminous coals; New Mexico (NM) subbituminous coal; and Texas (TX) lignite) were obtained from the Oak Ridge National Laboratory. All samples were obtained from power plant stack control devices; sampling and chemical analysis of these materials have been described (14). A seventh ash

used was an analytical standard (AR) obtained from Alpha Resources, Stevensville, Mich. An eighth ash, Kaneb (KA), was a high carbon ash obtained from a stack collection device of a power plant experiencing operating difficulties at the time of collection. Elemental analyses of these ashes are listed in Table 1, as are pH values for aqueous extracts of the ashes.

Other adsorbents included alumina (neutral, Brockmann activity I); silica gel; controlled porosity glass (100 Å average pore diameter, from Pierce Chemical Co., Rockford, Ill.); and flaked graphite (Southwestern Graphite Co. Burnet, Tex.). All adsorbents were sieved to pass a 45 μm screen, stored in the dark, and degassed at elevated temperatures by passing high purity nitrogen over them in an expanded bed (8) immediately prior to use. Porosities and surface areas were measured by BET nitrogen adsorption. Diffuse reflectance spectra were measured using a Varian Cary 14L spectrophotometer.

TABLE 1

BULK ELEMENTAL COMPOSITION AND AQUEOUS EXTRACT pH VALUES FOR COAL STACK ASHES[a,b,c]

Element	EA	ET	WK	IL	NM	TX	AR	KA
Si	23.4	30.0	23.4	22.7	28.1	25.7	29.0	na
Al	13.6	15.5	10.1	9.1	13.1	7.5	11.4	na
Fe	10.9	1.7	16.9	16.5	2.5	3.4	4.0	na
Ca	1.0	0.2	1.3	2.4	4.2	14.5	2.9	na
Mg	0.8	1.8	0.4	0.6	0.7	1.9	0.8	na
Na	0.3	0.2	0.2	1.7	1.4	0.4	0.8	na
K	2.4	2.0	2.2	1.6	0.6	0.5	0.9	na
C	1.8	0.5	0.3	0.3	1.0	0.5	0.3	2.8
pH	8.2	4.7	4.4	3.3	11.9	10.8	11.4	6.4

a All analytical data as weight percentages of the elements.
b See preceding page for abbreviations.
c Data not available indicated by "na".

Adsorption Techniques

PAHs were deposited on the adsorbents from the vapor phase immediately after the degassing procedure. Design details for the diffusion cell and expanded adsorbent bed are discussed in the literature (8,9).

Photochemical Techniques

Two illumination cells were used: a rotatable quartz tube (11) and a fluidized-bed photoreactor similar to that described by Daisey, et al. (15). The source was a Cermax xenon illuminator (ILC Technology, Sunnyvale, Cal.) operated at 180-320 W and situated 34-38 cm from the photolysis cell. The spectrum of this lamp closely simulates the solar spectrum in the 300-700 nm wavelength range. To avoid thermolysis of samples under illumination, the near infrared output of the lamp was attenuated by passing the beam through 20 cm of water. A portion of each adsorbent sample was stored in the dark, to serve as a control.

Analytical Procedures

After illumination of a sample, it was subjected to micro-Soxhlet extraction for 24 hr in the dark with methanol or toluene. A portion of the same sample, not illuminated, was extracted identically. Because many PAHs cannot be extracted quantitatively from coal ash (16), samples were subdivided into four portions after illumination but before extraction, so that the PAH recovery for each sample could

be expressed as a 95% confidence interval for quadruplicate extractions. The resulting solutions were analyzed for their extractable PAH content by UV-visible absorption or fluorescence spectrometry. Decisions as to whether a given PAH exhibited degradation on a particular adsorbent were based on differences between the extraction recoveries (as 95% confidence intervals) for illuminated and unilluminated samples.

Studies with NO_2

The photochemistry of adsorbed PAHs in the presence of NO_2 (12ppm in N_2) was studied. To remove traces of HNO_3 from the NO_2, the gas stream was passed through a 20 by 6.5 cm plastic tube packed tightly with nylon wool (17) and then through two 46-mm diameter nylon filters (18). Spectrophotometric analysis of the final nylon filter for nitrate (19) indicated that the system trapped all detectable quantities of HNO_3 present in the NO_2.

RESULTS AND DISCUSSION

Photoreactivities of adsorbed PAHs were classified in the following categories, based on 24 hr illuminations:

a) ++ : High reactivity (>50% loss of PAH)
b) + : Moderate reactivity (10-50% loss of PAH)
c) 0 : Little or no photochemical reactivity (0-10% loss of adsorbed PAH).

Using these classifications, the results are summarized in Table 2.

TABLE 2

PHOTOREACTIVITY OF ADSORBED PAHs[a,b]

PAH	EA	ET	WK	IL	NM	TX	AR	KA	Silica	Alumina	Glass	Graphite
Py	0	0	0	0	0	++	++	0	++	++	++	0
BaP	0	0	0	0	0	++	+	0	++	++	++	0
A	0	+	+	0	+	++	+	0	++	++	++	0
BaA	na	+	na	0	na	++	na	0	++	++	++	na
Ph	na	0	0	0	0	+	na	0	++	++	++	na

a See "Materials and Methods" for abbreviations for PAHs and ashes.
b Data not available indicated by "na".

Major generalizations from these observations include the following.

1) Greater photochemical reactivity is observed for each PAH on alumina, silica gel, or controlled porosity glass than on any coal stack ash substrate.

2) For each PAH, greater photochemical reactivity is observed on Texas lignite (TX) ash than any other ash.

3) No photochemical reactivity is observed for any of the five PAHs on the high carbon Kaneb (KA) ash. Also, pyrene, anthracene, and BaP fail to exhibit any measurable photoreactivity when adsorbed on graphite.

4) Of the five PAHs studied, anthracene is the most photoreactive on ET, WK, and NM ashes, but it appears less reactive than pyrene on the AR ash.

5) In contrast to the observations of Dlugi and Gusten (12), who examined the photochemistry of two PAHs on two ashes and reported much greater photoreactivity for both compounds on the more acidic ash (as estimated by the pH of aqueous extracts of the ashes), our two most "active" ashes (TX and AR) produce alkaline extracts. Several of the acidic ashes (IL,ET,WK) effectively suppress phototransformation of adsorbed PAHs. Likewise, one "alkaline" ash (NM) appears very effective at inhibiting the phototransformation of adsorbed PAHs. Hence, there does not appear to be an obvious relationship between ash surface acidity and the ability of that surface to suppress photodegradation of adsorbed PAHs.

6) A strong relationship is observed between the carbon content and the degree of inhibition of photochemical reactivity. A high iron content in the ash also appears to be related to suppression of phototransformation of adsorbed PAHs. Whether there is any relationship between these observations and the tendency for PAHs to be most strongly adsorbed on carbonaceous particles in stack ash (20) is not yet clear.

7) There is a pronounced general tendency for those ashes which are darkest in color (as noted visually and by uv-visible diffuse reflectance spectrometry) to be most effective in inhibiting photolysis of PAHs (see Figure 1). The lightest colored ashes (TX and AR) are those on which PAHs are photodecomposed most efficiently. The most deeply colored ashes (KA,EA,IL, and WK) effectively inhibit PAH phototransformation. Substrates which are virtually transparent throughout the 280-400 nm wavelength region, such as silica and alumina, show no inhibitive effect relative to solid or solution decomposition. Graphite, which absorbs strongly throughout this spectral region, appears to suppress photochemistry of adsorbed PAHs. In their earlier comparison of rates of photodegradation of anthracene and phenanthrene on two coal ashes, Dlügi and Gusten likewise noted that photodecomposition proceeded more rapidly on the lighter colored ash (12).

BET surface area and adsorption-desorption isotherm hysteresis measurements indicate that all adsorbents examined in this work possess pores of proper size to accomodate PAH molecules studied. The possibility exists, as earlier suggested by Nielsen, et al. (1), that PAHs "deposited inside porous particles... can easily be shielded from the incident light". It seems likely that such an "inner-filter effect" is a factor responsible for the variation in PAH photoreactivity between different ashes.

8) When pyrene or BaP is adsorbed on TX, ET, or IL ash or on silica gel, no detectable decomposition of either PAH is observed in the presence of NO_2 in the absence of light, provided that precautions are taken to remove the nitric acid impurity from the NO_2.

In the presence of both NO_2 and light (but in the absence of HNO_3), decomposition of pyrene and BaP is observed on silica gel and TX ash, but no evidence of nitro-substituted PAH is found.

These observations seem to corroborate the conclusions of Grosjean, et al. (18) that HNO_3, but not NO_2, effects nitration of adsorbed PAHs, irrespective of whether samples are illuminated or exposed to co-pollutants in the dark.

ACKNOWLEDGEMENTS

We thank D. A. Lee (Analytical Chemistry Division, Oak Ridge National Laboratory) for the surface area and porosity measurements. This work was supported by Contract AS05-81ER60006 with the Office of Health and Environmental Reasearch, U. S. Department of Energy.

REFERENCES

1. Nielsen, T.; Ramdahl, T.; Bjørseth, A. Environ. Health Perspect. 1983, 47, 103-114.
2. Pitts, J. N., Jr. Environ. Health Perspect. 1983, 47, 115-140.
3. Edwards, N. T. J. Environ. Quality 1983, 12, 427-441.
4. Van Cauwenberghe, K.; VanVaeck, L. Mutat. Res. 1983, 116, 1-20.
5. Nikolaou, K; Masclet, P.; and Mouvier, G. Sci. Total Environ. 1984, 32, 103-132.
6. Fisher, G. L.; Natusch, D. F. S. in "Analytical Methods for Coal and Coal Products"; Karr, C., Ed. Academic Press: New York, 1979, pp. 489-541.
7. Hulett, L. D.; Weinberger, A. J. Environ. Sci. Technol. 1980, 14, 965-970.
8. Miguel, A. H.; Korfmacher, W. A.; Wehry, E. L.; Mamantov, G.; Natusch, D. F. S. Environ. Sci. Technol. 1979, 13, 1229-1232.
9. Korfmacher, W. A. Ph.D. Thesis, University of Illinois, Urbana, IL., 1978.
10. Korfmacher, W. A.; Natusch, D. F. S.; Taylor, D. A; Mamantov, G.; Wehry, E. L. Science 1980, 207, 763-765.

11. Korfmacher, W. A.; Wehry, E. L.; Mamantov G.; Natusch, D. F. S. Environ. Sci. Technol. 1980, 14, 1094-1099.
12. Dlügi, R.; Gusten, H. Atmos. Environ. 1983, 17, 1765-1771.
13. Pitts, J. N., Jr.; Van Cauwenberghe, K. A.; Grosjean D.; Schmid, J. P.; Fitz, D. R.; Belser, W. L., Jr.; Knudson, G. B.; Hynds, P. M. Science 1978, 202, 515-519.
14. Lauf, R. J. Application of Materials Characterization Techniques to Coal and Coal Wastes. ORNL/TM-7663, Oak Ridge National Laboratory, 1981.
15. Daisey, J. M.; Lewandowski, C. G.; Zorz, M. Environ. Sci. Technol. 1982, 16, 857-861.
16. Griest, W. H.; Caton, J. E. in "Handbook of Polycyclic Aromatic Hydrocarbons", Bjørseth, A., Ed. Marcel Decker: New York, 1983, pp 95-148.
17. Sanhueza. E.; Plum, C. N.; Pitts, J. N., Jr. Atmos. Environ. 1984, 18, 1029-1031.
18. Grosjean, D.; Fung, K.; Harrison, J. Environ. Sci. Technol. 1983, 17, 673-679.
19. Mullin, J. B.; Riley, J. P. Anal. Chim. Acta 1955, 12, 464-480.
20. Griest, W. H.; Tomkins, B. A. Sci. Total Environ. 1984, 36, 209-214.

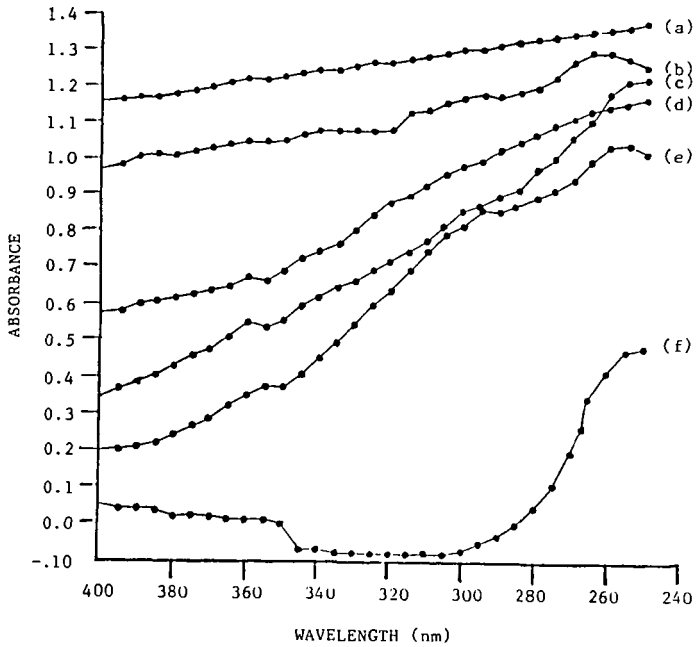

Figure 1. Graphical Representation of Data obtained from the Diffuse Reflectance Spectra of (a) Western Kentucky Bituminous, (b) Kaneb, (c) East Tennessee Bituminous, (d) New Mexico Subbituminous, and (e) Texas Lignite Coal Fly Ashes and, (f) Silica Gel.

CARBON ISOTOPES AS TRACERS OF BIOGENIC AND FOSSIL FUEL DERIVED CARBON TRANSPORT IN THE ATMOSPHERE

Roger L. Tanner and Jeffrey S. Gaffney

Environmental Chemistry Division
Department of Applied Science
Brookhaven National Laboratory
Upton, NY 11973

INTRODUCTION

Carbonaceous aerosols in the atmosphere are complex in nature and are derived from a variety of sources. Improved methods for characterization of organic and elemental fractions of these materials are urgently needed, especially to assess the contributions to carbonaceous aerosols from biogenic and anthropogenic sources of their gaseous and primary particulate precursors. As pointed out previously by several groups(1-5), carbon isotopes (^{13}C and ^{14}C) can be used to obtain new information on carbon source terms. The measurement of ^{14}C content by microscale gas proportional counting (6,7) or by direct ^{14}C atom counting with high energy nuclear accelerators (8) can provide direct evidence of the quantitative role of fossil fuel emissions (evaporation and combustion) vis-a-vis natural emissions from vegetation and human-derived emissions from biomass combustion with respect to the atmospheric carbon cycle.

The additional measurement of $^{13}C/^{12}C$ ratios in carbonaceous aerosols by isotope-ratio mass spectrometry provides information concerning fractionation processes but also can distinguish between biomass combustion sources involving C-3 plants (slash burning of corn, sugar cane) and C-4 plants (wood-burning)(9). This paper discusses recent data acquired at BNL demonstrating the value of ^{14}C and ^{13}C measurements in source allocation of carbonaceous aerosol fractions in the atmosphere. We further discuss the potential application of these techniques for mixed-phase studies of organic oxidant formation of direct relevance to acidic deposition in non-urban and remote atmospheres.

EXPERIMENTAL

Organic/elemental carbon speciation is performed on μg-sized samples using a thermal evolution technique (10) in which carbon is evolved in 2 discrete steps at 400°C in He and at 650°C in 10% O_2/He, then measured as CO_2 by NDIR spectroscopy. $^{13}C/^{12}C$ measurements are made by isotopic ratio mass spectrometry (Nuclide Corp) also after conversion to CO_2; ratios in samples of as little as 0.5 mg can be determined to ± 0.1 δ units.

Carbon-14 content is measured by specially designed gas proportional counters (7). Aerosol samples are first converted to CO_2 by combustion in a macroscale version of the thermal evolution technique. A clam shell oven was used to heat the sample for sequential evolution of organic and elemental carbon under equivalent conditions. Due to the possibility of thermal gradients, conditions in the macroscale apparatus were adjusted to produce the same recoveries of total carbon (μg C per cm^2 of filter area) as for the microscale apparatus. Carbon-14 data are reported as % contemporary carbon. Aldehyde data referred to in this paper were obtained by impinger sampling in dinitrophenylhydrazine/acetonitrile solution and analysis of the derivatives by HPLC with UV detection (11). Olefin measurements were made by a specially designed

ozone-chemiluminescence apparatus (12); difficulties in calibration accuracy and background drift with temperature limit its use to inferences of relative reactive hydrocarbon levels.

RESULTS AND DISCUSSION

Summaries of the aerosol carbon data obtained as part of the POLlutant-TERpene CAnopy Interaction STudies (Poltercaist I and II) conducted at the NOAA Atmospheric Turbulence and Diffusion Laboratory (ATDL) site near Oak Ridge, TN in cooperation with NOAA-ATDL and Oak Ridge National Laboratory (ORNL) staff are reported in Tables 1 and 2. Table 1 concentrates on the organic and elemental carbon data obtained at the Oak Ridge site. Compared to previously reported data (5) from urban and rural sites in the N.E. USA and from Barrow, AK in winter Artic haze episodes, concentrations of both organic and especially elemental carbon were quite high. Organic/total C (total = organic + elemental C) ratios were quite low and suggest the presence of substantial local sources of aerosol carbon in both summer and late winter seasons.

Some significant differences in measured organic/total C ratios by macro- and microscale techniques were observed, with the macroscale apparatus yielding higher ratios. This suggests that improvement in the macroscale technique to better simulate the rapid, uniform heating of the microscale apparatus is in order. However, differences were not large enough to affect the conclusion that local sources, possibly due to incineration, make dominant contributions to local aerosol carbon levels, and that levels of aerosol carbon make a non-trivial contribution to aerosol loadings and concommitant visibility effects. This contrasts with the summertime results in the nearby Great Smoky Mountains (13) in which aerosol carbon effects on visibilitiy were much smaller than those produced by aerosol sulfate levels. Summertime levels of aerosol sulfate were comparably high in both studies.

Table 2 presents the data for $^{13}C/^{12}C$ ratios and ^{14}C content of aerosols collected at the ATDL/Oak Ridge site. The ^{14}C results for two samples in which both organic and element ^{14}C carbon were measured on the same sample are in agreement with predictions that elemental carbon (soot) in atmospheric aerosols is due to primary emissions from combustion of fossil fuels to a greater extent than is organic carbon in aerosols, leading to lower ^{14}C content. The organic carbon may come from a large range of biomass materials of recent origin (leaf litter, carbon in resuspended soil, pollen, etc.) as well as primary and secondary combustion aerosols. In contrast, all soot must come from combustion sources and, although wood combustion makes a major impact on aerosol elemental carbon in some locations especially in winter (3), most elemental carbon is thought to be derived from fossil fuel burning. The high levels of contemporary elemental carbon samples even in the summer season strongly suggests that there are local soot sources from combustion of contemporary carbon-containing fuels other than wood.

In addition to aerosol measurements within and above the canopy during Poltercaist I and II studies, reactive trace gases (HNO_3, O_3, NO_x, olefins, reduced sulfur compounds and aldehydes) were also measured (14). In summer, 1983, increased levels of olefins (~ 2-fold) sampled after a significant rainfall were accompanied by increases in formaldehyde (HCHO) levels but not of acetaldehyde (CH_3CHO) levels. Isoprene emissions from the deciduous forest canopy are deduced to be the cause of increased HCHO levels, indicating biogenic contributions to gas phase organic oxidant precursors, but not directly to organic aerosol carbon formation. Much lower ratios of $HCHO/CH_3CHO$ were observed during winter, 1984, sampling when the deciduous canopy was dormant. Additional measurements are required in coniferous forest canopies in which emissions are different in nature (terpenes vs. isoprene) and emitted in a more

Table 1

POLTERCAIST I and II
Organic/Elemental Carbon
Oak Ridge, TN; July,1983 and March, 1984

Sample	Sampling Time	Sample Wt., mg	Microanalysis Org C $\mu g/m^3$	Microanalysis Elem C $\mu g/m^3$	Microanalysis Org/Total	Macroanalysis Org/Total C
I:C-1 (Org)	1937, 7/14 to 2005, 7/15	7.5	5.26	5.32	0.50	0.55
I:C-1 (Elem)		6.2				
I:C-2 (Elem)	2015, 7/15 to 0843, 7/18	10.2*	3.52	4.63	0.43	NA
I:C-4 (Total)**	1105, 7/20 to ?	7.1	3.59	4.25	0.46	0.75
I:C-5 (Total)	1008, 7/21 to 0852, 7/22	11.4	5.02	4.42	0.53	0.62
II:C-1 (Total)	2050, 3/8/84 to 0939, 3/10	10.1	3.30	7.2	0.31	0.54
II:C-2 (Org)	0940, 3/10 to 1356, 3/12	6.5	5.9	6.2	0.49	0.59
II:C-3,4 (Org)	1357, 3/12 to 0933, 3/16	14.1	8.3	4.7	0.64	0.66
II:C-3,4 (Elem)		7.4	6.8	5.4	0.56	

* Weight of elemental fraction only, organic fraction lost.

** Total samples are weight-averaged for elemental and organic carbon content.

Table 2

POLTERCAIST I and II
Organic/Elemental Carbon, $^{13}C/^{12}C$ and ^{14}C Data
Oak Ridge, TN; July, 1983 and March, 1984

Sample	Sample Wt., mg	Microanalysis Org/Total+	Macroanalysis Org/Total+	$^{13}C/^{12}C$, δ	^{14}C, % Contemporary*
I:C-1 (Org)	7.5	0.50	0.55	-25.5	74
I:C-1 (Elem)	6.2			-24.9	47
I:C-2 (Elem)	10.2	0.43	NA	-25.0	63
I:C-4 (Total)**	7.1	0.46	0.75	-25.2	99
I:C-5 (Total)	11.4	0.53	0.62	-25.4	78
II:C-1 (Total)	10.1	0.31	0.54	-24.3	48
II:C-2 (Org)	6.5	0.49	0.59	-24.7	75
II:C-3,4 (Org)	14.1	0.64	0.66	-25.2	76
II:C-3,4 (Elem)	7.4	0.56		-24.6	53

+ Org/Total = organic carbon/(organic + elemental carbon).

* Corrected to 1978 standard.

** Total samples are weight-averaged for elemental and organic carbon contents.

continuous pattern (15). For both types of canopy studies new isotopic ratio-based techniques are required, especially ^{14}C-measurements of ultra-high volume samples of gaseous species such as formaldehyde and, ultimately, of organic oxidants (PANs, ROOHs) and weak acids in atmospheric water samples, in order to trace the biogenic or anthropogenic origin of oxidized organics and other sinks from the atmosphere.

ACKNOWLEDGEMENT

We acknowledge the assistance of M. Phillips, J. Forrest, and D. Spandau of our group and of Dr. R.W. Stoenner (Chemistry Department, BNL) in performing the measurements reported here. We also acknowledge the Office of Health and Environmental Research, U.S. Department of Energy for their long-term support of this program.

REFERENCES

(1) Currie, L.A., Kunen, S.M., Voorhees, K.J., Murphy, R.B. and Koch, W.F. Analysis of carbonaceous particulates and characterization of their sources by low-level radiocarbon counting and pyrolysis/gas chromatography/mass spectrometry. Proc. Conf. Carbonaceous Particles in the Atmosphere, Univ. California, Berkeley, 1978, p. 36-48.

(2) Currie, L.A., Noakes, J. and Breiter, D. Measurement of small radiocarbon samples: Power of alternative methods for tracing atmospheric hydrocarbons. In Radiocarbon Dating, Berger, Rainer and Suess, H.E., eds. Proc. 9th International Radiocarbon Conf., Berkeley/Los Angeles, Univ. California Press, 1979, p. 58-175.

(3) Cooper, J.A., Currie, L.A. and Kleidal, G.A. Application of carbon-14 measurements to impact assessment of contemporary carbon source on urban air quality. Environ. Sci. Technol. **15** (1981) 1045-1050.

(4) Gaffney, J.S., 1982. Organic air pollutants: setting priorities for long-term research needs. Report BNL 51605 UC-11 (Environ. Control Technol. and Earth Sci., TIC-4500) 1982.

(5) Gaffney, J.S., Tanner, R.L., and Phillips, M. Separating carbonaceous aerosol source terms using thermal evolution, carbon isotopic measurements, and C/N/S determinations. The Science of the Total Environment **36** (1984)53-60.

(6) Currie, L.A., Klouda, G.A. and Cooper, J.A. Mini-radiocarbon measurements, chemical selectivity, and the impact of man on environmental pollution and climate. Radiocarbon **22** (1980) 349-362.

(7) Harbottle, G., Sayre, F.V. and Stoenner, R.W. Carbon-14 dating of small samples by proportional counting. Science **206** (1979) 683-685.

(8) Muller, R.A. Radioisotope dating with accelerators. Science **196** (1977) 489-494.

(9) Gaffney, J.S., Irsa, A.P., Friedman, L. and Slatkin, D.N. Natural $^{13}C/^{12}C$ ratio variations in human populations. Biomed. Mass. Spectr. 5 (1978) 495-497.

(10) Tanner, R.L., Gaffney, J.S. and Phillips, M. Determination of organic and elemental carbon in atmospheric aerosol samples by thermal evolution. Anal. Chem. **54** (1982) 1627-1630.

(11) Tanner, R.L. and Meng, Z. Seasonal variations in ambient atmospheric levels of formaldehyde and acetaldehyde. Environ. Sci. Technol. **18** (1984) 723-726.

(12) Kelly, T.J., Allar, W.J., Premuzic, E., Tanner, R., and Gaffney, J. Temperature dependence of ozone-hydrocarbon chemiluminescence. Possible hydrocarbon class monitor. Presented at the Symp. on Atmospheric Chemistry, Div. of Physical Chemistry, 182nd ACS National Meeting, New York, NY., Aug., 1981.

(13) Stevens, R.K., Dzubay, T.G., Shaw, R.W., McClenny, W.A., Lewis, C.W. and Wilson, W.E. Characterization of the aerosol in the Great Smoky Mountains. Environ. Sci. Technol. **14** (1980) 1491-1498.

(14) Tanner, R.L. and Gaffney, J.S. Biogenic and anthropogenic carbonaceous aerosols and their precursors within a forest canopy. Proc. 77th Annual Mtg., Air Pollution Control Assoc., San Francisco, CA, June 24-29, 1984, Paper No. 84-162.

(15) Yokouchi, Y., Okaniwa, M., Ambe, Y. and Fuwa, K. Seasonal variation of monoterpenes in the atmosphere of a pine forest. Atmos. Environ. **17** (1983) 743-750.

Characterization of Surfaces, Environmental Molecules and Oil Shales by Positron Annihilation

K. Venkateswaran, X. Luo, K.L. Cheng, S.L. Chong[+] and Y.C. Jean[*]
Departments of Physics and Chemistry
University of Missouri-Kansas City
Kansas City, Missouri 64110
+Western Research Institute, Laramie, WY 82071

Abstract

Positronium annihilation lifetime technique has been employed to investigate the physical and chemical properties of surfaces and gas adsorptions on various porous media, such as XAD resins zeolites, and alumina. Positronium lifetimes and formation probabilities vary as a function of adsorbate concentrations. By measuring the positronium chemical reaction rate constant of adsorbate, we are able to obtain useful information about the chemical state and mobility of adsorbed molecules, such as NO_2, SO_2, Ni^{++} and Co^{++} on the surfaces. We found a correlation between the total surface area and positronium formation probabilities in these systems. Applications of positronium annihilation technique to surface analysis, environmental science, and fossil fuels are discussed.

Introduction

The investigation of surface and microvoid properties has become one of the most interesting problem in catalytic, environmental science and fossil fuel research today. Most of catalytic reactions and adsorptions only take place on the surface of porous materials, such as graphites, powders and gel systems, which often form a structure with high surface area. One of the most intriguing problems in chemical research is on the understanding of the surfaces and properties of adsorbates inside these porous media.[1]

Modern surface analytical methods can be broadly categorized as: ex-situ, and in-situ techniques. Most of the existing techniques that have evolved using the conventional probes[1] such as photons, electrons, and ions are ex-situ methods. Each of the ex-situ probes approaches the surfaces of interest from outside the sample, and requires an ultra-high-vacuum ($<10^{-8}$ torr) condition. However, most of real surface applications are under atmosphere pressure. Unfortunately, there are very few good techniques that can be considered in-situ. One of the most significant advantages of in-situ methods is that, they can be used to study practical or "real" systems such as catalysts in fine powder and porous forms, as opposed to the ex-situ probes where the investigation are primarily carried out on single cryostat faces. In catalyst and environmental science research, the current interest is to understand how they work on the atomic scale. The major problem is to identify the active sites where bond breaking and rearrangements take place. The activity and selectivity of a catalyst is determined by the surface structure and composition. Most catalytic systems contain high surface area which have a complicated network of porous structure. Characterization of these complex but practical catalyst systems are not very feasible by using ex-situ probe, since many catalytically significant sites are in the closed pores or inner surfaces. It is therefore evident that a probe, preferably in-situ, and microscopic, to atomic scale, is an ideal surface probe to study the chemisry of catalytic systems.

Positronium annihilation spectroscopy (PAS)[2] is a new analytical technique which is capable of investigating the microvoid and inner-surface properties of porous materials. The advantages of using PAS are based on two facts. First, positronium (Ps), which consists of a positron (anti-electron) and an electron, will annihilate

at a specific rate which is controlled by the electronic density of systems under study. Gas-solid surfaces are the locations where the electronic densities are relatively low. Ps lifetimes are relatively long because Ps lifetime is inversely proportional to the electronic density. A longer lifetime of Ps annihilation has effectively increased the sensitivity using PAS for chemical analysis. The annihilation photons, whose energies are few-tenths of MeV, can be easily detected by standard nuclear technique. Thus Ps annihilation signals contain the electronic density information of materials under study.

The second advantage is that positron possesses unique surface speciality. Contrary to an electron probe, a positron possesses a negative work function in most of solids, i.e. a positron is preferentially diffused or localized to the surface instead of stayed inside the bulk of solids. Because of the surface speciality and sensitivity of positron, Ps annihilation signals are thus mainly characterized by surface states even in complicated porous materials.

Since the positrons emitted from neutron deficient radioisotopes will be thermalized in the bulk of materials in a few picoseconds, these positrons can finally diffuse into the microvoids or interfacial spaces. These positrons approach the surfaces internally, thus PAS is catalogued as an in-situ method which is rarely available in the surface research today. In this paper, we wish to present a series of results in applying positronium annihilation spectroscopy to chemical analysis (PASCA) for catalytic, environmental and fossil fuel systems.

Experimental:

(1) Positronium Annihilation Spectroscopy

Positronium atoms are formed in most of organic substrates. The detection of positronium annihilation is usually carried out by a positron lifetime method which has been known for a few decade in material science and solid state research. Other PAS techniques, such as Doppler broadening and angular correlation measurements of annihilation photons, offer similar or complementary information of lifetime method. In chemical applications, the positron lifetime method gives chemical reaction rate constants which are particularly fruitful.

The positron lifetime measurements were carried out by a conventional fast-fast coincident method, which monitors the starting signal (1.28 MeV γ-rays) from the positron annihilation in the material studied. The resolution of the spectrometer, which was employed in this study as shown in the schematic diagram of Fig. 1, was found to be 380 ps by measuring the coincident photons from a ^{60}Co source. The obtained lifetime spectra were resolved into a function with a sum of multinegative exponential terms by a computer program-POSITRONFIT EXTENDED with two Gaussian resolution functions. The lifetimes were fitted into three components with a source correction of 5% in Mylars, which support ^{22}Na sources. The 5% source correction was determined from a lifetime result in a sample of nitrobenzene in which the solution completely quenches Ps, thus permitting us to determine the proportion of positrons annihilated in Mylar.

(2) Sample Preparations:

XAD resins are copolymers of styrenedivinyl benzene. They are obtained from Rohm and Haas Co., (Philadelphia, Pa.). They are organic copolymers with varying functiona groups. All the XAD resins were subjected to a Soxhlet

extraction procedure with dichloromethane and methanol, water to remove non-polar and polar organic contamiants from the surfaces respectively. The pore structure of XAD resins is stable under this cycling treatments and the observed lifetime results are reproducible at the end of each cycling treatment. Detailed descriptions of these materials can be found in our previous paper.[3]

Linde molecular sieve zeolite-Y was obtained from Alfa Chemicals (Danvers, Ma) in the powder form. The zeolite-Y belongs to the faujasite family of crystalline alumino-silicates. Their framework structure consists of alternating silica and alumina tetrahedra. The zeolite-Y powder (in the Na^+-form) was activated at 400°C for six hours under a vacuum of 10^{-6} torr. The zeolite-Y powder in the Na^+ form was employed as the starting material for preparing metal-ion zeolites (Li^+, Fe^{+3}, Ni^{+2}, Cu^{+2}) by impregnating the metal nitrate solutions.

NO_2 and SO_2 were obtained from Linde Division (Speciality Gases) of Union Carbide Co. (research grade purity). The gases were introduced into a calibrated gas manifold system prior to adsorption on to a solid support in a specially designed sample cell. The adsorption of gases and the positron lifetime measurements were performed at 25°C.

The oil shale[4] was Green River oil shale from the Mahogany zone of the Piceance Creek Basin near Rifle, Co. The raw material contained about 35 wt% kerogen and2.3 wt% benzene-extractable bitumen. The particle size was about 150 μm (~100 mesh). The positron experiments were performed at room temperature under He atmosphere for different baking temperature.

Applications of PASCA:

(1) Total Surface Determined by PAS

We have measured the positron lifetimes in six different kinds of resins, namely XAD2, XAD4, XAD7, XAD8, XAD11, and XAD12. We observed three lifetime components in each of these resins, 0.4 nsec, 4.5 ± 1.0 nsec, and a long lifetime > 30 nsec. It is the second and third components that are useful in characterizing the chemical and physical properties of resins. Figure 2 shows a plot of I_3%, i.e. o-Ps componet versus surface area of these resins. It is obvious that the o-Ps intensity (I_3) is proportional to the surface area. We found a good linear relationship between I_3 and surface area. I_3 is found to be nearly independent of chemical functionality. The existing results of different high surface area systems: oxides,[5] graphites,[6] and silicagel,[7] fall into the same linear equation:

$$I_3 = 3.0 + 0.033\ S\ (>70\ m^2/g) \qquad (1)$$

$$I_3 = 0.080\ S \qquad (<70\ m^2/g) \qquad (2)$$

where S is the surface area (m^2/gm) and I_3 is the observed longest o-Ps component intensity in the media. The accuracy of obtaining S values by the above equations is abut 7%.

(2) Adsorption Studies of Environmental Important Molecules

By employing the lifetime technique we have studied the chemical

reactivities of NO_2, SO_2, NO and O_2, Ni^{++}, Cu^{++}, and Co^{++} in porous media. Two long-lived components ($\tau_2 \sim 5$ nsec, and $\tau_3 > 30$ nsec) have been attributed to positron annihilation on surface and in the microvoids of the media. The observed chemical reactivities between positronium atoms and gas molecules in microvoids are found to be smaller than those reported free gas due to caging effect. The chemical reactivities on the surface between Ps and adsorbed molecules on the surface, which in anionic forms, are reported for the first time and are found higher than those in the microvoids. The chemical reaction rate constant (k) were calculated by using Ps kinetic equation as:

$$\lambda_v = \lambda_v^o + k_v [M]_v \quad (3)$$

$$\lambda_s = \lambda_s^o + k_s [M]_s \quad (4)$$

where subscripts v, s, signify o-Ps annihilation rate void and surface respectively. Figures (3) and (4) show plots of the annihilation rates in the voids and the equilibrium pressure of SO_2 (P_E), as well as the annihilation rate on the surface and the ΔP (amount of SO_2 adsorbed). In all the systems, we observe the anti-inhibition effect of the surface component (I_2%). The distinct k_s and k_v values for each molecule are new information for chemical analysis applications.

(3) Preliminary Studies of Oil Shale by PAS

The investigation of the chemical and physical structure of combustible minerals and oil-shales has been attempted by PAS. We have measured the positron lifetime for the Green-River oil shale[4] as a function of baking temperatures. The result is shown in Fig. 5. The measurements were made at room temperature under He atmosphere in order to avoid any further reactions after baking. Inspite of the fact that the chemical constituents in such an oil shale are still not known exactly by coventional means, the lifetime results are very interesting in many respects.

The long-lived o-Ps lifetime (~1.3 nsec) indicates that the shale structure consists of interfacial spaces. The quantitative fraction of these layer spaces equals to 4% as measured by o-Ps component. The decomposition of internal organic compounds takes place at 340°C where o-Ps lifetime starts to increase. The optimal decomposition temperature takes place at 350°C as shown in Fig. 5. The decomposition continues up to the temperature about 450°C. Above 450°C, the shale structure becomes void-like since all organic molecules have escaped. The void concentration of the shale increases from 5% to 20% as the temperature increases from 450°C to 600°C as measured by o-Ps intensity. However, the void size (diameter) decreases as a function of temperature. If we employ the known correlation between the void diameter and the positron lifetime for solid substrates,[8] we obtain the void size diameter varying from 2.5 Å to 1.2 Å from 450°C to 600°C. More systematic studies of positron lifetime and different oil shales are in the progress in our laboratory.

Acknowledgement

This research is supported by NSF (Jean) of USA and WSEF (Cheng) at University of Missouri-Kansas City.

References

1. For example, see G.A. Somorjai, "Chemistry of Two-Dimensional Surfaces," Cornell University Press, Ithaca, NY, 1982.

2. See H. Ache, "Positronium and Muonium Chemistry," Adv. Chem. Ser. #175 (1979), ACS Pub. Washington D.C.

3. K. Venkateswaran, K.L. Cheng and Y.C. Jean, J. Phys. Chem. 88, 2465 (1984).

4. S.-L. Chong, "Chemical and Geochemical Aspects of Fossil Energy Extraction" ed. T.F. Yen, F.K. Kawahara and K. Hertzberg, Ann Arbor Pub. Mi. p. 143 (1983).

5. R. Paulin, G. Ambrosio, J. Phys. (Orsay, Fr.) 29, 263 (1968).

6. Y.C. Jean, K. Venkateswaran, E. Parsai and K.L. Cheng, Appl. Phys. A. 35, 169 (1984).

7. S.Y. Chuang, S.J. Tao, Can. J. Phys. 52, 749 (1970).

8. K. Venkateswaran, K.L. Cheng and Y.C. Jean, J. Phys. Chem. (submitted).

9. M. Eldrup, Positron Annihilation, Elsevier Pub. Amsterdam (1982).

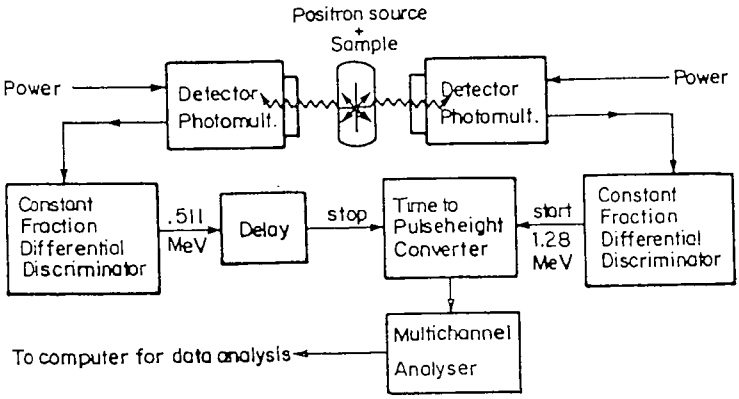

Fig. 1. A schematic diagram for a positron lifetime spectrometer at the University of Missouri-Kansas City.

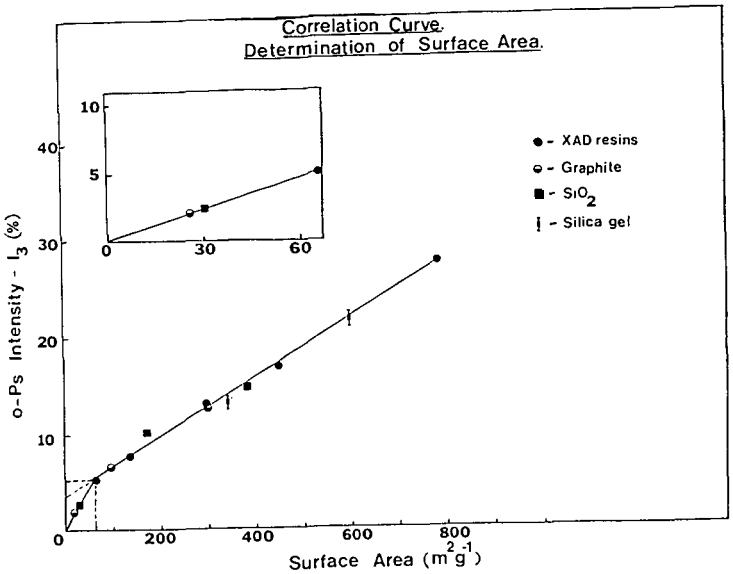

Fig. 2. Plot of o-Ps intensity vs. surface area measured by BET (Ref. 3).

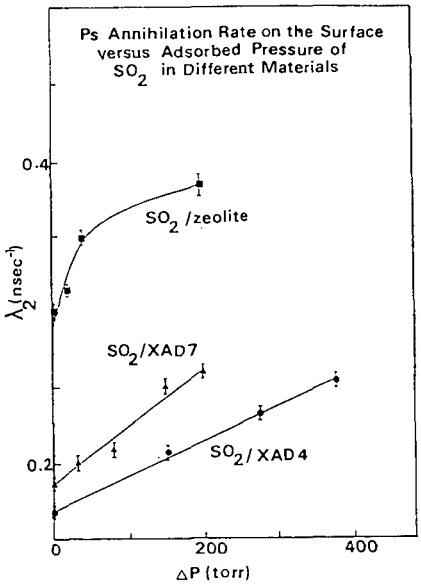

Fig. 3. Plot of the Ps annihilation rate on the surface vs. adsorbed pressure of SO_2.

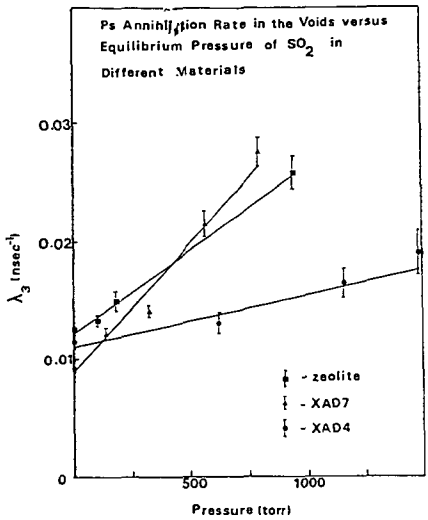

Fig. 4. Plot of the Ps annihilation rate on the surface vs. SO_2 pressure.

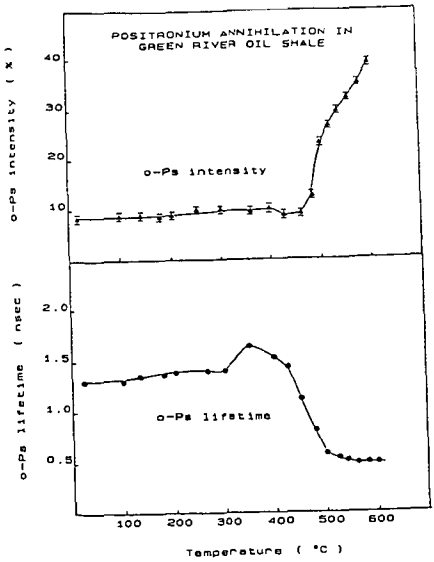

Fig. 5. Plot of the o-Ps lifetime and intensities vs. baking temperature in an oil shale.

DEVELOPMENT OF AN ACID-BASE-NEUTRAL SEPARATION SCHEME AND ITS APPLICATION TO ALTERNATIVE FUEL MIXTURES

Fernando M. Lanças, E.M. Soares, H.S. Karam
Universidade de São Paulo
Instituto de Física e Química de São Carlos
13560 - São Carlos (SP) - BRASIL

and

Harold M. McNair
Virgina Polytechnic Institute and State University
Blacksburg, VA, 24061 - U.S.A.

INTRODUCTION

Alternative fuels, such as solvent-refined coal (SRC), shale oil, and biomass, are gaining more importance as energy sources, as the scarcity of crude oil increases. Fractionation of these fuels into acidic, basic and neutral components is a generally accepted method of separation that has been widely applied for the characterization of coal-derived liquids (1-6) and shale oil (7,8). Various schematics have been utilized for this kind of separation, among which aqueous extraction (1,7,10,11), ion exchange chromatography (6,9, 12) and selective isolation of N-containing compounds by HCl-precipitation (2,3,5) or organometallic-coordination chromatography (6,12,13) have been the most commonly used.

Many of these schematics possess a number of disadvantages and/or limitations. The limited solubility of the protonated bases in the aqueous acid (aqueous acid extraction) (11,14) and the selective precipitation of the aromatic bases by HCl (HCl precipitation) (15) are just examples. The work by several authors (10,11,14,15) demonstrates that the basic fractions generated by different base isolation methods are not identical, and in some cases posses significant structural differences (15).

The inadequacy of the existing methods, in their present form, suggested to us that there is a need for a general and integrated acid base-neutral separation schematic. Such a schematic should be applicable to various kinds of liquid fuels, should avoid any extraction or precipitation steps and rely instead on chromatography. We have undertaken the development of this separation scheme using a large number of standards that represent the various chemical classes generally found in liquid fuels.

One "silica gel modified with KOH" column and one cation exchange resin column were employed for the fractionation. Mixtures of the various standards, as well as the alternative fuels, were separated into acids, bases and neutrals fractions which were then characterized by Gas Chromatography/Mass Spectrometry (GC/MS).

EXPERIMENTAL

Preparation of the packing materials for column-chromatography

Amberlyst 15, the cation-exchanger utilized, and the silica treated with KOH, were prepared according to the literature (9,16). In this work, 20 gm of the

cation-exchange resin,slurried in tetrahydrofuran; and 20 gm of the KOH treated silica, slurried in isopropanol-chloroform mixture, each was mechanically stirred for 30 minutes before being introduced into a 500 x 11 mm I.D. glass colunm fitted with a teflon stopcock and a piece of glass wool to retain the packing material. The modified silica column was then washed with 100 ml of chloroform while the resin column with 100 ml of n-hexane, each solvent of which serving as a first eluent.

Fractionation of standard mixtures on both columns

Separate mixtures of acids, bases and neutrals standards were prepared so as to contain 300 mg/ml of tetrahydrofuran. The composition of these standards appears in Table 1. The retention behaviour of the separate mixtures, on both columns, was monitored gravimetrically (and later studied by GC/MS) by injecting 1 ml of each mixture on each of the two columns and collecting fractions in vials of 5 ml each. Fractions were evaporated to constant weight by placing the vials in a, home-made, water bath-heated block, set at 70°C and passing Nitrogen at a low pressure. Figure 1 outlines the schematic used to fractionate a total mixture of the standards, and later applied to the liquid fuels, along with the eluents utilized to provide the optimum conditions for the separation.

Gas Chromatography-Mass Spectrometry: Experimental Conditions

The GC/MS system used was an HP 5995 B equipped with a library search system. The mass spectrometer was used in the electron impact (EI) mode with an ionization potential of 70 eV. Gas Chromatographic conditions appear as a footnote in Table 1. Standards were chromatographed individually and in their respective mixtures of acids, bases or neutrals to determine their retention characteristics and the best resolution conditions.

RESULTS & DISCUSSION

Chromatogram 1 shows the total mixture of acids, bases and neutrals standards before fractionation, while chromatograms 2, 3 and 4 are for the acidic, basic and neutral fractions, respectively, after the total mixture has been successively separated on cation-exchange and silica modified columns, according to the developed schematic in Fig. 1. Chromatograms 2 - 4 were generated under identical chromatographic conditions for comparison purposes. These conditions along with peak numbers identification appear in Table 1.

Chromatogram 1, in addition to being complex, shows that co-elution of several of the components is inevitable, even with the slow temperature programm employed. These problems are overcome after the total mixture is fractionated, as chromatograms 2 - 4 confirm.

Chromatogram 2 shows that the acidic fraction is pure; no overlap of basic or neutral components has been detected by GC/MS. Chromatogram 3 demonstrates that the basic fraction is slightly contaminated with some acidic components (peaks 31, 33, 39 and 41). The contamination levels are low as indicated by the relative peak areas measurement. The only contamination of the neutral components, in this same chromatogram, comes from 2-methyl indole (peak 34). This compound behaves as a week base and can easily be trapped by a strong cation-exchanger. This phenomenon is further emphasized in chromatogram 4 for the neutral fraction which shows the complete absence of 2-methyl indole.

The strong overlap of 2-sec-butylphenol (peak 24) and 3-t-butylphenol (peak 25) with the neutral fraction in chromatogram 4, could be due to the steric hindrance of the bulky buthyl groups to adsorption of these respective phenols on the basic silica surface.

Chromatogram 5 shows a basic fraction isolated form a typical Brazilian SRC (Mina do Leão) using the developed schematic. Conditions are the same as in Table 1 except that a 5°C/min temperature programn was used.

A portion of the total ion chromatogram (T.I.C.) for this same fraction is displayed in chromatogram 6. Both the gas chromatogram and the total ion chromatogram indicate that the various basic components have been well resolved which makes their identification (not attempted) quite possible specially knowing that this fraction should contain the basic compounds as the results in chromatogram 3 indicate.

In conclusion, this work suggests that using the developed schematic any mixture containing acidic, basic and neutral components can be effectively separated into its respective chemical classes, with a minimum overlap among these classes. The method can be refined a little more so as to yield even purer fractions. Work along these lines is under study.

REFERENCES

(1) Paudler, W. and M. Cheplen, Fuel 58, 775 (1979).

(2) Hausler, D., J.W. Hellgeth, L.T. Taylor, J. Borst and W.B. Cooley, Fuel 60, 40 (1981).

(3) Bockrath, B.C., C.L.D. Donne, F.K. Schweighardt, Fuel 57 (1) 4 (1978).

(4) Dutta, P.K. and R.J. Halland, Fuel 63, 197 (1984).

(5) Sternberg,H.W., R. Raymond and F.K. Schweighardt,Science 188, 149 (1975).

(6) Francisco, M.A. and J.G. Speight, Am. Chem. Soc. Fuel Chem. Div. Prepr. 29 (1) 26 (1984).

(7) Hertz, H.S., J.M. Brown, S.N. Chesler and S.A. Wise, Anal. Chem. 52, 1650 (1980).

(8) McKay, T.F., M.M. Boduszynski and D.R. Laltham,Liquid Fuels Technology 1 (1) 35 (1983).

(9) Jewell, D.M., J.H. Weber, J.W. Bunger, H. Planchar and D.R. Laltham, Anal. Chem. 44 (8) 1391 (1972).

(10) Burchill, P., A.A. Herod and E. Pritchard, J. Chrom. 246, 271 (1981).

(11) Burchill, P. A.A. Herod and E. Pritchard, Fuel 62, 20 (1983).

(12) Altgelt, K.H. D.M. Jewell, D.R. Laltham and M.L. Selucky, Chromatogr. in Pet. Anal., Marcel Dekker, New York, Ch. 9, pp. 185-214 (1979).

(13) Ibid, Ch. 11, pp. 273-286.

(14) Burchill, P., A.A. Herod, J.P. Mahon and E. Pritchard, J. Chrom. 265, 223 (1983).

(15) Finseth, D.H., Z.T. Przyslski and C.E. Schmidt, Fuel 6, 1174 (1982).

(16) Ramijak, Z., A. Šolc, P. Arpino, J.M. Schmitter and G. Guiochon, Anal. Chem. 49, 1222 (1977).

TABLE 1- Composition of Standards Utilized for Preparative Acid-Base-Neutral Separation. Numbers Correspond to Peaks in Chromatograms 1-4*

PEAK NUMBER	COMPONENT	PEAK NUMBER	COMPONENT	PEAK NUMBER	COMPONENT
1	Cyclohexyl Acetate	15	8-Methyl-Quinoline	29	3-t-Butyl Phenol
2	Phenetole	16	Phenol	30	2-Amino Teralin
3	5-Ethyl, 2-Methyl Pyridine	17	O-Cresol	31	P-Methoxy Phenol
4	Benzyl-Ethyl-Ether	18	Diphenyl Ether	32	Indole
5	N, N-Dimethyl Aniline	19	1,2,3,4-Tetrahydro-Quinoline	33	m-Methoxy Phenol
6	2,3-Dihydro,2-methyl-Benzofuran	20	2,6-Dimethyl-Quinoline	34	2-Methyl Indole
7	2,3-Dihydro-Benzofuran	21	P-Cresol	35	2,3-Dimethyl Indole
8	N-Methyl Aniline	22	1-Indanol	36	Dibenzothiophene
9	Aniline	23	4-Ethyl Phenol	37	7,8-Benzoquinoline
10	2,4-Dimethyl Aniline	24	2-Sec-Butyl Phenol	38	Acridine
11	O-Ethyl Aniline	25	2-Phenyl-Pyridine	39	2-Naphthol
12	Benzyl Alcohol	26	3-Phenyl-Pyridine	40	1,2,3,4-Tetrahydro-Carbazole
13	2-Amino Pyridine	27	Dibenzofuran	41	Resorcinol
14	Quinoline	28	Capric Acid	42	Carbazole

* CHROMATOGRAPHIC CONDITIONS: 50 m x 0.2 mm I.D. Fused Silica Carbowax 20 M Capillary; Column Temperature: 60°C Isothermal for 5 min, then 2°C/min temperature program to 240°. Flame Ionization Detector 280°C; Injector 250°C. Carrier Gas Helium at 1 ml/min. Split Ratio 1:15.

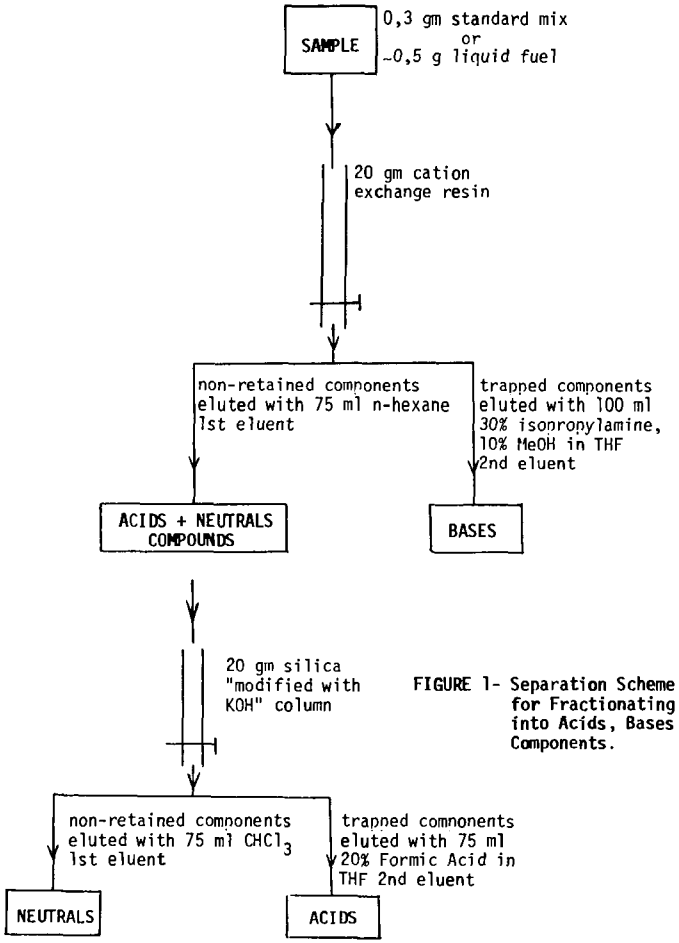

FIGURE 1- Separation Scheme Developped for Fractionating Liquid Fuels into Acids, Bases and Neutrals Components.

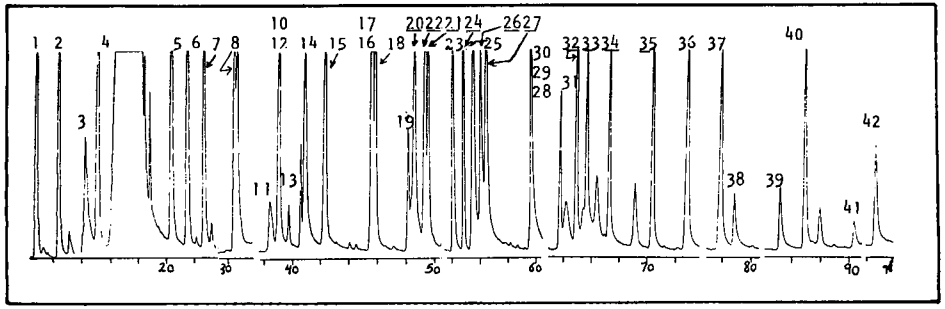

Figure 1. TOTAL MIXTURE OF ACIDS, BASES AND NEUTRALS STANDARDS BEFORE FRACTIONATION. CONDITIONS SAME AS TABLE 1.

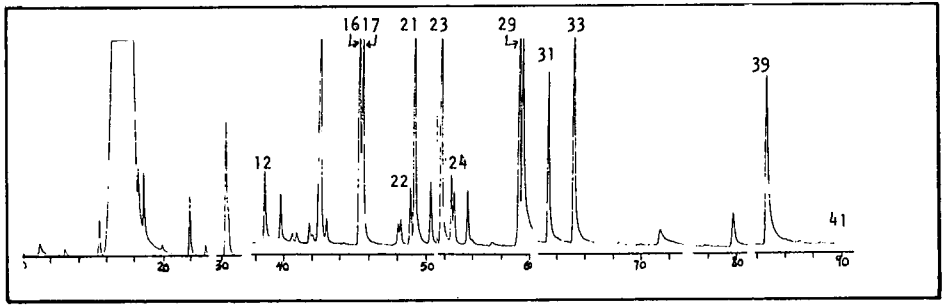

Figure 2. ACID FRACTION OBTAINED AFTER FRACTIONATION. CONDITIONS SAME AS TABLE 1.

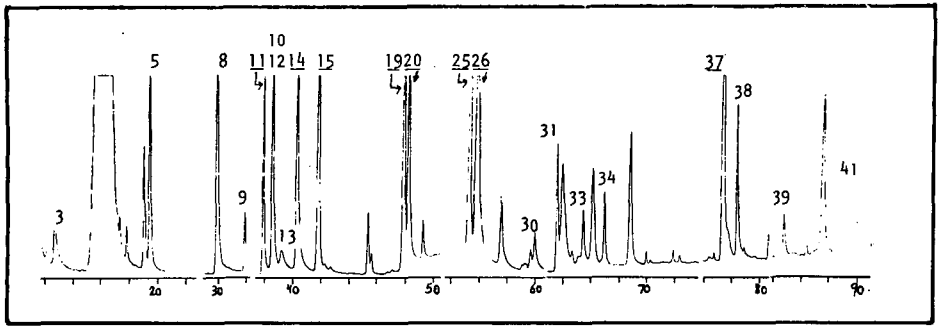

Figure 3. BASIC FRACTION OBTAINED AFTER FRACTIONATION. CONDITIONS SAME AS IN TABLE 1.

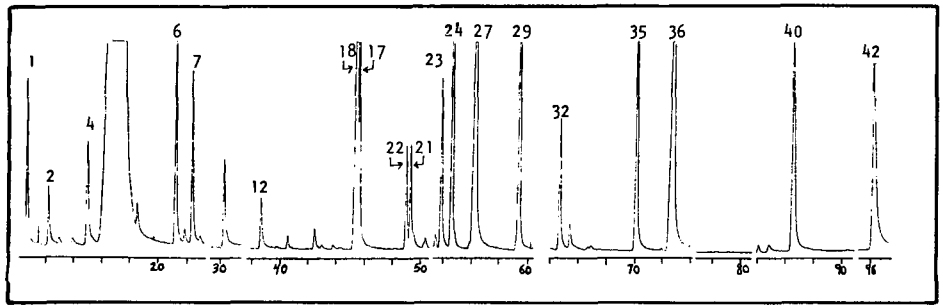

Figure 4. NEUTRAL FRACTION OBTAINED AFTER FRACTIONATION. CONDITIONS SAME AS IN TABLE 1.

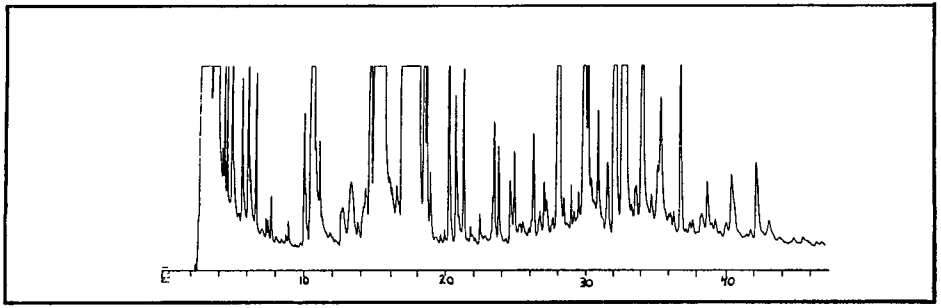

Figure 5. BASIC FRACTION ISOLATED FROM BRAZILIAN SRC (Mina do Leão). CONDITIONS SAME AS IN TABLE 1, EXCEPT TEMPERATURE PROGRAMN 5ºC/MIN.

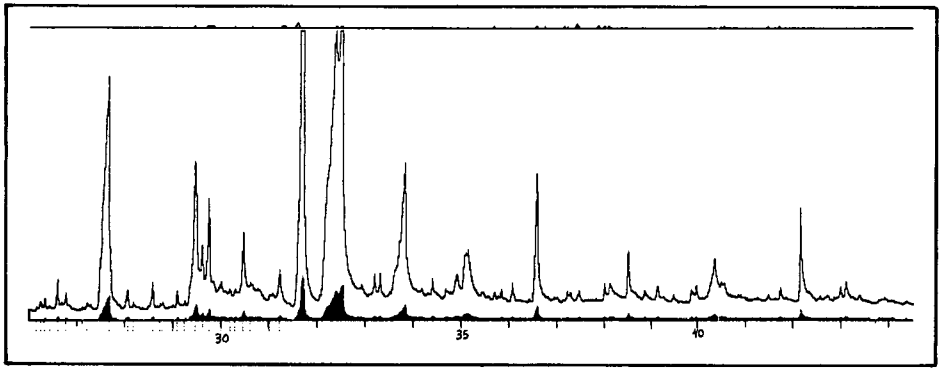

Figure 6. A PORTION OF THE TOTAL ION CHROMATOGRAM(T.I.C.) FOR BASIC FRACTION ISOLATED FROM Mina do Leão SRC. CONDITIONS SAME AS IN FIGURE 5.

CHEMICAL AND BIOLOGICAL EVALUATION OF OILS AND TARS PRODUCED UNDER VARYING COAL DEVOLATILIZATION CONDITIONS

Vassilis C. Stamoudis

Geochemistry Section
Energy and Environmental Systems Division
Argonne National Laboratory
Argonne, IL 60439

INTRODUCTION

Oils and tars are among the major coal-gasification by-products having potentially adverse health and environmental consequences. The production of oils and tars during gasification, pyrolysis, and hydropyrolysis is related to the initial coal devolatilization reactions. The yield has been shown to vary with temperature, pressure, residence time, gas/solid contact, gaseous environment, and presence of catalytic surfaces. Further, coal-gasification oils and tars have been shown to contain toxic chemicals, including polynuclear aromatic amines and hydrocarbons [1-4]. A comprehensive report of an extensive study relating process conditions to chemical and toxicological characteristics of coal-gasification oils and tars has been published [5]. A summary of some of the results and important findings is presented here.

EXPERIMENTAL

Experiments were conducted in a 2-lb/hr entrained-flow reactor operated by the Mellon Institute, in close cooperation with Environmental Research and Technology, Inc. The samples were analyzed by Argonne National Laboratory. Forty-nine successful runs of the reactor covered the following conditions: (a) reactor temperatures = 600°C, 800°C, and 1000°C; (b) gas-phase residence times = 0.2 s and 1.3 s; (c) reactor pressures = 3 atm and 10 atm; (d) reactant gases = He, H_2, CO_2, and steam; and (e) coal types = lignite and subbituminous coal. The organic by-products were trapped by means of three successive traps, and the trapped condensates were combined in proportion to the amounts produced. The combined oil/tar samples were then analyzed for organic compounds using computer-controlled, fused-silica, capillary-column gas chromatography (GC) (Hewlett-Packard 5880A). The aromatic relative retention index (RRI) [5,6] and the concentration of each peak were calculated and printed using custom software. GC/mass spectrometry (GC/MS) was used as necessary to confirm that the correct name was assigned to each RRI.

The Ames mutagenicity of the heavy tar trap samples was measured using the Ames assay (Salmonella TA98 strain with S-9 activation) [5]. All process conditions and chemical and toxicological data were entered into a mainframe computer, where the data were analyzed with great ease and flexibility by applying statistical analysis routines (CMS/SAS).

RESULTS AND DISCUSSION

The chemical composition of the combined oil/tar samples (Fig. 1), varied considerably, but the samples consisted mainly of aromatic compounds of one to four rings (Fig. 2). Therefore, the combined oil/tar samples were monitored routinely by RRI-GC for 62 chemicals, mainly one- to four-ring aromatic hydrocarbons (ranging from benzene to chrysene), and certain phenols and naphthols, acetophenone, indole, benzothiophene, benzofurans, and dibenzofuran.

In general, the most important of the process variables affecting chemical composition and mutagenicity was temperature. As seen in Fig. 1, the 1000°C-run samples were simpler mixtures in which phenols were absent and the level of alkylation was much reduced (Fig. 3). The amount of chromatographable material in these samples was very high. The mutagenicity of the heavy tar trap samples from the 1000°C runs was moderate (Fig. 4). Because the 600°C-run mixtures were much more complex, an additional 44 chemicals were monitored for several of these samples. The amount of phenols was high, and more polar and higher molecular weight materials were present, making the amount of nonchromatographable material higher. However, the mutagenicity associated with the 600°C-run heavy tar trap samples was very low. The 800°C-run combined oil/tar samples had both of the above characteristics -- a clearly higher degree of alkylation, intermediate chromatographability, and high mutagenicity (Fig. 4).

CONCLUSIONS

The results of this study suggest that changes in coal devolatilization conditions can significantly alter the chemical composition and toxicological properties of by-product oils and tars. The results also emphasize the importance of computer-assisted chromatographic analysis and data handling. Further, information of this kind is very useful in helping managers and engineers to design and build energy efficient and environmentally acceptable coal-conversion facilities.

ACKNOWLEDGMENTS

This work was supported by the U.S. Department of Energy's Morgantown Energy Technology Center as part of its Surface Gasification Environmental Program.

REFERENCES

[1] Stamoudis, V.C., S. Bourne, D.A. Haugen, M.J. Peak, C.A. Reilly Jr., J.R. Stetter, and K. Wilzbach, *Chemical and Biological Characterization of High-Btu Gasification (The HYGAS Process), I: Chemical Characterization of Mutagenic Fractions*, in Coal Conversion and the Environment: Chemical, Biological, and Ecological Considerations, D.D. Mahlum, R.H. Gray, and W.D. Felix, eds., U.S. Department of Energy, CONF-80-1039, pp. 67-95 (1981).

[2] Stamoudis, V.C., D.A. Haugen, M.J. Peak, and K.E. Wilzbach, *Bio-Directed Chemical Characterization of Condensates from Synfuel Processes*, in Advanced Techniques in Synthetic Fuel Analysis, C.W. Wright, W.C. Weimer, and W.D. Felix, eds., U.S. Department of Energy, CONF-81-1160 (PNL-SA-11552), pp. 201-214 (1983).

[3] Haugen, D.A., M.J. Peak, K.M. Suhrbier, and V.C. Stamoudis, *Isolation of Mutagenic Aromatic Amines from a Coal-Conversion Oil by Cation-Exchange Chromatography*, Analytical Chemistry, 54:32-37 (1982).

[4] Haugen, D.A., V.C. Stamoudis, M.J. Peak, and A.S. Boparai, *Isolation of Mutagenic Polycyclic Aromatic Hydrocarbons from Tar Produced during Coal Gasification*, in Polynuclear Aromatic Hydrocarbons: Formation, Metabolism, and Measurement, M. Cook and A.J. Dennis, eds., Battelle Press, Columbus, Ohio, pp. 607-620 (1983).

[5] Fillo, J.P., V.C. Stamoudis, J.R. Stetter, and S.W. Vance, *Influence of Coal Devolatilization Conditions on the Yield, Chemistry, and Toxicology of By-Product Oils and Tars*, U.S. Department of Energy, DOE/ET-14746-11 (ANL/SER-2), 243 pp. (1983).

[6] Stamoudis, V.C., *A Gas Chromatographic Scheme, Based on Relative Retention Indices, for Rapid Quantitative and Qualitative Analysis*, Pittsburgh Conf. on Analytical Chemistry and Applied Spectroscopy, Atlantic City, N.J., Paper No. 72, (March 1982).

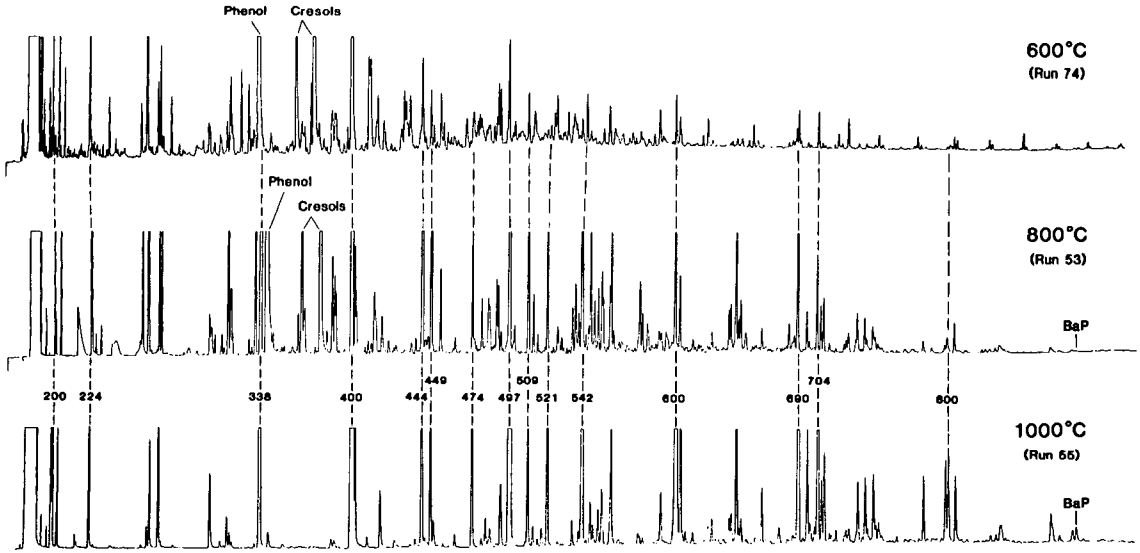

FIGURE 1 Typical GC Chromatograms for Combined Oil/Tar Samples Produced at 600°C, 800°C, and 1000°C (Peaks are labeled with the RRI: 200, benzene; 224, toluene; 338, indene; 400, naphthalene; 444, 2-methylnaphthalene; 449, 1-methylnaphthalene; 474, biphenyl; 497, acenaphthylene; 509, acenaphthene; 521, dibenzofuran; 542, fluorene; 600, phenanthrene; 690, fluoranthene; 704, pyrene; 800, chrysene; BaP, benz[a]pyrene. GC conditions: 50 m x 0.23 mm OV-101 fused-silica capillary column from Hewlett-Packard; initial oven temperature (20°C for 2 min) raised to 270°C at 2°C/min and held at 270°C for 20 min; splitless injection; He carrier gas)

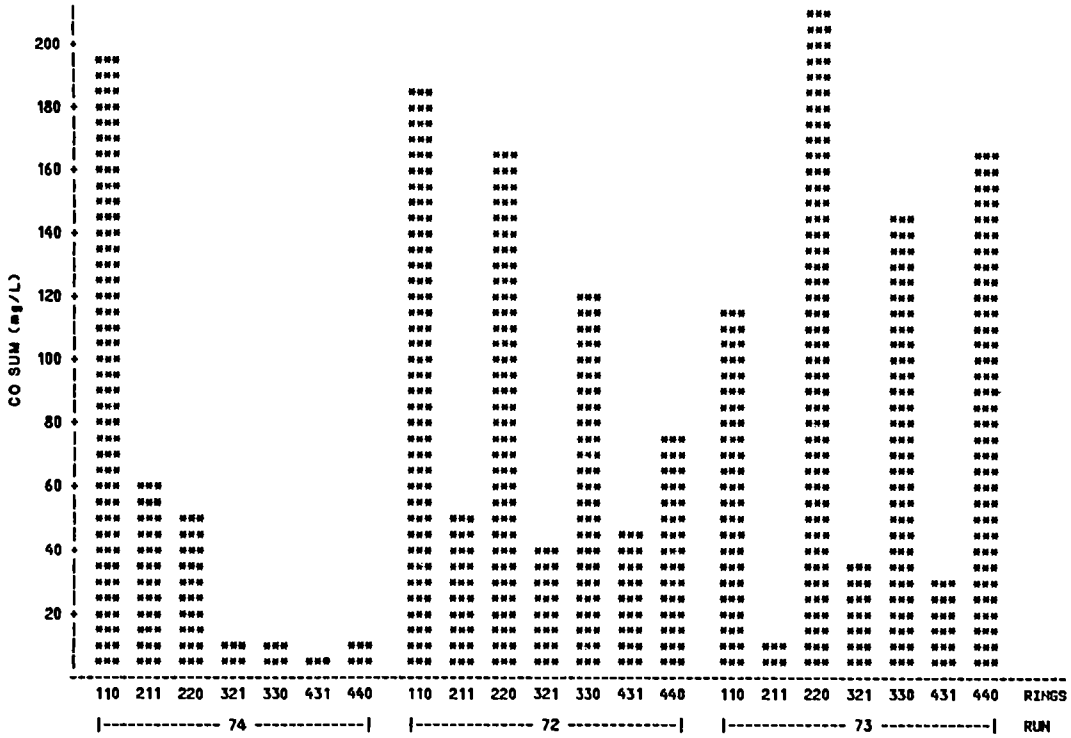

FIGURE 2 Analysis of Total Chromatographable Organics in Combined Oil/Tar Samples Versus Ring Structure for Reactor Runs 74 (600°C), 72 (800°C), and 73 (1000°C) (in the three-digit ring index, first digit = total number of rings, second digit = number of aromatic rings, and third digit = number of alicyclic rings)

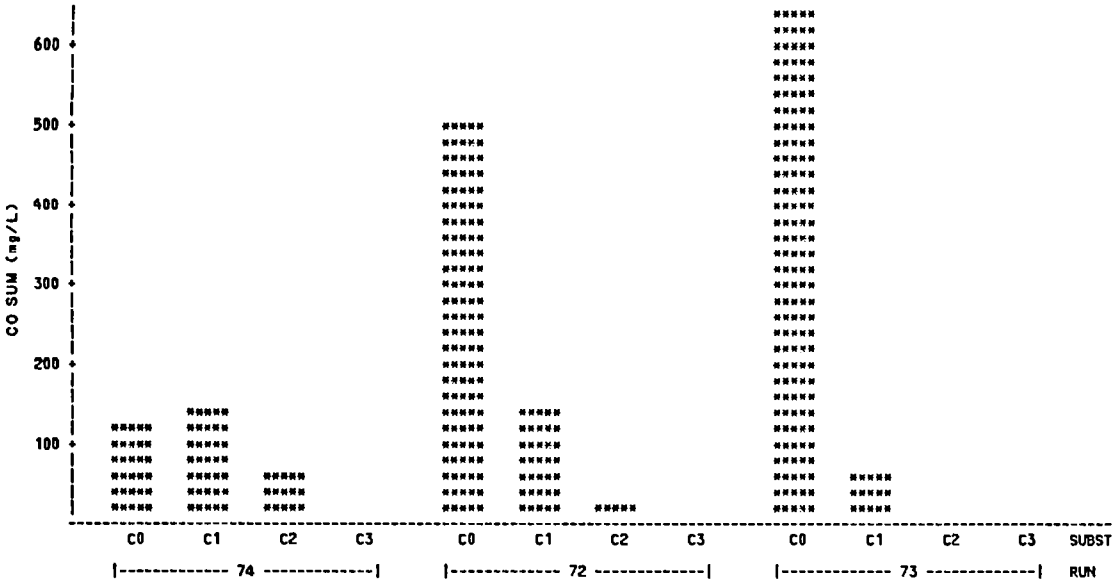

FIGURE 3 Analysis of Total Chromatographable Organics in Combined Oil/Tar Samples Versus Alkyl Substitution for Reactor Runs 74 (600°C), 72 (800°C), and 73 (1000°C)

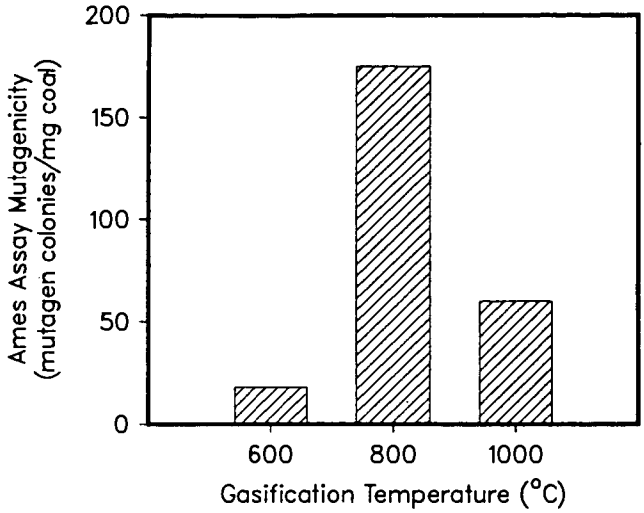

FIGURE 4 Mutagen Formation in Coal Devolatilization (calculated from dose response mutagenicity measurements)

THE FORMATION OF HYDANTOINS IN GASIFIER CONDENSATE WATER

E.S. Olson, J.J. Worman, and J.W. Diehl

University of North Dakota Energy Research Center
Box 8213, University Station
Grand Forks, North Dakota 58202

A number of 5,5-diakyl and 5-alkylhydantoins have been detected in the condensate water from the gasification of Indian Head (ND) lignite in the UNDERC slagging fixed bed gasifier (1, 2). These compounds were characterized by extensive GCMS studies (3) and quantitatively analyzed in samples of process water resulting from various stages in a pilot scale gasifier water treatment plant at UNDERC (4, 5). 5,5-Dimethylhydantoin and 5-ethyl-5-methylhydantoin constitute the major portion of the organic compounds remaining in the condensate water after extraction with diisopropyl ether and steam stripping (5). Because of their biological activity, they represent a potential health hazard in the effluents from a commercial gasifier. Although hydantoins can be adsorbed on activated carbon (3) and degraded by a bacterial nitrification system (6), the expense of removal from the water justifies an effort to gain a better understanding of the formation of hydantoins in the condensate water with the goal of predicting the extent to which the reaction will occur under various conditions.

The hydantoins do not form directly in the gasifier. They were shown to be either absent or present in low concentrations in water samples which were collected from a side stream sampler on the UNDERC gasifier and quickly frozen. When this side stream condensed water was heated in a constant temperature bath at 40°C, hydantoin concentrations increased in an approximately second-order manner. The formation is believed to proceed by the Bucherer-Berg reaction, the same reaction used in commercial hydantoin synthesis, from ammonia, carbonate, hydrogen cyanide and various ketones and aldehydes at a pH of 8.5.

A kinetic study was undertaken to obtain useful rate data for this reaction (7). Reliable and reproducible concentration data for acetone and cyanide were impossible to obtain for the raw gasifier condensate water because of the presence of reversible addition products of cyanide such as acetone cyanohydrin and 2-amino-2-methylpropanonitrile as well as large amounts of sulfide. Thus a model system was investigated where acetone cyanohydrin was reacted with excess ammonium carbonate at concentrations approaching those obtained in the condensate water, 0.020M and 0.25M, respectively. The reaction was studied at 50°, 70°, and 90°C using a capillary GC (OV351 phase) for the analysis of 5,5-dimethylhydantoin (DMH) using 4-methoxyphenol as the internal standard (4).

Linear second order plots were obtained for this reaction at the three temperatures. Table I gives the calculated pseudo second-order rate constants and linear regression fit.

Table I. Pseudo Second-Order Rate Constants and Least Squares Fit at Various Temperatures.

t(°C)	50	70	90
k_2' ℓ $mole^{-1}hr^{-1}$	1.86	3.60	4.62
r^2	0.999	0.998	0.997

The initial concentrations of acetone and cyanide were varied in order to determine their effect on the rate of formation of DMH. When the acetone concentration was doubled, keeping the original cyanide, ammonia, and carbonate concentrations constant, the rate of the reaction doubled at 90°C. A decrease in cyanide concentration to one-half of its original value decreased the rate by one-half. Table II gives the values of the initial rates of formation of DMH at 90°C varying acetone and cyanide concentrations.

Table II. Initial Rate of DMH Formation at Varying Acetone and Cyanide Concentrations. Ammonia and Carbonate Concentrations Were Held Constant at 0.50M and 0.25M, Respectively.

Initial Rate (mmoles $\ell^{-1}hr^{-1}$)	Acetone Concentration (M)	Cyanide Concentration (M)
123	0.02	0.02
220	0.04	0.02
60	0.02	0.01

In order to verify that the rate also depends on the concentrations of ammonia and carbonate, which were present in large excess in these experiments, the 90°C experiment was repeated using 0.02M acetone cyanohydrin and changing the concentration of ammonium carbonate to 0.20M. The expected pseudo second order behavior was again exhibited (r^2 = 0.998) and the observed rate constant was 2.8 liters $mole^{-1}hr^{-1}$. The value expected for 0.8 times the concentration of ammonia and carbonate is 2.9 liters $mole^{-1}hr^{-1}$.

This established that the rate of formation of DMH was first order in all of the reactants as expressed by the following equation:

$$\text{Rate of formation of DMH} = k\,[\text{Acetone}]\,[\text{HCN}]\,[NH_3]\,[CO_2]$$

This kinetic data is valuable in predicting the rate of formation of DMH in coal gasification condensate water, provided the model is applicable. The pH of the model solution and the condensate water remained constant at around 8.4, but the effects of small changes in pH on the rate are not fully known.

In the earlier experiment with sidestream condensate water, it was noted that the concentration of acetone decreased by one-half at the endpoint when the hydantoin concentration no longer increased. This implies that the limiting species for formation of hydantoins in the UNDER gasifier water is cyanide. The hydrogen cyanide peak in the GC analysis had also disappeared. When condensate water was analyzed from initial runs of the Great Plains Gasification Plant which uses coal of the same Beulah-Zap seam as Indian Head coal, negligible hydantoins and HCN were found.

Similarly when Indian Head lignite was used in the METC gasifier, the condensate water contained negligible hydantoins and HCN. In both cases acetone and 2-butanone concentrations were significant.

Data on actual HCN concentrations in the raw gas and quenched gas are not available for these gasifiers. A thorough study was reported by Anastasia on the HYGAS gasifier using Illinois No. 6 coal (8). Although 10% of the nitrogen in the coal was converted to HCN, only 1% of the total HCN entered the condensate water. Most of the HCN (80%) remained in the gas phase (quenched gas) and the

rest dissolved in the oil-tar phase. We expect that significant amounts of HCN are also produced in the gasification of lignite and the factors which determine how much of the HCN ends up in the condensate water are of importance.

One major factor for determining the cyanide concentration in the condensate water is how long the aqueous phase is in contact with the gas phase and oil-tar phase. Diffusion of the HCN at the interface of the aqueous phase with the gas and oil phases and subsequent reaction with acetone and acetone imine over a long period of time will build up the concentration of cyanide addition products which reversibly interconvert and eventually proceed to hydantoin. The residence times for water in the UNDERC spray washer (quench water system) and tar-oil-water separator are several hours which can allow for considerable diffusion buildup of the cyanide conjugates which form significant amounts of hydantoin.

Literature Cited

1. Mohr, D.H., Jr. and King, C.J. Report LBL-13584, Lawrence Berkeley Lab., November 1981, in "Processing Needs and Methodology of Contaminated Water Streams from Synfuel Processes," DOE Symposium, Germantown, Maryland, June 1981.

2. Olson, E.S.; Diehl, J.W.; and Miller, D.J. ASMS 30th Annual Conference on Mass Spectrometry and Allied Topics, Honolulu, Hawaii (1982); Abstracts, p. 818.

3. Olson, E.S.; Diehl, J.W.; and Miller, D.J. Anal. Chem., 1983 55, 1111.

4. Olson, E.S. and Diehl, J.W. 186th ACS National Meeting, Washington, D.C. (1983); Abstracts, ANYL 63.

5. Willson, W.G.; Hendrikson, J.G.; Mann, M.D.; Mayer, G.G.; and Olson, E.S. In report DOE/METC/84-13 (Feb. 1984) Twelfth Biennial Lignite Symposium: Technology and Utilization of Low-Rank Coals Proceedings, Vol. I, ed. by Kube, W.R.; Sondreal, E.A.; and Rao, C.D., p. 265-299.

6. Personal communication, G.G. Mayer and J. Gallagher (UNDERC).

7. Diehl, J.W.; Olson; E.S., and Worman, J.J., Fuel, accepted for publication.

8. L.J. Anastasia in Advanced Techniques in Synthetic Fuels Analysis, ed. by Wright, C.W.; Wiemer, W.C.; and Felix, W.D., Tech. Inform. Ctr., USDOE (1983), p. 105.

A STUDY OF THE REDUCTION, ALKYLATION, AND REDUCTIVE ALKYLATION OF A VOLATILE BITUMINOUS COAL

Narayani Mallya and Leon M. Stock

Department of Chemistry, University of Chicago, Chicago, IL 60637

INTRODUCTION

Reduction, alkylation, and reductive alkylation have been investigated by several different research groups to increase the solubility of coals for structural studies and to develop a greater understanding of the chemical factors essential for the conversion of the intractable coal molecules into soluble or liquid products (1,2). Several lines of evidence suggest that the higher ranking bituminous coals with 88 to 89% C(daf) are more readily converted to products that are soluble in common organic solvents than the lower ranking bituminous or subbituminous coals. The structural factors responsible for the facile reduction reactions of the higher ranking coals have not, as yet, been established. Accordingly, we have undertaken astudy of the relative effectiveness of reduction, alkylation, reductive alkylation and other reactions for the conversion of a vitrinite-rich, low volatile bituminous coal from the lower Kittanning seam in Pennsylvania--PSOC 1197--to soluble products and compared the results obtained in this work with the results obtained in previous studies of lower ranking coals.

EXPERIMENTAL PART

The coal sample was obtained from the Pennsylvania State University Sample Bank. The sample was ground to -325 mesh and then dried in vacuum at 60°C to constant weight.

Reduction.--The coal was reduced in three different ways: A) the coal (1 g) was suspended in liquid ammonia (200 ml) with 64 mmoles of potassium; B) the coal (1 g) was suspended in liquid ammonia (200 ml) with 110 mmoles of potassium; C) the coal (1 g) was suspended in liquid ammonia (200 ml) with 68 mmoles of potassium and 68 mmoles of 2-methyl-2-butanol. All the reactions were carried out at -78°C for 6 hours. Ammonium chloride was added to the reaction mixture to destroy any residual potassium and, thereby, interrupt the reaction. The ammonia was then evaporated and dilute aqueous hydrochloric acid was added to the residue. The mixture was filtered and the solid coal product was collected and dried in a vacuum oven at 60°C.

Alkylation.--The sample of PSOC-1197 was also alkylated in three different ways. Reductive butylation was carried out as described in a previous publication from this laboratory (3). About 60 mmoles of potassium and 80 mmoles of butyl iodide were used in the reaction. Non-reductive butylation was conducted using sodium amide in ammonia at -78°C as described by Ignasiak and coworkers (4). In this reaction, the coal (1 g) was treated with sodium amide (15 mmoles) for 6 hours. 1-Butyl iodide (15 mmoles) in benzene (50 ml) was then added to the reaction mixture which was stirred for 48 hours. The reaction was terminated by the addition of dilute, aqueous hydrochloric acid. The acidified coal product was collected and dried in vacuum at 60°C. The conventional alkylation reaction was carried out as described by Liotta and his coworkers (5). The coal (1 g) was stirred with 22% tetrabutylammonium hydroxide (30 ml) for 3 hours. 1-Butyl iodide (15 mmoles) in tetrahydrofuran (50 ml) was added and the suspension was

stirred for 2 days. The reaction mixture was acidified by the addition of dilute hydrochloric acid. The product was then collected by filtration, washed with water, and dried in vacuum at 60°C.

Measurements.--The solubilities of the coals and the freshly prepared reaction products in pyridine and tetrahydrofuran were determined by Soxhlet extraction. Elemental analyses were obtained by the Huffmann Laboratories and by the Illinois State Geological Survey. The solid state carbon NMR spectra (CP/MAS) were measured at the National Science Foundation Regional Center at Colorado State University using a JEOL FX 60Q system. The acidities of the coals and the reaction products were determined using the procedures described by Schafer (6) and Mallya and Zingaro (7).

RESULTS AND DISCUSSION

The results obtained in this investigation of the reduction, alkylation, and reductive alkylation of a low volatile, bituminous coal with 88% C(daf) are summarized in Tables 1, 2, and 3. The original coal is only modestly soluble in tetrahydrofuran and in pyridine. However, the reduction reactions of this coal with potassium in liquid ammonia, reactions 1 and 2 in the Tables, proceed readily to yield substances that are much more soluble in the organic solvents than the original coal. The facility with which this coal is reduced is remarkable, but not unexpected in view of the results obtained by Given, Wender, and their associates in studies of the reduction of similar high ranking coals under more vigorous conditions, for example with lithium in ethylene diamine (2). In contrast, Illinois No. 6 coal is neither reduced nor rendered soluble to a significant degree by reduction in liquid ammonia (1,3).

The reduction of the Lower Kittanning coal with 110 mmoles potassium/g coal provides a much more soluble product than the reaction with 64 mmoles potassium/g coal. The reducing agent was not consumed in these reactions. The microanalytical data suggest that about 10 hydrogen atoms/100C are added to the coal in the reaction with 64 mmoles potassium/g coal and that about 12 hydrogen atoms/100C are added in the reaction with 110 mmoles potassium/g. While it is well known that the microanalytical determinations of the hydrogen content of coals and coal products are subject to relatively large errors, we have no reason to doubt the reliability of the data presented in Table 2. Thus, it seems quite pertinent that the difference in the degree of reduction of the two samples is very modest compared to the change in solubility from 25 to 78% in tetrahydrofuran and from 39 to 92% in pyridine. These two reaction products also have virtually identical acid contents, Table 3. Thus, ether cleavage reactions do not appear to be responsible for the much greater solubility of the reaction product obtained with the greater concentration of the reducing agent. The observations are compatible with the idea that additional carbon-carbon bond cleavage reactions occur when the concentration of the reducing agent is increased. Metals in ammonia both reduce and fragment hydrocarbons such as the tetraarylalkanes as illustrated in equation 1) (1,8). Accordingly, we postulate that the higher concentration of reductant leads to a greater steady state concentration of aromatic anions with the result that a somewhat greater fraction of these reactive intermediates undergo carbon-carbon bond cleavage reactions during the reaction interval to produce more soluble, lower molecular weight products. Only a few additional cleavage reactions are required to account for the observations.

$$Ar_2CHCHAr_2 \rightarrow [Ar_2CHCHAr_2]^{\cdot -} \rightarrow Ar_2CH^- + Ar_2CH\cdot \qquad 1)$$

The reduction of the Lower Kittanning coal with potassium and 2-methyl-2-butanol in liquid ammonia at low temperature provides an even more soluble product, Table 1, reaction 3. As in the previous case, this reaction is ineffective for the reduction or solubilization of Illinois No. 6 coal (1). The microanalytical data imply that about 14 hydrogen atoms/100C have been incorporated into the structure of the low volatile bituminous coal. The f(A) values determined at the National Science Foundation Center at Colorado State University, for the reduction product, f(A) = 0.69, and the coal, f(A) = 0.82, imply that 21 hydrogen atoms/100C have been added to the coal. The large change in aromaticity strongly suggests that the aromatic anions and carbanions formed in the initial reduction reactions of this coal are efficiently trapped by the proton donor and converted to alkylaromatic compounds, dihydroaromatic compounds, and similar kinds of materials. The fact that a much more soluble product is formed in this reaction in which the aromatic anions of unstable compounds are rapidly protonated by the alcohol implies that reduction is as important as carbon-carbon bond cleavage in the solubilization of this coal as illustrated in equation 2)

$$[HArCH_2CH_2ArH]^- \begin{cases} \rightarrow HArCH_2\cdot + HArCH_2^- \\ \xrightarrow{H^+} HArCH_2CH_2ArH_2 \end{cases} \qquad 2)$$

The lower Kittanning coal contains 3.3 oxygen atoms/100C. Consequently, we also investigated the role of ether cleavage reactions in its reduction reactions. The original coal contains about 0.5 meq/g of acidic hydroxyl groups; hence there is 0.6 reactive hydroxyl group per 100 carbon atoms. Within the limits of the experimental error, the acidic hydroxyl group content of the reduction products is the same as that of the original coal. To examine this issue in another way, we alkylated the product of the reduction reaction with carbon-13 labeled methyl iodide and recorded the NMR spectrum of the products. No resonance signals were observed for O-methylation derivatives between 50 and 63 ppm. Thus, there are few acidic hydroxy groups in the coal product and ether cleavage reactions do not contribute in an important way to the solubilization of this high rank coal during reduction reactions in liquid ammonia. These results are compatible with the idea that the coal contains heterocyclic ethers such as dibenzofuran. Compounds of this type are reported to undergo reduction rather than carbon-oxygen bond cleavage when treated with metals in liquid ammonia (9).

The lower Kittanning coal was alkylated in two ways. First, the reaction was carried out with a relatively mild base, tetrabutylammonium hydroxide, and 1-butyl iodide in aqueous tetrahydrofuran as described by Liotta and his coworkers (5). This reaction was ineffective for the solubilization of the coal which has less than one acidic hydroxyl group per 100 carbon atoms. In a second attempt to alkylate this coal, the reaction was carried out with sodium amide in liquid ammonia using 1-butyl iodide using a modification of the procedure developed by Ignasiak and his coworkers (4). This method provided a product that was 69% soluble in tetrahydrofuran and 83% soluble in pyridine. The result contrasts sharply with the findings obtained previously for the Illinois No. 6

coal which was not solubilized by this technique (1). The microanalytical data and the carbon NMR spectrum of the product obtained in a non-reductive alkylation with carbon-13 enriched methyl iodide are incompatible with a high degree of alkylation of the coal. These observations, therefore, imply that base-catalyzed carbon-carbon bond cleavage reactions, equation 3) are more important for the solubilization of this coal than the alkylation reactions of the carbanions formed during the reaction.

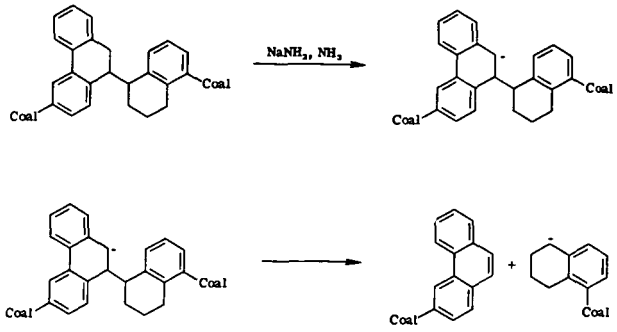

3)

Reductive alkylation of lower Kittanning coal with potassium and 1-butyl iodide provides virtually complete conversion of the material into soluble products. The exact weight gain could not be measured because it was not possible to remove the organic contaminants, for example residual 1-butyl iodide, without also dissolving the reductively butylated coal. The microanalytical data imply that more than six butyl groups/100C have been incorporated into the structure. The degree of solubilization of this coal is significantly greater than the degree of solubilization of the Illinois No. 6 coal realized in the same reaction. The carbon-13 NMR spectrum of the reductive methylation product obtained in the reaction with carbon-13 enriched methyl iodide exhibits an intense band in the C-methyl region from 15 to 40 ppm, but only very weak, almost imperceptible resonances in the O-methyl region between 55 and 65 ppm. Thus, as in the other reduction reactions of this coal, O-alkylation is an insignificant process. The resonances of the C-methyl groups added to the coal appear in three distinct regions near 22, 28, and 35 ppm, respectively. Unfortunately, the resonances are quite broad and it will be necessary to examine other C-alkylation products to assign these resonance signals with confidence.

CONCLUSION

Generally, coals are regarded as insoluble, intractable substances because of their macromolecular character, significant hydrogen bonding interactions, and the intermolecular interaction between unbonded aromatic molecules in different fragments of the structure. Solubilization can be realized when these interactions are disrupted or when the molecular weight is reduced.

Inasmuch as there are few acidic hydroxyl groups in the lower Kittanning coal, hydrogen bonding interactions do not play an important role in determining its behavior in solubilization. Thus, O-butylation of the original coal results in only a very modest increase in solubility. Moreover, no O-alkyl groups are introduced into this coal during reductive alkylation.

The carbon-oxygen and carbon-carbon bond cleavage reactions can reduce the molecular weight of coal molecules. Several lines of evidence indicate that ether cleavage reactions play an insignificant role in the reactions of the lower Kittanning coal. First, there is no increase in the content of acidic hydroxy groups after reduction. Second, there are only traces of O-alkylation products in the reduced coals. Thus, carbon-carbon bond cleavage reactions are much more probable under the conditions of these experiments. The fragmentation reactions of anion radicals such as the simple reaction illustrated in equation 1) occur during reduction and reductive alkylation. Base-catalyzed carbon-carbon bond cleavage reactions of hydrocarbons, as illustrated in equation 3) may occur in the presence of the strongly basic reagents during the non-reductive alkylation reactions. The available results indicate that reduction alone leads to significant increase in solubility and that reductive butylation using the same quantity of reducing agent yields an even more soluble product. Also, previous studies by Wachowska and her associates (10) indicate that the introduction of the large butyl and octyl groups has a large impact on the solubility of the higher rank coals. All these observations are in accord with the suggestion originally made by Wender and his associates that the introduction of hydrogen atoms into coals with significant aromatic character resulted in a disruption of the structure and a reduction of the attractive forces between non-bonded aromatic structures. The impact of the addition of hydrogen atoms is augmented, of course, by the introduction of large alkyl groups. Hence, reduction and alkylation when accompanied by the facile carbon-carbon cleavage in the highly aromatic coal structures provide quite soluble products.

ACKNOWLEDGEMENT

The authors wish to thank Dr. Chaven of Illinois State Geological Survey for obtaining the elemental analysis and the workers at the NSF Regional NMR Center at Colorado State University for measuring the C-13 CP/MAS NMR spectra. Technical assistance of Mr. Joseph Duran in this work is highly appreciated. The United States Department of Energy and the Illinois Department of Energy and Natural Resources supported this work.

REFERENCES

1) L.M. Stock, "Coal Science", 1 161 (1982)

2) I. Wender, L.A. Heredy, M.B. Neuworth and I.G.C. Dryden in "Chemistry of Coal Utilization" ed. M.A. Elliott, John Wiley and Sons, NY, (1981) pp. 437

3) C.I. Handy and L.M. Stock, Fuel, 61, 699 (1982)

4) B. Ignasiak, D. Carson and M. Gawlak, Fuel, 58, 883 (1979)

5) R. Liotta, Fuel, 58, 724 (1979)

6) H.N.S. Schafer, Fuel, 49, 197 (1970); ibid. 49, 271 (1970)

7) N. Mallya and R.A. Zingaro, in "The Chemistry of Low-Rank Coals" ed. H.H. Schobert, American Chemical Society, Washington, D.C. (1984) pp. 133

8) H. Smith in "Organic Reactions in Liquid Ammonia" John Wiley and Sons, NY (1963) pp. 156

9) M. Smith, in "Reduction" ed. R.L. Augustine, M. Dekker, Inc., NY, (1968) pp. 125

10) H.M. Wachowska, Fuel, 58, 99 (1979)

Table 1. A Summary of the Results Obtained in the Reduction, Alkylation, and Reductive Alkylation of a Low Volatile Bituminous Coal from the Lower Kittanning Seam (PSOC 1197).

Sample Origin	Result: Weight Gain (%)	Extractability (%, daf)[a]: Tetrahydrofuran	Pyridine
Original coal	-	4	6
1. Reduction, K(64 mmoles/g), NH_3, -78°C, 6 hrs	3	25	39
2. Reduction, K(110 mmoles/g), NH_3, -78°C, 6 hrs	2	78	92
3. Reduction, K(68 mmoles/g), t-C_4H_9OH, NH_3, -78°C, 6 hrs	5	94	96
4. Alkylation, $N(C_4H_9)_4OH$, C_4H_9I (13 mmoles/g), THF, Ambient T, 48 hrs	1	16	10
5. Alkylation, $NaNH_2$, C_4H_9I (13 mmoles/g), NH_3, -78°C, 6 hrs	2	69	83
6. Reductive alkylation, K(60 mmoles/g), NH_3, 6 hrs, -78°C, C_4H_9I (80 mmoles/g), THF Ambient T, 48 hrs	-	98	93

[a]The precision realized in replicate experiments is about ± 2%.

Table 2. Microanalytical Data for the Lower Kittanning Coal (PSOC 1197) and Its Reaction Products

Sample Origin	Analytical Data (%, daf)			
	C	H	N	Ash[c]
Original coal[a]	87.4	4.8	1.4	11.3
Reduction, reaction 1[a]	84.9	5.2	1.5	10.3
Reduction, reaction 2[a]	82.9	5.1	1.6	10.3
Reduction, reaction 3[b]	86.4	5.5	1.1	10.8
Alkylation, reaction 4[a]	88.1	4.8	1.7	13.7
Alkylation, reaction 5[a]	88.9	4.8	1.8	10.3
Reductive alkylation, reaction 6[a]	82.5	8.0	1.6	5.7

[a]The analysis was performed by Dr. C. Chaven, Illinois Geological Survey.

[b]The analysis was performed by Huffmann Laboratories, Wheatridge, Colorado.

[c]The analysis was performed in this laboratory.

Table 3. Aromaticity and Acid Group Concentration in the Lower Kittanning Coal (PSOC 1197) and Its Reduction Products.

Sample	Acidity (meq/g, daf)		
	Total	Carboxylic Acid	f(A)[a]
Original coal	0.40	<0.01	0.82
Reduction, reaction 1	0.36	-[b]	
Reduction, reaction 2	0.54	-[b]	0.76
Reduction, reaction 3	0.50	<0.01	0.69

[a]The fraction of aromatic carbon content, f(A) = [(C-C(Aliphatic)/C] where C = Area of All Carbon Resonance Signals and C(Aliphatic) = Area of the Aliphatic Carbon Resonance Signal, was determined using CP/MAS NMR spectroscopy.

[b]The carboxylic acid content was not determined.

CATALYTIC HYDRODENITROGENATION OF AN SRC-II COAL LIQUID. EFFECT OF HYDROGEN SULFIDE

Albert S. Hirschon, Robert B. Wilson, and Richard M. Laine*

SRI International
333 Ravenswood Avenue
Menlo Park, CA 94025

The first step in coal liquefaction yields coal liquids which are high in nitrogen, sulfur, and oxygen. These heteroatoms must be removed before these coal liquids can be transformed into synfuels or petrochemical substitutes. However, the catalytic removal of nitrogen (HDN) and oxygen (HDO) consumes excessive amounts of hydrogen. This excess hydrogen is consumed in the hydrogenation of aromatics. If it were possible to remove the nitrogen and oxygen from coal liquids with a minimum of hydrogen and at lower temperatures than currently used, coal could become an economically viable energy source.

Workers have shown that HDN catalysis of model systems undergoes significant rate enhancement in the presence of H_2S (1-5), and some enhancement in the presence of H_2O (6,7). Other workers (8,9) have shown that the acidity of the support is important in the enhancement of HDN activity.

We have recently suggested, based on mechanistic studies of HDN of nitrogen heterocycles that nucleophiles such as H_2S, H_2O, and perhaps NH_3 can enhance catalysis by promoting heterocyclic ring opening via nucleophilic attack on the metal-complexed heterocycle (10). We have also seen in our work that the addition of acids aids in the hydrogenation of nitrogen containing heterocycles (11). Thus it may be possible to increase the rate of hydrogenation of heterocycles while not effecting the rate of hydrogenation of other aromatics.

The objective of this work is to develop an understanding of how nucleophiles such as H_2S, SH^-, and $S^=$, H_2O, NH_3, and added acids effect the HDN process of coal liquids under catalysis conditions. From the results of our work we have found that the addition of H_2S or added acids to an SRC-II coal liquid enhances the removal of nitrogen under standard HDN conditions.

Experimental Procedures and Materials

SRC-II middle distillate was obtained from the Pittsburg and Midway Mining Co. SRC pilot plant at Fort Lewis, Washington. The cobalt-molybdenum catalyst, HT-400 (3 wt% CoO, 15.1 wt% MoO_3, on Al_2O_3) was obtained from Harshaw Chemical Company. Hydrogen sulfide (H_2S) was obtained from Matheson. Hydrogen (H_2), nitrogen (N_2), and an H_2S(10%)/H_2 gas mixture were obtained from Liquid Carbonic.

Apparatus

Hydrogenation reactions were performed in a 300-mL Autoclave Engineers (AE) Magnedrive stirred reactor, heated with a 1000-W electric furnace (AE). The temperature was controlled with a model CP temperature controller (AE). The autoclave was connected through a sample gas vent to a Carle Series S gas chromatograph (GC) adapted by Carle to analyze C_1-C_3, H_2, O_2, N_2, and H_2S.

Analytical Procedures

Nuclear magnetic resonance (NMR) spectra were obtained on a JEOL FX 90Q spectrometer. NMR samples were prepared by mixing one part by weight of coal liquid with two parts of $CDCl_3$. The conditions for obtaining the ^{13}C NMR spectra were as follows. Samples were made 0.025 M in $Cr(AcAc)_3$. The pulse width was 6 μs and pulse delay

15 s. The NNE option (heterodecoupling with no Nuclear Overhauser enhancement) was chosen for quantitative ^{13}C analyses.

The infrared (IR) spectra were obtained on a Perkin-Elmer 281 spectrophotometer. Elemental analyses were obtained from Galbraith Laboratories. (Nitrogen was determined by the Kjeldahl method).

Catalyst Preparation

The HT-400 cobalt-molybdenum catalyst was ground and sieved to obtain a 60- to 200- mesh powder. The catalyst was activated at 400°C in a flowing mixture of H_2S (10%) in H_2 for 24 h, then stored in a Vacuum Atmospheres Dri-box under N_2. (Before the catalyst was sulfided, it was heated for 2 h at 400°C under flowing synthetic air, pretreated with H_2S/H_2 mixture for 1 h at room temperature, then slowly heated to 400°C over a 2-h period). Anal.: Mo, 7.8%; S, 7.75%.

Standard Reaction Procedures

The autoclave was filled under N_2 with the desired quantity of activated catalyst and SRC-II liquid. The reactor was then charged with 1200 psi of H_2 (or H_2/H_2S). For those reactions using H_2S only or when NH_3 was added, the following procedure was used: A tared 20-mL minireactor was filled with H_2S or NH_3 to the desired weight. The minireactor was then connected to the 300-mL autoclave and the system was purged with N_2. The 300-mL reactor was cooled with dry ice, and the gas was condensed into the autoclave.

The system was heated to 400°C and maintained at 400°C for 1 h, at which time the heating furnace was removed. When the reactor had cooled to room temperature, GC analyses were performed on the product gases. The liquid products were removed and filtered to remove the catalyst. Duplicate runs were made at either end of the concentration range (analyzed nitrogen content deviates no more than 0.02% in the duplicate runs).

Results and Discussion

Treatment of SRC-II with Hydrogen Sulfide (without catalyst)

The data from the reactions of H_2S or H_2S/H_2 with the SRC-II liquid are shown in Table 1. When the SRC-II was treated with H_2S alone, we observed some evolution of gases (1.96 mmol gas/g coal liquid) due to H_2, ethane, and propane. The evolution of gases affects the quality of the remaining coal liquids. As determined by NMR, the fraction of aliphatic hydrogen and carbon decreased from 0.66 to 0.60 and 0.32 to 0.30, respectively, and the H/C ratio decreased from 1.20 to 1.15 from the original SRC-II liquid. In contrast, the treatment of the coal liquid with the H_2S/H_2 mixture resulted in essentially no change in hydrogen content from the original. The IR spectra of these reaction products are similar to that of the original liquid and show no absorptions in the region of 2550 to 2600 cm^{-1} where we expected to see SH stretches. Elemental analyses of the products from the H_2S and H_2S/H_2 reactions showed an increase in sulfur content from 0.30% to 0.54 and 0.43% respectively. These results are in accord with what might be expected based on Stenberg's work at higher temperatures (12) (450°C vs 400°C used here).

Treatment of SRC-II with Sulfided Catalyst

In experiments 3 through 9 we treated 50 g of the coal liquid using a 1% concentration of sulfided catalyst. As seen from Table 1 the addition of nucleophiles such as H_2S, HS^-, $S^=$, H_2O, or NH_3, or added acids such as trifluoroacetic acid (TFA), do not have a dramatic effect of the hydrogen uptake (by H/C ratio) or on the aliphatic to aromatic ratios (by NMR) nor were there significant difference in the IR spectra of the products from the runs. However, as seen from the elemental analyses of these

products, the nitrogen content of 0.74% (exp 3) in the baseline run with H_2 decreased to 0.56% (exp 4) in the H_2S/H_2 run, and decreased to 0.42% (exp 9) in the TFA/H_2 run. Figure 1 shows that as the H_2S or TFA concentration increases, the nitrogen concentration of the resultant hydrotreated product decreases. The addition of $S^=$ as Na_2S (exp 7) or the addition of H_2O (exp 5) to the standard reaction resulted in no enhancement over that of exp 3. The addition of NH_3 seemed to inhibit the HDN reaction (exp 6), whereas the combination of NH_3 and H_2S resulted in only a slight inhibition of the HDN reaction (exp 8).

Table 1. Reactions with 1% Sulfided Catalyst at 400°C for 1 h with 1200 psig of H_2 (or H_2S/H_2)

Experiment[a]	Additive (mole wt%)[b]	%N	%S	H/C	$\%H_{alip}$	$\%C_{aliph}$
SRC-II	--	0.98	0.30	1.20	66	32
1[c,d]	H_2S (0.27)	1.00	0.54	1.16	60	30
2[d]	H_2S (0.084)	0.92	0.43	1.21	67	33
3	--	0.74	0.04	1.28	71	38
4	H_2S (0.084)	0.56	0.12	1.23	72	40
5	H_2O (0.14)	0.75	--	1.27	72	38
6	NH_3 (0.084)	0.99	0.03	1.24	72	37
7	Na_2S (0.084)	0.72	0.18	1.20	73	38
8	NH_4HS (0.084)	0.87	0.15	1.23	73	39
9	TFA (0.054)	0.42	0.15	1.22	70	37

[a]Duplicate runs.
[b]Moles of additive per 50 g of coal liquid.
[c]No hydrogen used.
[d]No catalyst used.

Conclusions

The addition of free H_2S under coal liquid upgrading conditions aids in the HDN process. These results validate the HDN modeling studies of Bhinde et al. (1) and those of Satterfield (2-5) and are in accord with our predictions (10). Furthermore, in contrast to the runs without catalyst, the addition of H_2S with catalyst leads to the product that has a reduced sulfur content. Our results also show that TFA aids in the HDN process. Although the HDN enhancement resulting from the addition of TFA is most likely due to its acidic properties, since it decomposes during the HDN reaction it is difficult to determine at what step in the HDN process the acceleration occurs. However our preliminary results are encouraging and with further experimentation we may be able to make substantial improvement in the HDN process which will result in considerable cost benefit.

Acknowledgement

We wish to thank the Pittsburg and Midway Mining Companies for the supply of SRC-II coal liquid. The research reported was supported by Grant Number DE-FG22-83PC60781 from the Department of Energy.

REFERENCES

1. M.V. Bhinde, S. Shih, R. Zawadski, J.R. Katzer, and H. Kwart, "Chemistry and Uses of Molybdenum," 3rd Int. Conf. (1979) 184-187.

2. C.N. Satterfield and S. Gultekin, Ind. Eng. Chem. Proc. Des. Dev. (1981) 20, 62-68.

3. J.F. Coccheto and C.N. Satterfield, Ind. Eng. Proc. Des. Dev. (1981) 20, 49-53 and 53-61.

4. Yang, S. H. and C. N. Satterfield, Ind. Eng. Chem., Process Des. Dev., 23, 20 (1984).

5. Gultekin, S., S. A. Ali, and C. N. Satterfield, Ind. Eng. Chem., Process Des. Dev., 23, 179 (1984).

6. C. N. Satterfield and D. L. Carter 2nd Eng. Proc. Des. Dev. (1981) 20, 538-540.

7. L. Berg, F. P. McCandless, H. Bhatia, and A. Yeh, Energy Progress (1983) 3 248-251.

8. A. M. Tait and A. L. Hensley, Am. Chem. Soc. Div. Fuel Chem., preprints (1982) 27, 187-200.

9. B. M. Lok, F. P. Gortsema, C. A. Messina, H. Rastelli, and T.P.S. Izod, Am. Chem. Soc. Div. of Pet, Preprints (1982) 27, 470-480.

10. R.M. Laine, Catal. Rev.-Sci., (1983) 25, 459-474.

11. R. M. Laine, SRI International, 1983, private communication.

12. Stenberg, V. I., W. G. Wilson, D. E. Severson, G. G. Baker, C. L. Knudson, T. C. Owens, and J. R. Rindt, "Low Rank Coal Liquefaction Employing H_2S as a Homogeneous Catalyst," in Synfuels' first Science and Technology Symposium: A Selection of Papers, Abstracts, and Data, McGraw-Hill (1982).

FIGURE 1

EFFECT OF ADDITIVE ON HDN*

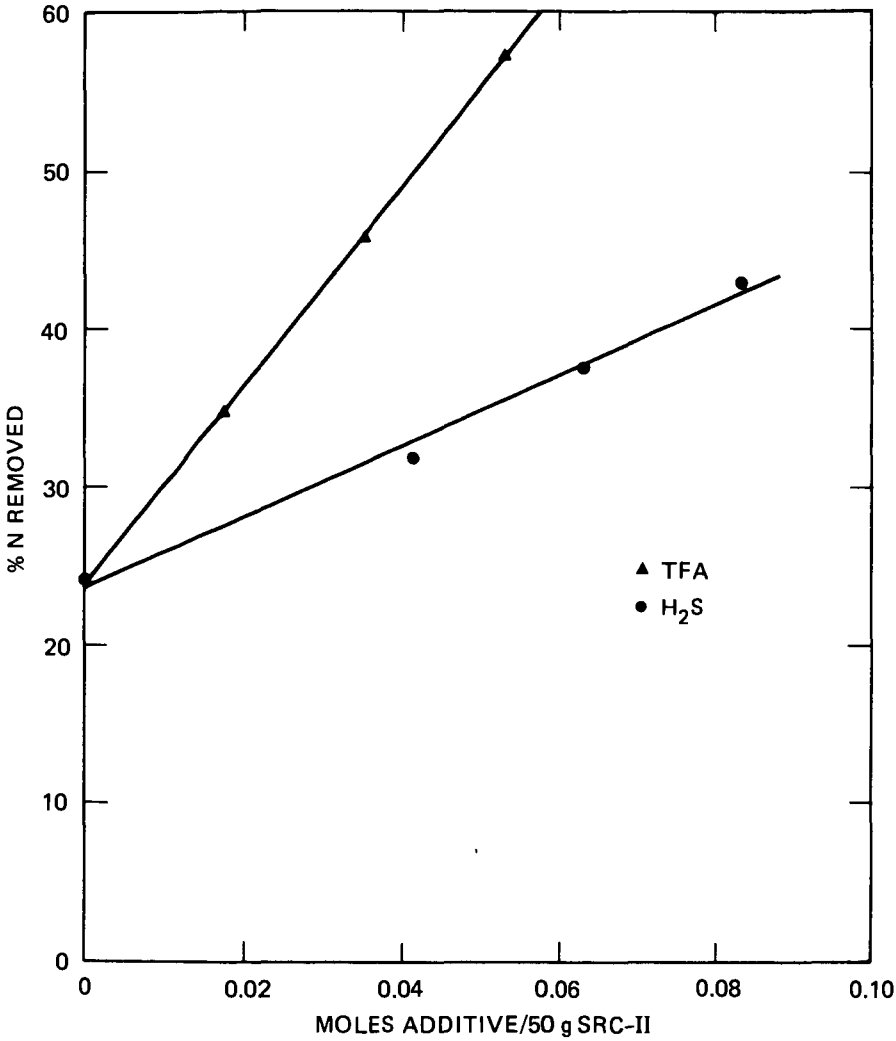

*1 h reaction of SRC-II liquid at 400°C with 1% sulfided CoMo catalyst and 1200 psig H_2

JA-327522-76

INTERACTIVE EFFECTS IN NITROGEN COMPOUND INDUCED STORAGE INSTABILITY IN SHALE DERIVED DIESEL FUEL

John V. Cooney,* Erna J. Beal and Bruce D. Beaver[1]

Combustion and Fuels Branch, Code 6180
Naval Research Laboratory, Washington, D. C. 20375-5000

INTRODUCTION

The autoxidation of middle distillate fuels during periods of storage has been a continuing problem in the utilization of these liquids by the government and commercially. With diesel fuels, instability is commonly defined by the formation of sediments, gums, color bodies and by the accumulation of hydroperoxides. Gravimetric accelerated storage stability tests conducted with model compounds as dopants in otherwise stable distillate fuels have demonstrated that oxidative condensation reactions of polar heterocycles are often deleterious to stability (2-15). In particular, nitrogen containing aromatics (pyrroles, pyridines, indoles, etc.) appear to be very harmful. Correlation of model dopant studies with results obtained with actual unstable fuels has indicated that the autoxidation processes are usually not isolated reactions but are sensitive to the presence of other fuel constituents (11, 13). Certain oxygen and sulfur compounds have been found to markedly alter the extent of model nitrogen compound induced storage instability in both middle distillate and model fuels (3, 4, 6, 16-18). Little is known about the chemical mechanisms of such interactive effects in fuel instability, and possible explanations include acid/base catalysis of oxidation and condensation pathways as well as involvement in radical chain processes. Interactions between different types of nitrogen compounds have also been studied to a limited extent (6, 10), and may similarly be of great importance in actual complex fuels.

As part of an effort to learn more about potential interactive effects, we have examined the autoxidation of two model nitrogen compounds, 2,5-dimethylpyrrole (DMP) and 3-methylindole (3-MI), in a shale diesel fuel in the presence of a second model dopant (t-butylhydroperoxide, an organic acid, or an organic base). The decision to examine DMP and 3-MI as nitrogen compound dopants was based upon a body of earlier work which analyzed the autoxidation behavior of these compounds (in the absence of other externally added active species) in the identical shale base fuel and under identical storage stability test conditions (10-12, 14, 15).

EXPERIMENTAL

Storage Test Techniques

The accelerated storage stability test method used has been described in detail (10-12). Hydroperoxide values were determined in stressed fuel samples following filtration through glass fiber filter paper by iodometric titration (ASTM D-1583-60).

Instrumental Methods

Infrared spectra were obtained as KBr pellets on a Perkin-Elmer Model 681 instrument with a Model 3600 data station (PECDS software). Solution proton nmr spectra were obtained in d_5-pyridine or deuterated chloroform with a Varian EM-390 90 MHz instrument. Elemental analyses were accomplished with a Carlo Erba Model 1106 elemental analyzer. Routine GC separations were made on either a Varian Model 3700 or a Perkin-Elmer Model 3920B gas chromatograph equipped with fused silica capillary columns (OV-101, 50 m x 0.3 mm) and FID detection.

Reagents

The base fuel for the present study was diesel fuel refined from Paraho crude shale oil by SOHIO. This fuel was produced in the U.S. Navy's Shale-II demonstration and is well-characterized (10). A quantity of this fuel was available which contained 24 mg/l of 2,4-dimethyl-6-t-butylphenol (AO-30) as the only additive (designated at NRL as fuel sample "D-11"). The D-11 fuel contained 15 ppm N (w/v) and exhibited good storage stability (10). All compounds used as dopants were pure by nmr, capillary GC, and/or mp. Fresh DMP was stored frozen under a nitrogen atmosphere to prevent autoxidation and it remained colorless under this storage. The concentration matrices for the interactive experiments were prepared so that effects of concentration (of both the DMP or 3-MI and the co-dopant) and of venting of test flasks could be assessed. In instances where the co-dopant was appreciably soluble in the D-11, two concentration levels were used (9.64×10^{-3}M and 3.21×10^{-2}M), which correspond to equivalent nitrogen compound (DMP or 3-MI) concentration levels of 135 and 450 ppm N (w/v). The construction of a 2 x 2 test matrix with both dopanta then involved duplicate test flasks at each possible pairing, with additional flasks providing baseline "blank" values for D-11 doped with just the nitrogen compound, just the co-dopant, and the undoped D-11 fuel. In cases where the co-dopant exhibited only limited solubility in the D-11 fuel, a saturated solution was employed.

RESULTS AND DISCUSSION

Autoxidation of DMP and 3-MI in the Presence of t-Butylhydroperoxide (TBHP)

Previous storage stability tests employing DMP and 3-MI as dopants in a stable shale diesel fuel base indicated that while both compounds deteriorated the quality of the fuel, the nature of their instability processes differed substantially (11, 14). The results obtained with DMP and 3-MI are compared below:

Table 1
Comparison of DMP and 3-MI Induced Storage Instability

Property	3-MI	DMP
Induction Period:	yes	not observed
Peroxide Level After Stress (Relative to Fuels Blanks):	slightly less (80°C) slightly more (43°C)	much less (80°C) much less (43°C)
Effect of Venting:	large	minimal
Effect of AO-30:	large	minimal
Reaction Order in Dopant:	?	1.0
Formula of Dopant:	C_9H_9N	C_6H_9N
Empirical Formula of Sediment:	$C_{15.8}H_{15.2}NO_{2.6}$	$C_{6.3}H_{6.7}NO_{1.6}$

Since the storage stability characteristics of these dopants had been examined in detail, it was considered of interest to compare both of these compounds in the context of interactive experiments. The initial study involved the addition of a model nitrogen compound to fuel D-11 together with a hydroperoxide as co-dopant. The hydroperoxide selected was t-butylhydroperoxide since it is available commercially in high purity. The goal of the experiments was to survey the importance of the accumulation of hydroperoxides in a complex fuel in influencing the formation of insolubles during stress when a particular class of nitrogen heterocycles is present.

Accelerated storage stability tests employing DMP and TBHP as co-dopants in fuel D-11 were run at both 80°C (7 and 14 days) and 43°C (49 and 92 days). The gravimetric results, summarized in Table 2, indicated that a definite positive (synergistic) interaction existed between the DMP and TBHP under all conditions examined. The concentration matrix which was studied used DMP at two levels: Lo DMP

= 135 ppm N w/v, equivalent to 9.64×10^{-3} M; and Hi DMP = 450 ppm N (3.21×10^{-2}M). The levels of TBHP used corresponded to the same molar concentration values. Thus, the relative concentration matrix which was used was therefore (expressed as moles of TBHP added/moles of DMP added): Lo TBHP/Lo DMP = 1.0, Lo TBHP/Hi DMP = 0.3, Hi TBHP/Lo DMP = 3.3, Hi TBHP/Hi DMP = 1.0. The results of hydroperoxide analyses also appear in Table 2, and are given as peroxide numbers (ASTM D-1583-60).

Table 2
Storage Stability Test Results for the DMP/TBHP Interaction

Sample*	Total Insolubles, mg/100 ml (Peroxide Number, meq ROOH/kg fuel) 80°C/7d	80°C/14d	43°C/49d	43°C/92d
Fuel Blanks	0.5(0.9)	0.0(3.0)	0.0(0.3)	0.0(1.0)
Lo TBHP Blanks	0.4(39.5)	0.9(34.2)	0.0(58.9)	0.0(17.2)
Hi TBHP Blanks	0.5(80.8)	0.7(84.6)	0.0(100.5)	0.0(60.9)
Lo DMP Blanks	30.2(0.2)	47.4(0.4)	25.4(0.0)	42.6(0.0)
Hi DMP Blanks	89.6(0.0)	171.4(0.2)	97.3(0.0)	153.7(0.0)
Lo TBHP/Lo DMP	37.9(18.8)	80.0(47.1)	33.2(70.6)	59.1(12.6)
Lo TBHP/Lo DMP/v	37.0(16.0)	81.3(70.4)	32.2(63.2)	60.5(10.2)
Lo TBHP/Hi DMP	101.3(7.5)	183.9(12.4)	113.8(22.4)	200.6(5.8)
Lo TBHP/Hi DMP/v	101.3(6.0)	193.9(7.3)	134.5(0.8)	215.2(4.2)
Hi TBHP/Lo DMP	62.7(63.3)	92.0(80.8)	79.4(33.4)	93.7(61.2)
Hi TBHP/Lo DMP/v	66.1(64.0)	95.7(93.8)	72.8(39.2)	95.5(116.5)
Hi TBHP/Hi DMP	160.4(25.0)	257.0(28.0)	233.2(57.3)	277.8(11.2)
Hi TBHP/Hi DMP/v	171.8(15.2)	267.5(20.7)	249.9(106.0)	325.3(47.8)

*The vented test flask trials are those denoted by "v".

In all instances, the presence of TBHP significantly increased the yield of insolubles produced when DMP was also present. Furthermore, the presence of Hi TBHP levels was always associated with more sediment than the corresponding Lo TBHP trials. In examining the peroxide number data, it will be noted that the correlation between the ultimate hydroperoxide levels and the yields of sediment are not good, which is an expected result (10, 11). The peroxide number of unstressed, doped D-11 fuel containing Lo TBHP was 20.7, and 68.9 for Hi TBHP. When DMP was not present, the TBHP dopant did not exert a significant destabilizing effect upon the fuel as measured by sediment generation. The effects of venting of test flasks were seen to be small and variable. Curiously, high levels of hydroperoxide were often observed in some Hi DMP trials after stress when TBHP had been present. Earlier work from our laboratory had indicated that DMP, in the absence of externally added hydroperoxide, was associated with very low peroxide numbers after stress.

A similar experimental matrix was used in the study of the potential interaction between 3-MI and TBHP. Interest in examining this interaction originated with our earlier studies of 3-MI induced fuel instability (11, 14), which showed that 3-MI is able to promote the formation of sediment and gum, but only in the absence of a hindered phenol antioxidant (AO-30). This result, coupled with the existence of a long induction period in the autoxidation of 3-MI in our shale diesel fuels, suggested that a classical free radical mechanism may be involved, which should, in turn, be sensitive to the presence of hydroperoxide present in the fuels.

Storage stability test results for the 3-MI/TBHP interaction are given in Table 3. These results indicate that a synergistic effect is present. Comparison of the 7 and 14 day results at 80°C suggest that an induction period was present. It will be noted that in the absence of externally added TBHP, 3-MI does not effectively promote sediment formation in the D-11 fuel, which contains AO-30. There is little doubt that the addition of TBHP rapidly overwhelmed the antioxidant, present at a level which was somewhat less than 24 mg/l, thereby allowing the autoxidation of 3-MI to proceed. The highest amounts of total insolubles were formed in the 43°C tests.

Venting of the test flasks generally led to a marked increase in the amount of sediment which formed. In these respects, the TBHP induced oxidation of 3-MI in fuel D-11 appears to be very similar to the simple autoxidation of this model nitrogen compound in fuel D-1 (a fuel which is identical in all respects to fuel D-11 except that it does not contain antioxidant) (11). Table 3 also shows peroxide analysis data for one of the stress sets (43°C/91d), which clearly indicates that high levels of hydroperoxide were present in all of the experimental flasks.

Table 3
Storage Stability Test Results for the 3-MI/TBHP Interaction

Sample*	Total Insolubles, mg/100 ml (Peroxide Number, meq ROOH/kg fuel) 80°C/7d	80°C/14d	43°C/49d	43°C/91d
Fuel Blanks	0.0	0.1	0.2	0.0(0.8)
Lo TBHP Blanks	0.0	0.4	0.0	0.0(16.2)
Hi TBHP Blanks	0.6	0.7	0.0	0.0(60.5)
Hi 3-MI Blanks	0.2	0.8	---	---
Lo TBHP/Lo 3-MI	0.7	1.1	0.3	0.0(50.2)
Lo TBHP/Lo 3-MI/v	0.4	3.9	0.5	0.0(76.6)
Lo TBHP/Hi 3-MI	1.5	11.7	2.2	53.6(46.3)
Lo TBHP/Hi 3-MI/v	2.3	12.5	70.7	129.0(36.6)
Hi TBHP/Lo 3-MI	0.7	3.8	2.5	3.7(112.5)
Hi TBHP/Lo 3-MI/v	0.6	4.1	1.5	9.3(159.9)
Hi TBHP/Hi 3-MI	1.7	8.7	33.0	0.7(64.2)
Hi TBHP/Hi 3-MI/v	1.9	17.2	81.2	149.5(56.3)

*The vented test flask trials are those denoted by "v".

Analyses of the sediments obtained with both DMP and 3-MI in the course of these TBHP interactive experiments have indicated that they are very similar, both in elemental composition and spectroscopic character, to sediments obtained in the absence of TBHP. For DMP, a typical sediment obtained in the presence of TBHP is 10.7% N, 60.1% C and 5.5% H; for 3-MI, a typical analysis is 5.5% N, 71.3% C and 5.6% H (these compare favorably with the empirical formulas in Table 1). Thus, it would appear that the TBHP functions as a catalyst or radical initiator rather than as a reactant in sediment formation.

Autoxidation of DMP and 3-MI in the Presence of Organic Acids and Bases

In an extension of our study of interactive effects in the autoxidation of DMP and 3-MI, ten organic acids and bases were examined as co-dopants in fuel D-11. This work was intended to determine whether the autoxidation of the nitrogen compounds is subject to acid or base catalysis, or if condensation products could form in lieu of true catalysis. Ten co-dopants were selected for study: acetic acid (HOAc), hexanoic acid (HA), decanoic acid (DA), p-toluenesulfonic acid (p-TsOH), dodecylbenzene sulfonic acid (DBSA), nicotinic acid (NA), 3-pyridinesulfonic acid (3-PSA), tri-n-butylamine (TBA), N,N-dimethylaniline (DMA) and 4-dimethylaminopyridine (4-DMAP). Most of the co-dopants were examined at two concentration levels ("Hi" and "Lo", as with TBHP); however, some of the compounds were only slightly soluble in D-11, so that a saturated solution was used for these (p-TsOH, NA, 3-PSA). Accelerated storage stability was assessed at 80°C (14d).

With DMP, the carboxylic acids (HOAc, HA and DA) all interacted in a synergistic fashion to increase the amount of sediment generated. A typical set of data is given in Table 4 for the DMP/DA experimental set. The results with the sulfonic acids were more difficult to interpret. Thus, DBSA exhibited a very strong positive interaction with DMP when present at levels of 0.3 or 1.0 equivalent. Yet when all four test flasks (vented and unvented) of the Hi DBSA/Lo DMP interaction were examined (these contain 3.33 equiv. of DBSA relative to DMP) a strong negative

interactive effect was seen. The interactive effects for p-TsOH were seen to be small in magnitude and variable. A very potent base catalyst, 4-DMAP, was observed to interact with DMP in a positive fashion whenever it was present. By contrast, interaction with other base catalysts (TBA, DMA) or low-solubility zwitterionic species (NA, present at ca. 0.3 ppm N w/v, and 3-PSA, present at less than 0.2 ppm N w/v) did not lead to significant synergism under these test conditions.

Table 4
Storage Stability Test Results for the DMP/DA Interaction
Fuel D-11 - 80°C/14 days - mg/100 ml

Sample*	Filtered Sediment	Adherent Gum	Total Insolubles
Fuel Blanks	0.1	0.0	0.1
Lo DA Blanks	0.1	0.1	0.2
Hi DA Blanks	0.1	0.1	0.2
Lo DMP Blanks	45.0	2.4	47.4
Hi DMP Blanks	165.2	6.2	171.4
Lo DA/Lo DMP	82.7	3.0	85.7
Lo DA/Lo DMP/v	84.2	2.6	86.8
Lo DA/Hi DMP	247.7	5.8	253.5
Lo DA/Hi DMP/v	238.8	5.3	244.1
Hi DA/Lo DMP	78.4	2.3	80.7
Hi DA/Lo DMP/v	96.2	2.6	98.8
Hi DA/Hi DMP	264.0	5.0	269.0
Hi DA/Hi DMP/v	279.2	5.3	284.5

*The vented test flask trials are denoted by "v".

Elemental and spectroscopic analyses were applied to the samples of DMP induced sediment from these interactive experiments. It was not possible to obtain an elemental analysis from the sediment formed in the DMP/DBSA trials, as their tarry/waxy nature precluded proper sampling technique. However, the incorporation of molecules of DBSA into the sediment is implied by: (a) the fact that such a large amount of sediment (up to 1300 mg/100 ml) was generated that the DMP alone is unable to account for the mass, and (b) a number of complex absorption peaks appear in the S=O/S-O region of the infrared. Thus, the DBSA may serve as a reactant in addition to or instead of serving as a catalyst. The incorporation of sulfur into DMP-derived sediments has been observed by other workers when thiophenol was used as a co-dopant (16-18); it has been considered possible that in situ oxidation of thiols to sulfonic acids may be a viable pathway (4, 6). The DMP-derived sediments produced in all nine other interactive experiments proved to be remarkably similar to the insoluble material generated by DMP without co-dopant. Thus, it would appear that the carboxylic acids and 4-DMAP are serving as true catalysts.

In a similar manner, the interaction of 3-MI with the ten acid/base co-dopants was examined in D-11 fuel using 80°C-14d storage stability tests. With the three carboxylic acids (HOAc, HA and DA), synergism was noted, with the highest levels of insoluble material present in Hi 3-MI flasks (ca. 6-60 mg/100 ml of sediment was generated, as compared with 0.8 mg/100 ml in the flasks which contained only 3-MI). Venting of test flasks seemed to be associated with higher levels of sediment. As was the case for DMP, the interactive effects of 3-MI with the sulfonic acids were difficult to interpret. With p-TsOH, the interactive effect was uniformly small and indeterminant. With DBSA, it was possible to generate small quantities of sediment under most conditions, but only one set of conditions (Hi DBSA/Hi 3-MI/unvented) led to the formation of large amounts of solids (ca. 70 mg/100 ml). With 4-DMAP, base catalysis of 3-MI autoxidation was not evident. In light of the superior catalytic nature of 4-DMAP, this result was somewhat unexpected, especially in light of a recent suggestion that base-catalyzed oxidation of 3-MI could be significant (19). Nicotinic acid (NA) was found to be catalytic in its interaction with 3-MI, with a maximum of ca. 30 mg/100 ml of sediment formed in the Hi 3-MI/vented trials (a

saturated solution of NA was used, 0.3 ppm N w/v). Despite the apparent failure of 4-DMAP, dimethylaniline (DMA) exhibited synergism with 3-MI, but the effect was largest when DMA was present at a "Lo" level. Tri-n-butylamine (TBA) actually appeared to inhibit the autoxidation of 3-MI slightly. The final co-dopant, 3-pyridinesulfonic acid (3-PSA) showed a very slight positive interactive effect, forming ca. 6 mg/100 ml of solids in the Hi 3-MI flasks.

Analysis of the sediments generated in the 3-MI interaction experiments was limited by the small amounts of materials isolated on the glass fiber filter pads. Elemental analyses could only be conducted on the sediments from the carboxylic acid interactions; these all contained ca. 5.7% N, 72.5% C and 5.8% H, and so are almost identical in elemental composition to 3-MI induced sediment which formed in the absence of the co-dopants. Spectroscopic examination of the sediments confirm that the heterogeneous material generated is also similar. Table 5 is a qualitative summary of the results obtained with DMP and 3-MI where an organic acid or base was present as a co-dopant.

Table 5
Summary of Relative Interactive Effects with Organic Acids and Bases

	Interactive Effect*	
Co-Dopant**	DMP as Dopant	3-MI as Dopant
HOAc	++	++v
HA	++	++v
DA	++	++
p-TsOH	i	i
DBSA	++	++v
NA	i	++v
3-PSA	i	+
TBA	+v	-
DMA	i	+
4-DMAP	+	i

*Key to symbols: ++ = strong synergism, + = weak synergism
- = weak inhibition, i = indeterminate effect
v = sensitive to venting of test flasks
**Refer to the text for the identity of the abbreviations.

CONCLUSIONS

Hydroperoxide dissolved in a shale derived diesel fuel can interact in a strong synergistic fashion with polar nitrogen heterocyles to lead to the formation of significant amounts of sediment and gum. Carboxylic and sulfonic acids similarly assist in the degradation of fuel quality by interacting with alkylpyrroles and indoles. Interactions with organic bases appear to be of a smaller magnitude.

ACKNOWLEDGMENT

The authors thank the Department of Energy for sponsoring this work under contract number DE-AI-81BC10525. Dr. Robert N. Hazlett is gratefully acknowledged for his continued support, encouragement and helpful discussions. References to brand names were made for identification only and do not imply endorsement by DOE or NRL.

REFERENCES

1. NRC/NRL Cooperative Research Associate Postdoctoral Fellow, 1984-1986.
2. J. W. Goetzinger, C. J. Thompson and D. W. Brinkman, DOE Report No. DOE/BETC/IC-83/3, October 1983.

3. J. W. Frankenfeld, W. F. Taylor and D. W. Brinkman, DOE Report No. DOE/BC/10045-12, February 1981.
4. J. W. Frankenfeld, W. F. Taylor and D. W. Brinkman, DOE Report No. DOE/BC/10045-23, March 1982.
5. J. W. Frankenfeld, W. F. Taylor and D. W. Brinkman, Ind. Eng. Chem. Prod. Res. Dev., 22: 608 (1983).
6. J. W. Frankenfeld, W. F. Taylor and D. W. Brinkman, Ind. Eng. Chem. Prod. Res. Dev., 22: 615 (1983).
7. K. E. Dahlin, S. R. Daniel and J. H. Worstell, Fuel, 60: 477 (1981).
8. J. H. Worstell and S. R. Daniel, Fuel, 60: 481 (1981).
9. J. H. Worstell, S. R. Daniel and G. Frauenhoff, Fuel, 60: 485 (1981).
10. R. N. Hazlett, J. V. Cooney and E. J. Beal, DOE Report No. DOE/BC/10525-4, June 1983.
11. J. V. Cooney, R. N. Hazlett and E. J. Beal, DOE Report No. DOE/BC/10525-8, June 1984.
12. J. V. Cooney, E. J. Beal and R. N. Hazlett, Preprints, Div. of Petro. Chem., ACS, 28(5): 1139 (1983).
13. J. V. Cooney, E. J. Beal and R. N. Hazlett, Preprint, Div. of Petro. Chem., ACS, 29(1): 247 (1984).
14. J. V. Cooney, E. J. Beal, M. A. Wechter, G. M. Mushrush and R. N. Hazlett, Preprints, Div. of Petro. Chem., ACS, 29(4): 1003 (1984).
15. J. V. Cooney, E. J. Beal and R. N. Hazlett, Liq. Fuels Tech., 2(4): 395 (1984).
16. N. F. Yaggi, S. H. Lee, J. Ge and N. C. Li, Preprints, Div. of Fuel Chem., ACS, 29(1): 178 (1984).
17. S. H. Lee, J. H. S. Ge and N. C. Li, Preprints, Div. of Petro. Chem., ACS, 29(4): 996 (1984).
18. L. Jones, R. N. Hazlett, N. C. Li and J. Ge, Fuel, 63: 1152 (1984).
19. Z. Yoshida, Heterocycles, 21: 331 (1984).

THE EFFECT OF ACTIVATION AND PROMOTION ON A FISCHER-TROPSCH CATALYST

H.W. Pennline, J.M. Stencel, M.F. Zarochak, S.S. Pollack, and R.R. Anderson

U.S. Department of Energy
Pittsburgh Energy Technology Center
P.O. Box 10940
Pittsburgh, Pennsylvania 15236

INTRODUCTION

Since the late 1970's, an interest in the production of gasoline and other transportation fuels from synthesis gas has been renewed. A conceptual scheme for the production of gasoline from low-ratio synthesis gas is the two-stage method developed by Mobil [1]. In this process, mixtures of hydrogen and carbon monoxide are reacted in a slurry bubble column containing a conventional Fischer-Tropsch catalyst in the first stage. The product from this step is then sent to the second-stage reactor that contains the shape-selective zeolitic catalyst ZSM-5. One of the goals of the indirect liquefaction research program at the Pittsburgh Energy Technology Center is to investigate catalyst systems in the slurry phase that are potential candidates for the first-stage process. These catalyst systems should process low ratios (0.5/1 to 1/1 of H_2/CO) of synthesis gas to produce a high yield of light olefins and gasoline-range hydrocarbons.

Certain results in the literature indicate that synthesis gas conversions with iron-manganese oxide catalysts yield a suppressed C_1-fraction and a large C_2-C_4 light-hydrocarbon fraction that deviates from that predicted by Schulz-Flory kinetics [2,3]. A recent three-phase study with iron-manganese catalysts of various compositions found that hydrogenation of olefins occurred along with olefin isomerization reactions [4]. The C_2-C_4 content of the hydrocarbon distribution followed Schulz-Flory kinetics and did not exceed the 56 weight percent maximum predicted by Schulz-Flory. Since these results with iron-manganese catalyst were not as good as those reported in the patent literature, two areas of interest -- catalyst activation and promotion -- were investigated with the intent of improving olefin selectivity and catalyst activity and stability.

In this study, the activation and promotion of a 21Fe/79Mn catalyst were investigated in a slurry reactor. The effects of the process parameters of temperature, pressure, and reducing gas composition on the activation step and on the subsequent catalyst activity and product selectivity were studied. Also, the alkali promotion of the iron-manganese catalyst with potassium carbonate was investigated. Slurry samples were taken at various times on stream, and the catalyst was analyzed by surface techniques so that the catalyst properties could be correlated with process results.

EXPERIMENTAL

The catalyst was prepared in a continuous, stirred precipitation reactor similar to a unit used by Kölbel and Ralek [5]. Nitrates of iron and manganese were reacted with ammonium hydroxide. Batches of the washed

and vacuum-dried coprecipitate were crushed, sieved through a 100-mesh screen, and homogenized by rolling. A portion of the total batch was further crushed and sieved through 325 mesh (44 μm). Catalyst for all the tests in this study was obtained from this portion. The fresh catalyst was about 14 weight percent iron and 52 weight percent manganese.

The slurry studies were conducted in a one-liter stainless steel stirred reactor as described elsewhere [6]. Typically, fifty-one grams of iron-manganese catalyst that were sieved through 325 mesh (44 μm) were placed in the reactor with the molten medium wax to make a 13.5 weight percent suspension based on unreduced catalyst weight. The high-boiling paraffinic wax (P-22 from Fisher Scientific Company) had an average carbon number of 28. The reactor system was sealed, cooled, leak-tested, and purged with helium. At the desired activation pressure, the temperature was increased to the desired activation temperature under a flow of helium. Isothermal conditions within the reactor were established by means of a sliding thermocouple in a thermowell in the reactor. The impeller was stopped and gas flow was decreased to a small amount, at which time the unexpanded slurry level was lowered to 0.5 liter by using the reactor pressure to force the excess wax through a dipleg and filter and into a heated wax trap. The impeller was then restarted, and once isothermal and isobaric conditions were reestablished, the inert flow was stopped and the activation gas was introduced. Unless specified, activation usually lasted for twenty-four hours. At the end of this activation, the liquid level was again readjusted, and the system pressure and temperature were adjusted to 200 psig and 275°C, respectively. Synthesis feed gas was introduced in increments over the next hour until a weight hourly space velocity (WHSV) of 1.21 hr^{-1} was reached. (WHSV is defined as grams of gas per hour per gram of charged catalyst.) Trap drainings, flows, and gas analyses were measured on a twenty-four hour basis for material balance determinations. Unless otherwise stated, tests in this study used a $1H_2$:1CO feed gas.

The gaseous and liquid products were characterized by various analytical techniques. Gas exiting the reactor system was analyzed for hydrogen, carbon monoxide, carbon dioxide, nitrogen, and hydrocarbons up to C_8 by gas chromatography. The liquid condensate in the trapping system was collected and physically separated into an aqueous fraction and an oil fraction. The aqueous phase was analyzed by mass spectrometry to detect oxygenates, and the water content was determined by the Karl Fischer reagent technique. The liquid hydrocarbon samples were characterized by fluorescent indicator adsorption (FIA) ASTM D-1319 to determine the functionality of the liquid oil, and by bromine number ASTM D-1159 to check the olefin content. Infrared studies were also performed on the oil fractions. Relative amounts of terminal, trans-internal, and beta-branched-terminal olefins were determined by infrared spectral analysis. The wax fraction, which was dependent on the trapping system, and selected liquid oil samples for a particular period of time were also analyzed by gas chromatography with a capillary column.

Slurry samples were withdrawn from the reactor at various times on stream. The wax-encapsulated iron-manganese catalysts were characterized by X-ray photoelectron spectroscopy (XPS) and X-ray diffraction (XRD). A mild washing of the slurry-catalyst samples by sonication in toluene was performed before the XPS analysis. These washed samples still contained

slurry wax, but it was at a level that permitted XPS data acquisition while simultaneously preventing oxidation of the catalyst surface. The samples were then either spread onto holders or pressed into thin wafers for subsequent XPS data acquisition. Preliminary XPS data were also obtained from activation of an iron-manganese catalyst treated in situ with hydrogen in the XPS. These data were acquired from wafered samples after gaseous treatment at pressures near 1.5 atm and temperatures between 275°C and 450°C. Preliminary results of various activations with iron-manganese catalyst in a thermogravimetric analyzer (TGA) were also obtained.

RESULTS AND DISCUSSION

In a previous study with various iron-manganese catalysts [4], a standard activation with carbon monoxide was used. With the 21Fe/79Mn catalyst used in this study, the catalyst was activated with carbon monoxide as the base-line case at 2.25 WHSV, 275°C, and 200 psig for 24 hours. All activations were conducted in situ. Activation parameters investigated were temperature (275°C versus 300°C), pressure (0 psig versus 200 psig), and gas composition (CO, CO followed by H_2 -- Kölbel-type [3], synthesis gas, and hydrogen). Slurry reactor results for selected periods during a test are shown in Table 1. Synthesis process conditions for all the tests were 1.21 WHSV of $1H_2/1CO$ feed gas, 275°C, and 200 psig unless otherwise indicated. In the tests where carbon monoxide was used to reduce the catalyst, the carbon dioxide was monitored in the exit gas by an infrared detector. In all cases, after the beginning of the carbon monoxide reduction, the carbon dioxide concentration reached a maximum during the first two hours and thereafter asymptotically approached a zero concentration.

As in past work with iron-manganese catalysts, the functionality of the product in the base-line test SL-54 changed with time on stream. As seen in Table 1, the light olefin content decreased with synthesis time due to olefin hydrogenation. This is paralleled by FIA results on the liquid oil, which reveal that with time on stream, the oil becomes more paraffinic and less olefinic. Also with catalyst aging, the olefinic products exhibit more double-bond isomerization. If the 2-butene/1-butene ratio is used as an index for olefin isomerization, this ratio -- thus, isomerization -- increased in the C_4 fraction with time. Similarly, by infrared analysis of the liquid oils, the ratio of internal to terminal olefins also increased with time.

The catalyst in test SL-57 was activated identically to the base-line test except at 300°C. This higher temperature of activation increased the initial activity of the catalyst but also increased the deactivation rate of the catalyst. A lower pressure (0 psig) of activation was used in test SL-60, and this increased the initial activity over the base-line test. A Kölbel-type of activation in test SL-58 (CO treatment for 24 hours at 275°C and 200 psig, followed by H_2 treatment at 275°C and 200 psig) had activity results similar to those of the base-line test SL-54.

The trends in the product selectivity were the same for all the tests (see Table 1). With time on stream, the hydrocarbon selectivity shifted to a lighter fraction; the olefin content decreased; and a larger percentage of olefin isomers occurred. A minor exception is noted in the Kölbel-type

activation test, where the internal-to-terminal olefin ratios in both the gas and oil phases went through a minimum during the first part of the test.

The major differences in the activation studies occurred when the catalyst was activated at 275°C and 200 psig with hydrogen or synthesis gas ($1H_2/1CO$) as compared to carbon monoxide. No catalyst activity occurred with hydrogen activation, and only slight conversion (<2%) occurred with a synthesis gas activation. Investigating a higher iron-to-manganese ratio catalyst, Maiti et al. [7] claimed that a $MnFe_2O_4$ spinel and MnO were the major phases at hydrogen reduction temperatures below 300°C. The XPS information in the latter section will clarify this point.

The addition of a structural promoter to the 21Fe/79Mn catalyst was attempted to stabilize the activity and maintain a high light-gas olefin content. Schulz and Gokcebay [8] claimed that potassium addition to their iron-manganese catalysts reduced secondary olefin hydrogenation and isomerization reactions. Based on this, several batches of 21Fe/79Mn catalyst were impregnated with various amounts of potassium. Three different potassium levels were investigated: 0.1, 0.4, and 1.3 weight percent. Results are listed in Table 1. An activation with carbon monoxide at 2.25 WHSV, 275°C, and 0 psig for 24 hours was done in situ for each test.

As compared to test SL-60 that had an unpromoted catalyst, the activity of the 0.1% potassium catalyst was about the same except after 119 hours on stream, where the potassium-promoted catalyst had deactivated significantly. The 0.4 and 1.3 weight percent potassium-promoted catalysts had very high initial activities [50 mole percent (H_2 + CO)-conversion] but decreased after 200 hours on stream to values comparable to the unpromoted catalyst.

The hydrocarbon distribution for the unpromoted iron-manganese shifts to a lighter fraction with time and to a lower olefin content with a larger fraction of olefin isomers. The lowest loading of 0.1 weight percent potassium did not seem to change these trends. However, for the catalyst with the 0.4 weight percent potassium loading, the product distribution shifts to a higher carbon number with time. The percent olefinic product actually increases with time, and the internal/terminal olefin ratio decreases -- indicating less olefin isomerization. At the highest potassium loading in test SL-62, the hydrocarbon distribution is relatively constant and is shifted to higher molecular weights. The olefin content is high (85 weight percent), and the internal/terminal olefin ratio is about an order of magnitude less than with the unpromoted iron-manganese catalyst. With this iron-manganese catalyst, a high loading of potassium is evidently needed to prevent olefin hydrogenation and isomerization reactions. However, the product distribution is shifted so that only about 30 weight percent of the hydrocarbon product is C_2-C_4 rather than the 40 weight percent obtained with the unpromoted catalyst.

The XPS analysis of the wax-encapsulated iron-manganese catalysts determined the surface atomic ratios Fe/Mn and C/Mn (see Table 2). These results can be correlated with the activity of a catalyst during three-phase testing. For example, the (H_2+CO) conversion in SL-61 was negligible throughout the slurry run. Such inactivity is mirrored in the C/Mn ratios that are constant throughout the test and are lower than C/Mn for other slurry tests. In relation to test SL-61, XRD and in situ XPS results with

an unpromoted iron-manganese catalyst under hydrogen with temperatures ranging from 275°C to 450°C revealed that metallic iron was not produced. Instead, a solid solution of FeO-MnO and/or a Fe-Mn spinel is formed. Hence, the constant and low C/Mn ratio in SL-61 suggests that iron is not available for iron carbide formation during synthesis gas exposure, and thus, no conversion/activity is observed during the test.

The variations in the atomic ratios for slurry tests SL-54 through SL-60 are related to differences in the activation gas sequence and the activation parameters for the unpromoted iron-manganese catalyst. In general, the trend in these tests is for the Fe/Mn values to decrease with time on stream. Correspondingly, the C/Mn values increase with time on stream and can be related to carbon deposition as a function of time on stream and/or as a difference in the amount of slurry wax retained by the catalysts after toluene sonication. In all cases, the catalyst deactivated to some extent over the first 200 hours on stream. More specifically, an increased carbon content was found on the catalyst activated under carbon monoxide at 300°C (SL-57) compared to the catalyst activated under carbon monoxide at 275°C (SL-54) with synthesis time. This increased C/Mn ratio, as independently confirmed by TGA results, is probably related to an enhanced amount of iron carbide and/or carbon formation during the activation and usage stages of SL-57. Such enhancement paralleled the faster deactivation rate for SL-57. The corresponding C/Mn ratios for SL-58 show that H_2 reduction after CO exposure (Kölbel-type activation) decreases the carbon content on the catalyst to levels below SL-57. Such a decrease may be related to greater formation of metallic Fe after the hydrogen reduction, as indicated by the high Fe/Mn ratio after 48 hours on stream.

Table 2 also reports XPS results from the potassium-promoted tests SL-62 through SL-64. In general, for these tests, the Fe/Mn ratio increases with time on stream, unlike results with the unpromoted catalysts. Also, the C/Mn ratio increases with time on stream. In all cases with the promoted catalyst, the potassium appears to enhance the surface iron concentration during a test. The potassium also appears to increase surface carbon deposition during a test. The catalyst in test SL-64 deactivated significantly during the experiment, and this could be related to the rapidly increasing C/Mn ratio during the test.

SUMMARY

The effects of various activations of an iron-manganese catalyst on synthesis gas conversion were investigated in a slurry reactor. Although the activation temperature and pressure did affect catalyst activity, olefin hydrogenation and isomerization reactions still appear to be significant in all cases. The activating gas composition had the most dramatic effect, with the catalyst exhibiting no activity after a hydrogen activation. Potassium promotion of the iron-manganese catalyst succeeded in increasing the activity and increasing the percentage of olefins in the light gas fraction. However, the hydrocarbon distribution was shifted to a higher average molecular weight. The XPS results of catalyst slurry samples at various process times were correlated with the catalytic process results to explain the particular catalyst performance.

DISCLAIMER

Reference in this report to any specific commercial product, process, or service is to facilitate understanding and does not necessarily imply its endorsement or favoring by the United States Department of Energy.

ACKNOWLEDGMENT

The authors wish to thank R.R. Schehl, R.E. Tischer, E.R. Bauer, and D.H. Finseth for contributions to this project.

REFERENCES

[1] Mobil Final Report, U.S. DOE Contract No. DE-AC22-80PC30022, June 1983.

[2] Bussemeier, B.; Frohning, C.D.; Horn, G.; Kluy, W. German Patent 2 518 964, 1976.

[3] Kölbel, H.; Tillmetz, K.D. U.S. Patent 4,177,203, 1979.

[4] Pennline, H.W.; Zarochak, M.F.; Tischer, R.F.; Schehl, R.R. Paper No. 14c, presented at the AIChE Summer National Meeting, Philadelphia, Pa., August 1984.

[5] Kölbel, H.; Ralek, M. Catal. Rev. Eng. 1980, 21, 225.

[6] Zarochak, M.F.; Pennline, H.W.; Schehl, R.R. DOE/PETC/TR-84/5, U.S. Department of Energy, 1984.

[7] Maiti, G.C.; Malessa, R.; Baerns, M. Applied Catal. 1983, 5, 151.

[8] Schulz, H.; Gokcebay, H. Proc. Organic React. Conf., Charleston, S.C., April 1982.

Table 1: Results of Activation and Promotion Studies.

Test	SL-54				SL-57			SL-58			SL-60		
Synthesis Time on Stream, hr*	47	118	142	191	47	119	167	43	115	187	48	120	204
CO-Conversion, mole percent	27.4	26.9	27.3	20.6	36.3	25.9	16.2	25.2	26.5	16.3	35.7	32.4	29.1
(H_2+CO)-Conversion, mole percent	29.8	27.5	29.0	24.1	38.3	29.2	15.8	25.0	25.5	19.7	35.6	33.1	30.1
Hydrocarbon Distribution, wt%													
CH_4	8.0	8.8	8.4	9.2	6.8	9.1	14.0	8.9	9.4	10.7	6.9	7.2	7.8
C_2-C_4	41.7	43.0	42.4	44.2	37.2	37.1	45.8	43.9	43.5	40.3	38.3	39.1	40.7
C_5+	50.2	48.2	49.2	46.6	56.0	53.8	40.2	47.2	47.1	49.1	54.8	53.7	51.5
Olefin Content C_2-C_4 Fraction, wt%	76.5	70.8	70.7	69.4	74.2	62.2	50.5	73.5	71.9	63.9	76.8	72.3	68.8
Internal/Terminal-Olefin Ratio	1.1	1.5	1.7	1.9	0.94	2.3	--	2.1	1.6	1.9	0.67	1.1	1.8
2-Butene/1-Butene Ratio	0.30	0.45	0.53	0.56	0.29	0.69	1.0	0.35	0.30	0.55	0.21	0.30	0.44

Test	SL-63			SL-64			SL-62		
Potassium Loading, wt%	0.1			0.4			1.3		
Synthesis Time on Stream, hr*	48	119		46	118	187	47	119	191
CO-Conversion, mole percent	32.9	14.6		56.3	32.9	18.0	59.5	40.5	30.4
(H_2+CO)-Conversion, mole percent	32.8	15.2		50.2	29.5	18.6	50.0	33.9	25.9
Hydrocarbon Distribution, wt%									
CH_4	7.0	16.6		9.4	9.5	6.6	3.7	3.6	3.8
C_2-C_4	32.3	48.8		37.6	37.1	29.3	21.0	23.4	25.1
C_5+	60.7	34.6		53.0	53.4	64.1	75.3	73.0	71.1
Olefin Content C_2-C_4 Fraction, wt%	65.4	45.4		65.2	67.4	69.3	83.8	84.8	85.9
Internal/Terminal-Olefin Ratio	1.4	3.0		1.5	1.2	0.63	0.14	0.16	0.23
2-Butene/1-Butene Ratio	0.50	0.25		0.45	0.33	0.11	0.03	0.04	0.05

*Slurry Synthesis Conditions: 1.21 WHSV of 1H_2/1CO, 275°C, 200 psig.

Table 2: Fe/Mn and C/Mn Atomic Ratios from XPS Analysis of Iron-Manganese Slurry Catalysts Sampled From the Slurry Reactor After Specified Activation Step(s) and After Specified Times on Stream.

Slurry Test	SL-54	SL-57	SL-58	SL-61	SL-60	SL-63	SL-64	SL-62
Fe/Mn								
CO-Activation	0.23	0.30	0.34		0.16	0.18	0.29	
H_2-Activation			0.32	0.29				
~48 hours	0.22	0.20	0.43	0.29	0.16	0.20	0.53	0.16
~100 hours				0.29		0.28		
~200 hours	0.16	0.14	0.19		0.15		0.50	0.24
C/Mn								
CO-Activation	4	6	10		10	7	8	
H_2-Activation			6	6				
~48 hours	6	12	10	4	19	13	23	16
~100 hours				4		15		
~200 hours	7	28	16		52		59	34

CATALYTIC SYNTHESIS OF METHANOL FROM HYDROGEN AND CARBON MONOXIDE ON A COPPER-ZINC OXIDE SUPPORTED CATALYST

Rajesh M. Agny and Christos G. Takoudis

School of Chemical Engineering
Purdue University
W. Lafayette, IN 47907

INTRODUCTION

Most kinetic studies of methanol synthesis over Cu/ZnO catalysts have been carried out using mixtures of carbon monoxide and hydrogen. But in some cases (1) the synthesis gas has also contained carbon dioxide (2). Power rate laws as well as complicated rate expressions have been proposed over the years. The detailed kinetics of the surface processes is virtually unknown. With the exception, perhaps, of the near-atmospheric work by Saida and Ozaki (3), investigations of the kinetics of methanol synthesis over Cu/ZnO catalysts have been done at pressures on the order of 75 atm (1,4-8). A major drawback of several such kinetic studies is the use of integral reactors.

In this study, we investigate the kinetics of methanol synthesis over a commercial $Cu/ZnO/Al_2O_3$ eatalyst in a differential reactor at pressures in the range from 3 to 15 atm and temperatures between 250 and 290° C (9).

EXPERIMENTAL METHOD

A high pressure unit is used for the kinetic experiments (9). The reactor system consists of a U-tube made of stainless steel 304, 0.95 cm OD and 0.09 cm thick. The U-tube is suspended vertically in a Techne fluidized sand bath SBS-4. In the direction of flow, the U-tube contains a length of glass wool, a preheating section of Potters silica glass spheres P-047, a second length of glass wool to isolate the catalyst bed from the glass spheres and a final glass wool plug above the catalyst bed to prevent carry-over of the catalyst (9). Omega iron-constantan thermocouple probes TT-J-30 are used for temperature measurements. Our data reveal that the fixed bed we use is isothermal (9). The reactor system is pressurized by a Grove back pressure regulator 91W. The reactor effluent is led to a Carle sampling valve 7707. During analysis, the effluent sample is carried by the carrier gas (hydrogen) to a Varian Aerograph Gas Chromatograph 202-B. A Chromosorb 102 column permits separation of CO, CO_2, and methanol. The gas chromatograph is coupled with a Houston Instrument chart recorder A521X-14K to enable qualitative and quantitative analysis of the effluent. Based on gas chromatographic analysis of CO bubbled through methanol at different temperatures, it is concluded that the weight percent of the components in the reactor effluent can be estimated by using Dietz's thermal conductivity weight factors (10).

A 5 g $Cu/ZnO/Al_2O_3$ catalyst sample (C79-2-01 of United Catalysts, Inc., Kentucky.) of average size equal to 0.077 cm is reduced with hydrogen at 1 atm and 290° C for 15 hours (9). No further pretreatment is done during the rest of the experimental span. A reaction interval of one hour is found to be sufficient to produce reproducible steady-state product distributions. Steady state reaction data are collected at temperatures between 250 and 290° C, pressures in the range of 3 to 15 atm, H_2/CO = 2.1 - 2.4

and total flow rates between 70 and 120 cc/min (STP). The catalyst composition measured with a Dispersive Analyzer is on an oxygen free basis: 40.6 wt.% Cu, 50.3 wt.% Zn and 9.1 wt % Al. The specific surface area of this catalyst, determined by BET with N_2, is 37.8 m^2/G.

RESULTS

The $Cu/ZnO/Al_2O_3$ catalyst is tested at three temperatures, 250, 270 and 290 °C. Typical measured steady state conversions are summarized in Table 1 along with the conditions used. No deactivation of the catalyst is observed at the experimental conditions studied, based on periodic tests conducted at "standard conditions" which were chosen to be 11.2 atm, 250 °C and H_2/CO ratio equal to 2.3. As a consequence of a rigorous design of our differential reactor, beat and mass transfer effects are negligible (9).

Methanol is the main product at the conditions studied. Carbon dioxide and water (in trace amounts) are formed as side products. No other by-products are observed at the conditions used. It is observed that tbe reaction rate increases as the temperature increases in the temperature range 250 to 290 °C. Also, the reaction rate increases as the total pressure increases at constant temperature and H_2/CO ratio (Table 1). Note that at 250 and 270 °C the metbanol synthesis reaction in our system is far from equilibrium whereas at 290 °C the reverse reaction becomes important.

Starting with power rate laws, several rate expressions were tried to fit our data. Emphasis was laid, on rate expressions containing a small number of parameters. The reaction rate was found to be approximately proportional to the total pressure. This enabled us to eliminate several rate expressions if the observed dependence of rate on total pressure was not followed (9).

Since evidence for the formyl (CHO-) and the methoxy (CH_3O-) species has been reported for Cu/ZnO catalysts during methanol synthesis (1,2,11), two parameter and three parameter kinetic models which can be derived from Langmuir-Hinshelwood type rate expressions were tried. These contained rate determining steps involving a bimolecular surface reaction between an absorbed hydrogen atom and either a methoxy or a formyl adsorbed species. The form of such rate expressions examined is

$$r = k\left\{P_{CO}P_{H_2}^2 - \frac{P_{MeOH}}{K_{eq}}\right\} \cdot P_{CO}^l \cdot P_{H_2}^m \qquad 1)$$

It is found that the best possible fit is obtained with the rate expression (9)

$$r = k\left\{P_{CO}P_{H_2}^2 - \frac{P_{MeOH}}{K_{eq}}\right\}(P_{CO}P_{H_2}^{0.5})^n \qquad 2)$$

where $k = k_o \exp\left(\frac{-E}{RT}\right)$ and $n = -1.30 \pm 0.03$. The Arrhenius plot of the temperature dependence of k is presented in Figure 1. With a single pre-exponential factor and a single overall activation energy obtained from linear regression of the rate constant data, large deviations (30-40%) are observed between predicted and measured reaction rates. Therefore, it is proposed that there is a decrease in the overall activation energy with temperature (Fig. 1). The overall activation energies and the corresponding pre-exponential factors computed at each temperature from Figure 1, are presented in Table 2. The error

accompanying the estimation of the activation energy is about ± 1000 cal/gmol based on the error involved in calculating the activation energy from the Arrhenius plot and the 15% maximum relative error in observed reaction rates. Equation 2 fits all our data with a maximum relative error of less than 15% (Fig. 2).

DISCUSSION

From the structure of rate Equation 2 we note that (i) the kinetics of the reverse reaction is accounted for; (ii) this rate expression contains only two parameters, the rate constant and an empirical constant, n (1,3,6,9); (iii) the reaction rate depends on a positive power of partial pressure of hydrogen and on a negative power of the partial pressure of carbon monoxide (1,9); and (iv) the measured overall activation energy decreases with increasing temperature (Table 2).

The term $P_{CO}P_{H_2}^{0.5}$ (Eq. 2) represents a formyl species, CHO-, formed by a reactive collision between CO and an adsorbed hydrogen atom. Mechanisms proposed by Herman *et al.*, (4) and Kung (11) involve the formyl species as one of the surface intermediates. Assuming the formyl species to be the most abundant surface intermediate and the last reaction step of both mechanisms to be rate determining, a rate expression similar to Equation 2 can be derived (9,12).

In the mechanism reported in (4), the intermediates are proposed to be bonded to the surface cation via the carbon atom. Such a proposal is feasible for noble-metal catalysts because relatively strong metal carbon bonds can be formed, and there is ample evidence that CO adsorbs molecularly on these metals with the carbon end pointing towards the metal (11). However, it is proposed that the large dipole moments and the relatively uneven electron density distribution on oxide surfaces favor bonding of the surface to the oxygen atom of the intermediate (11). Thus a methoxy type derivative should be more likely.

In the mechanism proposed in (11), the formation of the methoxy intermediate from the formyl species involves rupture of two bonds and formation of three bonds. An elementary step is expected not to involve multiple bond ruptures and formations. This proposed elementary step of such a mechanism must therefore be looked upon cautiously in the absence of independent evidence that supports such a step.

The indication of the formyl species from the kinetics observed and the examination of the shortcomings of the mechanisms proposed in (4,11) allow us to suggest the mechanism (9)

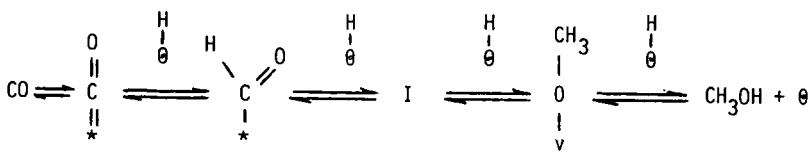

for the supported Cu/ZnO catalyst we used. Here the symbols *, θ and v represent a metal cation, a zinc or an oxygen site, and an oxygen vacancy respectively. "I" represents a likely intermediate between the formyl and methoxy species (9). Its possible structure needs to be investigated.

Rate equation 2 can be derived from this mechanism by assuming that the formyl species is the most abundant surface intermediate and that the surface reaction between the methoxy species and an

adsorbed hydrogen atom is the rate determining step (Agny, 1984). The main difference between this mechanism and the mechanism reported in (11) is the addition of an intermediate I between the formyl and methoxy intermediates.

Recently, coadsorption of CO and H_2 on ZnO and Cu/ZnO catalysts has been investigated at 270 K and subatmospheric pressures by Saussey *et al.*, (13). The infrared spectrum of a mixture of CO and H_2 adsorbed on ZnO or Cu/ZnO reveals a pair of weak bands which have been assigned to vibrations of a surface formyl species. This is to our knowledge, the first report presenting direct evidence for a formyl species resulting from CO and H_2 interaction on Cu/ZnO catalysts. Deluzarche et al. (14) claim to have identified, by reactive scavenging, the formyl species on nickel. Kung (11) presents certain organometallic chemistry analogs to substantiate the formyl and methoxy species as intermediates in the mechanism he has proposed for methanol synthesis on ZnO and Cu/ZnO catalysts. These findings support our suggestion that adsorbed formyl species can be the most abundant surface intermediate (9), although further studies are necessary for such a proposal.

Formaldehyde has never been observed as an intermediate in methanol synthesis over ZnO or Cu/ZnO catalysts. A plausible explanation, perhaps, is that formaldehyde being a highly reactive intermediate undergoes rapid conversion in some species like the methoxy. Saida and Ozaki (3), who have studied the kinetics of methanol synthesis over a $Cu/ZnO/Cr_2O_3$ catalyst at near atmospheric pressures, conclude that quantitative interpretation of their data is possible only by assuming a reaction sequence involving formaldehyde. In a very recent work, Tawarah and Hansen (15) have investigated the kinetics of methanol decomposition over ZnO in the temperature range 563 to 613 K. Based on their observations, they confirmed the presence of formaldehyde in the reactor effluent with a mass spectrometer and with chemical methods. Invoking the principle of microscopic reversibility, it may be concluded that some of those intermediates (15) participate in the methanol synthesis reaction.

Ample evidence exists for the methoxy species on ZnO and ZnO/Cr_2O_3 catalyst (16-19). Since the active forms appear to be the metal cations for both ZnO and Cu/ZnO catalysts, it seems reasonble to assume the formation of methoxy species on the Cu/ZnO catalysts. Recently, the methoxy species has also been observed on a Cu/ZnO catalyst during methanol synthesis (20). For Cu/ZnO catalysts it is proposed that the intermediates, in the course of their progress towards the product methanol, orient themselves to form the more favorable oxygen-surface bond (11). These arguments lend support to the inclusion of a methoxy intermediate in the mechanism proposed for methanol synthesis over a $Cu/ZnO/Al_2O_3$ catalyst.

There can be considered to be three possible ways of CO_2 formation (i) the Boudouard reaction, (ii) the water gas shift reaction, and (iii) oxidation-reduction of the catalyst. In our reaction system, the carbon and oxygen balances based on CO in the feed and CO, CO_2 and CH_3OH in the reactor effluent are always closed. This enables us to suggest that the Boudouard reaction can be eliminated as a source of CO_2 (9).

Van Herwijnen and Dejong (21) have investigated the kinetics and mechanism of the water gas shift reaction on a Cu/ZnO catalyst in the range of 172 to 230 °C and pressures ranging from 1 to 6 atm. With a feed mixture containing CO, N_2 and small amounts of H_2O, they find their Cu/ZnO catalyst to be active in the forward direction of this reaction. This finding allows us to suggest that at our experimental conditions (250–290 °C, 3–15 atm), such a reaction is likely.

Herman *et al.*, (4) have tested a $Cu/ZnO/Al_2O_3$ catalyst for a H_2/CO (76/24) mixture without CO_2. Although this catalyst is found to be selective to methanol, it is rapidly and irreversibly deactivated. Their examination of the catalyst by optical spectroscopy reveals only the pink color that is characteristic of copper. They attribute this to oxidation-reduction of the catalyst.

In view of these arguments and lack of any spectroscopical analysis of our catalyst, both the water gas shift reaction and oxidation-reduction of the catalyst are probably responsible for the formation of CO_2 at the conditions of our experiments.

SUMMARY

The kinetics of methanol synthesis from carbon monoxide and hydrogen over a commercial $Cu/ZnO/Al_2O_3$ catalyst has been investigated at temperatures between 250 and 290 °C and pressures between 3 and 15 atm. The highest catalytic activity is observed at 290 °C. A two parameter kinetic model that quantitatively describes the observed patterns is presented. It is also proposed that the formyl species, CHO-, appears to be the most abundant surface intermediate, and the rate determining step seems to be the surface reaction between the methoxy intermediate and an adsorbed hydrogen atom. Based on this study and current knowledge of supported Cu/ZnO catalysts, a mechanism for the methanol synthesis is proposed. The main feature of this mechanism is the shift from a carbon-surface bond to an oxygen-surface bond during the course of reaction.

NOMENCLATURE

E = Activation energy, cal/gmol

k = Rate constant, gmol/g•cat/sec/atm

k_o = Pre-exponential factor, gmol/g•cat/sec/atm

K_{eq} = Equilibrium constant of the methanol synthesis reaction

n = Empirical constant

r = Reaction rate, gmol/g•cat/sec

R = Universal gas constant, cal/gmol/K

T = Temperature of reaction, K

REFERENCES

1. Klier, K., Chatikavanij, V., Herman, R.G., and Simmons, G.W., *J. Catal. 74,* 343, 1982.
2. Henrici-Olive, G., and Olive, S., "Catalyzed Hydrogenation of Carbon Monoxide", Springer-Verlag, New York, 1984.
3. Saida, T.,and Ozaki, A., *Bull. Chem. Soc. Jpn. 37,* 1817, 1964.
4. Herman, R.G., Klier, K., Simmons, G.W., Finn, B.P., and Bulko, J.B., *J. Catal. 56,* 407, 1979.
5. Shimomura, K., Ogawa, K., Oba, M., and Kotera, Y., *J. Catal. 52,* 191, 1978.
6. Leonov, V.E., Karabaev, M.M., Tsybina, E.N., and Petrishcheva, G.S., *Kinet. Katal. 14,* 970, 1973.
7. Rozovskii, A.Y., Kagan, Y.B., Lin, G.I., Slivinskii, E.V., Loktev, S.M., Liberov, L.G., and Bashkirov, A.N., *Kinet. Katal. 16,* 810, 1975.
8. Kagan, Y.B., Rozovskii, A.Y., Liberov, L.W., Slivinskii, E.V., Lin, G.I., Loktev, S.M., and Bashkirov, A.N., *Dokl. Akad. Naukk SSSR 224,* 1081, 1975.
9. Agny, R.M., "Catalytic Synthesis of Methanol from Carbon Monoxide and Hydrogen over a Commercial $Cu/ZnO/Al_2O_3$ Catalyst", M.S. Thesis, Purdue University, 1984.
10. Dietz, W.A., *J. Gas Chromat. 5,* 68, 1967.
11. Kung, H.H., *Catal. Rev. Sci. Eng. 22,* 235, 1980.
12. Vannice, M.A., *J. Catal. 37,* 462, 1975.
13. Saussey, J., Lavalley, J., Lamotte, J., and Rais, T., *J. Chem. Soc. Chem. Commun.,* 278, 1982.
14. Deluzarche, A., Hinderman, J.P., and Kieffer, R., *Tegrahedron Lett.,* 2787, 1978.
15. Tawarah, K.M., and Hansen, R.S., *J. Catal. 87,* 305, 1984.
16. Deluzarche, A., Kieffer, R., and Muth, A., *Tetrahedron Lett.,* 3357, 1977.
17. Nagarjunan, T.S., Sastri, M.V.C., and Kuriacose, J.C., *J. Catal. 2,* 223, 1963.
18. Borowitz, J.L., *J. Catal. 13,* 106, 1969.
19. Ueno, A., Onishi, T., and Tamaru, K., *Trans. Faraday Soc. 67,* 3585, 1971.
20. Griffin, G.L., and Roberts, D.L., "Multi-component Adsorbate Interactions of Cu/ZnO Methanol Synthesis Catalysts", paper presented in the 75th Annual Meeting AIChE, November 14-18, 1982, in Los Angeles, California.
21. Herwijnen, T.V., and Dejong, W.A., *J. Catal 63,* 83, 1980.

ACKNOWLEDGEMENTS

Support was provided by NALCO and CONOCO Companies through the Coal Research Center, Purdue University.

TABLE 1.

Steady State Data of Methanol Synthesis of $Cu/ZnO/Al_2O_3$ Catalyst C79-2-01 of United Catalysts, Inc.

Run #	Reactor Temperature (°C)	Reactor Pressure (atm)	$\frac{H_2}{CO}$	F	Flow Rate at STP (cc/min)	Conversion of CO to Methanol (%)	Reactor Effluent Composition (%)				
							CO	H_2	CH_3OH	CO_2	H_2O
1	250	14.3	2.4		102	0.27	29.4	70.5	0.08	a	a
2	250	12.6	2.4		100	0.24	28.9	70.9	0.07	a	a
3	250	11.2	2.2		77	0.22	31.1	68.8	0.07	a	a
4	250	9.4	2.2		79	0.19	31.6	68.3	0.06	a	a
5	250	7.7	2.1		83	0.15	32.5	67.4	0.05	a	a
6	250	6.2	2.2		79	0.13	31.6	68.3	0.04	a	a
7	270	14.2	2.3		104	0.91	29.4	70.0	0.26	0.27	a
8	270	11.0	2.2		112	0.61	30.9	68.8	0.18	0.09	a
9	270	9.5	2.4		101	0.54	29.5	70.2	0.16	0.07	a
10	270	7.8	2.2		100	0.42	30.9	68.9	0.13	0.07	a
11	270	6.2	2.2		103	0.32	30.9	68.9	0.11	0.06	a
12	270	3.4	2.1		106	0.16	32.0	67.9	0.05	a	a
13	290	14.3	2.4		101	1.35	29.0	70.0	0.40	0.51	a
14	290	11.2	2.3		116	0.96	29.8	69.6	0.30	0.26	a
15	290	9.5	2.2		100	0.81	30.6	68.8	0.27	0.27	a
16	290	7.7	2.1		103	0.63	31.4	68.1	0.20	0.24	a
17	290	6.2	2.2		97	0.48	30.7	69.0	0.15	0.14	a
18	290	3.5	2.2		99	0.22	31.3	68.6	0.07	a	a

[a] Trace amounts.

TABLE 2.

Pre-exponential Factors and Overall Activation Energies for Methanol Synthesis over $Cu/ZnO/Al_2O_3$ Catalyst C79-2-01 of United Catalysts, Inc.

Temperature (°C)	Pre-exponential Factor (gmol/g·cat/sec/atm)	Overall Activation Energy (cal/gmol)
250	13,600	34,000 ± 1,000
270	1,890	29,500 ± 1,000
290	48	25,000 ± 1,000

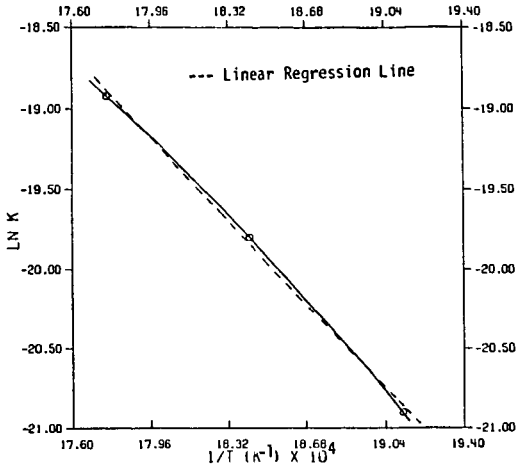

Figure 1. Arrhenious Plot for the Methanol Synthesis Reaction in our System (Eq. 2).

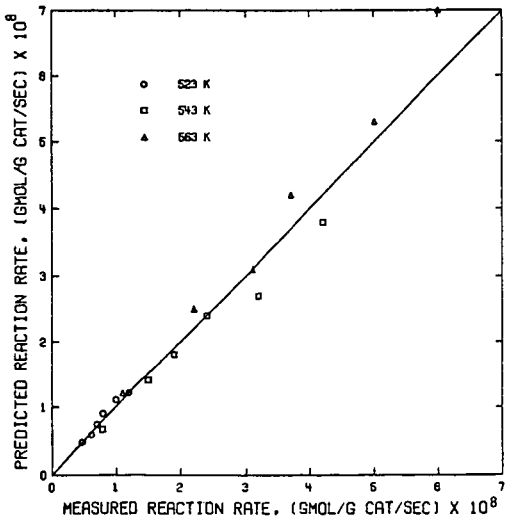

Figure 2. Comparison Between Measured Reactions Rates and Predicted Reaction Rates (Eq. 2).

STEAM PYROLYSIS OF SHALE AND PETROLEUM GAS OIL MIXTURES

by
Harry P. Leftin and David S. Newsome

The M. W. Kellogg Company
Research & Development Center
16200 Park Row
Houston, Texas 77084

ABSTRACT

Light gas oil and heavy gas oil from Paraho shale oil and their mixtures with a petroleum light gas oil were pyrolyzed in the presence of steam at 880-900°C and contact times between 60 and 90 milliseconds in a nonisothermal bench scale pyrolysis reactor. Blending of petroleum LGO into the shale oil feeds provided product yields that were the weighted linear combination of the yields of the individual components of the blends. Partial denitrogenation and a pronounced decrease in the rate of coke deposition on the reactor walls was observed when petroleum gas oil was blended with the shale gas oils.

INTRODUCTION

Steam pyrolysis of hydrocarbons in tubular reactors is the key process for production of gaseous olefins that serve as major raw materials for the petrochemical industry. While the recent concern regarding cost, supply and availability of petroleum derived feedstocks for petrochemicals production has subsided, at least temporarily, the long term outlook remains sufficiently clouded that the present breathing spell affords an opportunity to examine potential alternative feed sources. These concerns have lead to several investigations[11,12,13] of shale oil as feed for olefins production. Indeed, the M. W. Kellogg Company have recently completed a study[4] to evaluate shale oil fractions and hydrotreated shale oil fractions as feed for olefins production in conventional pyrolysis. The authors concluded from this study that shale oil distillates produce ethylene, propylene and benzene yields similar to those from petroleum, however coking rates were unacceptably high for all except the lightest fraction. Mild hydrotreating improved the tube wall fouling rate of the shale oil naphtha and light gas oil fractions to the range typical of petroleum light gas oil (LGOP); that for the heavy gas oil (HGOS) was improved but still unacceptable. In another study[5], more extensive prerefining by hydrotreating reduced the heteroatom concentration and provided yields of olefins comparable with or exceeding those from petroleum fractions. Substantially lower ethylene yield was obtained from severely hydrotreated TOSCO II distillate due to steam reforming during pyrolysis. Coking rates and liquid products yields were not reported.[5]

While it is clear that shale oil has the potential to eventually be a major source of hydrocarbon for both fuel and chemical production, the near term prospects call for limited production from subsidized programs. Since dedicated refineries and petrochemical plants cannot be justified to utilize this material, it will be necessary either to upgrade the shale oil to its petroleum equivalent or to improve its processability by blending it with conventional petroleum. Indeed, even when shale oil production begins to expand as petroleum declines, the blending of these to produce feedstocks will presage the smooth evolution of shale oil specific processing technology.

The literature on steam pyrolysis of shale oil distillates is limited but adequate to indicate its potential as feedstock, particularly after some prerefining. The literature on steam pyrolysis of petroleum distillates is extensive. However, no literature exists in the cocracking of shale and petroleum distillates. Cocracking of petroleum derived feedstocks has been shown to provide expected product yields, that is, yields which are the linear combination of yields of the individual components of the blend. However, coking behavior of such feedstock mixtures showed[7] remarkable effects where the coking rate of a suitably blended feedstock mimicked the rate of the less coking feed component.

The present study was undertaken to determine the cracking and coking behavior of shale oil distillates under conditions of millisecond pyrolysis and the effects of admixture of petroleum LGO on these properties. Particular interest was paid to liquid products.

EXPERIMENTAL:

Apparatus:

The bench scale pyrolysis furnace and flow system have been described previously in detail.[8,9,10]

The experimental arrangement for pyrolysis comprised a feed system, vaporizer preheater, an electrically heated furnace and product recovery system. Liquid feedstocks were fed from Ruska metering pumps into the vaporizer where they were mixed with superheated steam before passing through the preheater and into the reactor. The reaction zone was an annulus between a reactor tube and a coaxial thermowell, both of 310 stainless steel. Temperature profiles were measured with a calibrated chrome-alumel thermocouple manually driven along the length of the reactor. On leaving the reaction zone, the process stream was rapidly cooled by admixture with a recycled stream of cooled product gas.[6] The quenched products were further cooled against chilled water in an indirect heat exchanger and water condensate plus liquid products were separated by means of a small cyclone separator which was an integral part of the product gas recycle quench system.

To avoid formation of carbon oxides due to steam reforming reactions, as was observed in other studies with hydrotreated shale oil distillate,[5] the walls of the stainless steel reactor were maintained in a catalytically inactive form by sulfiding and the pyrolysis experiments were performed in the presence of 50 ppm sulfur which was introduced to the system as ethyl mercaptan contained in the process feed water.

At the completion of a pyrolysis run the amount of coke deposited on the reactor tube wall during the run was determined by burning out with a steam-air mixture.[10] To accomplish this, the pyrolysis system is modified by replacement of the quenching system with a CO_2 collection system. Air and water rates are controlled by rotameters and needle valves. Contaminant CO_2 is removed from both the water and bottled air used in the burn-off. After the combustion gases leave the reactor, the bulk of the unreacted water is removed with a room temperature trap, and residual water vapor is removed with a drying agent. The dry gases then enter a CuO bed maintained at high temperature to convert any CO to CO_2 and is then passed through another drying agent prior

to being absorbed in a preweighed ascarite/magnesium perchlorate tube. Total carbon deposited in the reactor is calculated from the weight of CO_2 collected. A gas chromatograph in the system periodically measures the CO_2 level in the combustion gas stream to determine when a burnout is completed.

After a pyrolysis run/burnout cycle is completed, the reactor tube is conditioned for the next run by reducing and sulfiding the reactor walls with a flow of hydrogen and hydrogen sulfide.

Product Analysis:

Two gas samples, for duplicate analysis by mass spectrometry, were taken in the first third and final third of the run period. Results of duplicate mass spectrometric determinations fell within the established limits for this analytical method, and the averaged values were then used.

Liquid product, after separation from process steam condensate, is assayed into gasoline (36-218°C), light fuel oil (218-343°C) and heavy fuel oil (343°C$^+$) by gas chromatographic simulated distillation (GCSD) as defined in ASTM method D-2887. Yields of individual C_6-C_8 aromatics (BTX) were obtained by G.C.

Total organic nitrogen present in the C_5^+ liquid products from selected runs was determined by the Kjeldahl method. Boiling range distribution of nitrogen was determined using a gas chromatographic simulated distillation method modified by use of a detector specific for organic nitrogen. The method involves injecting a sample into a chromatographic column equipped with effluent splitter leading to a Thermionic Specific Detector (TSD) for nitrogen and a Flame Ionization Detector (FID) for carbon. The area from the TSD for each time interval is recorded on magnetic tape while the area from the FID over the entire chromatogram is recorded separately. From these data and previously determined calibration factors, nitrogen concentration and boiling range distributions may be determined using the conventional GCSD temperature vs time plot. A Varian 3700 G.C. equipped with TSD and FID was employed for this work.

Feedstocks

Shale light gas oil (LGOS) and heavy gas oil (HGOS), prepared by distillation from Paraho shale oil, were samples of the same materials used in an earlier steam pyrolysis study (4). An Arabian light gas oil comprised the petroleum derived light gas oil (LGOP) used in this study. Blends of shale gas oils and the petroleum gas oil were prepared to contain 20, 40, 60 and 80 wt% petroleum gas oils. Thus a total of ten feedstocks were examined. Inspection data for these feedstocks and blends are summarized in Table I.

DATA AND DISCUSSION

Runs were carried out at maximum temperatures (Tm) of a parabolic temperature profile (9) between 744°C and 899°C with steam dilution corresponding to steam/hydrocarbon weight ratios between 0.5 and 1.0. All runs were isobaric at

a total pressure of 13-15 psig (90-105 kPa). Most of the runs were carried out under millisecond contact times (less than 0.1 seconds); however, one run on each of the neat shale gas oils (LGOS and HGOS) was carried out at conventional contact time (about 0.3 seconds) to determine the effect of this variable on product yields. With the exception of those runs where excessive reactor coking (Runs 11,12 & 13) forced early run termination, material balances fell between 95% and 100%.

Tables II and III summarize the individual run conditions and the observed yields and conversions for all runs with light and heavy shale gas oils (LGOS and HGOS), respectively. Runs No. 1 and 10 were carried out under conventional contact time conditions similar to those used in an earlier study.[4] Results for both the neat LGOS and HGOS are in excellent agreement with the earlier data.[4]

Comparison of runs 1 and 2 show the effect of conventional vs millisecond conditions on pyrolysis of neat LGOS. These data show an enhancement in selectivity to ethylene as described previously[3] for operations at increased temperature and decreased contact time. A similar comparison (Runs 10 & 11) for pyrolysis of heavy shale gas oil (HGOS) was precluded by the rapid coking of the reactor.

Pyrolysis of Shale-Petroleum Gas Oil Blends:

Gaseous Product:

In runs No. 3,4,5,6 and 7, blends of an Arabian light gas oil (LGOP) and shale light gas oil (LGOS) were pyrolyzed under closely identical operating conditions. Conversion and product yields changed monotonically in the mixtures between those for neat LGOS and for neat LGOP. Figure 1 illustrates the changes in conversion and yields of major gaseous products for the LGOS/LGOP feedstock blends. Yields of major products for these blends are the arithmetic weighted average of the yields for the individual feedstocks in the blends. Accordingly, full yield benefits normally attainable from separate steam pyrolysis of shale LGO may be realized by cocracking the shale feed with petroleum gas oil in an existing gas oil pyrolysis furnace. Since the shale oil feed, in this case, is intrinsically poorer in terms of ethylene yield, a proportional penalty in furnace ethylene capacity will obtain. To some extent, this penalty can be compensated by increasing severity or decreasing hydrocarbon partial pressure, e.g. runs no. 2 vs 3.

Due to the higher coking rates attendant to the pyrolysis of the shale heavy gas oil (HGOS), fewer data are available for this feedstock. Figure II summarizes the conversion and yields of major gaseous products for cocracking HGOS/LGOP blends. While these data are limited to blends at the low end of the HGOS content, extrapolation to 100% HGOS provides an estimate yield that might be realized from high severity pyrolysis of neat HGOS. The extrapolated results appear reasonable in view of those obtained from HGOS under milder conditions (Run 10).

Liquid Products:

Gasoline and fuel oil become major products of olefins production processes when liquid hydrocarbon feedstocks are used in steam pyrolysis. These, so-called, co-products comprise from 35-55 wt% of the feed depending on feed properties and pyrolysis conditions. Consequently, these liquid co-products exert a large effect on the economics of naphtha and gas oil pyrolysis for both petroleum or shale oil derived feedstocks.

With the exception of a related study (4) which reports the gasoline and fuel oil yields from pyrolysis of shale oil distillates, no literature exists on the effects of operating conditions on yields or on the quality of these liquid products. In the present work both of these topics were investigated.

Yields of boiling range fractions of the pyrolysis liquids as determined by gas chromatographic simulated distillation (GCSD) (ASTM method D-2887) are summarized in tables II and III. Gasoline yield from LGOS appears to be somewhat greater than that for the petroleum gas oil studied. This result may not be unique, however, since gasoline yield is known to depend on characteristics of various petroleum gas oils. It is of greater interest that the yield of potential motor gasoline appears to change little with either pyrolysis severity or with composition of the blended feedstocks. Since gasoline yields for LGOS are comparable to those of petroleum feedstock, it is of interest to determine the quality of this for use as motor fuel. A special gas chromatographic method was used to provide data needed for calculation of Research Octane Number (RON) of the gasoline fraction in the pyrolysis liquid from Run #9 (60% LGOS/40% LGOP). According to this method, a cutting column is used to separate the gasoline from the higher boiling materials which are discarded in a back flush. The gasoline cut is fed to a capillary column for quantitative analysis and identification of the components in the gasoline. The Research Octane Number calculated from this G.C. analysis using the method of Anderson et al (1) was found to be 99.4.

Light and heavy fuel oil yields are greater for the shale oil feedstocks and these vary linearly with composition for the blended feedstocks.

Nitrogen Distribution:

Shale oil as well as its distillate fractions have a high content of organic nitrogen, typically between 1 and 2 wt percent. Since nitrogen is a catalyst poison for current refinery operations and a detriment to liquid fuel products, most schemes for utilization of shale oil require upgrading by severe hydrotreating. While steam cracking (a non catalytic process) is not inhibited by organic nitrogen, the quality and hence the value of liquid products are adversely affected. Typically in steam pyrolysis of liquid feedstocks approximately one half of the feed is converted to gaseous products which contain no organic nitrogen. It becomes very interesting then to determine to what extent, if any, this gasification involves net denitrogenation of feedstock and also to determine the distribution of remaining nitrogen among the liquid products.

Boiling range distribution of organic nitrogen in the LGOS feedstock and in the pyrolysis liquid products from runs with neat LGOS (Run #8) and with LGOS/LGOP blend (Run #9) were determined by gas chromatography. Results are illustrated in Figure III and summarized in Table IV.

TABLE IV

Nitrogen Distribution in Pyrolysis Liquid Fractions

Run No.	8		9	
	Wt% of Feed	Wt% N	Wt% of Feed	Wt% N
Liquid Fraction				
C_5-218°C (Liquid only)	17.0	2.34	17.9	0.26
C_5-218°C Total gasoline[a]	21.7	1.83	21.6	0.22
218-354°C Fuel Oil	21.1	2.72	20.6	0.71
354°C + Hy Fuel Oil	11.9	4.08	10.7	4.23
Whole Liquid Product	50.0	2.92	49.2	1.39
% Nitrogen Balance[b]	98.6		72.5	
Apparent Denitrogenation %	1.4		27.5	

(a) Includes C_5,C_6 gasoline components contained in the gas samples.

(b) Total Nitrogen in Liquid Products/N in Feed.

In Figure III, the results of gas chromatographic determination of cumulative nitrogen content as a function of boiling point (retention time) is plotted against the analogous data for cumulative carbon (GCSD) in the liquid samples. In this way, the retention time is eliminated from the plot and a distribution curve relating the nitrogen content with the carbon content is obtained in which the slope of the curve at any point is the concentration of nitrogen in the fraction of the sample boiling below that point. Thus a straight line with unit slope (45°) indicates uniform nitrogen concentration in all fractions of the total liquid.

Nitrogen in the LGOS feedstock is fairly uniformly distributed over the entire boiling range (Figure III-a). The liquid produced from pyrolysis of neat LGOS contains almost all of the organic nitrogen from the feed and this nitrogen is also broadly distributed over the boiling range of this product (Figure II-b). In this case, there is a small trend toward increasing nitrogen concentration with increasing boiling range.

A pronounced change in nitrogen distribution (Figure III-c) is found in the liquid product from cracking a blend of LGOS and LGOP. In this case, the nitrogen concentration is strongly shifted into the heavier portion of the pyrolysate and a significant part of the feed nitrogen appears to have been removed. Partial denitrogenation by steam pyrolysis provides a clear economic benefit from cocracking shale oil/petroleum blends. Additional benefits may be derived from the reduced nitrogen content of the gasoline and light fuel oil products which, although they still require upgrading, can be denitrogenated with less severe hydrotreating than would be required for denitrogenation of the entire feedstock or the products from separate cracking of LGOS. Disposition of the heavy fuel is an equivalent problem in either case. In any event, cocracking of shale oil and petroleum feedstocks offers an interesting alternative to severe hydrotreating of shale oil.

Reactor Tube Wall Fouling:

The high fouling rate exhibited by heavier shale oil fractions has been identified (4) as being the major hurdle that must be overcome in its utilization as feedstock for olefins production. Partial hydrotreatment of the pyrolysis feed resulted in reducing the fouling rate (4) but not to an acceptable level, especially for the heavy gas oil (HGOS). Severe hydrotreatment, on the other hand, reduced fouling adequately (5) but at considerable expense due to high hydrogen consumption and the high pressures required (2).

Inhibition of tube wall coking in pyrolysis furnace tubes by cocracking in the presence of a low coking hydrocarbon has recently been described (7). It has now been found that an analogous phenomenon occurs in the cocracking of shale gas oils in admixture with a low coking petroleum gas oil. Figure IV illustrates this effect for both the HGOS/LGOP and LGOS/LGOP feed blends. With the addition of less than 40% LGOP to LGOS, the fouling rate of the feedstock combination is substantially reduced and closely approaches the rate characteristic of the petroleum gas oil itself. Substantially more LGOP must be added to suppress the fouling rate of HGOS. This is in accord with the intrinsically higher coking propensity of the heavier shale feedstock.

While the fouling behaviour of the HGOS and LGOS blends with LGOP is in qualitative agreement with the coke inhibition index (CII) concept,(7) it does not agree quantitatively with the correlation developed for petroleum feedstocks. High organic oxygen and nitrogen contents of the shale liquids exert a positive influence on their coking properties as evidenced by the observed (5) decrease in coking rate upon removal of these heteroatoms.

According to the observed coking behavior of mixtures of shale and petroleum distillates, acceptably low coking rates can be expected from blends containing significant quantities of shale liquid. This provides an interesting alternative to hydrotreating prior to pyrolysis.

CONCLUSIONS:

Shale oil distillates may be a substitute feed for olefins production in high severity pyrolysis. Cocracking in admixture with suitable petroleum derived feedstocks offers a potential alternative to costly hydrotreating by providing partial denitrogenation of the liquid fuel coproducts as well as by largely overcoming the barrier due to the inherent excessive tube wall fouling characteristics of the shale oil liquids.

REFERENCES

1. P. C. Anderson, J. M. Sharkey & R. P. Walsh, J. Inst. Petr. 58 ,84 (1972).

2. R. F. Anderson, et al, D.O.E. Report No. FE-2315-25, (May 1978).

3. B. P. Ennis, H. P. Boyd & R. Orriss, Chem. Technol. 5 ,(11) 693 (1975).

4. H. J. Glidden & C. F. King, Chem. Eng. Prog. 76 ,(12) 47 (1980).

5. C. F. Griswold, A. Ballut, H. R. Kavianian, D. F. Dickson & V. F. Yesavage, Chem. Eng. Prog. 75 ,(9) 78 (1979).

6. J. Happel & L. C. Kramer, Ind. Eng. Chem., 59 ,39 (1967).

7. H. P. Leftin & D. S. Newsome, U.S. 4,176,045, Nov. 27, 1979.

8. H. P. Leftin, D. S. Newsome, T. J. Wolfe & J. C. Yarze, "Industrial and Laboratory Pyrolysis", Am. Chem. Soc. Symposium Series 32 ,373 (1976).

9. H. P. Leftin and A. Cortes, Ind. Eng. Chem. Proc. Des. & Dev. 11 ,613 (1972).

10. D. S. Newsome & H. P. Leftin, Chem. Eng. Prog. 76 ,(5) 76 (1980).

11. C. G. Rudershausen & J. B. Thompson, Prepr. Div. Pet. Chem. Am. Chem. Soc. 23 ,(1) 241 (1978).

12. E. G. Shultz, J. B. Guyer & H. R. Linden, Ind. Eng. Chem. 47 ,2479 (1955).

13. P. D. Smith, P. F. Dickson & U. F. Yesavage, Prepr. Div. of Pet. Chem. Am. Am. Chem. Soc. 23 ,(2) 756 (1978).

TABLE I

FEEDSTOCK INSPECTIONS

TYPE	SHALE	LIGHT GAS OIL BLENDS			PETROLEUM	SHALE	HEAVY GAS OIL BLENDS			
Feed Designation	LGOS	L-1	L-2	L-3	LGOP	HGOS	H-1	H-2	H-3	H-4
Wt% Shale oil	100	80	60	40	0	100	80	60	40	20
Wt% Petroleum LGO	-	20	40	60	100	0	20	40	60	80
ASTM Dist'n (°F)										
IBP	424	-	-	-	335	662	-	-	-	-
10%	458	-	-	-	427	714	-	-	-	-
30%	497	-	-	-	478	756	-	-	-	-
50%	536	-	-	-	512	797	-	-	-	-
70%	572	-	-	-	546	844	-	-	-	-
90%	614	-	-	-	599	889	-	-	-	-
E.P.	637	-	-	-	638	918	-	-	-	-
°API	28.9	31.0	33.1	35.3	39.9	19.7	23.3	27.2	31.2	35.4
Molecular Wt(1)	210	212	213	215	218	371	325	290	261	238
Elemental Analysis (Wt%)										
C	85.16	85.39	85.61	85.84	86.29	85.41	85.59	85.76	85.94	86.15
H	12.36	12.57	12.79	13.00	13.43	11.38	11.79	12.20	12.61	13.02
N	1.49	1.20	0.90	0.60	N.D.	2.14	1.71	1.28	0.86	0.43
S	0.76	0.63	0.49	0.35	0.09	0.64	0.53	0.42	0.31	0.20
O	1.78	1.42	1.07	0.71	N.D.	1.64	1.31	0.98	0.66	0.33
H/C Atom Ratio	1.73	1.75	1.78	1.80	1.85	1.59	1.64	1.69	1.75	1.80

(1) Calculated

TABLE II

STEAM PYROLYSIS OF SHALE LIGHT GAS OIL
AND MIXTURES WITH PETROLEUM LIGHT GAS OIL

Run #	1	2	3	4	5	6	7	8	9
Feed Composition:									
Wt% LGOS	100	100	100	80	60	40	0	100	60
Wt% LGOP	0	0	0	20	40	60	100	0	40
Temp. max (°C)	766	899	899	899	899	899	899	882	879
Log Mean O (Sec)[a]	0.32	0.073	0.086	0.086	0.088	0.093	0.091	0.090	0.094
H_2O/Oil (g/g)	1.00	1.02	0.50	0.50	0.50	0.50	0.50	0.50	0.50
Outlet Pressure (Psig)	13	13	15	15	15	15	15	15	15
Conversion (1-C_5+)	49.8	48.0	46.1	46.4	51.6	53.1	61.6	44.4	46.9
Yields (Wt%)(Basis Output)									
H_2	0.44	0.73	0.72	0.68	0.72	0.73	0.84	0.55	0.59
CH_4	8.70	10.9	10.7	9.87	10.6	10.8	11.5	9.08	8.21
C_2H_2	0.06	0.88	0.82	0.76	0.74	1.05	0.90	0.29	0.32
C_2H_4	15.6	20.4	18.1	18.7	21.9	22.7	27.5	16.3	19.0
C_2H_6	3.63	2.01	2.37	2.32	2.49	2.39	2.59	2.70	2.13
C_3H_4	1.14	0.65	0.64	0.60	0.56	0.63	0.82	0.38	0.31
C_3H_6	11.6	7.56	7.63	7.93	8.79	8.94	10.2	8.90	9.36
C_3H_8	0.60	0.18	0.08	0.11	0.15	0.30	0.12	0.31	0.40
C_4H_6	3.28	3.23	3.26	3.37	3.84	3.59	4.78	3.15	3.05
C_4H_8	4.71	1.49	1.67	1.93	1.93	1.89	2.20	3.24	3.45
C_4H_{10}	0.10	0.01	0.15	0.13	0.02	0.01	0.17	0.06	0.09
C_5+ (liq)	49.0	51.3	53.2	52.9	48.1	46.6	38.2	54.7	52.9
Coke	1.24	0.72	0.70	0.66	0.31	0.28	0.21	0.35	0.21
Gasoline (C_5-218°C)	20.6	20.2	21.3	19.3	21.2	21.2	18.7	21.7	21.6
Fuel Oil (218°-343°C)	20.4	19.0	20.0	20.3	17.1	17.3	13.0	21.1	20.6
Fuel Oil (343°-454°C)	6.43	7.49	7.89	8.26	6.27	5.34	4.45	8.48	8.71
Pyrolysis Tar (454°C+)	1.57	4.61	4.01	5.08	3.52	2.76	2.05	3.43	1.98
BTX[b]	4.3	4.4	5.8	6.2	7.4	7.5	7.0		5.1
Tube Wall Fouling:									
Run Length (Min.)	237	89	111	69	120	120	120	131	135
Wt of Coke Product (gm)	1.03	0.85	1.59	0.96	0.79	0.71	0.54	1.41	0.83
Coking Rate (mg/min)	4.53	9.60	14.3	13.8	6.59	5.91	4.51	10.8	6.15
Nitrogen Wt%									
Gasoline	-	-	-	-	-	-	-	1.83	0.22
Fuel Oil	-	-	-	-	-	-	-	2.72	0.71
Fuel Oil + Tar	-	-	-	-	-	-	-	4.08	4.23
Nitrogen Balance Prod/Feed (%)	-	-	-	-	-	-	-	98.6	72.5
RON (C_5-218°C)									99.4

(a) Temperatures between 600°C and Tmax.
(b) Benzene, Toluene, O,M & P Xylene, Ethylbenzene and Styrene.

TABLE III

STEAM PYROLYSIS OF SHALE HEAVY GAS OIL AND MIXTURES WITH PETROLEUM LIGHT GAS OIL

Run #	10	11	12	13	14	15	16
Feed Composition:							
Wt% HGOS	100	100	80	60	40	20	0
Wt% LGOP	0	0	20	40	60	80	100
Temp. Max (°C)	744	899	899	899	899	899	899
Log Mean O (Sec)[a]	0.33	0.07	0.07	0.07	0.073	0.071	0.063
H_2O/Oil (g/g)	1.00	0.75	0.74	0.76	0.75	0.77	0.79
Outlet Pressure (Psig)	13	15	15	15	15	15	15
Conversion ($1-C_5^+$)	36.5	(b)	(b)	(b)	52.7	59.4	66.6
Yields (Wt%) Basis (output)							
H_2	0.45	-	-	-	0.67	0.79	0.82
CH_4	9.66	-	-	-	9.74	11.0	11.4
C_2H_2	0.05	-	-	-	0.81	1.10	0.81
C_2H_4	10.6	-	-	-	23.2	26.6	28.1
C_2H_6	3.74	-	-	-	2.17	2.36	2.42
C_3H_4	0.42	-	-	-	0.53	0.74	1.01
C_3H_6	7.51	-	-	-	9.06	10.2	12.6
C_3H_8	0.52	-	-	-	0.20	0.25	0.30
C_4H_6	1.45	-	-	-	3.85	4.34	5.57
C_4H_8	2.00	-	-	-	2.26	2.08	3.40
C_4H_{10}	0.08	-	-	-	0.16	0.03	0.01
C_5^+(liq)	49.2	-	-	-	46.9	40.4	33.3
Coke	14.3	-	-	-	0.40	0.20	0.13
Gasoline (C_5-218°C)	-	-	-	-	23.4	19.4	19.9
Fuel Oil (218°-343°C)	-	-	-	-	12.8	12.0	8.77
Fuel Oil (343°-454°C)	-	-	-	-	6.04	5.40	3.35
Pyrolysis Tar (454°C$^+$)	-	-	-	-	4.66	3.60	1.28
BTX[c]	-	-	-	-	5.5	3.6	7.1
Tube Wall Fouling:							
Run Length (min)	77	12	29	47	100	123	120
Wt of Coke Produced (gas)	4.27	0.56	1.06	0.94	0.80	0.49	0.32
Coking Rate (mg/min)	55.5	46.6	36.5	20.0	9.97	3.98	2.65

(a) Temperatures between 600°C and Tmax.
(b) Run terminated due to reactor pressure drop buildup from rapid coking.
(c) Benzene, Toluene, O,M & P Xylene, Ethylbenzene and Styrene.

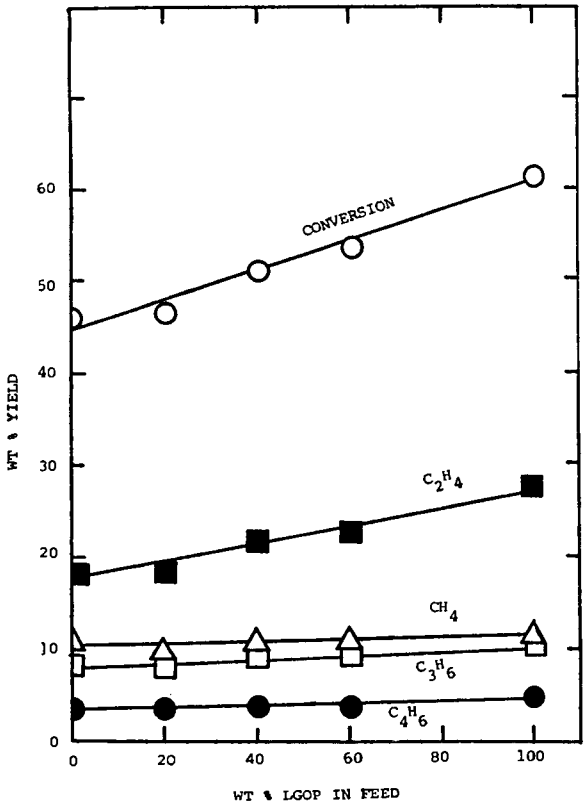

FIGURE 1. PYROLYSIS OF SHALE & PETROLEUM GAS OIL BLENDS (LGOS+LGOP). PRODUCT DISTRIBUTIONS.

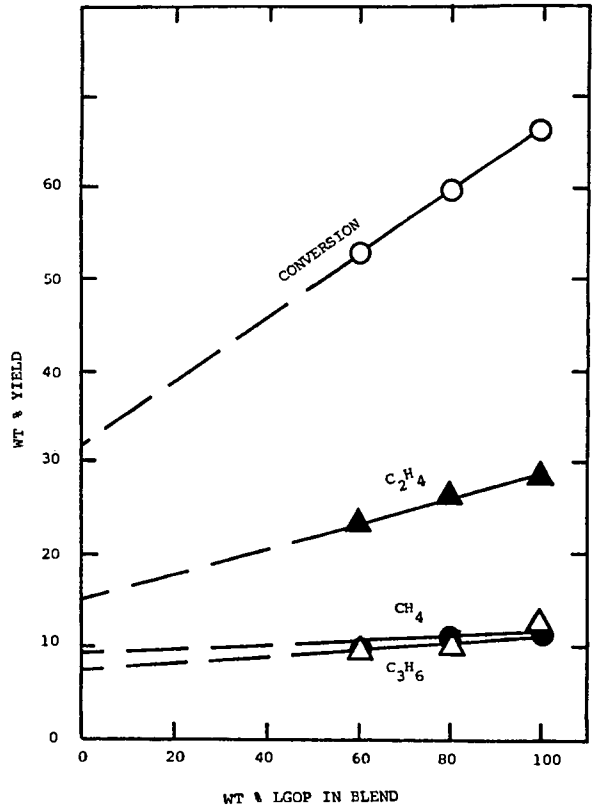

FIGURE 2. PYROLYSIS OF SHALE+PETROLEUM GAS OIL BLENDS (LGOS + LGOP). PRODUCT DISTRIBUTION.

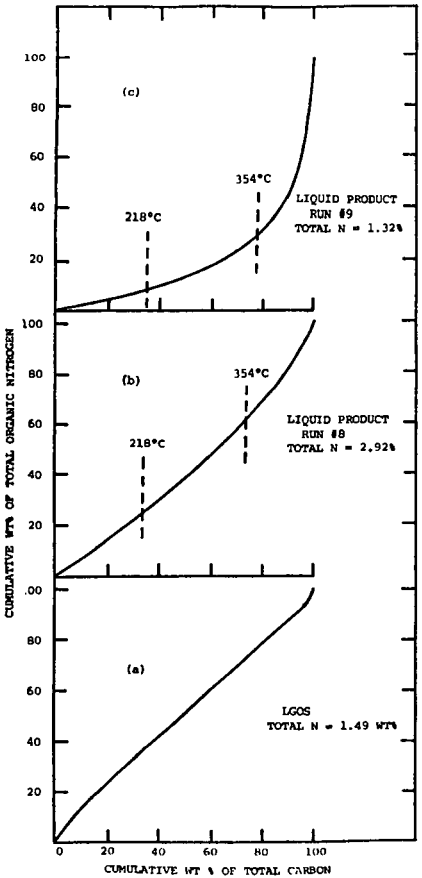

FIGURE 3. ORGANIC NITROGEN DISTRIBUTIONS

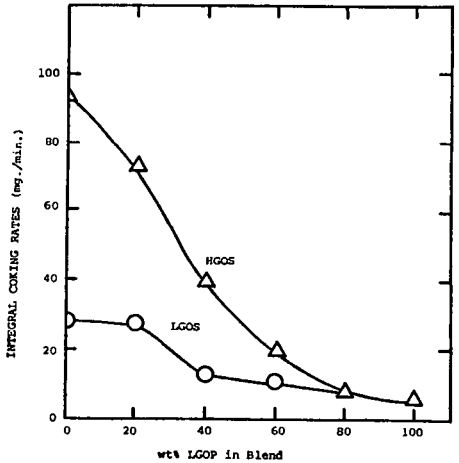

FIGURE 4. REACTOR FOULING RATES
SHALE/PETROLEUM GAS OIL BLENDS

DETERMINATION OF HYDROGEN DONATING PROPERTIES OF COAL LIQUEFACTION PROCESS SOLVENTS

Douglas W. Later and Donald M. Camaioni

Pacific Northwest Laboratory
Richland, Washington 99352

INTRODUCTION

The hydrogen donating properties of solvents used in direct coal liquefaction processes are of key importance in determining conversion efficiencies and overall product qualities. The reduction of fluorenone to fluorene at 400°C has recently been used in this laboratory to study the hydrogen donating properties of process solvents from different direct liquefaction technologies. Choi and Stock [1,2] have elucidated the mechanism of the reduction of fluorenone by hydrogen donating compounds and have demonstrated the utility of this reduction for evaluating the hydrogen atom transfer properties of coal and coal macerals.

The reduction reaction for fluorenone occurs in three stages [1]. Stage 1 is a radical process which produces 9-hydroxyfluorene as the intermediate product. In stage 2, this intermediate is transformed into bis(9-fluorenyl) ether by a non-radical process. The ether decomposes in stage 3 to produce fluorene and fluorenone via a radical process. In the study by Choi and Stock, it was shown that radical initiators, such as benzyl phenyl thioether or coal, accelerate the reactions of stages 1 and 3. The mechanisms of stages 1 and 3 are formulated in Scheme I. In the absence of initiator, a bimolecular molecule-assisted homolysis reaction [3-5] between fluorenone and donor initiates the reduction reaction:

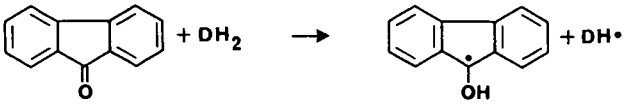

Reductions conducted in the absence of added initiators measure the ability of the solvent to both initiate the reduction and transfer hydrogen to radicals, whereas reductions carried out in the presence of initiators serve to measure the hydrogen donor ability of the solvent. Thus, the fluorenone reduction reaction provides a simple procedure to assess the relative abilities of process solvents and solvent components to participate in these radical initiating and hydrogen transfer reactions which are important to coal liquefaction.

EXPERIMENTAL

SAMPLES

Fluorenone was prepared by air oxidation [6] of fluorene (Aldrich Chemical) and was recrystallized from methanol to yield material >99% pure as determined by capillary column gas chromatography (GC). Process solvents from two direct coal liquefaction technologies were used in these experiments: (1) a Solvent Refined Coal (SRC)-I process solvent; and (2) a recycle pasting solvent from the Wilsonville, AL integrated two-stage liquefaction (ITSL) process. The physical and chemical properties of these materials are discussed in detail elsewhere [7,8]. Briefly, the SRC-I solvent had a boiling range of 480-850°F and the ITSL pasting solvent was a 650°F+/solid resids material. These liquefaction materials are from

developmental processes and should not necessarily be considered representative of future commercial coal liquefaction products.

The crude solvents were each tested individually for fluorenone conversion efficiency. In addition, chemical class fractions of these materials were obtained by alumina adsorption chromatography. Details of this procedure have been previously reported [9]. Briefly, the crude coal liquefaction materials were separated into four chemical classes: (1) aliphatic hydrocarbons, (2) neutral polycyclic aromatic hydrocarbons (PAH), (3) nitrogen-containing polycyclic aromatic compounds (N-PAC) and (4) hydroxylated PAH (Hydroxy-PAH).

Fluorenone Reduction Reactions

Fluorenone reductions were conducted at 400°C for 1 hr in sealed evacuated quartz tubes. Generally, benzene solutions of reactants were prepared and aliquots were transferred by microliter syringes to 6 mm o.d. quartz tubes (1 mm wall thickness), so as to provide 50 µL total volume containing approximately 5 mg donor and 0.025 mmol fluorenone. Reactions with the ITSL crude process solvent necessitated weighing the material directly into the tubes due to its insolubility in benzene. Loaded reaction tubes were freeze-thaw degassed on a vacuum line prior to flame sealing and thermostating in a Tecam SB-4 fluidized sandbath with TC4D temperature controller.

Quantitative Analyses

Quantitative analyses of the fluorenone reaction products were performed by capillary column GC. A Hewlett-Packard (HP) model 5880A gas chromatograph equipped with a 30 m x 0.25 mm i.d. fused silica DB-5 (J&W Scientific) capillary column was used. The splitless injection technique was used for sample introduction in conjunction with an HP7671A auto sampling device. Each sample was analyzed in triplicate using a flame ionization detector with peak response information stored and manipulated by the HP5880 microprocessor-controlled integrator. 2-Chloroanthracene was added to all reaction products at a concentration of 100 ng/µL and was used as internal standard for all GC quantitative analyses. Calculations for the conversion of fluorenone to fluorene were done on a mole basis with the conversion amounts reported for fluorene as a percentage of the initial fluorenone present in the reaction. This value was then adjusted to reflect a weight-normalized conversion based on a 5 mg quantity of coal liquid used in the fluorenone reduction reaction. Replicate analyses were performed with the mean and standard deviation reported in Table 1. Recovery percentages were also calculated and reported.

RESULTS AND DISCUSSION

The conversion yields for the reduction of fluorenone to fluorene by the crude process solvents and their chemical class fractions are presented in Table 1. For comparison, 9,10-dihydroanthracene was run and was observed to produce a 21±2% conversion of fluorenone; this is in close agreement with the results of Choi and Stock for the same compound [1,2]. Recoveries of fluorenone plus fluorene were greater than 90% for the unfractionated process solvents indicating that little adduction of intermediate fluorene-based radicals with solvent constituents had occurred. The aliphatic hydrocarbon and neutral PAH fractions showed recoveries similar to the crudes; greater than 85%. But, the more polar constituents exhibited lower recoveries (70-80%), which suggests that adduction of fluorenone reduction intermediates with N-PAC (A_3) and hydroxy-PAH (A_4) components occurred under these reaction conditions. Ionic reactions of the 9-hydroxfluorene with these polar fractions likely divert the reduction reaction producing fluorenyl adducts to the

activated aromatic rings. Choi and Stock [1] observed that reductions of benzophenone in the presence of phenol lead to diphenylmethylphenols and other side products.

The SRC-I solvent showed lower conversion (38%) than the ITSL process solvent (88%) from the new generation two-stage liquefaction technology. The chemical composition of the process solvents investigated in these experiments have been characterized and compared previously [7]. Table 2 provides information regarding their relative chemical class compositions. The ITSL material contained a wide range of high boiling, high molecular weight constituents while the SRC-I process solvent had intermediate boiling point and molecular weight ranges. The ITSL recycle pasting solvent contained the highest levels of aliphatic hydrocarbons and had the lowest combined levels of nitrogen and oxygen heteroatomic PAH. Furthermore, from detailed chemical analyses by GC and GCMS [7,8], hydroaromatic compounds such as dihydropyrene, which are known to be excellent hydrogen-donating compounds, were major constituents of the ITSL process solvents.

If the relative conversion yields for the different chemical classes are compared for a given coal liquefaction solvent (see Table 1), the chemical class producing the lowest conversion was the aliphatic hydrocarbon fraction (A_1), followed by the neutral PAH isolate (A_2). The N-PAC (A_3) and hydroxy-PAH (A_4) classes provided the highest yields for the conversion of fluorenone to fluorene. Hence, it is apparent that the polar constituent of coal liquefaction process solvents participate well in both the radical initiating and hydrogen donating steps shown in Scheme I. This observation is consistent with model studies which showed that 1,2,3,4-tetrahydroquinoline produced higher conversions to fluorene than tetralin or 9,10-dihydroanthracene [1,2]. Thus, the reduced levels of N-PAC in the SRC I versus the ITSL process solvent is one possible reasons for the relatively lower conversion yields observed for the SRC I material.

Considerable variability in the conversion yields of the neutral PAH fractions (A_2) of these two process solvents was observed. It was therefore of interest to compare the chemical/physical properties of these isolates. The neutral PAH isolates of the SRC-I process material displayed only a 7% conversion yield. This isolate was mostly 2- to 5-ring parent PAH with relatively low levels of alkylated and hydroaromatic PAH [9]. The neutral PAH isolate (A_2) from the ITSL recycle pasting solvent had a higher fluorenone conversion yield, 44%, and was characterized by high levels of alkylated PAH and hydroaromatic compounds. The mean molecular weight of this isolate was much higher than the SRC I process solvent [7]. The presence of significant levels of greater than 5-ring PAH in this isolate was responsible for the shift to higher average molecular weight. Larger aromatic ring systems provide greater resonance stabilization of radicals derived from PAH components of this fraction. Greater resonance stabilization energies of radicals cause lower energies of activation (E_a) for initiation and hydrogen transfer reactions which equates with increased reaction rates and higher conversions.

SUMMARY

In summary, it is evident from the data presented in this paper using the fluorenone-fluorene conversion model system that comparative assessments of recycle solvents with different chemical and physical properties are possible. The polar constituents of these process materials, the N-PAC and hydroxy-PAH, appeared to be the most efficient radical initiators and hydrogen donators. The effectiveness of neutral PAH chemical fractions as reductants was dependent on the amounts of alkylated and hydroaromatic compounds present, as well as the size distribution of aromatic ring systems which make up the fraction. The ITSL neutral PAH fraction showed a better conversion efficiency than the analogous SRC-1 fraction. The addition of a radical initiating agent, such as coal, is expected to alter the net

fluorenone conversion efficiencies of these crude solvents and solvent fractions, presumably to reflect relative hydrogen donating abilities.

ACKNOWLEDGEMENTS

This work was supported by the US Department of Energy Office of Basic Energy Sciences and Office of Fossil Energy under Contract DE-AC06-76RLO 1830.

REFERENCES

1 Choi, C.; Stock, L. M., J. Org. Chem. (in press).
2 Choi, C.; Stock, L. M., "Chemistry and Characterization of Coal Macerals"; Winans, R. E., Ed.; American Chemical Society; Washington D.C., 1984.
3 Franz, J. A.; Camaioni, D. M.; Beishline, R. R.; Dalling, D. K., J. Org. Chem. 1984, 49, 3563.
4 King, H. H.; Stock, L. M., Fuel, 1981, 60, 748.
5 Pryor, W. A., in "Organic Free Radicals"; Pryor, W. A., ed. American Chemical Society; Washington, D.C., 1978; ACS symposium series 69; pp. 33-46.
6 Sprinzak, Y., J. Amer. Chem. Soc., 1958, 80, 5449-5455.
7 Later, D. W. "Two-Stage Coal Liquefaction Process Materials from the Wilsonville Facility Operated in the Non-Integrated and Integrated Modes: Chemical Analysis and Biological Testing"; PNL-5215, NTIS, Springfield, VA, 1984.
8 Mahlum, D. D. "Chemical, Biomedical and Ecological Studies of SRC-I Materials from the Fort Lewis Pilot Plant: A Status Report"; PNL-3474, NTIS, Springfield, VA, 1981.
9 Later, D. W.; Lee, M. L.; Bartle, K. D.; Kong, R. C.; and Vassilaros, D. L.; Anal. Chem. 1981, 53, 1612-1620.

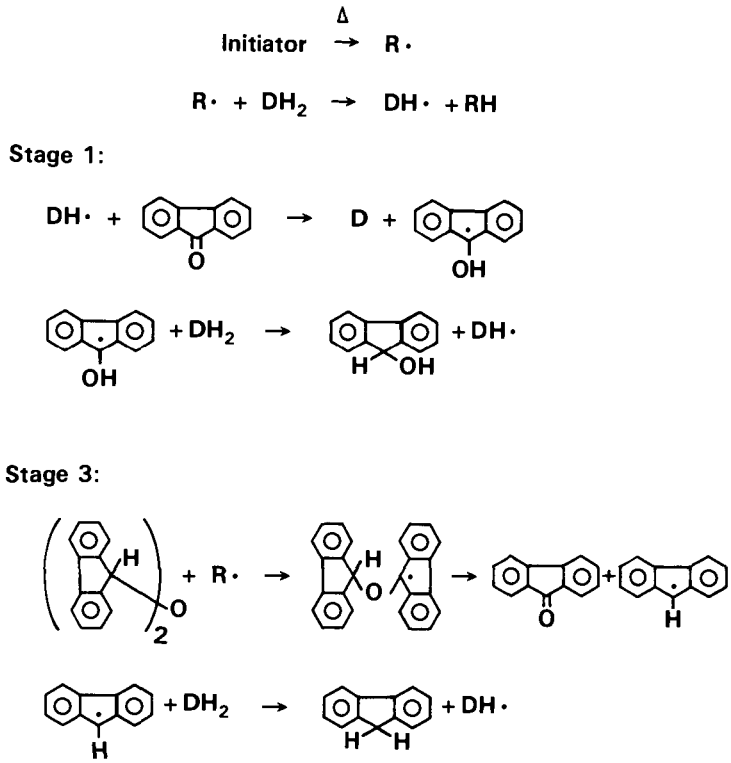

Scheme I. Radical Mechanism for the Reduction of Fluorenone by Hydrogen Donors

TABLE 1. Conversion of Fluorenone to Fluorene by Two Coal Liquids and Their Chemical Fractions

Sample	Fraction[a]	% Conversion[b]	% Recovery[c]
SRC-I Process Solvent:	Crude	38 ± 2	91
	A_1	1 ± 1	89
	A_2	7 ± 1	95
	A_3	45 ± 4	78
	A_4	43*	81*
ITSL Recycle Pasting Solvent:	Crude	88 ± 1	97
	A_1	9 ± 3	86
	A_2	44 ± 11	91
	A_3	65*	82*
	A_4	57 ± 1	78
Fluorenone Only	---	0	85

(a) Key: A_1 = aliphatic hydrocarbons; A_2 = neutral PAH; A_3 = N-PAC; and A_4 = hydroxy-PAH.
(b) % conversion is quantity of fluorene in moles versus the initial fluorenone quantity normalized to 5 mg of sample.
(c) % recovery is the sum of both fluorene and fluorenone as compared with the initial fluorenone quantity.
* Single point determination.

TABLE 2. Comparative Chemical Class Composition of Process Solvents from Two Different Direct Coal Liquefaction Technologies

	Aliphatic Hydrocarbons	Neutral PAH/ Hydroaromatic	N-PAC	Hydroxy-PAH
SRC-I Process Solvent	13.9	47.5	13.5	25.1
ITSL Recycle Pasting Solvent	25.9	41.0	21.1	12.0

THE KINETICS OF CATALYTIC HYDROGENATION OF POLYNUCLEAR AROMATIC COMPONENTS IN COAL LIQUEFACTION SOLVENTS*

H. P. Stephens and R. J. Kottenstette

INTRODUCTION

Although the importance of polynuclear aromatic hydrocarbons (PAHs) as hydrogen transfer agents in coal liquefaction has been well established (1,2), there have been few studies of the kinetics of the formation of hydroaromatic donor forms by catalytic hydrogenation. This paper presents the results of hydrogenation experiments performed with single component PAH solutions in an inert solvent and with a complex, multicomponent coal-derived liquid. The rate of hydrogenation of one PAH component found in coal-derived liquids, pyrene, was followed and used to illustrate the impact of reaction conditions on the kinetics and thermodynamics of catalytic hydrogenation of PAHs in liquefaction solvents. The results show that the catalytic hydrogenation behavior of PAHs in complex coal-derived liquids is analogous to that of a single component system. In addition, this study clearly demonstrates PAHs in coal-derived liquids can be quantitatively hydrogenated to donor-solvent products at temperatures as low as 100°C.

EXPERIMENTAL

To establish the thermodynamic behavior of the hydrogenation of pyrene to 4,5-dihydropyrene, reactions were performed over a wide range of conditions: temperatures from 275 to 400°C and pressures from 500 to 2000 psig. Subsequent kinetic experiments with pyrene and the coal-derived liquefaction solvent were performed at 100 and 300°C and hydrogen pressures of 100 and 500 psig.

Materials

Pyrene and n-hexadecane, an inert solvent for the pyrene experiments, were used as received from Aldrich Chemical Company. The coal-derived liquid studied was a hydrogenated Koppers creosote oil used as a start-up solvent in pilot two-stage coal liquefaction experiments (3). Prior to use, it was catalytically dehydrogenated under nitrogen at 425°C. This converted all but approximately 10% of the hydropyrenes to pyrene. Two catalysts were employed for these experiments. Shell 324 M, a Ni-Mo/Alumina catalyst currently used in the second stage of integrated two-stage pilot plant operations (4), was added in its presulfided form to experiments at 275°C and above. Because Shell 324 has a low activity at temperatures below 250°C, reactions performed at 100°C were

* This work supported by the U. S. Department of Energy at Sandia National Laboratories under contract DE-AC04-76DP00789.

catalyzed with a novel catalyst under development, palladium hydrous titanate (5,6). Both catalysts were added to the reactors as -200 mesh powders. High purity hydrogen was used in all experiments.

Apparatus and Procedure

Batch reactions were performed in stainless steel microreactors (7), equipped with thermocouples and pressure transducers. Four reactors could be operated simultaneously. After the reactors were charged with the reactants and catalyst, they were pressurized with hydrogen and heated to temperature (heat-up time $\approx$ 1 min) in a fluidized sand bath while being horizontally shaken at 160 cycles/min. Temperatures and pressures were recorded with a digital data acquisition system during the course of the experiments. Following the heating period, the reactor vessels were quenched (time of quench $\approx$ 10 sec), and the products were removed for analysis.

A separate set of experiments was used to establish that catalyst particle size and reactor agitation rate were sufficient to prevent reaction rate retardation due to mass transfer limitations. It was estimated from reactor heat-up and quench rates that time at temperature could be determined to within 0.5 min. Temperatures and pressures were maintained at the nominal values to within $\pm$ 2°C and $\pm$ 20 psig respectively.

Product Analyses

The products were washed from the reactor with toluene, filtered to remove catalyst and transferred to a volumetric flask. Following the addition of internal standards, 2-methylnaphthalene for the hydrogenation of pyrene in n-hexadecane and n-tridecane for the creosote oil experiments, the product solutions were brought to a known volume and analyzed by gas chromatography.

Packed column chromatography [Hewlett-Packard 5840A with flame ionization detection (FID)] was sufficient for analysis of the products from the pyrene reactions. Column and chromatographic conditions were: 1/8 in x 10 ft. column with Supelco 10% Sp-2100 on 100/120 Supelcoport, 220°C, 20 cm^3/min nitrogen carrier gas. However, separation of the product components of the creosote oil experiments required high-resolution chromatography (Hewlett Packard 5880A with FID) and a capillary column: 0.2 mm ID x 30 m long SE 54; 0.56 cm^3/min helium carrier flow; 100:1 split ratio injection; and a temperature ramp from 120 to 270°C at 2°C/min.

Gas chromatography/mass spectrometry techniques were used to identify the order of elution of pyrene and hydrogenated products. An external standard consisting of a solution of the internal standard, pyrene, n-hexadecane and 1,2,3,6,7,8-hexahydropyrene was used to establish FID response factors relative to the internal standards. The weights (W) of each

component of the product mixture were calculated from the chromatograph area (A), the response of the standard (R_s) and the relative response factor (R_r):

$$W = R_r \cdot R_s \cdot A$$

RESULTS AND DISCUSSION

Thermodynamic Behavior

Qualitative aspects of the hydrogenation of pyrene in n-hexadecane at the higher temperatures of this study can be observed in Figure 1, a plot of the ratio of 4,5-dihydropyrene (H_2Py) to pyrene (Py) concentration as a function of time for experiments performed at 300°C and 500 psig. As can be seen, $[H_2Py]/[Py]$ approaches a constant value which indicates that hydrogenation proceeds by a reversible reaction:

$$H_2 + Py \underset{k_{-1}}{\overset{k_1}{\rightleftharpoons}} H_2Py$$

Thus, the maximum (equilibrium) concentration of dihydropyrene $[H_2Py]_e$ which can be formed is limited by the hydrogen pressure P and the value of the equilibrium constant K_p for the reaction:

$$[H_2Py]_e = P\ K_p[Py]_e$$

Results of the experiments at 300°C and 500 psig with creosote oil, Figure 2, have established that the dihydropyrene to pyrene ratio exhibits a similar, though much slower, approach to an equilibrium value.

Results of more than 50 catalytic hydrogenation experiments with pyrene over a wide range of temperatures (275 to 400°C), hydrogen pressures (500 to 2000 psig) and reaction times (5 to 120 minutes) have established the temperature dependence of K_p, as calculated from the pressures and equilibrium concentration ratios of $[H_2Py]_e$ to $[Py]_e$:

$$K_p = \frac{1}{P}\ \frac{[H_2Py]_e}{[Py]_e}$$

A van't Hoff plot of these values is given in Figure 3. Linear regression of the data yields the temperature (degrees Kelvin) dependence of K_p for the hydrogenation of pyrene to dihydropyrene:

$$\ln K_p = \frac{5330}{T} - 15.86$$

Extrapolation of this equation shows that low temperature hydrogenation greatly favors the formation of dihydropyrene. For example, consider hydrogenation at 500 psig and two temperatures 400°C and 100°C. Although conversion of pyrene to dihydropyrene is limited to 15% at 400°C, equilibrium

conversion at 100°C is greater than 99%. Thus, at high temperatures pyrene hydrogenation is a reversible process, while at low temperatures, it is essentially an irreversible process. In addition, higher values of K_p at low temperatures permit a substantial reduction in hydrogen pressure to achieve comparable or better conversions.

Kinetics

For reversible reactions, the approach to equilibrium can be modeled as a first-order process with an effective rate constant equal to the sum of the forward and reverse rate constants (8):

$$\ln \frac{X_e}{X_e - X_t} = (k_1 + k_{-1})t$$

where X_t and X_e are the extents of reaction at time t and at equilibrium. For pyrene

$$X_t = \frac{[H_2Py]_t}{[Py]_t + [H_2Py]_t}$$

and

$$X_e = \frac{P\ K_p}{1 + P\ K_p}$$

Figure 4 shows a plot of ln $(X_e/(X_e-X_t))$ vs time at 300°C and 500 psig for the hydrogenation of pyrene in n-hexadecane and Figure 5 shows a similar plot for the hydrogenation of pyrene in creosote oil. As can be seen, although the rate of hydrogenation of pyrene in the complex solvent may be modeled by pseudo first-order reversible kinetics, the rate constant on a catalyst weight basis is two orders of magnitude smaller. This can be attributed to the presence of many other species in the creosote oil which compete with pyrene for active sites on the catalyst.

That catalytic hydrogenation of pyrene proceeds by an essentially irreversible reaction path at low temperatures is demonstrated by the results of experiments with pyrene in n-hexadecane catalyzed with palladium hydrous titanate at 100°C and 100 psig. Two major products, 4,5-dihydropyrene (H_2Py) and 4,5,9,10-tetrahydropyrene (H_4Py) are formed under these conditions. Initial experimentation showed that although the concentration of H_4Py increased monotonically with reaction time, the concentration of H_2Py reached a maximum, then decreased. Because this behavior indicates an irreversible series reaction path,

$$Py \xrightarrow{k_1} H_2Py \xrightarrow{k_2} H_4Py$$

the results of additional experiments (% conversion to H_2Py vs % conversion to H_4Py) were plotted on a series reaction diagram, Figure 6. An excellent fit of the data to a hyperbolic series reaction path expression was obtained:

$$Y + S(X-100) = S(Y+X-100)^{1/S}, \quad S \neq 1$$

where Y = % conversion to H_2Py
X = % conversion to H_4Py
S = selectivity = k_1/k_2 = 1.5

Therefore, the rate of disappearance of pyrene can be modeled, as shown by Figure 7, by irreversible first-order kinetics:

$$\ln \frac{[Py]_t}{[Py]_o} = k_1 t$$

where $[Py]_o$ is the initial concentration of pyrene.

That pyrene in a complex liquefaction solvent can be hydrogenated irreversibly at low temperatures was demonstrated by hydrogenation of creosote oil at 100°C and 500 psig for 30 minutes with palladium hydrous titanate catalyst. No pyrene could be detected in the hydrogenated creosote oil following the reaction. It was completely converted to hydrogenated products.

CONCLUSION

The ultimate application of this study is to provide guidance for establishing optimum conditions for hydrogenation of coal liquefaction process solvents. The results presented here show that high temperature catalytic hydrogenation of PAH hydrogen donor precursors such as pyrene is reversible and that the maximum conversion to dihydropyrene is thermodynamically limited by a low value for the equilibrium constant K_p. Because a higher value of K_p at low temperatures favors formation of the hydroaromatic product, conversion at low temperatures is kinetically limited. However, advantages of low temperature hydrogenation include quantitative conversion of PAHs to hydroaromatics and a substantial reduction of the hydrogen pressure. Additionally, this study has clearly demonstrated that satisfactory hydrogenation rates at low temperatures may be achieved by using more active catalysts, such as palladium hydrous titanate.

REFERENCES

1. D. D. Whitehurst, T. O. Mitchell and M. Farcasiu, Coal Liquefaction, Academic Press, New York (1980).

2. E. Gorin, "Fundamentals of Coal Liquefaction," p. 1845-1918, in Chemistry of Coal Utilization, 2nd Supplementary Volume, Martin A. Elliot, Ed., Wiley-Interscience, New York (1981).

3. H. D. Schindler, J. M. Chen, M. Peluso and J. D. Potts, "Liquefaction of Eastern Bituminous Coals by the ITSL Process," Proceedings of the 7th Annual EPRI Contractors Conference on Coal Liquefaction, Palo Alto, CA, May 12, 1982, Electric Power Research Institute (1982).

4. M. J. Moniz, R. S. Pillai, J. M. Lee and C. W. Lamb, "Process Studies of Integrated Two-Stage Liquefaction at Wilsonville," Proceedings of the 9th Annual EPRI Contractors' Conference on Coal Liquefaction, May 8-10, 1984, Palo Alto, CA, Electric Power Research Institute.

5. H. P. Stephens, R. G. Dosch and F. V. Stohl, Preprints of Papers, American Chemical Society, Fuel Division, Vol. 28, No. 1, p. 148 (1983).

6. H. P. Stephens, R. G. Dosch and F. V. Stohl, Ind. Engr. Chem., Prod. R&D, in press (1985).

7. R. J. Kottenstette, SAND-82-2495, Sandia National Laboratories, Albuquerque, NM, March 1983.

8. J. W. Moore and R. G. Pearson, Kinetics and Mechanisms, 3rd Ed., John Wiley & Sons, New York (1981).

FIGURE 1. $[H_2Py]/[Py]$ vs. time for hydrogenation of pyrene (100 mg) in n-hexadecane (1.0 g), 300 C, 500 psig, 15 mg 324M

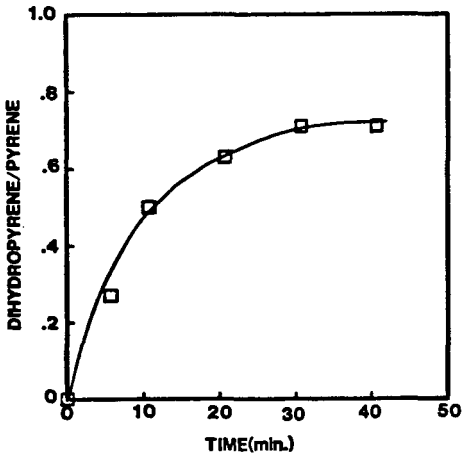

FIGURE 2. [H_2Py]/[Py] vs. time for hydrogenation of dehydrogenated creosote oil (1.0 g), 300 C, 500 psig, 100 mg 324M

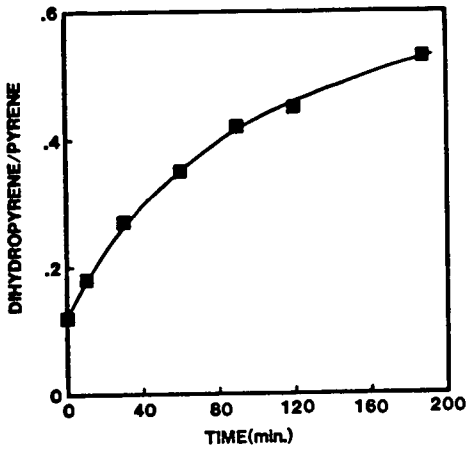

FIGURE 3. van't Hoff plot for hydrogenation of pyrene to dihydropyrene, 275 to 400 C

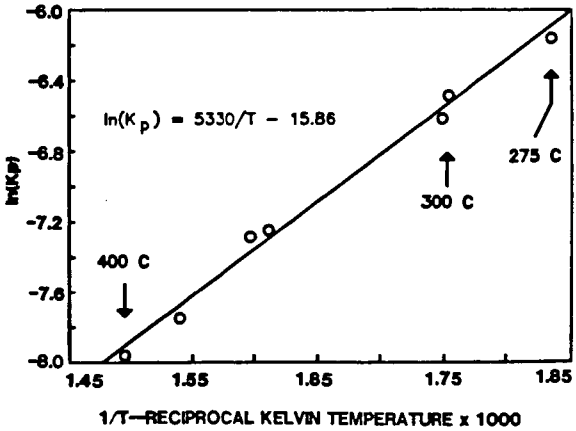

FIGURE 4. Pseudo first-order reversible kinetic plot for hydrogenation of pyrene in n-hexadecane

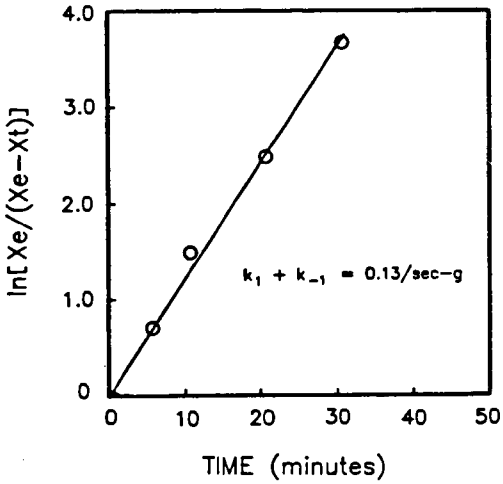

FIGURE 5. Pseudo first-order reversible kinetic plot for hydrogenation of pyrene in dehydrogenated creosote oil

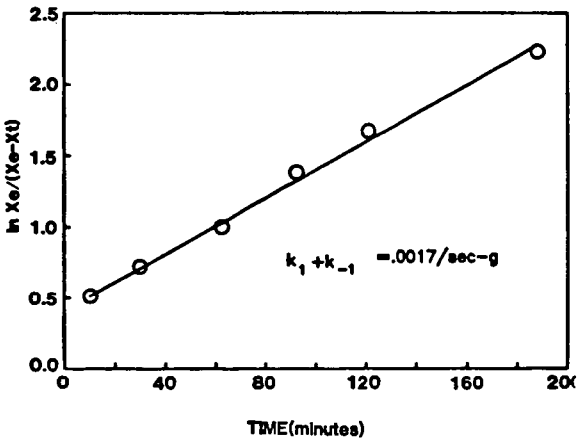

FIGURE 6. Series reaction diagram for hydrogenation of pyrene to di- and tetrahydropyrenes, 100 C, 100 psig

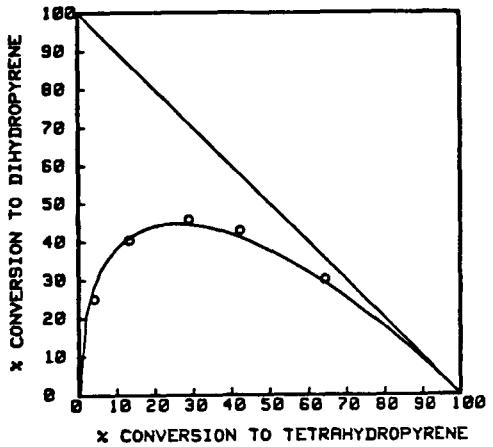

FIGURE 7. Irreversible kinetic plot for hydrogenation of pyrene (100 mg) in n-hexadecane (1g), 100 C, 100 psig, 18 mg Pd titanate

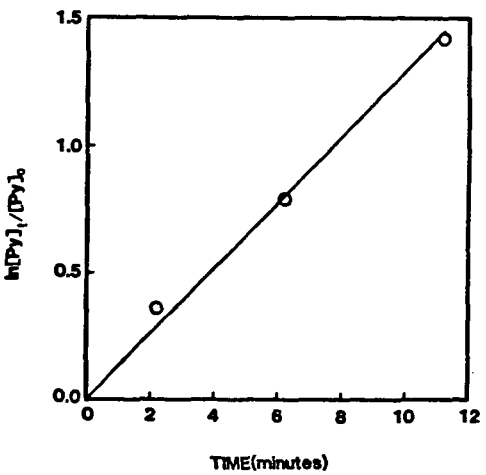

COAL LIQUEFACTION WITH ^{13}C LABELLED CARBON MONOXIDE

S.A. Farnum, A.C. Wolfson, D.J. Miller,
G.E. Gaides, and D.D. Messick

University of North Dakota Energy Research Center
Box 8213, University Station
Grand Forks, North Dakota 58202

Low-rank coals may be successfully liquefied under pressure using CO or mixtures of CO and H_2O or CO and H_2. Following a suggestion in the literature in 1921 (1), Appel and Wender in 1968 reported conversions of both bituminous coal and lignite with CO/H_2O (2). The reaction with lignite was found to be rapid, converting 1:1 lignite/H_2O to benzene-soluble tar plus gases in 87% yield (maf) coal at 2,000 psi initial CO pressure and 380°C. Successful continuous liquefaction of lignite in a Process Development Unit for 28 day runs was demonstrated by Severson and co-workers at the University of North Dakota Chemical Engineering Department's Project Lignite (3, 4). During these runs the wet, as-received coal was processed with 50/50 CO/H_2 (syngas) at about 440°C and 2,500 psig. The heavy product prepared was called "Solvent-Refined Lignite", SRL. Batchelder and Fu evaluated some of the syngas technology in 1979 with respect to process commercialization (5).

The University of North Dakota Energy Research Center has continued to investigate low-rank coal liquefaction using mixtures containing CO. The use of H_2S along with syngas has resulted in much improved processing (6). Recently, low temperature reactions (below 400°C) using CO as the reductant have shown exceptional promise (7).

Several mechanisms for reduction reactions with CO have been proposed. Previous studies at UNDERC have shown that CO apparently reacts more rapidly with coal than does H_2, and that the amount of CO that reacts increases as more as-received lignite is added (8). Whether the CO reacts directly with the coal organic structure or with the water in the coal to produce H_2 *in situ*, is unknown. The catalytic effect of coal ash on the shift reaction ($CO + H_2O = CO_2 + H_2$) may also be a significant factor. Finally, it has been suggested that hydrogen formed from closely bound coal water may be especially active "nascent hydrogen" (2, 9).

We carried out a high temperature study of the reaction of isotopically labelled syngas ($^{13}CO/H_2$) with a Texas lignite at 450°C and 3400-3700 psi in coal-derived solvent (10). This study was designed to determine the amount of CO incorporation into the distilled products and hydrocarbon gases. No incorporation of the ^{13}C was seen, thus eliminating Fischer-Tropsch type reactions, and direct incorporation reactions, such as carbonylation reactions. The only labelled product found was $^{13}CO_2$. At that time we did not examine the insoluble products for ^{13}C incorporation.

The present study was designed to investigate low temperature reactions of three coals of differing rank, Big Brown Texas lignite, Wyodak subbituminous, and Powhatan bituminous coal, with pure CO. The conditions chosen also provide baseline data simulating the first stage in a two-stage liquefaction process. Additional development of analytical methods insured that each part of the product could be examined for ^{13}C incorporation and the gases were more carefully analyzed for $^{13}C/^{12}C$ ratios in each gaseous carbon-containing product by GC/MS.

Experimental

Reactions were carried out in a multiple minireactor assembly designed for simultaneous use of up to twelve 22 mL tubes. The stainless steel tubes each contained a stainless steel stirring bar which mixed slurry and gases when the assembly was agitated in a fluidized sand bath. Five grams of a 40% as-received coal slurry in a coal-derived recycle solvent distillate was charged. Labelled gas, 50/50

$^{13}CO/CO$, or unlabelled CO gas was introduced, via a manifold system, to a pressure of 1,000 psig cold. The assembly was lowered into the bath preheated to the selected temperature, 300°, 340°, or 380°C for 1 hour, rapidly quenched to room temperature, and allowed to equilibrate. Gas weight was obtained by collecting the gas in a preweighed evacuated bomb of known volume relative to the reaction vessel.

The analysis scheme used is outlined in Figure 1. Gas analyses were performed using an automated refinery gas analyzer and $^{13}C/^{12}C$ ratios for the gaseous products were obtained using capillary GC/MS.

A portion of the recovered product was extracted with tetrahydrofuran (THF) and a second portion was microdistilled. A third portion of the recovered product was extracted with CH_2Cl_2 and the solvent was removed with a rotary evaporator at room temperature. A 50 MHz ^{13}C NMR spectrum was obtained for the CH_2Cl_2 soluble fraction using a gated pulse sequence with the decoupler on only during data acquisition. Samples in CD_2Cl_2 with TMS and $Cr(AcAc)_3$ present were pulsed about two hours until the signal to noise ratio was adequate. These spectra were compared with those of samples from reactions performed in the same manner with unlabelled CO. The CH_2Cl_2 insoluble products were examined by 50 MHz Cross Polarization/Magic Angle Spinning (CP/MAS) solid ^{13}C NMR employing total sideband suppression using TOSS dephasing and foldback pulsing before acquisition (11). These spectra were also compared with those of products from reactions run at the same time with unlabelled CO.

Results and Discussion

The weights of product gas, THF insolubles, distillation residue, water, and ash were used to calculate conversions for these reactions. For the purpose of this experiment ^{13}CO and CO were assumed to react at the same rate so that labelled and unlabelled runs could be averaged to obtain yield structures (Table I). The low-rank coals gave better conversion at 300°C but the Powhatan bituminous coal gave better conversions at 340° and 380°C.

Tracer reactions with ^{13}CO are expected to give easily recognizable labelled products because the natural abundance of ^{13}C is only 1.1%. An incorporation of 1% ^{13}C should double the signal. When identical samples for runs with unlabelled CO are compared, an incorporation of only 0.5% should be recognized without difficulty.

The ^{13}C spectra of the soluble and the insoluble products of labelled reactions were carefully compared with those run without labelled CO. No differences were seen for any of the three coal products at 300°, 340°, or 380°C. A comparison of the CH_2Cl_2 insoluble solid spectra from runs using labelled and unlabelled CO are shown in Figure 2.

Gas analyses for selected runs analyzed by capillary GC/MS and GC were used to determine the ratios of ^{13}CO to ^{12}CO and $^{13}CO_2$ to $^{12}CO_2$ and the number of moles of each isotopic compound in the product. The number of moles of CO_2 that was produced from CO was easily calculated since a 50% labelled ^{13}CO was used. The remaining CO_2 produced was assumed to arise from the coal, the only other carbon source present. The number of moles of H_2 found in the product was less than 1/5 the moles of CO_2 formed from CO during the reaction of the two low-rank coals at 300°C. However, during reaction of the bituminous coal, Powhatan (POW1), less CO_2 was formed from the CO added (Figure 3), possibly because the number of moles of water present in the charged coal, POW1, was much smaller, which could limit the shift reactions during the POW1 liquefaction at 300°C. The absence of coal moisture does not, however, limit the conversion of POW1 by CO at higher temperatures, since water may be released by coal thermolysis at 340° and 380°C which could react readily with CO (12).

Table I. Multiple Minireactor Reactions of CO With 40% Coal Slurries for 60 Minutes

No. Runs Averaged	Coal	Temperature, °C	Average Yield (wt % of maf coal) Conversion	Gas	Distillate	Soluble Residuum	Average Closure
5	BB1*	300	20	13.5	3.6	8	92
3	WYO1**	300	24	18	3.7	16	95
3	POW1***	300	16	4.3	6.4	14	96
2	BB1	340	62	24	11.8	27	95
1	WYO1	340	51	30.5	2.0	17.5	94
2	POW1	340	83	29	6.2	46	88
2	BB1	380	77	2	9.3	40	92
2	WYO1	380	72	39	-3.0	35	95
2	POW1	380	87	26	1.9	59	101

Solvent was UNDERC CPU Run 66 D1160 Distillate.

*BB1 - Big Brown Texas lignite, 8.12% ash, 24.40% water.
**WYO1 - Wyodak, Wyoming subbituminous coal, 8.37% ash, 24.03% water.
***POW1 - Powhatan, Ohio bituminous coal, 10.78% ash, 2.02% water.

Summary

No ^{13}C incorporation into products other than CO_2 was detected after reactions of Big Brown Texas lignite, Wyodak subbituminous coal, or Powhatan bituminous coal with 50/50 $^{13}CO/CO$ at 300°, 340° or 380°C in recycle solvent for 1 hour. No evidence for a Fischer-Tropsch type mechanism, CO insertion, or carbonylation reactions was found.

These data are consistent with a mechanism involving CO entering into the shift reaction with *in situ* water. The differing response of the coals can be explained by invoking coal ash liquefaction and shift catalysis and the amount of water intimately connected with each coal (13, 14). The change in response by Powhatan at higher temperatures may be due to a shift mechanism initiated by water released from thermal reactions (12). The success of low temperature CO liquefaction would not be unexpected if a shift reaction mechanism were in operation since the equilibrium constant for the shift reaction favors H_2 and CO_2 at lower temperatures.

Acknowledgment

UNDERC carried out this work for the U.S. Department of Energy under Cooperative Agreement No. DE-FC21-83FE60181.

Literature Cited

1. Fischer, F. and Schrader, H., 1921, Brennstoff - Chem. 2, 257. (cf. Ref. 2).
2. Appell, H.R. and Wender, I., 1968, Am. Chem. Soc. Div. Fuel Prepr. 12(3), 220.

3. Severson, D.E., Souby, N.M. and Baker, G.G., 1977, Am. Chem. Soc. Div. Fuel Prepr. 22(6), 161.
4. Severson, D.E., Souby, A.M. and Owens, T.C., 1982, "Energy Sources", Vol. 6, No. 3, 173, Crane, Russak and Co., Inc.
5. Batchelder, R.F. and Fu, Y.C., Ind. Eng. Chem. Process Des. Dev., 1979, 18(4), 594.
6. Sondreal, E.A., Willson, W.G. and Stenberg, V.I., 1982, Fuel, 61, 925.
7. Rindt, J.R. and Cisney, S.J., "Low-Temperature Liquefaction of North Dakota Lignite", DOE/FE/60181-21.
8. Knudson, C.L., Willson, W.G., and Baker, G.G. Am. Chem. Soc. Div. Fuel Prepr., 1981, 26(1), 132.
9. Takemura, Y. and Ouchi, K., 1983, Fuel, 62, 1133.
10. Low-Rank Coal Research Under the UND/DOE Cooperative Agreement, Quarterly Technical Progress Report, April - June 1983, DOE/FE/60181-17, 5-17-5-24.
11. Dixon, W.T., Schaefer, J., Sefik, M.D., Stejskal, E.O. and McKay, R.A., 1982, J. Mag. Reson. 49, 341.
12. Suuberg, E.M., Peters. W.A., and Howard, J.B., in "Thermal Hydrocarbon Chemistry", Advances in Chemistry Series, 183, 1979, Chapter 14, American Chemical Society, Washington, D.C.
13. Lee, J.M., Tarrer, A.R., Guin, J.A., and Prather, J.W., 1977, Am. Chem. Soc. Fuel Div. Prepr. 22(6), 120.
14. Given, P.H. Cronauer, D.C., Spackman, W., Lovell, H.L., Davis, A. and Biswas, B., 1975, Fuel, 54, 34.

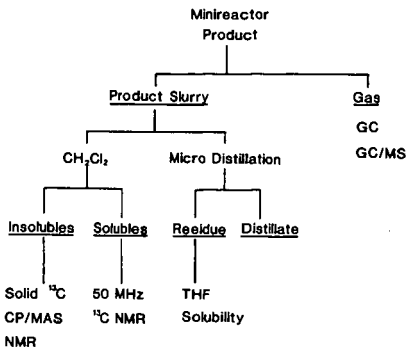

Figure 1. Analysis scheme for minireactor products.

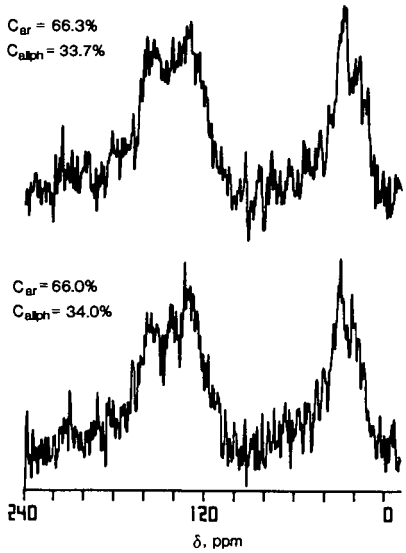

Figure 2. 50 MHz CP/MAS ^{13}C NMR Spectra of insoluble heavy ends from CO reaction with Big Brown lignite (top) and 50/50 $^{13}CO/CO$ reaction with Big Brown lignite (bottom).

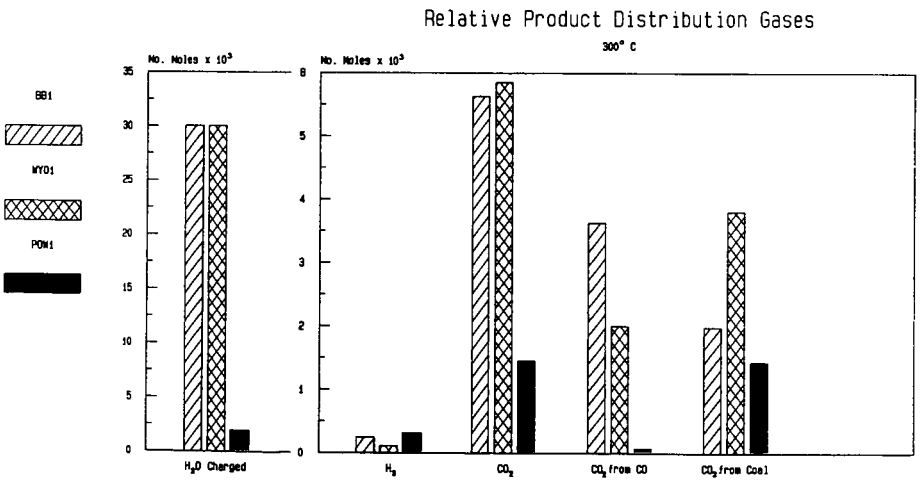

Figure 3. Gaseous product distribution at 300°C from reactions with 50/50 $^{13}CO/O$.

WATER-ASSISTED AND NONDONOR-VEHICLE-ASSISTED COAL LIQUEFACTION

B.D. Blaustein, B.C. Bockrath, H.M. Davis, S. Friedman, and E.G. Illig

Pittsburgh Energy Technology Center
U.S. Department of Energy
Pittsburgh, PA 15236

and

M.A. Mikita

Department of Chemistry
University of Colorado at Denver
Denver, CO 80202

In continuous coal liquefaction operations, the recycle vehicle has several functions. First, it serves as the medium in which to slurry the fresh coal feed and transport it through the preheater into the reactor. Second, it often acts as a source of hydrogen, i.e., it is a hydrogen donor. Much of the chemistry of coal liquefaction can be explained by reactions of hydrogen-donor vehicles with coal or the free radicals generated by thermolysis of coal. In the usual coal liquefaction process, much of the liquid product serves as recycle vehicle, since the slurry fed to the reactor is typically two parts recycle vehicle to one part coal. The throughput of coal for a given reactor might be increased if a lesser quantity of a readily available material could be substituted for the coal-derived recycle vehicle. One possible substitute would be water, at least as far as acting as a slurry medium for fresh coal feed.

Water has been used in the past in the liquefaction or the extraction of coal for a variety of reasons. When used in combination with carbon monoxide and a suitable catalyst, water was a source of hydrogen for the reduction of coal [1,2]. In this work, an organic solvent was frequently used in combination with water. Liquefaction under carbon monoxide has also been carried out with slurries composed of coal and either water or aqueous base without an organic solvent [3,4]. In some cases, water served to carry dissolved metal salts used as homogeneous catalysts as well as acting as the liquefaction medium [5]. Thus, the elimination of coal-derived recycle solvents commonly used in liquefaction in favor of water -- a simple, cheap, and readily available substitute -- has already been accomplished in the laboratory. In comparison with conventional organic liquefaction solvents, water has been shown to be quite effective when used in combination with H_2S, in particular under synthesis gas rather than hydrogen [6]. Aqueous liquefaction using impregnated catalysts has also been combined in a single operation with supercritical water distillation to separate the oil and asphaltene from the coal char residue [7]. The results clearly show that the liquids produced by hydrogenation can be extracted by supercritical water and transported away from insoluble coal residues. It has also been shown that the simple treatment of coal with supercritical water in the absence of hydrogen or catalysts renders a substantial portion of the treated coal extractable by tetrahydrofuran after the product was cooled and recovered from the autoclave [8]. The amount of extract obtained depended on the density of the supercritical water. Higher yields were obtained when coal was injected into supercritical water, thus providing a rapid heat-up of the coal, than when a coal-water slurry was heated to operating temperature. From these extraction studies, it is apparent that water is able to assist the diffusion and dispersal of liquefaction products and reactants. In addition to these roles, it has also been reported that water may directly participate as a reactant in the thermolytic chemistry of certain model

compounds. In the presence of water, dibenzyl ether decomposes at 400°C by both pyrolytic and hydrolytic pathways, the latter leading to the formation of benzyl alcohol [9]. The removal of nitrogen from heterocyclic compounds, such as isoquinoline, was also reported to be accelerated in the presence of supercritical water [10].

Taken together, these studies indicate that under various conditions, supercritical water may act as a good liquefaction medium, dissolve or extract coal-derived liquid products, promote the cleavage of certain bonds likely to be found in coal, provide hydrogen through the water-gas shift reaction, and possibly assist the contacting of coal with catalysts or hydrogen. It has also now been made clear by the successful preparation of coal-water mixtures for direct combustion that pumpable slurries can be made at ambient conditions using as little as 30% by weight of water. The present study is intended to evaluate further the role of water, near or above its critical temperature, in the conversion of coal to a liquefaction product. Specifically, we wish to determine whether it is possible, feasible, and, finally, advantageous to use water as a replacement for all or part of the recycle vehicle used for slurrying coal in conventional liquefaction practice. Since water is not a hydrogen donor in the usual sense, the behavior of other nondonors was also examined. It should be pointed out that for coal hydrogenation alone, no vehicle is needed. Much of the previous work on coal hydrogenation was done by simply subjecting dry powdered coal in batch units to a high pressure of gaseous hydrogen, sometimes under the influence of an impregnated catalyst [11].

EXPERIMENTAL

A multireactor consisting of five individual microautoclaves, each of approximately 45-mL capacity and attached to a single yoke, was used to study these reactions [12]. The entire assembly was immersed rapidly into a preheated, fluidized sand bath, allowing heat-up to reaction temperature in 4-6 minutes. Immersion in a second fluidized sand bath held at room temperature provided rapid quenching. The autoclaves were agitated by a rapid horizontal-shaking motion, assuring good mixing of heterogeneous, multiphase mixtures. Individual thermocouples allowed continuous temperature monitoring of each microautoclave. For all experiments reported here, the reactors, once pressurized, were isolated from the gas-handling manifold by a valve and a short length of tubing of negligible volume. This prevented loss of water from the reaction zone due to condensation in the unheated portion of the system. Separate experiments using different reactors, in which it was possible for water to migrate to unheated regions of the system, indicated that such water loss had a profound but erratic effect on measured values for pressure and coal conversion, and generally led to misleading data.

The pressure at reaction temperature was not measured directly in these experiments. Using van der Waal's equation, the partial pressure of water was estimated as 1700 psi at 385°C in those cases where 1.7 g of water was charged. When 3.4 g was charged, the partial pressure was estimated at 2670 psi. At this temperature, the partial pressure due to hydrogen is estimated to be about 2600 psi. Total pressures are thus about 4300 psi or 5300 psi. The density of supercritical water was 0.05 g/mL when 1.7 g was charged and 0.11 g/mL when 3.4 g was charged.

Table 1 gives the analyses of the Illinois No. 6 (River King Mine) bituminous coal and the vehicles used in these experiments.

Most of the conversion values were obtained by the centrifugation method given below. Conversions for run 13 and the three series HD2, HD3, and HD4 were determined by a somewhat different method based on filtration of the insolubles.

TABLE 1. Elemental Analyses of Coal and Vehicles.[a]

Material	C	H	N	O	S
Illinois No. 6 Coal, River King Mine[b]	73.7	5.6	1.5	14.8	4.5
SRC-II Distillate	87.1	8.0	1.4	3.0	0.4
Lummus Vehicle[c]	89.8	6.8	1.0	1.8	0.5

[a] wt.%, daf basis, Huffman Labs, Wheatridge, Colo.

[b] Moisture-free ash content was determined to be 13.6 wt.% for the River King Coal. As used, the coal contained 3 wt.% water.

[c] Obtained from operations of the integrated two-stage Lummus liquefaction plant at Bloomfield, N.J., on Illinois No. 6 coal.

Separate experiments established that similar values were obtained by both methods.

Following gas collection and measurement via water displacement, the reactors were washed out with tetrahydrofuran (THF) together with physical scraping of the reactor walls. The THF was distilled before use to remove the inhibitor. The reactor and contents were sonicated to aid the dissolution and/or dispersion of the products in THF. This was repeated until the THF solution was clear and the reactor tare weights before and after reaction agreed to within ±0.01 gram. The total volume of THF so accumulated (~300 mL) was evaporated in a hood to a volume of about 50 mL and transferred to a tared 250 mL centrifuge bottle. Additional THF was added to bring each volume up to ~150 mL, and the bottles were centrifuged at 3500 rpm for 20 minutes. The THF solution was then decanted and an additional 150 mL of THF was added to each residue in the bottle with stirring. This centrifugation/decantation/solvent addition sequence was repeated until the opaque solution became amber and opalescent. Experience indicated that such a process was necessary twice in the higher conversion runs and up to 5 times with lower conversions. The residues (THF-insolubles) were then dried overnight in their bottles in a vacuum oven at 110°C under an aspirator-maintained vacuum. The oven was purged with nitrogen until the temperature was below 60°C, and the bottles with residues were allowed to cool in air and were then weighed. The percent conversion was equal to

$$100 - \frac{\text{wt. THF-insoluble residue - wt. ash}}{\text{wt. moisture, ash-free coal}} \times 100$$

The reproducibility was usually within 1-2%.

The THF solutions obtained from the above procedure were roto-evaporated under an aspirator vacuum in tared, 250-mL round-bottom flasks. When no more solvent was seen to condense, the flasks were dried and the THF-soluble products were thus obtained. In some cases, cyclohexane solubles were isolated using a similar procedure. The THF extracts were transferred to 250-mL centrifuge tubes with 25.0 ± 1 mL of hot THF with the aid of sonication. To these solutions, 125 mL of cyclohexane was added and the centrifugation process employed, followed

by a second extraction with an additional 150 mL of pure cyclohexane. The extracts were recovered by roto-evaporation of the solutions and drying in the vacuum oven at 110° overnight.

For a typical run, the gas analysis showed CO_2 and H_2S were the major gases produced, along with the much lesser amounts of methane, ethane, and propane. The yields for one run were 4.2 wt.% for CO_2, and 0.3 wt.% each for methane, ethane, and propane, on a daf coal basis.

In experiments 6E and 6F of Table 3, where a coal/water/catalyst slurry was used, the procedure was as follows. Catalyst was added to 8.5 mL of solution of 200 ppm Aerosol OT surfactant (American Cyanamid) in water in a round-bottom flask, and the mixture slowly added to 10 g coal with physical mixing, followed by immersion in a sonic bath for 5 minutes, followed by rotation on a roto-evaporator at atmospheric pressure while submerged in a ice bath for 15 minutes. This slurry did not appear to settle with time. The slurry was mixed by hand again just prior to transfer of 7.4 g to the microautoclave. In experiment 6D, an aqueous solution of catalyst was added to the coal in the autoclave; and in 6G, 6H, and 6J, a solution of catalyst containing 200 ppm Aerosol OT was added. In experiment 6K, a slurry made as in 6E and 6F above was dried in a vacuum oven before use. In experiment 6I, such a dried slurry was added to the autoclave with fresh water.

RESULTS AND DISCUSSION

Table 2 shows the results of runs made to measure conversion of Illinois No. 6 (River King Mine) bituminous coal under a variety of conditions selected to uncover effects of water addition. Since this work was directed toward replacing or reducing the amount of organic recycle vehicle normally employed, all of the experiments reported here were conducted with the relatively low vehicle-to-coal ratios of 0.5 or less. Experiments with higher ratios showed no better conversions. As may be seen, without addition of water, conversions for these high coal-content slurries are quite low at the very moderate reaction temperatures employed. The addition of 0.42 parts water based on coal (the amount contained in a 70/30 coal/water slurry) increases conversion significantly. Evidently, reasonable conversions can be obtained using this minimal amount of water provided the loading of recycle vehicle is not too low, that is 1.6 g or above in the case of HD3-1, -2, and -3. We also note that under these mild, non-catalytic conditions the nature of the reducing gas had little effect, since in one experiment (HD4-2), the substitution of carbon monoxide for hydrogen had little effect on the conversion. The use of the more severe conditions of 1200 psi hydrogen (cold) and 427°C produced a small increase in conversion as expected (13 and HD2-3). However, variables other than reaction severity may have more significant effects, since still higher conversions were obtained at 385°C by appropriate choice of the organic vehicle, as discussed later.

A second series of experiments was run under conditions chosen to reveal the effect of the nature of the organic vehicle used in noncatalytic aqueous liquefaction. In a general way, conversions increased moderately as the organic vehicle was changed from one usually considered to be a poor hydrogen donor (1-methylnaphthalene) to vehicles considered to be better hydrogen donors (tetralin and 9,10-dihydroanthracene). Thus, the usual concepts of hydrogen-donor liquefaction chemistry may also be applied usefully to this series of less conventional liquefaction systems.

If good conversion in a noncatalytic system requires a minimal amount of an organic vehicle and also benefits from the addition of some water, it is reasonable to ask if the combination of organic vehicle and water is superior to either used separately. The final set of experiments in Table 2 indicates that this is the case. Conversion was poor without either (HD29-4), much improved with water alone (HD29-3), and still better with SRC-II distillate vehicle alone

(HD19-3,4). A combination of SRC-II distillate and water (HD18-3,4) produced a conversion better than either used separately.

Cyclododecane is a high-boiling hydrocarbon expected to be a poor hydrogen donor. When it was used as a nondonor vehicle, the conversion fell between the value for water and that for SRC-II distillate used in a lesser amount. When used in combination with SRC-II distillate, the conversion was not improved over that of SRC-II distillate alone. This stands in contrast to the result obtained for the combination of SRC-II distillate plus water. This different behavior indicates that addition of the second component to SRC-II distillate is not acting simply to dilute the relatively small amount of the recycle vehicle used in these experiments.

Table 3 contains data for the catalytic liquefaction of coal in the presence of water. When various forms of molybdenum are added to the coal, conversions are substantially increased. Clearly, high temperatures are not required for these molybdenum catalysts to influence liquefaction. More important, with catalyst present, the organic vehicle may be totally replaced by water without loss in conversion. As was seen in Table 2, this result was not obtained in the absence of catalyst. The important function of water is also underscored by the rather low conversion obtained with added catalyst but with no vehicle of any kind, i.e., a dry hydrogenation (6K).

Conversion increases continually with catalyst loading up to at least 1000 ppm molybdenum on coal (6A, HD30-1, -2, -3). Of the several methods used for application of the catalyst, none seemed to give notably superior results insofar as THF conversion values are concerned. However, there are indications now under study that the yield of lighter products may change significantly according to the method of catalyst application.

The surfactant, Aerosol OT, used to assist the preparation of coal/water/catalyst feed slurries had a small beneficial effect on conversion in both the presence of catalyst (HD30-4 vs. HD30-1) and the absence of catalyst (HD29-3 vs. 6A). At this point, it is only possible to speculate that the surfactant enhances the action of the water by improving the wetting of the coal.

In one case (6F), a low-boiling ether, THF, was substituted for water. The conversion was unexpectedly high, albeit the catalyst loading was twice that used with water. Tetrahydrofuran is quite effective in swelling River King coal at room temperature. The connection between this property and the liquefaction result is presently unclear, but investigation of a series of lower molecular weight vehicles may shed more light on the structural requirements for superior performance. These and related experiments are in progress.

Table 4 gives the data for analyses of the THF-solubles isolated from runs HD19-1,2 in which 1000 ppm Mo was used as catalyst in conjunction with surfactant. Except for the higher-than-usual oxygen content, these are typical analyses for a coal liquefaction product. The infrared spectrum of the cyclohexane solubles obtained from a dilute CH_2Cl_2 solution shows that about 2.1 wt.% of oxygen is in phenolic OH and the remaining 5% is presumably in ethers. The carbon aromaticity of the THF solubles was determined by ^{13}C-CP/MAS NMR to be 0.72, which is virtually identical to that of the feed coal. The data for characterization of the products in hand so far are in accord with the rather mild conditions used to bring about the conversions.

The preliminary results obtained so far form a basis for an encouraging outlook on liquefaction with water or other nondonor vehicles. High coal conversions were obtained at modest temperatures with use of little or no organic recycle vehicle. Thus, it is possible and feasible to use water as a substitute liquefaction medium. The advantage in doing so in continuous units is still to be

TABLE 4. Elemental Analyses and Molecular Weights of HD19-1,2 Product Fractions.[a]

Elemental Analysis (wt.%)[b]	Cyclohexane Solubles	Tetrahydrofuran Solubles[c]	Tetrahydrofuran Insolubles[c]
C	82.9	81.8	24.5
H	7.3	5.9	1.4
O	7.1	7.3	7.5
N	1.2	1.9	0.5
S	1.8	1.9	6.9
Ash (wt.%), 750°C	---	---	66.2
Molecular Weight, $\bar{M}_n$		1300[d]	

a Huffman Laboratories, Wheatridge, Colo.

b Average of duplicate microanalyses.

c Dried to constant weight @ 30°C under vacuum before analysis.

d VPO in pyridine at 90°C.

demonstrated. At the least, a different line of investigation is now open whereby important questions regarding the mechanism of liquefaction may be addressed. Since no organic vehicle need be used, the coal-derived products of liquefaction may be analyzed without interference. At the same time, the presence of a fluid medium provides better heat transfer and better dispersion of the reactants than possible with dry hydrogenations. It is expected that further work will be fruitful by determining how the course of liquefaction is affected by the chemical and physical properties of water or other nondonors and by uncovering the important variables associated with the use of dispersed catalysts at mild liquefaction temperatures.

TABLE 2. Liquefaction of Illinois No. 6 (River King Mine) Bituminous Coal.[a]

Run Number(s)	H_2 Pressure cold, psig	Temp., °C	Time at Temp., min.	Vehicle g.	Vehicle Type	H_2O g.	Conv.[b] %	Notes
HD3-5	800	370	60	1.62	LUM	0	55	Lummus vehicle
HD3-4	800	370	60	2.00	LUM	0	67	
HD3-3	800	370	60	1.29	LUM	1.70	61	
HD3-2	800	370	60	1.60	LUM	1.70	80	
HD3-1	800	370	60	2.00	LUM	1.70	79	
HD4-2	800(CO)	370	60	1.60	LUM	1.72	82	
13,HD2-3,4	1185	427	60	1.98	LUM	1.70	86,87	
HD10-3,4	1200	385	40	1.50	MEN	1.70	77,79	1-Methylnaphthalene
HD10-1,2	1200	385	40	1.50	LUM	1.70	82,84	
HD12-3,4	1200	385	40	1.50	SRC-II	1.70	85,87	SRC distillate
HD12-1,2	1200	385	40	1.50	TET	1.70	88,90	Tetralin
HD15-1,2	1200	385	40	1.50	DHA	1.70	91,93	9,10-Dihydroanthracene
HD29-4	1200	385	30	0	---	0	25	
HD29-3	1200	385	30	0	---	3.4	52	
HD19-3,4	1200	385	30	1.50	SRC-II	0	72,74	
HD18-3,4	1200	385	30	1.50	SRC-II	1.7	86,88	
HD29-2	1200	385	30	3.4	CDOD	---	67	Cyclododecane
HD29-1	1200	385	30	1.50	SRC-II	1.7 CDOD	72	Cyclododecane

[a]Coal charge in each case was 4.0 g.

[b]Based on THF extractions.

TABLE 3. Catalytic Experiments and Associated Base Cases in Water-Assisted Liquefaction of Illinois No. 6 Coal.[a]

Ex. #	Vehicle	Water, g.	Catalyst[b]	Precursor/Application[c]	THF Conv.
6C	SRC II	1.7	----		86,88
6D	SRC II	1.7	1000 ppm Mo	aqueous sol. $MoS_4^{=}$	90,92
6E	SRC II	1.7	1000 ppm Mo	NH_4 molybdate/sol. slurry	89,91
6F	SRC II	1.7, THF	2000 ppm Mo	$Mo_2(OAc)_4$/sol. slurry	90
6A	--	3.4	----	surfactant	67
6G	--	3.4	1000 ppm Mo	$MoS_4^{=}$/surfact. soln.	86,90
6H	--	3.4	1000 ppm Mo	NH_4 molybdate/surfact. soln.	85,87
6I	--	3.4	1000 ppm Mo	$MoS_4^{=}$ impreg. coal, then water	91
6J	--	3.4	1000 ppm Mo	$MoS_4^{=}$/surfact. soln.	89,91
6K	--	---	1000 ppm Mo	NH_4 molybdate impreg. coal	76,78
HD30-1	--	3.4	1000 ppm Mo	NH_4 molybdate/surfact. soln.	87
HD30-2	--	3.4	250 ppm Mo	NH_4 molybdate/surfact. soln.	80
HD30-3	--	3.4	100 ppm Mo	NH_4 molybdate/surfact. soln.	73
HD30-4	--	3.4	1000 ppm Mo	NH_4 molybdate/aqueous soln.	84

[a] Reaction conditions: 4.00 g River King coal; 385°C; 30 minutes at temperature; 1200 psig (cold) hydrogen, using 1.50 g SRC-II distillate where indicated.

[b] ppm metal on coal. See Experimental Section for details.

[c] When the use of a surfactant is indicated, aerosol OT was employed at ≈200 ppm in water.

REFERENCES

[1] H.R. Appell, I. Wender, and R.D. Miller, Chem. Ind., 1703 (1969).

[2] H.R. Appell, Energy, 1, 24 (1976).

[3] D.S. Ross and J.E. Blessing, Fuel, 57, 379 (1978).

[4] D.S. Ross, J.E. Blessing, Q.C. Nguyen, and G.P. Hum, Fuel, 63, 1206 (1984).

[5] D.S. Ross, Q.C. Nguyen, and G.P. Hum, Fuel, 63, 1211 (1984).

[6] V.I. Stenberg, R.D. Hei, P.G. Sweeny, and J. Nowok, Am. Chem. Soc. Div. Fuel Chem. Preprints, 29(5), 63 (1984).

[7] P. Barton, Ind. Eng. Chem., Process Des. Dev., 22, 589 (1983).

[8] G.V. Deshpande, G.D. Holder, A.A. Bishop, J. Gopal, and I. Wender, Fuel, 63, 956 (1984).

[9] M.E. Paulaitis, M.T. Klein, and A.B. Stilles, DOE Quarterly Report, DE-FD22-82PC50799, July-September, (1983).

[10] D.M. Tiffany, T.J. Houser, M.E. McCarville, and M.E. Houghton, Am. Chem. Soc. Div. Fuel Chem. Preprints, 29(5), 56 (1984).

[11] C.O. Hawk and R.W. Hiteshue, "Hydrogenation of Coal in the Batch Autoclave," U.S. Dept. of the Interior, Bureau of Mines, Bulletin 622, (1965).

[12] R.R. Anderson and B.C. Bockrath, Fuel, 63, 329 (1984).

ACKNOWLEDGMENT

M.A. Mikita was a Faculty Research Participant for the summer of 1984 and was appointed to the Pittsburgh Energy Technology Center by Oak Ridge Associated Universities. The authors wish to thank the personnel from the PETC Division of Coal Science for careful analyses of the various materials and products.

DISCLAIMER

Reference to a brand or company name is made to facilitate understanding and does not imply endorsement by the U.S. Department of Energy.

AQUEOUS LIQUEFACTION OF ILLINOIS NO. 6 COAL

Bogdan Slomka, Tetsuo Aida,
and Thomas G. Squires

Ames Laboratory*
Iowa State University
Ames, Iowa 50011

INTRODUCTION

Near its critical point (T_c = 374°C, P_c = 218 atm.), water is a good solvent for organic (1) as well as inorganic materials while, at ambient conditions, most organics are insoluble in water. Water is also thermally stable, even at temperatures above 450°C, and has a large heat capacity. Finally, water is very cheap compared to other solvents.

By virtue of this combination of properties, water has great potential as a solvent for coal liquefaction and has drawn the attention of a number of investigators in recent years (2-6). These researchers have established a number of advantages for water including:

i. Ease of separation of solvent and product;
ii. Minimal char production (2);
iii. Use of soluble catalysts (3,4); and
iv. Relatively high liquefaction yields.

Recently, we developed a unique flow mode reactor (7) which has enabled us to isolate processes contributing to coal liquefaction and to investigate them dynamically. Using this reactor with a variety of solvents, we established 300°C as the threshold temperature for thermal chemical solubilization of Illinois No. 6 Coal; and in the 360-420°C range, we obtained conversions ranging from 15% in hexane to 44% in toluene.

Our recent investigations have focused on two important components of coal conversion: thermal chemical reactions and dissolution of coaly material (including thermolysis products) in the solvent; and we are exploring the effects of temperature and pressure on these processes. Here, we report the initial results of our investigation of these effects in the aqueous liquefaction of coal and compare these results to those obtained with other solvents.

EXPERIMENTAL

General

Illinois No. 6 coal from the Ames Lab Coal Library was used in these studies. This coal has the following ultimate analysis (dmmf basis): 78.82% C; 5.50% H; 1.59% N; 2.29% S_{org}; and 10.05% ash. Prior to use, this coal was ground, sized to 60 x 100 mesh, and dried at 110°C overnight under vacuum. Conversions were measured gravimetrically and are reported as % weight loss on a raw coal basis.

*Operated for the U.S. Department of Energy by Iowa State University under contract No. W-7405-Eng-82.

Flow Mode Extraction of Coal

The liquefaction experiments were carried out in the apparatus shown schematically in Figure 1. Typically, the reactor was loaded with 500 mg. of coal (leaving a free volume of 0.70 ml); and the system was filled with solvent and brought to operating pressure (usually 3000 psi). Heating (rate $\sim$ 150°C/min) and solvent flow (1.0 ml/min) were initiated simultaneously; and constant temperature and pressure were attained within three minutes. Extraction was continued for one or, in some cases, two hours. In some experiments, conditions were changed at predetermined points during the run. After cooling and flushing with nitrogen, the residue was removed from the reactor, dried at 110°C overnight under vacuum, and weighed.

RESULTS AND DISCUSSIONS

The advantages of the Flow Mode Extractor used in these experiments has been established in a previous report from this laboratory (7). These advantages are analogous to those reported for other rapid heating, continuous product removal techniques (e.g. heated grid vacuum pyrolysis (8)) and include suppression of retrogressive reactions and dynamic observation of changes which occur during the course of the conversion.

Flow Mode Extraction of Coal with Water

Our initial experiments were conducted for the purpose of comparing aqueous extraction yields to those which had been obtained using a series of nominally unreactive organic solvents (9). Figure 2 shows a comparison of the extraction yields for these solvents at 420°C and 3000 psi with that of water at 400°C and 3580 psi. Clearly, water is one of the best "nonreactive" solvents for the thermal liquefaction of coal. This conclusion also holds at 370 and 400°C, the other temperatures included in this investigation.

We can find only one basis for comparing batch and flow mode systems in the aqueous liquefaction of Illinois No. 6 Coal. At 400°C Vasilakos reports batch mode conversions of 34.0% (3580 psi) and 29.5% (3070 psi) (10). Under identical conditions in our reactor, we find extraction yields of 38.2% and 33.6%, respectively.

Temperature and Pressure Effects on Aqueous Liquefaction

Because of the unusually high critical pressure of water (P_c = 3206 psi; cf. benzene: P_c = 716 psi), interesting temperature/pressure/conversion relationships were expected for aqueous extraction of coal. The effects of temperature and pressure on conversion are reported in Table 1. Trends in this behavior are more apparent in Figure 3 which plots conversion vs. density for a series of isotherms.

At 370°C, conversion begins to decrease quite rapidly as the density approaches 0.15 g/ml, and we believe that there are similar "threshold" densities at the higher temperatures. However, pressures fluctuated wildly during the latter experiments, and we were unable to obtain meaningful data under these conditions. In the low density

Table 1. Effect of Temperature and Pressure on the Aqueous Extraction of Illinois No. 6 Coal

Expt. No.	Temperature (°C)	Pressure (psi)	Density[a] (g/ml)	Weight Loss (%)
16	370	1925	0.061	14.6
17	370	2950	0.151	31.8
18	370	3207	0.485	34.9
22	380	2950	0.128	34.3
11	380	3220	0.174	35.4
21	380	3750	0.482	35.6
19	400	3070	0.113	33.6
20	400	3580	0.163	38.2

a. For pure water (11).

region, it appears that conversion is limited by solubility since thermal processes should proceed at about the same rate under both high and low density conditions.

Our final series of experiments were designed to determine whether the "extract" remaining in the low density residue after extraction for one hour at 370°C and 1925 psi was recoverable by simply increasing the pressure to 2950 psi. We suspected that, at 370°C, much of this material would be fixed by retrogressive reactions during the period of low density extraction. Surprisingly, in a two stage experiment at 370°C (first stage 1925 psi, extraction time 1 hour; second stage 2950 psi, extraction time 1 hour), we obtained an extraction yield of 31.6% compared to 31.8% conversion for one stage extraction at 2950 psi. We are puzzled by this behavior and plan to continue our investigations by analyzing products at discrete intervals during the course of the conversion.

ACKNOWLEDGEMENT

This material was prepared with the support of the U. S. Department of Energy, Grant No. DE-FG22-82PC50786 for which we are grateful. However, any opinions, findings, conclusions, or recommendations expressed herein are those of the authors and do not necessarily reflect the views of DOE.

REFERENCES

1a. Barton, P.; Fenske, M. R. Ind. Eng. Chem. Process Des. Dev. **1970**, 9, 18.

1b. Barton, P.; Hajnik, D. F. In "Adsorption and Ion Exchange with Synthetic Zeolites," ACS Symposium Series 135, Flank, W. F., Ed., American Chemical Society, Washington, D. C., **1980**, Chapter 12.

2. Modell, M.; Reid, C.; Amin, S. I., U. S. Patent 4,113,446, **1978**.

3. Barton, P. Ind. Eng. Chem. Process Des. Dev. **1983**, 22, 589.

4. Ross, D. S.; Nguyen, Q. C.; Hum, G. P. Fuel **1984**, 63, 1211.

5. Ross, D. S.; Blessing, J. E.; Nguyen, Q. C.; Hum, G. P. Fuel **1984**, 63, 1206.

6. Deshpande, G. V.; Holder, G. D.; Bishop, A. A.; Gopal, J.; Wender, I. Fuel **1984**, 63, 956.

7. Squires, T. G.; Aida, T.; Chen, Y. Y.; Smith, B. F. Prepr. Pap.-Am. Chem. Soc., Div. Fuel Chem. **1983**, 28(4), 228.

8. Freihaut, J. D.; Zabielski, M. F.; Seery, D. J. Nineteenth Symposium (International) on Combustion, The Combustion Institute, **1982**, p. 1159 and references cited therein.

9. Unpublished results from this laboratory.

10. Vasilakos, N. P.; Dobbs, J. M.; Parisi, A. S. Prepr. Pap.-Am. Chem. Soc., Div. Fuel Chem. **1983**, 28(4), 212.

11a. Canjar, L. N.; Manning, F. S. "Thermodynamic Properties and Reduced Correlations for Gases," Gulf Publishing Company, Houston, Texas.

11b. Keenan, J. M.; Keyes, F. H. "Thermodynamic Properties of Steam," John Wiley & Sons, Inc., **1951**.

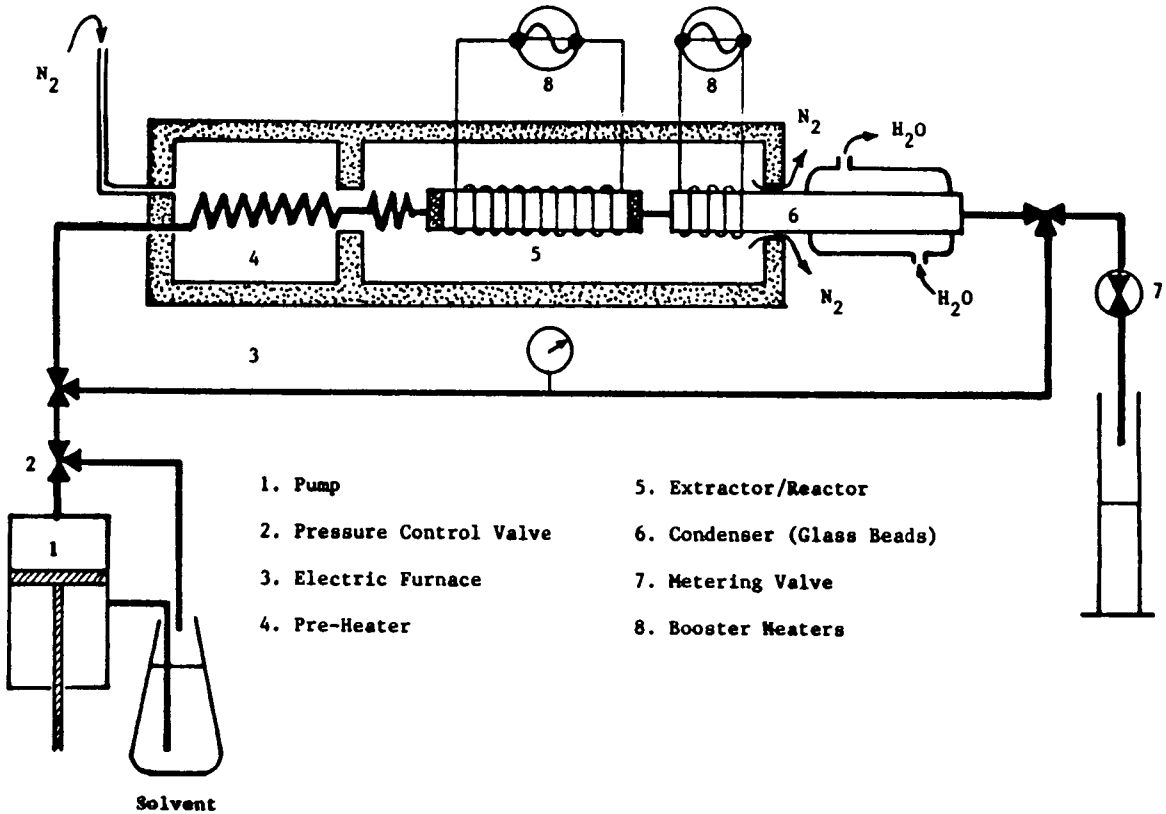

FIGURE 1. Rapid Heating Flow Mode Reactor

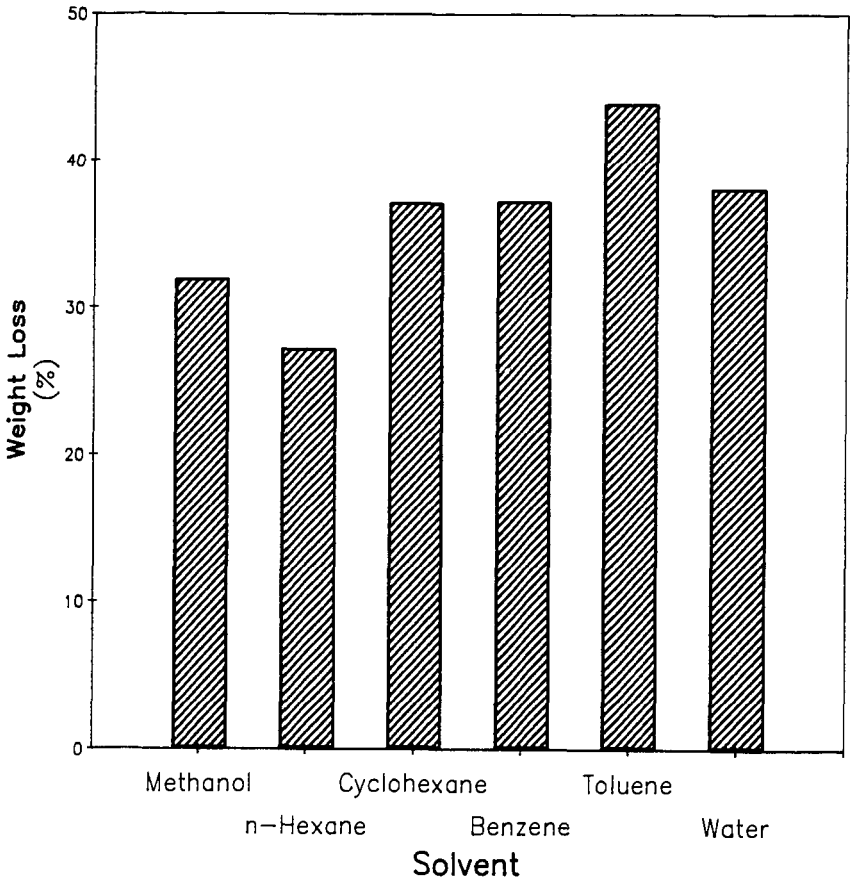

FIGURE 2. Solvent Extraction of Illinois No. 6 Coal at 420°C[a] and 3000 psi[a] (2 Hours[b])

a. Aqueous extraction conducted at 400°C, 3580 psi.

b. Benzene and water extractions reported for 1 hour.

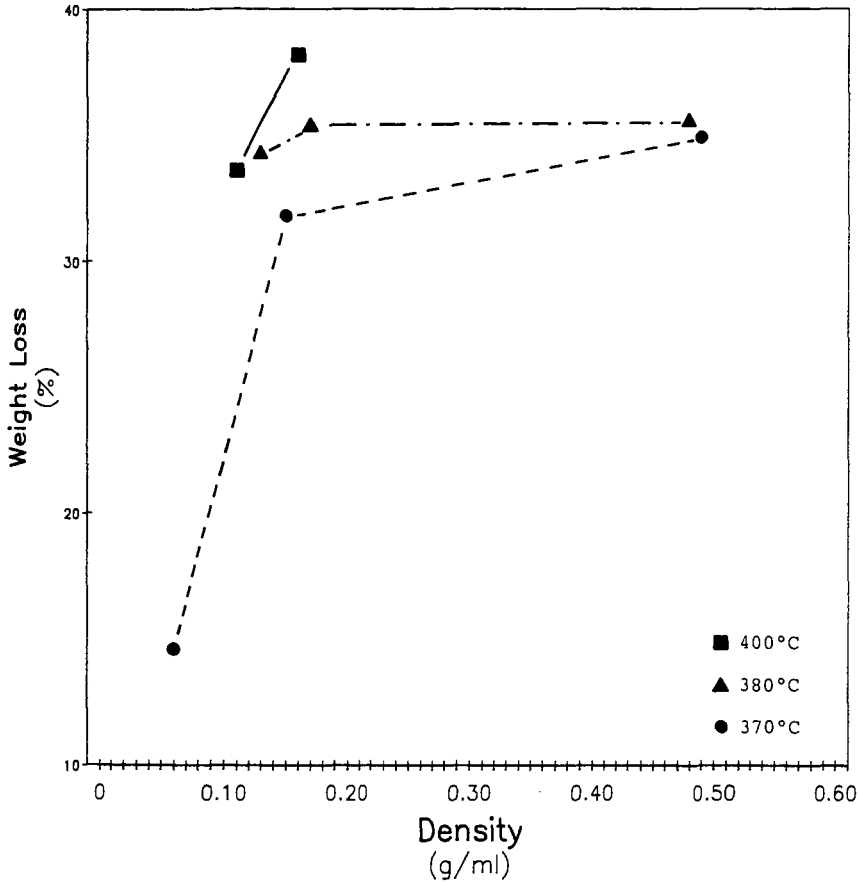

FIGURE 3. Density and Temperature Effects in the Aqueous Extraction of Illinois No. 6 Coal